National Library of Canada
Bibliothèque nationale du Canada

Canadian Theses Service
Service des thèses canadiennes

Ottawa, Canada
K1A 0N4

NOTICE

The quality of this microform is heavily dependent upon the quality of the original thesis submitted for microfilming. Every effort has been made to ensure the highest quality of reproduction possible.

If pages are missing, contact the university which granted the degree.

Some pages may have indistinct print especially if the original pages were typed with a poor typewriter ribbon or if the university sent us an inferior photocopy.

Reproduction in full or in part of this microform is governed by the Canadian Copyright Act, R.S.C. 1970, c. C-30, and subsequent amendments.

AVIS

La qualité de cette microforme dépend grandement de la qualité de la thèse soumise au microfilmage. Nous avons tout fait pour assurer une qualité supérieure de reproduction.

S'il manque des pages, veuillez communiquer avec l'université qui a conféré le grade.

La qualité d'impression de certaines pages peut laisser à désirer, surtout si les pages originales ont été dactylographiées à l'aide d'un ruban usé ou si l'université nous a fait parvenir une photocopie de qualité inférieure.

La reproduction, même partielle, de cette microforme est soumise à la Loi canadienne sur le droit d'auteur, SRC 1970, c. C-30, et ses amendements subséquents.

NL-339 (r. 88/04) c

Canada

THE UNIVERSITY OF ALBERTA

Geotechnical Properties of Oil Sands and Related Strata

by

KEITH MICHAEL KOSAR

A THESIS

SUBMITTED TO THE FACULTY OF GRADUATE STUDIES AND RESEARCH

IN PARTIAL FULFILMENT OF THE REQUIREMENTS FOR THE DEGREE

OF DOCTOR OF PHILOSOPHY IN GEOTECHNIQUE

DEPARTMENT OF CIVIL ENGINEERING

EDMONTON, ALBERTA

Spring, 1989

National Library of Canada
Canadian Theses Service
Ottawa, Canada
K1A 0N4

Bibliothèque nationale du Canada
Service des thèses canadiennes

The author has granted an irrevocable non-exclusive licence allowing the National Library of Canada to reproduce, loan, distribute or sell copies of his/her thesis by any means and in any form or format, making this thesis available to interested persons.

The author retains ownership of the copyright in his/her thesis. Neither the thesis nor substantial extracts from it may be printed or otherwise reproduced without his/her permission.

L'auteur a accordé une licence irrévocable et non exclusive permettant à la Bibliothèque nationale du Canada de reproduire, prêter, distribuer ou vendre des copies de sa thèse de quelque manière et sous quelque forme que ce soit pour mettre des exemplaires de cette thèse à la disposition des personnes intéressées.

L'auteur conserve la propriété du droit d'auteur qui protège sa thèse. Ni la thèse ni des extraits substantiels de celle-ci ne doivent être imprimés ou autrement reproduits sans son autorisation.

ISBN 0-315-52945-8

Canada

THE UNIVERSITY OF ALBERTA

RELEASE FORM

NAME OF AUTHOR KEITH MICHAEL KOSAR

TITLE OF THESIS **Geotechnical Properties of Oil Sands and Related Strata**

DEGREE FOR WHICH THESIS WAS PRESENTED DOCTOR OF PHILOSOPHY IN GEOTECHNIQUE

YEAR THIS DEGREE GRANTED Spring, 1989

Permission is hereby granted to THE UNIVERSITY OF ALBERTA LIBRARY to reproduce single copies of this thesis and to lend or sell such copies for private, scholarly or scientific research purposes only.

The author reserves other publication rights, and neither the thesis nor extensive extracts from it may be printed or otherwise reproduced without the author's written permission.

(SIGNED) .....K.M. Kosar.....

PERMANENT ADDRESS:

47 Templemont Road N.E.

CALGARY, Alberta

T1Y 5A3

DATED January 6, 1989

THE UNIVERSITY OF ALBERTA

FACULTY OF GRADUATE STUDIES AND RESEARCH

The undersigned certify that they have read, and recommend to the Faculty of Graduate Studies and Research, for acceptance, a thesis entitled **Geotechnical Properties of Oil Sands and Related Strata** submitted by KEITH MICHAEL KOSAR in partial fulfilment of the requirements for the degree of DOCTOR OF PHILOSOPHY IN GEOTECHNIQUE.

.....

Supervisor

.....

.....

.....

.....

.....

External Examiner

Date..... January 6, 1989

ABSTRACT

The geotechnical response of an oil sands reservoir to in situ heating or to fluid pressure increase results in stresses and deformations which affect hydraulic fracture propagation, formation shearing, well casing performance, the stability of underground openings (uncased wells, tunnels and shafts), and the magnitude of surface heave. The analytical procedures used to model the above mechanisms must simulate fully-coupled thermal-mechanical-fluid flow behaviour (heat consolidation analysis). For these procedures to be utilized for quantitative geotechnical design, material models must be developed and implemented based on an intimate and fundamental understanding of the geotechnical behaviour of the geologically complex and variable reservoir materials. The research documented in this thesis investigates and evaluates the geotechnical behaviour of oil sands and related strata through representative laboratory testing.

The geomechanical behaviour of Athabasca and Cold Lake oil sands, as well as that of overlying, underlying and interbedded strata over a range in temperature of 20°C to 300°C and effective confining stresses to 7 MPa was investigated. The fundamental influence of temperature, pressure, stress and temperature path, time and history of stress on shear strength, stress-strain and thermal volume change behaviour is examined. The use of geological and geotechnical facies to analyze and interpret laboratory test

results is described.

The mechanical properties of Athabasca and Cold Lake formation materials were found to be dependent on temperature, pressure and stress path followed during the test. Cold Lake Clearwater Formation oil sands were weaker and more deformable than Athabasca McMurray Formation oil sands and contained minerals which were more susceptible to pressure and temperature induced grain breakage. As a result, the geotechnical properties vary significantly for the two oil sands. The geotechnical behaviour of oil sands was also found to be dependent on the amount of fines present in the specimen. The Clearwater Formation shale properties were strongly affected by temperature. During heating, the shale shows a volume decrease due to structural breakdown. After slow heating, the shales exhibit higher strengths and modulii. The majority of geotechnical properties of oil sands and associated strata vary non-linearly with pressure and temperature.

ACKNOWLEDGEMENTS

Funding for the research documented in this thesis was provided by the Alberta Oil Sands Technology and Research Authority in the form of a research grant and a graduate student scholarship. The research was supervised by Professor J.D. Scott, who provided guidance and encouragement throughout the study.

Oil sands core materials used in the research program were provided by Petro-Canada Resources, Husky Oil Company, BP Resources Canada Limited and the Alberta Oil Sands Technology and Research Authority.

The technical assistance provided by Denis Gagnon, Hal Soderberg, Jan Radziszewski, Steve Gamble, Gerry Cyre and other staff members is greatly appreciated.

Table of Contents

Chapter		Page
1.	INTRODUCTION	1
	1.1 Statement of Problem	1
	1.2 Research Objectives	4
	1.3 Scope of Thesis	5
	1.4 Organization of Thesis	8
2.	BACKGROUND	10
	2.1 Effect of Geological Factors on Constitutive Behaviour	10
	2.1.1 General	10
	2.1.2 Environment of Deposition	10
	2.1.3 Geological History	16
	2.1.4 Athabasca Oil Sands and Related Strata	19
	2.1.5 Cold Lake Oil Sands and Related Strata	31
	2.2 Effect of Temperature on Constitutive Behaviour	38
	2.2.1 Rock	38
	2.2.2 Soils	42
	2.3 Effect of Effective Confining Stress on Constitutive Behaviour	50
	2.3.1 Introduction	50
	2.3.2 Soils	51
	2.3.3 Rock	67
	2.4 Effect of Stress Path	70
	2.5 Geotechnical Properties of Oil Sands at Ambient Temperatures	76
	2.5.1 Mechanical Properties	76
	2.5.2 Physical and Thermal Properties	80

2.6 Geotechnical Properties of Oil Sands at Elevated Temperatures 81

3. OIL SANDS GEOTECHNICAL RESEARCH FACILITY 83

3.1 Geotechnical Test Facility 83

3.2 Sample Preparation and Test Procedures 87

3.3 Compliance Testing 98

4. GEOLOGICAL DETAILS OF MATERIALS STUDIED 99

4.1 Athabasca Materials 99

4.1.1 Underground Test Facility 99

4.1.2 Southern Athabasca McMurray Formation Oil Sands 118

4.1.3 Northern Athabasca Clearwater Formation Oil Sands 119

4.1.4 Summary 120

4.2 Cold Lake Materials 122

4.2.1 Cold Lake Location No. 1 124

4.2.2 Cold Lake Location No. 2 128

4.2.3 Cold Lake Location No. 3 128

4.2.4 Cold Lake Location No. 4 130

4.2.5 Summary 131

5. THERMAL VOLUME CHANGE OF ATHABASCA MATERIALS 135

5.1 Materials Studied 135

5.2 Drained Thermal Volume Change 137

5.2.1 Oil Sands 142

5.2.2 Clearwater Shale 159

5.2.3 Devonian Limestone 165

5.3 Undrained Thermal Volume Change 167

5.4 Summary and Conclusions 172

6. COMPRESSIBILITY OF ATHABASCA MATERIALS 175

6.1 Materials Studied 175
6.2 Methods and Procedures 180
6.3 Oil Sands 182
6.4 Clearwater Shale 196
6.5 Devonian Limestone 201
6.6 Summary and Conclusions 202
7. SHEAR STRENGTH OF ATHABASCA OIL SANDS 207
7.1 Materials Studied 207
7.2 Methods and Procedures 209
7.3 Passive Drained Compression Stress Path 215
7.4 Passive Undrained Compression Stress Path 241
7.5 Drained Unloading Stress Paths 255
7.6 Effect of Elevated Temperatures 270
7.7 Summary 285
8. SHEAR STRENGTH OF ATHABASCA RELATED STRATA 288
8.1 General 288
8.2 Materials Studied 293
8.3 Methods and Procedures 295
8.4 Shear Strength and Stress-Strain Behaviour of Clearwater k_{cc} Shale 299
8.5 Shear Strength and Stress-Strain Behaviour of Devonian Limestone 313
8.6 Summary and Conclusions 323
9. THERMAL VOLUME CHANGE OF COLD LAKE MATERIALS 328
9.1 Materials Studied 328
9.2 Oil Sands 328
9.3 Clearwater Shale 348
9.4 Clearwater Carbonate Rock 351

9.5 Summary and Conclusions 353
10. COMPRESSIBILITY OF COLD LAKE MATERIALS 356
10.1 Materials Studied 356
10.2 Oil Sands 357
10.3 Clearwater Shale 372
10.4 Summary and Conclusions 372
11. SHEAR STRENGTH OF COLD LAKE OIL SANDS 377
11.1 Materials Studied 377
11.2 Methods and Procedures 378
11.3 Cold Lake Location No. 1 Oil Sands 380
11.4 Cold Lake Location No. 2 Oil Sands 419
11.5 Cold Lake Location No. 3 Oil Sands 423
11.6 Cold Lake Location No. 4 Oil Sands 430
11.7 Summary and Conclusions 436
12. SHEAR STRENGTH OF COLD LAKE RELATED STRATA 441
12.1 Materials Studied 441
12.2 Clearwater Shale 444
12.3 Carbonate Cemented Sand 454
12.4 Summary and Conclusions 457
13. CONCLUSIONS AND RECOMMENDATIONS 459
13.1 General 459
13.2 Athabasca Materials 464
13.3 Cold Lake Materials 478
13.4 Comparison of Athabasca and Cold Lake Materials 487
13.5 Recommended Future Research 492
BIBLIOGRAPHY 497
A. EQUIPMENT DETAILS 568

B. SAMPLE PREPARATION AND TEST PROCEDURES 593
C. COMPLIANCE TESTING 607
D. ATHABASCA MATERIALS: COMPRESSIBILITY TEST RESULTS .635
E. COLD LAKE MATERIALS: COMPRESSIBILITY TEST RESULTS .665
F. SPECIMEN DATA 706

List of Tables

Table		Page
1.1	Major Factors Affecting Soil or Rock Constituents	3
2.1	Stratigraphy in Area of UTF	23
3.1	Equipment Modifications During Research Program	88
4.1	Results of Gamma Ray Log (Borehole AO-27)	105
4.2	Laboratory Particle Size Distribution (Borehole AO-27)	106
4.3	Results of Caliper Log (Borehole AO-27)	108
4.4	Results of Resistivity Log (Borehole AO-27)	110
4.5	Results of Density Log (Borehole AO-27)	112
4.6	Core Disturbance, With and Without Repressurization	116
4.7	Summary of Athabasca Materials Used in Experimental Program	123
4.8	Summary of Cold Lake Materials Used in Experimental Program	132
5.1	Athabasca Thermal Volume Change Specimens	136
5.2	Athabasca Oil Sands Drained Thermal Volume Change Test and Specimen Data	143
6.1	Isotropic Compressibility of Athabasca Oil Sands	179
6.2	One-Dimensional Compressibility of Athabasca McMurray Formation Oil Sands (Interbedded Specimens)	187
6.3	Isotropic Compressibility of Athabasca McMurray Formation Oil Sands (Interbedded Specimens) at 20°C	191
6.4	Isotropic Compressibility of Athabasca McMurray Formation Oil Sands (Interbedded Specimens) at 225°C	194

Table		Page
7.1	Consolidated Passive Drained Triaxial Tests - Athabasca McMurray Formation Oil Sands	218
7.2	Consolidated Passive Drained Triaxial Tests - Athabasca Clearwater Formation Oil Sands	231
7.3	Consolidated Passive Drained Triaxial Tests - Athabasca McMurray Formation Oil Sands (Interbedded Specimens)	238
7.4	Consolidated Passive Undrained Triaxial Tests - Athabasca McMurray Formation Oil Sands	248
7.5	Consolidated Drained Stress Path Triaxial Tests - Athabasca McMurray Formation Oil Sands	261
7.6	Effect of Stress Path on Initial Tangent Modulus of Deformation	267
7.7	Consolidated Passive Drained Triaxial Tests - Athabasca McMurray Formation Oil Sands at 225°C	274
7.8	Consolidated Passive Undrained Triaxial Tests - Athabasca McMurray Formation Oil Sands at 225°C	280
8.1	Athabasca Clearwater k_{cc} Shale - Initial Conditions	294
8.2	Athabasca Clearwater k_{cc} Shale - After Isotropic Consolidation and Drained Heating	297
8.3	Athabasca Clearwater k_{cc} Shale - Consolidated Passive Triaxial Tests	301
8.4	Summary of Geotechnical Properties of Devonian Limestone at UTF Site	316
9.1	Cold Lake Clearwater Formation Thermal Volume Change Specimens	329
9.2	Cold Lake Oil Sands Thermal Volume Change Test and Specimen Data	331
10.1	One-Dimensional Compressibility of Cold Lake Clearwater Formation Oil Sands (Location No. 1)	358

Table		Page
10.2	Isotropic Compressibility of Cold Lake Clearwater Formation Oil Sands (Location No. 1) at 20°C	359
10.3	Isotropic Compressibility of Cold Lake Clearwater Formation Oil Sands (Location No. 1) at 225°C	360
10.4	Compressibility of Cold Lake Clearwater Formation Oil Sands (Location No. 2)	361
10.5	Compressibility of Cold Lake Clearwater Formation Oil Sands (Location No. 3)	362
10.6	Compressibility of Cold Lake Clearwater Formation Oil Sands (Location No. 4)	363
11.1	Consolidated Drained Triaxial Tests - Cold Lake Clearwater Formation Oil Sands (Location No. 1)	381
11.2	Consolidated Undrained Triaxial Tests - Cold Lake Clearwater Formation Oil Sands (Location No. 1)	395
11.3	Consolidated Drained Triaxial Tests - Cold Lake Clearwater Formation Oil Sands at 225°C (Location No. 1)	406
11.4	Consolidated Drained Triaxial Tests - Cold Lake Clearwater Formation Oil Sands (Location No. 2)	420
11.5	Consolidated Drained Triaxial Tests - Cold Lake Clearwater Formation Oil Sands at 225°C (Location No. 2 and No. 3)	427
11.6	Consolidated Drained Triaxial Tests - Cold Lake Clearwater Formation Oil Sands (Location No. 3 and No. 4)	428
11.7	Consolidated Undrained Triaxial Tests - Cold Lake Clearwater Formation Oil Sands (Location No. 4)	433
12.1	Cold Lake Clearwater Formation Shale - Initial Conditions	442
12.2	Cold Lake Clearwater Shale - After Isotropic Consolidation and Drained Heating	445

Table		Page
12.3	Consolidated Triaxial Tests - Cold Lake Clearwater Shale	446
13.1	Results of X-ray Diffraction Analyses	488
C.1	Calibration Factors For Electronic Measuring Devices	609

List of Figures

Figure		Page
1.1	Solution Strategy to Geotechnical Problems During In Situ Thermal Recovery	6
2.1	Major Oil Sands Deposits of Alberta	11
2.2	Geology of Alberta Oil Sands	13
2.3	Stratigraphic Column of McMurray Formation in Athabasca Oil Sands Mining Area	21
2.4	Grain Size Distribution for Athabasca Oil Sands	26
2.5	Limestone Stratigraphy at UTF Site	28
2.6	Stratigraphic Columns of Clearwater Formation in Northern Cold Lake Area	34
2.7	Composition of Cold Lake Clearwater Oil Sands	36
2.8	Thermal Expansion of Sand at Different Densities	49
2.9	Compressibility of Sands and Gravels	54
2.10	Crushing of Soils with Different Initial Grain Sizes	55
2.11	Grain Crushing of Angular and Subrounded Coarse Sand	56
2.12	Particle Crushing of Rounded and Angular Sand	58
2.13	Components of Shear Strength in Confined Drained Tests on Sand	60
2.14	Confined Drained Compression Tests on Dense Ottawa and Sacramento Sand	62
2.15	Confined Drained Compression Tests on Dense Chatahoochee River Sand	63
2.16	Confined Drained Compression Tests on Saturated Ham River Sand	65
2.17	Fracture Types in Triaxial Compression	68
2.18	Laboratory Stress Paths	71

Figure		Page
4.1	UTF Site - Isopack Map of Main Pay Zone	100
4.2	UTF Site - Underground Development Phase A Pilot	101
4.3	Clearwater Oil Sands Core Sample (Cold Lake Location No. 1)	125
4.4	Clearwater Shale Core Sample (Cold Lake Location No. 1)	127
4.5	Clearwater Oil Sands Core Sample (Cold Lake Location No. 2)	129
4.6	Clearwater Carbonate Rock Core Sample (Cold Lake Location No. 4)	133
5.1	Drained Thermal Volume Change of Saline Creek Oil Sands	144
5.2	Thermal Volume Change of Saline Creek Oil Sands Structure	147
5.3	Drained Thermal Volume Change of UTF Oil Sands Specimen UFCOS1	149
5.4	Drained Thermal Volume Change of UTF Oil Sands	152
5.5	Thermal Volume Change of Soil Structure of UTF Oil Sands	155
5.6	Drained Thermal Volume Change of Medium Plastic UTF Clearwater Shale	160
5.7	Time Dependent Drained Thermal Volume Change of UTF Shale	163
5.8	Drained Thermal Expansion of UTF Devonian Limestone	166
5.9	Undrained Thermal Expansion of UTF Oil Sands	169
5.10	Undrained Thermal Volume Change of UTF Smectite Rich Shale	171
6.1	Isotropic Compressibility of Athabasca Oil Sands	185
6.2	One-Dimensional Compressibility of Athabasca Interbedded Oil Sands	188

Figure Page

6.3 Isotropic Compressibility of Athabasca Interbedded Oil Sands 192

6.4 Isotropic Compressibility of Athabasca Clearwater k_{cc} Shale 197

6.5 One-Dimensional Compressibility of Athabasca Clearwater k_{cb} Shale 199

6.6 Thermal Consolidation of Athabasca Clearwater k_{cb} Shale 200

6.7 One-Dimensional Compressibility of Athabasca Devonian Limestone 203

7.1 Field Stress Paths for Steam Injection 211

7.2 Laboratory Stress Paths 213

7.3 Drained Passive Compression Tests on Athabasca McMurray Formation Oil Sands 216

7.4 Grain Contacts in McMurray Formation Oil Sands Specimen 220

7.5 Cemented Grains in McMurray Formation Oil Sands Specimen 221

7.6 Shear Strength of Athabasca Oil Sands from Triaxial Tests 224

7.7 Variation of E with Confining Pressure at Axial Strain = 0.25% 226

7.8 Variation of Poisson's Ratio with Confining Pressure at Axial Strain = 0.25% 228

7.9 Drained Passive Compression Tests on Athabasca Clearwater Formation Oil Sands 232

7.10 Drained Passive Compression Tests on Athabasca McMurray Formation Interbedded Oil Sands 236

7.11 Shear Strength of Athabasca Interbedded Oil Sands From Triaxial Tests 240

7.12 Undrained Passive Compression Tests on Rich Oil Sands 242

7.13 Stress Path for Undrained Passive Compression Tests on Rich Oil Sands 246

Figure Page

7.14 Undrained Passive Compression Tests on McMurray Formation Interbedded Oil Sands 249

7.15 Tangent Modulus at 0.25% for Undrained Triaxial Compression Tests on Oil Sands 251

7.16 Undrained Shear Strength of Athabasca Oil Sands 252

7.17 Stress Path Testing of Rich, Low Fines McMurray Oil Sands 256

7.18 Effect of Stress Path on Shear Strength of Low Fines Oil Sands 259

7.19 Stress Path Testing of McMurray Formation Interbedded Oil Sands 262

7.20 Shear Strength of Athabasca Interbedded Oil Sands from Stress Path Tests 264

7.21 Axial Strain Contours for Various Stress Paths 269

7.22 Effect of Temperature on Strength of Low Fines Oil Sands 271

7.23 Drained Passive Compression Tests on McMurray Formation Oil Sands at 225°C 275

7.24 Effect of Temperature on Stress-Strain Behaviour of High Fines Oil Sands 277

7.25 Drained Passive Compression Tests on Low Fines McMurray Formation Oil Sands at Elevated Temperatures 278

7.26 Effect of Temperature on High Fines Oil Sands 281

7.27 Undrained Passive Compression Tests on McMurray Formation Oil Sands at 225°C 282

7.28 Effect of Temperature on Undrained Strength of Interbedded Oil Sands 284

8.1 Drained Passive Compression Tests on Clearwater k_{cc} Shale at 20°C 302

8.2 Drained passive Compression Tests on Clearwater k_{cc} Shale at 225°C 303

Figure		Page
8.3	Undrained Passive Compression Tests on Clearwater k_{cc} Shale	304
8.4	Triaxial Test Results on Clearwater k_{cc} Shale	306
8.5	Drained Strength of Clearwater k_{cc} Shale	308
8.6	Variation of Drained Modulus - Clearwater k_{cc} Shale	312
8.7	Generalized Geological Cross-Section at UTF Site	314
8.8	Passive Compression Tests on Devonian Limestone	318
8.9	Triaxial Compression Tests on Devonian Limestone	320
8.10	Shear Strength of Athabasca Oil Sands and Related Strata	326
9.1	Drained Thermal Volume Change of Cold Lake Oil Sands (Location No. 1)	333
9.2	Drained Thermal Volume Change of Cold Lake Oil Sands (Location No. 2)	336
9.3	Thermal Volume Change of Cold Lake Oil Sands (Location No. 3)	338
9.4	Thermal Volume Change of Cold Lake Oil Sands (Location No. 4)	340
9.5	Drained Thermal Volume Change of Cold Lake Oil Sands	342
9.6	Thermal Volume Change of Sand Structure of Cold Lake Oil Sands	345
9.7	Thermal Volume Change of Cold Lake Clearwater Shale	349
9.8	Drained Thermal Expansion of Cold Lake Clearwater Carbonate Rock	352
10.1	One-Dimensional Compressibility of Cold Lake Oil Sands	364
10.2	Grain Size Distribution Before and After One-Dimensional Loading and Drained Heating	365

Figure		Page
10.3	Isotropic Compressibility of Cold Lake Oil Sands	370
10.4	One-Dimensional Compressibility of Cold Lake Clearwater Shale	373
10.5	Isotropic Compressibility of Cold Lake Clearwater Shale	374
11.1	Passive Drained Compression of Cold Lake Clearwater Oil Sands (Location No. 1)	382
11.2	Scanning Electron Micrograph of Specimen CL1TOS4 (Magnification 55X)	384
11.3	Energy Dispersive X-ray Analysis of Crushed Grain in Specimen CL1TOS4	385
11.4	Energy Dispersive X-ray Analysis of Specimen CL1TOS4	387
11.5	Relative Crushing of Cold Lake Location No. 1 Oil Sands	388
11.6	Drained Compression Tests on Cold Lake Clearwater Oil Sands (Location No. 1)	390
11.7	Variation of Drained Modulus - Cold Lake Clearwater Oil Sands (Location No. 1)	393
11.8	Passive Undrained Compression of Cold Lake Clearwater Oil Sands (Location No. 1)	396
11.9	Undrained Compression Tests on Cold Lake Clearwater Oil Sands (Location No. 1)	399
11.10	Variation of Undrained Modulus - Cold Lake Clearwater Oil Sands (Location No. 1)	403
11.11	Passive Drained Compression at 125°C	407
11.12	Passive Drained Compression at 225°C (Location No. 1)	410
11.13	Scanning Electron Micrograph of Specimen CL1TOS14 (Magnification 55X)	411
11.14	Passive Drained Compression Test on Specimen CL1TOS15	414

Figure Page

11.15 Scanning Electron Micrograph of Specimen CL1TOS15 (Magnification 110X) 416

11.16 Summary of Passive Drained Compression Tests on Cold Lake Oil Sands (Location No. 1) 417

11.17 Passive Drained Compression Tests on Cold Lake Oil Sands (Location No. 2) 421

11.18 Passive Drained Compression Test on Specimen CL2TOS4 424

11.19 Passive Drained Compression Test on Cold Lake Oil Sands (Location No. 3) 425

11.20 Scanning Electron Micrograph of Specimen CL3TOS2 (Magnification 72X) 429

11.21 Passive Drained Compression Test on Specimen CL4TOS1 431

11.22 Passive Undrained Compression Test on Specimen CL4TOS2 434

11.23 Grain Size Distribution Before and After Undrained Shear at 20°C 435

12.1 Passive Drained Compression Test on Cold Lake Clearwater Shale 447

12.2 Passive Undrained Compression Test on Cold Lake Clearwater Shale 449

12.3 Passive Undrained Compression Test on Cold Lake Clearwater Shale at 225°C 451

12.4 Passive Compression Tests on Cold Lake Clearwater Shale 453

12.5 Passive Drained Compression Test on Cold Lake Cemented Sand 455

12.6 Passive Drained Compression Test on Cold Lake Cemented Sand at 225°C 456

A.1 High Temperature Triaxial Compression Cell With Internal Load Cell 569

A.2 Sketch of Installation and Wiring of Internal Load Cell and Vertical Strain Arms 571

Figure		Page
A.3	High Temperature Consolidometer	573
A.4	Schematic of High Temperature and Pressure Triaxial Cell and Pressure Systems	575
A.5	Schematic of Room Temperture Triaxial Cell and Pressure Systems	576
A.6	Schematic of High Tempertaure Consolidometer and Pressure Systems	577
A.7	High Pressure Air-Actuated Pump	579
A.8	Servo-Controller: Block Function Diagram	580
A.9	Ennis Measuring Accumulator	582
A.10	Bellows Volume Change Device	583
A.11	Loading Frame	585
A.12	Steam Generator	587
A.13	Mould for Forming Triaxial Membranes	592
C.1	Variation of Piston Friction with Confining Pressure at 225°C	611
C.2	Loading System Stiffness	613
C.3	Loading System Stiffness Test at 225°C	616
C.4	Vertical Compression of Aluminum Cylinder at 20°C	617
C.5	Vertical Compression of Aluminum Cylinder at 225°C	618
C.6	Vertical Thermal Expansion of Aluminum Cylinder	621
C.7	Thermal Expansion of Water (54 mm Ring)	626
C.8	Thermal Expansion of Water (76 mm Ring)	627
C.9	Vertical Expansion of Oedometer	629
C.10	Oedometer Compression for Different Temperatures	630
C.11	Oedometer Piston Friction	634

Figure Page

D.1 Isotropic Compressibility Test AMTOS1 636

D.2 Isotropic Compressibility Test AMTOS2 637

D.3 Isotropic Compressibility Test AMTOS3 638

D.4 Isotropic Compressibility Test ACTOS1 639

D.5 Isotropic Compressibility Test ACTOS2 640

D.6 Isotropic Compressibility Test ACTOS3 641

D.7 Isotropic Compressibility Test ACTOS4 642

D.8 One Dimensional Compressibility Test UFCOS1 643

D.9 One Dimensional Compressibility Test UFCOS2 644

D.10 One Dimensional Compressibility Test UFCOS3 645

D.11 One Dimensional Compressibility Test UFCOS4 646

D.12 One Dimensional Compressibility Test UFCOS5 647

D.13 Isotropic Compressibility Test UFTOS1 648

D.14 Isotropic Compressibility Test UFTOS2 649

D.15 Isotropic Compressibility Test UFTOS3 650

D.16 Isotropic Compressibility Test UFTOS5 651

D.17 Isotropic Compressibility Test UFTOS6 652

D.18 Isotropic Compressibility Test UFTOS7 653

D.19 Isotropic Compressibility Test UFTOS8 654

D.20 Isotropic Compressibility Test UFTOS9 655

D.21 Isotropic Compressibility Test UFTOS10 656

D.22 Isotropic Compressibility Test UFTOS12 657

D.23 Isotropic Compressibility Test UFTOS14 658

D.24 Isotropic Compressibility Test UFHTTOS1 at 225°C 659

Figure Page

D.25 Isotropic Compressibility Test UFHTTOS2 at 225°C 660

D.26 Isotropic Compressibility Test UFHTTOS3 at 225°C 661

D.27 Isotropic Compressibility Test UFHTTOS4 at 225°C 662

D.28 Isotropic Compressibility Test UFHTTOS5 at 225°C 663

D.29 Isotropic Compressibility Test UFHTTOS6 at 225°C 664

E.1 One Dimensional Compressibility Test CL1COS1 666

E.2 One Dimensional Compressibility Test CL1COS2 at 225°C 667

E.3 One Dimensional Compressibility Test CL1COS3 at 225°C 668

E.4 Isotropic Compressibility Test CL1TOS1 669

E.5 Isotropic Compressibility Test CL1TOS2 670

E.6 Isotropic Compressibility Test CL1TOS3 671

E.7 Isotropic Compressibility Test CL1TOS4 672

E.8 Isotropic Compressibility Test CL1TOS5 673

E.9 Isotropic Compressibility Test CL1TOS6 674

E.10 Isotropic Compressibility Test CL1TOS7 675

E.11 Isotropic Compressibility Test CL1TOS8 676

E.12 Isotropic Compressibility Test CL1TOS9 677

E.13 Isotropic Compressibility Test CL1TOS10 678

E.14 Isotropic Compressibility Test CL1TOS11 at 125°C 679

E.15 Isotropic Compressibility Test CL1TOS12 at 225°C 680

E.16 Isotropic Compressibility Test CL1TOS13 at 225°C 681

Figure Page

E.17 Isotropic Compressibility Test CL1TOS14 at 225°C 682

E.18 Isotropic Compressibility Test CL1TOS15 at 225°C 683

E.19 One Dimensional Compressibility Test CL2COS1 684

E.20 Isotropic Compressibility Test CL2TOS1 685

E.21 Isotropic Compressibility Test CL2TOS2 686

E.22 Isotropic Compressibility Test CL2TOS3 687

E.23 Isotropic Compressibility Test CL2TOS4 at 225°C 688

E.24 One Dimensional Compressibility Test CL3COS1 689

E.25 One Dimensional Compressibility Test CL3COS2 690

E.26 One Dimensional Compressibility Test CL3COS2 at 225°C 691

E.27 One Dimensional Compressibility Test CL3COS3 at 225°C 692

E.28 One Dimensional Compressibility Test CL3COS4 693

E.29 Isotropic Compressibility Test CL3TOS1 694

E.30 Isotropic Compressibility Test CL3TOS2 at 225°C 695

E.31 One Dimensional Compressibility Test CL4COS1 at 250°C 696

E.32 One Dimensional Compressibility Test CL4COS2 697

E.33 One Dimensional Compressibility Test CL4COS2 at 100°C 698

E.34 One Dimensional Compressibility Test CL4COS2 at 200°C 699

E.35 One Dimensional Compressibility Test CL4COS2 at 200°C 700

Figure Page

E.36 One Dimensional Compressibility Test CL4COS3 at 200°C 701

E.37 One Dimensional Compressibility Test CL4COS4 702

E.38 Isotropic Compressibility Test CL4TOS1 703

E.39 Isotropic Compressibility Test CL4TOS2 704

E.40 Isotropic Compressibility Test CL4TOS3 at 225°C 705

1. INTRODUCTION

1.1 Statement of Problem

Thermal in situ recovery processes are the most common methods used to extract bitumen from oil sands reservoirs buried at depth. The main techniques include cyclic steam stimulation, steam drive and fire flooding. All of these techniques involve drilling injection and production wells from the ground surface with the exception of AOSTRA's Underground Test Facility which entails gaining access to the oil sands reservoir from underground drilling tunnels. During in situ recovery, stresses and deformations occur in the oil sands formation and adjacent strata caused by changes in stress, pore fluid pressure and temperature. The response of the oil sands reservoir to fluid pressure change or to in situ heating results in shear and compressive deformations in the formation and affects hydraulic fracture propagation, formation shearing, well casing performance, the stability of underground openings (uncased wells, tunnels and shafts), and the magnitude of upward heave.

Heating of oil sands and adjacent or interbedded strata (principally shales and limestones) during in situ thermal recovery induces heat transfer by conduction and convection, pore fluid pressure generation and dissipation through fluid flow and/or volume change and stress and deformation effects due to temperature, pore fluid pressure and volume changes. These phenomena occur simultaneously and are mutually

dependent and, therefore, require fully compatible coupled analyses for determining the temperature, pore fluid pressure, stress and deformation distribution in the geological materials affected by the bitumen recovery process. The phenomena involved have been coupled together within a concept termed "Heat Consolidation".

The constitutive behaviour representing a particular interaction between heat flow, pore fluid pressure changes and mechanical deformation are generally complex due to the individual response of the soil or rock constituents: particulate, mineral structure and pore fluids (liquids and gases). The combined behaviour of the material components is also highly dependent on geological processes such as environment of deposition and physical, mechanical and chemical alteration over geological time. Laboratory evaluation of these effects are often obscured by sample disturbance caused by core expansion and inadequate preparation and testing procedures.

The major factors affecting soil or rock constituents are summarized in Table 1.1. In general, processes contributing to a physical, chemical or mechanical change to a material constituent result in non-linear and irreversible behaviour of the overall geological material. For example, the mechanical characteristics of soil systems may be highly non-linear and inelastic due to diagenetical alteration of mineral grains and soil fabric (Dusseault, 1977; Barnes, 1980), stress induced particle degradation (Bishop, 1965;

Table 1.1 Major Factors Affecting Soil or Rock Constituents

Soil or Rock Constituent	Ambient Conditions		Sample Disturbance	Thermal Recovery			
	Environment of Deposition	Geological History		Stress Path	Temperature	Effective Stress Level	Pore Fluid Pressure
Individual Particulate	Mineral - type - shape - surface texture Amount of each mineral	Diagenesis -Authigenesis -Recrystallization	Dehydration Hydration	Distortion Compression Yield	Expansion Distortion Yield Chemical alteration Dehydration Crystallization Phase change Oxidation	Distortion Compression Yield	Compression/ Expansion
Structure	Grain size distribution Fabric Stratification Inhomogeneities	Fabric Interparticle contact/ bonding Interparticle forces Jointing/ Fissuring	Fabric Fracturing Bedding plane separation	Fabric (geometric arrangement of particles) Interparticle contact/bonding (cohesion or cementation) Frictional resistance Interparticle forces Shearing or fracturing			
Fluids (bitumen, water, dissolved gases)	Pore fluid composition	Bitumen/ water proportions Dissolved/ free gas Pore fluid pressure	Degree of fluid saturation Gas evolution	Pore pressure equalization or drainage	Density Viscosity Pore pressure Phase change Gas soluability Gas evolution	Pore pressure	Phase change Gas solubility

Vesic and Clough, 1968; Janoo, 1986), or temperature induced structural changes (Mitchell and Campanella, 1968; Houston, et al, 1985; Scott and Kosar, 1985). Clearly, the necessary constitutive relations required for the formulation of heat consolidation theory must be developed and implemented based on a fundamental understanding of the processes involved.

1.2 Research Objectives

The constitutive models used to represent the coupling effects between various phenomena require realistic material parameters which are determined from laboratory tests which employ temperatures, pressures and stress paths appropriate to the in situ process being used. The objective of this study is, therefore, to investigate and identify the major factors governing the constitutive behaviour of oil sands and related strata associated with each of the three pairs of coupling processes (thermal-mechanical, hydro-thermal and hydro-mechanical) through representative laboratory testing. This objective requires the development of relatively complex laboratory equipment and the formulation of specialized sample preparation and testing techniques.

The research focuses on relevant strata from the Athabasca and Cold Lake oil sands deposits. These deposits are of particular interest since each supports significant in situ recovery activity and each was formed under different geological depositional environments and were subjected to different geological histories.

1.3 Scope of Thesis

Geotechnical engineering in in situ oil sands development involves predicting the stresses and deformations that occur in formation strata caused by changes in stress, pore fluid pressure and temperature. The geotechnical response of an oil sands reservoir and associated strata to in situ heating or to fluid pressure increase requires complex and powerful computational methods which can simulate fully-coupled thermal-mechanical-fluid flow behaviour (heat consolidation analysis). For these computational procedures to be utilized for quantitative geotechnical design, however, they must be developed and implemented based on an intimate and fundamental understanding of the geotechnical behaviour of the geologically complex and variable reservoir materials.

An overall approach for rational analysis for geotechnical problems associated with in situ processes is put forth in Figure 1.1. The methodology takes into account the strong influence geology and sampling, sample preparation, and testing procedures have in developing reliable constitutive models for soil behaviour. This methodology forms the framework for the present research.

The geological factors which influence the constitutive behaviour of sediments have been documented in Chapter 2 based on a review of the geological literature. These factors arise from depositional and epigenetic processes and affect mineral particles, grain structure and pore fluids

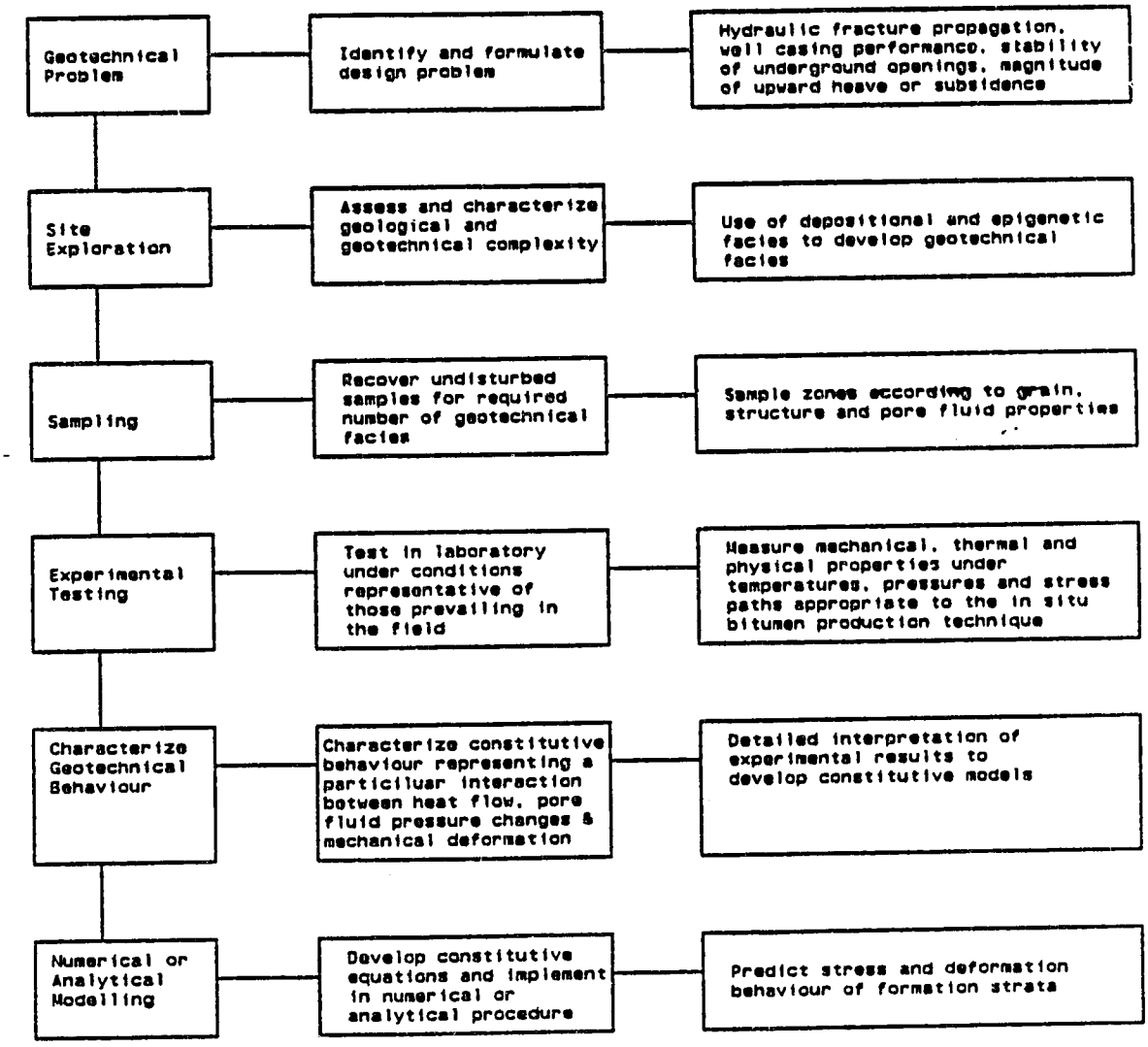

Figure 1.1 Solution Strategy to Geotechnical Problems During In Situ Thermal Recovery

and, therefore, influence the geotechnical behaviour of the overall soil or rock system. Facies models applied to depositional and epigenetic processes and the development of geotechnical facies have proved useful to organize, analyze and interpret geotechnically complex materials. Generalized interpretations of the depositional environments and geological history of pertinent Athabasca and Cold Lake deposits strata have been presented.

The bulk of the experimental work on each set of materials is separated into three broad categories of constitutive behaviour:

1. Triaxial compression tests were carried out to measure the stress-strain behaviour and strength of strata over a range in temperature from 20°C to 225°C and effective confining stresses to 7 MPa. Several stress paths indicative of actual field conditions were investigated.

2. Compression behaviour in response to both one-dimensional and triaxial loading conditions was measured over the temperature range of 20°C to 300°C.

3. Thermal volume change behaviour under various loading conditions and stress histories was measured over the temperature range of 20°C to 300°C.

1.4 Organization of Thesis

The influence of temperature change, stress path, effective stress level and pore fluid pressure changes on the constitutive behaviour of soil and rock based on a review of the relevant literature is presented in Chapter 2. An overview of previous studies involving the laboratory measurement of the geotechnical properties of oil sands at ambient and elevated temperatures is also included in this section.

Chapter 3 outlines the geotechnical high temperature and pressure test facility developed during this research program and summarizes sample preparation and test procedures. Detailed descriptions and specifications of the testing equipment are included in Appendix A. Detailed sample preparation and test procedures used to determine the geotechnical properties of oil sands and related strata under temperature, pressure and stress path conditions associated with in situ thermal bitumen recovery methods are given in Appendix B. Procedures for calibrating electronic measuring devices and results of compliance testing to isolate experimental system response due to temperature and pressure changes are documented in Appendix C.

The geological details of the formation strata studied in the research program are documented in Chapter 4.

The laboratory investigation is divided into two major parts. Athabasca oil sands and related strata are considered in Chapters 5 to 8, inclusive. Cold Lake oil sands and related strata are studied in Chapters 9 to 12, inclusive.

Physical properties such as density, porosity, water and bitumen saturation, grain size distribution, specific gravity and mineral composition were measured for each test to assess the quality and homogeneity of the test specimen and to aid in the interpretation of test results. Physical properties data of test specimens are summarized in Appendix F.

Geotechnical parameters and experimental results derived from the laboratory investigations are summarized and discussed at the conclusion of each chapter. The thesis concludes with a summary of the important findings of this research, discussion of the practical implications and recommendations for further research.

2. BACKGROUND

2.1 Effect of Geological Factors on Constitutive Behaviour

2.1.1 General

The geotechnical behaviour properties of porous sediments are significantly influenced by geological agents. For example, mineralogy, fabric and structure of reservoir and confining strata are controlled by the depositional environment. Subsequent geological activity which causes changes in formation temperature, pressure and pore fluid composition may significantly alter soil fabric and structure (eg. interparticle-contacts, bonding and forces). In situ clastic deposits therefore exist under the influence of many geological factors which vary from deposit to deposit and may vary through the vertical and lateral extent of a particular deposit. As a consequence the fundamental affects of geology on constitutive behaviour must be understood and evaluated to provide an adequate and realistic analytical framework.

2.1.2 Environment of Deposition

Athabasca, Cold Lake, Peace River and Wabasca are the four major oil sands deposits in Alberta (Figure 2.1). These deposits have estimated in-place reserves of about 214.6 x 10^9 m^3, almost 90% of which are contained in the Cretaceous sands of the Athabasca (146.5 x 10^9 m^3) and Cold

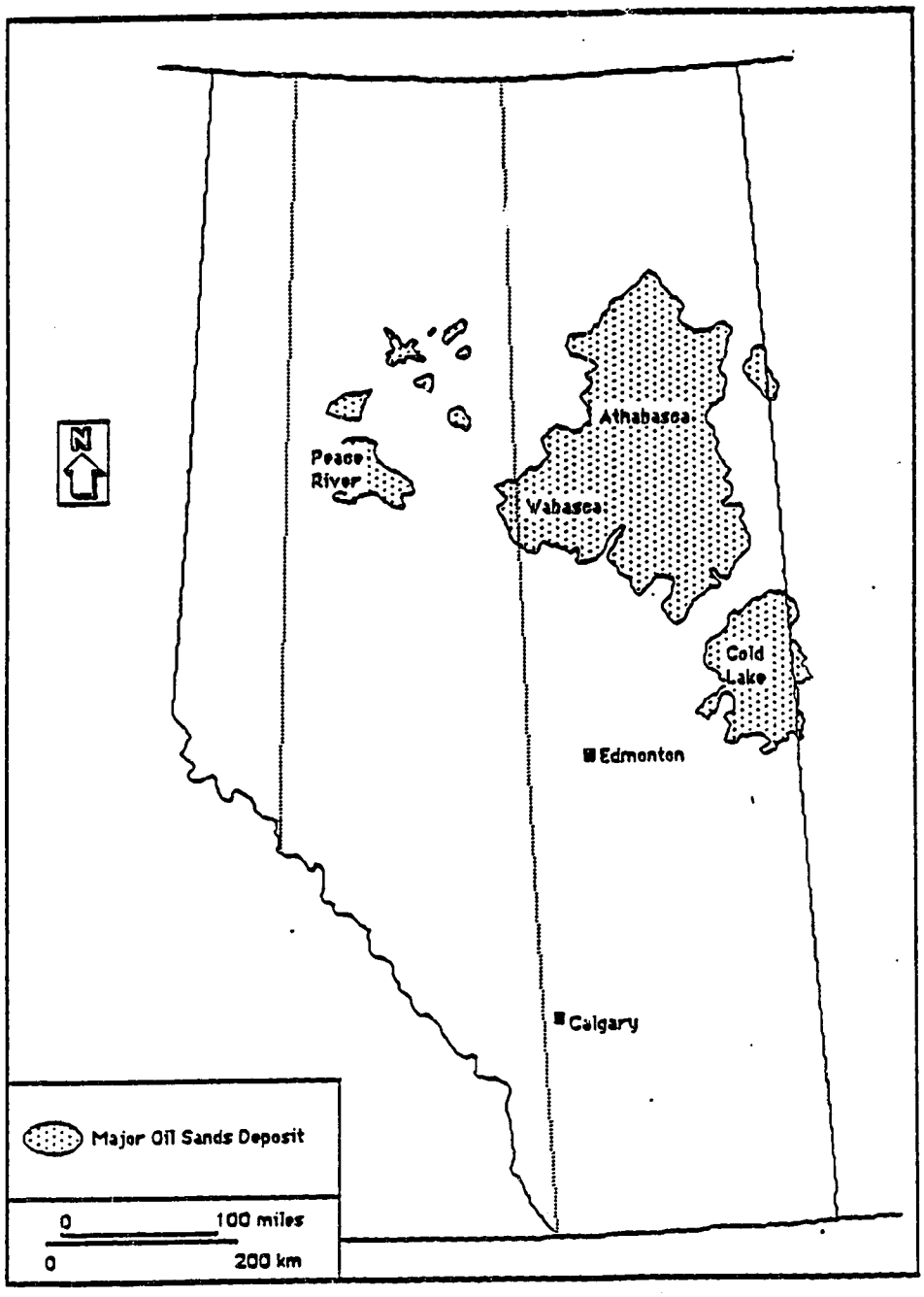

Figure 2.1 Major Oil Sands Deposits of Alberta

Lake (43 x 10^9 m^3) deposits (Outtrim and Evans, 1978). Almost all of the oil bearing sands are contained within the Lower Cretaceous Manville Group and its equivalents (Figure 2.2).

The sedimentology and petrology of the various reservoir formations have been studied extensively as a result of exploitation of bitumen reserves by surface mining and in situ recovery technologies. In general, the literature indicates oil sands formation strata consists of a variable sequence of uncemented clastic sediments (primarily sands and shales) deposited in a variety of marine and continental environments. As a result of the complex stratification oil sands geological strata is commonly described and characterized in terms of facies models.

Briefly, a sedimentary facies is a group of features, such as lithology, sedimentary structures or organic structures, which are significantly different from those in other parts of the stratigraphic unit and indicate its particular environment of deposition (see Walker, 1979 for a review of relevant work and discussion). A facies model is then a group of facies which can be representative of a particular geological process; that is, a general summary of a specific sedimentary environment. Facies models are commonly used to reconstruct paleogeography due to tectonic events such as uplift, erosion or subsidence, conditions of transport and deposition as well as sedimentary environment.

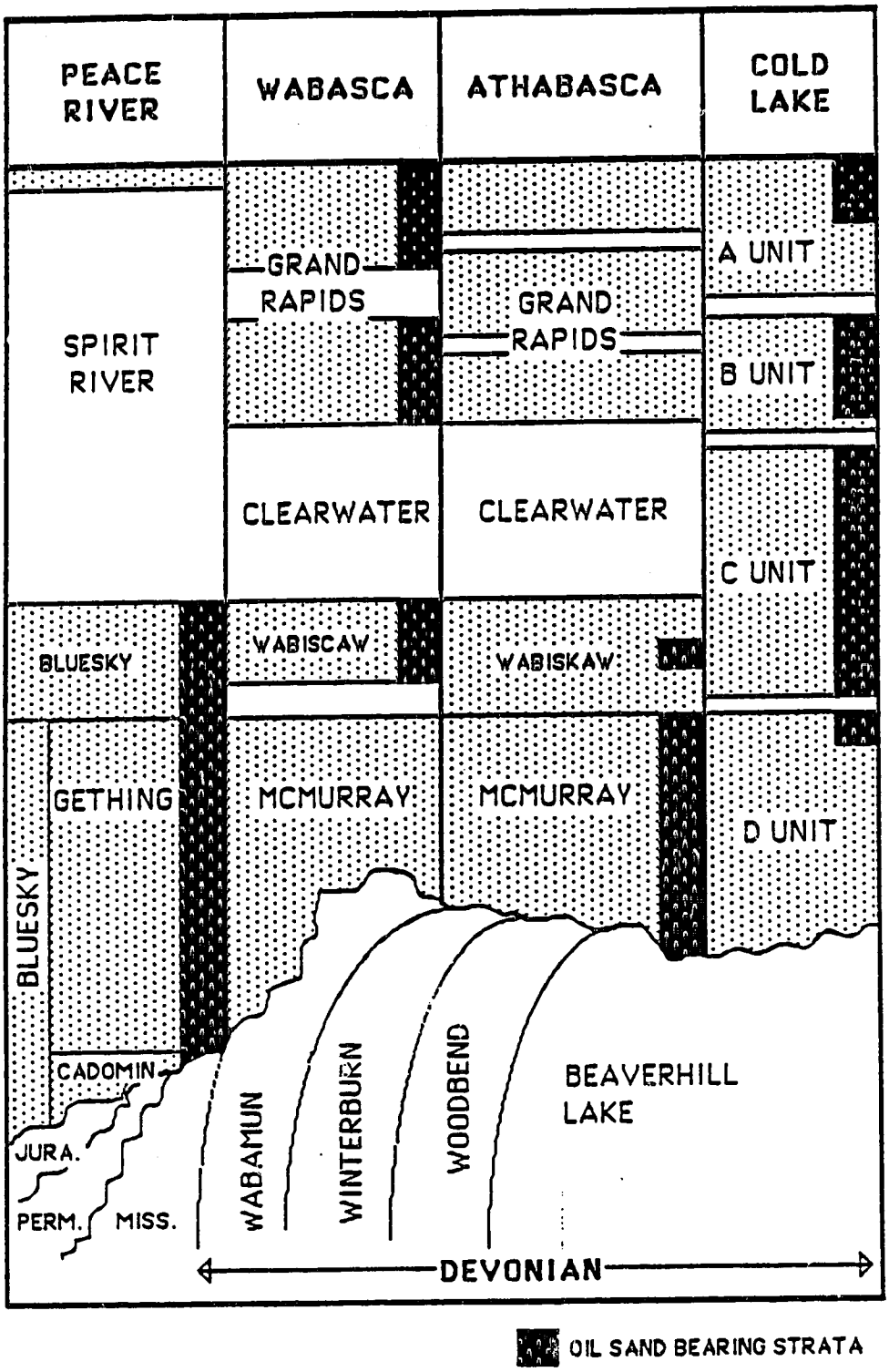

Figure 2.2 Geology of Alberta Oil Sands

Facies models are used in geological research to study factors which affect reservoir variability in order to forecast the size, shape and homogeneity of oil sands reservoirs peripheral to core holes.

Walker (1979) states that in addition to being a summary of sedimentary environment, a facies model must satisfy the following objectives:

1. It must be normalized so as to provide an adequate basis for comparison.

2. It must provide a framework and guide for future observations.

3. It must function as a predictor in new geological situations.

4. It must function as a foundation for the hydrodynamic system or environment that it represents.

Facies models have an important role in the interpretation, characterization and prediction of geotechnical constitutive behaviour. For example, facies

models have been utilized by the U.S. Corps of Engineers in studying the geotechnical behaviour of Mississippi Delta sediments (Kolb, 1962). Barton (1975) coupled geological and engineering investigations, which he termed "geotechnical facies analysis", of Quanternary sediments underlying Westernport Bay, Australia in the design of harbour facilities. In an important paper Morgenstern and Cruden (1979) describe the fundamental importance of geological considerations in geotechnical analysis and design:

> "In the solution of geotechnical problems the engineer is used to employing numerical models in his calculations, physical models in his design, and statistical models in his analysis of data and assessment of reliability. These are all design tools that are particularly valuable after the design problem has been identified and formulated. Geotechnical complexity has been defined as conditions where geotechnical properties vary considerably over the scale of the project under consideration. Projects of this kind present many difficulties to the designer and an analysis of the geotechnical complexity is a prerequisite to rational site investigation and final design formulation. Geotechnical complexity can be analyzed by applying the concept of facies to the genetic, epigenetic, and weathering processes that affect geotechnical properties".

2.1.3 Geological History

A sediment may undergo significant physical and chemical alteration during burial over geologic time. Post-depositional changes in temperature, effective stress and groundwater conditions (composition, availability and flow) may affect mineral particles and grain structure and, therefore, may have a profound influence on the constitutive behaviour of the overall soil or rock system.

The processes that produce the changes that occur in a sediment's composition and structure after deposition are combined together in the geological literature in the term diagenesis. The dominant diagenetic processes are cementation, pressure solution phenomena, mineral authigenesis, recrystallization and compaction (Blatt et al, 1972). A more general term, epigenesis, which also includes post-depositional modification due to deformational processes such as tectonic rebound, has been put forth by Morgenstern and Cruden (1979).

Diagenetic processes which affect both individual clastic grains and soil or rock structure are well documented in the geological literature. For example, diagenetic chemical and physical processes may corrode or dissolve mineral grains (eg. Weyl, 1959), induce grain growth by crystallized overgrowth (eg. Pittman, 1972), cause fracturing or plastic deformation of grains by compaction forces (eg. Atwater and Miller, 1965) or mineral authigenesis and recrystallization (eg. Larson and

Chilinger, 1967).

The grain structure of sand sediments, fine grained sediments (silt and clay) and chemically precipitated crystalline sediments (limestone, salt, gypsum, etc.) generally respond differently to diagenetic actions. Detrital silicate or carbonate sand grains usually acquire tangential grain contacts during deposition although a relatively small number of these contacts may be long contacts (grains sharing a common surface) (Taylor, 1950). Over time, the number of long contacts may increase and a portion of contacts may become concavoconvex or surated due to lithostatic pressures and pressure solution (Weyl, 1959; Thomson, 1959). Compaction (consolidation) may also further reduce the void ratio of the sediment as pore space is occupied by fragments of weaker particles which are crushed or plastically deformed. Grain fabric and grain contacts may also be affected by diagenetic processes involving chemical reactions between grain matrix and groundwater solutions resulting in authigenic overgrowth, cementation and pore filling clay mineral authigenesis and recrystallization. Diagenesis in sand sediments tends to reduce porosity and increase grain contact area. Constitutive behaviour may or may not be affected depending on the intensity of the diagenetic changes that take place. For instance, hydraulic conductivity and compressibility may decrease due to reduced porosity while mechanical parameters such as shear strength and stress-strain moduli may increase due to increased grain

contact shearing resistance and decreased void ratio.

Fine grained sediments can exhibit complex structural variation due to diagenetic processes. Changes in temperature, pressure and/or pore fluid composition over time can lead to the formation of interparticle bonds, reduction in pore space due to authigenesis and transformation of one mineral type to another. Weaver (1959) found montmorillonite converted to mixed layer montmorillonite-illite below 3000 m in several locations studied. Burst (1969) reports hydrated structures decrease dramatically at depths greater than 2500 m (formation temperatures above 95°C) for Eocence sediments of the Gulf coast. Conversion of clay minerals from expansive to non-expansive form is due to the removal of water layers under lithostatic pressures and is believed to be driven by both increases in pressure (generally burial below 3000 m) and temperature (to about 100°C). An increase in chlorite and decrease in montmorillonite and montmorillonite-illite mixed layer minerals may occur in shales at depth (Weaver and Pollard, 1973). Cementation of clayey sediments increases sensitivity and results in an apparent preconsolidation pressure (Mitchell, 1956).

Calcareous sediments are susceptible to diagenetic alteration by cementation, dissolution and replacement (eg. Friedman, 1964; Land, 1967). Dissolution leads to increased porosity as carbonate minerals are removed by differential solution and subsequent leaching. Cementation reduces

porosity due to the growth of newly formed crystals. Replacement (the concurrent dissolution and precipitation of crystals) may or may not affect overall void space but may significantly alter grain structure.

Experimental assessment of constitutive behaviour of oil sands and related strata requires recognition of the processes contributing to in situ composition, shape and orientation of mineral particles and mineral structure. Morgenstern and Cruden (1979) have demonstrated that facies models applied to depositional and epigenetic processes are useful to organize and analyze the characterization of geotechnically complex materials. The procedure involves developing geotechnical facies (zones of strata which display common constitutive response) by superimposing epigenetic facies on the various sedimentary facies.

2.1.4 Athabasca Oil Sands and Related Strata

The depositional history of the Athabasca oil sands has been subject to intense study for a number of years. The majority of work has been concentrated in the area of the two commercial surface mining projects (Suncor Inc. and Syncrude Canada Ltd.) in the northern part of the deposit. Geological research has involved identifying facies patterns in order to predict the geometry, grade and fines content of the oil sands reservoir and the thickness and extent of overlying, underlying and interbedded shale strata. Results of facies analyses are used in mine planning and design to

estimate economic factors, such as waste to ore ratios, and to delineate unfavourable weak strata that may have an adverse effect on mine slope stability.

The vast majority of reserves are contained within the Lower Cretaceous sands of the Lower Mannville McMurray Formation. In general, the geological literature indicates that the stratigraphy of the McMurray Formation in the Athabasca Deposit is complex and highly variable. The McMurray Formation is commonly divided and characterized as three stratigraphic units (upper, middle and lower members), each representing a distinct sedimentary facies pattern. Mattison (1987) identifies over 40 geological reports and papers which interpret the depositional history of the McMurray Formation using deltaic, fluvial and estuarine theory on both a local and regional scale.

A generalized stratigraphic column for the McMurray Formation developed by Mattison (1987) based on sedimentologic, ichnologic and paleontologic criteria in the Athabasca oil sands mining area is schematically depicted in Figure 2.3. At the base of the sequence are coarse grained sands (generally barren of bitumen) exhibiting cross-stratification (fluvial channel sands) overlain by silts and shales (floodplain deposits). It is noted that the lower member (as defined by Mattison) is often neglected in overall facies analyses performed by other researchers (eg. Mossop, 1980) due to its localized development in the lows of the underlying Devonian limestone surface. The middle

(After Mattison, 1987)

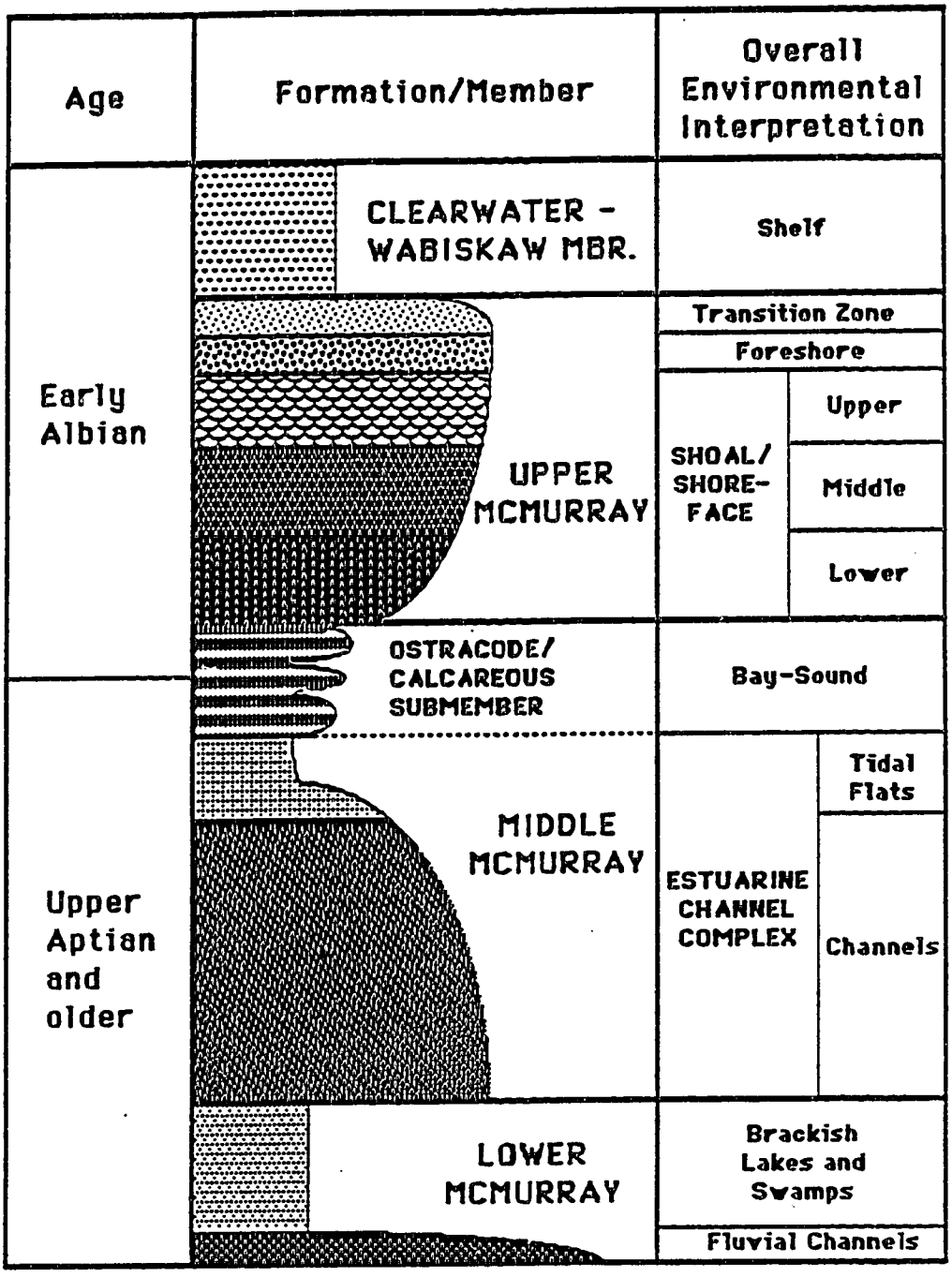

Figure 2.3 Stratigraphic Column of McMurray Formation in Athabasca Oil Sands Mining Area

McMurray is dominated by sands deposited in an estuarine channel complex (channels, mid-channel bars and point bars, and channel margins) overlain by shale and shaley sands (tidal flat deposits) which are, in turn, overlain by shale with interbedded sand (bay sound deposits). The uppermost facies group consists of shoal/shoreface sands overlain by shaley and glauconitic sands of the transitional shelf-shoreface zone and the shefal Wabiskaw Member of the Clearwater Formation.

The Wabiskaw Member contains oil bearing sands in the western region of the Athabasca Deposit (Ranger, 1982). The Wabiskaw member consists of three sands (Wabiskaw A - youngest, Wabiskaw B, and Wabiskaw C - oldest) with interbedded shale. The sands are believed to have originated from the upper Paleozoic sedimentary rocks of the Wainwright Ridge to the southwest and deposited in a marine, shallow shelf environment. Bitumen is trapped stratigraphically and structurally and accumulations of natural gas occur randomly on localized structures.

The majority of Athabasca oil sands considered in this thesis were obtained from AOSTRA's Underground Test Facility (UTF) located approximately 45 km north of Fort McMurray. The McMurray Formation is approximately 38 m thick and is overlain by about 128 m of strata (Pleistocene-recent, Grand Rapids Formation and Clearwater Formation) at this location as shown in Table 2.1 (AOSTRA, 1986). The facies pattern has been interpreted as (occurrence from oldest to youngest)

Table 2.1 Stratigraphy in Area of UTF

Age	Formation	Member	(Thickness) at Site	Material
Quaternary	Pleistocene - Recent	-	3-5 m	Till, glaciolacustrine and glaciofluvial sediments, organics
		EROSIONAL UNCONFORMITY		
Upper Cretaceous	Grand Rapids	-	54.2 m	Interbedded, poorly indurated, claystone, siltstone and glauconitic sandstone, with significant silty and clayey sand zones.
Lower Cretaceous	Clearwater Formation	Kcg	-	Predominantly claystone, minor siltstone and sandstone.
		Kcf	18.5 m	Sand and silt, with claystone and siltstone lenses. Three sandstone lenses.
		Kce	5.1 m	Predominantly claystone and siltstone, minor silt and sandstone.
		Kcd	13.6 m	Claystone at top of unit; remainder predominantly sands, sandstone and siltstone.
		Kcc	22.1 m	Thick claystone unit, with siltstone lenses.
		Kcb	5.5 m	Predominantly claystone at top and sand at bottom.
		Kca	3.7 m	Predominantly claystone.
		Kcw (Wabiskaw)	0.6 m	Thin glauconitic sandstone
	McMurray Formation	Marine	9 m	Fine to medium-grained locally glauconitic. Wet sand at top overlying muddy and silty, fine-to very fine-grained sands and silty muds.
		Estuarine	29 m	Oil impregnated to varying degrees fine-to medium-grained quartz sands, occasional siltstone and claystone layer.
		EROSIONAL UNCONFORMITY		
Upper Devonian	Waterways Formation	Moberly	28.5 m	Thin bedded, argillaceous limestone and massive limestone.
		Christina	22(+) m	Calcareous shale and argillaceous limestone.

upper estuarine channel sand sequence, lower estuarine channel sand, tidal flat/estuarine shoreface group, lower marine shoreface and upper beach/shoreface. The sequences of facies exhibited at the Underground Test Facility are similar to those developed in the surface mining area about 15 km to the east (Mattison, 1987).

It is apparent that a number of geotechnical facies must be delineated, sampled and characterized to adequately define the overall constitutive behaviour of the McMurray Formation. The number of geotechnical facies requiring detailed laboratory assessment, however, would depend on the geotechnical problem under consideration. Mine slope design would require characterization of potential weak zones while numerical modeling of heat consolidation during in situ thermal recovery would require a comparatively large number of geotechnical facies to be sampled and characterized.

High grade oil bearing sands of the Athabasca Deposit are predominantly fine to medium grained and uniformly graded quartz sand. Rich oil sands generally consist of approximately 95 percent quartz, 2 to 3 percent feldspar grains, 2 to 3 percent mica and clay minerals, and traces of other minerals (Mossop, 1978). The grains are primarily subangular with moderate sphericity (Mossop, 1980).

Athabasca oil sands are composed of a dense interlocking grain fabric developed during the time of burial in which diagenetic processes occurred with dissolution and recrystallization of quartz at grain

boundaries. Unlike typical dense sands which exhibit tangential grain contacts, Athabasca oil sands have a large number of concavo-convex and long contacts (Dusseault, 1977; Barnes, 1980). The sand grains are water wet with the majority of the water in elements, known as pendular rings, surrounding the grain-to-grain contact points (Takamura, 1982). The water forms a continuous phase throughout the oil sands matrix. Bitumen occupies the remaining pore space and also forms a continuous phase throughout the oil sands structure. Peacock (1986) reports that the pore liquids are saturated with gas (75% to 90% methane and 10% to 25% carbon dioxide) under in situ conditions. The Combined Solubility Coefficient for the combined gases was found to be approximately 0.20 ($cm^3/cm^3/101$ kPa for bitumen (the small volume of water in the rich oil sands specimens tested by Peacock contained very little gas in solution).

Dusseault (1977, 1980) reports saturated bulk densities for uniformly graded, rich oil sands of 2.05 to 2.18 Mg/m^3 and porosities of 28 to 36 percent. Mossop (1978) reports oil and water saturations of rich oil sands in the Athabasca Deposit of 18 and 2%, respectively. The grain size distribution for Athabasca oil sands is given in Figure 2.4.

In the Athabasca Deposit the McMurray Formation rests primarily on the truncated limestones and calcareous shales of the Waterways Formation, but towards the west they are underlain by the slightly younger carbonate rocks of the Woodbend Group (eg. Norris, 1973; Stewart and MacCallum,

(After Edmunds et al, 1987)

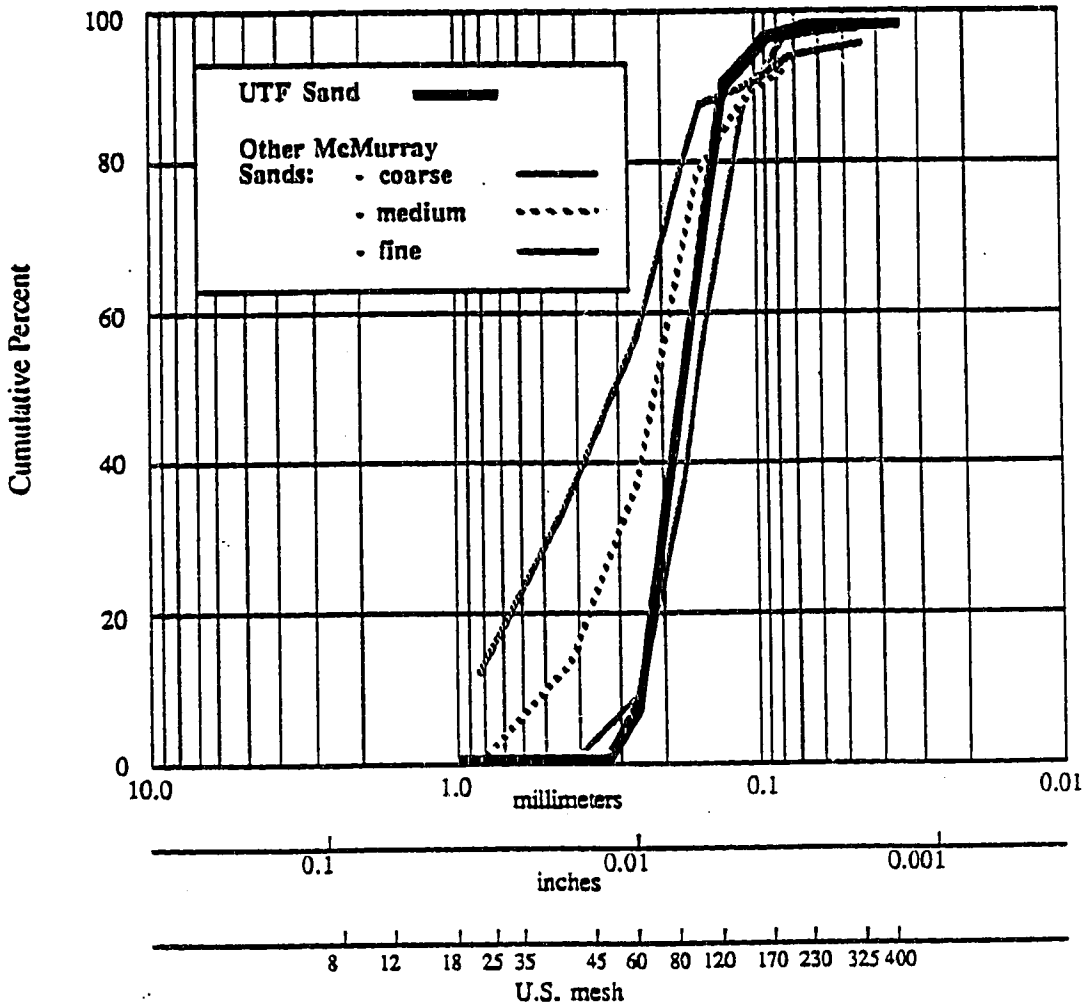

Figure 2.4 Grain Size Distribution for Athabasca Oil Sands

1978; Mossop, 1978; Mathews et al, 1980). The Waterways Formation was deposited during Upper Devonian time and prior to the deposition of the McMurray Formation was uplifted, tilted and eroded. During the Pre-Cretaceous unconformity, a drainage system developed on the Devonian strata. Erosional carving, weathering and kastification of the exposed strata occurred accompanied by salt solution of the underlying Prairie Evaporate Formation. The overlying Devonian beds collapsed forming a broad basin draining to the north. The floor of the basin was covered by shales and shaley limestones of the Waterways Formation. The drainage basin was filled during Cretaceous time as the sea flooded it from the north.

Two major near-orthoganal joint sets have been identified in the Moberley Member of the Waterways Formation (Babcock, 1975). One set of joints has a mutual trend of 000° and 090° while the other system is normal and parallel to the trend of the Rocky Mountain Cordillera (050° and 145°).

The Waterways Formation in the vicinity of the Underground Test Facility consists of interbedded shales and limestones transitional to relatively competent limestone at depth (Figure 2.5). AOSTRA (1986) classifies the Moberley/Mildred Lake Members, the uppermost units of the Waterways Formation, into the following distinct limestone types:

(After AOSTRA, 1986)

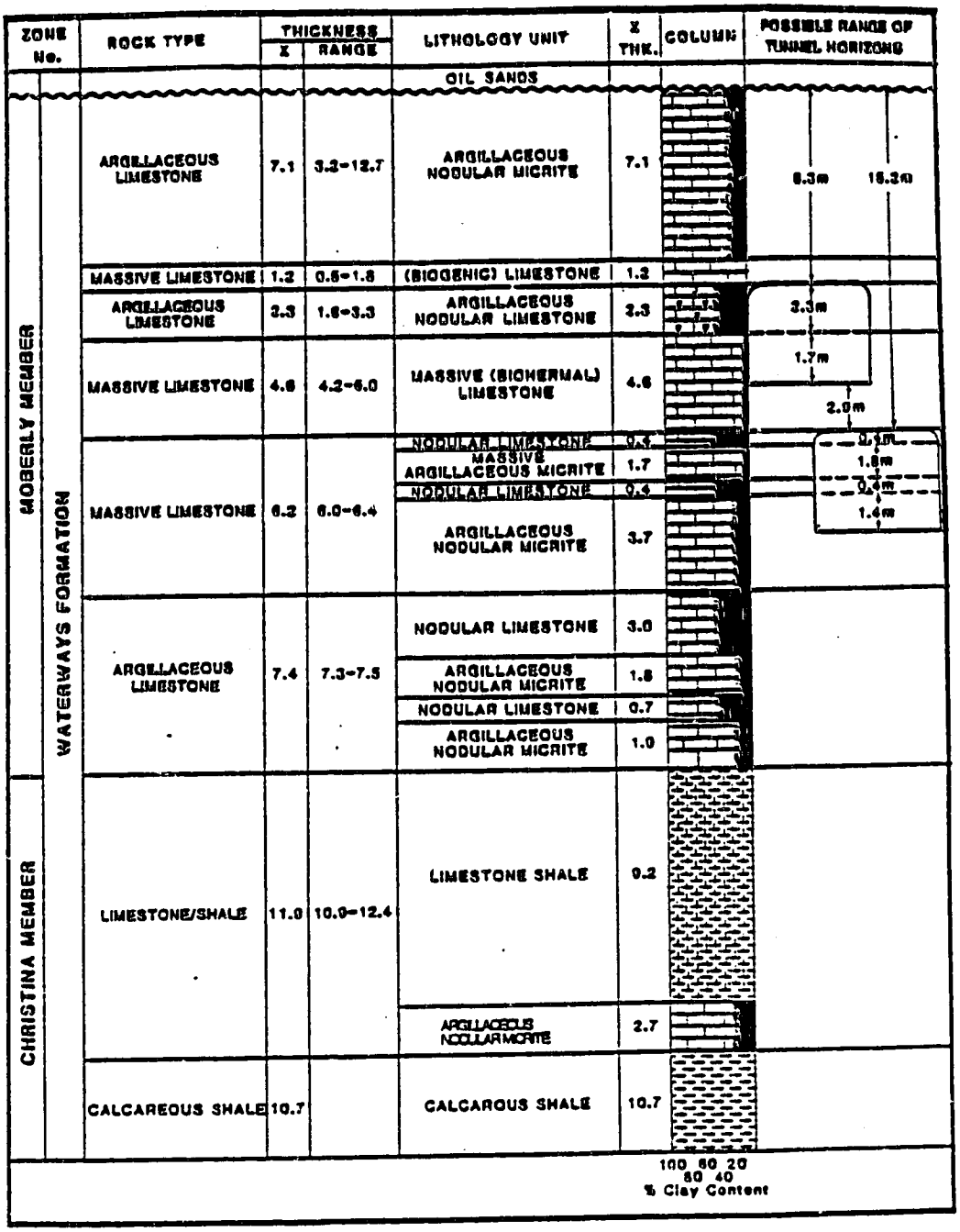

Figure 2.5 Limestone Stratigraphy at UTF Site

- argillaceous micritic limestone,
- argillaceous nodular micrite,
- biogenic limestone,
- nodular limestone, and
- biohermal limestone.

Occasional thin clay interbeds have also been reported. Argillaceous micritic limestone is generally the uppermost strata in the sequence and biogenic or nodular limestone underlies the micrite. AOSTRA (1986) describes all limestone units as being "quite hard and moderately competent" and reports no evidence of solution activity. The surface of the limestone at UTF slopes gently to the west at about 5 m/km. Bedding dips at approximately 2° and joints are vertical and tight.

The Clearwater Formation is a Lower Cretaceous unit which forms the reservoir cap in the Athabasca Deposit. It consists primarily of laterally extensive, flat lying clay shales, clay silts and fine grained sands deposited in a shallow marine environment (Table 2.1). Since the geotechnical behaviour of the Clearwater Formation strata has an influence on the method of overburden removal as well as foundation and slope design at surface mining projects, a substantial amount of geological and geotechnical work has been performed on these strata (eg. Lobb, 1982; Issac and Dusseault, 1984; Issac et al, 1982; Mossop and Flach, 1983).

Issac and Dusseault (1984) and Issac et al (1982) have conducted extensive studies on the Clearwater Formation at the Syncrude Canada Ltd. leases east of the Underground Test Facility. The pertinent results of these studies may be summarized as follows:

1. The Clearwater Formation conformly overlies the McMurray Formation oil sands and is widespread and uniform and has not been subjected to appreciable tectonic or diagenetic forces.

2. The formation has been separated into several units (k_{cw} and k_{ca} through to k_{cf}) with each unit having fairly consistent geological and engineering index properties such as grain size, fabric, moisture content and mineralogy.

3. Units k_{cd} and k_{cw} consist of a mixture of sand, silt and clay with remaining units composed primarily of high plastic clays or clayey silts. Three zones of high smectite content and low density zones have been identified as well as several layers of cemented siltstone of substantial lateral extent throughout the formation.

4. The strata is highly overconsolidated with liquidity indices ranging from -0.03 to -0.27. The mean activities of plastic strata range from 0.78 to 2.02. Water contents vary from 18% for silty strata to 33% for low density smectitic strata.

5. The unweighted clay separation of the clay sizes fraction is illite (44%), smectite (34%), koalinite (11%) and chlorite (11%). The illite content is approximately constant with depth, while the smectite content increases with depth and the kaolinite and chlorite contents decrease with depth.

At the Underground Test Facility site the Clearwater Formation is found between depths of 54 and 125 m (Table 2.1). AOSTRA (1986) describes the Wabiskaw Member at the base of the Clearwater Formation as primarily glauconitic sandstone, units k_{cb}, k_{cd} and k_{cf} as predominantly silts and very fine sands with lesser clays, and units k_{ca}, k_{cc}, k_{ce} and k_{cg} as dominantly shale. Detailed descriptions are contained in Table 2.1.

2.1.5 Cold Lake Oil Sands and Related Strata

The Cold Lake oil sands considered in this study are from the Lower Cretaceous Clearwater Formation of the Upper

Mannville Group. The Clearwater Formation in the Cold Lake Deposit was deposited as nearshore marine sands and associated marine shales (Waywanko, 1982; Visser et al, 1985). The underlying McMurray Formation and overlying Grand Rapids Formation are non-marine sediments (Outtrim and Evans, 1978; Minken, 1974; Putman and Pedskalny, 1983).

The Clearwater Formation was deposited into the Western Cretaceous interior which was exposed to the boreal seas to the north and was closed to the south (Visser et al, 1985). At the beginning of Clearwater time, the Boreal Sea had reached its maximum southward transgression between the North American Craton to the east and the rising Cordillera to the west (Kramers, 1974). Sequential deposition of shales, silty and sandy shales, interbedded shale and sands and massive sands occurred during the retreat of the Boreal Sea in the Wabiskaw area. North and west of the Cold Lake Deposit the Clearwater Formation is composed primarily of marine shales. To the south and east, sands and shales occurring from transitional marine environments dominate the Clearwater Formation (Kirk, 1986). Wightman (1984) interprets the Upper Mannville Deposit as occurring in a river dominated deltaic system. The Cold Lake Clearwater Formation contains facies which are delta-fringe shales and silts, lower delta front shale and sands and upper delta front beach sand and stream mouth bar sands (Harrison et al, 1981).

In the northern part of the deposit the Clearwater Formation has been subdivided into three depositional facies (Visser et al, 1985):

1. Offshore
2. Offshore-transitional
3. Shoreface

Two stratigraphic columns of the Clearwater Formation illustrating the three bitumen reservoirs (C-1, C-2 and C-3) are shown in Figure 2.6. In general, the Clearwater Formation is composed of an upward coarsening trend underlying an overall upward fining trend. This pattern is interpreted by Visser et al (1985) as a regressive sequence followed by a transgressive sequence. The offshore facies is dominated by shale with lesser amounts of silts and sands and grades into the offshore-transitional facies. The offshore-transitional facies is composed of interbedded sands, silts and shales and forms a relatively sharp contact with the shoreface facies. The shoreface facies is dominated by fine grained glauconitic sand with frequent shale partings and thin shale beds near the base.

The mineralogy in the Clearwater Formation varies in the lateral and vertical directions (Kirk, 1986). Putnam and Pedskalny (1983) classify the mineralogy and grain composition of Clearwater sands as feldspathic litharenites

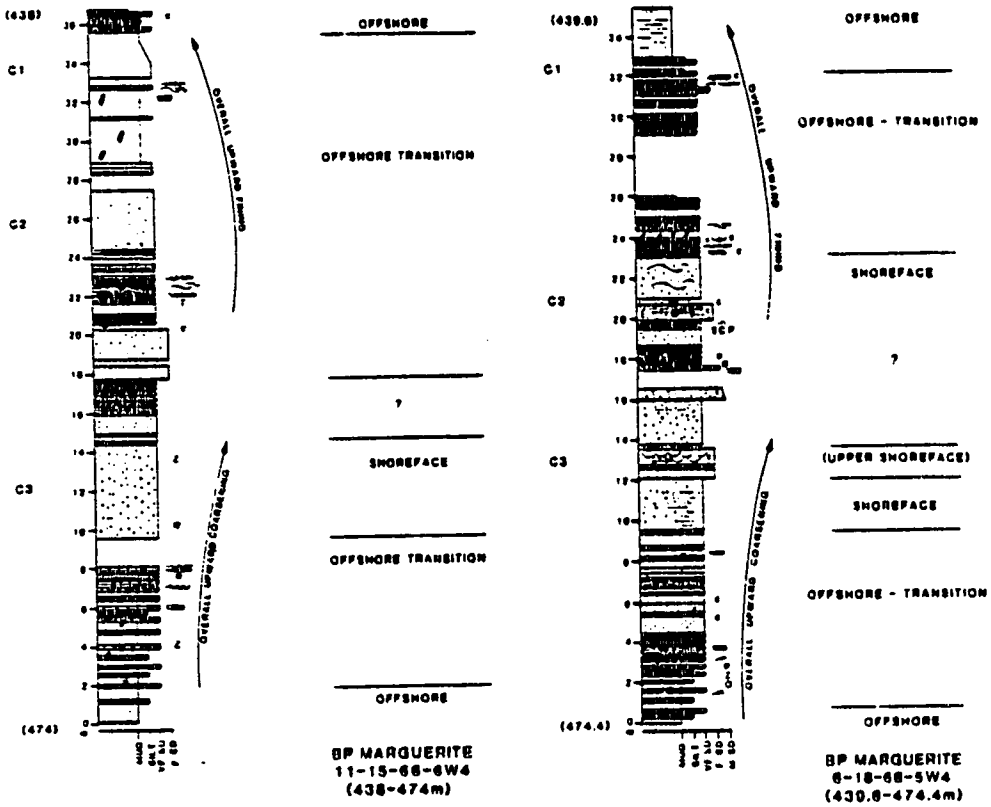

Figure 2.6 Statigraphic Columns of Clearwater Formation in Northern Cold Lake Area

and litharentites (Figure 2.7). Litharenites are sands which contain less than 75% quartz and the remaining grains are comprised of less than 25% feldspar and more than 75% rock fragments and chert. Feldspathic litharenites are sands which contain less than 75% quartz with the remaining grains consisting of 25 to 50% feldspar and 50 to 75% rock fragments and chert. Generally, the Clearwater oil sands of the Cold Lake Deposit contain more rock fragments than detrital minerals (Putnam and Pedskalny, 1983; Kirk, 1986; Harrison et al, 1981; Bowman et al, 1983). The rock fragments may consist of volcanic, shale, sandstone, siltstone, metamorphic and plutonic rock fragments. The primary detrital minerals are quartz, K-feldspar, chert, plagioclase and carbonate. The source of the Clearwater Formation sediments is not clear but, based on the large amount of volcanic rock fragments in the sands, possible sources are the Cordillera in British Columbia or the Precambrian Shield to the east (Putnam and Pedskalny, 1983; Harrison et al, 1981).

Visser et al (1985) describe C-3 reservoir sands as very fine to fine grained, angular to subangular with low sphericity and moderately to well sorted with porosities ranging from 30 to 40%. The clay mineral content ranges from 5% at the base to 1% at the top. Detrital smectite and mixed layer illite-smectite are dispersed throughout the zone. Authigenic chlorite and illite are the primary clays at the top of the interval while authigenic koalinite is the major

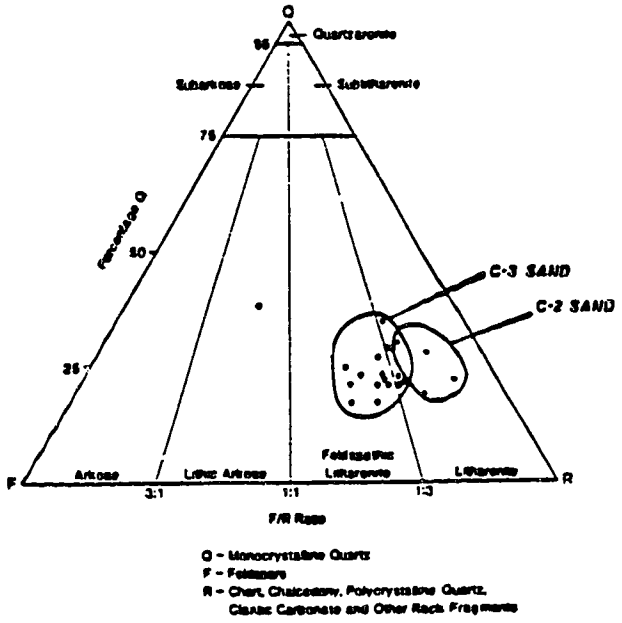

(After Visser et al, 1985)

Figure 2.7 Composition of Cold Lake Clearwater Oil Sands

clay at the base. The C-2 reservoir sands are depicted as very fine grained and subangular with medium sphericity and moderately sorted with porosities ranging from 30 to 35%. This sand contains approximately 2% clay minerals, the majority of which are illite-smectite. Illite-Smectite is believed to be detrital in origin and has a spongy fabric. Also present locally is authigenic koalinite and platey chlorite. The C-1 reservoir sands are considered as being of poor reservoir quality and, therefore, have not been as extensively studied.

The C-3 sands form the thickest (12 to 20 m) and richest (up to 14 wt.% bitumen) reservoir. Horizontal to vertical permeability ratios are often high due to frequent clay laminae and occasional discontinuous calcite cemented sandstones (Visser et al, 1985). The C-3 reservoir is underlain by thick shale (1 to 5 m) of the offshore facies (Figure 2.6) and is overlain by the fining upward trend (C-2 and C-1 sands). The C-2 reservoir has a thickness of 2 to 5 m and the thickness of the C-1 sands range from 2 to 5.5 m. The C-2 and C-1 reservoirs are separated by shale 3 to 5 m thick and 3 to 4 m of shale overlies the C-1 reservoir.

The in situ pore fluid pressure in the C-3 reservoir is approximately 2700 kPa and has a virgin temperature of 15°C (Visser et al, 1985). The C-3 reservoir is generally subjected to in situ steam injection while the C-2 and C-1 reservoirs are generally only produced if sufficient heat

transfer occurs to these overlying reservoirs.

The stratigraphy of the Clearwater Formation varies laterally in the Cold Lake Deposit. Waywanko (1982) reports that a regional core survey indicates that the major deltaic deposit lies to the southeast of the deposit. In general, the reservoir sands in the southern part of the deposit are more fluvially dominated and are coarser grained, have less interbedded shale and higher bitumen content while toward the north and west the marine influence is stronger resulting in more offshore deposits which are finer grained and shalier (Visser et al, 1985; Harrison et al, 1981).

2.2 Effect of Temperature on Constitutive Behaviour

2.2.1 Rock

Extensive laboratory and field studies have been carried out to characterize the influence of temperature change on the thermal, mechanical and physical behaviour of rock masses. The majority of work has been conducted in the areas of geological, geophysical and rock mechanics research (see Agar, 1984 for a review).

Crystalline and cemented rock masses subjected to changes in temperature may undergo significant structural change caused by the development of thermally induced fissuring or the propagation of pre-existing fractures. Thermal degradation may cause a significant change in mechanical properties such as strength, stiffness and

compressibility, as compared to intact values. In addition, thermal properties such as thermal expansion, thermal conductivity and thermal diffusivity and physical properties such as hydraulic conductivity may also be significantly altered due to the formation or extension of thermally induced fissures.

Thermally induced cracking of intact rock masses has been investigated by Lo and Wai (1982), Cooper and Simmons (1977), Richter and Simmons (1974), Berthomieu and Jouanna (1984), Johnson et al (1978), Johnson and Gangi (1980) and others.

Lo and Wai (1982) conducted a series of thermal expansion tests on limestone and granitic gniess over the temperature range of 20 to 400°C. In the experimental procedure, some intact rock specimens were heated slowly at a rate of 2°C per minute or less while others were subjected to an instantaneous temperature increase. Thermally induced cracking was found to be controlled by both temperature and the rate of temperature increase. Lo and Wai identified a "threshold temperature" above which significant fracturing occurs. They postulate that thermal cracking in heterogeneous cemented rock is caused by differential thermal expansion of mineral grains resulting in separation along grain boundaries. In homogeneous crystalline rock, thermal cracking was believed to be caused by differential thermal expansion of randomly aligned anisotropic minerals resulting in the development of internal tensile stresses

which exceed the tensile strength of the rock. The thermal cracking process was found to be enhanced in specimens containing pre-existing micro-cracks. Lo and Wai conclude during initial heating of intact rock specimens, thermally induced cracks form above the threshold temperature even for slow rates of heating. The critical temperature for slow heating for initially crack-free limestone was found to be 210°C and about 100°C for initially micro-fissured granitic gniess.

Similar results to those obtained by Lo and Wai were reported by Richter and Simmons (1974), Cooper and Simmons (1977), Johnson et al (1978) and Johnson and Gangi (1980). In contrast to the above studies, Berthomieu and Jouanna (1984) investigated cracking of granitic rock due to thermal cooling and proposed a method, based on laboratory tests, for estimating the critical cooling temperature for which thermal cracking occurs.

Several studies have demonstrated that the thermal expansion characteristics of rock are significantly influenced by the thermal cracking process (eg. Cooper and Simmons, 1977; Heard, 1980; Lo and Wai, 1982; Page and Heard, 1981, Richter and Simmons, 1974; and Wong and Brace, 1979). The formation of thermal fractures during initial heating increases the measured expansion as compared to specimens that remain intact when subjected to the same increase in temperature. This disparity generally accounts for the wide variation in published thermal expansion values

for similar rock types as noted by Richter and Simmons (1974). Caution must, therefore, be exercised when using numbers obtained from the literature for numerical analyses if the experimental procedures used to derive those specific values are not known. Further, heating of fissured rock specimens may result in measured thermal expansion values which are less than the sum of the thermal volume change of the individual mineral components, as a portion of the expansion is taken up in the expansion of grains into the pre-existing fractures. On a larger scale, the development of thermal strains and stresses is therefore dependent on the severity of jointing in the rock mass (see Witherspoon et al, 1981 and Cook, 1983).

Heat transfer properties have been studied by Durham and Abey (1981), Walsh and Decker (1966), Lo and Wai (1982), Somerton (1958), Anand et al (1973) and many others (see Seto, 1985 for a review). Porosity increases arising from thermally induced fissuring tends to impede thermal transport in dry rock. Thermal diffusivity and thermal conductivity exhibit temperature and temperature history dependencies due to the phenomenon of thermal cracking.

The fluid flow properties of a rock mass may also be affected by the thermal cracking process. The degree of significance, however, depends on the frequency of pre-existing joints or fractures and the interaction between the pore fluid and mineral constituents. While thermal cracking tends to increase porosity, the effect may be

offset or eliminated by the closure of existing discontinuities or the migration or precipitation of fines which may clog pores and restrict fluid transport. Useful experimental data and discussion regarding the permeability of rock at elevated temperatures may be found in Somerton (1982), Heard and Page (1982), Summers et al (1978) and Brace (1980).

Mechanical properties of rock subjected to increases in temperature have been studied by Wai and Lo (1981), Heard (1982), Heuze (1983) and others (see Agar, 1984 for a review). In general, the literature indicates that the mechanical properties of crystalline or cemented intact rock are adversely affected by temperature due to thermal cracking. The stiffness and strength reduces while the compressibility increases at elevated temperatures.

2.2.2 Soils

The effect of heating on the geotechnical properties of soils has been under investigation by a number of researchers for several years. Early research concentrated on the influence of temperature increases on soil properties with particular reference to construction in permafrost, highway design and soil stabilization. In recent years attention has focussed primarily in the areas of high-level radioactive waste disposal and energy resource development.

Finn (1951) carried out a series of consolidation tests on remolded clay over the temperature range of 4 to 27°C.

The results of the study indicated that although the coefficient of consolidation varied with temperature, the amount of compression associated with incremental increases in pressure was independent of temperature. The temperature dependency of the coefficient of consolidation was attributed to the variation of permeability due to changing pore water viscosity.

To isolate volume change response to temperature effects Paaswell (1967) performed a number of thermal consolidation tests on remolded shale to temperatures up to 85°C. The rate of temperature increase applied to the specimens varied from 10°C in 2.5 hours to 55°C in 0.25 hours. For all rates of thermal loading volumetric strain was found to increase as the temperature was increased. Also, the magnitude of strains was greater for larger temperature increases at a given constant stess level.

A theoretical analysis for predicting volume changes in soils resulting from temperature variations and pore pressure changes due to undrained heating has been developed by Campanella and Mitchell (1968) and examined further by Mitchell (1976). Under fully drained conditions the volume change of a soil subjected to increases in temperature arises from the expansion of the individual mineral grains and structural changes in the soil matrix. Under completely undrained conditions the volume change of a fully saturated soil experiencing a temperature increase under no effective confining stress results from the expansion of the

individual mineral grains and pore fluid. Pore pressure response depends on both the thermal expansion and compressibility of the individual components. The material properties required in the Mitchell and Campanella analyses are coefficients of thermal volume change and the coefficients of compressibility for each of the soil components.

The influence of temperature on soil compressibility was investigated by Plum and Esrig (1969). The amount of consolidation due to temperature loading was found to increase with increasing soil compressibility, and a heating and cooling cycle resulted in behaviour characteristic of a loading and unloading cycle. Further, an illite specimen subjected to an overconsolidation ratio of 1.7 experienced no consolidation when heated from 24 to 50°C. Plum and Esrig attributed volume reductions due to temperature increase to decreased effective stress and strength at mineral contacts caused by double layer expansion resulting in increasing repulsive forces. This assertion was later discounted by Mitchell (1969).

Sherif and Burrous (1969) conducted a series of unconfined compression tests on kaolinite specimens over the temperature range of 24 to 66°C. Prior to testing the specimens were consolidated isotropically in the range of 140 to 675 kPa at 24°C. The unconfined compression strength was found to decrease with temperature for specimens tested at the same water content. In contrast, Laguros (1969)

reports an increase in strength with temperature for several soils over the temperature range of 2°C to 41°C. It should be noted, however, that these specimens were consolidated and tested at the same temperature and as a consequence exhibited lower void ratios at the higher temperatures. Laguros also found a decrease in liquid limit with increasing temperature for the soils tested. Noble and Demirel (1969) conducted direct shear tests on highly plastic clay over the temperature range of 2°C to 60°C. Shear strength determinations were made from tests performed at or below the consolidation temperature. Their test results indicate for specimens consolidated under the same temperature, shear strength decreases with increasing temperature. They also found the shear strength increased for a given constant temperature test with increasing consolidation temperature. Murayama (1969) carried out a series of unconfined triaxial compression tests on undisturbed high plastic clay over the temperature range of 5°C to 45°C. The modulus of deformation was found to decrease with increasing temperature and is attributed to a reduction in effective confining stress caused by pore fluid pressure increases caused by undrained heating.

Williams (1982) conducted consolidated undrained triaxial tests on saturated remolded illite over the temperature range of 4°C to 200°C. Williams found that specimens maintained under a constant effective confining stress consolidate in response to a temperature increase.

The amount and rate of consolidation increased with increasing temperature. Thermal consolidation was attributed to a reduction in attraction between mineral particles at elevated temperatures resulting in weaker particle bonds which necessitates rearrangement of particles into a denser packing to carry the applied load. Williams describes the reduction in attraction in terms of a viscous component of the shear strength of the double layer and adsorbed cations. The shear strength of remolded illite was found to increase with increasing temperature and was attributed to an increase in density arising from consolidation due to heating. It was concluded that although viscosity reduction in response to heating may cause a reduction in strength, this effect is small in terms of the increase in strength and stiffness due to compaction during drained heating.

Green (1984) carried out a series of consolidated undrained triaxial tests on undisturbed illite and smectite-rich saturated clays over the temperature range of 4°C to 200°C. The important observations and conclusions arising from this study may be summarized as follows:

1. During drained heating under constant effective confining stress the laboratory specimens increased in density. The magnitude of compression increased with increasing temperature and was attributed to a reduction in attractive forces between soil particles

which caused a decrease in interparticle shearing resistance.

2. Undrained heating caused the pore fluid pressure to increase, the magnitude of which increased with decreasing void ratio and increasing specimen stiffness.

3. Specimens heated to test temperature under fully drained conditions showed increasing stiffness and peak shear strength with increasing temperature.

4. Peak shear strength of specimens with similar initial water contents were found to be dependent on the amount of volumetric strain experienced during consolidation for the particular soil and fabric and independent of the test temperature.

Much of the experimental work on the effects of elevated temperature on the geotechnical properties of soft clays performed by Green (1984) and Williams (1982) is summarized in Houston et al (1985).

Kosar (1983) performed a series of one-dimensional thermal volume change tests on compacted quartz sand over the temperature range of 20°C to 200°C. The constant vertical effective confining stress applied to each specimen prior to heating was varied from 0.05 MPa to 3.5 MPa and the initial density of the specimens ranged from 1.46 to 1.65 Mg/m^3. For each thermal expansion test conducted (Figure 2.8) a negative volume change was observed for the first heating increment (20°C to 50°C). The loosest sand specimen (initial density of 1.46 Mg/m^3 at 20°C) displayed the greatest volume decrease (0.36%) over this temperature range. The sample initially compacted to a density of 1.62 Mg/m^3 at 20°C showed a volume decrease of 0.08% over the temperature range from 20°C to 50°C. After completion of this test (to approximately 200°C) the specimen was allowed to cool. At room temperature a net volume decrease of 0.10% was measured indicating that the volume decrease was due to a compaction of the soil structure.

Since this sand was tested in the dry state with the grains in mineral to mineral contact and each grain undergoing thermal expansion, relative movement or reorientation of the sand grains must have occurred during the temperature increase to 50°C to allow an overall volume decrease. Campanella and Mitchell (1968) suggest such behaviour results from a temperature induced change in interparticle forces that occurs to allow the sand structure to support the same effective stress.

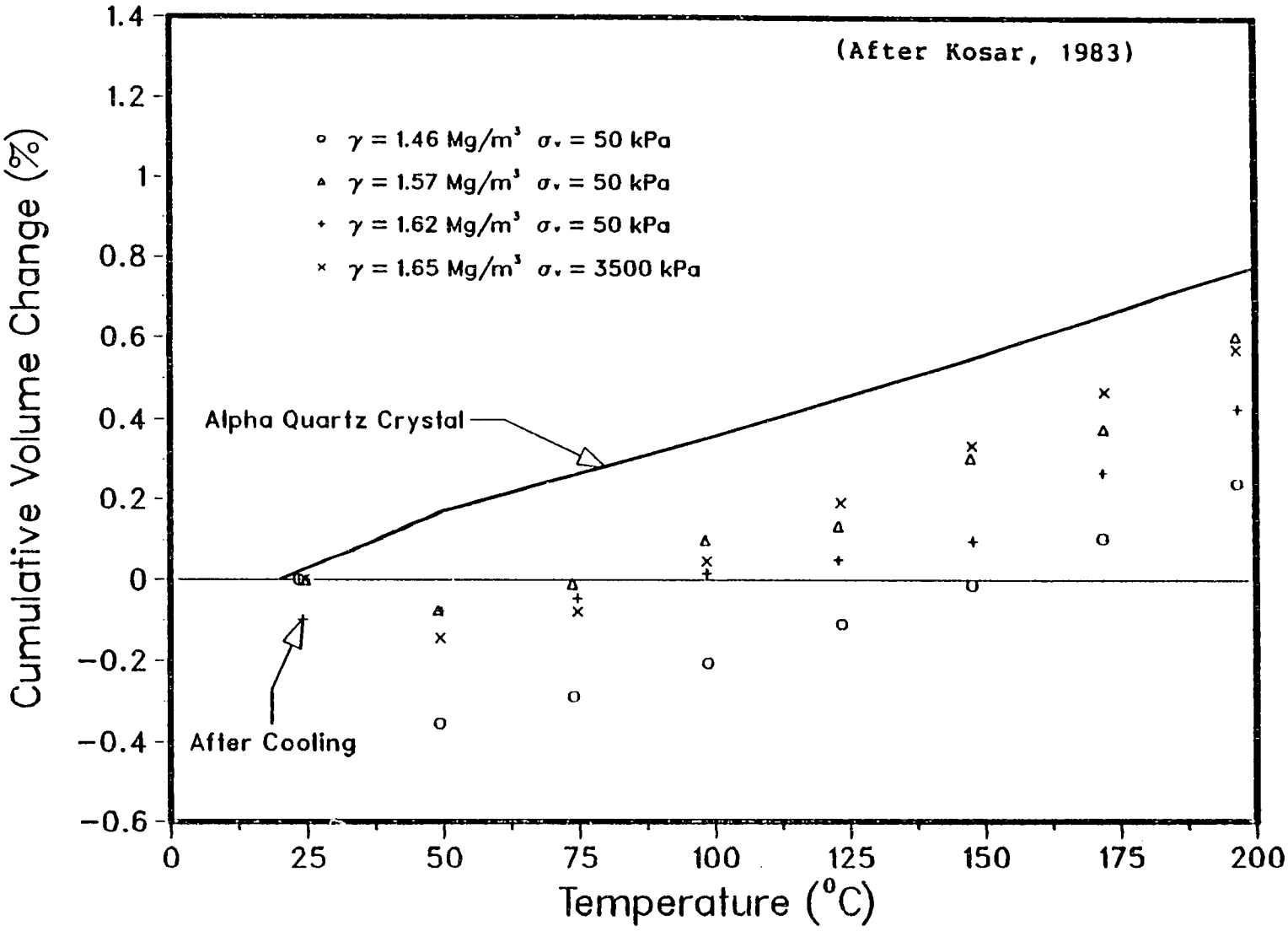

Figure 2.8 Thermal Expansion of Sand at Different Densities

Over the temperature range of 50 to 200°C all specimens display a volume increase roughly paralleling that of a quartz crystal. This behaviour tends to suggest the soil structure has achieved a tight packing arrangement at 50°C (grain slippage no longer occurring or negligible) and the subsequent volume increase with temperature results only from the thermal expansion of the individual grains. The comparison of the volume change of the sand mass with that of a solid quartz mass allows the thermal volume change of the soil structure and of the individual sand grains to be separated.

2.3 Effect of Effective Confining Stress on Constitutive Behaviour

2.3.1 Introduction

Oil sands formation strata may exist under high effective confining stresses. For example, Clearwater Formation oil sands in the Cold Lake Deposit at a burial depth of 450 m, assuming a mean overburden unit weight of 2.2 Mg/m^3 and an in situ pore fluid pressure of 2.7 MPa (Visser et al, 1985), is subjected to an effective overburden stress of about 7 MPa. At the AOSTRA Underground Test Facility in the Athabasca Deposit, the maximum principal stress in the McMurray Formation oil sands at a depth of about 155 m is horizontal and estimated to be between 2 and 3 MPa (AOSTRA, 1986). Although these stresses

are generally higher than those normally encountered in conventional geotechnical practice, there does exist a class of geotechnical problems in which soil or rock experience high stresses. Common examples include foundations of high dams, deep foundations of offshore platforms and zones peripheral to deep wells or tunnels.

This section provides a general overview of published work concerning the constitutive behaviour of soil and rock under elevated pressures.

2.3.2 Soils

Terzaghi and Peck (1948) conducted a number of one-dimensional compression tests on sand and on sand containing various amounts of mica (0 to 20%) to stresses over 100 MPa. The results of these tests demonstrated that the magnitude of deformation was dependent on the density of the sand and the compressibility increased dramatically with increasing mica content. They concluded that the increased compressibility of sand at higher stresses was due to particle fracturing and crushing. Grain crushing for mica free sand was observed to occur at pressures exceeding 10 MPa.

The phenomenon of grain crushing during one-dimensional compression at high stresses was also investigated in a later study by Roberts and de Souza (1958). They tested a variety of sands to stresses of approximately 100 MPa. The major observations arising from this study are summarized as follows:

1. The amount of grain crushing was found to be dependent on the gradation of the soil. Uniformly graded soil was more susceptible to pressure induced grain degradation than well graded soils.

2. At relatively low confining stresses (about 2 MPa) sands consisting of angular grains displayed greater compressibility and tendency to crush than sands comprised of rounded grains. This disparity, however, was found to decrease with increasing confining stress.

3. Uniformly graded sands displayed significant particle degradation above 35 MPa.

4. Grain crushing was found to be a time dependent process.

Lee and Farhoomand (1967) conducted a number of isotropic and anisotropic triaxial compression tests on subrounded and angular granitic sands and gravels to confining stresses of approximately 14 MPa. The important conclusions which emerged from this study are summarized as follows:

1. Sand is quite compressible under an applied confining stress and is generally accompanied by some degree of grain breakage.

2. Coarse grained soils compress more and display more grain breakage than fine sands (Figures 2.9 and 2.10).

3. Soils comprised of angular grains show greater compressibility and particle degradation under applied stress than do soils consisting of rounded grains (Figures 2.9 and 2.11).

4. Uniformly graded soils display greater compressibility and crushing than well graded soils with the same maximum grain size (Soils A and F in Figures 2.9 and 2.10).

(After Lee and Farhoomand, 1967)

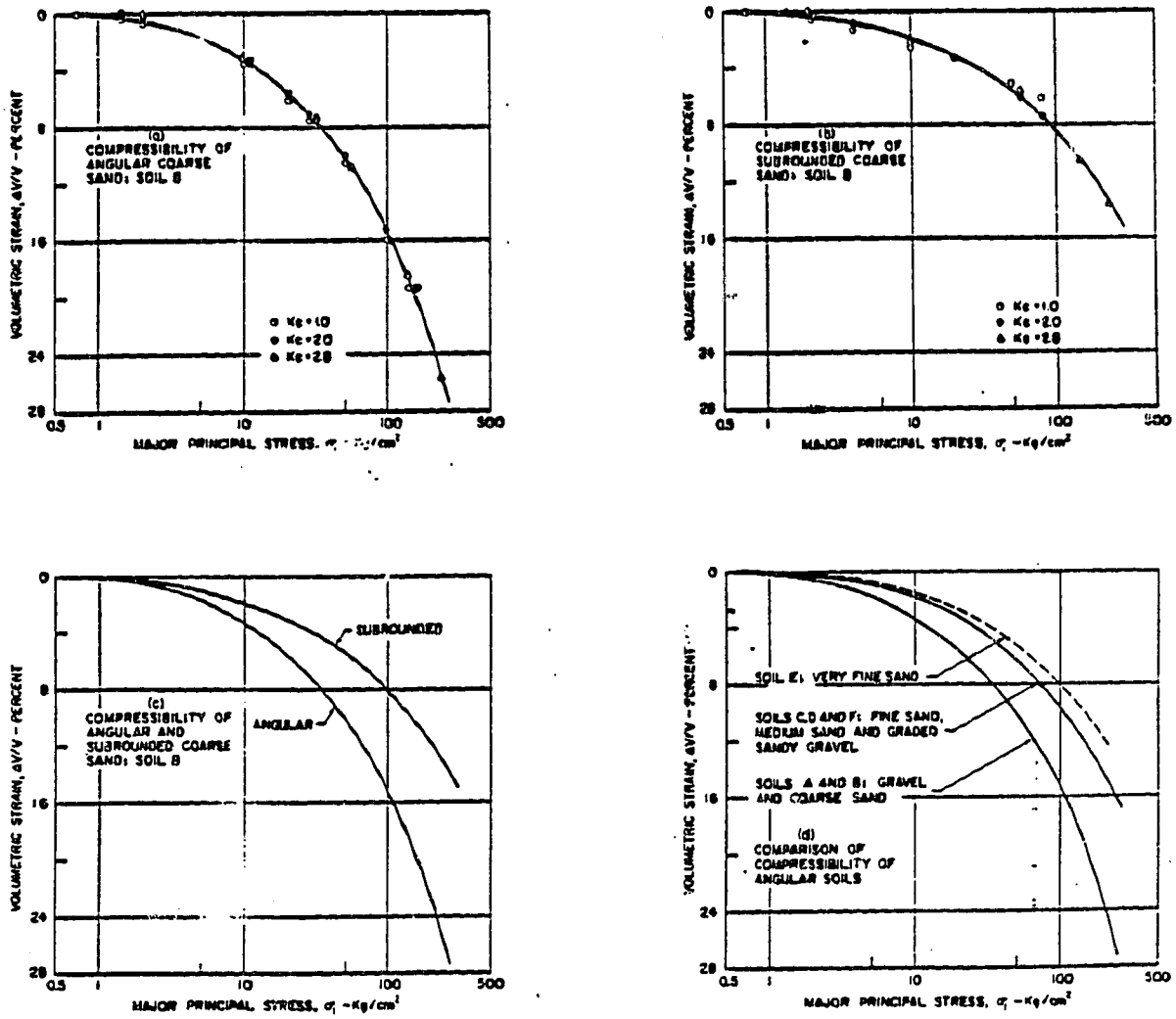

Figure 2.9 Compressibility of Sands and Gravels

(After Lee and Farhoomand, 1967)

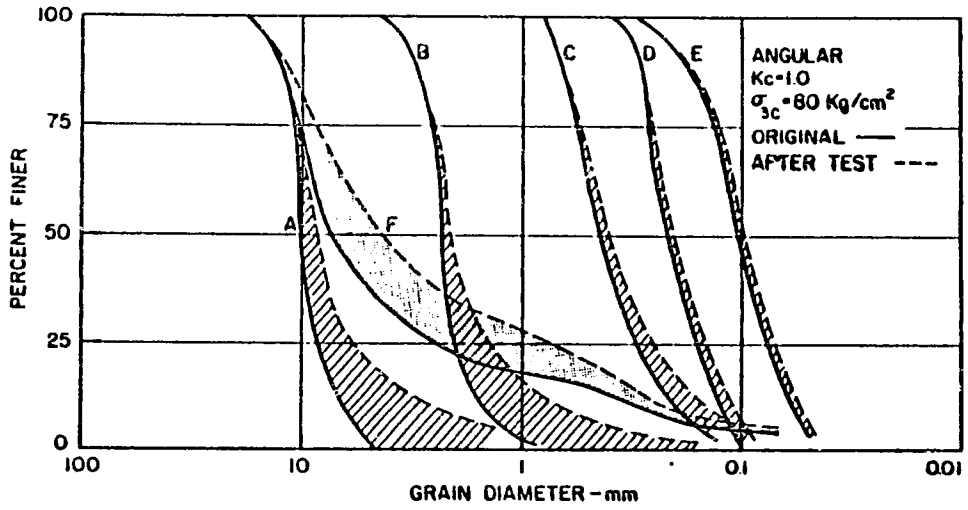

Figure 2.10 Crushing of Soils with Different Initial Grain Sizes

(After Lee and Farhoomand, 1967)

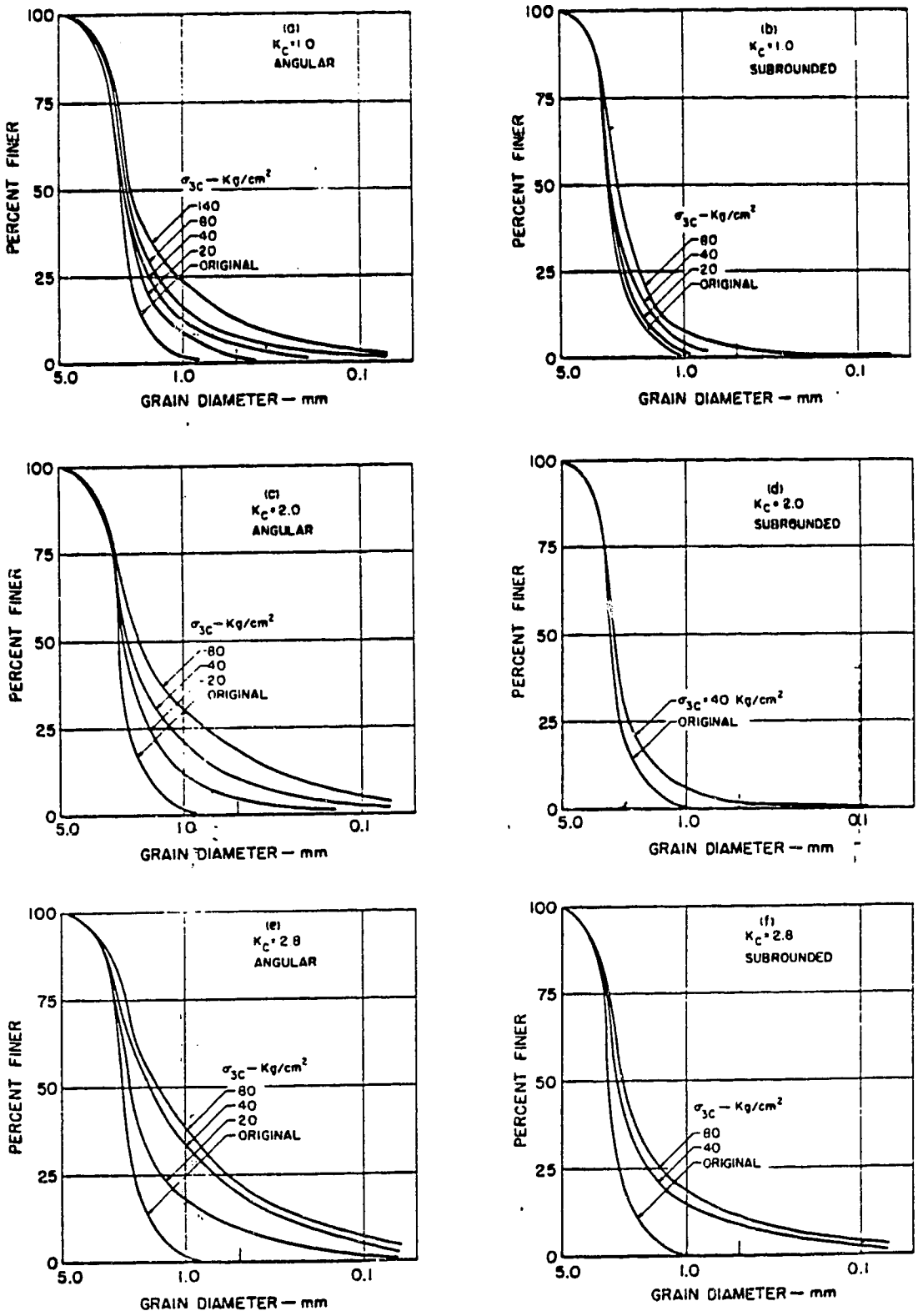

Figure 2.11 Grain Crushing of Angular and Subrounded Coarse Sand

5. Under a particular load, compression and grain breakage continue to increase at a decreasing rate for a long period of time.

6. A unique relationship was found between the volume change and the major principal stress (Figure 2.9) which was independent of the ratio of σ_1/σ_3 (or k_c). However, the higher the k_c ratio the greater the degree of particle breakage (Figure 2.12).

Hall and Gordon (1963) carried out triaxial tests on coarse grained soil to confining stresses of 4.5 MPa and found stress induced particle degradation was greater for uniform soils as compared to graded soil, the majority of which took place during shear. Similar results were reported by Vesic and Barksdale (1963) on tests performed on medium grained sand to 70 MPa confining stress.

Bishop (1966), based on tests performed on Ham River sand, concluded that the curvature in the failure envelope with increasing confining pressure for dense sands was due primarily to the decrease in the rate of dilatancy with increased pressure. This reduced rate of volume increase at failure at higher confining stresses results from crushing of sand grains which begins locally at grain contacts and may result in crushing of entire grains. This, in turn,

(After Lee and Farhoomand, 1967)

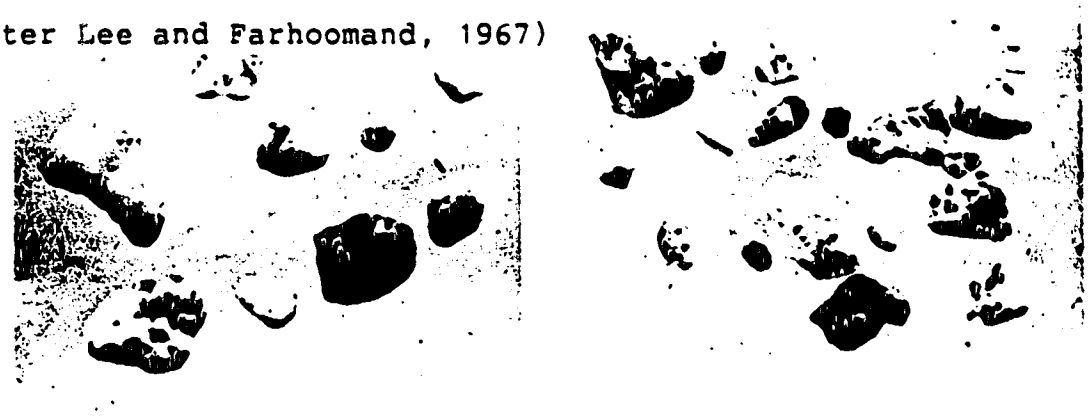

(a) Rounded: original

(d) Angular: original

(b) Rounded: σ_3=20 Kg/cm^2, K_c=2.0

(e) Angular: σ_3=20 Kg/cm^2, K_c=2.0

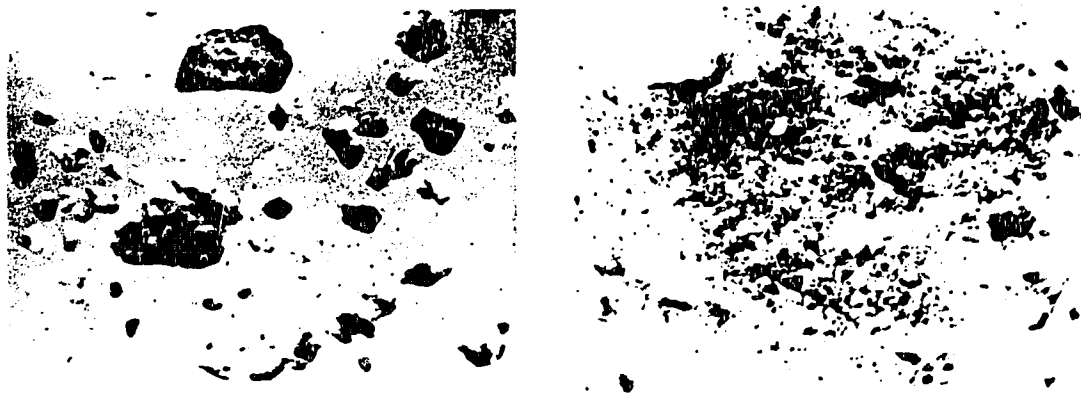

(c) Rounded: σ_3=80 Kg/cm^2, K_c=2.8

(f) σ_3=80 Kg/cm^2, K_c=2.8

Figure 2.12 Particle Crushing of Rounded and Angular Sand

results in a significant reduction in the overall effective angle of friction at failure.

Lee and Seed (1967) suggest that the shear strength of sand under drained conditions is composed of three components: sliding friction, dilatancy, and crushing and rearranging of sand grains. The relative contribution each of these components make to the angle of internal friction as the confining stress is increased is shown in Figure 2.13. Resistance to sliding friction is the dominant component of shear strength at all confining stresses, denoted by ϕ_μ in Figure 2.13.

Lee et al (1969) report values of ϕ_μ range from about 22° for quartz to about 37° for feldspar, with somewhat lower values for layer lattice minerals such as mica. In physical terms ϕ_μ represents the sliding friction of one mineral against another without contributing effects of volume change or grain breakage. Sand grains tend to slide over each other and little crushing occurs in dense samples at low confining stresses. The energy required for this dilation to occur has a significant effect on the shear strength at low confining pressures. Therefore, sliding friction and dilatancy are the major components of shear strength of dense sands at low confining stresses. At high confining stresses the sand particles tend to crush and reorient themselves with the broken fragments occupying the pore space between larger grains. Crushing of sand grains also requires energy and, therefore, affects the total

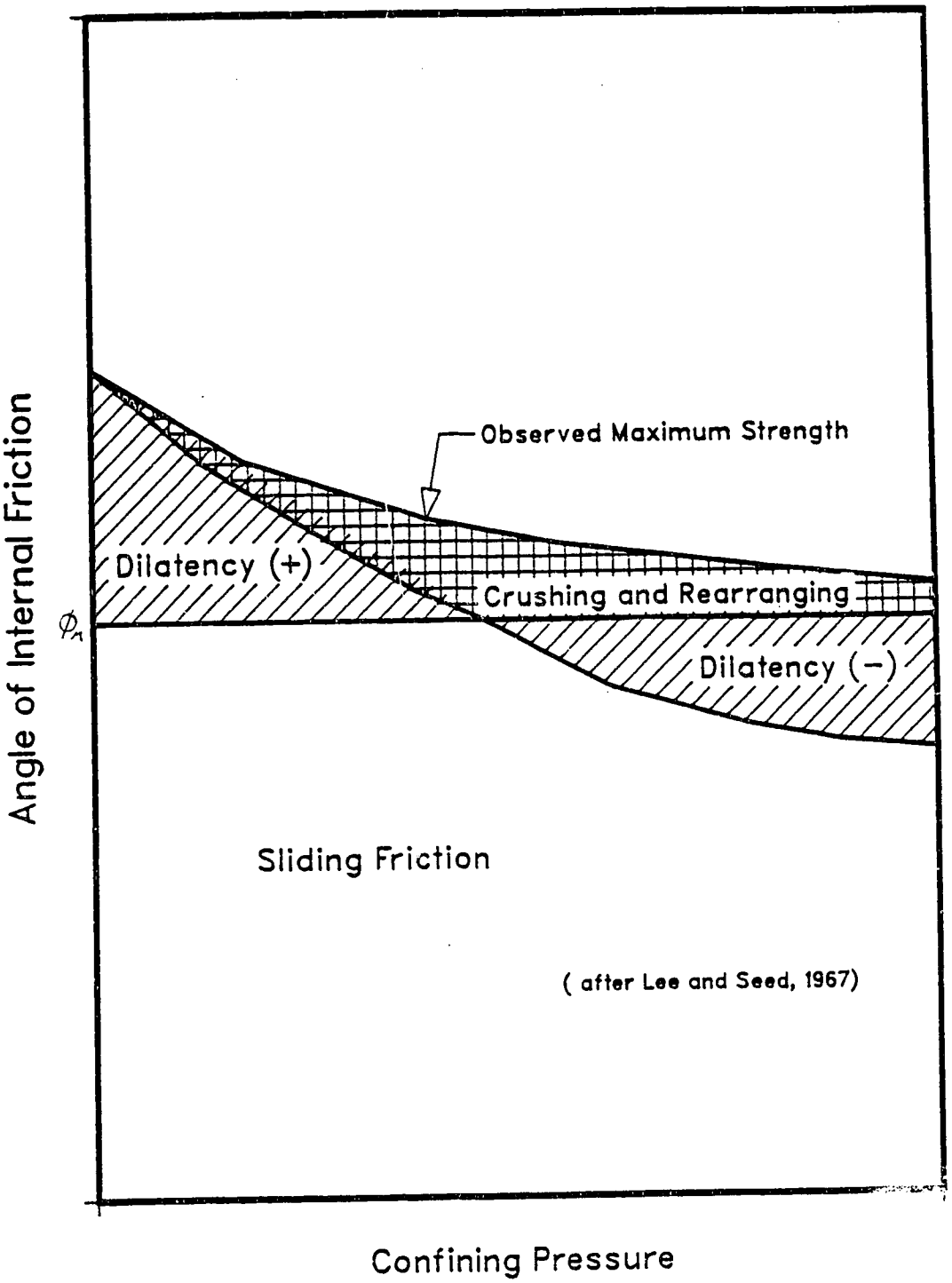

Figure 2.13 Components of Shear Strength in Confined Drained Tests on Sand

shearing resistance. Sliding friction and crushing are the major components of the drained shear strength of dense sands at high confining stresses.

Lee and Seed (1967a) conducted confined drained compression tests on Sacramento River sand (predominantly subangular and subrounded feldspar and quartz sand) and Ottawa sand (well rounded quartz sand) under confining pressures up to 14 MPa. They found that the failure envelope for Ottawa sand (Figure 2.14) displayed a continuous curvature and continued to flatten out over the entire range of confining pressures. The failure envelope for the Sacramento River sand on the other hand reached a minimum slope at confining pressures much less than 14 MPa as shown in Figure 2.14. They attribute the difference in behaviour of the two sands to the high crushing resistance of the Ottawa sand.

Vesic and Clough (1968) performed a series of confined drained compression tests on Chattahoochee River sand (a medium, uniform, quartz sand) and report intensive crushing of sand grains in the mean normal stress range of 1.0 to 10.0 MPa. This resulted in failure envelopes which were curved over this stress range. The overall effective angle of friction at failure decreased with increasing confining stress in this range, as shown in Figure 2.15. Vesic and Clough define a term called the breakdown stress as the stress at which all dilatancy effects disappear and above which grain crushing and sliding are the major mechanisms by

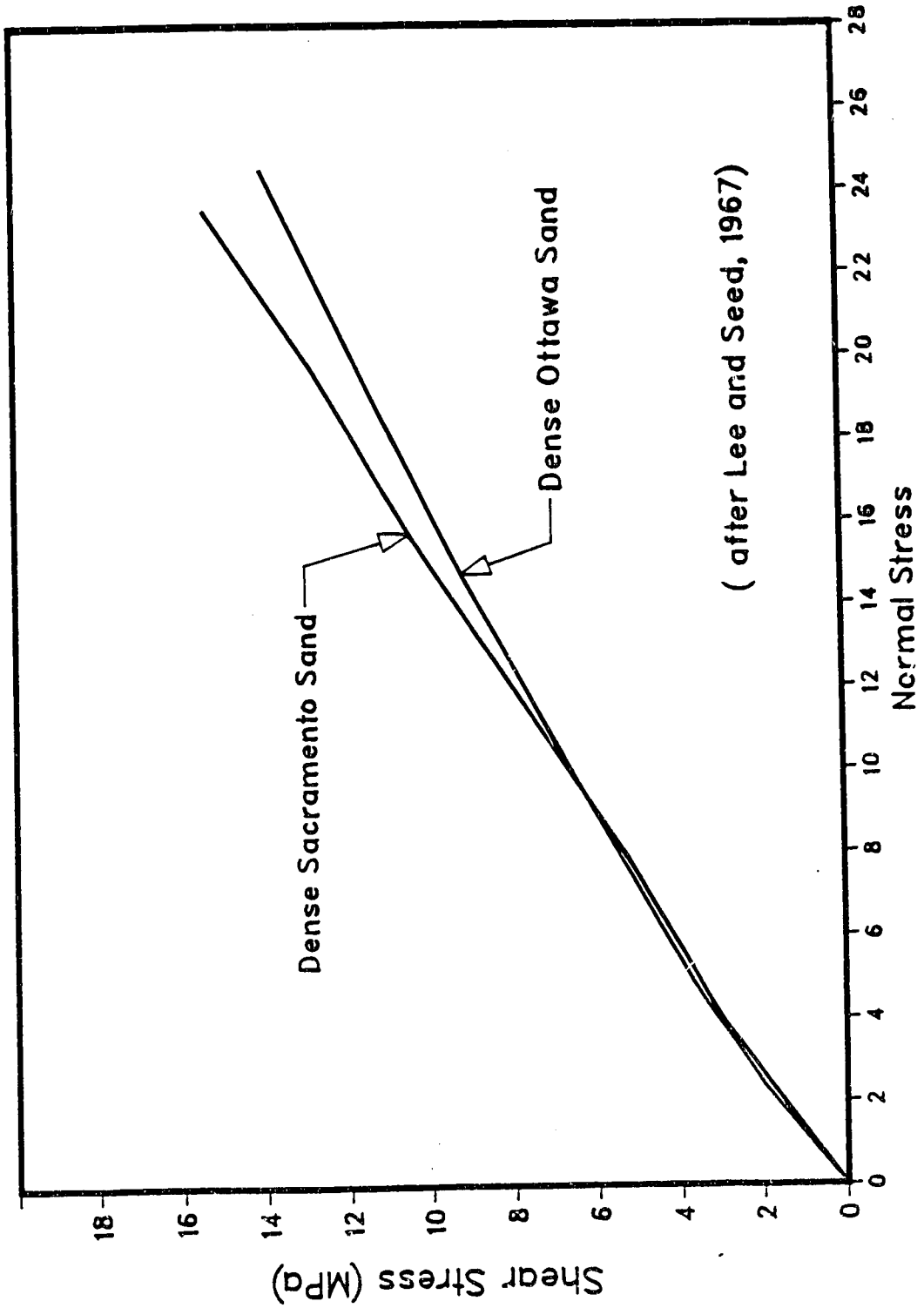

Figure 2.14 Confined Drained Compression Tests on Dense Ottawa and Sacramento Sand

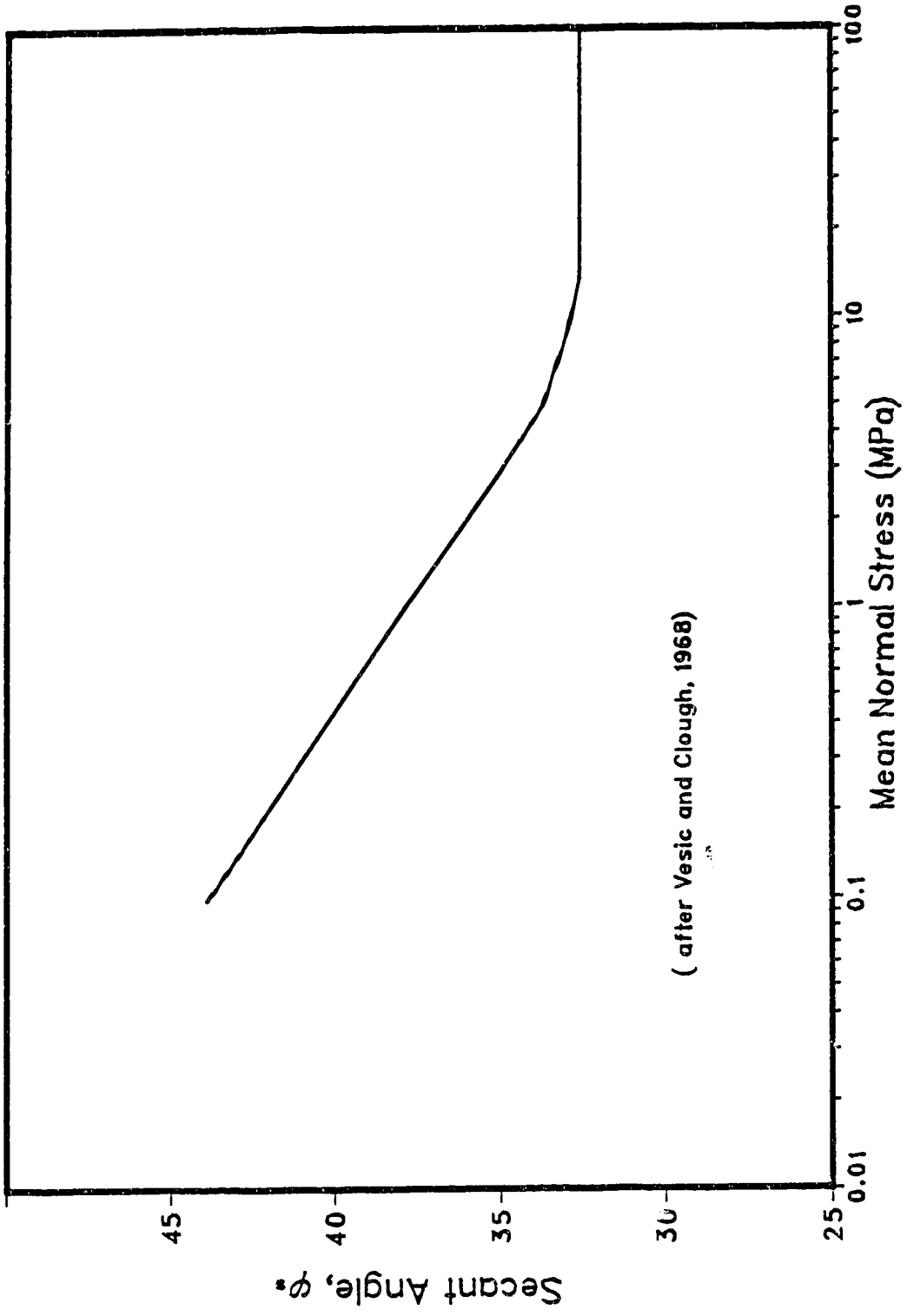

Figure 2.15 Confined Drained Compression Tests on Dense Chatahoochee River Sand

which shear deformation on slip planes is possible. Breakdown pressure of a particular sand is controlled by the composition, gradation and shape of sand grains. They report a breakdown stress of about 10 MPa for dense Chattahoochee River sand (Figure 2.15).

Lo and Roy (1973) investigated the effects of high confining pressure (up to 11 MPa) on the drained shear behaviour of artificially prepared granular materials. The materials used in the study were, in order of increasing particle strength, limestone, quartz and aluminum oxide. The sand grains used in the investigation were of an angular shape. They report a decrease in the effective angle of friction with increasing confining pressure. For quartz sand ϕ' was reduced from 42.5° at σ'_3 = 0.1 MPa to 36.8° at 11 MPa. For the weaker grained limestone sand the reduction in ϕ' was less, from 42.2° at 0.1 MPa to 38.3° at 11 MPa.

Bishop (1966) found that axial strains in the order of 20% were required to achieve the maximum shear strength of dense sand at 7 MPa effective confining pressure. This is due to the rate of grain crushing at larger strains and also due to the increasing hydrostatic component of the applied stress which also increases and results in the tendency for the sand to stiffen. The results of these confined drained tests performed on Ham River sand are shown in Figure 2.16.

Vesic and Clough (1968) conducted a series of confined drained compression tests on dense Chattahoochee River sand (a medium grained, uniform, quartz sand) and found the

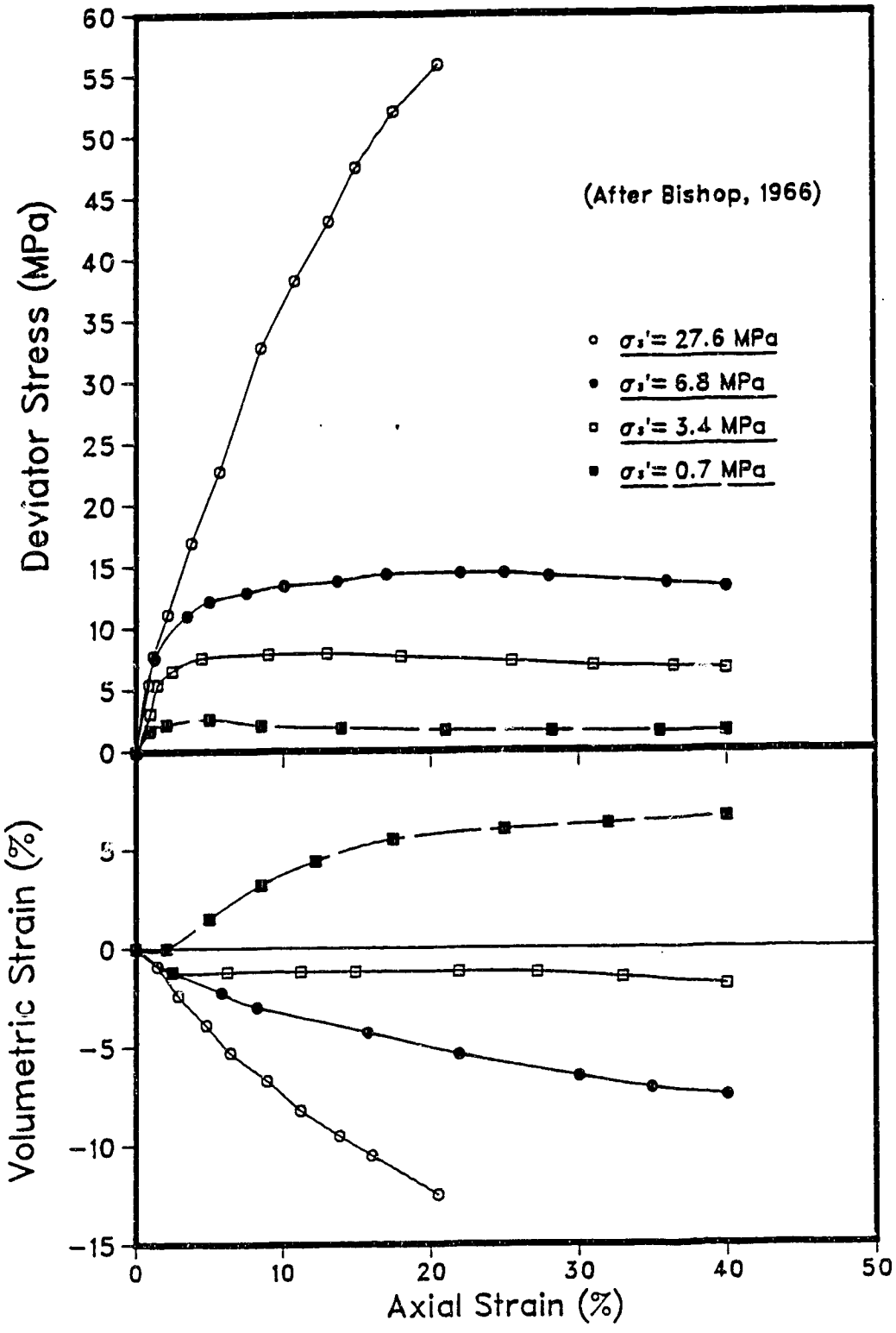

Figure 2.16 Confined Drained Compression Tests on Saturated Ham River Sand

failure strain increased from approximately 7% at cell pressures of 0.1 MPa to about 26% at cell pressures of 3 MPa. Lo and Roy (1973) performed drained triaxial tests on artificially prepared quartz and limestone sands and found axial strains to failure of over 30% were required for these materials at confining stresses exceeding 3 MPa. As a result, it is necessary to specify the axial strain at which failure strength is measured. Most researchers select failure strains arbitrarily depending on the type of problem under consideration.

Datta et al (1980) carried out isotropic compression and consolidated drained shear tests on calcareous and Ottawa sands at confining stresses up to 6.3 MPa. Calcareous sands with skeletal particles were found to be significantly more susceptible to crushing than Ottawa quartz sand. Crushing reduced the maximum principal effective stress ratio during drained shear and altered the stress-strain-volume change behaviour from a dilatant brittle to a more plastic material exhibiting volume contraction during shear.

Zoback and Byerlee (1976a, 1976b) conducted a series of permeability tests on Ottawa sand and crushed Westerly Granite subjected to isotropic compression and triaxial compression and extension at effective confining stresses up to 200 MPa. They report large permeability reductions during triaxial shear due to grain crushing. They conclude that relative changes in permeability are not uniquely related to

relative pore-volume changes due to the ability of debris from grain crushing to clog pore fluid channels and inhibit flow. Results of triaxial compression and extension tests show that if sufficient deformation occurs fluid flow can be anisotropic with the permeability in the direction of maximum compression significantly lower.

2.3.3 Rock

The stress-deformation behaviour of intact crystalline or cemented rock is dependent on confining stress (eg. Heard, 1960; Griggs and Handin, 1960; Mogi, 1966; Elliott and Brown, 1985). Intact rock displays more ductile behaviour as confining stress increases. Modes of failure during deviatoric compression generally progress from splitting parallel to the direction of maximum stress at low confining stress, to shear along a distinct failure plane at intermediate stress, to general yielding at high confining stress as shown in Figure 2.17 (Griggs and Handin, 1960). The strain to maximum shear strength increases as the rock progresses from strain-softening through to strain-hardening behaviour at high confining stress.

Read and Hegemier (1984) suggest, however, that strain-softening behaviour of intact rock at low confining stress measured in the laboratory is the result of inhomogeneous deformation and fracturing and is not a material property phenomenon. They conclude that strain-softening is a result of scaling the

(After Griggs and Handin, 1960)

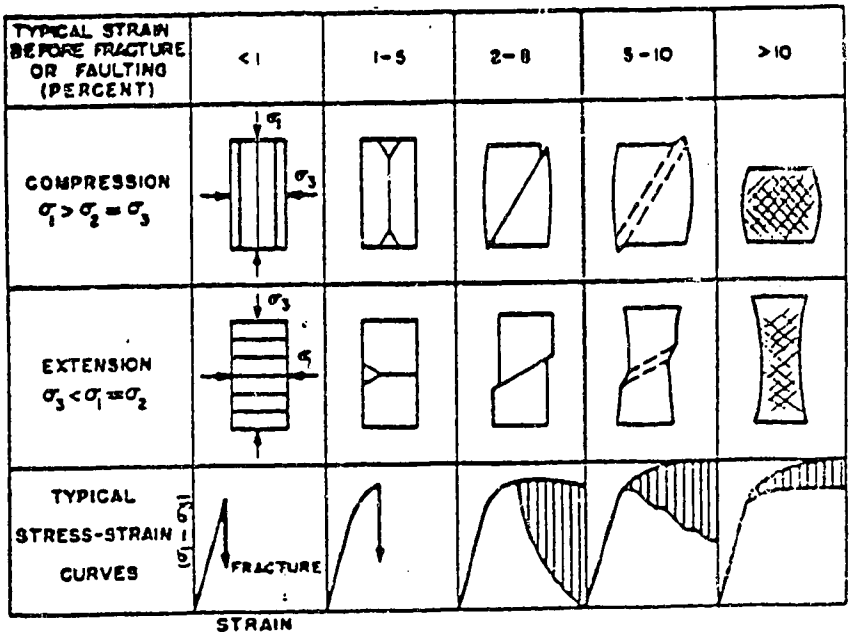

Figure 2.17 Fracture Types in Triaxial Compression

force-displacement data by the original cross-sectional area, instead of the true cross-sectional area of the unfractured material.

The mechanical behaviour of in situ rock masses is significantly influenced by the presence of discontinuities (eg. joints and fractures). In general, the literature indicates that the stiffness and shear strength of a highly fractured rock mass is lower than the intact rock. Jaeger and Cook (1979) suggest that rock masses consisting of randomly orientated, irregular shaped blocks behave in a manner similar to soils at low confining stress. As confining stress increases, however, due to the close packing of blocks of rock the behaviour is more nearly that of the rock than that of aggregate or soil.

Most intact rock is fissured and therefore its permeability is dependent on confining stress due to the opening and closure of discontinuities. The permeability of intact rock is affected by dilatant volume changes during deviatoric stress changes which is caused by the opening of micro-cracks (Mordecai and Morris, 1971; Zoback and Byerlee, 1976b).

Joints and fractures of in situ rock masses form a compressible network of flow channels which are confining stress dependent. Joints of rocks buried at depth are generally tight, however, and little permeability change would be anticipated from increases in confining stress (eg. Brace, 1980).

2.4 Effect of Stress Path

The stress-deformation behaviour of soil is dependent on the stress path followed during the test. A conventional diagram for showing stress paths in the laboratory is given in Figure 2.18. The vertical axis is the major principal effective stress, σ_1', and the horizontal axis is the resultant of the intermediate and minor principal effective stresses, σ_2' and σ_3' where $\sigma_2' = \sigma_3'$). The conventional stress paths accessible in laboratory testing are shown in Figure 2.18a. Consolidated drained passive compression and consolidated passive undrained compression are the more common triaxial tests which involve increasing the major principal total stress, σ_1', applied to the specimen while holding the intermediate and minor principal total stresses σ_2 and σ_3, constant and equal. Prior to these conventional triaxial tests the sample is consolidated to approximate in situ stress conditions following an isotropic compression stress path ($K_o = 1$ where $K_o = \sigma_3'/\sigma_1'$). The specimen may also be consolidated following a confined compression stress path in an oedometer cell where lateral straining of the specimen is prevented and the minor and intermediate principal stresses increase at a slower rate than the major principal stress.

Passive compression tests are generally useful for comparing the relative behaviour of different soils; however, these simple loading conditions are rarely representative of actual field problems and, in general,

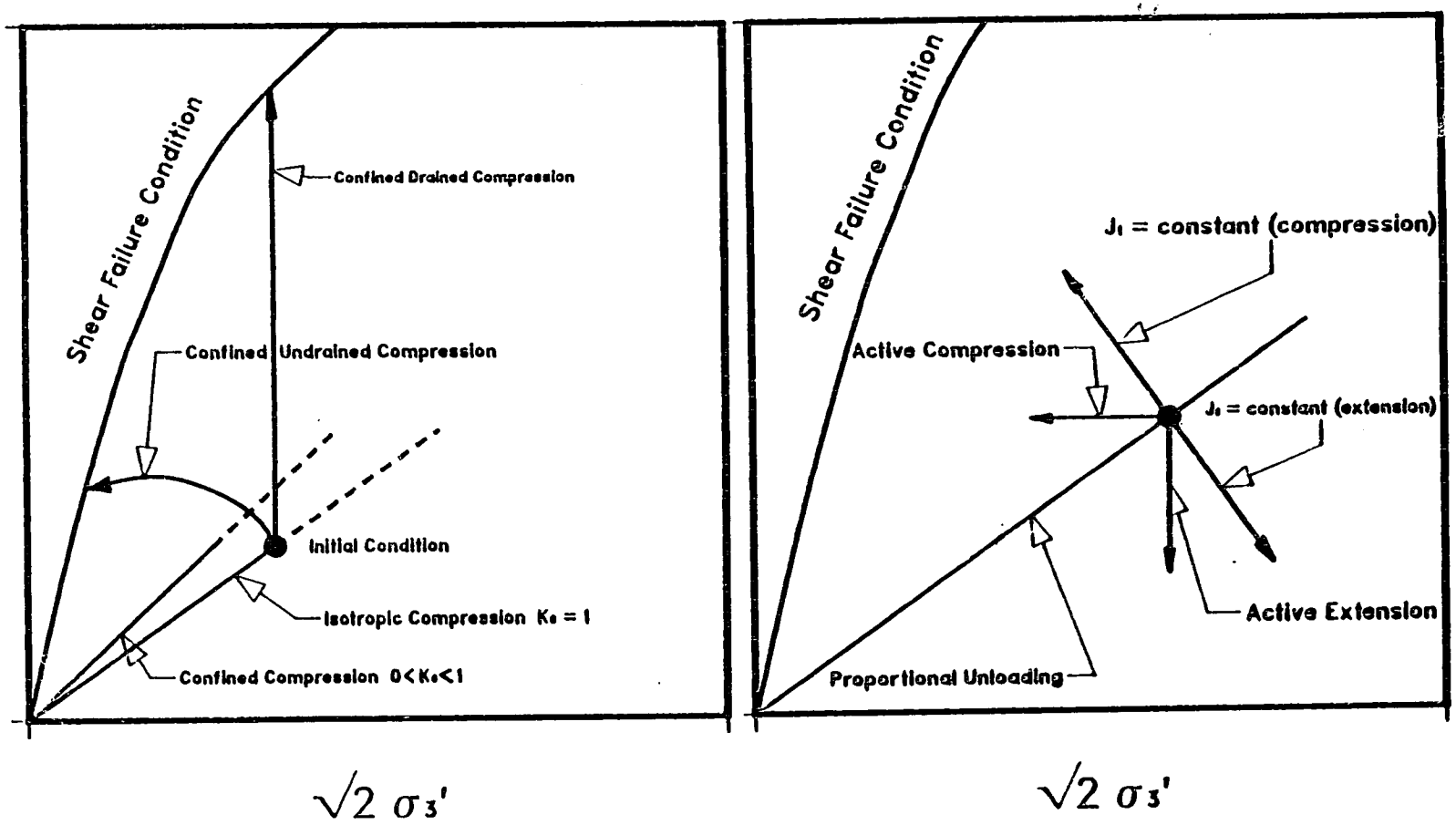

a) Conventional Laboratory Stress Paths in Triaxial and Oedometer Tests

b) Other Stress Paths Accessible in Triaxial Test

Figure 2.18 Laboratory Stress Paths

deformation data obtained from standard triaxial tests are not equivalent to those obtained by loading along other paths.

A variety of stress paths which are accessible in the triaxial test are shown in Figure 2.18b. Each test involves manipulating the principal effective stresses during the test to simulate the field stress path. The stress-strain response of soils varies with the stress path followed and, therefore, the stress history applied during the test must be representative of the field condition. For simplicity, most triaxial cells operate with $\sigma_2 = \sigma_3$ although special cells which control all three principal stresses are available.

The stress path dependency of soils has been demonstrated by several researchers. For example, Medeiros and Eisenstein (1983) studied the influence of different stress paths on the stress-deformation behaviour of glacial till and dense pre-glacial sand. They found that the stress-strain relationships of both the till and the sand showed strong path dependence. At corresponding stress and strain levels active compression and extension tests displayed larger moduli of deformation than did the conventional passive compression tests.

The results obtained by Medeiros and Eisenstein also indicated that based on tangent moduli for analogeous stress paths in triaxial and plane strain tests, the intermediate stress had a significant effect on the modulus of

deformation and angle of shearing resistance of the till. Similar results were obtained by Green (1971) for dense, medium fine Ham River sand and by Lee (1970) for Sacramento sand.

Vaid (1985) conducted a number of undrained triaxial stress-path tests on normally consolidated, undisturbed Haney clay (a marine, silty clay with liquid limit = 44% and plasticity index = 18%). He found that the deformation modulus was much higher for K_o consolidation than for corresponding conventional isotropic consolidation. Vaid also reports that Haney clay subjected to identical K_o consolidation history is stiffer along a plane-strain stress path than along a passive compression stress path. During extensional deformation of K_o consolidated clay triaxial stress path was found to either underestimate or overestimate the deformation modulus obtained by plane strain stress path depending on the deviatoric stress level.

Lambrechts and Leonards (1978) studied the effect of stress history on the stress-deformation behaviour of uniformly graded Ottawa quartz sand. The influence of stress path on the stress-deformation characteristics was evaluated by comparing the modulus values and the ranges in deviator stress over which they apply in reference to the respective stress history. The major conclusions from this study are summarized as follows:

1. Minor differences in particle packing can affect the stress-strain behaviour of a uniform sand, even when the void ratio has been precisely duplicated.

2. The irreversible strain due to prestressing, including stress paths along the K_o line, can increase the reload modulus by more than an order of magnitude over that of the normally consolidated sample, even though no residual stresses due to prestressing are extant. The effect of a residual lateral stress equal to that under K_o preloading is to increase the modulus by an additional factor of about two.

3. The magnitude of the prestress that is applied and removed by K_o stressing, and the associated prestraining, significantly influences the stress level at which the deformation behaviour in the reloading mode ends and virgin loading begins; the higher the OCR, the higher the threshold (or yield) stress. Unloading along different stress paths to the same stress level does not result in the same subsequent reloading response. Thus, a stress ratio

criterion defining the mode of deformation to be expected (virgin, unloading, or reloading) is not generally applicable.

4. Neither prior stress history nor minor differences in particle packing, which may influence stress-strain behaviour very significantly, had any discernible effect on the shear strength of the sand samples tested.

Law (1981) studied the effect of stress path on the drained soil brittleness (difference between peak and post-peak strength) of very stiff, sensitive, fissured Champlain Sea clay. Law concludes that for a given soil at the same effective confining pressure, the conventional triaxial drained compression tests result in the highest brittleness, followed by constant σ_{oct}', constant p' and lastly by constant σ_1' (decreasing σ_3') tests. For soil consolidated to the same confining stress prior to shear under constant strain rate the same results occur. Soil brittleness was also found to increase with decreasing effective confining stress.

2.5 Geotechnical Properties of Oil Sands at Ambient Temperatures

2.5.1 Mechanical Properties

Several studies have shown that mechanical properties of oil sands are significantly affected by the method of sampling, sample preparation and by laboratory test procedures (eg. Kosar et al, 1987; Agar, 1984 and Dusseault, 1977). Agar (1984) observed a 25% reduction in maximum shear strength for Athabasca oil sands corresponding to an initial porosity difference of only about 1%. For experimental test results to be representative of in situ behaviour it is therefore necessary to preserve the in situ orientation of sand grains and the soil fabric in the laboratory. Kosar et al (1987) emphasizes the importance of conducting tests in the laboratory under conditions representative of those prevailing in the field.

The mechanical properties of oil sands have been studied extensively over the years as geotechnical problems associated with oil sands development have arisen. A fundamental understanding of the mechanical characteristics of oil sands and the methods and procedures required to measure representative properties has evolved from these investigations.

The first known endeavor to measure the mechanical properties of oil sands was made by Tustin (1949). One-dimensional and triaxial compression tests were carried

out on rich McMurray Formation oil sands specimens obtained from block and Shelby tube samples. The shear strength of "undisturbed" specimens were found to be only marginally higher than remolded strengths. Hardy and Hemstock (1963) recognized that conventional soil sampling procedures employed by Tustin were not adequate to yield undisturbed samples and therefore significantly underestimated the strength characteristics. They attributed the low laboratory strengths to non-dissipated gas pore pressure which caused a reduction in effective stress leading to a decrease in shear strength. Hardy and Hemstock, in an attempt to minimize the evolution of dissolved gases due to stress relief during coring utilized two specialized sampling techniques. The first involved freezing samples after coring and thawing under a confining stress in a triaxial cell. This method yielded shear strengths significantly higher than those measured by Tustin. In the second, a pressurized core barrel was used in conjunction with surface freezing. This method was unsuccessful primarily due to mechanical difficulties and poor sample preparation procedures. Although the work by Hardy and Hemstock was not successful in providing a good experimental assessment of in situ strength, it does serve to illustrate the important role sampling, sample preparation and laboratory procedures have in the laboratory determinations of mechanical characteristics of oil sands. It also identified gas evolution arising from the decrease in fluid pressure and confining stress during coring as the

primary cause of core expansion.

As a result of early experimental tests on oil sands, researchers have sought to improve oil sands sampling and preparation techniques. For example, oil sands core samples have been obtained using downhole freezing techniques by Dusseault (1977), oil sands block samples from an open pit mine were taken by Sterne (1981), frozen core samples from a natural valley exposure were obtained by Agar (1984) and Plewes (1987), oil sands cores were recovered with a pitcher sampler by Peacock (1986) and in situ freezing methods have been used by Dusseault and Van Domselaar (1982). A review of the influence of sample disturbance on laboratory characterization of oil sands and an evaluation of present and proposed sampling techniques has been provided by Dusseault and Scott (1984). In general, the literature indicates that methods which employ freezing, reduce clearance between core sample and liner and provide mechanical axial and radial restraint to core expansion are most successful at the present time in reducing sample damage. The literature also indicates that immediate surface freezing and maintained freezing through the transport, storage, sample preparation and specimen mounting phases is the most successful and reliable method of minimizing post-sampling expansion.

The majority of published data on mechanical properties of Athabasca McMurray Formation oil sands prior to 1984 has been compiled and summarized by Au (1984). Subsequent work

has been carried out by Agar (1984) and Plewes (1987). Limited mechanical data on Cold Lake oil sands has been published by Agar (1984) and Kosar et al (1987).

In general, oil sands may be characterized as a very dense, strong, incompressible, uncemented sand. Athabasca oil sands consist of a uniformly graded, predominantly quartz sand, whereas Cold Lake oil sands contain some additional minerals which are much weaker. The presence of bitumen in the voids of the sand matrix appears to have little or no effect on the compressibility, shear strength and elastic parameters of the oil sands. The bitumen does, however, have a controlling role in the permeability of the oil sands and, therefore, in the rate of pore pressure dissipation during shear. In addition, the bitumen may contain considerable gas in solution which can have a profound effect on maintaining pore fluid pressure as a decrease in confining stress allows gas bubbles to develop which retard the dissipation of pore pressures.

Gas evolution also causes sample disturbance during coring and sample preparation. As the mechanical properties are considerably affected by small amounts of sample disturbance, great care has to be taken during coring, handling, storage and sample preparation in order to measure realistic parameters in the laboratory.

2.5.2 Physical and Thermal Properties

Fluid flow properties of Alberta oil sands have been measured by Clark (1960), Camp (1970), Dusseault (1977), Starr et al (1979), Hackbarth and Nastasa (1979), Parsons and Hemstock (1983), Mainland (1983) and Agar (1984) (see Agar 1986 for a review). Gas evolution from oil sands has been examined by Peacock (1986) and Branco (1988). Oil sands microfabric has been studied by Barnes (1980) and Agar (1984). Thermal properties of oil sands have been examined by Clark (1944), Somerton (1973), Karim and Hanafi (1981), Cervenan et al (1981), Seki et al (1981), Smith-Magowan et al (1982), Cassis et al (1985) and Seto (1985).

In general, laboratory measurements of physical and thermal properties of oil sands are sensitive to sample disturbance and test procedures. Tests performed on specimens which are disturbed or not fully saturated can yield erroneous results. For example, Dusseault (1977) and Agar (1984) report that sample disturbance by core expansion results in an overestimation of in situ permeability as the increase in pore space is filled by water during testing. Seto (1985) illustrates that thermal conductivity tests on remolded, unsaturated oil sands are lower than values obtained from high quality, saturated specimens. Peacock (1986) discusses sampling, storage, preparation, and testing methods required to provide reliable gas properties measurements of oil sands. Dusseault and Scott (1984) report that water content, reserves calculations, free gas content

and other calculations can be influenced by sample expansion during coring.

2.6 Geotechnical Properties of Oil Sands at Elevated Temperatures

Published information on the geotechnical properties of oil sands at elevated temperatures is limited. The mechanical properties of Athabasca McMurray Formation oil sands have been measured by Agar (1984) over the temperature range of 20°C to 200°C. Agar also reports thermal expansion, compressibility and permeability data at temperatures up to 300°C. Boga et al (1980) conducted a limited number of triaxial tests on McMurray Formation oil sands to 90°C. Kosar (1983) studied the thermal expansion of McMurray oil sands over the temperature range of 20 to 200°C. Seto (1985) measured the thermal properties of high quality, fully saturated McMurray Formation oil sands over the temperature range of 20 to 200°C. Thermal properties of remolded or disturbed oil sands at temperatures up to 500°C have been measured by Clark (1944), Somerton (1973), Karim and Hanafi (1981), Cervanan et al (1981), Seki et al (1981), Smith-Magowan et al (1982) and Cassis et al (1985).

The strength of Athabasca McMurray Formation oil sands somewhat decreases at elevated temperatures (Agar, 1984). The effect of temperature was found to lower the effective strength 10% over a 200°C range of temperature. Temperature increase, however, also significantly increases the pore

fluid pressure and if pore pressure dissipation cannot occur at the same rate as the temperature increase, the drop in effective stress can cause a considerable decrease in the shear strength.

Agar (1984) also reports that the compressibility and absolute permeability of McMurray Formation oil sands are not significantly affected to temperatures up to 300°C. The predominantly quartz sand matrix was found to be virtually unaltered at elevated temperatures with small variations in measured values attributed to pore volume changes due to heating or drained compression. The properties of the pore fluids (bitumen, water and dissolved gases), however, were found to be significantly affected by changes in temperature. Heating causes a reduction in the dynamic viscosity of pore bitumen and water which, in turn, increases pore fluid mobility.

Seto (1985) found that the thermal conductivity and thermal diffusivity of partially or fully saturated Athabasca McMurray Formation oil sands decreases with increasing temperature. The rate of decrease was found to increase with increasing bitumen content. In contrast, the thermal conductivity of the dry quartz sand grains increased with increasing temperature.

3. OIL SANDS GEOTECHNICAL RESEARCH FACILITY

3.1 Geotechnical Test Facility

The geotechnical oil sands research laboratory was developed to carry out tests to determine the geotechnical properties of oil sands and associated strata (shale, limestone, etc.) under high temperature and pressure. The test facility consists of two triaxial cells, two oedometers and a hot water or steam injection system.

The laboratory facility includes two separate and independent triaxial compression systems. The high temperature and high pressure triaxial cell can measure the compressibility and shear strength properties of oil sands and related strata under confining stresses up to 27 MPa and temperatures up to 315°C. Loads up to 440 kN can be applied to shear the sample. Pore fluid pressure, vertical and lateral strains and volume change of the test specimen can be measured. Hot water or steam can be passed through the sample by the pressure injection system at pressures up to 20 MPa and temperatures up to 315°C to flush bitumen out of or into an oil sands sample and to measure the permeability of the specimen.

The laboratory facility also includes a room temperature and medium pressure triaxial cell which can operate at confining pressures up to 14 MPa, pore pressures up to 14 MPa and vertical compression loads up to 175 kN. The disparity in load and pressure capabilities between the

two triaxial compression systems reflects the high back pressures required to maintain the pore fluids in the liquid phase at elevated temperatures. For example, to maintain water in the liquid phase at 300°C requires a back liquid pressure of approximately 10 MPa.

Both triaxial cells are equipped with internal strain gauge load cells mounted directly on the test specimens during the triaxial testing which allows a direct measure of stress on the specimen, eliminating the uncertainty of piston friction and providing a fast, accurate measure of stress. The high temperature and high pressure triaxial cell includes an internal axial strain measuring device to accurately measure the axial strain of the test specimen.

The odeometer systems can measure compressibility and thermal expansion properties of oil sands and related strata under loads up to 30 MPa and temperatures up to 315°C. Vertical compression, pore fluid pressure and volume change of the test specimen can be measured. The pressure injection system can also be used with the oedometers to remove bitumen and to measure permeability.

The oil sands geotechnical research facility was originally constructed in 1980. It consisted of:

1. A high temperature and high pressure triaxial cell and loading frame with servo-controlled axial loading.

2. A high temperature and high pressure oedometer cell.

3. High pressure air actuated pumps to provide back pressure and confining pressure.

4. Heaters and temperature control systems.

5. A data acquisition system.

The technical aspects of the original equipment are detailed in Agar (1984).

Observations made during the experimental testing by Agar indicated that modifications were required to improve the efficiency and economic performance of the laboratory equipment. Further, with the addition of certain components to the equipment the accuracy of measured data could be greatly improved and more geotechnical properties measured. Slight modifications to the equipment were also required to provide a safer environment for operational personnel and to reduce exposure of fragile components of the equipment to possible damage.

Due to the unique design and operational use of the high temperature and pressure components of the laboratory

equipment, modifications often required the design, machining and construction of specialized hardware components (such as internal load cells, end caps, etc.) or adaptation of materials designed for other engineering applications (such as seals and membranes). Emphasis during equipment upgrading concentrated on:

1. Providing greater control of pressure, temperature and load during testing to improve the quality of measured results.

2. Developing the capability to apply a history of stress during testing which was more representative of actual field operations (or stress path testing capability).

3. Eliminating or modifying components, such as seals and membranes, which are susceptible to degradation or failure at elevated temperatures and pressures.

4. Isolating the triaxial and oedometer systems such that each system could operate independently and a number of geotechnical tests could be performed simultaneously.

The measures employed to reduce the original limitations of the equipment are summarized in Table 3.1 and were implemented over a one year period. Laboratory equipment specifications and drawings are detailed in Appendix A.

3.2 Sample Preparation and Test Procedures

During core sampling from boreholes in situ confining stresses and pore fluid pressures are reduced rapidly and gas evolution from the bitumen and water may occur. This formation of gas bubbles combined with the lack of cementation and, therefore, cohesive strength between sand grains results in expansion of the oil sands fabric. If the amount of sample disturbance caused by core expansion is significant, the interlocking contacts at grain boundaries are lost and the overall grain surface contact area reduced as grain movement and rotation occur. As a result, during confined compression of highly disturbed oil sands specimens the ability of sand grains to slide and rotate during shear deformation is increased resulting in reduced shearing resistance and, in most cases, contractive rather than dilatant behaviour.

Early laboratory determinations of strength-deformation behaviour of Athabasca McMurray Formation oil sands (Brooker, 1975; Carrigy, 1967; Hardy and Hemstock, 1963; et al) underestimate the shear strength properties due to sample disturbance caused by inadequate core sampling,

Table 3.1 Equipment Modifications During Research Program

Component	Design Limitation	Modification
High temperature triaxial cell and high temperature oedometer	Test specimens required to be 76.2 mm in diameter. Therefore limited to core samples greater than 76.2 mm.	Design and machining of hardware components to enable testing of 54 mm and 63.5 mm specimens. Permitted testing of smaller diameter or slabbed core and provided flexibility to reduce amount of sample preparation.
High temperature O-ring seals	O-ring seals originally supplied with the equipment by the manufacturer (Kalrez Compound 3018, manufactured by Dupont) proved susceptible to degradation through thermal cycling.	Adopted O-rings composed of chemical compounds commercially referred to as Viton and Kalrez compounds 1050 and 1018. These compounds are more resistant to degradation over the operational temperature range of the equipment, are more compatible with petroleum products and are more stable during frequent thermal cycling. Steam generators were equipped with metal O-rings.
Volume change measuring device	Practical operating range of metal bellows is 75 ml with absolute maximum capacity of 100 ml. Differential pressure cannot exceed 450 kPa when bellows is fully extended or contracted. Can only be routed to one experimental system at a time. May require recharging between triaxial or oedometer tests and during permeability tests.	Laboratory equipment supplemented with two "Enniss" Measuring Accumulators (EMA). Each accumulator has a working capacity of 500 ml and can replace a volume change and pressuring device.
High pressure air actuated pumps	May fluctuate about the desired pressure level by as much as 200 kPa. Difficult to maintain small constant effective stresses on test specimens.	EMA devices and non-volume measuring accumulators were installed to eliminate rapid pressure fluctuations associated with air actuated pumps.
Loading frame of high temperature triaxial cell	1. Hydraulic ram at base of cell and required lifting of entire cell during shear. Utilized flexible manifold for back pressure lines connected to base of cell. Necessitated complex and cumbersome series of two-way swival fittings. 2. Limited machine stiffness negated accurate tracing of entire post failure stress-strain curve.	1. Hydraulic ram loading configuration reversed. Triaxial cell remains stationary during shear and the top mounted hydraulic ram pushes loading piston through top of cell. Back pressure lines remain stationary throughout test with possibility of leaks and fitting failure reduced. 2. Frame pre-stressed to 440 kN. Sleeves of 2.5 cm wall thickness installed over 5 cm diameter rods to accommodate pre-stressing.

... continued

Table 3.1 Equipment Modifications During Research Program (continued)

Component	Design Limitation	Modification
High temperature triaxial axial loading device	Axial deviatoric loading by a servo-controlled, electric motor powered hydraulic pump driving a 440 kN capacity hydraulic ram. Electronic servo-controller uses load cell transducer feedback to control the hydraulic pump loading rate. Therefore limited to constant rate of stress testing. Conversion to external LVDT feedback for strain controlled testing awkward due to cell pressure variations during sample seating. Generally poor control during sample shear from internal axial arms due to electronic noise from signal amplification.	Installation of positive displacement pump (Jeffri Pump). This pump can operate to 35 MPa and is controlled by a micro processor which can be programmed to supply fluid to ram at specified constant rate for constant rate of strain testing.
Internal load cells	Not included in original system. Required use of external load cell corrected for piston friction.	Addition of three internal load cells to accommodate 54, 63.5 and 76 mm diameter specimens.
High temperature triaxial membranes	RTV silicone rubber susceptible to swelling and depolymerization at elevated temperatures. Practical temperature limit of 200°C.	Teflon membranes adopted for triaxial testing at 225°C. Copper membranes machined from tubing were developed utilizing a tapered end cap o-ring sealing mechanism. Copper is non-reactive with oil cell fluid and is stable to 1000 C. However, the excessive cost and time to machine membranes prohibited routine usage.
High temperature triaxial cell fluid	Silicone oil resulted in degradation of RTV silicone rubber at elevated temperatures.	Replaced by "Essotherm N-69" oil which extended practical working range of RTV silicone rubber from 200°C to 225°C.

... continued

Table 3.1 Equipment Modifications During Research Program (continued)

Component	Design Limitation	Modification
Pressure transducers	To accurately span entire pressure range of equipment or to maintain small differential pressures required several transducers of varying capacities.	Inclusion of multiple range differential transducers. These transducers consist of a diaphragm mounted between two stainless steel blocks. Each transducer is supplied with a number of diaphragms each with a different working range. In addition to measuring pressures from various pumps and loading systems, differential transducers can be installed to measure the pressure gradient across a sample during permeability determinations.
Data acquisition system	Stores gathered information on magnetic tape. Storage procedure at times was extremely slow during which time the measuring devices could not be monitored	A great portion of this storage time was eliminated through the installation of a disc drive storage system.
Emergency shutoff valves	Not equipped.	Air operated valves were installed to allow equipment to be neutralized from a safe distance in event of equipment malfunction or breakdown during testing at elevated temperatures and pressures.
Protective shield	Not equipped.	As a safety precaution during operational use of the equipment, a safety shield was installed to protect laboratory personnel from escaping hot fluid.

sample preparation and test procedures. Dusseault (1977) recognized the need to minimize sand matrix expansion caused by gas evolution accompanying reductions in confining pressures. Dusseault employed borehole refrigeration techniques which entailed circulating chilled diesel fuel in the borehole prior to core sampling. Core samples were frozen upon reaching the surface and laboratory specimens were prepared while the oil sands were in the frozen state. Conventional soil testing procedures were then utilized for geotechnical properties determinations.

The above method reduced the amount of sand matrix disturbance compared to standard soil sampling techniques and provided a better characterization of the geotechnical properties of Athabasca McMurray Formation oil sands. However, standard soil testing procedures proved inadequate in producing geotechnical properties representative of in situ values. The need for specialized sampling and testing procedures for oil sands was further exemplified by Sterne (1981) and Barnes (1980). Sterne utilized test specimens cut from block samples taken from a mine face at the Suncor open pit mining operation north of Fort McMurray. Oil free specimens of the Grand Rapids Formation were taken by Barnes from a surface exposure on the Athabasca River, about 80 km southwest of Fort McMurray. The results of these studies indicate that sample preparation and test procedures are required which preserve or regain the integrity of the sand matrix to provide meaningful measurements of geotechnical

properties such as shear strength, stress-strain moduli and Poisson's ratio.

Plewes (1987) and Agar (1984) obtained samples from diamond coring of an oil sands outcrop in the Saline Creek Valley south of Fort McMurray. The stresses in the valley wall of Saline Creek have been reduced at a very slow rate during geologic time and, therefore, a significant portion of the gas initially present in the oil sands has drained without disruption of the oil sands soil structure. The oil sands were permitted to freeze in situ over the winter months and samples were cored in the late winter. Freezing of oil sands aids in preserving the structure of the oil sands by: greatly increasing the viscosity of the bitumen which considerably decreases the rate of gas diffusion and evolution; reducing by shrinkage the pore fluid pressures; and reducing the amount of gas evolution due to stress relief by improving the solubility of gas in the bitumen. This sampling procedure resulted in more reliable determinations of stress-strain-strength properties of Athabasca oil sands.

The method of sampling varies due to the accessibility of the oil sands. High quality samples could be obtained from oil sands at depth by in situ freezing or pressure coring but these techniques are complex and very expensive and are unlikely to be adopted by industry for routine usage. Present core sampling techniques utilize core barrels with a non-rotating inner barrel which contains a PVC liner

to collect the core sample. The inner barrel precludes washing of the sample with drilling fluid and the development of rotational shear of the sample. The effect of sample disturbance caused by core expansion on the geotechnical properties of oil sands can be significantly reduced by immediately sealing and freezing the PVC liner containing the oil sands after the core barrel reaches the surface and by adopting sample preparation and test procedures which preserve or regain the integrity of the sand matrix.

The sample preparation procedures used in this study, outlined in detail in Appendix B, involve storing, trimming and mounting the oil sands specimens in the test apparatus in the frozen state. To preclude structure expansion, the oil sands specimen is not allowed to thaw until it is under sufficient confining stress in the laboratory test cell. During the thawing period the volume of water entering or leaving the sample is monitored.

The test procedures used to measure the geotechnical properties of oil sands and associated strata involve applying the history of stress during the test which is representative of actual field conditions. Prior to testing, however, the disturbance caused by the core sampling procedures must be reduced and the quality of the test specimen must be assessed. The effects of core sampling disturbance are reduced by resaturating and consolidating the test specimen to approximate in situ conditions. The

pore pressure parameter B, which is the measure of the undrained pore fluid pressure response of the specimen to a change in isotropic stress, is used to determine the pore fluid pressure required to fully saturate the test specimen. After the test specimen has thawed completely (usually 12 hours) the confining and back pressures are raised in equal increments and the pore pressure parameter B is measured following each increment. By maintaining a constant effective confining stress on the sample during each increase in pore fluid pressure the soil structure does not compress and the pore fluid saturation pressure is determined when the B parameter becomes constant. For most oil sands specimens the pore fluid saturation pressure is approximately 2000 to 2500 kPa for the test time employed.

The pore pressure parameter B is also useful as an indicator of sample quality. The greater the increase in pore fluid pressure, the greater the soil skeleton compressibility. For most soils, the B parameter is usually very close to one. However, due to the dense soil structure of oil sands and the compressibility of the bitumen, rich oil sands commonly have values considerably less than one.

The B parameter was used in conjunction with initial bulk density and index of disturbance for assessing the degree of sample disturbance caused by core expansion. In the past, bulk density has been the major factor in evaluating sample disturbance. The greater the microfabric disturbance the lower the bulk density. Bulk density,

however, suffers as a quality indicator because it is greatly influenced by the amount of fines in the sample. In contrast, the fines content of an oil sands sample has little effect on the B value. The index of disturbance, developed by Dusseault and Von Domselaar (1982), is used to compare the in situ porosity n of a given oil sand with laboratory derived porosity n_e and is defined as:

$$I_D = (n_e - n) / n \qquad (3.1)$$

In situ porosity can be determined from geophysical logging performed on the cored holes. Since the presence of free gas in an oil sands reservoir is rare, however, in situ porosity can be calculated by:

$$n = \frac{M_w/G_w + M_b/G_b}{M_w/G_w + M_b/G_b + M_s/G_s} \qquad (3.2)$$

where:

M_w = mass of water

M_b = mass of bitumen

M_s = mass of mineral grains

G_w = specific gravity of water

G_b = specific gravity of bitumen

G_s = specific gravity of mineral grains

To obtain representative values of geotechnical and petrophysical properties, Dusseault and Von Domselaar recommend an index of disturbance of less than 10 percent.

After full pore fluid saturation is achieved, as determined by the B tests, cyclic compressibility tests are carried out on each sample. Increments of effective confining stress are applied to the sample up to 2 MPa above the in situ vertical effective confining stress and the volume change of the specimen is measured. During compression the pore fluid pressure is maintained above the pore fluid saturation pressure. The effective confining stress is cycled up to three times above and below the in situ confining stress and the B test is repeated following the completion of the cyclic compression. The B value after cyclic compressibility of a high quality oil sands specimen is approximately 0.6. The magnitude of reduction in the B value from initial saturation to after cyclic compression reflects the amount of sample disturbance during coring and preparation.

Since the geotechnical properties of oil sands, as well as the properties of associated strata, depend not only on the existing stresses but also on the stresses experienced by the formation over geological time, the above test procedures are carried out on all specimens prior to measurement of geotechnical properties such as shear strength, stress-strain moduli and thermal expansion or compression. These latter test procedures are discussed in detail in Appendix B.

The processes used to recover bitumen from oil sands subject the formation to changes in effective stress, pore

fluid pressure and temperature. During the stages of the in situ bitumen recovery process oil sands, as well as associated strata, undergo several different stress paths. Oil sands near a well casing during cyclic steam recovery, for example, experience a complex history of stress corresponding to each phase of the process such as well excavation, grouting, hydraulic fracturing, steam injection and pumping. The geomechanical behaviour depends on the series of stress changes applied to the oil sands. For instance, an oil sands specimen tested under a stress history associated with hydraulic fracturing would produce a stress-strain relationship which differs significantly from the one obtained from a test representative of the stress path followed during steam injection.

Due to the stress dependency of the oil sands and associated strata, testing procedures are followed to ensure the geotechnical properties measured in the laboratory are representative of those existing in the formation. The stress paths explored in this study include passive drained compression, passive undrained compression, active drained compression, J_1 = constant drained compression and extension, isotropic and constrained compression, and drained and undrained constrained heating. Each of these test procedures is outlined in Appendix B.

3.3 Compliance Testing

During experimental testing the apparatus response to changes in load, stress and temperature must be separated from the test specimen response. The equipment behaviour was isolated by testing substances whose material properties are well established, such as aluminum and water, over a wide range of temperatures and pressures.

Compliance testing methods, procedures and results are outlined and discussed in detail in Appendix C.

4. GEOLOGICAL DETAILS OF MATERIALS STUDIED

4.1 Athabasca Materials

The formation strata studied in this phase of the research program were collected from three separate well locations in the Athabasca Deposit. The depths of the oil sands reservoirs at these locations ranged from 150 to 300 m.

4.1.1 Underground Test Facility

The majority of the Athabasca samples for the experimental study were obtained from Well AO-27 (13-07-093-12W4) at the AOSTRA Underground Test Facility located approximately 45 km north of Fort McMurray. At the well site, the main pay zone (defined as continuous oil sands grading greater than 10% by weight) is about 24 m thick (Figure 4.1) and is overlain by about 138 m of overburden (AOSTRA, 1986). Overburden materials are defined as Quarternary Sediments (primarily glacial till) and the shales and sands of the Grand Rapids Formation, Clearwater Formation as well as the predominantly shaley strata of the Upper McMurray Formation. Well AO-27 is located 335 m directly west of the two 3 m diameter access shafts (Figure 4.2).

Borehole AO-27 was triconed to a depth of 100 m and then cored continuously until the Devonian limestone was encountered at a depth of 162.2 m. Core sampling was carried

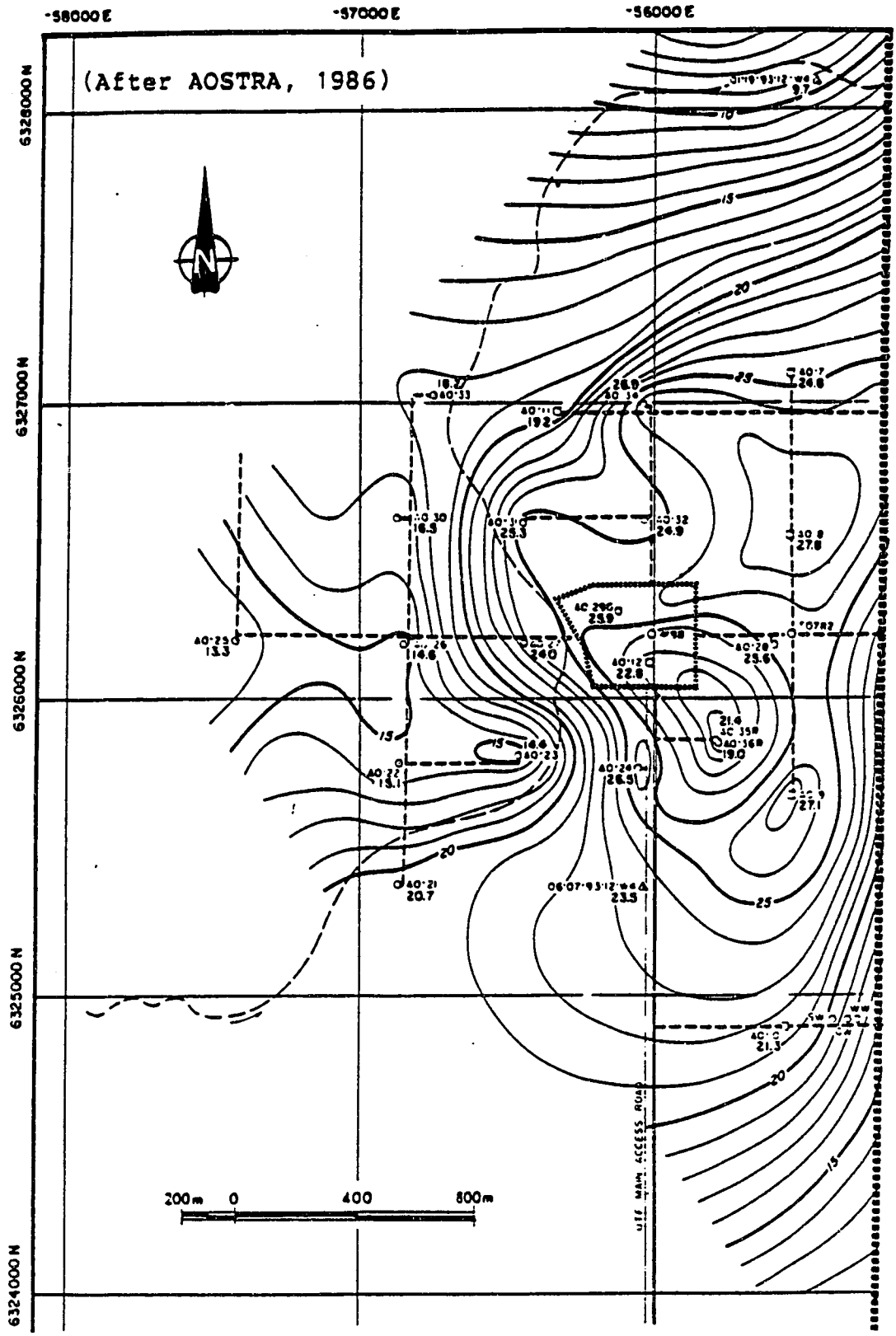

Figure 4.1 UTF Site - Isopack Map of Main Pay Zone

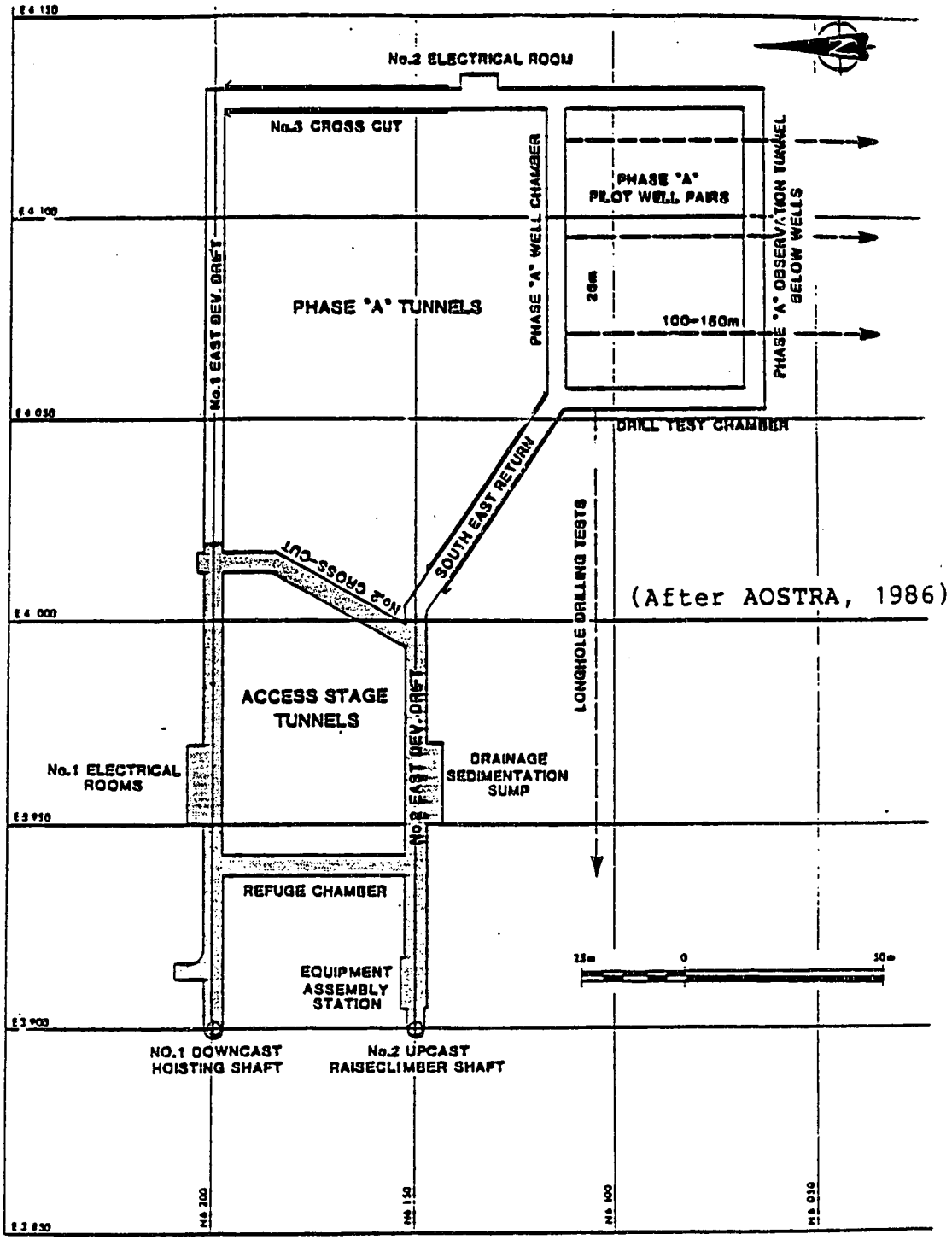

Figure 4.2 UTF Site - Underground Development Phase A Pilot

out using a triple tube Christianson core barrel with an inner PVC liner 71 mm inside diameter (HQ core).

Cores of shale taken from the Clearwater Formation (depth interval of 100 m to 125 m) were capped and sealed and stored at room temperature. The overall core recovery in the Clearwater Formation was approximately 72%. The true depth of the shale core recovered was based on comparison of a geophysical field log (natural gamma ray log) and gamma ray logging in the laboratory of recovered core lengths. After core recovery from the borehole the 10 m plastic core liner was cut into lengths of 1.5 m or less. During cutting it was noted that the core liner was permitted to flex and may have resulted in some cracking of the shale to occur. There did not appear to be any significant amount of core expansion as the core emerged from the borehole. However, 8 of the 15 core samples throughout the core interval experienced some degree of expansion during transport and storage. A maximum axial expansion of 4 cm (over 1.5 m of core) occurred between the depth interval of 117 to 118.5 m.

Prior to coring the bottom portion of the McMurray Formation strata (depth interval of 152 to 161 m) the inner plastic liner was perforated with 2 mm holes to allow evolving gases to escape. Holes were drilled on four sides of the core liner at a spacing of approximately 10 mm. Immediately after coring the oil sands were observed to fit loosely in the liners and it was estimated that the coring bit was overcutting the oil sands strata by 1 to 1.5 mm. The

3 m long PVC core tubes from each of the three coring runs were cut into 1 m sections and were capped and sealed. Two samples were put in containment cells and pressurized to 1.5 MPa with nitrogen gas and chilled to -25°C. The third sample from each run was placed directly in the freezer to be used as a control to enable evaluation of the effectiveness of the pressurization procedure in inhibiting core expansion due to gas evolution.

After transport to the University the pressure vessels were stored in a cold room at -18°C for 13 days after which each was slowly depressurized at a rate of 150 kPa per day. After complete depressurization was obtained the solids, bitumen and water content of each tube sample was carefully determined and later used in conjunction with down hole geophysics data to calculate in situ porosity to assess the degree of sample disturbance.

Subsequent to coring a number of geophysical measurements were carried out in Borehole AO-27. The log suite included Bulk Density, Gamma Ray, Resistivity and Caliper logs.

Gamma ray logs are used to measure the amount of naturally occurring gamma rays in a formation strata. In general, shales are more radioactive than either sands or limestones and therefore gamma ray measurements are a good indicator of the shaliness of a formation. Gamma ray logs provide a means for interpreting depositional environments (or facies patterns) and lithologic variations.

The gamma ray index, I_{GR}, is commonly used to normalize gamma ray readings between clean sand (I_{GR} = 0) and a shale I_{GR} = 1), that is:

$$I_{GR} = (GR_{log} - GR_{min})/(GR_{max} - GR_{min}) \quad (4.1)$$

where:

GR_{log} = gamma ray reading of formation

GR_{min} = minimum gamma ray reading (clean sand or carbonate)

GR_{max} = maximum gamma ray reading (shale)

The minimum and maximum gamma ray deflections were determined to be 43 and 150 API units, respectively. The results of the gamma ray log performed in Borehole AO-27 are summarized in Table 4.1. The gamma ray survey indicates the presence of the estuarine channel sand sequence between depths of 137 m to 163 m (I_{GR} ranging from 0.30 to 0.39) overlain by shale and shaley sands of the tidal flat or estuarine shoreface group and lower marine shoreface between depths 128 to 137 (I_{GR} = 0.53) which in turn is overlain by coarsening upward sand sequence of the upper beach/shoreface and the sands of the Shefal Wabiskaw Member between depths 125 to 128 m (I_{GR} = 0.16). The gamma ray log results in the McMurray Formation correlate well with laboratory particle size distributions shown in Table 4.2.

Table 4.1 Results of Gamma Ray Log (Borehole AO-27)

Depth (m)	Gamma Ray Log Reading	Gamma Ray Index	Shale Content
6 - 20	140	0.907	high
20 - 52	110	0.626	medium
52 - 56	135	0.860	high
56 - 60	85	0.393	low
60 - 92	100	0.533	medium
92 - 116	125	0.766	high (Kcc unit)
116 - 121	95	0.486	medium (Kcb unit)
121 - 125	125	0.766	high (Kca unit)
125 - 128	60	0.159	low
128 - 137	100	0.533	medium
137 - 148	75	0.299	low
148 - 163	85	0.393	low

Table 4.2 Laboratory Particle Size Distribution (Borehole A0-27)

Depth (m)	Mass Fraction > 325 Sieve	Mass Fraction < 325 Sieve
126.1 - 127.6	0.7955	0.2045
128.5 - 135.8	0.4360	0.5640
135.8 - 137.9	0.5254	0.4746
137.9 - 139.9	0.9063	0.0937
140.0 - 142.5	0.5902	0.4098
142.5 - 145.4	0.6324	0.3676
145.4 - 147.9	0.7819	0.2181
147.9 - 151.9	0.5372	0.4628
152.0 - 162.1	0.8248	0.1752

Dusseault (1984) notes that the use of natural gamma logs as a clay content indicator may be unreliable in shale strata in which the illite content, as a percentage of the total clay mineral, is highly variable. This is because the gamma log uses ^{40}K as the assumed source and illite is the major host of ^{40}K in clay minerals while other clays have significantly less amounts. Dusseault cites results from gamma ray traces taken in the Clearwater Formation at the Syncrude Canada Ltd. mine lease in which smectite-rich zones display a suppressed natural gamma ray response. This effect has been noted in Borehole AO-27 in the k_{cb} unit of the Clearwater Formation which contains a significant amount of montmorillonite as verified by laboratory index testing. For example, at a depth of 118.5 m the liquid limit and plasticity index of the shale strata were determined to be 181% and 140.4%, respectively. As noted previously, the shale core from this depth displayed significant swelling after sampling.

The results of the caliper log are given in Table 4.3. Caliper diameters are fairly uniform (average of 13.4 cm) through the McMurray Formation (125 to 163 m). The measured diameters are more variable in the shale strata of the overlying Clearwater and Grand Rapids Formations. The highest measurements occurred in the k_{cb} unit of the Clearwater Formation between depths of 116 and 121 m reflecting the swelling and subsequent washing of the low density, high montmorillonite strata.

Table 4.3 Results of Caliper Log (Borehole AO-27)

Depth (m)	Caliper Reading (cm)	Comments
1 - 56	16.2	Fluctuates occasionally
56 - 92	14.6	Fluctuates occasionally
92 - 116 (Kcc unit)	15.0	Fluctuates
116 - 121 (Kcb unit)	17.8	Peak of 20.2 cm at 118.5 m
121 - 125 (Kca unit)	15.4	Fairly Uniform
125 - 163	13.4	Uniform

The electrical resistivity of a formation strata is defined as:

$$R = rA/L \qquad (4.2)$$

where:

R = electrical resistivity in ohm-meters

A = area the current is flowing through in m^2

L = length of the material in m

r = electrical resistance in ohms

In hydrocarbon rich zones the resistivity readings are generally high because hydrocarbons are non-conductors. The resistivity of oil and gas may be in the order of millions of ohm-meters (Hilche, 1982). The resistivity of water varies with the amount of salt in solution and ranges from 0.1 ohm-meters for salt saturated water to over one million for distilled water. In general, the resistivity of shales is relatively low but increases with increasing sand content. The magnitude of the increase, however, is limited to where enough sand is present to create permeability and porosity. The resistivity of permeable strata may be influenced by the invasion of mud filtrate which generally has a higher resistivity than formation water.

The resistivity log carried out in Borehole AO-27 (Table 4.4) correlates well with the shale content distribution as interpreted from the gamma ray log results.

Table 4.4 Results of Resistivity Log (Borehole AO-27)

Depth (m)	Shale Content (based on gamma ray log)	Resistivity (ohm-m)	Productivity of Oil Sands
20 - 52	medium	> 7.5	
52 - 56	high	>> 7.5	
56 - 60	low	30.0	
60 - 92	medium	>30.0	
92 - 116	high	>>10.0	
116 - 121	medium	> 7.0	
121 - 125	high	>> 7.0	
125 - 128	low	20.0	
128 - 137	medium	>10.0	
137 - 148	low	60.0	high
148 - 163	low	40.0 **	high

** Note : Peak resistivity readings of - 400 ohm-m at 154 m depth
300 ohm-m at 160 m depth

High shale content units show relatively low resistivities. The bitumen bearing sands of the estuarine channel sequence (depth range of 137 to 163 m) display the greater resistivity measurements.

Compton Scattering of gamma rays are used by density logs to measure the bulk density of formation strata. The density measuring instrument normally consists of a gamma ray source and two detectors (Hilchie, 1982). Electrons orbiting the atoms in the formation strata scatter the gamma rays emitted from the source. Compton Scattering causes a loss of energy of the gamma rays. Dense strata causes more scattering and absorption of gamma rays and therefore less gamma rays reach the detector. Density logs are usually calibrated in water saturated limestone formations.

The results of a geophysical density log carried out in Borehole AO-27 are given in Table 4.5. Density measurements in the first 5 m of depth were relatively high (2.65 Mg/m^3) and may reflect boundary conditions associated with the coring process (well casing, etc.). Through the depth interval of 5 to 51 m, density measurements were fairly uniform, averaging 2.10 Mg/m^3, although occasional localized fluctuations in density readings, ranging from 1.60 Mg/m^3 to 2.65 Mg/m^3, were observed. Low density readings in this zone were coincidental with positive "spikes" in the caliper log indicative of localized washing of formation strata. High density measurements may reflect the presence of thin, hard, low porosity, cemented siltstone layers of the Grand Rapids

Table 4.5 Results of Density Log (Borehole AO-27)

Depth (m)	Average Density Log Reading (apparent Mg/m3)
2 - 5	2.65
5 - 51	2.10 (occasional larger values)
51 - 116	2.20
116 - 121 (Kcb unit)	1.90 (1.60 Mg/m3 at 118.5 m depth)
121 - 163	2.20

Formation as previously shown in the generalized stratigraphy in the area of the Underground Test Facility (Table 1.2). Over the depth interval of 51 to 116 m density measurements fluctuate about a reading of 2.20 Mg/m³ with localized peaks as high as 2.80 Mg/m³ but generally averaging 2.60 Mg/m³. Localized readings below 2.20 Mg/m³ were less common and on average were about 2.10 Mg/m³. Density readings through the Clearwater k_{cb} unit (depth interval of 116 to 121 m) were consistently low (1.90 Mg/m³) reflecting the swelling and subsequent washing of the high montmorillonite strata in this zone.

Gamma ray density log measurements through the McMurray Formation (depth interval of 125 to 162.5 m) varied between 2.04 Mg/m³ to 2.56 Mg/m³. Density readings generally decreased with depth and averaged approximately 2.20 Mg/m³ through the interval.

The in situ porosity, n_d, may be derived from bulk density measurements obtained from gamma ray density logs using the following expression (Dusseault and Van Domselaar, 1982):

$$n_d = \frac{G_s - D}{G_s - G_w + S_o (G_w - G_o)} \qquad (4.3)$$

where:

G_s = mineral grain mean density

G_o = specific gravity of oil

G_w = specific gravity of water

S_o = oil saturation

D = bulk density measured from gamma ray density log

The above formulation assumes that no free gas is present in the oil sands reservoir which is valid for the vast majority of oil sands reservoirs in Alberta (Dusseault and Van Domselaar, 1982).

In situ porosities were calculated from the geophysical density log for the oil sands core samples retained for experimental testing. It was observed, through correlation of the gamma ray and density logs, that bulk density readings in the McMurray Formation generally increase with increasing amounts of shale interbedding. The mineral grain mean density (G_s in Equation 4.3) was therefore calculated by considering the relative proportion of oil sands to shale based on gamma ray index values (IGR) for the particular sampling depth. In calculating porosities from the density log it was assumed that:

1. McMurray Formation oil sands consist of primarily quartz sand with a mean specific gravity of 2.65 Mg/m^3.

2. Minerals forming the shale interbedding have an overall average grain density of 2.70 Mg/m^3.

3. Pore water and pore bitumen have equivalent specific gravities of 1.01 mg/m^3.

Intact porosities calculated in this manner are given in Table 4.6a. In situ porosities back calculated from laboratory samples taken at the same depths assuming no free gas in situ (Chapter 3, Equation 3.2) are given in Table 4.6b for comparative purposes.

The majority of data in Table 4.6 suggests that in situ porosities back calculated from laboratory samples overestimate the true in situ porosity as measured by the density log. This may be due to water infiltration into laboratory samples caused by expansion of the pore space caused by stress relief and swelling (hydration) of clay. It should be noted, however, that the oil sands core samples contained thin, discontinuous shale seams ranging from 1 mm to a few cm in thickness and the laboratory samples were relatively small (approximately 2.5 cm thick). The back calculated porosity values are therefore highly dependent on the proportion of oil sands to shale in the particular

Table 4.6 Core Disturbance, with and without Repressurization

a) based on geohpysical logs

Depth (m)	GR (API units)	IGR	Bulk Density (Mg/m3)	Gs	Porosity nd (%)	Laboratory Porosity (%)	Index of Disturbance (%)	Pressurized ?
152.5	110	0.626	2.26	2.68	25.2	30.8	22.2	No
153.0	75	0.299	2.22	2.66	26.9	35.9	33.5	No
153.5	53	0.093	2.11	2.65	33.1	39.2	18.4	Yes
154.0	50	0.065	2.08	2.65	34.9	37.2	6.6	Yes
154.2	80	0.346	2.16	2.67	30.6	40.9	33.7	Yes
155.0	95	0.486	2.26	2.67	24.9	36.6	47.0	No
155.75	105	0.579	2.20	2.68	28.8	37.8	31.7	No
156.0	70	0.252	2.16	2.66	30.8	35.8	17.8	Yes
156.75	85	0.393	2.14	2.67	31.2	35.2	10.3	Yes
160.0	60	0.159	2.10	2.66	33.5	40.5	19.5	Yes
160.5	65	0.206	2.10	2.66	34.7	39.7	16.8	Yes

b) based on laboratory results

Depth (m)	Bitumen ** Content (weight %)	Water ** Content (weight %)	Solids ** Content (weight %)	Porosity (%)	Laboratory Porosity (%)	Index of Disturbance (%)	Pressurized ?
152.5	6	7	87	27.9	30.8	10.4	No
153.0	11	4	85	31.3	35.9	14.7	No
153.5	11	4	85	31.3	39.2	25.2	Yes
154.0	10	4	86	31.1	37.2	20.6	Yes
154.2	--	-	--	31.1	40.9	31.5	Yes
155.0	7	7	86	30.6	36.6	19.6	No
155.75	9	6	85	31.7	37.8	19.2	No
156.0	9	6	86	30.7	35.8	16.6	Yes
156.75	11	4	85	31.6	35.2	11.4	Yes
160.0	13	4	83	35.4	40.5	14.4	Yes
160.5	13	4	83	35.4	39.7	12.2	Yes

** Data rounded to nearest percentage point

specimen. The density log tool in contrast does not distinguish thin shale seams (less than 10 cm thick) (Hilche, 1982) and treats the shale laminated oil sands as a homogeneous shaley sand. In addition, the density log measures the density on one side of the borehole only and therefore may obscure the discontinuous nature of the shale interbedding.

The results shown in Table 4.6 suggest that core repressurization in this case did not have a significant influence in reducing sample damage caused by core expansion. Further, high index of disturbance values (as high as 47% from geophysical log and as high as 32% back calculated from laboratory specimens) indicate that there was little benefit derived from drilling gas release holes along the core liner axis.

Devonian limestone core samples for the experimental study were obtained from Well AO-32 (03-18-93-12W4) located approximately 400 m north of the two 3 m diameter access shafts at the Underground Test Facility site (Figure 4.2). The three 1.5 m HQ core samples originated at the Pre-Cretaceous unconformity, separating McMurray and Waterways Formations, at 151 m and terminated at a depth of 155.5 m. The core consisted of microcrystalline limestone with thinly interbedded shale with the interbedding becoming less frequent and continuous with depth.

The limestone core was taken by triple tube core barrel and was frozen on site. Due to the high shale content in the

upper 3 m of core, the freezing process caused the majority of this core to break up.

4.1.2 Southern Athabasca McMurray Formation Oil Sands

Core samples obtained at an average depth of 295 m by triple tube core barrel from the McMurray Formation in the southern portion of the Athabasca Deposit (about 50 km southwest of Fort McMurray) were provided for geotechnical analysis. No detailed geological or geophysical data was available at this site. The McMurray Formation at this location is approximately 40 m thick and consists of an overall fining upward sequence, ranging from rich, low fines content oil sands at the base to sandy shale at the top of the formation.

Approximately 2 m of 76 mm diameter core samples were collected from the lower portion of the formation. The core sample consisted of rich (bitumen content 15% by weight), uniformly graded oil sands with a fines content (less than 0.074 mm of the grain sized distribution) of approximately 5%. The core had been frozen on the surface with dry ice and stored in a cold room at -18°C. Back calculated in situ porosities (assuming no free gas in situ) indicated that the index of disturbance of the core sample ranged from 11 to 18%.

The in situ pore fluid pressure at sampling depth for this location was reported to be approximately 2200 kPa.

4.1.3 Northern Athabasca Clearwater Formation Oil Sands

At a site approximately 90 km northwest of Fort McMurray a 3 m (76 mm diameter) core length of Clearwater Formation (Wabiskaw Member) oil sands was obtained for geotechnical testing. The oil sands strata was cored using a triple tube core barrel and had been frozen on site and subsequently stored in a cold room (-18°C) prior to testing.

The core sample consisted of fairly homogeneous oil sands with a bitumen content of about 12% by weight and a fines content (less than 0.074 mm of the grain size distribution) ranging from 5 to 20%. Back calculated in situ porosities (assuming no free gas in situ) indicated that the index of disturbance of the core sample ranged from 15 to 21%.

No detailed geological or geophysical information was available from this well location. However, the Wabiskaw Member at this location is at least 24 m thick and consisted of an overall fining upward sequence ranging from low fines oil sands at the base to sandy shale at the top of the unit. The core sample was taken from the lower portion of the unit.

The depth of the core sample was approximately 220 m and the in situ pore fluid pressure at this depth was reported to be 800 kPa.

4.1.4 Summary

The materials comprising the Athabasca Deposit are geologically complex and extremely variable in-place. Geological complexity is characterized primarily by rapid changes in grain size, material structure and mineralogy and reflects the non-uniform manner in which the sediments were deposited.

McMurray Formation oil sands intersecting Borehole AO-27 at the UTF site display significant vertical variability. This variability is characterized by changes in grain size distribution of the oil sands and by the presence of discontinuous shale seams and clasts which range in thickness, frequency and spacing. Significant spacial variability of the McMurray Formation across the UTF site has been reported by AOSTRA (1986).

The complex stratigraphy of the McMurray Formation at the UTF site is indicative of a complex depositional environment. The geological history of the McMurray Formation at the UTF site has been interpreted by AOSTRA (1986) as consisting of two broad environments of deposition encompassing a number of sedimentary processes:

1. An estuarine environment composed of an estuarine channel sand facies, an estuarine channel breccia facies, a lower estuarine channel sand facies, an estuarine muddy and sandy flat facies, and an estuarine sandy flat facies.

2. A marine environment consisting of a lower marine shoreface facies and an upper beach/shoreface facies.

The stratigraphical sequence of sediments varies spacially and vertically according to the particular sedimentary environment. For example, low fines oil sands are generally restricted to channel sands and associated channel bar sands which are representative of high flow environments within the lower portion of the formation. Shale interbedding in the lower portion of the formation is indicative of estuarine channel margin sedimentation and periods of waning flow within the depositional system. Further variability arises due to the transitory nature of the estuarine channel complex which results in depositional features being reworked through time by active migration of main channel trends (Mattison, 1987).

It should be noted that geological complexity of Athabasca sediments cannot be entirely attributed to changes in depositional environments. For example, the Clearwater Formation was deposited in a regionally extensive marine environment and yet contains significant variations in clay mineralogy as well as localized cemented siltstone layers. Therefore, geological variability is also associated with changes in the nature of the source rocks and diagenetic changes.

The Athabasca core materials collected for geotechnical analysis are summarized in Table 4.7. Geological facies interpretation was based on geophysical data, core examination and local or regional experience. Sedimentary processes appear to be a good general indicator of the variability of soil properties and constitutive behaviour in a particular sequence of sediments.

4.2 Cold Lake Materials

The majority of bitumen production in the Northern Cold Lake Deposit is obtained from the Clearwater Formation. The Clearwater Formation contains three vertically stacked reservoir units designated as C-1, C-2 and C-3 sands. The lowermost C-3 reservoir unit in Northern Cold Lake is the thickest and richest reservoir and therefore is generally subjected to in situ thermal recovery methods (Visser et al, 1985). The C-2 reservoir sands are generally less rich and continuous and are not usually targeted for direct thermal stimulation. However, C-2 sands may be subject to future recovery if sufficient heat migrates from the underlying heated C-3 reservoir.

Cold Lake Deposit specimens used for laboratory testing were taken from four separate well locations northwest of Cold Lake. The core includes both the C-2 and C-3 reservoir oil sands as well as the intervening formation strata (typically interbedded sands, silts and shales). The Clearwater Formation strata was cored using triple tube core

Table 4.7 Summary of Athabasca Materials Used in Experimental Program

Location	Geological Unit	Depth (m)	Geological Facies	Core Description
UTF	Clearwater (Kcc)	100 - 116	Marine Sequence	Medium to high plastic shale, occassional siltstone lenses, minor silt and sand interbedding
UTF	Clearwater (Kcb)	116 - 121	Marine Sequence	High plastic shale, frequent thin seams of smectite dispersed throughout interval
UTF	Clearwater (Kca)	121 - 125	Marine Sequence	Medium to high plastic shale, fairly uniform
UTF	McMurray	152 - 161	Estuarine Channel Complex	Fine to medium grained oil sands, containing thin discontinuous shale seams and clasts (1mm to a few cm thick)
UTF	Waterways	151 - 155.6	Argillaceous Nodular Micrite	Microcrystalline limestone with discontinuous calcareous shale and clasts (1 mm to a
Southern Athabasca	McMurray	295	Estuarine Channel Sand Sequence (Assumed)	Rich uniformly graded oil sands, medium grained, low fines content (approximately 5 %)
North West Athabasca	Clearwater (Wabiskaw)	220	Shelf (Assumed)	Rich uniformly graded oil sands, medium grained, fines content ranging from 5 to 20% cm thick)

barrels and was received at the University in 89 mm inside diameter plastic core liners which were sealed and frozen.

4.2.1 Cold Lake Location No. 1

A 17.5 m core length of Clearwater Formation strata was obtained for geotechnical testing. The depth of the core ranged from 441 m to 458 m, the top of the Clearwater C-3 oil sands reservoir. The C-3 oil sands were observed to be highly damaged (fractured and broken) and were therefore not salvageable for geotechnical testing.

The majority of core samples consisted of interbedded oil sands, silts and shales. A portion of the core (depth of 443 m to 447 m), however, was composed of fairly continuous oil sands (C-2 reservoir sands). A 1 m thick massive shale bed was found extending over the depth interval of 449.5 to 450.5 m. These two materials were selected from the core interval for laboratory testing.

The C-2 oil sands reservoir core sample consisted of fine grained oil sands with frequent discontinuous shale seams and clasts up to 5 mm thick (Figure 4.3). The bitumen content of the core length ranged from 4.5% to 10.7% by weight and the fines content (less than 0.074 mm) of the grain size distribution ranged from 9% to 49% by weight. Back calculated in situ porosities (assuming no free gas in situ) indicated that the index of disturbance of the core sample ranged from 13 to 20%.

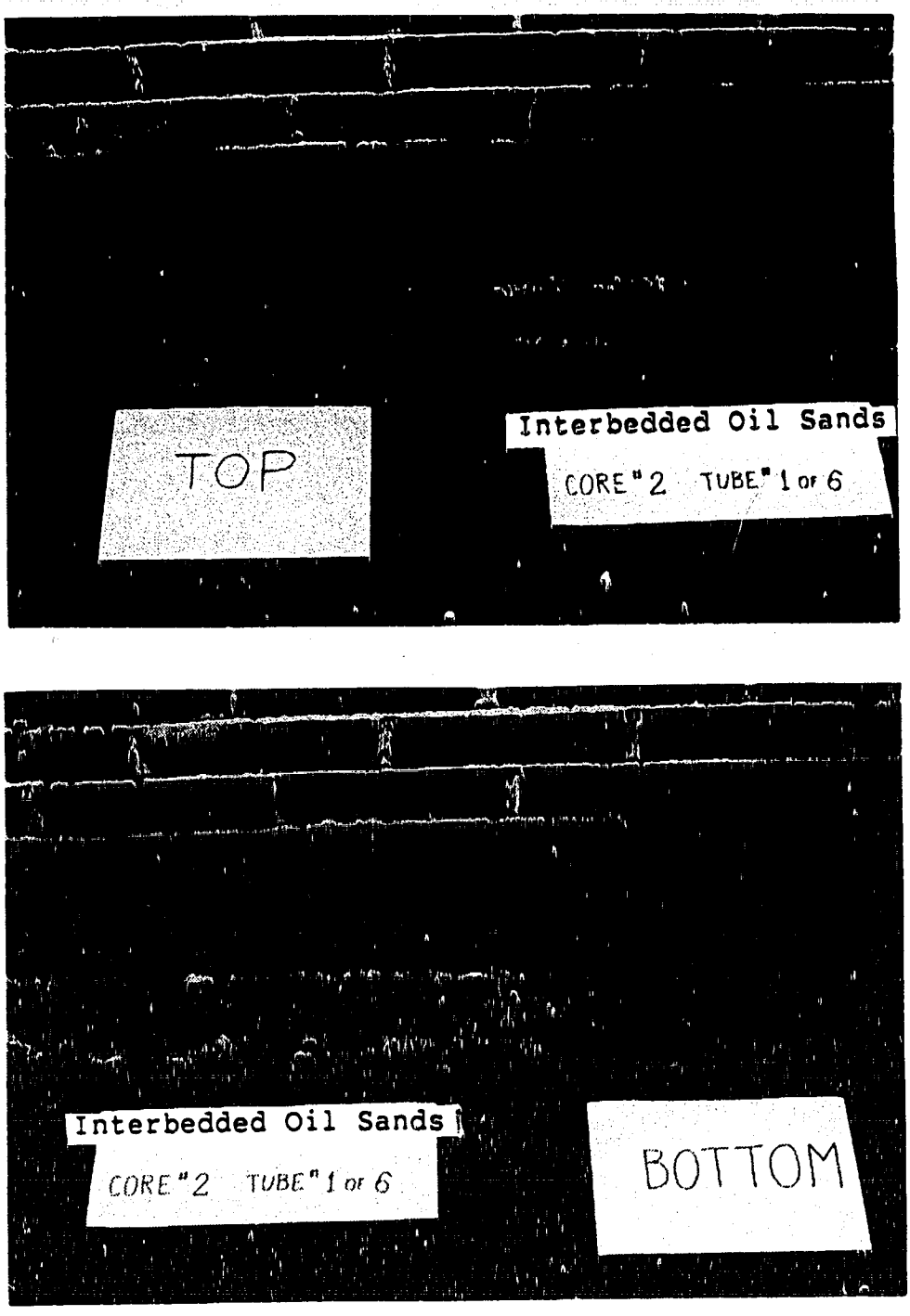

Figure 4.3 Clearwater Oil Sands Core Sample (Cold Lake Location No. 1)

The shale over the depth interval of 449.5 to 450.5 m was hard, highly fissile, highly plastic and dark grey to black in colour (Figure 4.4). The bulk density and initial water contents were 2.15 Mg/m^3 and 16%, respectively. The shale had a liquid limit of 70% and a plastic limit of 28%. The initial void ratio of the core interval was about 0.4 with an initial saturation of 95%. The occasional lens of silt or fine sand a few mm thick was observed in the core sample. Frequent partings or fracturing parallel to stratification was noted. Spacing of the discontinuities was highly variable and ranged from 0.5 mm to 20 cm, with the majority 0.5 mm to a few mm.

The material forming the core interval was representative of an offshore-transitional depositional facies. This facies reflects deposition in a marine offshore-transition zone where clay deposition from suspension is the dominant sedimentation mechanism interrupted by episodic influxes of sand and silt (Visser, et al, 1985). Due to the complex geological depositional environment a number of geotechnical facies may be derived based on grain size distribution and the proportion of shale, sand and silt in a particular depth interval. The materials selected for geotechnical analysis represent two such geotechnical facies indicative of the two extremes of materials resulting from the non-uniform depositional environment.

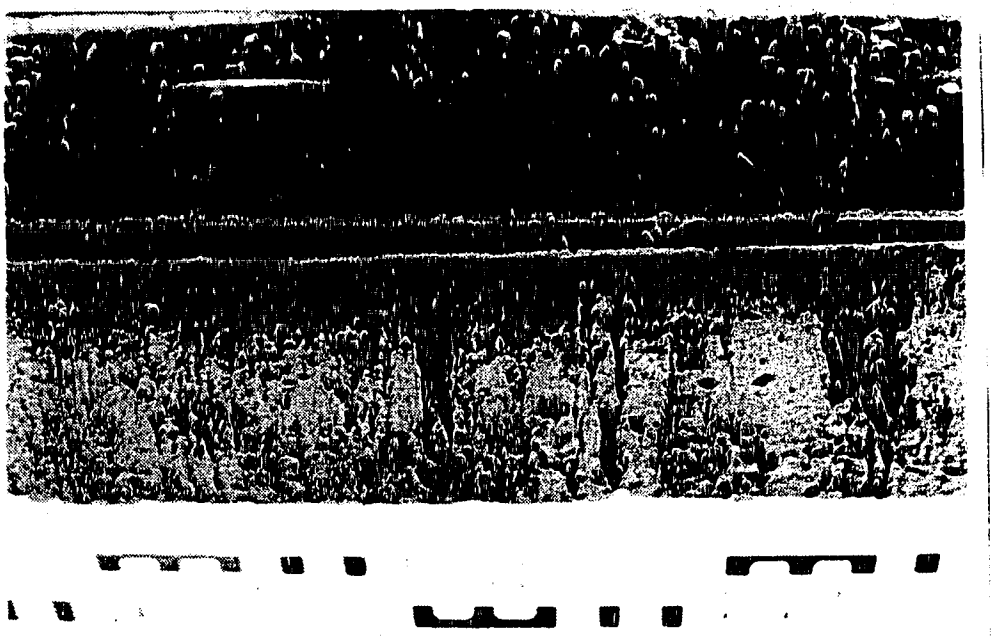

Figure 4.4 Clearwater Shale Core Sample (Cold Lake Location No. 1)

4.2.2 Cold Lake Location No. 2

A 1.5 m thick core sample of the main Clearwater oil sands (C-3 sands) at a depth of 460 m was provided for geotechnical analysis (Figure 4.5). The core sample consisted of fine grained, rich (bitumen content of up to 12% by weight), uniform oil sands with a fines content ranging from 6 to 10% by weight. Back calculated in situ porosities (assuming no free gas in situ) indicated that the index of disturbance of the core sample ranged from 18 to 31%.

The C-3 oil sands are interpreted by Visser et al (1985) of being deposited in a shoreface zone. Sand typical of a shoreface facies is fine grained and may contain thin shale beds or partings (usually at the base of the unit) up to 2.5 cm thick. The oil sands core sample did not contain any visible shale discontinuities and therefore, in this particular case, geological and geotechnical facies coincide.

4.2.3 Cold Lake Location No. 3

A 1.5 m core sample obtained at an average depth of 487 m from the Clearwater Formation in Northern Cold Lake was collected for laboratory testing. The core sample was composed of fine grained oil sands of low bitumen content (8% by weight) with frequent interbedded shale seams varying in thickness from 1 mm to a few cm. The fines content (less than 0.074 mm) of the grain size distribution was

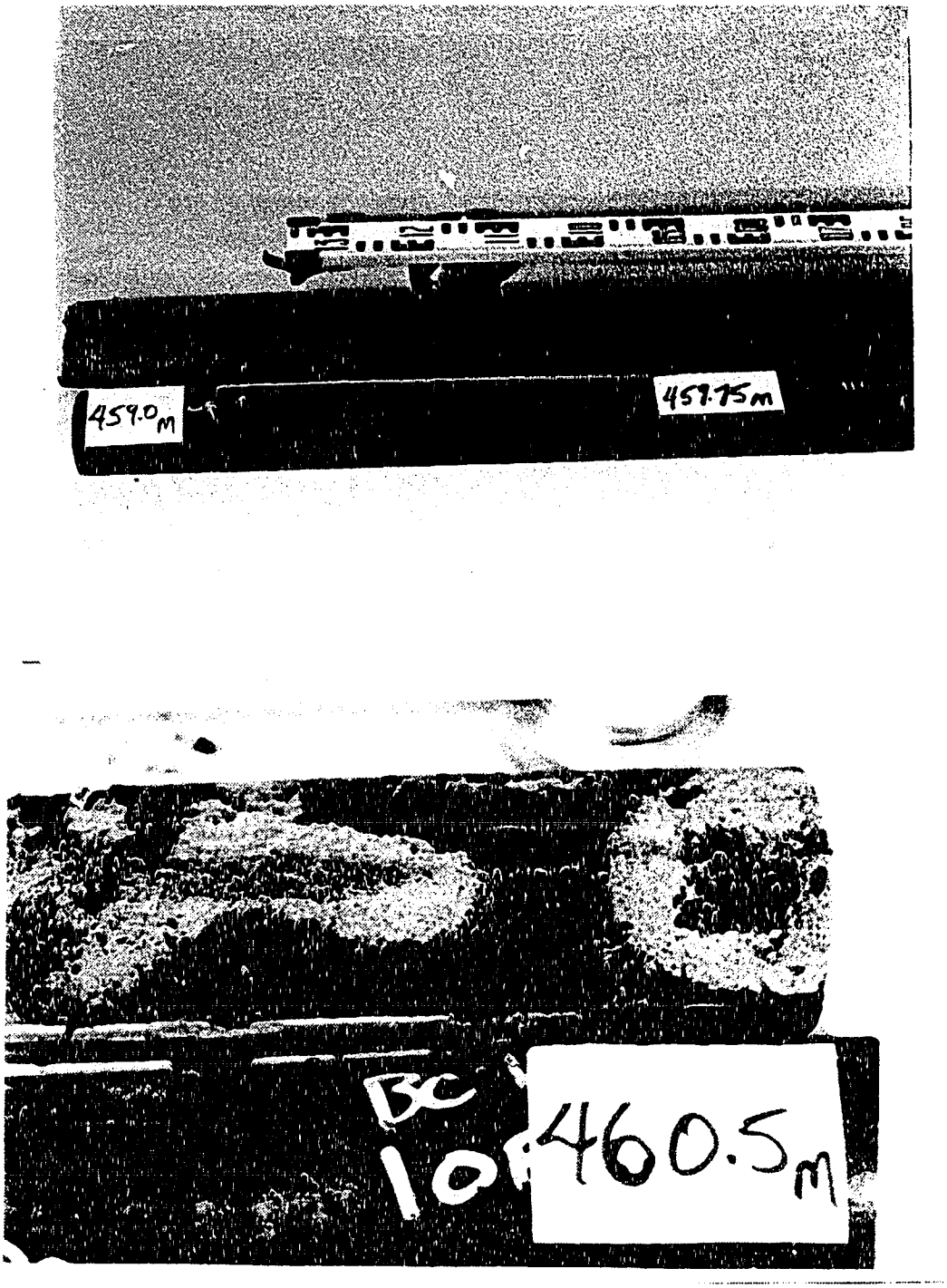

Figure 4.5 Clearwater Oil Sands Core Sample (Cold Lake Location No. 2)

approximately 15% by weight. The index of disturbance of the core sample based on back calculated in situ porosities (assuming no free gas in situ) ranged from 11% to 18%.

No detailed geological or geophysical information was available from this well location. The relatively high proportion of shale within the interval, however, is indicative of quiet water sedimentation and, therefore, reflects an offshore-transitional depositional facies.

4.2.4 Cold Lake Location No. 4

An 18 m core length of Clearwater Formation strata was obtained from Cold Lake Location No. 4. The depth of the core ranged from 460 m to 478 m. The majority of core samples consisted of interbedded oil sands, silts and shale. A 0.9 m thick carbonate rock bed was identified at a depth of 466 m. In general, the core interval consisted of an overall upward fining sequence with the frequency and thickness of oil sands beds increasing with depth.

The majority of the oil sands core was highly fractured and not suitable for geotechnical testing. A limited amount of intact oil sands core, however, at a depth of 474 m was of sufficient quality for laboratory testing. The test specimens were lean, silty, fine grained oil sands with bitumen contents of about 8% by weight. Each specimen contained thin, discontinuous shale seams and clasts. The fines content (less than 0.074 mm) of the grain size distributions were fairly consistent at about 30% by mass.

Back calculated in situ porosities (assuming no free gas in situ) indicated that the index of disturbance of this section of core ranged from 11 to 19%.

The carbonate rock at a depth of 466 m was grey, very fine grained, strong and massive with occasional thin (less than 1 mm), discontinuous brown (iron) staining parallel to bedding planes (Figure 4.6). Visser et al (1985) report a similar occurrence of a ferron calcite cemented, indurated sand 50 to 120 cm thick at the base of the Clearwater C-2 reservoir traceable over most of the Wolf Lake area in Northern Cold Lake.

4.2.5 Summary

The Cold Lake core materials collected for geotechnical analysis are summarized in Table 4.8. The materials forming the Clearwater Formation in Northern Cold Lake are geologically complex and reflect a non-uniform marine depositional environment. As in the case of Athabasca Deposit sediments, geological complexity is characterized by rapid changes in grain size, material structure and mineralogy.

A number of geotechnical facies were selected for laboratory testing to provide an overall indication of the constitutive behaviour of the Clearwater Formation strata. Geotechnical zoning was carried out by selecting core intervals of similar lithology and was limited to some extent due to excessive core damage caused by inadequate

Table 4.8 Summary of Cold Lake Materials Used in Experimental Program

Location	Geological Unit	Depth (m)	Geological Facies	Core Description
Northern Cold Lake No. 1	Clearwater	445	Offshore Transitional	Fine grained oil sands, low bitumen content, frequent interbedded shale seams up to 5 mm thick
Northern Cold Lake No. 1	Clearwater	450	Offshore Transitional	Shale, highly fissile, highly plastic, hard, occasional lense of fine grained sand, frequent partings or fractures parrallel to stratification (spacing ranges from 0.5 mm to 20 cm)
Northern Cold Lake No. 2	Clearwater	460	Shoreface	Fine grained oil sands, uniform, high bitumen content
Northern Cold Lake No. 3	Clearwater	487	Offshore Transitional	Fine grained oil sands, low bitumen content, frequent interbedded shale seams varying in thickness from 1 mm to a few cm
Northern Cold Lake No. 4	Clearwater	474	Offshore Transitional	Fine grained oil sands, low bitumen content, frequent interbedded shale seams varying in thickness from 1 mm to a few cm
Northern Cold Lake No. 4	Clearwater	466	Offshore Transitional	Carbonate rock, very fine grained, strong, massive, occassional discontinuous thin (less than 1mm) brown staining parrallel to bedding planes

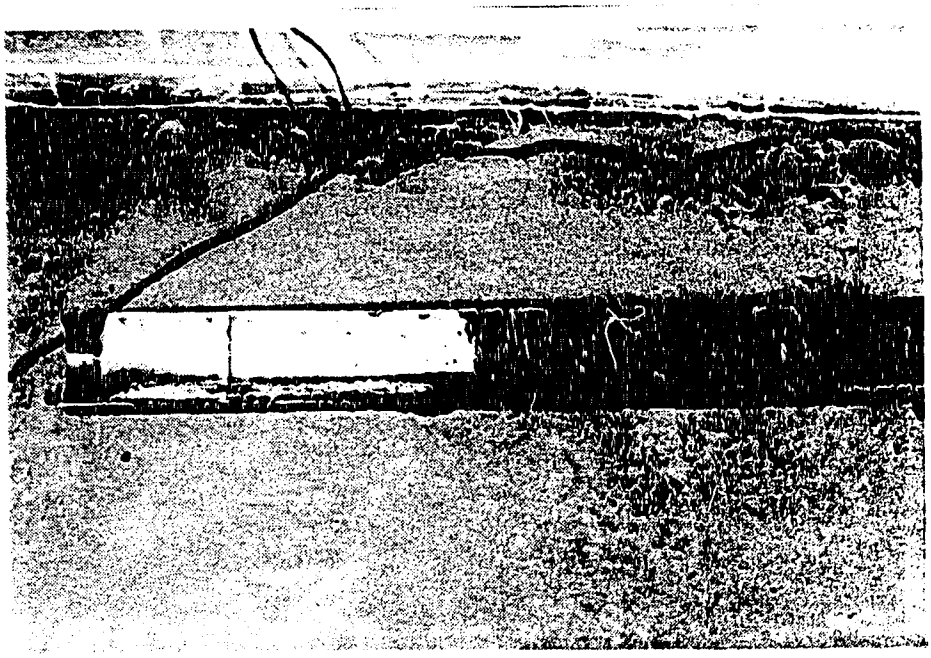

Figure 4.6 Clearwater Carbonate Rock Core Sample (Cold Lake Location No. 4)

transportation and storage procedures which occurred prior to delivery to the University.

5. THERMAL VOLUME CHANGE OF ATHABASCA MATERIALS

5.1 Materials Studied

The materials comprising the Athabasca Deposit which may be subjected to either direct thermal stimulation or peripheral heating exhibit both geological and geotechnical complexity. Laboratory specimens used in the experimental program to develop representative relationships which characterize thermal volume change behaviour of these materials were derived from four geological units at the Underground Test Facility site (Table 5.1).

The strata was separated into geotechnical facies based on interpretation of geological facies, core examination and index testing (grain size distribution; bitumen, water and solids content; and Atterberg limit testing). The geological facies under consideration include:

1. **Clearwater k_{cc} Shale.** A medium plastic, silty shale of very stiff to hard consistency. Its colour varied from dark grey to black.

2. **Clearwater k_{cb} Shale.** A medium plastic, silty shale of very stiff to hard consistency. Its colour ranged from dark grey to black.

Table 5.1 Athabasca Thermal Volume Change Specimens

Test Number	Depth (m)	Geological Unit	% water (mass)	% bitumen (mass)	% solids (mass)	% fines (<0.074 mm)	liquid limit (%)	plastic limit (%)
UFCCS1	100.4	Clearwater (kcc)	15.3	0	84.7	----	50.5	23.3
UFCCS3	117.3	Clearwater (kcb)	14.1	0	85.9	----	46.2	21.0
UFCCS4	117.9	Clearwater (kcb)	20.2	0	79.8	----	180.8	40.4
UFCCS5	118.0	Clearwater (kcb)	20.2	0	79.8	----	180.8	40.4
UFCOS1	157.8	McMurray	9.4	4.3	86.3	47.5	-	-
UFCOS2	157.8	McMurray	9.4	4.3	86.3	47.5	-	-
UFCOS3	157.8	McMurray	9.4	4.3	86.3	47.5	-	-
UFCOS4	155.2	McMurray	6.9	4.9	88.2	44.8	-	-
UFCOS5	155.2	McMurray	5.3	8.3	86.4	51.8	-	-
UTFCL1	155.4	Waterways	2.1	0	97.9	----	-	-

3. **Clearwater k_{cb} Shale.** A high plastic shale of very stiff consistency. Its colour varied from dark grey to black with frequent brownish smectite rich bands. The bands were essentially horizontal with thicknesses ranging from 1 mm to several mm.

4. **McMurray Oil Sands.** A fine to medium grained, lean oil sands. Brownish grey to black in colour. Pockets and lenses of silty shale were encountered randomly throughout the specimens. Shale interbedding ranged from 1 mm to several mm thick.

5. **Waterways Limestone.** A microcrystalline limestone. The specimen was uniform and massive. Its colour varied from light to medium grey.

5.2 Drained Thermal Volume Change

Under fully drained conditions the volume change of a soil subjected to increases in temperature arises from the expansion of the individual mineral grains and structural changes in the mineral skeleton. Pore fluid pressures must remain constant throughout the specimen during drained heating to prevent mechanical deformations caused by changes in effective confining stresses. This requires the specimen to be heated slowly to allow thermally generated pore fluid

pressures to drain simultaneously with application of the temperature increase.

When a homogeneous soil with grains in particle to particle contact undergoes a temperature change, each mineral experiences the same volumetric strain and the entire structure will experience the same volumetric strain, $\alpha_s \Delta T$ (Campanella and Mitchell, 1968). Subsequent volume changes may arise from changes in intergranular forces due to temperature which entails relative movement or reorientation of particles to allow the soil mass to support the same effective stress. This change in volume is denoted by $(\Delta V_{st})_{\Delta T}$. As a result the net volume change of a soil mass subjected to a change in temperature under fully drained conditions is:

$$(\Delta V_m)_{\Delta T} = \alpha_s \, V_m \Delta T + (\Delta V_{st})_{\Delta T} \qquad (5.1)$$

where:

α_s = volumetric coefficient of thermal expansion of the mineral grains.

V_m = volume of soil mass

ΔT = change in temperature.

The structural volume change of the soil structure due to a change in temperature may be expressed as:

$$(\Delta V_{st})_{\Delta T} = \alpha_{st} V_m \Delta T \qquad (5.2)$$

where:

α_{st} = coefficient of structural volume change of soil structure due to change in temperature.

Combining Equations 5.1 and 5.2 gives:

$$(\Delta V_m)_{\Delta T} = (\alpha_s + \alpha_{st}) V_m \Delta T \qquad (5.3)$$

Thermal volume change of mineral grains are recoverable, whereas structural changes are non-recoverable.

The volume of pore fluid drained (under constant effective confining stress) from a fully saturated soil specimen experiencing a change in temperature can be expressed as:

$$(\Delta V_d)_{\Delta T} = (\Delta V_f)_{\Delta T} + (\Delta V_s)_{\Delta T} - (\Delta V_m)_{\Delta T} \qquad (5.4)$$

where:

$(\Delta V_f)_{\Delta T}$ = volume change of pore fluids due to change in temperature

$(\Delta V_s)_{\Delta T}$ = volume change of sand grains due to change in temperature.

The volume change of pore fluids experiencing a change in temperature (materials containing both water and bitumen in the pores, such as oil sands) can be stated mathematically as:

$$(\Delta V_f)_{\Delta T} = a_w V_w \Delta T + a_b V_b \Delta T \qquad (5.5)$$

where:

a_w = coefficient of thermal volume change of water

V_w = volume of pore water

a_b = coefficient of thermal volume change of bitumen

V_b = volume of pore bitumen.

The volume change of the mineral grains due to change in temperature is denoted by:

$$(\Delta V_s)_{\Delta T} = \alpha_s V_s \Delta T \tag{5.6}$$

Combining Equations 5.3, 5.5 and 5.6 gives:

$$(\Delta V_d)_{\Delta T} = \alpha_w V_w \Delta T + \alpha_b V_b \Delta T + \alpha_s V_s \Delta T - (\alpha_s + \alpha_{st}) V_m \Delta T \tag{5.7}$$

or:

$$(\Delta V_d)_{\Delta T} = \alpha_w V_w \Delta T + \alpha_b V_b \Delta T - \alpha_s \Delta T (V_m - V_s) - \alpha_{st} V_m \Delta T \tag{5.8}$$

where:

$V_m - V_s$ = volume of the voids.

The amount of fluid expelled from a soil specimen during a drained thermal volume change test is therefore the sum of the volume change of the fluids less the change in void volume and structural volume change. If the structure expands $(\Delta V_{st})_{\Delta T}$ is positive and would be subtracted or, contrastingly, if the structure contracts $(\Delta V_{st})_{\Delta T}$ is negative and would be added.

5.2.1 Oil Sands

McMurray Formation Estuarine Sand

Agar (1984) and Kosar (1983) conducted a series of drained thermal volume change tests on undisturbed specimens of oil sands over the effective confining stress range of 0.02 MPa to 6 MPa. The oil sands specimens were obtained from core samples taken from an oil sands outcrop at Saline Creek, approximately 1 km south of Fort McMurray. The pertinent test specimen data is given in Table 5.2.

Saline Creek oil sands is a uniformly graded (uniformity coefficient, D_{60}/D_{10}, of approximately 2) quartz sand with a fines content (less than 0.074 mm of the grain size distribution) of about 3% by mass. These oil sands specimens typically had bitumen saturations of about 80% and water saturations of about 20% of the pore volume. These sands are representative of a high flow depositional environment and are consistent with a estuarine channel sand and associated channel bar sands facies as interpreted by Mattison (1987).

The results of the drained thermal volume change tests performed on Saline Creek oil sands are given in Figure 5.1. The drained thermal volume change test by Kosar (1983) under a back pressure of 2 MPa displays a rapid increase in volume

Table 5.2 Athabasca Oil Sands Drained Thermal Volume Change Test and Specimen Data

Test Number	Location	Effective Confining Stress (MPa)	% water (mass)	% bitumen (mass)	% solids (mass)	Bulk Density (Mg/m3)	Void Ratio	Index of Disturbance (%)
Kosar (1983)	Saline Creek	0.24	3.9	11.2	84.9	2.02	0.539	9.5
Agar (1984)	Saline Creek	6.00	2.1	15.5	82.3	1.97	0.635	7.2
Agar (1984)	Saline Creek	0.20	2.1	15.6	82.4	1.99	0.617	5.4
UFCOS1	AOSTRA UTF	2.50	9.4	4.3	86.3	2.00	0.540	18.0
UFCOS3	AOSTRA UTF	2.30	9.4	4.3	86.3	1.91	0.612	27.9
UFCOS4	AOSTRA UTF	2.50	6.9	4.9	88.2	2.00	0.505	27.8
UFCOS5	AOSTRA UTF	2.50	5.3	8.3	86.4	2.03	0.517	15.4

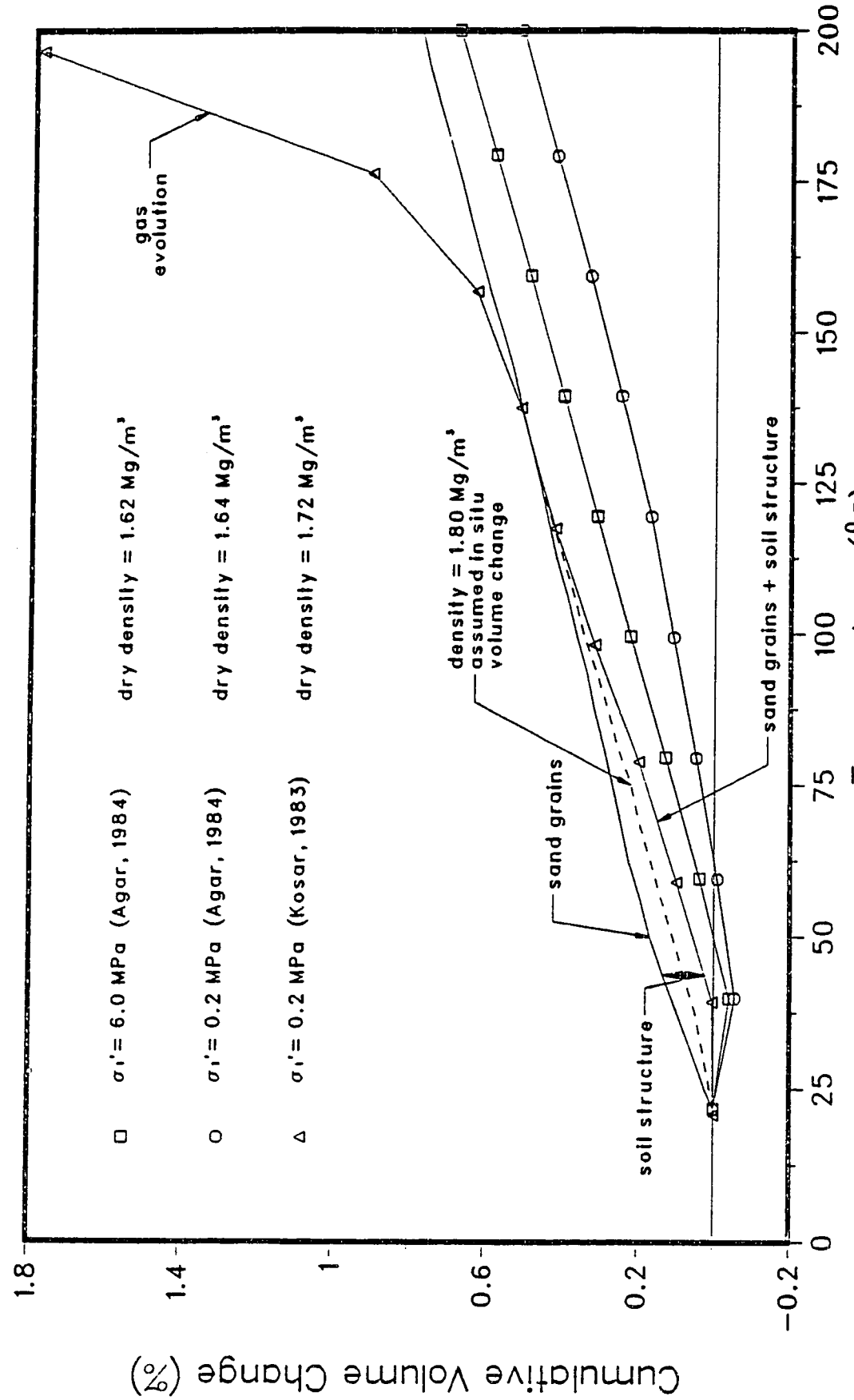

Figure 5.1 Drained Thermal Volume Change of Saline Creek Oil Sands

over the temperature range of 180°C to 200°C. The back pressure for this test was not sufficiently high enough over this temperature range to keep gases in solution. If gas evolution did occur over this temperature range, the gas bubbles at time of formation must have been at pressures exceeding the vertical confining stress of 2.2 MPa in order to disrupt the skeletal grains and force the cell confining piston upward. The gas bubbles would theoretically continue to expand until pressure equalization between the liquid and gases was achieved resulting in the steady state points (temperature stable and zero volume change) at 180 and 200°C. Because the gas bubbles form in the viscous bitumen, they cannot drain from the specimen and expand the sample even under drained conditions.

The volume change with temperature of the quartz sand grains is plotted with the drained thermal volume change tests on Saline Creek oil sands. Since the results of the drained tests on oil sands are a measure of the volume change of both the sand grains and soil structure, the difference between the two curves is the volume change of the soil structure. Testing of Saline Creek oil sands shows that the oil sands matrix undergoes some heat induced compaction at the onset of heating, the magnitude of which reflects the amount of sample disturbance (Agar, 1984; Kosar, 1983). Because heat compaction is unlikely in this very dense, uniformly graded quartz sand, an assumed volume change curve more representative of in situ oil sands is

also illustrated (Kosar, 1983).

A separate plot of the cumulative volume change of the soil structures alone is given in Figure 5.2. Temperature induced changes in the soil structure are significant over the temperature range of 20°C to 140°C and is greatest at approximately 50°C.

From the drained tests conducted on Saline Creek oil sands it is evident that volume increases of less than 1% are likely for drained conditions over the temperature range of 20°C to 200°C provided adequate back pressures are maintained to prevent gas evolution. The thermal volume increase appears to be independent of confining pressure. The dense, interpenetrative structure of this rich oil sands showed a negligible amount of thermal volume change. The vast majority of the volume increase was due to the thermal expansion of the quartz sand grains.

McMurray Formation Estuarine Channel Margin Sedimentation

The thermal volume change behaviour of oil sands from the Underground Test Facility site was tested to investigate the influence shale interbedding has on the oil sands matrix during heating. The specimens contained frequent discontinuous shale clasts and seams interspersed within the oil sands. The fines content (less than 0.074 mm) of the grain size distribution was approximately 48% by weight and the bitumen contents were about 5% by weight (Table 5.1).

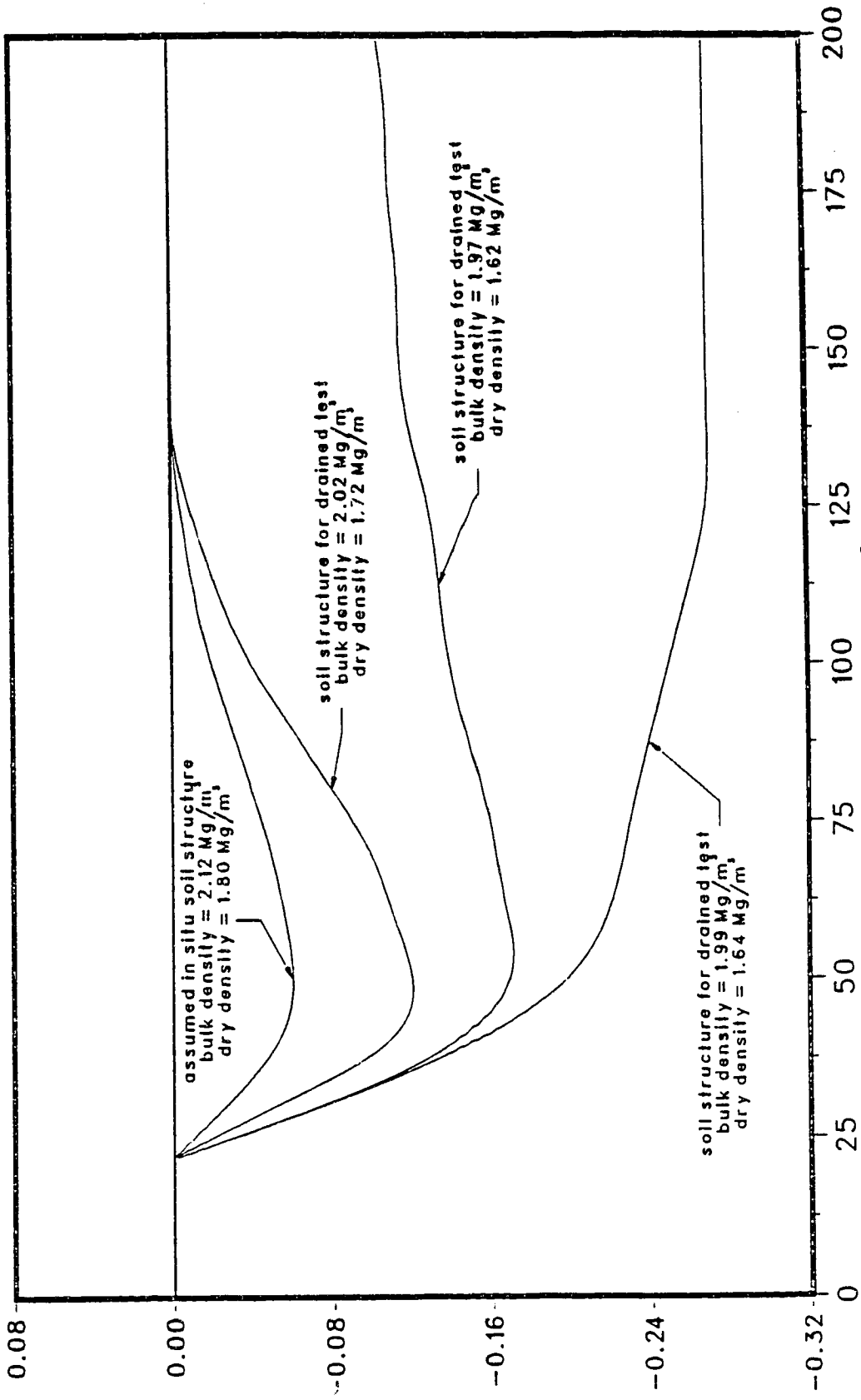

Figure 5.2 Thermal Volume Change of Saline Creek Oil Sands Structure

Shale interbedding is indicative of estuarine channel margin sedimentation and periods of waning flow within the depositional system (Mattison, 1987).

Drained thermal volume change was measured in several tests at a vertical effective confining stress of 2.5 MPa. A back pore fluid pressure of 10 MPa was maintained on each specimen during heating to prevent evolution of gases dissolved in the liquid phases from occurring. The pertinent test specimen data is given in Table 5.2.

The results of a drained thermal volume change test carried out on UTF oil sands are given in Figure 5.3. The specimen (UFCOS1) was compressed one-dimensionally to 3.4 MPa and cycled over the vertical effective stress range of 1 MPa to 3.4 MPa prior to heating under an effective confining stress of 2.5 MPa. Volumetric thermal volume change is plotted as a percentage of the original specimen volume. For comparative purposes, the cumulative volume change of a quartz sand grain is also shown. It is noted that the volumetric coefficient of thermal expansion of most clay particles is similar to that of quartz. For example, Mitchell and Campanella (1968) estimate the coefficient of thermal expansion of illite to be $3.5 \times 10^{-5} {}^{\circ}C^{-1}$ which is comparable to that of quartz which ranges from $3.4 \times 10^{-5} {}^{\circ}C^{-1}$ at 20°C to $5.0 \times 10^{-5} {}^{\circ}C^{-1}$ at 225°C (Clark, 1966).

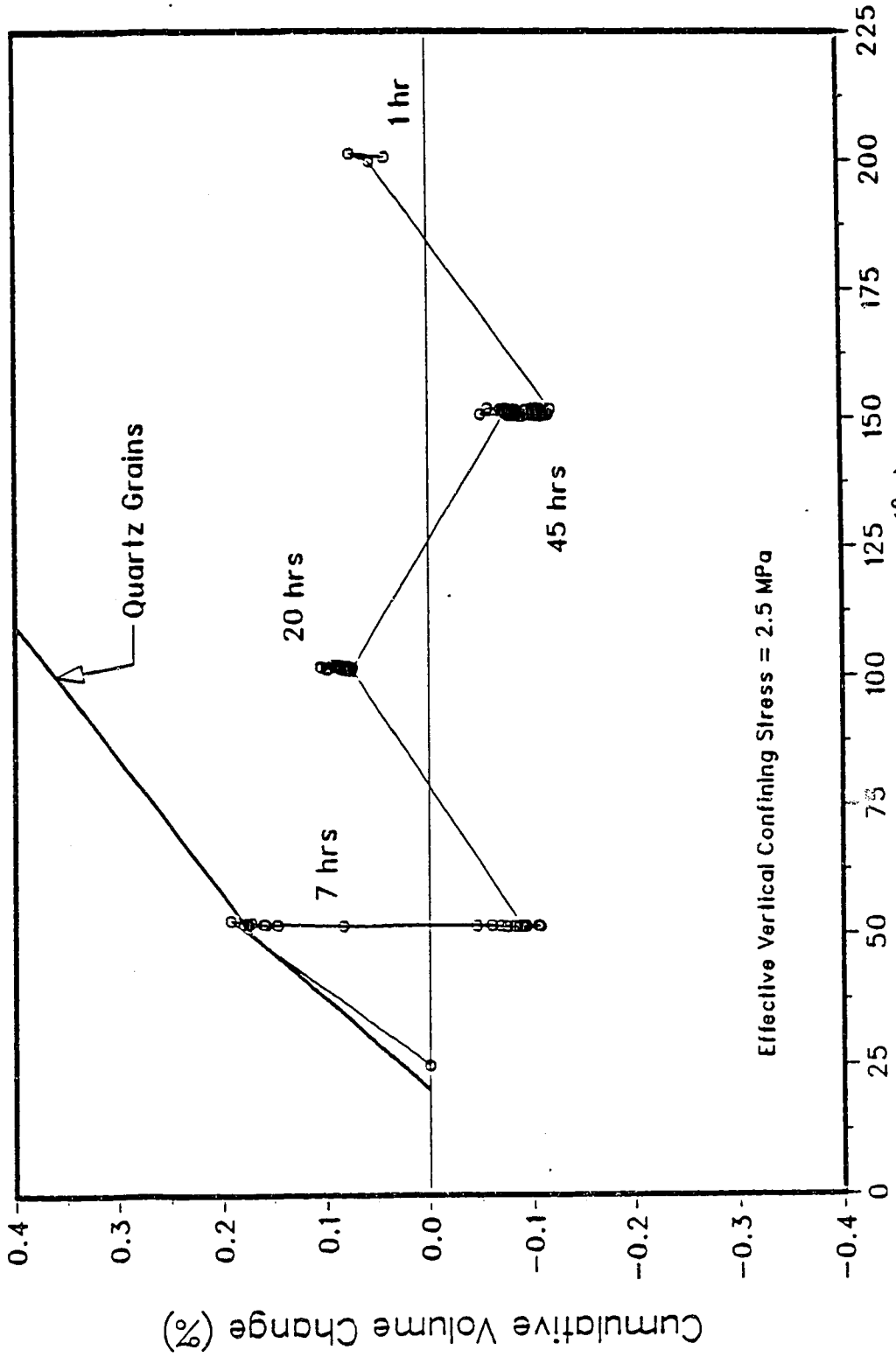

Figure 5.3 Drained Thermal Volume Change of UTF Oil Sands Specimen UFCOS1

The important behavioural characteristics concerning the drained thermal volume change of this shale interbedded oil sands derived from this test are summarized as follows:

1. Application of the first heating increment to 50°C produced an initial volumetric increase. The possible mechanisms contributing to this volume increase include: thermal expansion of the mineral grains, thermal expansion of any non-dissipated pore liquids and thermal volume change of the soil structure. Since the mineral grains are in contact, the mineral grains and soil mass must experience the same volumetric strain. The measured volume increase was the same as that expected for the mineral grains alone. This suggests that the pore liquids are draining from the specimen as they expand and structural changes are negligible during the onset of the temperature increase. The volume subsequently decreased over a 7 hour period resulting in a net volume decrease of 0.1%. This volume decrease indicates a significant rearrangement of the soil matrix is occurring.

2. During heating to 100°C the specimen underwent a volumetric increase. A volume change of less than 0.05% was measured over a 20 hour period. This volume

change was cyclic over this time period due to slight variations, less than 2°C, in temperature. The amount of time dependent volume change due to structural changes in the soil matrix was negligible.

3. During heating to 150°C the specimen experiences a volumetric decrease. Although the volume change was cyclic over a 45 hour period, due to temperature fluctuations, the specimen did show a slight overall decrease of about 0.03%.

4. The specimen expands during the final heating increment to 200°C.

The results of three additional fully drained volumetric thermal expansion tests carried out on this shaley oil sands are shown in Figure 5.4. In these tests Specimens UFCOS3 and UFCOS5 were heated at a rate of 25°C per hour while Specimen UFCOS4 was heated at 50°C per hour. Specimen UFCOS3 was compressed to 3.5 MPa and cycled over the vertical effective stress range of 1.5 MPa to 3.5 MPa prior to heating. The remaining specimens were consolidated to 2.5 MPa prior to testing. Again, for comparative purposes, thermal expansion of quartz grains is also shown.

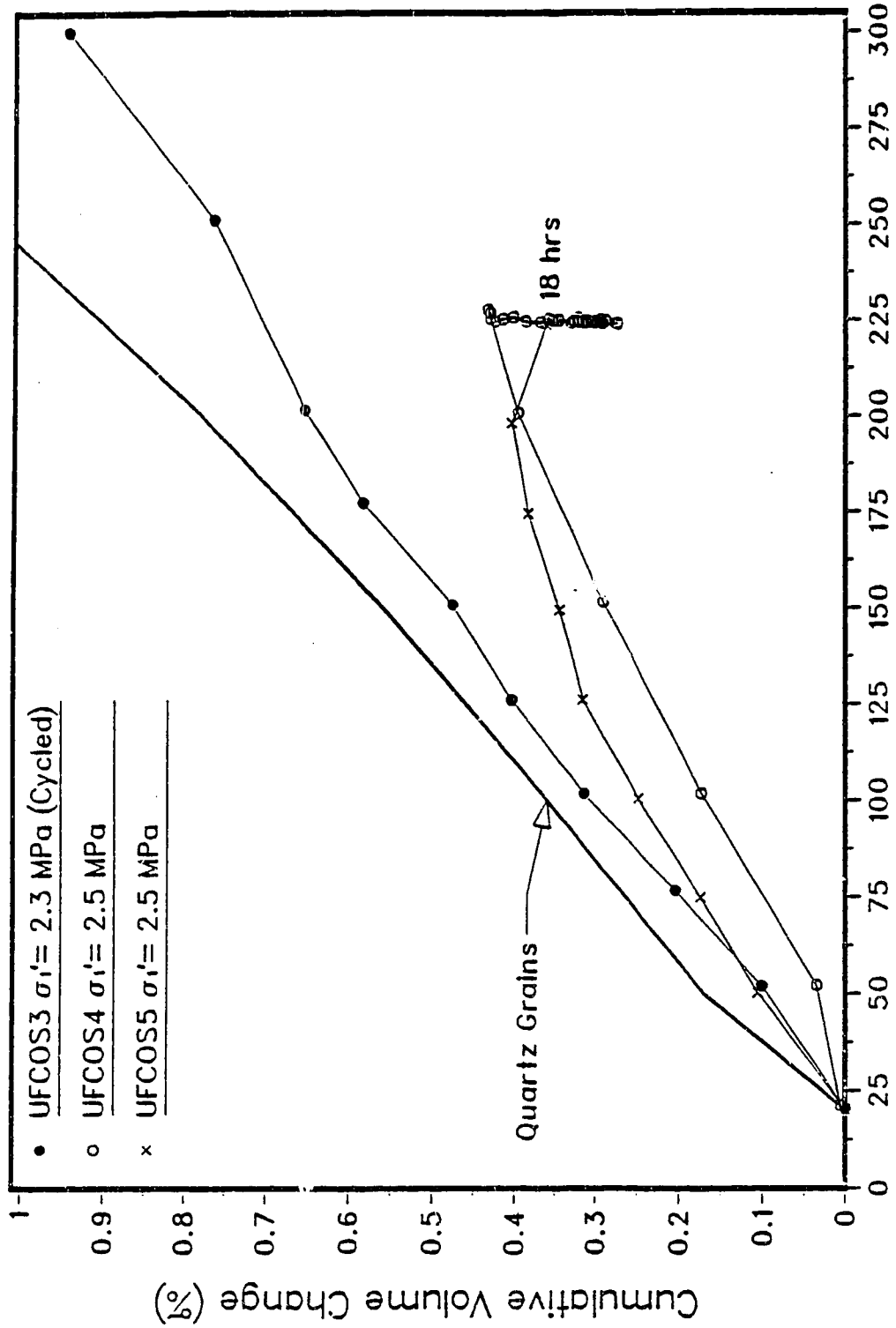

Figure 5.4 Drained Thermal Volume Change of UTF Oil Sands

Several noteworthy aspects regarding the constitutive behaviour of this oil sands due to rate of heating and load history are summarized as follows:

1. All three specimens show a cumulative volume increase during heating. Specimen UFCOS4, however, displays a time dependent volume decrease of about 0.15% over an 18 hour period at 225°C.

2. The specimen which underwent stress cycling before heating (UFCOS3) shows the greatest thermal volume increase even though the initial index of disturbance of this specimen was similar to UFCOS4 (28%) and significantly higher than UFCOS5 (15%).

3. The non-cycled specimens (UFCOS4 and UFCOS5) display approximately the same amount of thermal expansion (0.35%) at 225°C. The rate of thermal volume change varies during the tests. Specimen UFCOS4 shows a relatively small volume increase during the first heating increment to 50°C and the rate of thermal expansion is essentially linear over the temperature range of 50°C to 225°C. The rate of thermal expansion of Specimen UFCOS5, in contrast, decreases with increasing temperature throughout the test and is

negative over the final 25°C heating increment to 225°C.

The thermal volume change of the soil structure of this shaley McMurray Formation oil sands is shown in Figure 5.5. The cycled specimen (UFCOS1) heated slowly over a 73 hour period displayed the greatest structural collapse during heating. Thermal contraction of the soil structure was least for the cycled specimen heated at a rate of 25°C per hour. Non-cycled specimens heated at rates of 25°C per hour and 50°C per hour were intermediate to the above curves as illustrated in Figure 5.5.

Comparison of Geotechnical Facies

During one-dimensional compression in the oedometer shear stresses and shear strains develop due to:

1. Differential thermal expansion of the various mineral grains.

2. Transient heat transfer through the soil specimen.

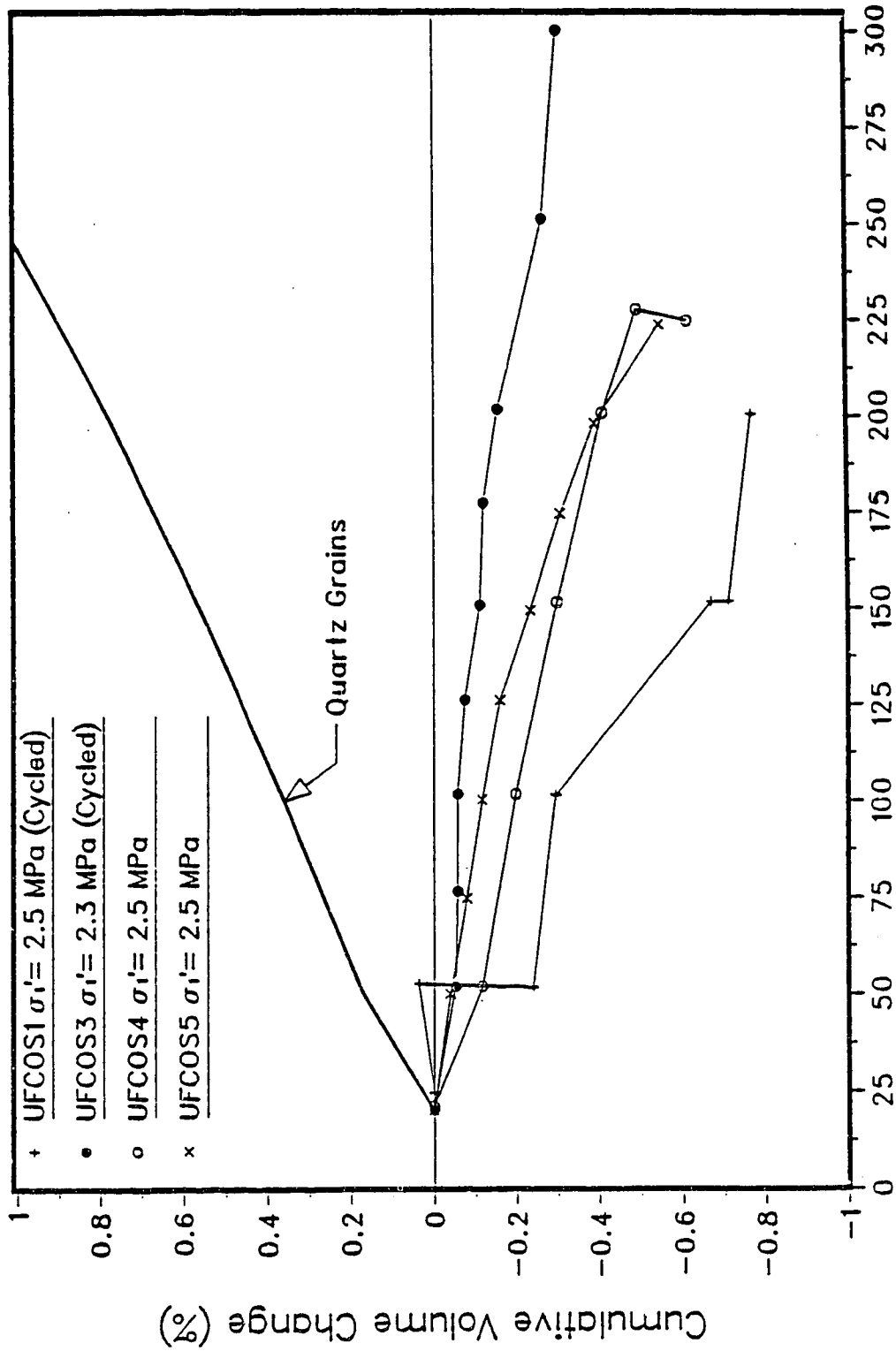

Figure 5.5 Thermal Volume Change of Soil Stucture of UTF Oil Sands

3. Non-uniform rates of heat transfer through different mineral grains.

4. Differential thermal expansion of test specimen and oedometer ring.

The stresses are opposed by frictional resistance of the individual interparticle contacts, cohesion or bonding between individual particles and the strength of the individual grains. If the thermally induced shear stresses overcome the overall shearing resistance of the soil matrix, the particles must move and reorientate into a denser configuration to carry the effective stress. This may involve the breaking of bonds between clay particles or crushing of weak sand grains in addition to sliding friction.

Agar (1984) and Kosar (1983) found a small volume decrease of rich Saline Creek oil sands specimens during the onset of heating (about 50°C). The more disturbed, lower density samples showed a higher degree of contraction of the soil structure. Subsequent thermal expansion of these specimens to temperatures of 300°C showed negligible change in the sand structure. Kosar (1983) also tested remoulded oil sands tailings samples at different initial densities and found that the amount of structural collapse at the

onset of heating increased as the initial density decreased. In all of the above tests on sands, structural changes were not time dependent over the effective stress range of 0.2 MPa to 6 MPa and temperatures up to 300°C.

Campanella and Mitchell (1968), Williams (1982) and Green (1984) report results of thermal tests performed on illite laboratory specimens at temperatures up to 200°C. Compression under constant effective stress and temperature was found to be time dependent with the rate of compression decreasing with increasing time. The amount of compression was reported to increase with increasing temperature and was attributed to a reduction in the attractive forces between clay particles with increasing temperature.

Rapid heating at 25°C or 50°C per hour of highly interbedded oil sands under drained conditions causes an increase in volume. The increase in volume is dominated by the thermal expansion of the mineral grains. Structural collapse of the soil matrix during rapid heating is resisted by frictional resistance and cohesion between particles. The cycled specimen expands more than the non-cycled specimens because the number and area of interparticle contacts are initially greater due to the cycling of stress. Structural changes occur when the thermally induced shear stresses exceed the friction resistance and the particles must rearrange into a dense packing to increase the frictional resistance in order to carry the 2.5 MPa effective confining stress.

During rapid heating, thermal consolidation of the shale clasts is inhibited by the time dependent slipping or rupture of bonds caused by a reduction in attractive forces and higher temperatures, by arching of the less compressible oil sands, and by small localized zones of non-dissipated pore fluid pressures. During slow or prolonged heating, the soil matrix slowly collapses until enough additional bonds are created to allow the soil structure to carry the effective stress, as shown in Figures 5.3, 5.4 and 5.5. The drained thermal volume change of highly interbedded oil sands is, therefore, "temperature path" dependent.

The structural collapse of the shale interbedding is also stress path dependent as illustrated in Figure 5.3. The soil matrix shows significant structural collapse over a 7 hour period at 50°C (Figure 5.5). Subsequent heating to 100°C produces little change in the soil structure even after 20 hours due to the formation of additional bonds and the increased frictional resistance due to densification of the soil structure. When the temperature was increased by an additional 50°C (to 150°C) collapse of the soil structure again occurs although the time dependency is smaller due to strengthening of the soil structure during heat consolidation at lower temperatures. The same mechanisms account for the difference in soil matrix collapse between cycled and non-cycled specimens during rapid heating.

5.2.2 Clearwater Shale

Medium Plastic Silty Shale

Drained thermal volume change of Clearwater Formation k_{cc} and k_{cb} shale was measured at vertical effective confining stresses of 0.2 MPa and 2.0 MPa, respectively. Both specimens had very similar water contents and liquid and plastic limits (Table 5.1) and were therefore zoned into the same geotechnical facies.

The test results shown in Figure 5.6 represent volume change as a percentage of the original sample volume after consolidation. Specimen UFCCS1 (k_{cc} shale) was heated at 1 hour increments of 10°C and Specimen UFCCS3 (k_{cb} shale) at 1 hour increments of 25°C. A back fluid pressure of 10 MPa was maintained during the tests to prevent gas evolution.

For comparative purposes, the volume change with temperature of illite clay particles is also shown in Figure 5.6. The volumetric coefficient of thermal expansion of illite was estimated to be 3.5×10^{-5} $°C^{-1}$ (Mitchell and Campanella, 1968). Illite is the principal clay found in Clearwater Formation k_{cc} shale in the Athabasca Deposit (Issac et al, 1982).

The specimen tested at 0.2 MPa effective confining stress shows a cumulative volume increase throughout the

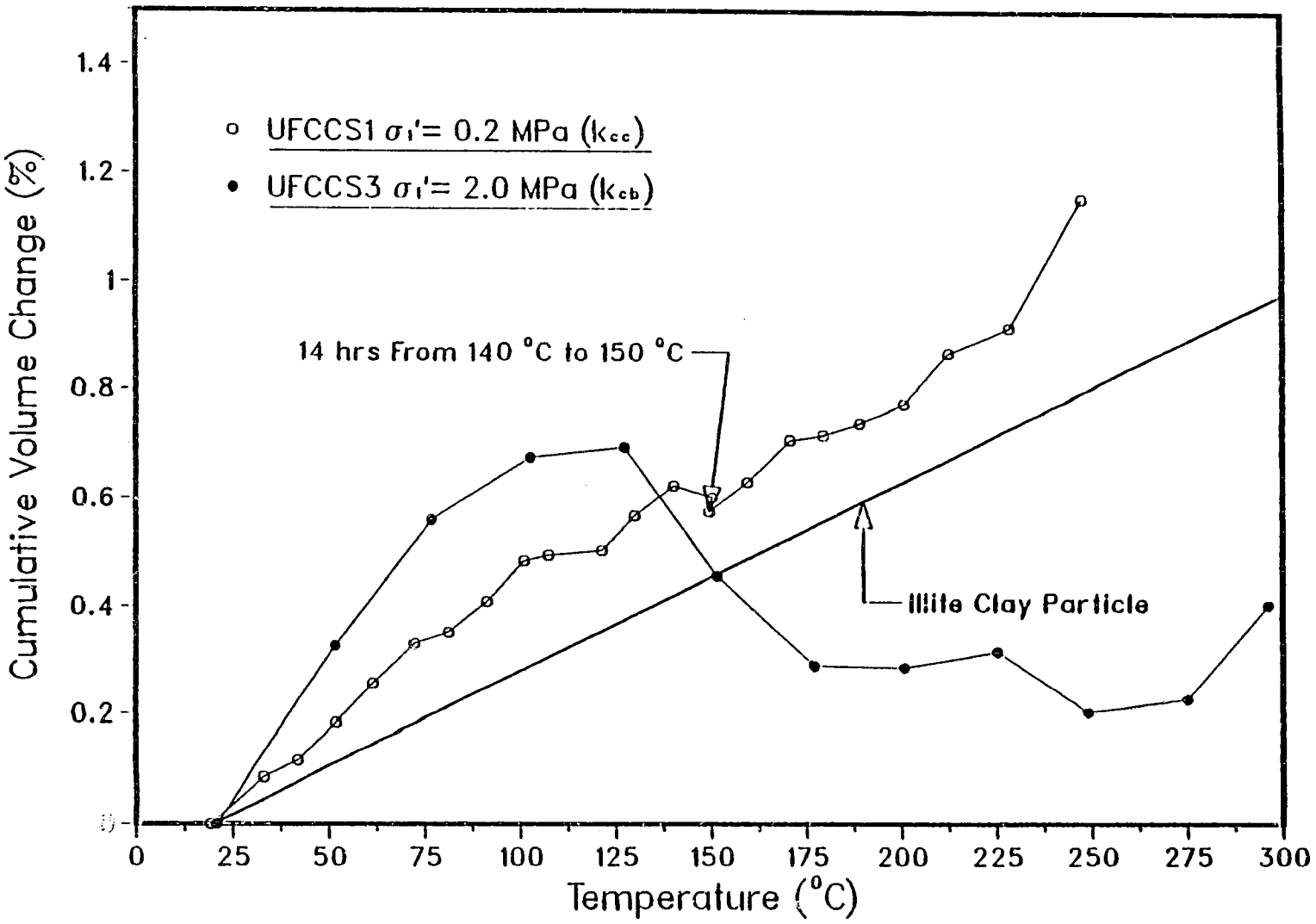

Figure 5.6 Drained Thermal Volume Change of Medium Plastic UTF Clearwater Shale

test. In contrast, the specimen tested at 2.0 MPa displays a cumulative volume increase to 125°C followed by a volume decrease which levels off at about 175°C.

Structural changes in the shale skeleton during drained heating is dependent on interparticle forces, frictional resistance and cohesion. The short term drained thermal volume change tests shown in Figure 5.6 suggest that structural changes are also dependent on the history of stress experienced by the specimen prior to heating. The specimen tested at 0.2 MPa effective confining stress was heated at a rate 2.5 times slower than the specimen at 2.0 MPa and displayed an overall cumulative volume increase to 250°C. At 150°C this specimen displays a very small volume decrease after 14 hours, whereas the specimen consolidated to 2.0 MPa prior to heating shows a significant volume decrease at that temperature. The step-like nature of the thermal expansion curve of the 0.2 MPa specimen suggests that small structural changes are occurring throughout the test.

The specimen consolidated to 2.0 MPa develops higher induced shear stresses as a result of lateral constraint in the oedometer. As the specimen is heated, additional thermally induced shear stresses develop and this, combined with a reduction in attractive forces between particles, results in the need for the structure to densify until enough bonds form to allow the shale structure to carry the 2.0 MPa effective stress. For the specimen consolidated to

0.2 MPa, the induced mechanical and thermal shear stresses are smaller and only minor structural changes are required for the matrix to carry the 0.2 MPa effective confining stress. As a result, the thermal expansion curve is "stepped" as shown in Figure 5.6.

High Plastic Shale

A long term thermal volume change test at 2.0 MPa effective confining stress carried out on high plastic k_{cb} shale is shown in Figure 5.7. Long term conditions for a particular temperature level were only reached when the thermal volume change had ceased. This condition is shown on the plot at intervals of 50°C. The time required to attain steady state conditions ranged from 4 to 20 hours.

During long term heating the high plastic k_{cb} shale shows negligible volume change to 50°C whereupon it decreases to 100°C and remains somewhat constant thereafter at a net volume decrease of 0.3%. For comparative purposes, the test performed on medium plastic k_{cb} shale at 2.0 MPa effective confining stress measured at 1 hour heating increments of 25°C (a short term test) is also shown. During short term heating the medium plastic shale shows a volume increase of about 0.7% to 125°C and decreases to 175°C and remains essentially constant thereafter at a net volume increase of 0.3%.

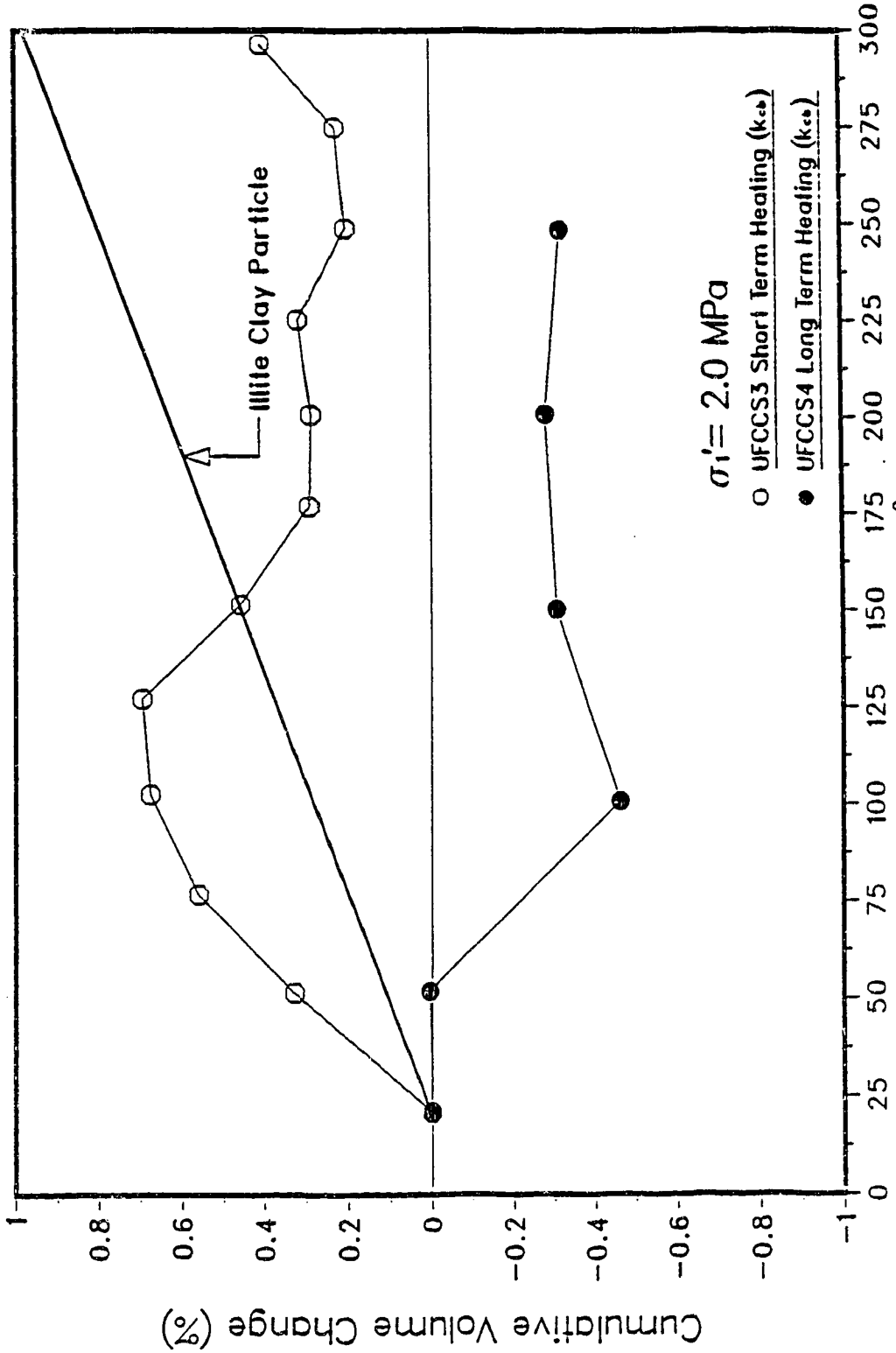

Figure 5.7 Time Dependent Drained Thermal Volume Change of UTF Shale

Comparison of Geotechnical Facies

Laboratory results demonstrate that the effect of temperature on the drained thermal volume change of Clearwater shale depends on stress history, rate of heating and the magnitude of the temperature increase. Structural collapse of shale is inhibited by the time dependent slippage or rupture of bonds caused by a reduction in attractive forces at higher temperatures and by localized zones of non-dissipated pore fluid pressure. The data obtained from thermal volume change tests carried out on two geotechnical shale facies from the Athabasca Clearwater Formation suggest:

1. The interparticle bonding of high plastic smectite-rich k_{cb} shale is initially relatively weak when compared to medium plastic k_{cb} and k_{cc} shale. Slow prolonged drained heating at 2 MPa effective confining stress (in situ conditions) may, therefore, represent an upper bound of thermally induced permanent volume decrease.

2. Rapid heating of medium plastic k_{cb} shale at 2 MPa effective confining stress may reflect a lower bound of structural deformation in situ stress condition

resulting in a net volume increase even though long term heating may cause a net volume reduction.

3. Drained heating of medium plastic k_{cc} shale at low effective confining stress may represent the maximum overall volume increase. Under low effective confining stresses the thermal volume change of the overconsolidated shale is relatively insensitive to the rate of heating as demonstrated in Figure 5.6.

5.2.3 Devonian Limestone

Drained thermal expansion of intact Devonian limestone was measured at an effective confining stress of 2.5 MPa. Volumetric thermal expansion results over the temperature range of 20 to 300°C are shown in Figure 5.8. The specimen was heated at a rate of 25°C per hour.

The cumulative volume increase is essentially linear to 300°C. The volumetric coefficient of thermal expansion of this limestone is approximately 3.9×10^{-5} °C^{-1}. The cumulative volume increase at 300°C was about 1.1%.

The thermal volume change test carried out on crystalline limestone generates volume increases of the mineral solids only, provided the cementation between grains remains intact during heating. No visual signs of specimen deterioration were observed after the test and the specimen did not display a volume change after cooling to 20°C.

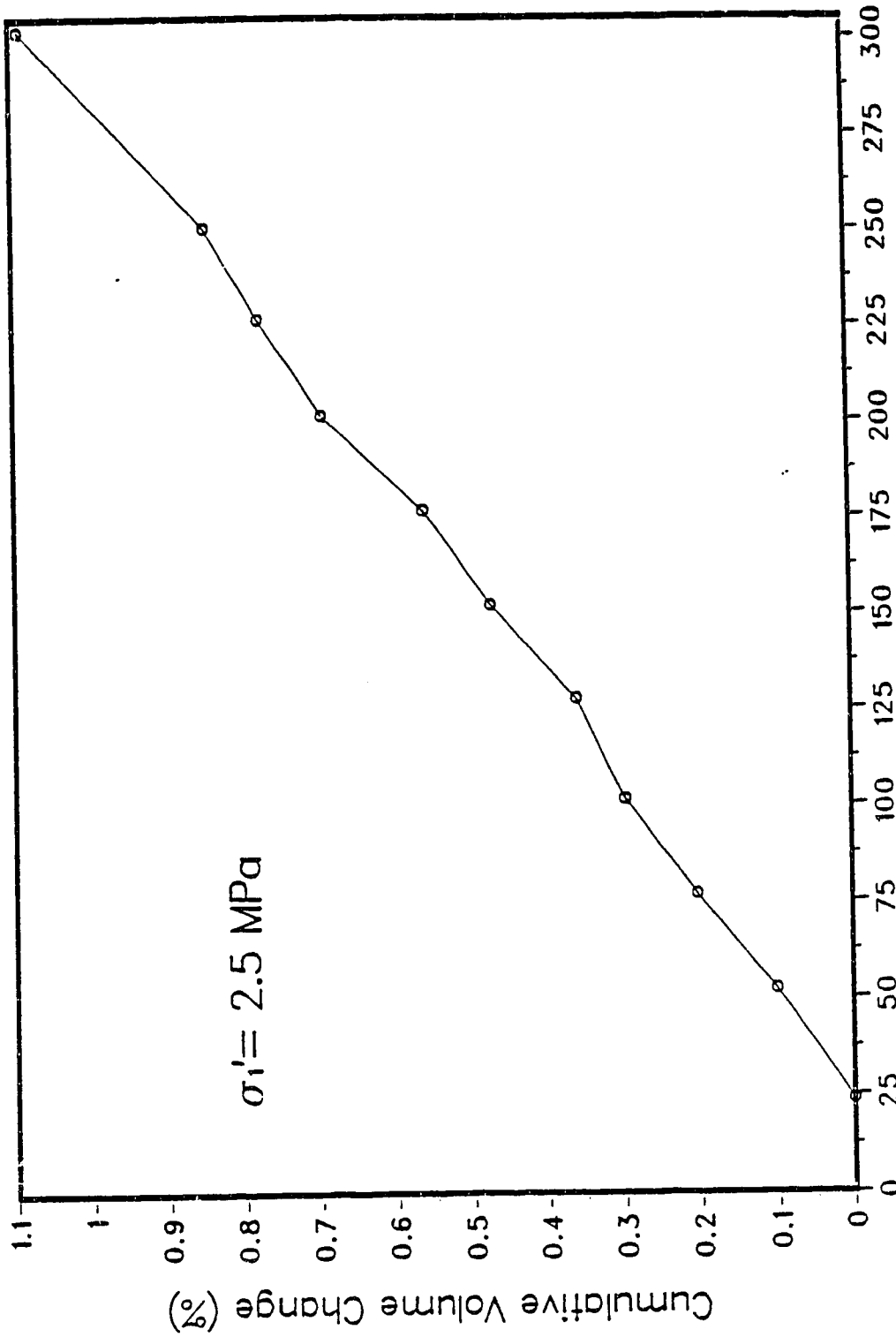

Figure 5.8 Drained Thermal Expansion of UTF Devonian Limestone

The results indicate that the cohesion between mineral grains is of sufficient magnitude to resist shear and tensile stresses developed due to heating. The coefficient of thermal expansion of the carbonate mineral grains (about 3.9×10^{-5}) is similar to the mineral grains found in the oil sands and in the Clearwater Formation shale.

5.3 Undrained Thermal Volume Change

Under fully undrained conditions the volume change of a fully saturated soil subjected to increases in temperature occurs from expansion of individual mineral grains and pore liquids. Structural changes in the soil skeleton do not occur during undrained heating provided pore fluid pressure and vertical total confining stress are constant and balanced during heating to prevent mechanically induced volume changes of the soil matrix.

The total volume change of a soil mass subjected to a change in temperature under completely undrained conditions (zero effective confining stress) is:

$$(\Delta V_m)_{\Delta T} = \alpha_w V_w \Delta T + \alpha_b V_b \Delta T + \alpha_s V_s \Delta T \qquad (5.9)$$

Undrained free expansion tests were performed under a constant pore fluid pressure. The pore fluid pressure was held constant during the test by heating slowly (usually 25°C/hour or less) and through manipulation of the applied

load to the piston in order to compensate for piston friction. After each application of heat, sufficient time was permitted to establish steady state conditions; that is, the temperature readings had stabilized and the thermal volume change ceased.

Oil Sands

The amount of thermal expansion depends on the proportion of mineral solid to pore liquid. A thermal volume increase of about 16% for shale interbedded oil sands can be expected during undrained heating to 300°C as shown in Figure 5.9.

The incremental coefficient of thermal expansion of liquid water varies from 2×10^{-4} °C^{-1} at 20°C to 1×10^{-3} °C^{-1} at 200°C and does not vary significantly with pore pressures up to 10 MPa. Kosar (1983) found Athabasca bitumen expanded slightly more than water. As shown previously, incremental coefficient of clay particles is not significantly different from the quartz sand grains, approximately 4×10^{-5} °C^{-1}. The undrained thermal volume change of oil sands is, therefore, not significantly affected by the presence of shale interbedding provided that the proportion of mineral solid to pore liquid does not vary significantly.

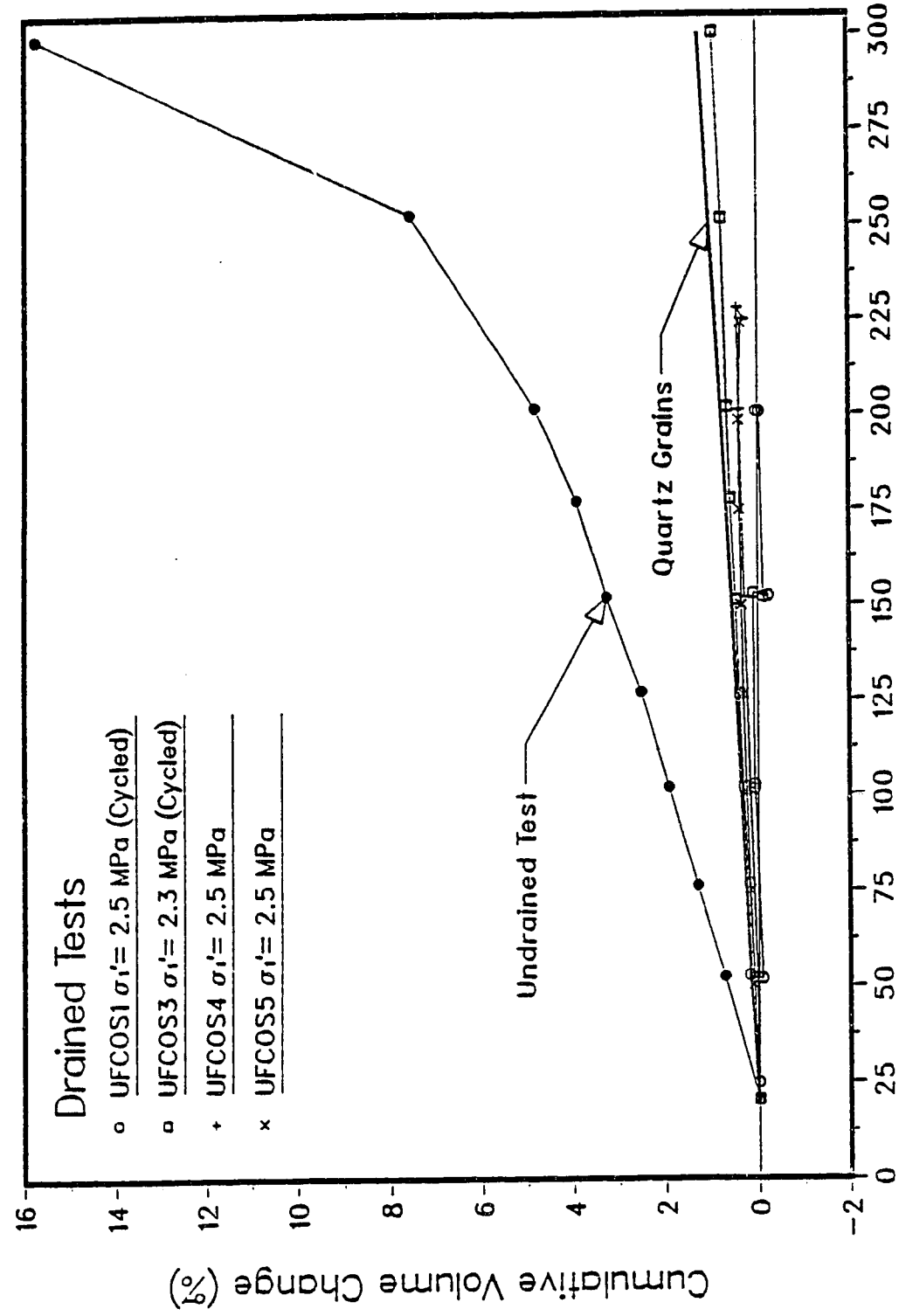

Figure 5.9 Undrained Thermal Expansion of UTF Oil Sands

Clearwater Shale

The results of a completely undrained thermal expansion test performed on smectite-rich k_{cb} shale are shown in Figure 5.10. The undrained thermal expansion test shows a volume increase of about 9% over the temperature range of 20 to 250°C. Also shown on the plot are the drained thermal volume change test results and the estimated curve for the illite clay particles.

Since the thermal volume change of water is well established over a range of pressures in the literature and the water content and volume of the specimen were measured prior to testing, it was possible to back calculate the thermal expansion behaviour of the clay particles. The back calculated thermal volume change of the mineral solids are also shown in Figure 5.10. The thermal expansion of clay particles determined from the undrained test is slightly larger than the estimated value for illite.

Assuming that the mineral grain expansion of illite, smectite, koalinite and chlorite (principal minerals in Clearwater shale) are similar, none of the shale specimens tested show a structural volume increase during heating. All of the drained thermal volume change results plot below the mineral grain expansion back calculated from the undrained test (Figure 5.10).

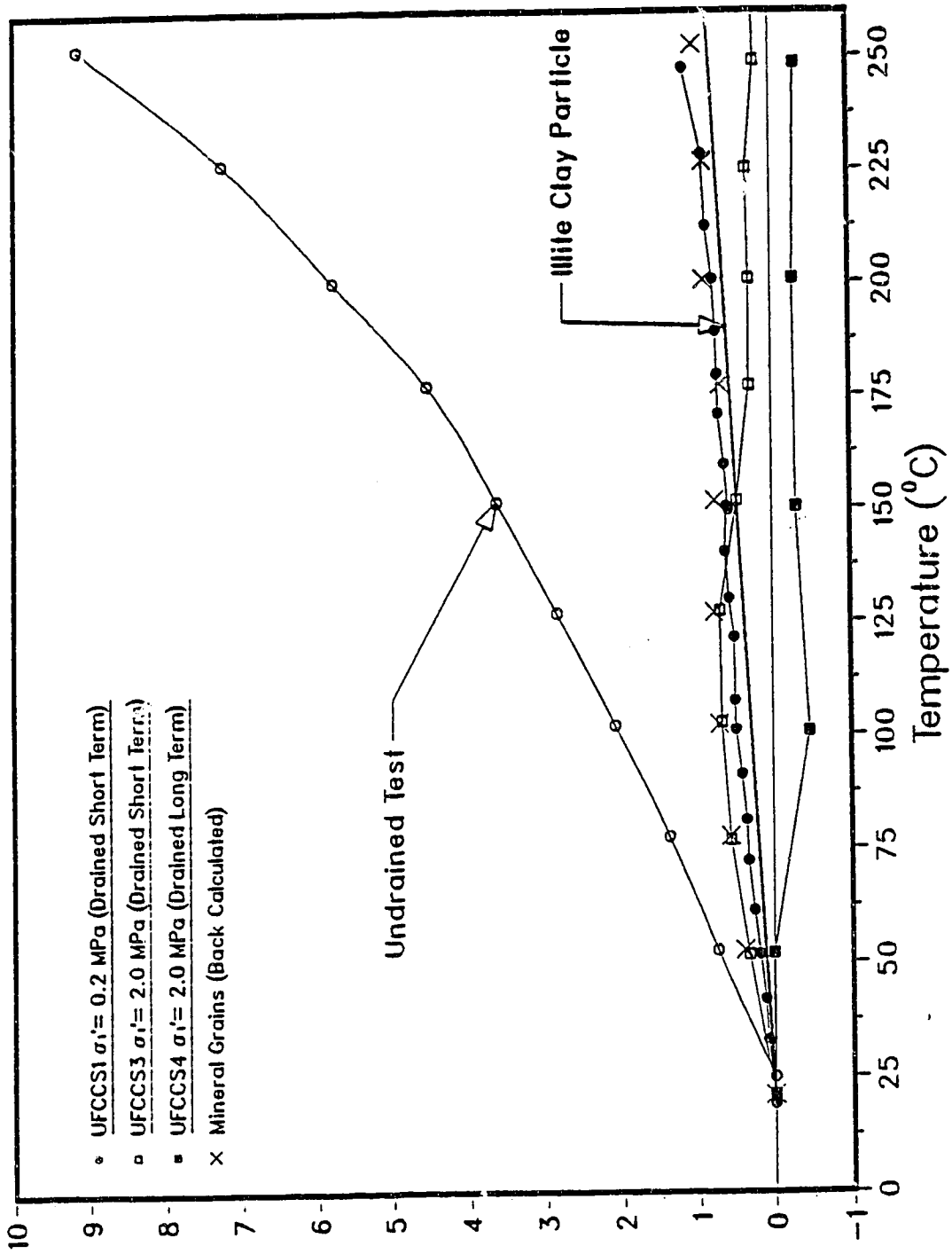

Figure 5.10 Undrained Thermal Volume Change of UTF Smectite Rich Shale

5.4 Summary and Conclusions

The thermal volume change of several geotechnical facies comprising the Athabasca Deposit which may be subject to direct or peripheral heating were studied. The mechanisms contributing to the constitutive behaviour of each horizon have been identified and documented.

Numerical methods used to calculate thermally induced ground deformations and stress changes during in situ production require as input the coefficient of thermal expansion. The coefficient of thermal expansion is maximum during undrained heating where volume change of the mineral solids and pore liquids occurs. The coefficient of thermal expansion is least during fully drained heating when the pore liquids drain as they expand. Volume change is due to expansion of the mineral grains and expansion or contraction of the soil structure.

Structural changes during drained heating have an important role in the thermal volume change behaviour of shale and interbedded oil sands. Structural changes are dependent primarily on the frictional resistance and cohesion of the individual interparticle contacts and the magnitude of thermally induced interparticle forces. These components are, in turn, dependent on the rate of heating, effective confining stresses and the history of stress experienced by the material. In other words, structural changes are stress and temperature path dependent.

During undrained heating against the confining stress, thermal strains, $\alpha\Delta T$, and compressive stresses required to suppress thermal strains, $\alpha E\Delta T$, are maximum. During in situ production, as flow takes place partial drainage occurs and eventually the fully drained condition may be attained. During the transition from undrained to drained conditions, the influence of pore liquids on the coefficient of thermal volume change decreases and the effects of structural changes increase. The coefficient also develops a stress and temperature path dependency.

Thermal stresses and strains during undrained heating of interbedded oil sands and shale always increase in situ due to thermal expansion of the mineral grains. The impact mineral grain expansion has on the in situ stress and strain field, however, is overshadowed by the response of the pore fluids during undrained heating. When the pore fluids can expand the thermal stresses and strains are much larger because the thermal expansion coefficient of the pore fluids is large compared to that of the mineral solids. If the pore fluids cannot expand the pore fluid pressure increases and will result in decreasing the vertical and horizontal effective stresses. This effect is also comparatively large since the pore fluids expand more rapidly than the solids.

Thermal stresses and strains during drained heating of rich Athabasca oil sands always increase in situ because the coefficient of thermal expansion is positive (Agar, 1984; Kosar, 1983). Drained heating of interbedded oil sands and

shale may cause an increase or decrease in stresses and strains depending on the in situ effective stress field and the rate of heating due to the time and pressure dependent thermal consolidation characteristics of the shale.

6. COMPRESSIBILITY OF ATHABASCA MATERIALS

6.1 Materials Studied

During in situ thermal recovery, volume changes accompanying changes in stress, pore fluid pressure and temperature are governed by the physiochemical characteristics of the soil matrix. The compressibility of a soil mass depends on such factors as the frictional resistance between soil particles, interparticle bonding, particle strength, void ratio and the size, shape and gradation of the mineral particles. Changes in volume of the soil structure can cause changes in strength and deformation properties and changes in porosity-dependent permeability. Compressibility is also a necessary parameter for assessing pore fluid pressure changes which may result from changes in stress or temperature under fully undrained or partially drained conditions.

The constitutive behaviour of materials from three different sites in the Athabasca Deposit were studied. The geotechnical facies examined included:

Underground Test Facility

1. Clearwater k_{cc} Shale. A high plastic shale of very stiff to hard consistency. The depth of the core sample was approximately 106 m. The liquid limit,

plastic limit and water content of the laboratory specimen were 64%, 25% and 15%, respectively. The initial void ratio was 0.43. Its colour varied from dark grey to black.

2. **Clearwater k_{cb} Shale.** A high plastic shale of very stiff consistency. The depth of the core sample was 118 m. The liquid limit, plastic limit and water content of the laboratory specimen were 181%, 140% and 25%, respectively. The initial void ratio was 0.62. Its colour varied from dark grey to black with frequent brownish smectite-rich bands. The bands were essentially horizontal with thicknesses ranging from 1 mm to several mm.

3. **McMurray Oil Sands.** A fine to medium grained, lean oil sands. Brownish-grey to black in colour. Pockets and lenses of silty shale were encountered randomly throughout the specimens. Shale interbedding ranged from 1 mm to several mm. Fines contents ranged from 36 to 72% by weight. Bitumen contents ranged from 4 to 9.5% by weight.

4. **Waterways Limestone.** A microcrystalline limestone. The specimen was uniform and massive. Its colour varied from light to medium grey.

Southern Athabasca

1. **McMurray Oil Sands.** A medium grained, uniformly graded, rich oil sands. Dark grey to black in colour. Bitumen content of about 15% by weight. A fines content of approximately 5% by weight. The depth of the core sample was about 295 m.

Northern Athabasca

1. **Clearwater Oil Sands.** A medium grained, medium rich oil sands. Dark grey to black in colour. Bitumen content of about 12% by weight and a fines content ranging from 5 to 21%. The depth of the core sample was about 220 m.

Athabasca oil sands materials considered in this study were formed under three different depositional environments.

South Athabasca McMurray Formation oil sands consist of a uniformly graded, low fines quartz sand (Table 6.1) which is indicative of a moderately strong and prolonged depositing current. These sands are similar in mineralogy and fabric to estuarine channel, mid-channel and point bar sands encountered over much of the area occupied by the Underground Test Facility (AOSTRA, 1986), surface mining projects (Mattison, 1987) and portions of the Saline Creek valley. These sands form the main reservoir unit in the Athabasca Deposit and are the most commonly studied geotechnical facies.

Clearwater Formation (Wabiskaw Member) sands obtained from North Athabasca were deposited in a shallow-water marine environment. These sands, although similar in appearance to the bitumen rich, low fines estuarine sands of the McMurray Formation, are less uniformly graded with fines contents up to 21% by weight and slightly lower bitumen contents (Table 6.1). This glauconitic sand is considered as a separate geotechnical facies in this study.

Shaley oil sands obtained from Borehole AO-27 at the Underground Test Facility are indicative of esturarine channel margin sedimentation. Although these sands contain from 36% to 72% shale in the form of discontinuous seams and clasts, on a macroscopic scale are considered in this study to be of sufficient homogeneity to be classed as one geotechnical facies.

Table 6.1 Isotropic Compressibility of Athabasca Oil Sands

Initial Conditions

Test Number	Bulk Density (Mg/m3)	Dry Density (Mg/m3)	% water (mass)	% bitumen (mass)	% solids (mass)	% fines (<0.074 mm)	Void Ratio e	Sr (%)	Index of Disturbance (%)
AMTOS1	1.85	1.52	2.6	14.9	82.5	5.6	0.74	76	18
AMTOS2	1.87	1.54	2.3	15.5	82.2	5.4	0.72	79	15
AMTOS3	1.89	1.54	3.3	15.5	81.2	9.2	0.73	85	11
ACTOS1	1.90	1.58	5.4	11.4	83.2	21.0	0.67	79	15
ACTOS2	1.91	1.58	5.0	12.0	83.0	18.0	0.67	80	15
ACTOS3	1.77	1.44	6.7	11.9	81.4	5.0	0.84	72	21
ACTOS4	1.86	1.53	6.6	11.5	81.9	20.0	0.74	80	15

Isotropic Compressibility

McMurray Formation Oil Sands			
Test Number	Average Effective Stress Range (MPa)	Bulk Modulus K (MPa)	
		Initial Loading	After Cycling
AMTOS1	3.4 - 6.3	180	600
AMTOS2	2.2 - 5.0	217	540
AMTOS3	5.1 - 9.0	259	750

Clearwater Formation Oil Sands			
Test Number	Average Effective Stress Range	Bulk Modulus K (MPa)	
		Initial Loading	After Cycling
ACTOS1	2.4 - 7.3	217	630
ACTOS2	5.0 - 8.9	509	1058
ACTOS3	1.1 - 4.7	146	478
ACTOS4	1.0 - 5.0	179	425

6.2 Methods and Procedures

The compressibility of a soil mass is normally measured either by isotropic compression in the triaxial cell or by confined compression in the oedometer. In principle, the compressibility of a soil mass can be determined experimentally in several ways by manipulating the principal effective stresses during the test. In cases where the field stress path can be identified, the compressibility parameters should be measured using the effective stresses and stress paths that have or will occur in the actual soil mass. Volumetric changes in the mineral structure associated with deviatoric stress changes are discussed separately in subsequent chapters.

During isotropic and confined compression, volume change is accommodated through sliding between mineral grains and deforming or crushing of individual particles. These mechanisms result in the development of shear forces at individual particle contacts. During isotropic compression these interparticle forces tend to balance out under the "all-around" confining stress. In contrast, during confined compression, because particle movement is limited primarily to one direction due to the lateral constraint, interparticle shear forces acting on surfaces common to contact points are anisotropic and therefore a net shear stress develops.

In the confined compression test the specimen experiences both shear strain and volume change, whereas

during isotropic compression the specimen does not undergo shear straining. As a result, the stress path followed by the specimen in each test is different and a distinction must be made between constrained modulus, D, measured in the oedometer and the bulk modulus, K, measured during isotropic compression in the triaxial cell.

When isotropic compressibility results are plotted in terms of volumetric strain, the inverse slope of the compression curve is the bulk modulus, K, or

$$K = \frac{\Delta\sigma'_o}{\Delta\epsilon_v} \tag{6.1}$$

where σ'_o = the average principal effective stress.

ϵ_v = volumetric strain.

The constrained modulus, D, is the ratio of axial stress to volumetric strain during confined compression, or

$$D = \frac{\Delta\sigma'_v}{\Delta\epsilon_v} \tag{6.2}$$

The isotropic and confined volume compressibility parameters are related through elastic theory as follows:

$$K = \frac{D\ (1 + \nu)}{3\ (1 - \nu)} \tag{6.3}$$

where ν = Poisson's ratio.

and similarly effective stress change between the two types of compressibility tests are

$$\sigma'_o = \frac{\sigma'_v (1 + \nu)}{3 (1 - \nu)} \qquad (6.4)$$

6.3 Oil Sands

McMurray Formation Estuarine Sand

Isotropic compressibility values for bitumen rich, low fines oil sands have been reported to range from 225 to 4000 MPa (Au, 1984). Plewes (1987) conducted cyclic compressibility tests on oil sands over a range of stress of 2 to 4 MPa and measured volume compressibility values of between 425 and 1140 MPa. Similar tests performed by Dusseault (1981) over a range of stress of 2.8 to 13.3 MPa and Agar (1984) over a range of 4.0 to 25.0 MPa resulted in bulk modulus values between 1250 and 4000 MPa.

Results of isotropic compressibility tests carried out on McMurray Formation oil sands from the southern portion of the Athabasca Deposit (test series AMTOS) are summarized in

Table 6.1. Details of the individual tests are included in Appendix D.

Oil sands specimens were subjected to up to three loading and unloading cycles. The compressibility of this oil sands is high upon initial loading but converges to a lower constant value after a loading and unloading cycle. These results indicate that the vast majority of the sand matrix recompaction is achieved during initial loading. This high initial compressibility (low bulk modulus) reflects the amount of sample disturbance during coring. Initial index of disturbance values for this oil sands range from 11 to 18% (Table 6.1). Repeatability of cycling results suggests that the oil sands are behaving in an elastic manner during stress cycling. It is, therefore, unlikely any appreciable amount of particle degradation is occurring. Bulk modulus values during stress cycling were found to range between 540 and 750 MPa over the effective confining stress range of 2 to 9 MPa.

The bulk modulus of McMurray Formation oil sands is dependent on the effective confining stress range over which the parameter is measured. For example, Plewes (1987) and Agar (1984) report volume compressibilities of 400 to 2700 MPa cycled at about 5 MPa effective confining stress. The initial bulk densities of these oil sands specimens were generally greater than 2.0 Mg/m^3 and index of disturbance values less than 10%. Differences in compressibility were attributed to disturbance of the sand structure during

coring and sample preparation. In general, a cyclic stress compressibility test performed on good quality, undisturbed oil sands specimens should provide a good indication of the in situ compressibility. The oil sands tested in this study were taken from a depth of 295 m using a triple tube core barrel and suffered significant sample disturbance. Initial bulk densities were less than 1.90 Mg/m^3 and index of disturbance values were as large as 18%. The bulk modulus of this oil sands was found to be in the lower range of values measured by Agar and Plewes.

Clearwater Formation Shefal Sands

The isotropic compressibility of Clearwater Formation (Wabiskaw Member) oil sands (test series ACTOS) obtained from the Northern part of the Athabasca Deposit is summarized in Table 6.1. Stress-volume change plots are included in Appendix D. Specimens were obtained from a core sample to a depth of 220 m and experienced a high amount of sample disturbance. The indices of disturbance of these specimens ranged from 15 to 21% with initial bulk densities of 1.91 mg/m^3 or less (Table 6.1).

The isotropic compressibility of Clearwater Formation oil sands is comparable to the McMurray Formation oil sands examined in this research program (Figure 6.1). The effect of differences in geological environment of deposition and

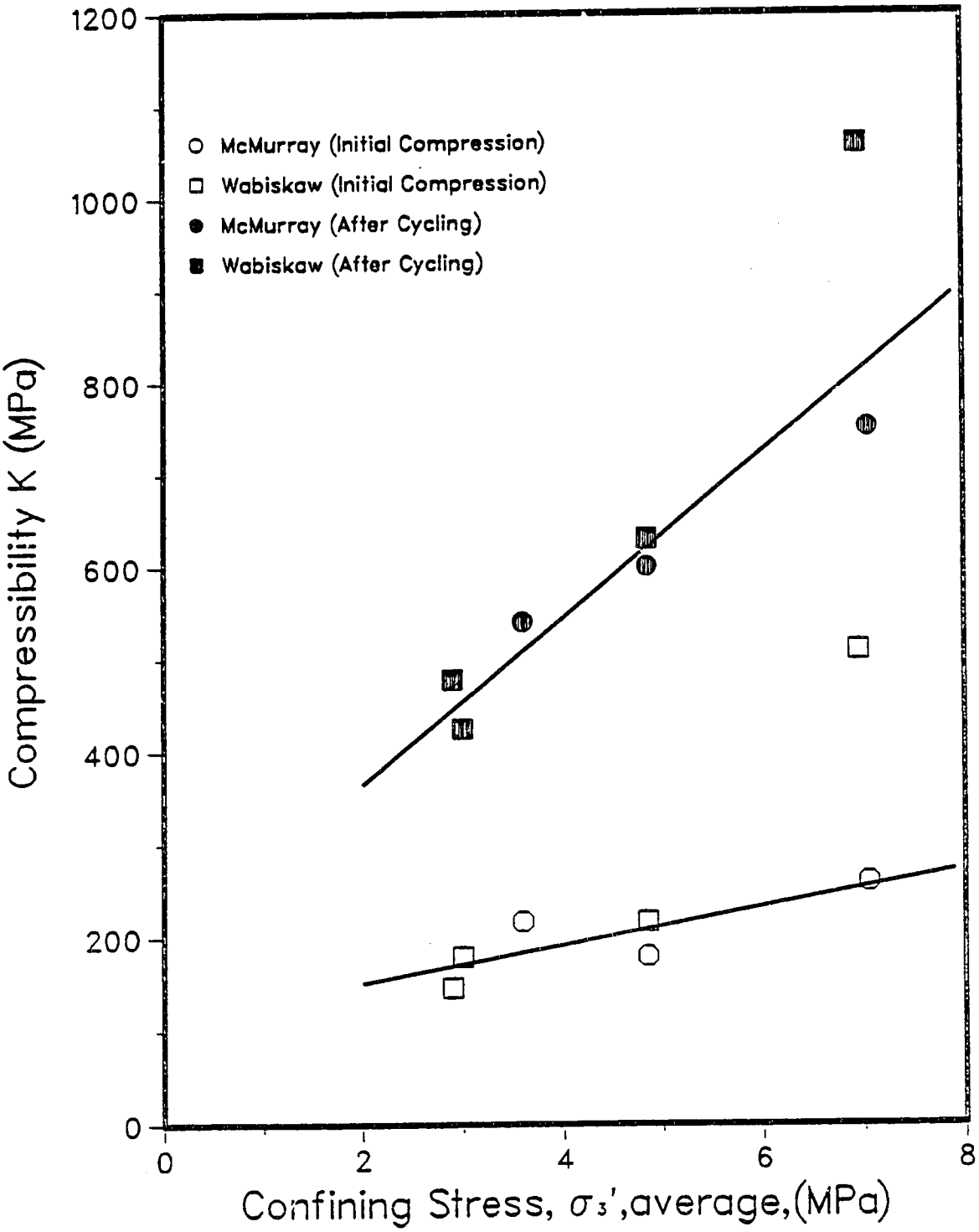

Figure 6.1 Isotropic Compressibility of Athabasca Oil Sands

geological history on the compressibility of these two oil sands may be overshadowed by the high degree of sample disturbance experienced by the samples during the conventional coring process.

McMurray Formation Estuarine Channel Margin Sedimenation

The one-dimensional compressibility of oil sands containing thin, discontinuous shale seams obtained from core samples taken at the AOSTRA Underground Test Facility (test series UFCOS) are summarized in Table 6.2. Individual stress-volume change plots are given in Appendix D.

Up to three cycles of loading and unloading were applied to oil sands specimens. A typical specimen experiencing two cycles of stress at 20°C is shown in Figure 6.2. The constrained modulus is low upon initial loading but converges to higher values after a loading and unloading cycle. This high initial compressibility and large amount of non-recoverable strain reflects the amount of sample disturbance during coring. A relatively small amount of permanent strain results from each cycle of stress after initial compression (that is, a relatively stable hysteresis loop is formed). The constrained modulus of this oil sands at 20°C was found to be about 1500 kPa.

Two one-dimensional compressibility tests performed at 225°C are also summarized in Table 6.2. The constrained

Table 6.2 One Dimensional Compressiblity of Athabasca McMurray Formation Oil Sands (Interbedded Specimens)

Initial Conditions

Test Number	Bulk Density (Mg/m3)	Dry Density (Mg/m3)	% water (mass)	% bitumen (mass)	% solids (mass)	% fines (<0.074 mm)	Void Ratio e	Sr (%)	Index of Disturbance (%)
UFCOS1	1.97	1.70	9.4	4.3	86.3	47.5	0.56	75	21
UFCOS2	1.91	1.65	9.4	4.3	86.3	47.5	0.61	69	27
UFCOS3	1.90	1.64	9.4	4.3	86.3	47.5	0.62	68	29
UFCOS4	1.99	1.76	6.9	4.9	88.2	44.8	0.51	70	29
UFCOS5	1.99	1.72	5.3	8.3	86.4	51.8	0.54	77	19

One Dimensional Compressibility

Test Number	Temp. (°C)	Measured							Calculated (assuming Poisson's ratio = 0.3)						
		Vertical Effective Stress Range (MPa)	Constrained Modulus D (MPa)						Average Principal Effective Stress Range (MPa)	Bulk Modulus K (MPa)					
			First Cycle		Second Cycle		Third Cycle			First Cycle		Second Cycle		Third Cycle	
			Load	Unload	Load	Unload	Load	Unload		Load	Unload	Load	Unload	Load	Unload
UFCOS1	20	1.6 - 3.3	306	813	693	960	933		1.0 - 2.0		503	429	594	578	
UFCOS2	20	2.0 - 3.9	491	1084	941	1255			1.2 - 2.4		617	583	777		
UFCOS3	20	1.6 - 3.4	517	1498	561	1351			1.0 - 2.1		927	347	836		
UFCOS4	225	2.5 - 5.0	1012	2599	1052	2013	1143		1.5 - 3.1		1609	651	1246	708	
UFCOS5	225	2.0 - 4.6	657	2051	872	1652	1553	1644	1.2 - 2.8		1270	540	1023	961	1018

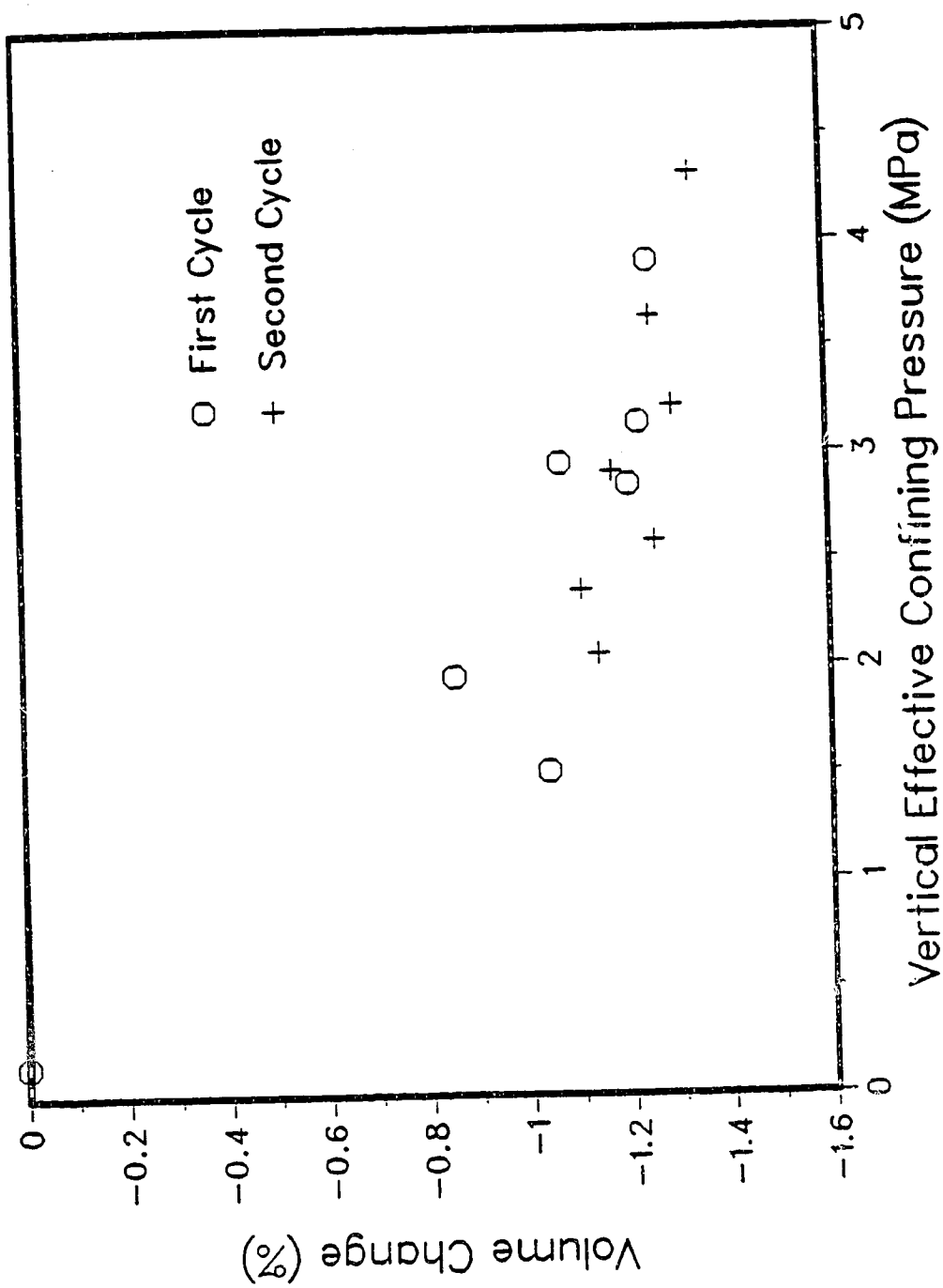

Figure 6.2 One Dimensional Compressibility of Athabasca Interbedded Oil Sands

modulus of these specimens is higher due to a volume reduction experienced during drained heating. The amount of permanent (non-recoverable plastic) strain obtained from each cycle of stress at 225°C is very small or negligible.

There is a significant increase in the cyclic constrained modulus from about 1500 MPa at 20°C to about 2600 MPa at 225°C. This increase in specimen stiffness may be attributed to heat induced consolidation of the oil sands matrix during heating and initial compression at the elevated test temperature. Agar (1984) reports a decrease in cyclic compressibility from 2000 MPa at 20°C to 3300 MPa at elevated temperatures for low fines, rich oil sands. It is noted, however, that these compressibility values were measured over significantly higher effective stresses (up to 19.5 MPa) and cumulative, non-recoverable strain occurred with each cycle of loading and unloading. This behaviour is indicative of particle degradation at high temperatures and pressure. Morgenstern (1981) also illustrated the effect temperature has on the confined compression of quartz sand. The compressibility of quartz sand under an applied pressure of 32 MPa was found to increase significantly with temperature due to grain breakage. Considering the relatively low vertical effective stress (less than 5 MPa) applied to the specimens in this study, and the high proportion of interbedded shale (up to 52% fines by weight) suggests that the decrease in volumetric compressibility at 225°C may be due to heat consolidation of the shale seams

and clasts.

The results of several isotropic compressibility tests (test series UFTOS) carried out at 20°C are summarized in Table 6.3. Stress-volume change plots for individual tests are presented in Appendix D.

A typical triaxial specimen undergoing three cycles of drained isotropic compression is shown in Figure 6.3. As in the case of the one-dimensional tests, non-linear inelastic behaviour is prominent during initial loading while essentially elastic behaviour is observed during stress cycling. It is noted for the particular test shown in Figure 6.3 (cycled over the effective confining stress range of 0.2 to 12 MPa) the stress volume change curve, although essentially elastic, is significantly non-linear.

During initial compression the amount of volume change is larger for isotropic compression than for one-dimensional compression. This is because for a given change in vertical stress, σ, the change in the sum of principal stresses is less during one-dimensional compression than for isotropic compression (Equation 6.4). Further effects of stress path on compressibility are apparent when Tables 6.2 and 6.3 are compared. Conventional elastic theory has been used to compare the results of the isotropic compression stress path and the one-dimensional compression stress path. Bulk and constrained moduli were calculated assuming a constant Poisson's ratio of 0.3. Reasonable agreement is noted between measured and calculated values during cycling of

Table 6.3 Isotropic Compressiblity of Athabasca McMurray Formation Oil Sands (Interbedded Specimens) at 20 °C

Initial Conditions

Test Number	Bulk Density (Mg/m3)	Dry Density (Mg/m3)	% water (mass)	% bitumen (mass)	% solids (mass)	% fines (<0.074 mm)	Void Ratio e	Sr (%)	Index of Disturbance (%)
UFTOS1	1.99	1.67	8.3	7.6	84.1	41.2	0.60	84	12
UFTOS2	2.06	1.77	8.3	5.6	86.1	55.2	0.51	85	12
UFTOS3	2.07	1.76	8.5	6.6	84.9	54.0	0.52	91	6
UFTOS4	2.12	1.84	6.4	6.5	87.1	52.9	0.45	87	10
UFTOS5	2.13	1.86	6.4	6.5	87.1	52.9	0.44	90	7
UFTOS6	1.92	1.59	2.8	14.1	83.0	3.4	0.68	80	14
UFTOS7	1.93	1.58	4.1	14.0	81.9	3.4	0.69	86	10
UFTOS8	2.05	1.75	7.3	7.4	85.3	57.3	0.53	87	10
UFTOS9	1.96	1.64	7.8	8.8	83.4	36.1	0.62	85	11
UFTOS10	2.06	1.77	6.6	7.3	86.1	71.9	0.50	86	11
UFTOS12	1.98	1.65	7.0	9.5	83.4	37.7	0.60	87	10
UFTOS14	1.91	1.56	2.7	15.5	81.8	3.0	0.70	85	11

Isotropic Compressibility

Test Number	Temp. (°C)	Calculated (assuming Poisson's ratio = 0.3)							Measured						
		Vertical Effective Stress Range (MPa)	Constrained Modulus D (MPa)						Average Principal Effective Stress Range (MPa)	Bulk Modulus K (MPa)					
			First Cycle		Second Cycle		Third Cycle			First Cycle		Second Cycle		Third Cycle	
			Load	Unload	Load	Unload	Load	Unload		Load	Unload	Load	Unload	Load	Unload
UFTOS1	20	14.9 - 19.7		2468	997	2203	1258	1323	9.2 - 12.2	644	1528	617	1364	779	819
UFTOS2	20	4.0 - 5.2		1346					2.5 - 3.2	253	833				
UFTOS3	20	5.7 - 9.2		1118	751	1284			3.5 - 5.7	315	692	465	795		
UFTOS4	20														
UFTOS5	20	3.2 - 5.7		829	470	835			2.0 - 3.5	190	513	291	517		
UFTOS6	20	4.8 - 8.2		1179	693				3.0 - 5.1	234	730	429			
UFTOS7	20	4.0 - 7.3		911	502				2.5 - 4.5	131	564	311			
UFTOS8	20	3.2 - 9.7		1003	898				2.0 - 6.0	769	621	556			
UFTOS9	20	2.6 - 7.3		732	594				1.6 - 4.5	190	453	368			
UFTOS10	20	3.2 - 7.3		819	669	1084			2.0 - 4.5	141	507	414	571		
UFTOS12	20	4.0 - 7.3		743	670	1069			2.5 - 4.5	165	460	415	662		
UFTOS14	20	2.4 - 7.3		1076	767	1200			1.5 - 4.5		666	475	743		

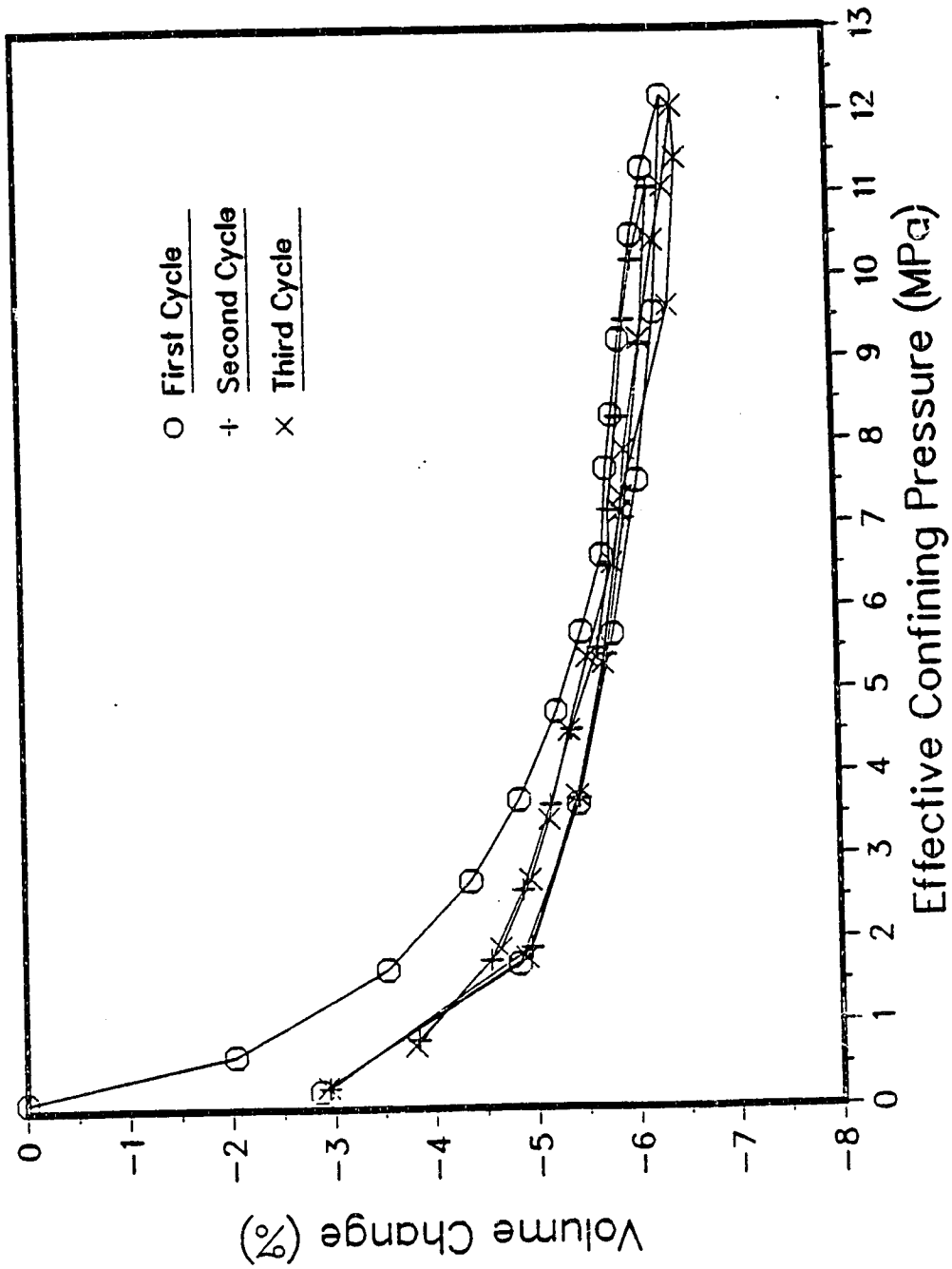

Figure 6.3 Isotropic Compressibility of Athabasca Interbedded Oil Sands

stress. This further supports the view that the oil sands is behaving in an elastic manner over the applied stress range and that grain crushing is not taking place.

A second series of isotropic compression tests (test series UFHTTOS) carried out on oil sands obtained from the Underground Test Facility site are summarized in Table 6.4. Each specimen in the series was subjected to cycles of drained isotropic compression at 20°C followed by slow drained heating to 225°C and further isotropic compression. The bulk moduli at 225°C are greater than those measured at 20°C, again reflecting the soil matrix densification observed during drained heating. It is noted that two of the oil sands specimens in this test series had relatively high bitumen contents (about 14% by weight) and relatively low fines contents (about 5% of the grain size distribution less than 0.074 mm by weight). Several interesting observations concerning the drained strength compression behaviour of oil sands may be derived from these test results:

1. Bulk modulus values for low fines oil sands at 20°C are low when compared to measurements made by other researchers on similar oil sands over the same stress range. Results of isotropic compression tests after drained heating to 225°C, however, are in agreement. This tends to suggest that mechanical recompression of rich oil sands specimens alone is not sufficient to eradicate the effects of sample disturbance when

Table 6.4 Isotropic Compressiblity of Athabasca McMurray Formation Oil Sands (Interbedded Specimens) at 225 °C

Initial Conditions

Test Number	Bulk Density (Mg/m3)	Dry Density (Mg/m3)	% water (mass)	% bitumen (mass)	% solids (mass)	% fines (<0.074 mm)	Void Ratio e	Sr (%)	Index of Disturbance (%)
UFHTTOS1	1.99	1.73	6.2	7.0	86.8	51.3	0.53	75	21
UFHTTOS2	1.96	1.65	0.8	14.8	84.4	5.2	0.60	81	14
UFHTTOS3	1.96	1.62	5.2	12.4	82.4	4.5	0.64	88	8
UFHTTOS4	2.04	1.77	4.5	8.6	86.9	48.4	0.49	81	16
UFHTTOS5	2.06	1.80	7.2	5.2	87.6	56.7	0.47	80	17
UFHTTOS6	2.04	1.75	7.8	6.3	85.9	65.5	0.51	85	12

Isotropic Compressibility

Test Number	Calculated (assuming Poisson's ratio = 0.3)			Measured		
	Vertical Effective Stress Range (MPa)	Constrained Modulus D (MPa)		Average Principal Effective Stress Range (MPa)	Bulk Modulus K (MPa)	
		20 °C	225 °C		20 °C	225 °C
UFHTTOS1	4.0 - 8.1	984	3643	2.5 - 5.0	609	2255
UFHTTOS2	6.5 - 9.7	1779	2612	4.0 - 6.0	1101	1617
UFHTTOS3	1.6 - 8.1	816	3554	1.0 - 5.0	505	2200
UFHTTOS4	4.0 - 7.3	759	2694	2.5 - 4.5	470	1668
UFHTTOS5	6.5 - 10.2	1210	3358	4.0 - 6.3	749	2079
UFHTTOS6	1.6 - 4.0	267	2200	1.0 - 2.5	165	1362

the initial sand structure is moderately disturbed (index of disturbance values slightly greater than 10%). As noted in Chapter 5, partial collapse of the grain structure during drained heating is required in order for a disturbed oil sand to carry the same applied effective confining stress at higher temperatures.

2. Bulk modulus values of oil sands containing at least 50% shale by weight in the form of thin, discontinuous seams and clasts are significantly lower than high quality, undisturbed, rich oil sands at 20°C. The presence of more compressible shale inclusions appears to have a significant influence on the mechanical behaviour of oil sands. Similar results have been reported by Plewes (1987) for isotropic cyclic compressibility tests conducted on interbedded oil sands from the Syncrude Canada oil sands lease. The fines content of these specimens ranged from 13.5 to 15.0% by weight. Plewes reports volume compressibilities as low as 62 MPa on the second load cycle over the stress range of 0.4 to 0.7 MPa.

3. The compressibility of the high fines specimens studied here increases after drained heating. The influence of shale interbedding on the compressibility of oil sands therefore decreases with the amount of heat consolidation experienced by the shale. If enough consolidation of the shale interbedding occurs, the compressibility of the oil sands becomes comparable to rich oil sands. The calculated constrained moduli from the high temperature tests are comparable to the one-dimensional tests over similar stress ranges.

6.4 Clearwater Shale

High Plastic k_{cc} Shale

The results of an isotropic compressibility test performed on high plastic k_{cc} shale from a depth of 106 m are shown in Figure 6.4. The bulk modulus during initial loading is 74 MPa at 2 MPa effective confining stress but increases to 122 MPa during recompression.

If it is assumed that the compressibility of low fines oil sands is approximately 1000 MPa and the characteristics of shale clasts found in oil sands comprising estuarine channel margin sediments are similar to this high plastic

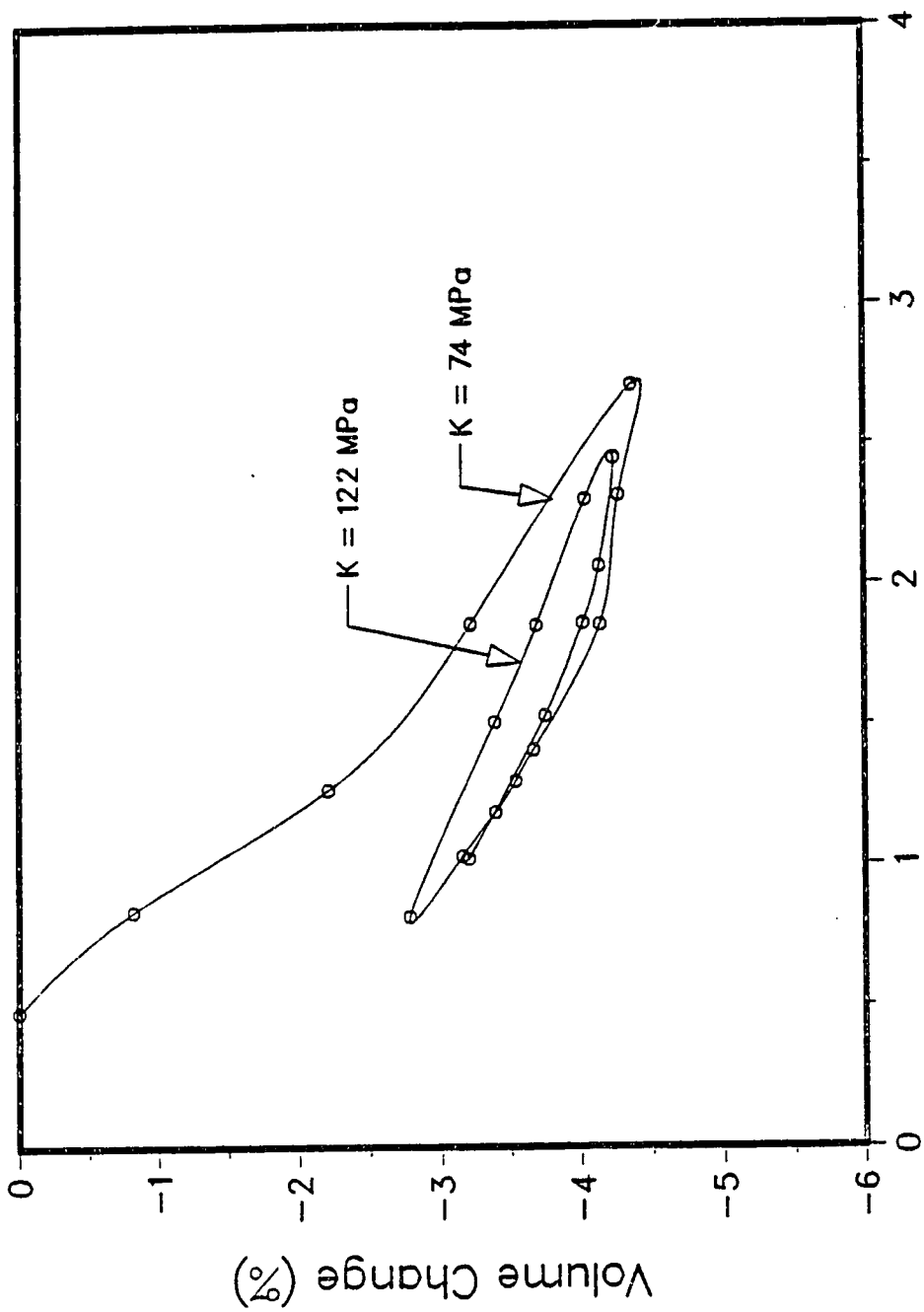

Figure 6.4 Isotropic Compressibility of Athabasca Clearwater Kcc Shale

shale, then the bulk modulus of an oil sands specimen comprised of 50% shale clasts by volume would be about 560 MPa. Measurements of bulk modulus on UTF oil sands containing 36 to 72% shale clasts by weight over a similar effective stress range vary between 415 and 740 MPa (Table 6.3). It may, therefore, be concluded that geological complexity of oil sands in the form of inclusions of more compressible argillaceous material may have a controlling effect on the compressibility characteristics of otherwise high quality oil sands.

High Plastic k_{cb} Shale

The results of a one-dimensional compression test performed on smectite-rich k_{cb} shale at 20°C are shown in Figure 6.5. The constrained modulus is 37 MPa during initial loading and converges to 354 MPa after an unloading and reloading cycle over the vertical effective stress range of 1.7 to 2.0 MPa.

The volumetric compressibility of this high plastic shale due to thermal loading after mechanical consolidation to a vertical effective confining stress of 2.0 MPa (Figure 6.5) under fully drained conditions is shown in Figure 6.6. These results are derived from the long term one-dimensional thermal volume change test (UFCCS4) described in the previous chapter.

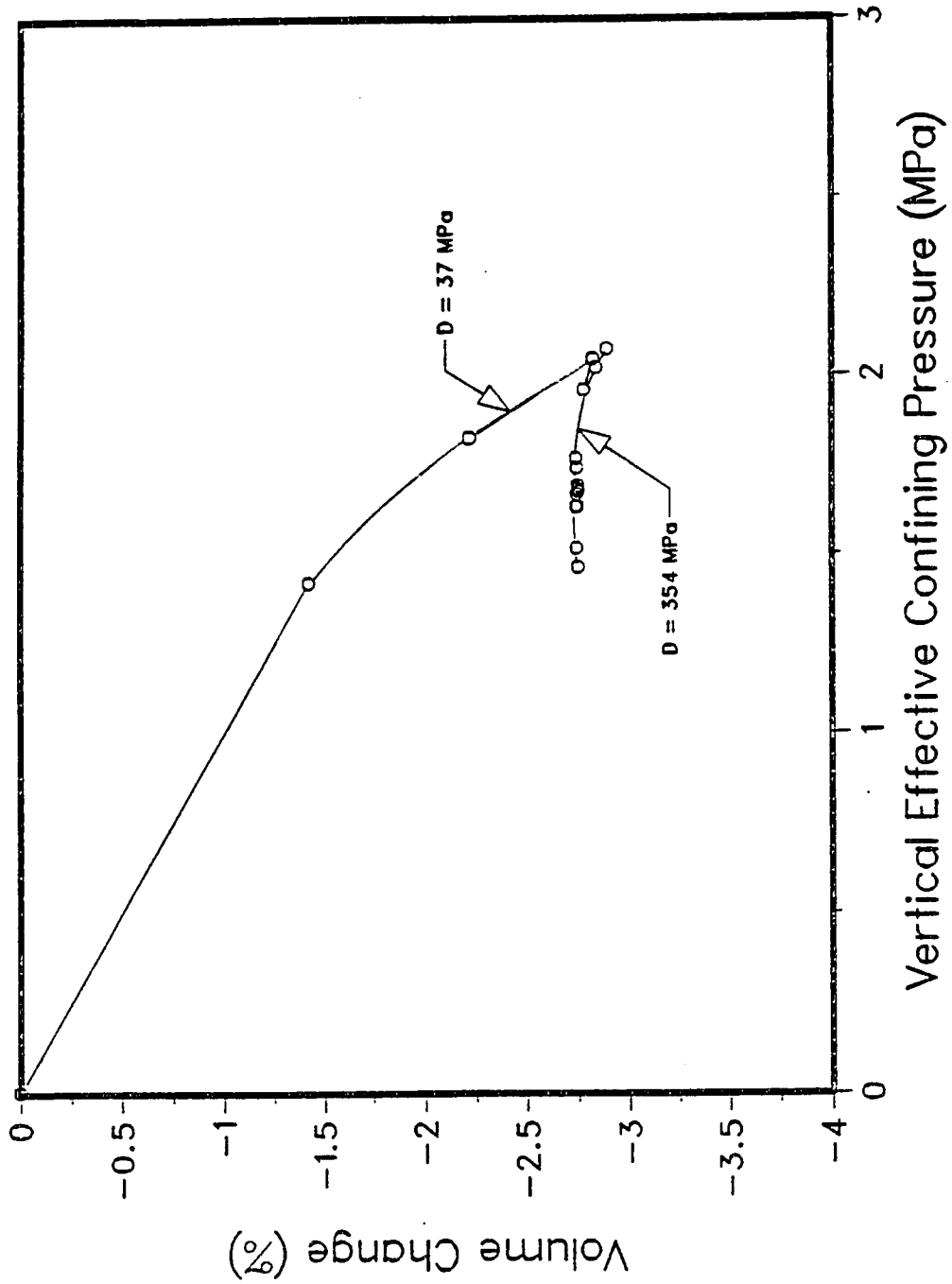

Figure 6.5 One Dimensional Compressibility of Athabasca Clearwater Kcb Shale

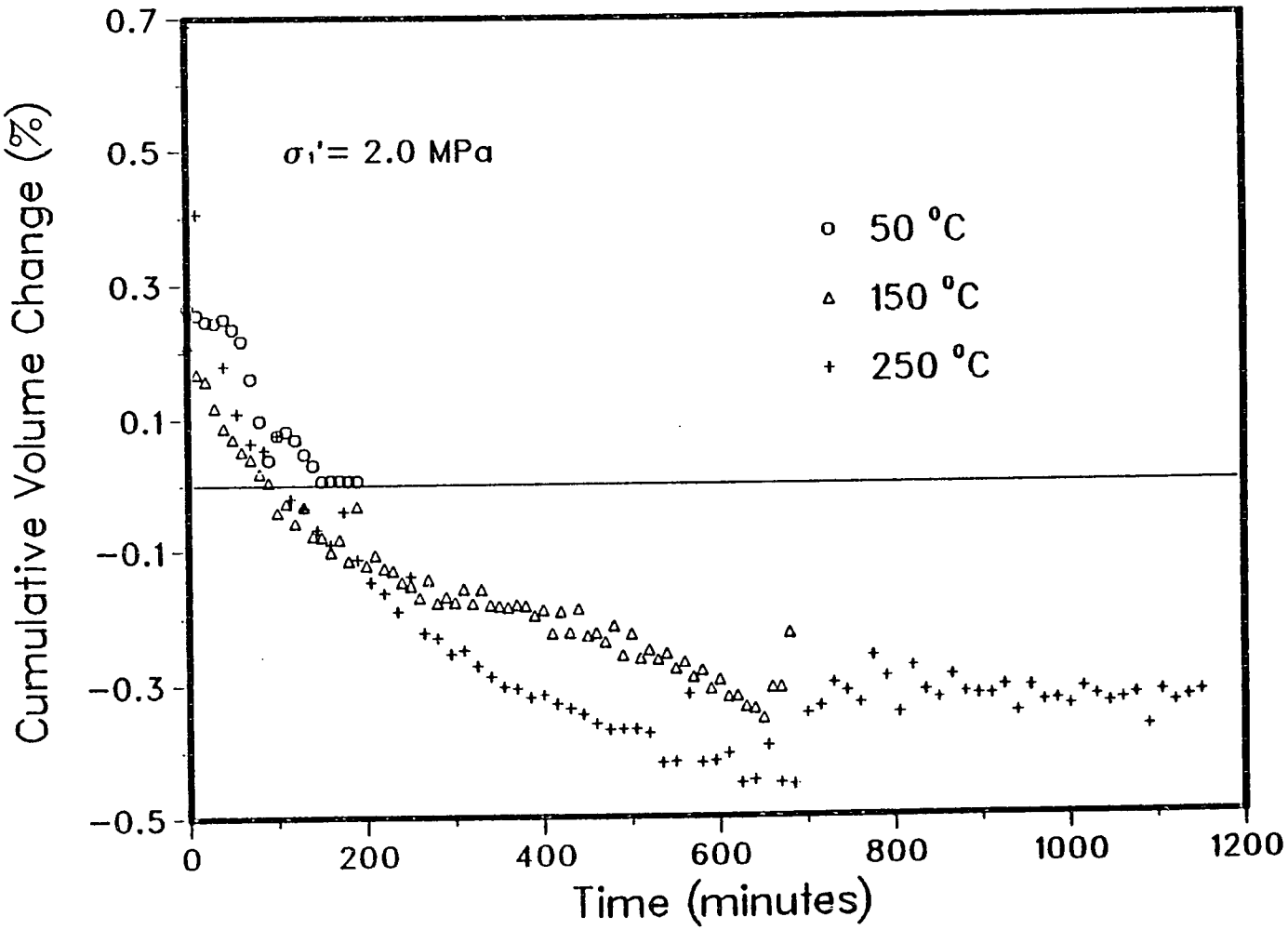

Figure 6.6 Thermal Consolidation of Athabasca Clearwater Kcb Shale

As previously discussed, as the specimen is heated additional thermally induced shear stresses develop at the particle contacts. The development of these shear stresses combined with a reduction in attractive forces between particles results in the structure densifying until enough bonds form to carry the 2.0 MPa effective confining stress. Slippage or rupture of bonds caused by the reduction in attractive forces during temperature loading is a time dependent process. The rate of thermal volume reduction decreases with increasing time as shown in Figure 6.6. For the temperature levels shown in the figure (50°C, 150°C and 250°C), the thermal volume change levels off in approximately 700 minutes or about 12 hours.

Consolidation due to thermal loading is highly dependent on stress history as illustrated in the thermal volume change testing. For this heavily over-consolidated shale, the amount of heat consolidation increases with increasing effective confining stress. For example, the specimen which was heated to 250°C under an effective confining stress of 0.2 MPa (Chapter 5) displays negligible heat consolidation.

6.5 Devonian Limestone

A one-dimensional compressibility test was carried out on intact Devonian limestone obtained from the Underground Test Facility site. The test specimen was taken from a core sample at a depth of 155 m. The test specimen consisted of

relatively competent limestone and was absent of any appreciable amounts of shale interbedding.

The specimen was loaded to 4.0 MPa vertical effective confining stress and subjected to a loading, unloading and reloading cycle over the stress range of 0.5 to 5.0 MPa (Figure 6.7). Non-linear behaviour is evident below 3.0 MPa and pronounced hysteresis is observed. As is common with cemented materials, the strain is recovered at the completion of the loading and unloading loop.

A constrained modulus of 4100 MPa was measured during loading over the stress range of 3.0 to 5.0 MPa. This intact limestone is approximately half as compressible as high quality, rich oil sands and about one-tenth as compressible as Clearwater high plastic k_{cb} shale.

6.6 Summary and Conclusions

The isotropic compressibility of McMurray Formation and Clearwater Formation oil sands obtained from depths of 300 m and 220 m, respectively, was examined. These core samples were obtained using conventional coring techniques and resulted in laboratory specimens which were highly disturbed (i.e., indices of disturbance, I_D, ranging from 11 to 21%). The cyclic compressibility values of these specimens were significantly lower than those reported by Agar (1984) for high quality (I_D less than 10%) oil sands obtained from the Saline Creek surface exposure. The cyclic compressibility values were, however, similar to the lower range of values

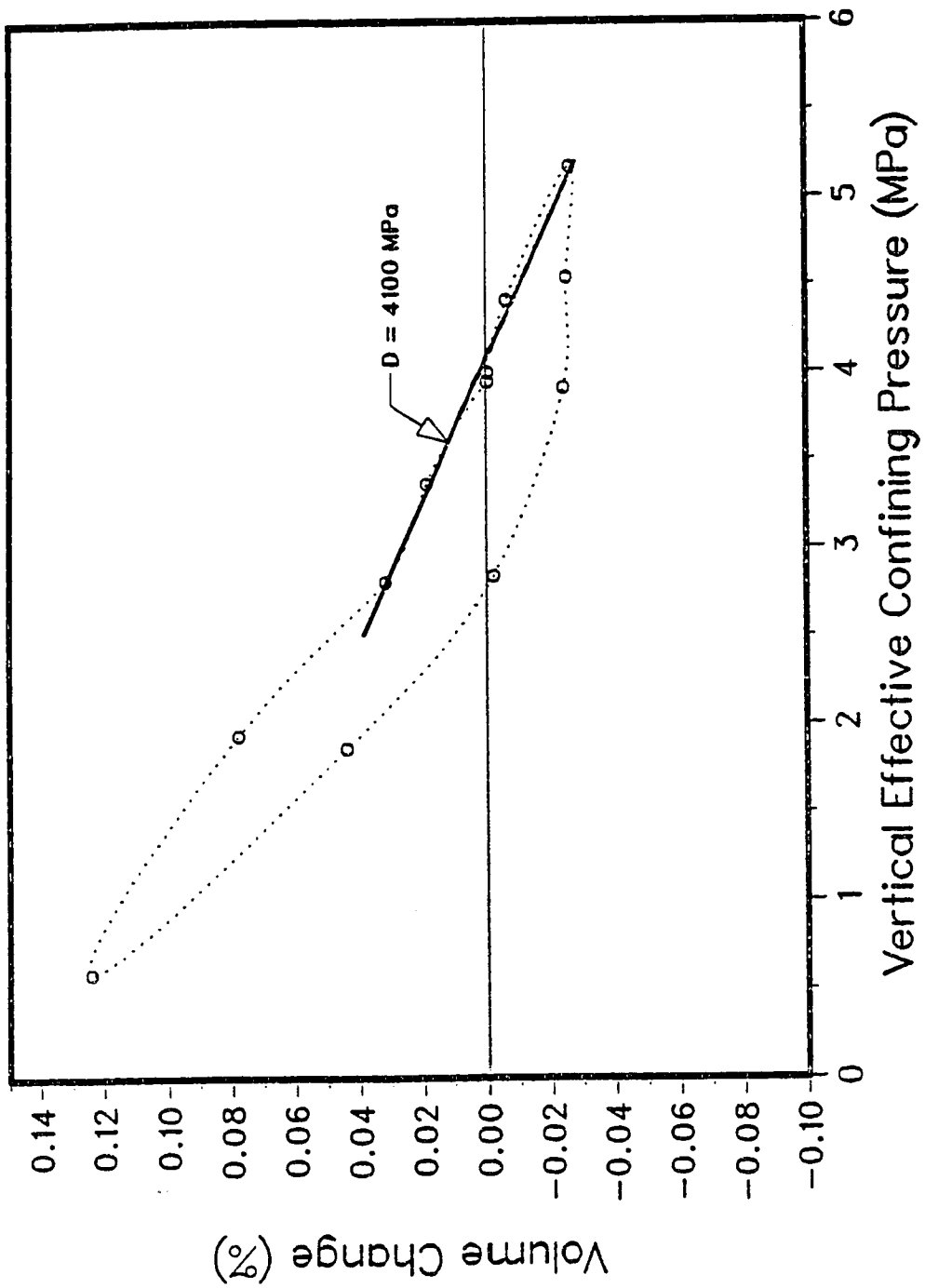

Figure 6.7 One Dimensional Compressibility Athabasca Devonian Limestone

reported by Plewes (1987) for Saline Creek oil sands. The initial indices of disturbance for these specimens ranged from 2.7 to 24% and generally higher compressibility values were associated with the more initially disturbed specimens.

The compressibility of oil sands depends on the physiochemical characteristics of the sand structure such as frictional resistance between sand grains, particle strength, void ratio and the size, shape and gradation of the mineral particles. These factors are, in turn, dependent on the sand grain mineralogy, geological environment of deposition and geological history. The similarity of compressibility results between the McMurray and Clearwater oil sands tested here and between the more disturbed Saline Creek oil sands suggests that excessive sample disturbance (I_D greater than 10%) from coring causes a sufficient amount of microfabric disturbance which is not recoverable during the stress cycling process. While cyclic compressibility tests performed on high quality oil sands specimens provide a good indication of the in situ compressibility, excessive disturbance may reduce the compressibility of oil sands of similar mineralogy and may eradicate the influence of geological processes between different oil sands.

It should be noted that factors which govern the compressibility of oil sands also govern the strength and deformation properties during shear. As a consequence, although stress cycling prior to shear generally produces specimen densities comparable to in situ densities, the

shear strength parameters may be significantly affected.

The presence of shale interbedding has a major influence on the compressibility of McMurray Formation oil sands. Discontinuous seams and clasts of more compressible shale interspersed in the oil sands matrix increases the overall compressibility of the oil sands. After drained heating, the compressibility of interbedded oil sands is reduced. The influence of shale interbedding on the compressibility of oil sands, therefore, decreases with the amount of consolidation experienced by the snale inclusions. In fact, if enough heat consolidation of the shale interbedding occurs, the compressibility of the oil sands becomes comparable to rich oil sands.

Generally volumetric strains associated with thermal consolidation of shale during first time heating are not recoverable (Green, 1984; Williams, 1982; Campanella and Mitchell, 1968). Improvements in strength and deformation properties associated with volume reductions caused by heat consolidation are likely to be retained after the initial in situ steam injection cycle. The gain in strength parameters are, however, at the expense of losses in porosity-dependent permeability. Temperature increase also significantly increases the pore fluid pressure and if pore pressure dissipation cannot occur at the same rate as the temperature increase, the drop in effective stress can cause a considerable decrease in the shear strength.

The volumetric compressibility of high plastic, smectite-rich Clearwater k_{cb} shale due to thermal loading is time dependent. The time required to complete heat consolidation under temperatures and pressures associated with in situ recovery is relatively small (about 12 hours) when compared to the steam injection phase of the in situ recovery cycle which is generally a month or more.

Intact, relatively shale-free limestone is about one-half as compressible as high quality, rich oil sands and approximately one-tenth as compressible as Clearwater shale. Based on observations on the effects of shale interbedding on the compressibility of oil sands, the shaley limestone near the uncomformable surface which separates McMurray and Devonian sediments is likely to be governed by the more compressible shale interbedding.

The compressibility of oil sands and shale is dependent on the temperature, pressure and stress path followed during the test. Analytical procedures used to model the stresses and deformations of formation strata must, therefore, utilize compressibility values representative of the actual formation response.

7. SHEAR STRENGTH OF ATHABASCA OIL SANDS

7.1 Materials Studied

The stress-deformation and strength behaviour of oil sands subjected to changes in deviatoric stress is controlled primarily by frictional resistance at mineral grain contacts, grain movement and reorientation and dilation or contraction of the mineral grain matrix. The relative movement of mineral grains as well as distortion and breakage of individual grains during shear deformation depends on:

a) The composition, the size and the shape of individual mineral grains.

b) The gradation, the packing and the nature of contact surfaces.

c) The history of stress experienced by the oil sands in situ.

d) The stress path followed by the oil sands during in situ thermal recovery.

e) The change in temperature.

f) The rate of deformation.

Consequently, stresses and deformations developed in the oil sands reservoir in and around heated production zones may vary significantly in different geotechnical facies. Additionally, the influence of (d), (e) and (f) above must be considered in laboratory testing in order that more realistic results may be obtained and used in the development of constitutive models for oil sands.

Oil sands materials from three different sites in the Athabasca Deposit, each representing a distinct geotechnical facies, were studied:

1. Underground Test Facility. Estuarine channel margin sediments of the McMurray Formation. Oil sands containing from 36% to 72% shale by weight in the form of discontinuous seams and clasts. The depth of the core samples was 152 to 161 m.

2. Southern Alberta. Estuarine sand of the McMurray Formation. Medium grained, uniformly graded, rich oil sands. A fines content of about 5% by weight. The depth of the core sample was about 295 m.

3. Northern Athabasca. Shallow-water marine sands of the Clearwater Formation (Wabiskaw Member). Medium grained, medium rich, glauconitic oil sands. A fines content ranging from 5 to 21% by weight. The depth of the core sample was about 220 m.

7.2 Methods and Procedures

Processes used to recover bitumen from oil sands subject the formation to changes in effective stress, pore fluid pressure and temperature. During the stages of the in situ bitumen recovery process oil sands may undergo several different stress paths. Oil sands near a well casing during cyclic steam recovery, for example, experience a complex history of stress corresponding to each phase of the process such as well excavation, grouting, hydraulic fracturing, steam injection and pumping. The geomechanical behaviour depends on the series of stress changes applied to the oil sands.

In situ stress changes are also controlled by geotechnical complexity. The field stress paths for steam injection in a relatively homogeneous oil sands formation

(estuarine channel, mid-channel bar or point bar sands) and a formation horizontally stratified with oil sands and shale layers (estuarine channel margin sedimentation) are shown on Figure 7.1. During this bitumen recovery process, steam is injected at pressures higher than the in situ pore pressures but below the fracturing pressure. During the early stages of steam injection, the vertical and horizontal effective stresses are increased by thermal expansion of the reservoir matrix. The series of stress changes applied to the oil sands result in two distinct stress paths as shown in Figure 7.1; that is:

1. Estuarine Sand. Increases in the pore fluid pressures from temperature increases and from the steam injection pressure result in decreasing both the vertical and horizontal effective stresses by the same amount.

2. Estuarine Channel Margin Sedimentation. Pore pressures increase due to thermal expansion of the pore fluids and by the steam injection pressure. The formation has a horizontal permeability much higher than the vertical permeability due to the stratification. Because of the higher horizontal permeability, the net effect on the horizontal effective confining stress could be a reduction in

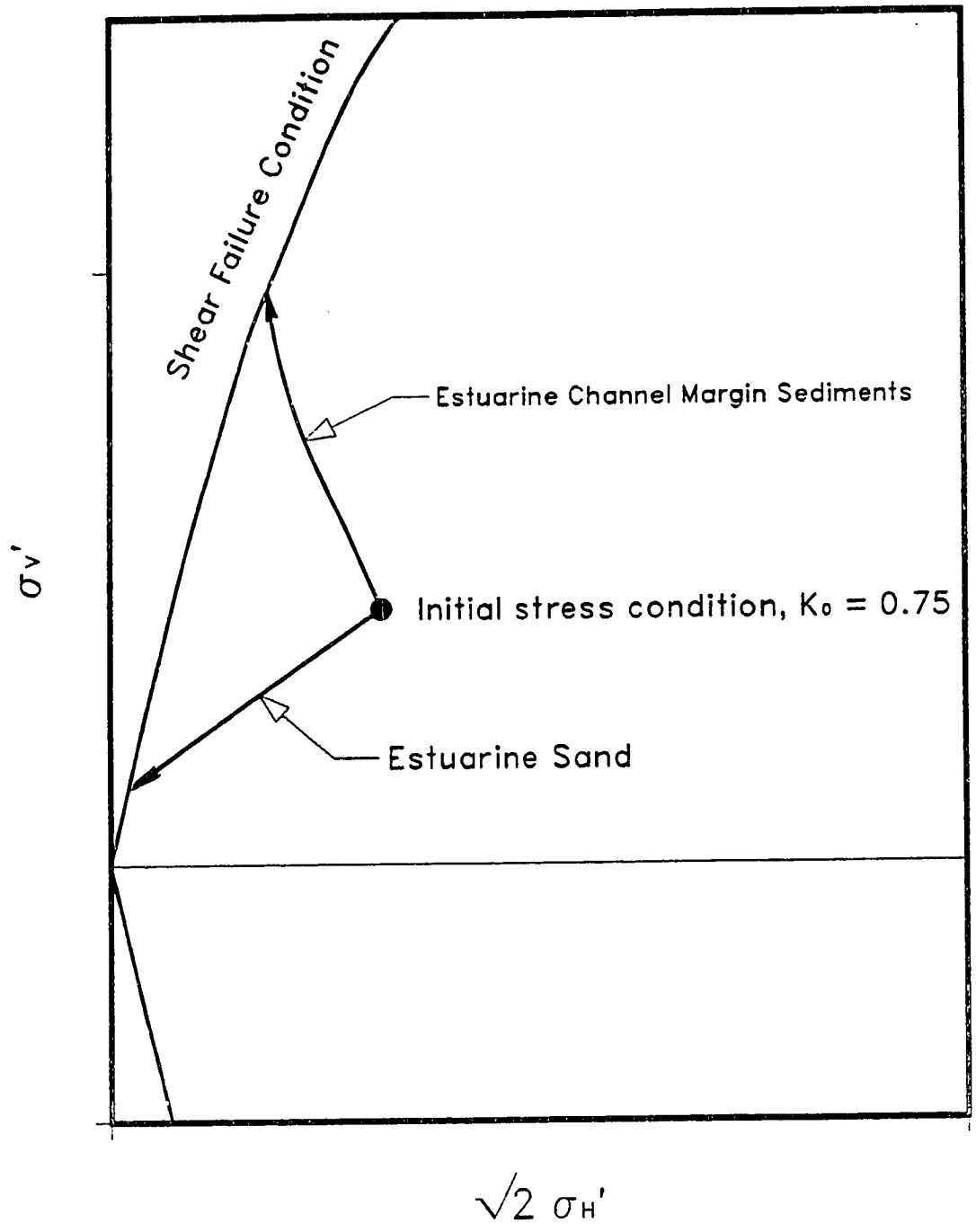

Figure 7.1 Field Stress Paths For Steam Injection

stress. Due to the low vertical permeability and the small area heated, the net effect on the vertical effective stress will be an increase in stress.

In both cases, as the stress conditions are approaching the shear failure envelope, shear deformations will take place. If the stress changes are sufficient, shear failure will be reached.

The stress paths shown in Figure 7.1 may be classed as "unloading stress paths" in which one or more of the in situ effective stresses are reduced during bitumen recovery. Effective stress reductions generally arise from temperature increases under fully undrained or partially drained conditions, unloading due to excavation of underground openings (wells, tunnels and shafts) and pore pressure increases due to fluid injection. Effective stress increases are generally limited to oil sands production zones where drainage and pore fluid pressures are controlled and reservoir volume changes arise from thermal expansion under fully drained conditions.

Five triaxial stress paths were studied during triaxial strength testing of Athabasca oil sands. The stress paths in triaxial stress space are shown in Figure 7.2. The stress paths may be described as follows:

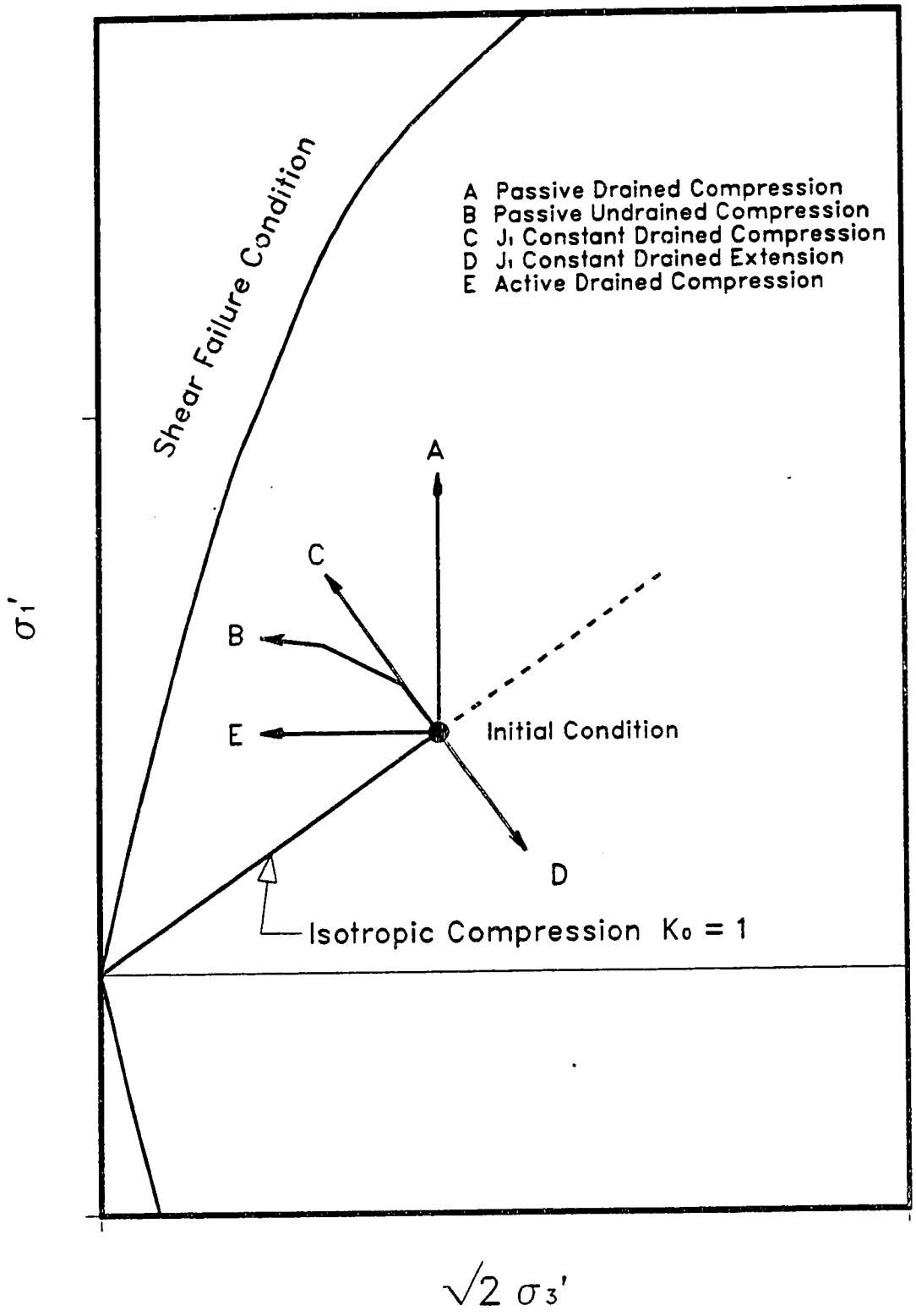

Figure 7.2 Laboratory Stress Paths

1. Passive Drained Compression. In this test the axial stress is increased and the radial stress remains constant. Pore fluid is allowed to drain freely during the test.

2. Passive Undrained Compression. In this test the axial stress is increased, the radial stress remains constant and drainage of pore fluids during the test is prevented.

3. J_1 Constant Drained Compression. In this test the average principal stress is held constant by increasing the axial stress and decreasing the radial stress. Drainage of pore fluids is permitted during the test.

4. J_1 Constant Drained Extension. In this test the average principal stress is held constant by decreasing the axial stress and increasing the radial stress. Drainage of pore fluid is permitted during the test.

5. Active Drained Compression. In this test the axial stress is held constant and the radial stress is decreased. Drainage of pore fluids is permitted during the test.

A total of 25 triaxial tests were carried out on Athabasca oil sands over a range of temperatures from 20°C to 225°C and effective confining stresses to 7 MPa.

7.3 Passive Drained Compression Stress Path

Estuarine Sand

The stress-strain and volume change relationships for high grade (well sorted sand with low fines content, less than 5% by weight) McMurray Formation oil sands tested following passive drained compression stress paths (test series AMTOS) are shown in Figure 7.3. The oil sands specimens were obtained from a core sample taken southwest of Fort McMurray at a depth of approximately 295 m. The effective confining stress applied to the specimens during each test varied. Specimen AMTOS1 was tested under an effective confining stress of 4.2 MPa which approximates the in situ average effective stress. Specimen AMTOS2 was tested under an effective confining stress of 2.5 MPa and Specimen AMTOS3 under 7.0 MPa. A cyclic stress compressibility test

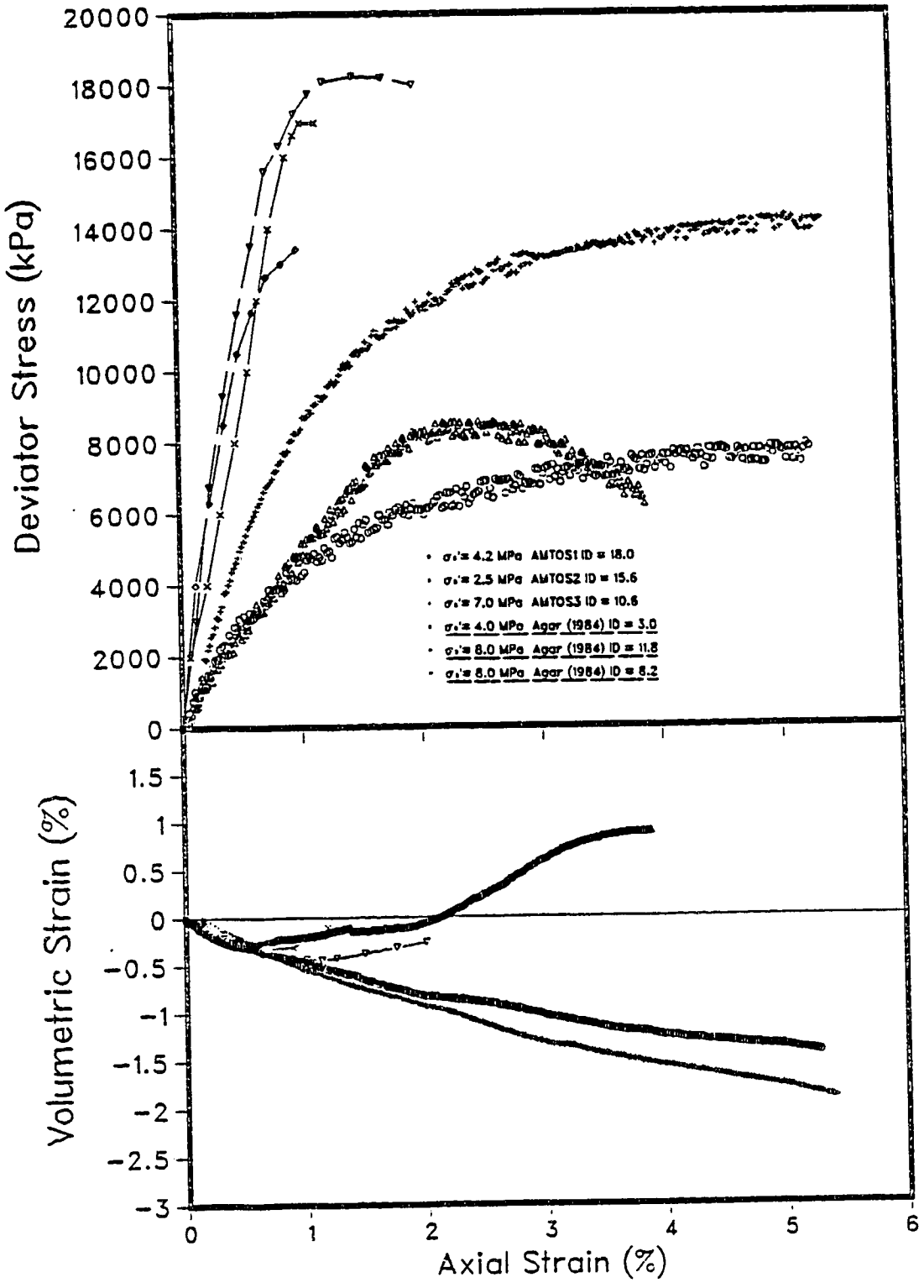

Figure 7.3 Drained Passive Compression Tests on Athabasca McMurray Formation Oil Sands

was performed on each specimen prior to the drained shear test. Each specimen was compressed isotropically to at least 2.0 MPa above the effective confining stress applied to the specimen during the shear test. Results for each phase of each test (initial conditions, isotropic compression and drained shear tests) are summarized in Table 7.1.

The stress-strain and volume change relationships for high grade oil sands from the Saline Creek outcrop, as reported by Agar (1984), are plotted on Figure 7.3 for comparison. The bitumen contents of these specimens were about 16.5% by weight and each specimen had a fines fraction of less than 5% by weight.

The shear strengths of the two Saline Creek oil sands specimens tested under an effective confining stress of 8 MPa differ significantly. The peak deviator stress of the specimen with an initial index of disturbance of 8.2% was 17.9 MPa as compared to 13.4 MPa for the specimen with an index of disturbance of 11.8%. Saline Creek oil sands are composed of a dense interlocking grain structure developed during the time of burial in which diagenetic processes occurred with dissolution and recrystallization of quartz at grain contacts. This oil sands has a large number of concavo-convex and long contacts. The dramatic reduction in shear strength is attributed to disruption of the locked sand structure. It is noted, however, that the initial tangent modulus and volume change during shear do not differ significantly.

Table 7.1 Drained Passive Triaxial Tests - Athabasca McMurray Formation Oil Sands

Initial Conditions

Test Number	Bulk Density (Mg/m3)	Dry Density (Mg/m3)	% water (mass)	% bitumen (mass)	% sand (mass)	Void Ratio e	Sr (%)	Pore Pressure Parameter B **	Index of Disturbance (%)
AMTOS1	1.85	1.52	2.6	14.9	82.5	0.74	76	1.00	18.0
AMTOS2	1.87	1.54	2.3	15.5	82.2	0.72	79	1.00	15.1
AMTOS3	1.89	1.54	3.3	15.5	81.2	0.73	85	0.99	10.6

** Note: At 0.2 MPa Effective Confining Stress after saturation at 2.5 MPa Back Pressure

Isotropic Consolidation

Test Number	Volume Change (%) from σ' = 0.2 to (•) MPa	Bulk Density (Mg/m3) σ' = (•) MPa	Dry Density (Mg/m3) at σ' = (•) MPa	K (MPa) Cycled from (• to •) MPa	Void Ratio e	Index of Disturbance (%)
AMTOS1	-5.87 (6.3)	2.01 (6.3)	1.62 (6.3)	600 (3.4 to 6.3)	0.64	8.0
AMTOS2	-4.68 (5.0)	2.00 (5.0)	1.61 (5.0)	540 (2.2 to 5.0)	0.64	7.3
AMTOS3	-7.07 (9.0)	2.03 (9.0)	1.65 (9.0)	750 (5.1 to 9.0)	0.60	-1.0

Drained Shear Test

Test Number	Effective Confining Stress (MPa)	Back Pressure (MPa)	B	Deviator Stress at failure (MPa)	Axial Strain at failure (%)	Volumetric Strain at failure (%)	Modulus of Elasticity (MPa)	Poisson's Ratio
AMTOS1	4.2	2.5	0.81	7.8	5.24	-1.42	632	0.20
AMTOS2	2.5	2.5	0.88	8.5	2.21	0.60	616	0.11
AMTOS3	7.0	2.6	0.74	14.0	4.39	-1.65	1215	0.15

The index of disturbance of Specimen AMTOS3 prior to testing was similar to the moderately disturbed Saline Creek specimen. Specimen AMTOS3 showed a slightly greater maximum shear strength of 14.0 MPa during drained passive compression under an effective confining stress of 7.0 MPa. However, the axial strain and volumetric strain to failure were significantly higher and the initial stiffness was considerably lower. During the shear test this specimen displayed strain hardening and contractive volume change behaviour in the post-peak region.

The grain structure of AMTOS series McMurray Formation oil sands prior to triaxial shear was studied with the aid of a scanning electron microscope. An Energy Dispersive X-ray analysis performed on the grains indicated that the specimen was almost entirely composed of quartz. Although the core sample was disturbed during the coring process, evidence of diagenetic alteration of the grain fabric characteristic of Saline Creek oil sands is clearly visible. Figure 7.4 illustrates a number of long and concavo-convex grain contacts while Figure 7.5 shows the development of crystal overgrowth into the pore space between grains and the resulting cementation of the grains.

Prior to shear testing Specimen AMTOS3 was subjected to isotropic compression and stress cycling to an effective confining stress of 9.0 MPa. During this procedure the porosity was reduced to slightly below the estimated in situ porosity resulting in a negative value for the index of

Figure 7.4 Grain Contacts in McMurray Formation Oil Sands Specimen

Figure 7.5 Cemented Grains in McMurray Formation Oil Sands Specimen

disturbance. This behaviour indicates a significant amount of grain movement and reorientation has occurred and the original grain structure altered. In other words, subjecting a disturbed oil sands specimen to high effective confining stresses may alter the grain contacts from an interlocking to a tangential configuration. Although the laboratory specimen attains a porosity similar to that found in situ, its maximum shear strength and deformation modulus would be significantly reduced from the decreased grain contact area.

Figure 7.3 also shows stress-strain and volume change plots for Saline Creek and AMTOS series oil sands tested under an effective confining stress of 4 MPa. The Saline Creek specimen displays dilatant behaviour during shear and this increase in volume during shear straining was accompanied by strain softening behaviour in the post-peak region. Specimen AMTOS1, however, shows strain hardening behaviour accompanied by contractive behaviour throughout the test. Initial index of disturbance values were 3.0% and 18.0% for the Saline Creek specimen and the South Athabasca specimen, respectively. Maximum deviator stresses were 17.0 MPa for the Saline Creek specimen and 7.9 MPa for Specimen AMTOS1. Despite isotropic stress cycling of Specimen AMTOS1 prior to shear testing the shear strength is significantly lower and much more deformable than the Saline Creek specimen. The vast difference in stress-strain and volume change behaviour is due to the significant difference in initial core sample disturbance.

In the undisturbed state, high grade McMurray Formation oil sands exhibits high dilatancy and post-peak strain softening behaviour during triaxial compression under low effective confining stresses. As the effective confining stress is increased, the amount of dilation decreases as more grain breakage and crushing occurs during shear deformations. In either case, the amount of grain movement and grain orientation prior to shear failure is relatively small. High dilatancy during shear and strain softening behaviour is evident only at low effective confining stress for disturbed AMTOS series oil sands (Specimen AMTOS2). As the effective confining stress increases the strength peaks are suppressed and the specimens trend toward strain hardening and contractive volume change behaviour.

Shear strength data obtained from consolidated passive compression tests carried out on high grade McMurray Formation oil sands by Dusseault (1983) are shown in Figure 7.6. Test specimens were subjected to isotropic stress cycling to effective confining stresses of 13 MPa prior to shearing. The average porosity of these specimens prior to and after stress cycling was 0.35 and 0.34, respectively. Initial index of disturbance values were not available for these tests. Results of drained passive compression tests carried out on AMTOS oil sands subjected to stress cycling prior to shear and the non-cyclically compressed test results reported by Agar (1984) are also shown in the figure.

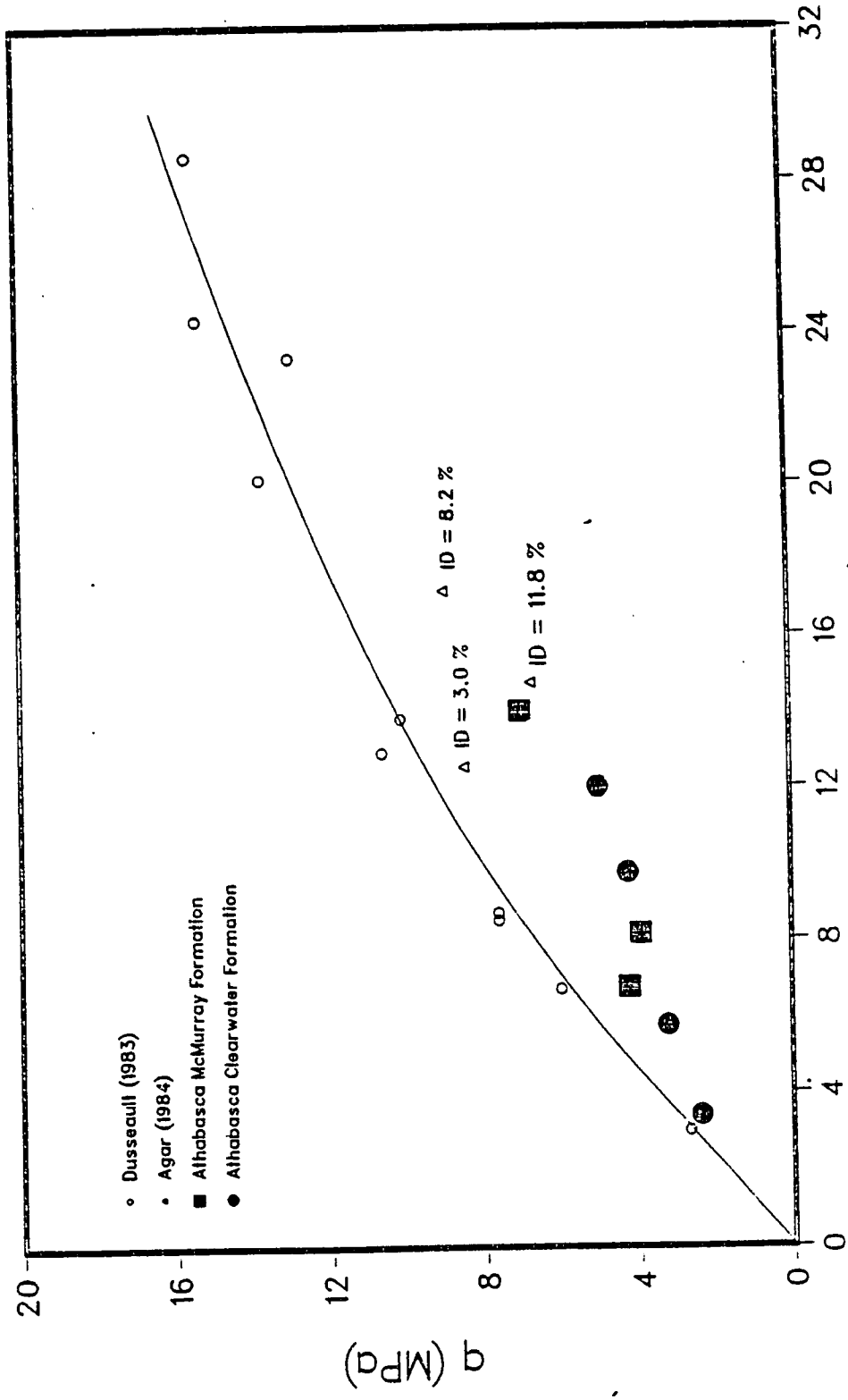

Figure 7.6 Shear Strength of Athabasca Oil Sands From Triaxial Tests

The cyclically compressed tests by Dusseault (1983) give slightly higher strength values than the non-cycled, high quality, undisturbed specimen (index of disturbance of 3.0%) of Agar (1984). The initial porosity of this specimen was 0.34. The more disturbed specimens tested by Agar (index of disturbance of 8.2% and 11.8%) plot considerably lower. The initial porosities of these specimens were 0.36 and 0.37, respectively. Given that the porosity of the specimens prior to isotropic compression and stress cycling were slightly less than the initial porosity of the non-cycled specimens, it is likely that the non-cycled specimens had higher porosity values prior to shear. The difference in shear strength may therefore be due to the lower porosities of the cycled specimens prior to shear.

The average porosities of disturbed AMTOS series oil sands before and after stress cycling were 0.42 and 0.38, respectively. The difference in shear strength between AMTOS series oil sands and those reported by Dusseault is due to the more densely packed sand structure which exhibits a higher resistance to shear. It is noted that the strengths of AMTOS series oil sands are similar to the results reported by Agar for more disturbed specimens.

The relationship between tangent modulus of elasticity and effective confining stress derived from drained passive compression tests carried out on high grade, low fines McMurray Formation oil sands is given in Figure 7.7. The drained elastic modulus increases with confining pressure.

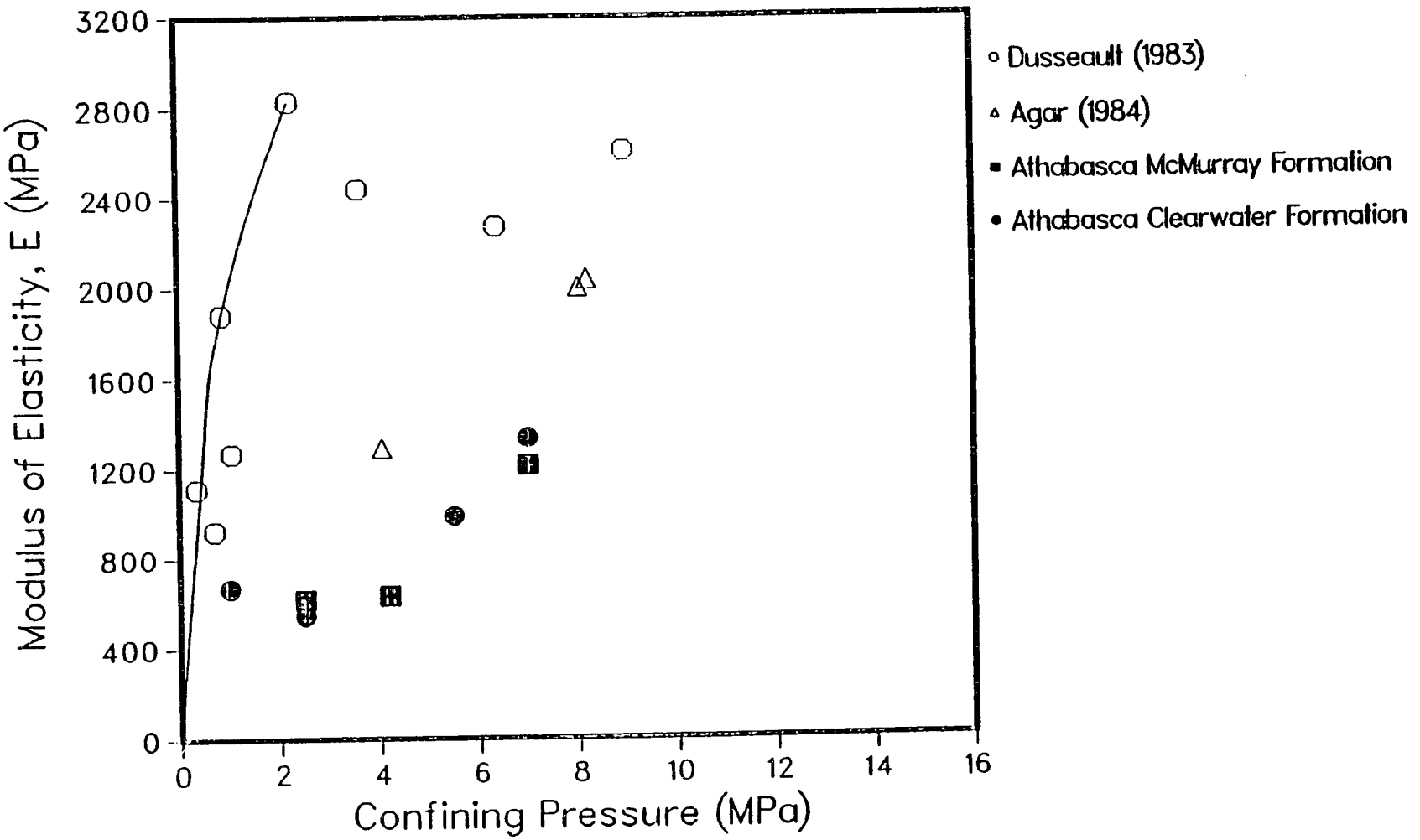

Figure 7.7 Variation of E with Confining Pressure at Axial Strain = 0.25 %

The rate of increase of the modulus, however, decreases with increasing confining pressure. The envelope shown in Figure 7.7 was obtained from tests where the effective confining stress was cycled prior to the shear test (Dusseault, 1983). By extrapolation, the drained modulus of elasticity is apparently zero or negligible at zero confining pressure.

Drained modulus values from tests performed on disturbed McMurray oil sands specimens obtained from depth and undisturbed McMurray oil sands from Saline Creek are also shown in Figure 7.7. The results indicate that sample disturbance has a significant effect on the drained modulus of elasticity of oil sands. Isotropic stress cycling results in specimens with higher modulus values. However, the benefit derived from stress cycling diminishes with the amount of initial sample disturbance experienced by the specimen during core sampling.

Comparing Figure 7.7 with Figure 7.6, it is apparent that, proportionally, sample disturbance does not reduce the shear strength of high grade oil sands as much as it reduces the drained modulus of elasticity. In other words, compared with the shear strength the drained modulus of elasticity is more sensitive to sample disturbance.

The variation of Poisson's ratio of high grade McMurray Formation oil sands with effective confining pressure is shown in Figure 7.8. Poisson's ratios measured on the oil sands obtained for this study are generally lower than those obtained in previous studies. These lower values reflect the

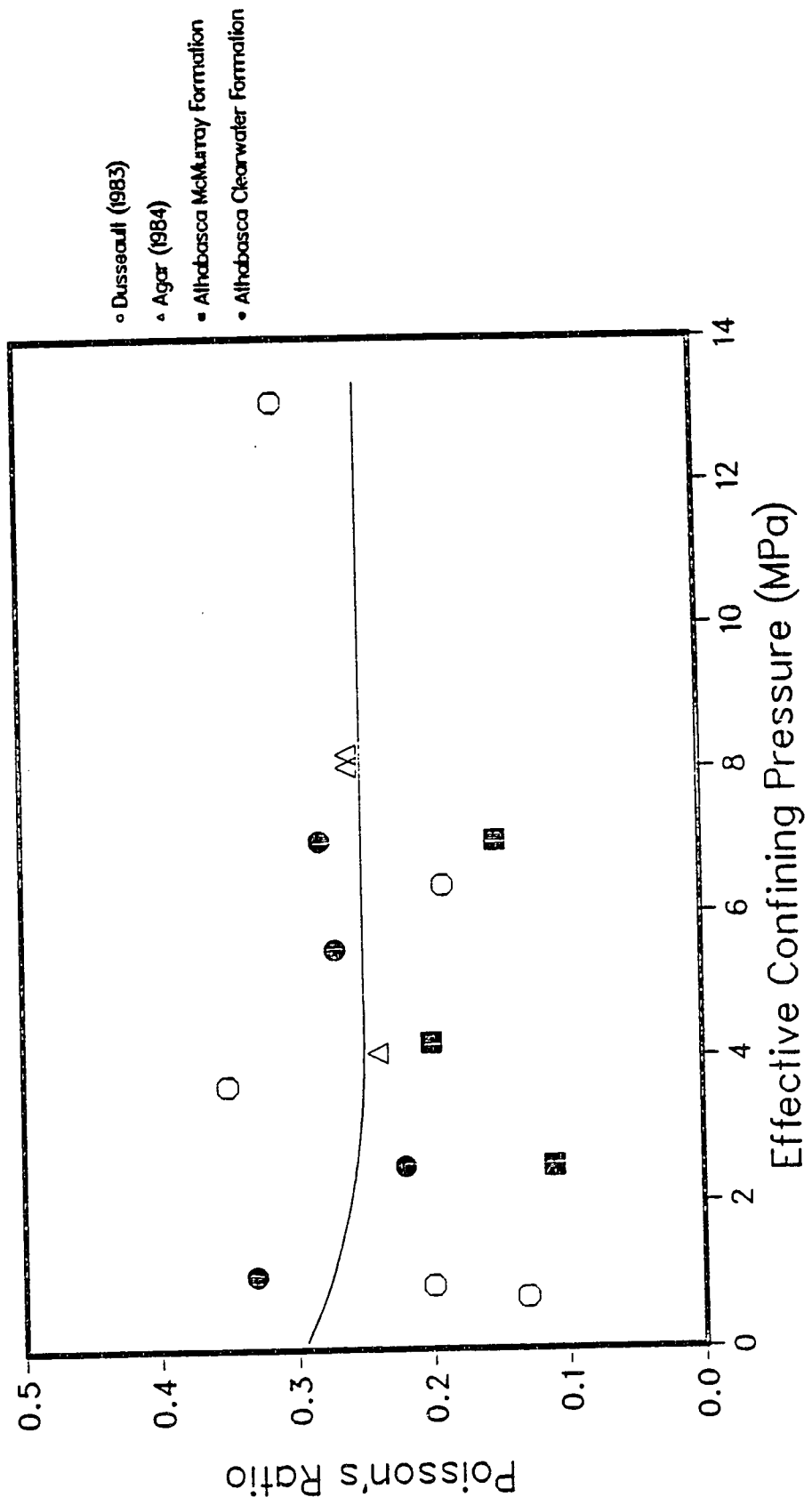

Figure 7.8 Variation of Poisson's Ratio with Confining Pressure at Axial Strain = 0.25 %

higher compaction of the disturbed oil sands structure during shear.

Two major conclusions may be drawn from the drained passive compression tests carried out on McMurray Formation oil sands:

1. Isotropic stress cycling of specimens prior to shear testing results in a significant improvement in measured geomechanical properties. These values may be more representative of in situ mechanical behaviour of oil sands. This test procedure, however, is effective only if the oil sands matrix has not undergone excessive sample disturbance during core sampling. The results obtained from the shear tests performed on disturbed specimens obtained from a depth of 295 m are significantly weaker and much more deformable despite isotropic stress cycling prior to triaxial compression.

2. From the specimens examined here it appears that conventional triple tube core sampling techniques used in the petroleum industry to obtain oil sands samples may result in test specimens which are initially highly disturbed and not adequate for representative geotechnical testing. It should be noted, however, that these core samples were not

obtained specifically for geotechnical purposes and may have experienced poor handling and storage procedures. Since the source of the sample disturbance is not apparent, core sample quality should be assessed on a site specific basis.

Clearwater Formation Shefal Sands

The stress-strain and volume change relationships for Athabasca Clearwater Formation oil sands (test series ACTOS) tested following drained passive compression stress paths are shown in Figure 7.9. The oil sands specimens were obtained from a core sample taken in the Wabiskaw Member of the Clearwater Formation, northwest of Fort McMurray. The depth of the core sample was approximately 220 m and the in situ average effective stress was about 5.5 MPa. Four drained triaxial shear tests were performed under effective confining stresses ranging from 1.0 to 7.0 MPa. Each specimen was compressed to at least 2.0 MPa above the effective confining stress applied to the specimen during the shear test and cycled. Results for each phase of each test are given in Table 7.2.

Under initial conditions (prior to isotropic consolidation) each specimen exhibited a high degree of core disturbance. Specimens ACTOS1, ACTOS2 and ACTOS4 possessed a bulk density of approximately 1.90 Mg/m^3 and an index of

Table 7.2 Drained Passive Triaxial Tests - Athabasca Clearwater Formation Oil Sands

Initial Conditions

Test Number	Bulk Density (Mg/m3)	Dry Density (Mg/m3)	% water (mass)	% bitumen (mass)	% sand (mass)	Void Ratio e	Sr (%)	Pore Pressure Parameter B **	Index of Disturbance (%)
ACTOS1	1.90	1.58	5.4	11.4	83.2	0.67	79	1.00	15.5
ACTOS2	1.91	1.58	5.0	12.0	83.0	0.67	80	0.98	14.6
ACTOS3	1.77	1.44	6.7	11.9	81.4	0.84	72	0.97	21.0
ACTOS4	1.86	1.53	6.6	11.6	81.9	0.74	80	0.95	14.6

** Note: At 0.2 MPa Effective Confining Stress after saturation at 2.6 MPa Back Pressure

Isotropic Consolidation

Test Number	Volume Change (%) from σ = 0.2 to (*) MPa	Bulk Density (Mg/m3) σ = (*) MPa	Dry Density (Mg/m3) at σ = (*) MPa	K (MPa) Cycled from (* to *) MPa	Void Ratio e	Index of Disturbance (%)
ACTOS1	-6.78 (7.3)	2.06 (7.3)	1.70 (7.3)	630 (2.4 to 7.3)	0.56	3.1
ACTOS2	-5.67 (8.9)	2.04 (8.9)	1.68 (8.9)	1058 (5.0 to 8.9)	0.58	4.4
ACTOS3	-5.65 (4.7)	1.95 (4.7)	1.53 (4.7)	478 (1.1 to 4.7)	0.74	12.4
ACTOS4	-4.33 (5.0)	1.99 (5.0)	1.60 (5.0)	425 (1.0 to 5.0)	0.66	7.5

Drained Shear Test

Test Number	Effective Confining Stress (MPa)	Back Pressure (MPa)	B	Deviator Stress at failure (MPa)	Axial Strain at failure (%)	Volumetric Strain at failure (%)	Modulus of Elasticity (MPa)	Poisson's Ratio
ACTOS1	5.5	2.5	0.78	8.5	2.14	-1.12	986	0.27
ACTOS2	7.0	2.5	0.68	10.0	3.30	-1.38	1335	0.28
ACTOS3	2.5	2.5	0.83	6.5	2.54	-0.74	542	0.22
ACTOS4	1.0	2.5	0.88	4.8	1.19	0.25	666	0.33

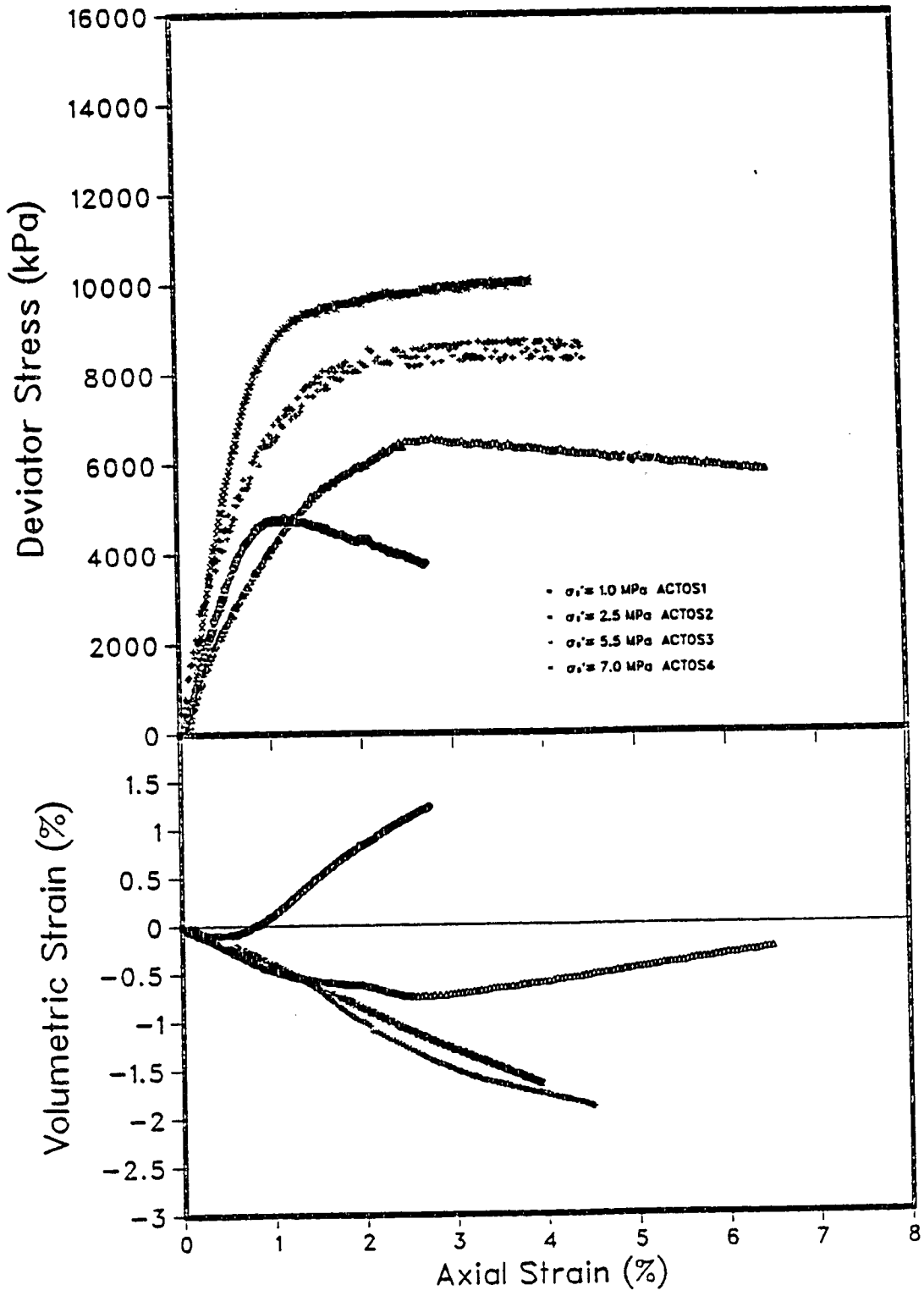

Figure 7.9 Drained Passive Compression Tests on Athabasca Clearwater Formation Oil Sands

disturbance of about 15%. Specimen ACTOS3 appeared to be somewhat more disturbed with an initial bulk density of 1.77 Mg/m^3 and an index of disturbance of 21%.

Clearwater oil sands exhibit high dilatancy during shear and strain weakening behaviour is evident at low effective confining stress. As the effective confining stress increases the strength peaks are suppressed and the specimens trend toward strain hardening and contractive volume change behaviour. These results are similar to those observed for disturbed Athabasca McMurray Formation oil sands (test series AMTOS).

Clearwater Formation oil sands test results are compared to McMurray Formation oil sands test results in Figures 7.6, 7.7 and 7.8. The following characteristics regarding the mechanical behaviour of Clearwater Formation Wabiskaw Member oil sands are noted:

1. The maximum shear strength of disturbed Wabiskaw oil sands is very similar to disturbed McMurray Formation oil sands. This is not surprising since Wabiskaw Member oil sands consist primarily of reworked McMurray sediments deposited in marine water during transgression of the Boreal Sea southward across the McMurray strata (Carrigy and Kramers, 1974). Drained shear tests performed on disturbed sands of similar mineralogy and similar void ratio prior to shear should yield similar results.

2. The elastic moduli obtained from McMurray and Clearwater oil sands specimens obtained from depth are very similar. These results are lower than the results obtained from high quality McMurray Formation oil sands isotropically consolidated and significantly lower than the good quality McMurray Formation oil sands subjected to stress cycling prior to shear.

3. Poisson's ratio is fairly consistent around 0.25 over a wide range of confining pressures. However, at low confining pressures, Poisson's ratio is about 0.3. These values are consistently higher than the disturbed McMurray Formation oil sands but are in fair agreement with undisturbed and good quality cycled McMurray specimens.

The strength-deformation behaviour of the oil bearing sands of the Wabiskaw Member of the Clearwater Formation within the Athabasca Deposit is very similar to McMurray Formation oil sands obtained from similar depths. It is noted, however, that both sets of laboratory specimens experienced severe disturbance to the oil sands matrix prior to testing due to poor core sampling and storage procedures. The effects of geological environment of deposition and

geological history on constitutive behaviour of Clearwater oil sands could not be evaluated in this case.

McMurray Formation Estuarine Margin Sedimentation

The stress-strain and volume change relationships for interbedded McMurray Formation oil sands (test series UFTOS) tested following drained passive compression stress paths are shown in Figure 7.10. Test specimens were obtained from core samples taken in the McMurray Formation at the AOSTRA Underground Test Facility over a depth range of 152 m to 161 m. The test specimens consisted of fine grained oil sands with overall bitumen contents ranging from 5.6 to 7.6% by weight. Each specimen contained thin, discontinuous shale seams. The fines content (less than 0.074 mm) of the grain size distribution was fairly consistent at approximately 50% by weight.

The effective confining stress applied to the specimens during the shear tests varied from 1.0 MPa to 4.0 MPa. Specimens UFTOS1 and UFTOS2 were sheared at the approximate in situ average effective stress of 2.5 MPa. A cyclic stress compressibility test was performed on Specimens UFTOS1, UFTOS2 and UFTOS3. Specimen UFTOS1 was compressed isotropically to 12 MPa, UFTOS2 to 3.2 MPa and UFTOS3 to 5.5 MPa prior to cycling. Specimen UFTOS4 underwent isotropic consolidation to 4.0 MPa and was not cycled prior to the drained shear test. Results for each phase of testing

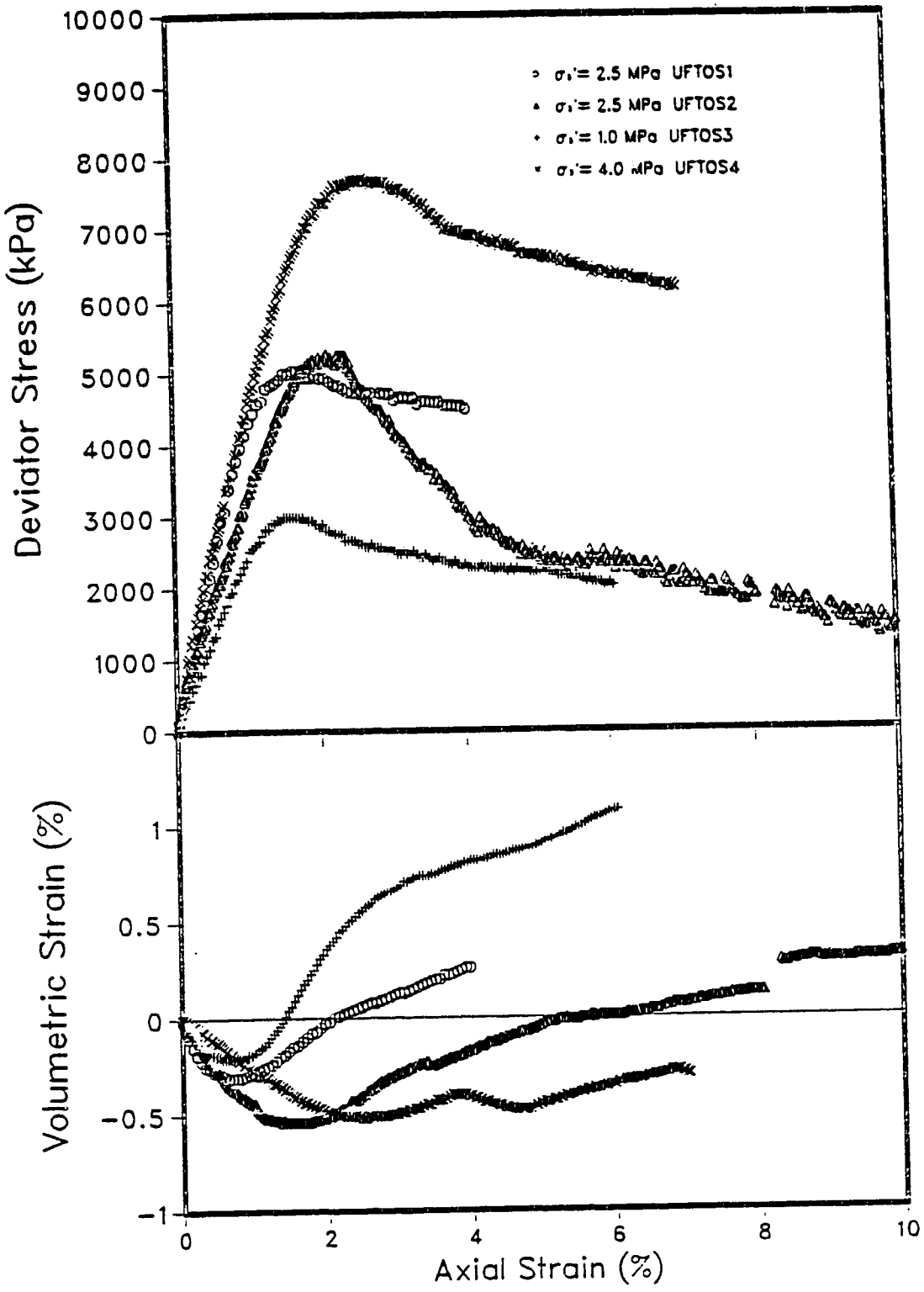

Figure 7.10 Drained Passive Compression Tests on Athabasca McMurray Formation Interbedded Oil Sands

are summarized in Table 7.3.

The peak shear strength and axial strain at failure increased with effective confining pressure while the volumetric strain at failure decreased. Specimens displayed strain softening and dilatant volume change behaviour in the post-peak region. The initial tangent modulus of elasticity also increased with increasing confining stress. Poisson's ratio varied from 0.26 to 0.35 and no direct correlation between Poisson's ratio and effective confining stress is apparent.

The significant influence of shale inclusions on both shear strength and stress-strain behaviour of McMurray Formation oil sands is clearly demonstrated in Figure 7.10:

1. Specimens UFTOS1 and UFTOS2 were compressed isotropically to 12.1 MPa and to 3.2 MPa, respectively. Both specimens were cycled prior to shear and then sheared under identical conditions at 2.5 MPa effective confining stress. The oil sands specimen containing the heavily overconsolidated shale (UFTOS1) was stiffer than the oil sands specimen containing the less overconsolidated shale despite having a higher void ratio prior to shear. Void ratios prior to shear were 0.50 and 0.45 for Specimens UFTOS1 and UFTOS2, respectively. The difference in void ratio values reflect the relative amount of fines in each specimen (fines contents were

Table 7.3 Drained Passive Triaxial Tests - Athabasca McMurray Formation Oil Sands (Interbedded Specimens)

Initial Conditions

Test Number	Bulk Density (Mg/m3)	Dry Density (Mg/m3)	% water (mass)	% bitumen (mass)	% solids (mass)	% fines	e	Sr (%)	Pore Pressure Parameter B **	Index of Disturbance (%)
UFTOS1	1.99	1.67	8.3	7.6	84.1	41.2	0.60	84	1.00	11.7
UFTOS2	2.06	1.77	8.3	5.6	86.1	55.2	0.51	85	1.00	12.1
UFTOS3	2.07	1.76	8.5	6.6	84.9	54.0	0.52	91	1.00	6.4
UFTOS4	2.12	1.84	6.4	6.5	87.1	52.9	0.45	87	0.99	10.0

** Note: At 0.2 MPa Effective Confining Stress after saturation at 2.5 MPa Back Pressure

Isotropic Consolidation

Test Number	Volume Change (%) from σ' = 0.2 to (*) MPa	Bulk Density (Mg/m3) σ' = (*) MPa	Dry Density (Mg/m3) at σ' = (*) MPa	K (MPa) Cycled from (* to *) MPa	Void Ratio e	Index of Disturbance (%)
UFTOS1	-6.48 (12.1)	2.12 (12.1)	1.79 (12.1)	142 (0.3 to 3.7)	0.50	-1.2
UFTOS2	-4.16 (3.2)	2.16 (3.2)	1.85 (3.2)	833 (2.5 to 3.2)	0.45	2.6
UFTOS3	-4.81 (5.5)	2.16 (5.5)	1.85 (5.5)	227 (1.0 to 2.8)	0.45	3.8
UFTOS4	-4.16 (4.0)	2.20 (4.0)	1.92 (4.0)	Not Done	0.39	-0.6

Drained Shear Test

Test Number	Effective Confining Stress (MPa)	Back Pressure (MPa)	B	Deviator Stress at failure (MPa)	Axial Strain at failure (%)	Volumetric Strain at failure (%)	Modulus of Elasticity (MPa)	Poisson's Ratio
UFTOS1	2.5	3.0	1.00	5.04	1.67	-0.12	469	0.26
UFTOS2	2.5	2.1	0.85	5.26	2.13	-0.49	323	0.27
UFTOS3	1.0	2.5	0.93	2.99	1.52	0.06	244	0.34
UFTOS4	4.0	2.0	0.89	7.73	2.68	-0.51	454	0.35

41.2% and 55.2% for Specimens UFTOS1 and UFTOS2, respectively). Increasing the pre-shear isotropic consolidation stress by a factor of 2 results in a 45% increase in the initial tangent modulus of elasticity. It is noted, however, that both materials show similar peak deviator stress values.

2. The peak strength of Specimen UFTOS2 exceeds the residual value by approximately 300% (5.26 MPa as compared to 1.29 MPa). The friction angles corresponding to peak and residual strengths were 31° and 13°, respectively. Significant displacement along a single well developed plane of weakness was observed in the specimen after the test. Deformation in this oil sands specimen was dominated by failure through the heavily overconsolidated shale strata. Failure initially involved rupture of interparticle bonds with basal plane slip in the clay minerals controlling at large strain leading to a significant reduction in friction angle.

The shear strength of interbedded McMurray Formation oil sands plotted in the form of a p'-q diagram is shown in Figure 7.11. For comparative purposes, a failure envelope for triaxial peak strength test data for high grade

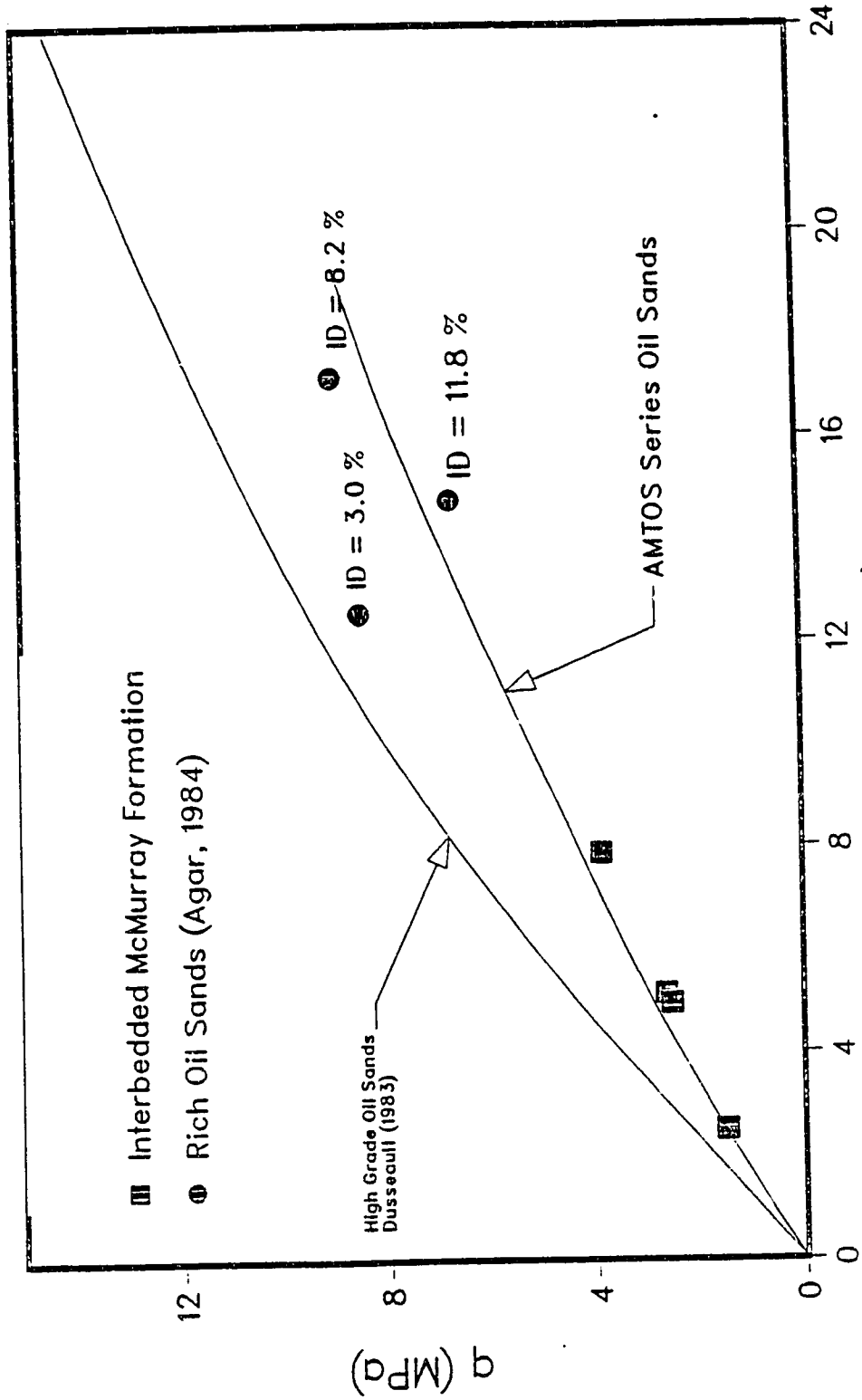

Figure 7.11 Shear Strength of Alhabasca Interbedded Oil Sands From Triaxial Tests

specimens (Dusseault, 1983), a failure envelope for disturbed AMTOS series oil sands, and peak strength data from Agar (1984) are also shown in the figure. The strengths of the interbedded oil sands specimens are approximately 25% weaker than rich, well consolidated, dense oil sands and have strengths similar to disturbed, rich oil sands.

7.4 Passive Undrained Compression Stress Path

McMurray Formation Estuarine Sand

A typical stress-strain and pore pressure change relationship for high grade, uniformly graded McMurray Formation oil sands tested following passive undrained compression stress path is given in Figure 7.12. The specimen was taken from a core sample obtained from the Saline Creek surface exposure. The specimen had an initial bulk density of 2.03 Mg/m^3, a bitumen content of 14.1% by weight and an index of disturbance of 9.7% (initial porosity of 0.36). The fines content (less than 0.074 mm) of the grain size distribution was 1.7% by weight.

The specimen displays an increase in pore fluid pressure at the beginning of the test due to compression of the sand matrix during the onset of straining. The reduction in effective confining stress results in strain hardening behaviour in the deviatoric stress-strain curve at low

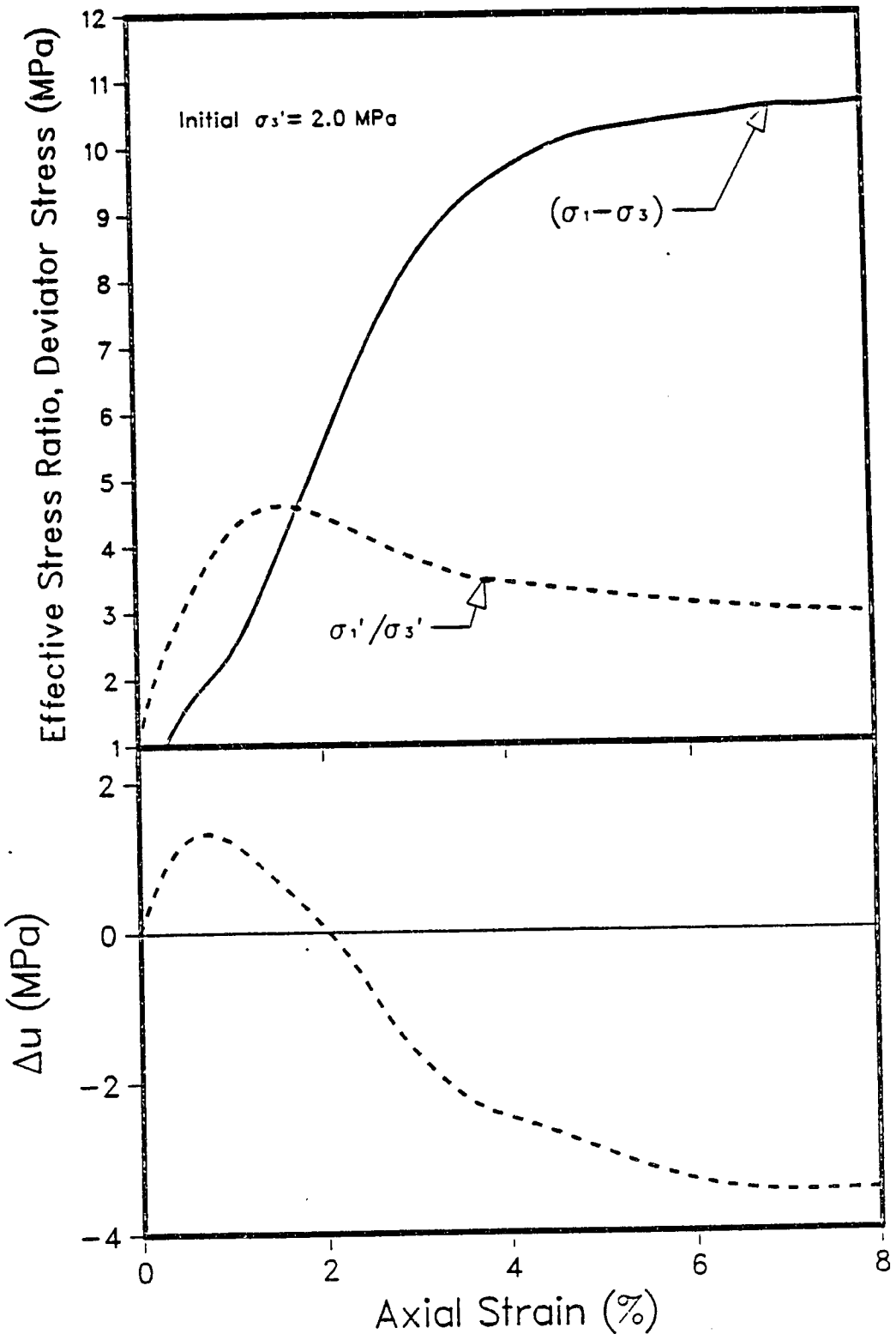

Figure 7.12 Undrained Passive Compression Tests on Rich Oil Sands

strains. As the specimen reaches its peak effective stress ratio, the pore fluid pressure decreases as the sand matrix has a tendency to dilate under the reduced effective confining stress. As the pore fluid pressure falls with continued straining the effective confining stress increases causing a progressive increase in stiffness in the deviatoric stress-strain curve. The pore fluid pressure continues to fall below the initial back pressure in the specimen resulting in a net increase in effective confining pressure of the specimen. The specimen eventually reaches its maximum strength of 10.7 MPa at 8.7% axial strain (not shown in the figure) when the pore fluid pressure levels out.

Plewes (1987) carried out a series of consolidated undrained passive compression tests on high grade Saline Creek oil sands. The important observations and conclusions arising from this study may be summarized as follows:

1. The maximum principal stress ratio decreases with increasing index of disturbance values. Laboratory specimens with index of disturbance values less than 14% and subjected to isotropic stress cycling prior to shear were found to provide adequate representation of in situ stress-strain and strength behaviour.

2. The initial tangent modulus of deformation is less following an undrained passive compression stress path than following a drained passive compression stress path. The undrained and drained modulus values were found to be essentially equivalent, however, when measured under similar stress and strain conditions (i.e., where $\Delta u/\Delta \epsilon = 0$ for undrained tests and where $\Delta v/\Delta \epsilon = 0$ for drained tests).

3. The strain required to reach the maximum stress ratio in undrained compression ranges between 1% and 2% and is equivalent to strains required in drained passive compression. The strain to maximum strength increases with the amount of the pore fluid pressure reduction during the test. Maximum or ultimate strength is reached at the critical confining stress as the dilatancy of the oil sands is suppressed by the higher confining stresses. The strain to failure ranges between 2% for $\sigma_3'_i = \sigma_{crit} = 7.3$ MPa and 14% for $\sigma_{3_i} = 0$.

4. The failure envelope in terms of maximum principal stress ratio representative of in situ strength is defined by Mohr Coulomb parameters $\phi' = 30°$ and $c' = 500$ kPa (mean stresses greater than 4.0 MPa).

The failure envelope is distinctly curved between 1.5 and 4.0 MPa. The failure envelope for undrained tests is less when compared to drained tests but is comparable when drained test results are corrected for volume change during testing by Rowe's stress-dilatancy theory.

5. The maximum or ultimate strength of oil sands following the undrained passive compression stress path is defined as the residual strength for oil sands ($\phi' = 30°$). The high strains required to reach the critical confining stress are sufficient to reduce the angle of shearing resistance of oil sands to the residual angle.

A typical undrained passive compression stress path for the test shown in Figure 7.12, plotted in terms of p'-q, is given in Figure 7.13. The stress path is initially curved toward the origin due to the reduction in σ_3' caused by the increase in pore fluid pressure at the beginning of the test due to compression of the sand matrix during the onset of the stress increase. The volume reduction of the sand matrix results in the pore fluids taking more of the load due to their inability to drain. As the specimen reaches its peak principal stress ratio the pore fluid pressure decreases as

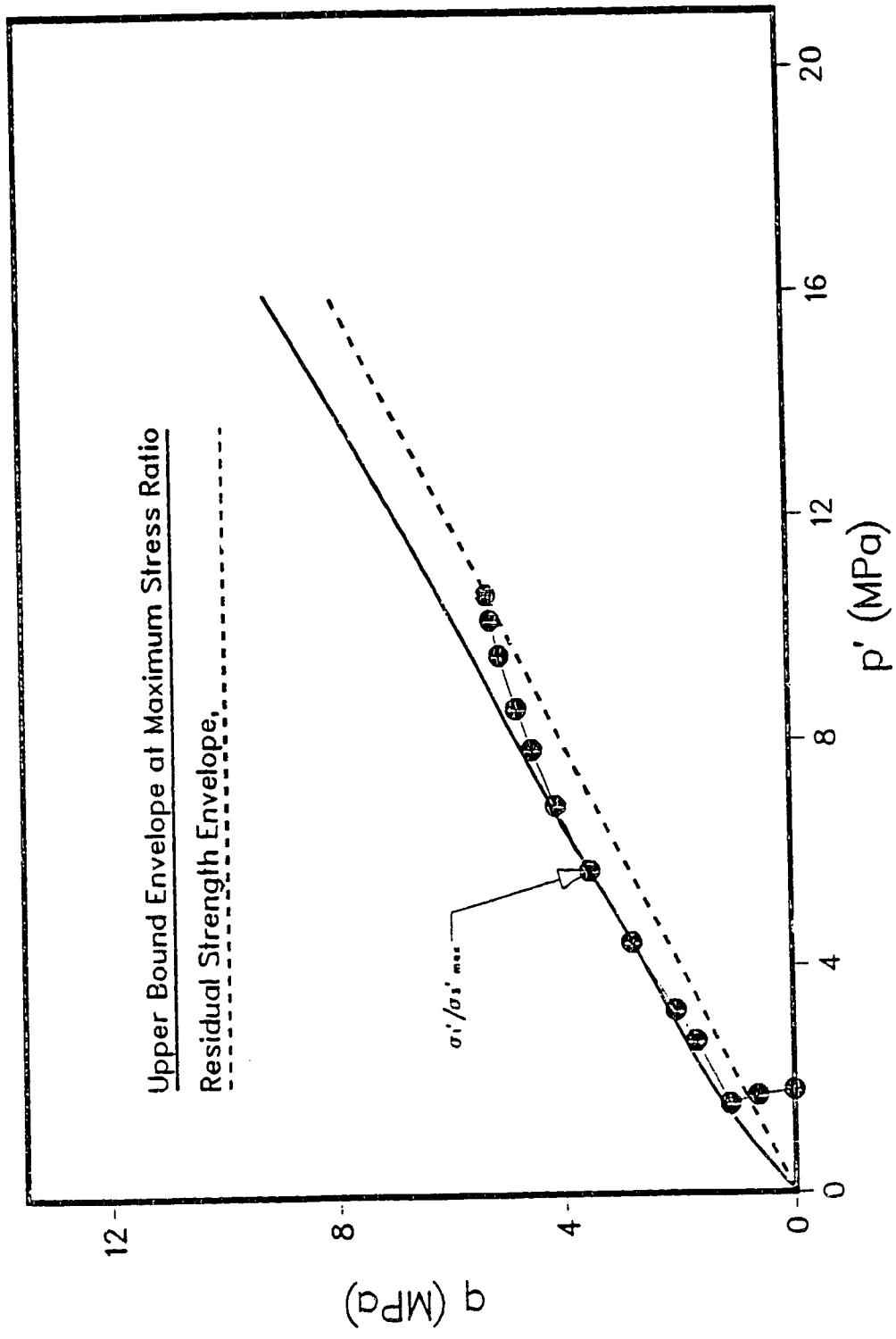

Figure 7.13 Stress Path for Undrained Passive Compression Test Rich Oil Sands

the sand matrix tendency to dilate under the shear strain is suppressed. After attaining its maximum stress ratio, the stress path trends toward the residual strength envelope.

McMurray Formation Estuarine Margin Sedimentation

The undrained shear strength deformation behaviour of McMurray oil sands from the AOSTRA Underground Test Facility site was studied over a range of initial effective confining stresses. Two specimens, UFTOS5 and UFTOS8, contained the discontinuous shale seams with fines content (less than 0.074 mm) of the grain size distributions of approximately 55% by weight. The overall bitumen contents were about 7% by weight. Specimens UFTOS6 and UFTOS7 were high grade, rich oil sands with a bitumen content of 14% by weight and a fines content of approximately 3.4% by weight.

The deviatoric stress-strain and pore pressure response relationships for these specimens tested following undrained passive compression stress paths are shown in Figure 7.14. The initial effective confining stress applied to the test specimens prior to shear ranged from 0.5 to 4.0 MPa. A cyclic stress compressibility test was performed on each sample prior to the undrained shear test. Results for each phase of testing are summarized in Table 7.4.

Rich oil sands Specimens UFTOS6 and UFTOS7 tested under initial effective confining stresses of 0.5 and 1.0 MPa, respectively, each display a slight increase in pore fluid

Table 7.4 Undrained Passive Triaxial Tests - Athabasca McMurray Formation Oil Sands

Initial Conditions

Test Number	Bulk Density (Mg/m3)	Dry Density (Mg/m3)	% water (mass)	% bitumen (mass)	% solids (mass)	% fines	e	Sr (%)	Pore Pressure Parameter B **	Index of Disturbance (%)
UFTOS5	2.13 *	1.86	6.4	6.6	87.1	52.9	0.44	90	0.99	7.3
UFTOS6	1.92	1.59	2.8	14.1	83.0	3.4	0.68	80	1.00	14.5
UFTOS7	1.93	1.58	4.1	14.0	81.9	3.4	0.69	86	0.98	9.8
UFTOS8	2.05 *	1.75	7.3	7.4	85.3	57.3	0.53	97	0.99	10.0

* Low grade, high fines oil sands.

** Note: At 0.2 MPa Effective Confining Stress after saturation at 2.5 MPa Back Pressure

Isotropic Consolidation

Test Number	Volume Change (%) from σ = 0.2 to (•) MPa	Bulk Density (Mg/m3) σ = (•) MPa	Dry Density (Mg/m3) at σ = (•) MPa	K (MPa) Cycled from (• to •) MPa	Void Ratio e	Index of Disturbance (%)
UFTOS5	-3.82 (3.3)	2.21 (3.3)	1.93 (3.3)	288 (2.5 to 3.2)	0.38	-2.4
UFTOS6	-3.86 (5.0)	2.04 (5.0)	1.66 (5.0)	485 (1.0 to 2.0)	0.61	7.7
UFTOS7	-4.85 (3.9)	2.04 (3.9)	1.66 (3.9)	316 (1.0 to 3.9)	0.61	1.6
UFTOS8	-3.46 (5.9)	2.13 (5.9)	1.81 (5.9)	556 (2.0 to 4.0)	0.47	2.5

Undrained Shear Test

Test Number	Effective Confining Stress (MPa)	Back Pressure (MPa)	B	Maximum Shear Strength (MPa)	Axial Strain at Max. Shear Strength (%)	Max. Stress Ratio at (% Strain)	Modulus of Elasticity (MPa)	A at Failure
UFTOS5	2.3	8.0	0.78	4.45	1.48	4.30 (1.32)	405	0.26
UFTOS6	0.5	8.0	0.88	9.75	3.19	5.82 (0.50)	586	-0.29
UFTOS7	1.0	8.0	0.90	5.53 ***	4.17	4.34 (2.81)	200	-0.09
UFTOS8	4.0	8.0	0.82	6.94	3.72	3.34 (1.54)	647	0.14

*** Test stopped prior to peak

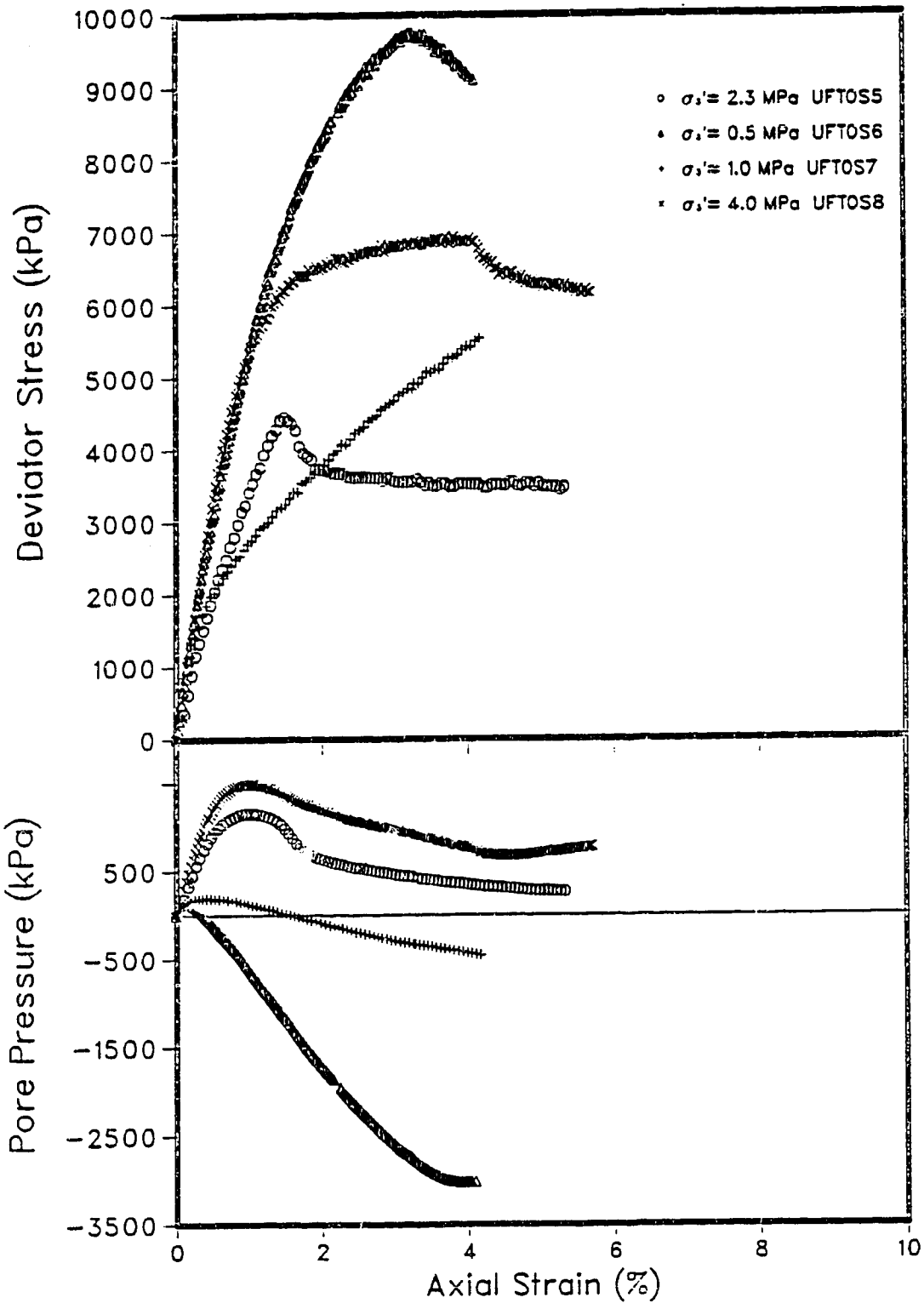

Figure 7.14 Undrained Passive Compression Tests on McMurray Formation Interbedded Oil Sands

pressure followed by a significant pore fluid pressure decrease which falls below the initial back pressure in the specimen resulting in a net increase in effective confining pressure of the specimen. The pore pressures parameter A for these tests were both negative indicating the relatively large decrease in pore fluid pressure during shear. Low grade, high fines content oil sands Specimens UFTOS5 and UFTOS8 tested under initial effective confining stresses of 2.3 and 4.0 MPa, respectively, each display an increase in pore fluid pressure at the beginning of the test. The pore fluid pressure for each specimen then decreases as the soil matrix tends to dilate and levels out and remains constant with a net pore pressure increase.

Initial undrained tangent modulus is plotted against the initial effective confining stress at an axial strain of 0.25% and is shown in Figure 7.15. An axial strain value of 0.25% was used to negate measurement errors associated with seating of the end porous stones and the top loading cap in the triaxial cell. Undrained modulus values obtained from consolidated passive compression tests carried out on high grade McMurray Formation oil sands by Plewes (1987) are also shown. The initial undrained deformation modulus for high fines content oil sands agree favourably with those obtained for rich oil sands.

Undrained failure envelopes plotted in terms of effective stress at the maximum stress ratio and at residual strength ($\phi_r' = 30°$) are shown in Figure 7.16. The failure

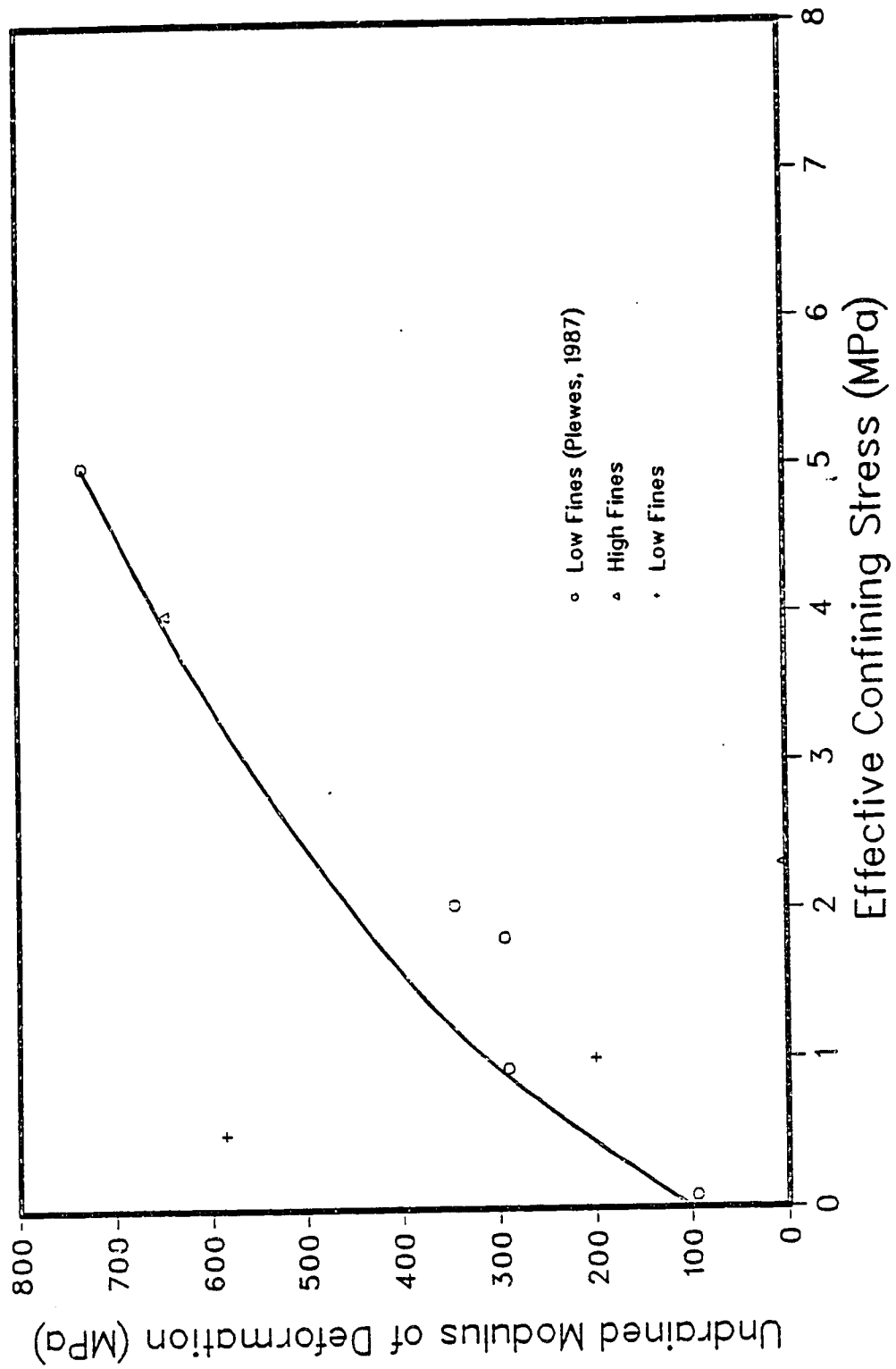

Figure 7.15 Tangent Modulus at 0.25% Strain for Undrained Triaxial Compression on Oil Sands

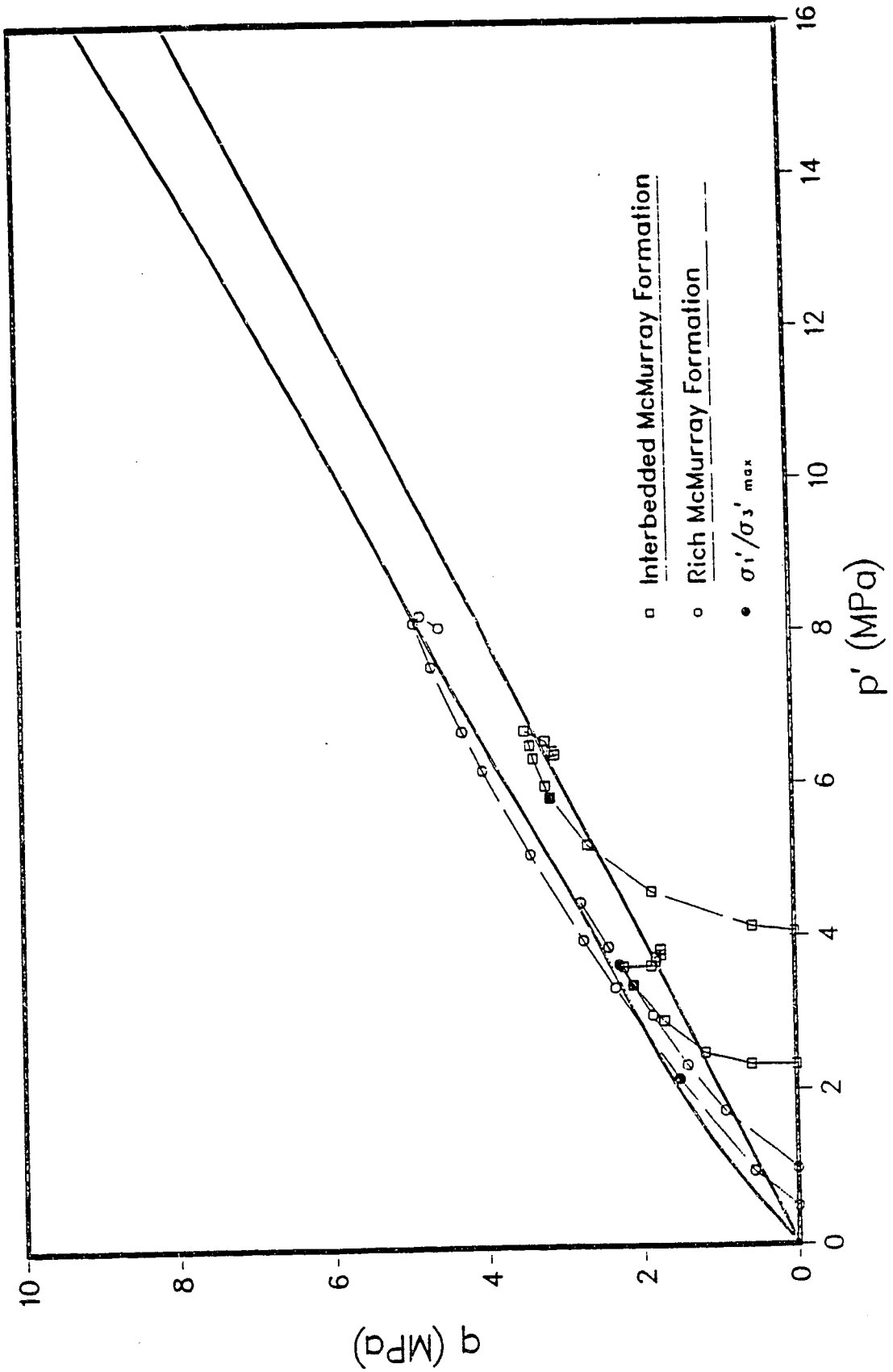

Figure 7.16 Undrained Shear Strength of Athabasca Oil Sands

envelopes, plotted in terms of p'-q are based on consolidated undrained passive compression tests performed on high quality, rich oil sands as reported by Plewes (1987). The effective stress paths for high grade, low fines oil sands and low grade, high fines oil sands obtained from the Underground Test Facility are also illustrated in Figure 7.16. The oil sands specimens approach the upper bound envelope when the maximum principal stress ratio is obtained and thereafter follow or parallel the failure envelope shown in Figure 7.16. The test involving Specimen UFTOS7 (a rich oil sands) was stopped prior to the maximum shear strength being realized. This test is represented in Figure 7.16 as the stress path originating from p' = 1.0 MPa and q = 0 MPa. Although the test was not completed, the maximum stress ratio was reached at the failure envelope and the stress path appears to follow the failure envelope.

The test results indicate that enough shear strain takes place at the maximum principal stress ratio to cause yield in the test specimen. The stress path continues to follow the failure envelope due to the increase in effective confining stress caused by the pore fluid pressure reduction during shear which increases the shearing resistance of the test specimen. The stress path only deviates from the failure envelope when the maximum strength is exceeded and the test specimen assumes a purely plastic state. Thus, the failure criteria for oil sands can be defined in terms of maximum principal stress ratio or maximum shear strength.

Failure in terms of the maximum stress ratio occurs at lower strains (Table 7.4) and is dependent on the pore pressure response of the test specimen which is controlled by the tendency to compress upon initial loading and the onset of shear dilatancy. The pore fluid pressure increase caused by matrix compression at the beginning of the test is the dominant factor in failure as defined by the maximum stress ratio. Failure in terms of the maximum or ultimate shear strength occurs at higher axial strains (Table 7.4) and is dependent on the pore fluid pressure response and the shearing resistance of the soil matrix.

In terms of maximum deviator stress low grade, high fines content oil sands are significantly weaker than rich oil sands tested at the same initial effective confining stress. The maximum deviator stress of rich oil sands specimen tested under an effective confining stress of 2 MPa (Figure 7.12) is approximately 10.5 MPa, twice that measured here for high fines oil sands tested at 2.3 MPa. This higher maximum deviator strength was also accompanied by much larger axial strains and much greater pore fluid pressure reductions which fell well below the initial pore fluid pressures applied to the specimens prior to shear. The high fines content oil sands tested here display a net pore fluid pressure increase which appears to be due to the presence of fines which reduces the oil sands' tendency to dilate at higher confining stresses. This effect was noted in drained passive compression tests shown in Figure 7.10.

The maximum stress ratio and axial strain to maximum stress ratios of high fines oil sands are similar to those reported by Plewes (1987) for rich oil sands measured on test specimens at similar initial effective confining stresses. This may be due to the similar compressibility characteristics at the onset of loading of the two materials which controls the pore pressure response of the materials at low strains. Because initial failure is defined by the maximum stress ratio, the two materials fall on approximately the same failure envelope as shown in Figure 7.16.

7.5 Drained Unloading Stress Paths

McMurray Formation Estuarine Sand

The deviatoric stress-strain and volume change relationship for a high grade, low fines McMurray Formation oil sands specimen tested following a drained J_1 constant compression stress path is shown in Figure 7.17. The J_1 constant compression stress path is a proportional loading stress path where the axial effective stress is increased while the radial stress is simultaneously decreased such that the first stress invariant J_1 $(\sigma_1' + \sigma_2' + \sigma_3'/3)$ remains constant. This stress path is shown in Figure 7.2 as a line perpendicular to the isotropic pressure line where

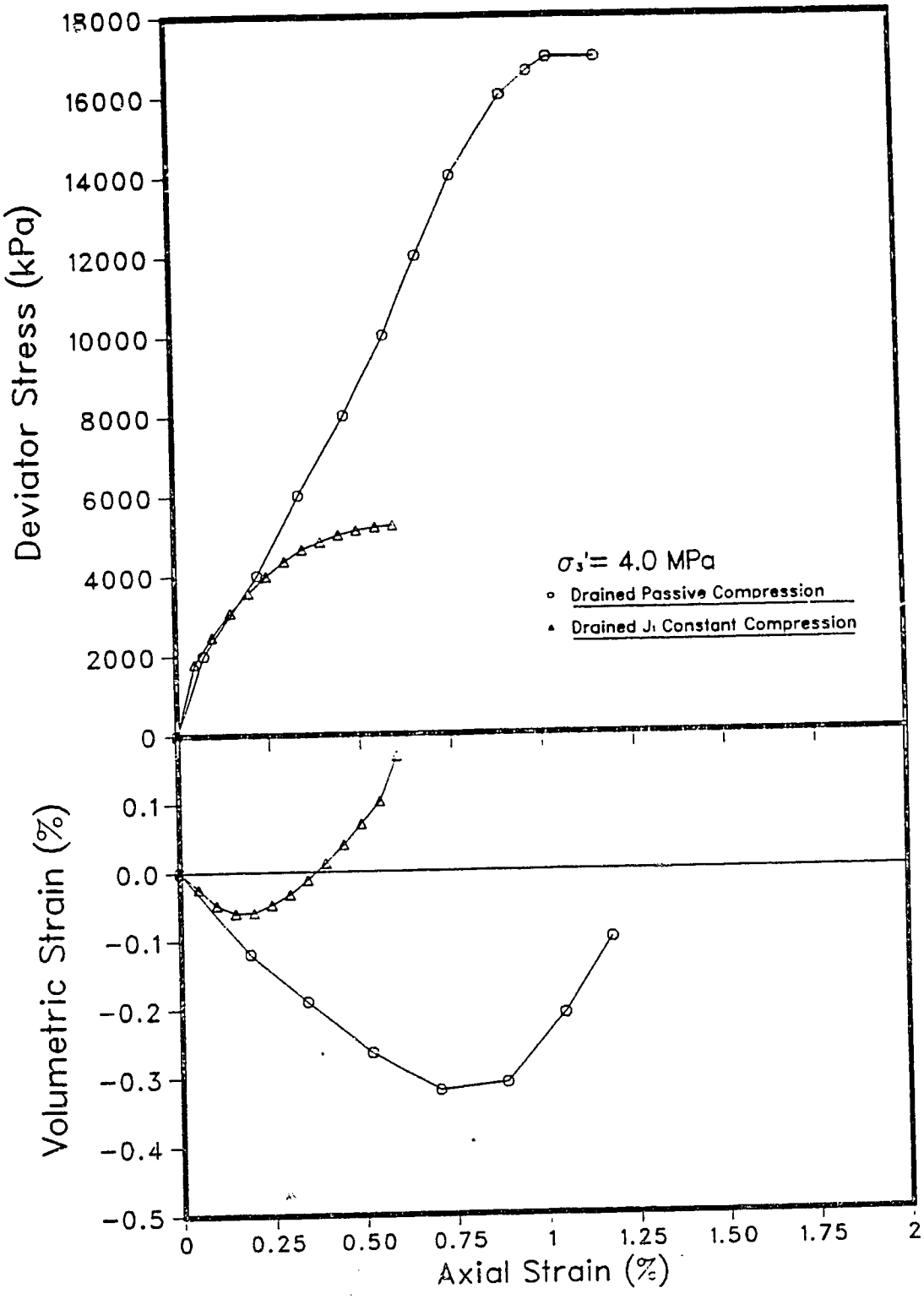

Figure 7.17 Stress Path Testing of Rich Low Fines McMurray Formation Oil Sands

the sum of the principal effective stresses is constant. Stress changes occurring around a deep well bore, shaft or tunnel during excavation are typical examples simulated by following this stress path. For comparative purposes, a rich oil sands specimen tested following the standard drained passive compression stress path is also shown. The initial index of disturbance values for both specimens were less than 8%.

The effects of varying the stress path applied to rich oil sands specimens on stress-strain behaviour are noted:

1. The peak deviator stress is significantly greater following the drained passive compression stress path than following the drained J_1 constant stress path. Both stress paths originate with all-round effective stresses equal ($\sigma_a' = \sigma_r'$) to 4 MPa. As external stresses are applied to the specimens the progressive combinations of effective stresses which act on each specimen during the shear tests are considerably different. During drained passive compression the axial stress (σ_a') is increased while the radial stress (σ_r') remains constant. The sum of the principal effective stresses ($\sigma_1' + \sigma_2' + \sigma_3'$) therefore increases and there is a substantial increase in average principal effective confining stress by the time failure is reached. In the J_1 constant compression test, however, the average

principal effective stress remains constant. As a result, the peak deviator stress or shear strength is higher in the passive compression test due to the higher effective confining stress.

2. There is a marked increase in dilatancy during J_1 constant compression, again reflecting the lower effective confining stress experienced by the specimen as shear stresses are applied.

3. The axial strain to failure is smaller and the initial tangent modulus is greater during J_1 constant compression. This reflects the smaller strain required to mobilize shear strength under the lower and constant effective confining stress.

A failure envelope plotted in terms of the major principal effective stress, σ_1', and the resultant of the intermediate principal effective stresses, σ_2' and σ_3', where $\sigma_2' = \sigma_3'$ is shown in Figure 7.18. The failure envelope is based on consolidated triaxial compression tests performed on high quality, rich oil sands as reported by Agar (1984). The shear strength of rich oil sands following the J_1 constant and passive compression stress paths are

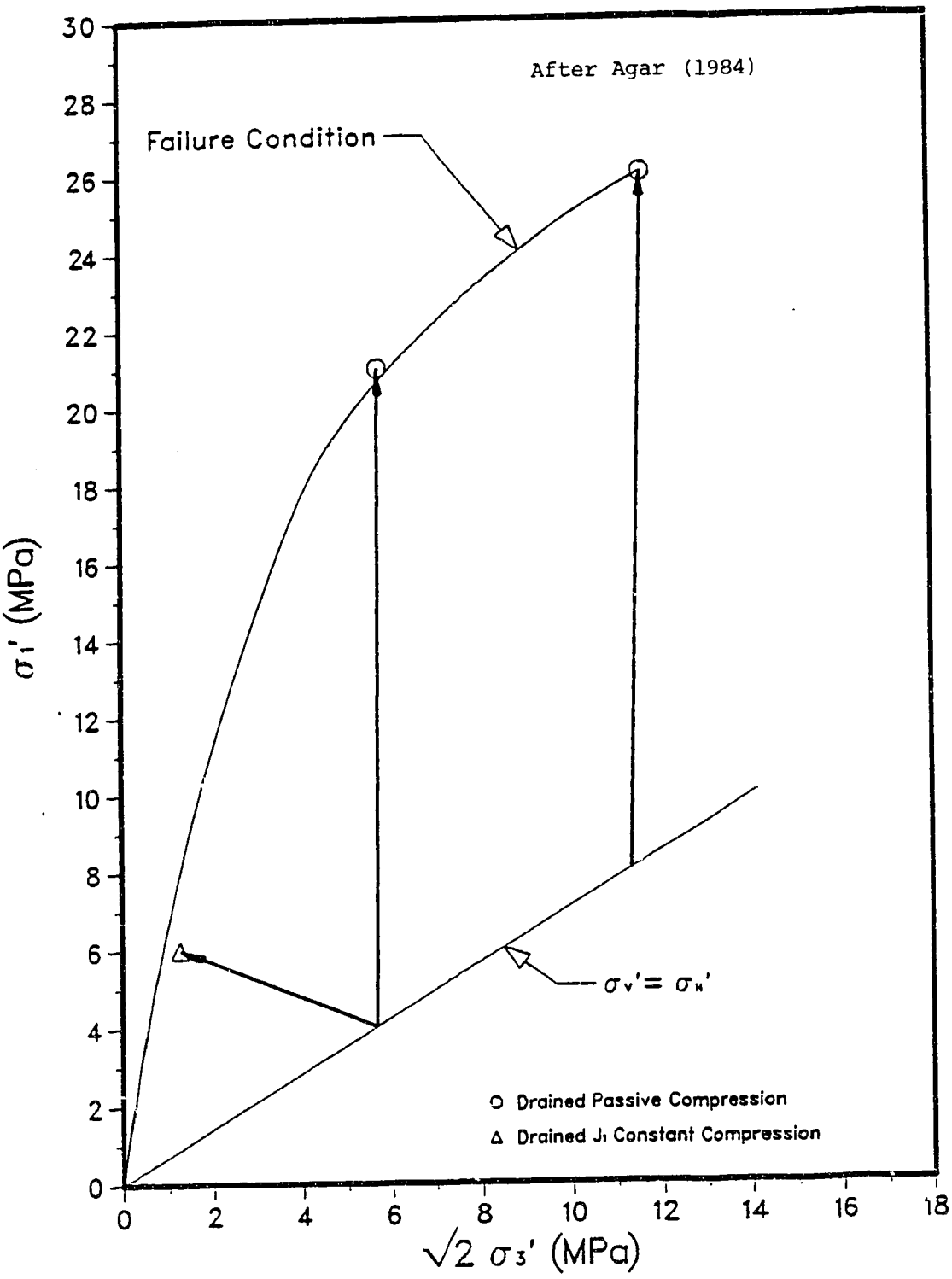

Figure 7.18 Effect of Stress Path on Strength of Low Fines Oil Sands

also shown. The stress paths terminate at failure points which lie approximately on the same failure envelope.

Estuarine Channel Margin Sedimentation

The deviatoric stress-deviatoric strain and volume change relationships for McMurray Formation oil sands tested following several drained unloading stress paths is shown in Figure 7.19. Test specimens were obtained from core samples taken in the McMurray Formation at the AOSTRA Underground Test Facility over a depth range of 152 m to 161 m. Test Specimens UFTOS9, UFTOS10 and UFTOS12 consisted of fine grained oil sands with overall bitumen contents ranging from 7 to 9.5% by weight. Each specimen contained thin, discontinuous shale seams. The fines content (less than 0.074 mm) of the grain size distribution ranged from 38 to 72%. Specimen UFTOS14 was a high grade, rich oil sands with a bitumen content of 15.5% by weight and a fines content of 3.0% by weight.

The specimens were tested under similar initial effective confining stresses of about 2.5 MPa which approximates the in situ average effective stress. A cyclic stress compressibility test was carried out on each specimen prior to performing the shear tests. Results for each phase of testing are summarized in Table 7.5.

The significant effect of stress path on stress-strain behaviour and peak deviatoric stress is demonstrated by

Table 7.5 Consolidated Drained Stress Path Triaxial Tests - Athabasca McMurray Formation Oil Sands

Initial Conditions

Test Number	Bulk Density (Mg/m3)	Dry Density (Mg/m3)	% water (mass)	% bitumen (mass)	% solids (mass)	% fines	e	Sr (%)	Pore Pressure Parameter B **	Index of Disturbance (%)
UFTOS9	1.96	1.64	7.8	8.8	83.4	57.3	0.62	85	0.99	10.9
UFTOS10	2.06	1.77	6.6	7.3	86.1	71.9	0.50	86	0.98	10.8
UFTOS12	1.98	1.65	7.0	9.5	83.4	37.7	0.60	87	0.97	9.6
UFTOS14	1.91	1.56	2.7	15.5	81.8	3.0	0.70	85	0.99	10.6

** Note: At 0.2 MPa Effective Confining Stress after saturation at 2.5 MPa Back Pressure

Isotropic Consolidation

Test Number	Volume Change (%) from σ = 0.2 to (*) MPa	Bulk Density (Mg/m3) σ = (*) MPa	Dry Density (Mg/m3) at σ = (*) MPa	K (MPa) Cycled from (* to *) MPa	Void Ratio e	Index of Disturbance (%)
UFTOS9	-4.12 (4.5)	2.06 (4.5)	1.71 (4.5)	461 (1.6 to 4.5)	0.55	3.2
UFTOS10	-4.39 (4.6)	2.15 (4.6)	1.85 (4.6)	413 (1.5 to 4.6)	0.43	0.6
UFTOS12	-4.11 (4.2)	2.07 (4.2)	1.72 (4.2)	416 (1.3 to 4.2)	0.54	1.8
UFTOS14	-2.99 (4.5)	2.00 (4.5)	1.61 (4.5)	475 (1.5 to 4.5)	0.65	5.7

Drained Shear Test

Test Number	Effective Confining Stress (MPa)	Back Pressure (MPa)	B	Deviator Stress at failure (MPa)	Axial Strain at failure (%)	Volumetric Strain at failure (%)	Modulus of Elasticity (MPa)	Stress Path
UFTOS9	2.5	2.5	0.88	3.00	2.11	0.05	1334	J1 (Compression)
UFTOS10	2.5	2.5	0.83	1.64	0.81	0.81	1014	Active Compression
UFTOS12	2.5	2.5	0.68	3.98	-3.05	0.10	875	J1 (Extension)
UFTOS14	2.3	2.5	0.62	4.08	1.05	0.91	2603	J1 (Compression)

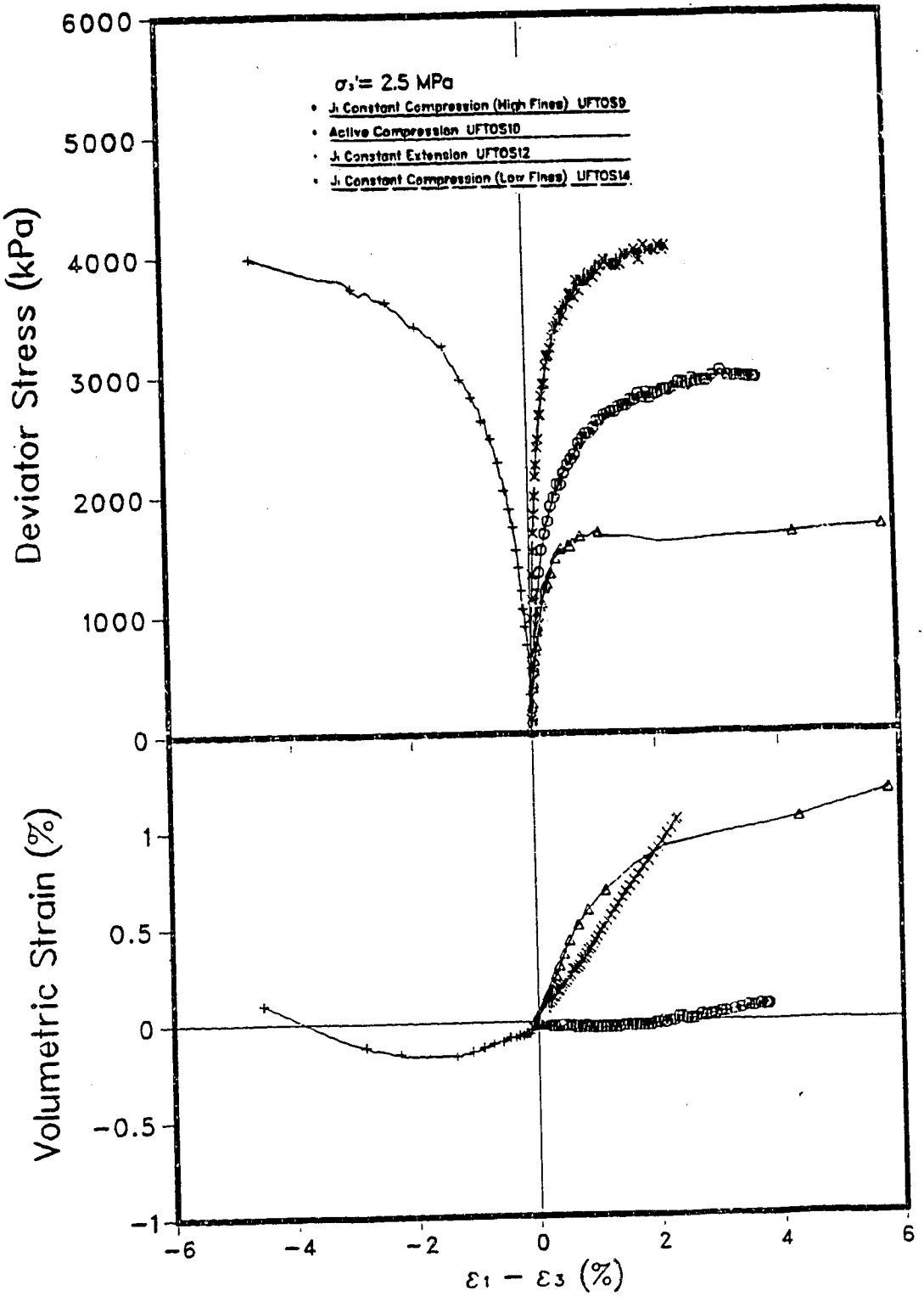

Figure 7.19 Stress Path Testing of McMurray Formation Interbedded Oil Sands

comparing Figure 7.19 and the stress path followed by each of the specimens, plotted in terms of p'-q, as shown in Figure 7.20.

1. The active compression stress path was performed by reducing the radial stress while holding the axial stress constant. This stress path is illustrated in Figure 7.2 as a line originating on the all-round effective stress line and moving horizontally toward the axial stress axis. During this test the specimen experiences a net reduction in average principal effective confining stress as shown in Figure 7.20. This results in a lower peak deviator stress, higher dilatancy and lower deviatoric strain to failure when compared to the other stress paths shown in Figure 7.19.

2. The J_1 constant extension stress path is a proportional unloading stress path where the axial effective stress is decreased while the radial stress is simultaneously increased such that the first stress invariant J_1 remains constant. This stress path is illustrated in Figure 7.2 as a line perpendicular to the isotropic pressure line where the sum of the principal effective stresses is constant. During this shear test the specimen does

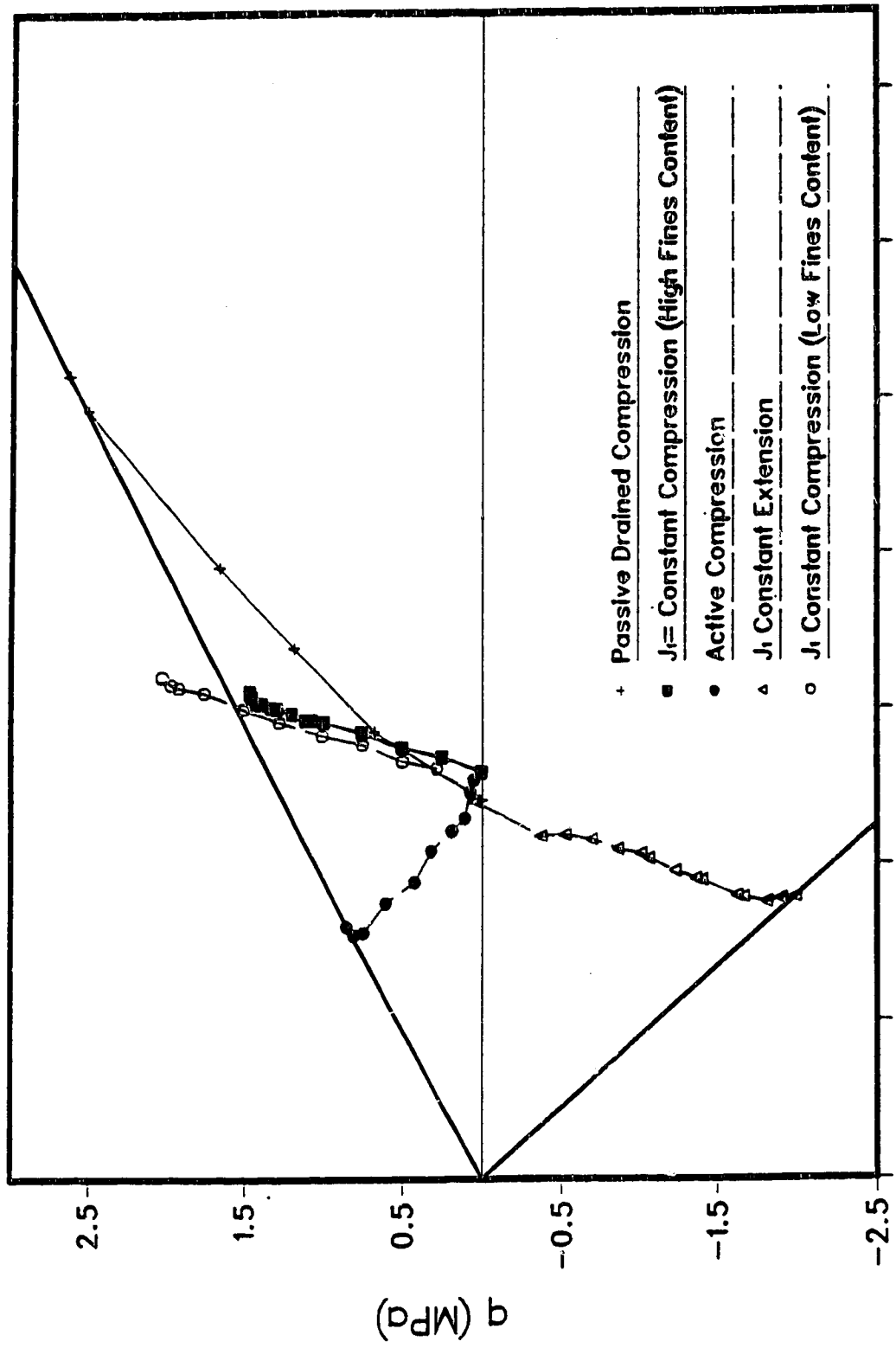

Figure 7.20 Shear Strength of Athabasca Interbedded Oil Sands From Stress Path Tests

not experience a net change in average principal effective confining stress. The peak deviator stress is higher, the dilatancy is less pronounced and the deviatoric strain to failure is higher than the shale interbedded specimens tested following the active compression stress path. It is noted that this specimen displays a significant strain hardening response (significant curvature in stress-strain curve to peak deviator stress).

3. The J_1 constant compression stress path is a proportional loading stress path where the axial effective stress is increased while the radial stress is simultaneously decreased such that the first stress invariant J_1 remains constant. This stress path is shown in Figure 7.2 as a line perpendicular to the isotropic pressure line. During this test the specimen, as in the case of the J_1 constant extension stress path, does not experience a net change in average principal effective confining stress. As expected, the specimen is stiffer and less dilatant than the specimen subjected to the active compression stress path.

It is noted that the rich oil sands specimen is stronger, stiffer and more dilatant than the shale interbedded specimen following the J_1 constant drained compression stress path (Figure 7.19). This trend was also observed during both passive drained and passive undrained compression stress path tests. The weaker, more compressible shale strata interbedded in the oil sands appears to have a significant effect on the overall stress-strain characteristics of the formation regardless of stress path followed.

A drained failure envelope (k_f-line) derived from passive compression, J_1 constant compression and active compression stress path tests on interbedded McMurray Formation oil sands is plotted in Figure 7.20. The failure line is defined by the Mohr-Coulomb parameters $c' = 0$ and $\phi' = 30°$. The J_1 constant extension stress path terminates at a failure point below the all-round pressure line shown in Figure 7.2 (p' axis in Figure 7.20). This point where the deviatoric stress is maximum is indicative of the extension failure envelope.

The stress-strain relationships of interbedded McMurray Formation oil sands shows a strong stress path dependency. This is illustrated by comparing the initial tangent modulus from different stress paths as shown in Table 7.6. The conventional passive drained compression test exhibited smaller moduli of deformation than did the J_1 constant compression, active compression and J_1 constant extension

Table 7.6 Effect of Stress Path on Initial Tangent Modulus of Deformation

Test Number	Initial Effective Confining Stress (MPa)	Stress Path	Fines Content (< 0.074 mm) % by mass	Initial Tangent Modulus, E (MPa)
UFTOS2	2.5	Passive Drained Compression	55.2	323
UFTOS5	2.3	Passive Undrained Compression	57.3	405
UFTOS9	2.5	J1 = Constant (Compression)	36.2	1334
UFTOS10	2.5	Active Compression	71.9	1014
UFTOS12	2.5	J1 = Constant (Extension)	37.7	875

tests. The results from passive drained and passive undrained compression tests, however, gave similar results. It is noted that the initial tangent moduli for the passive undrained and the J_1 constant compression stress paths should be similar due to the similarity in the initial stress increment direction (Figure 7.2, paths B and C). The dissimilar moduli values are attributed to specimen variability.

The strength variation with axial strain for the various drained stress paths is illustrated in Figure 7.21. The J_1 constant extension stress path yielded negative axial strains during shear. As noted in Figure 7.2 the results of this test appear below the isotropic stress line and terminate at a failure point on the extension failure envelope. Although this test is not directly comparable to the other compression stress paths, it is included in Figure 7.21 for illustrative purposes. The specimen subjected to the active compression stress path in which the average principal effective confining stress decreases during loading develops the vast majority of shearing strength at relatively low axial strains. For the J_1 constant compression and passive compression stress paths the initial rate at which shear strength develops decreases as the rate of effective confining stress applied to the specimen during the test is reduced.

Figure 7.21 demonstrates that the strains to failure vary significantly with stress path. This indicates that

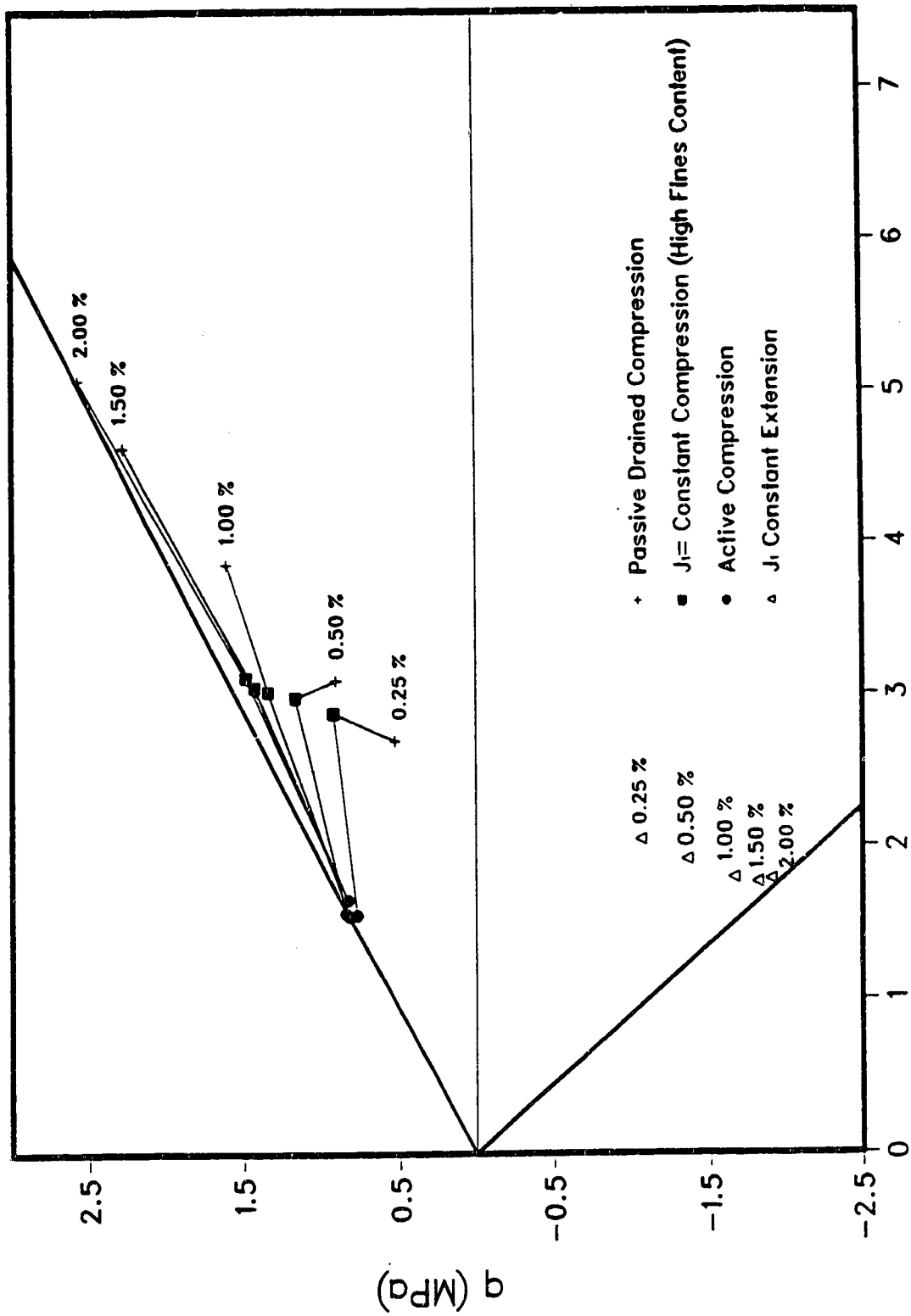

Figure 7.21 Axial Strain Contours for Various Stress Paths

depending on the stress path followed, the strain at which mobilization of shear strength occurs can be significantly different from the conventional passive drained compression test. Depending on the loading (or unloading) conditions, geotechnical parameters (particularly deformability) derived from standard triaxial testing and used in analyses will not correctly predict field performance. It is, therefore, important to test oil sands and related strata under conditions appropriate to the method of in situ production.

7.6 Effect of Elevated Temperatures

McMurray Formation Estuarine Sand

The effect of temperature increases on stress-strain behaviour and shear strength of high quality, low fines McMurray Formation oil sands has been studied by Agar (1984). Shear strength data at temperatures of 20°C, 125°C and 200°C as measured in drained triaxial tests are plotted in the form of a p'-q diagram as shown in Figure 7.22. The maximum shear strength of rich oil sands is relatively insensitive to temperatures up to 200°C.

The major conclusions reached by Agar (1984) regarding the influence of temperature on stress-strain behaviour are summarized below:

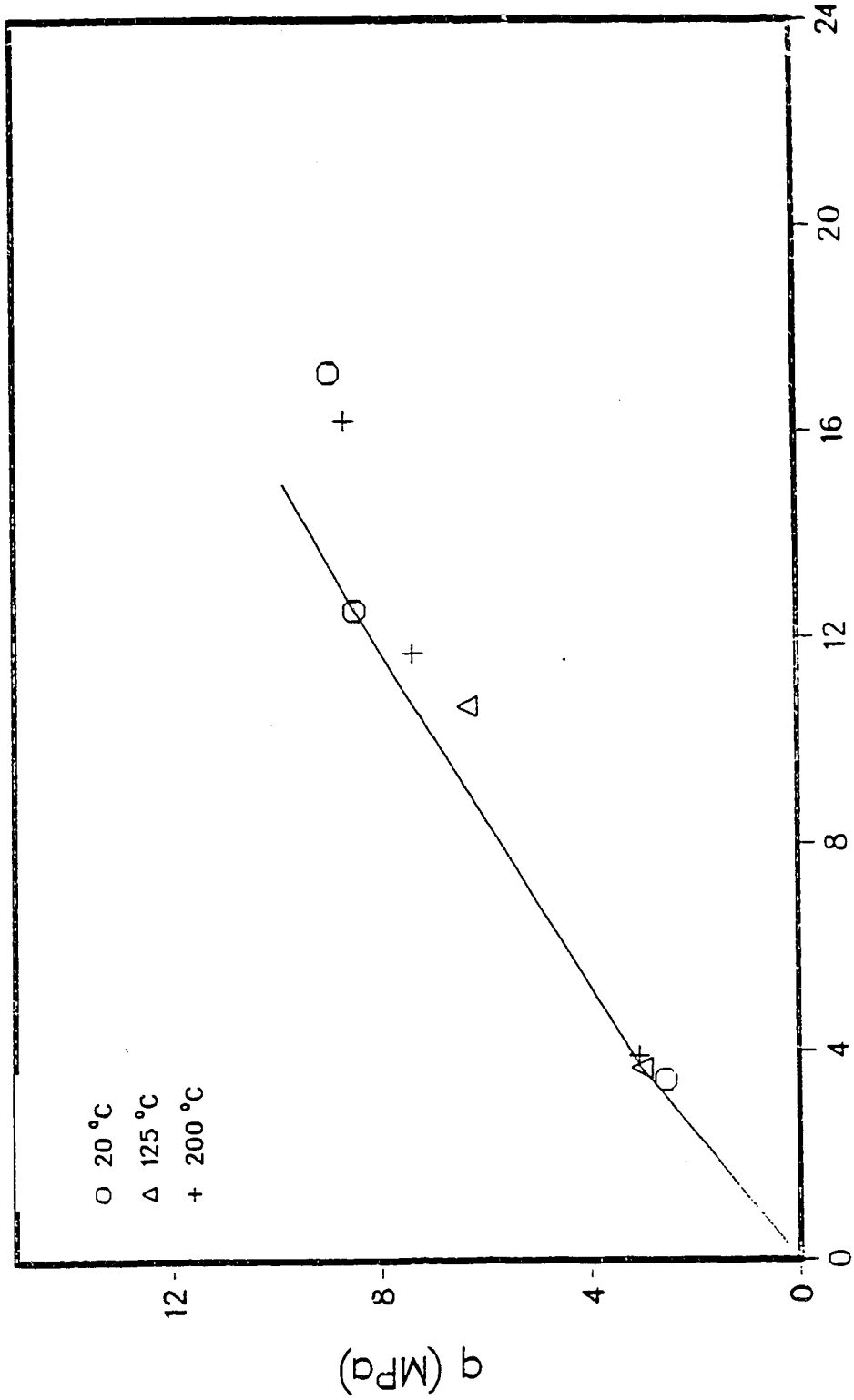

Figure 7.22 Effect of Temperature on Strength of Low Fines Oil Sands

1. Initial tangent modulus was found to increase slightly at elevated temperatures. The modulus, however, was observed to be higher at 125°C than at 200°C.

2. Volumetric compression during the application of shear stresses was suppressed slightly at elevated temperatures.

3. Dilatent volume change below peak deviator stress was increased at elevated temperatures. Dilatancy, however, was found to be higher at 125°C than at 200°C.

Rich McMurray Formation oil sands consist of a uniformly graded quartz sand. The shear strength and stress-strain behaviour of oil sands at elevated temperatures depends on the strength of the mineral grains at higher temperatures and on the amount of grain breakage and particle rearrangement which occurs during heating. The quartz sand grains appear to be highly resistant to physical breakdown during heating at elevated temperatures and pressures.

McMurray Formation Channel Margin Sedimentation

A series of triaxial tests performed on oil sands obtained from a core sample taken at the Underground Test Facility at a depth of approximately 155 m following the drained passive compression stress path at 225°C are shown in Figure 7.23. The procedure used in the high temperature tests was the same as that used in the 20°C tests up to and including the cyclic compressibility test. After isotropic consolidation the specimen was heated under fully drained conditions to 225°C under the effective confining stress to be used in the shear test. During the heating the volume of pore fluid leaving the specimen (heat consolidation) was monitored. After the specimen reached the test temperature a cyclic stress compressibility test was carried out to assess any changes in the sand matrix compressibility caused by heat consolidation. Each stage of each test is summarized in Table 7.7.

Specimen UFHTTOS1 was comprised of fine grained oil sands interbedded with frequent thin seams and clasts of shale. The overall bitumen content was 7% by weight and fines content (less than 0.074 mm) of the grain size distribution was 51% by weight. Specimens UFHTTOS2 and UFHTTOS3 consisted of uniform, rich oil sands with fines contents of about 5% by weight.

Figure 7.24 is a plot of stress-strain curves comparing passive drained compression tests for high fines content

Table 7.7 Drained Passive Triaxial Tests - Athabasca McMurray Formation Oil Sands at 225 °C

Initial Conditions at 20 °C

Test Number	Bulk Density (Mg/m3)	Dry Density (Mg/m3)	% water (mass)	% bitumen (mass)	% solids (mass)	% fines	e	Sr (%)	Pore Pressure Parameter B **	Index of Disturbance (%)
UFHTTOS1	1.99	1.73	6.2	7.0	86.8	51.3	0.53	75	0.99	21.2
UFHTTOS2	1.96	1.65	0.8	14.8	84.4	5.2	0.60	81	0.98	14.3
UFHTTOS3	1.96	1.62	5.2	12.4	82.4	4.5	0.64	88	0.93	8.1

** Note: At 0.5 MPa Effective Confining Stress after saturation at 2.5 MPa Back Pressure

Isotropic Consolidation and Drained Heating to 225 °C

Test Number	Volume Change (%) from σ = 0.2 to (•) MPa at 20 °C	K (MPa) at 20°C Cycled from (• to •) MPa	Total Vol. Ch. (%) 20-225 °C at σ = (•) MPa	K (MPa) at 225 °C Cycled from (• to •) MPa	Void Ratio e 20°C	Void Ratio e 225°C	Index of Disturbance (%) 20°C	Index of Disturbance (%) 225°C
UFHTTOS1	-3.24 (5.0)	609 (2.5-5.0)	-6.79 (2.5)	2255 (2.5-4.0)	0.48	0.43	13.6	4.7
UFHTTOS2	-3.44 (6.0)	1101 (4.0-6.0)	-7.49 (4.0)	1617 (4.0-5.0)	0.55	0.48	7.5	-1.1
UFHTTOS3	-3.83 (5.4)	505 (1.0-5.4)	-9.17 (1.0)	2200 (1.3-2.6)	0.58	0.49	1.3	-9.0

Drained Shear Test

Test Number	Effective Confining Stress (MPa)	Back Pressure (MPa)	B	Deviator Stress at failure (MPa)	Axial Strain at failure (%)	Volumetric Strain at failure (%)	Modulus of Elasticity (MPa)	Poisson's Ratio
UFHTTOS1	2.3	7.6	0.60	6.52	2.63	0.127	498	0.16
UFHTTOS2	3.8	7.6	0.60	14.72	1.79	0.326	1179	0.10
UFHTTOS3	1.1	7.5	0.68	4.66	1.09	1.208	567	----

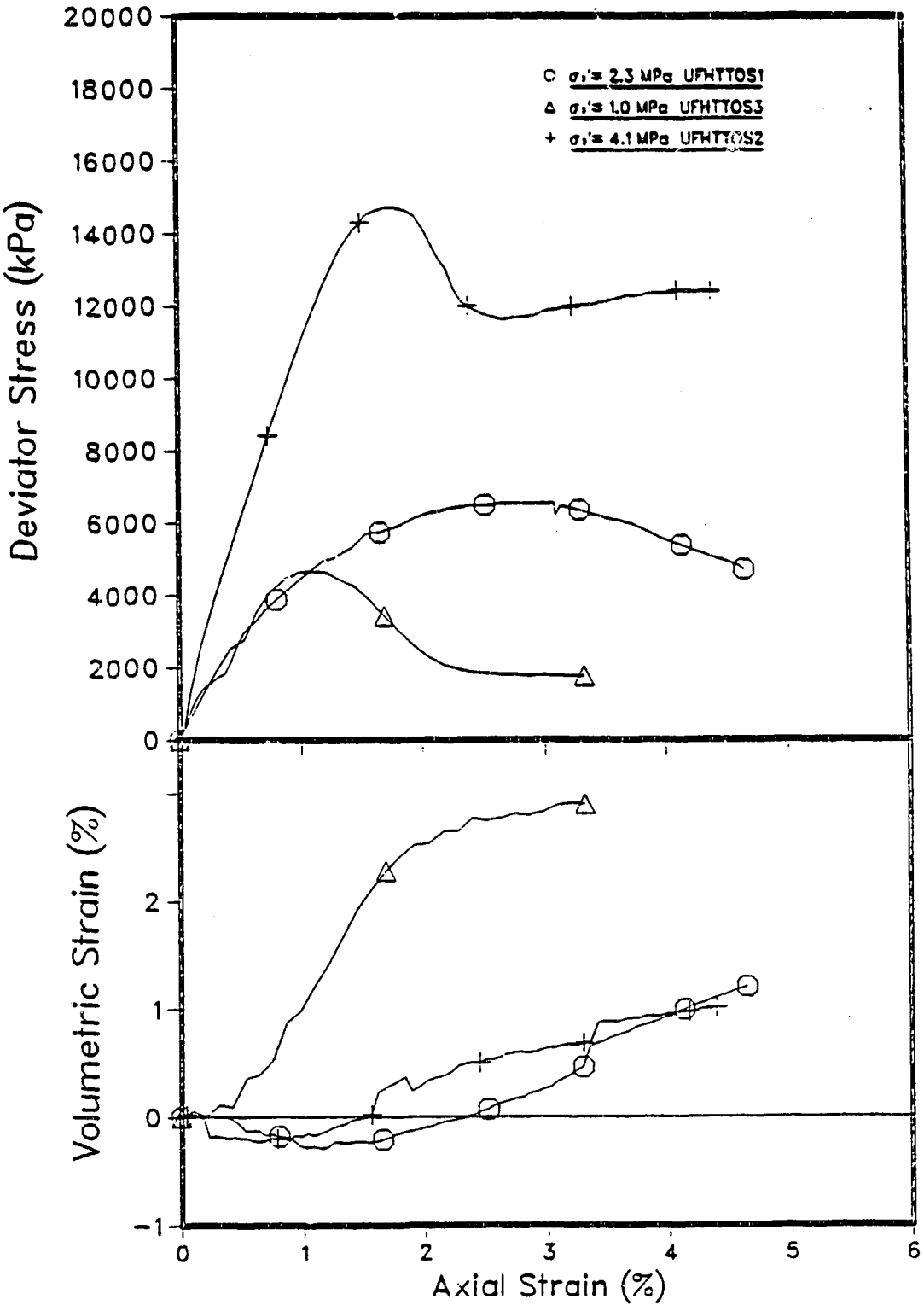

Figure 7.23 Drained Passive Compression Test on McMurray Formation Oil Sands at 225 °C

specimens UFTOS2 tested at 20°C and UFHTTOS1 tested at 225°C. The physical properties of both specimens were similar. Each specimen had a solids content of about 86% by weight, a fines content of about 50% by weight and an initial void ratio of about 0.52. Specimen UFHTTOS1 was slightly more compressible than UFTOS2 when cycled over a similar range of stress at 20°C but was significantly less compressible when cycled over the same range of stress at 225°C. The peak deviator stress and initial stress-strain modulus of high fines content McMurray Formation oil sands is higher at 225°C. The difference in shear strength and initial stiffness is attributed to heat consolidation of the thin, discontinuous shale seams as reflected in void ratio values prior to shear (0.45 for Specimen UFTOS2 and 0.43 for Specimen UFHTTOS1). Dilatant volume change is more pronounced at 225°C.

Figure 7.25 compares the stress-strain behaviour of low fines oil sands subjected to drained passive compression at elevated temperatures with 4 MPa effective confining stress. The specimen tested at 200°C was obtained from a surface outcrop south of Fort McMurray by Agar (1984). The fines content of this specimen was 5.2% by mass. A comparison between this test and Test UFHTTOS2 suggests that low fines McMurray Formation oil sands obtained from surface outcrops show similar strength-deformation behaviour at elevated temperatures as specimens obtained at depth.

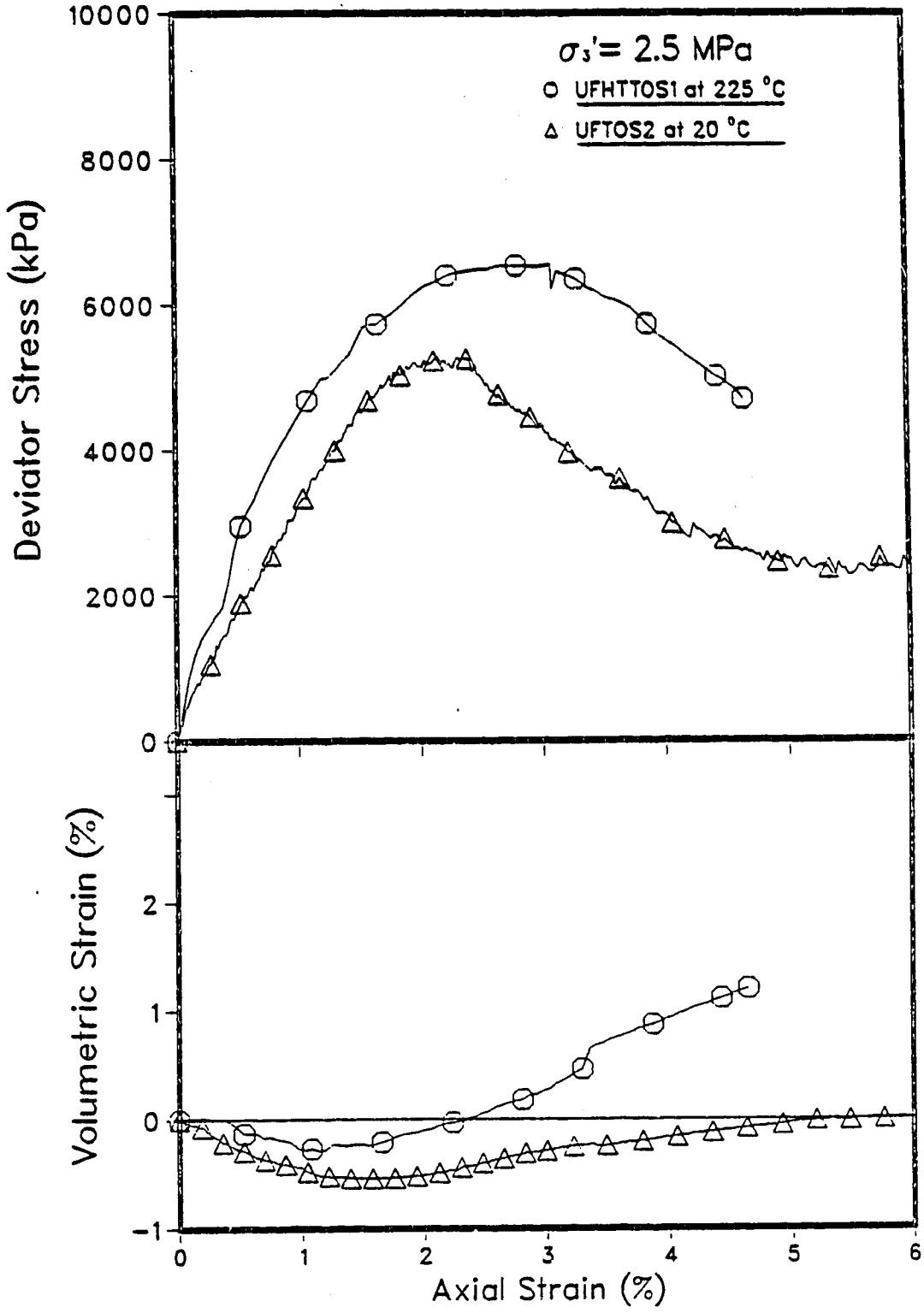

Figure 7.24 Effect of Temperature on Stress–Strain Behaviour of High Fines Oil Sands

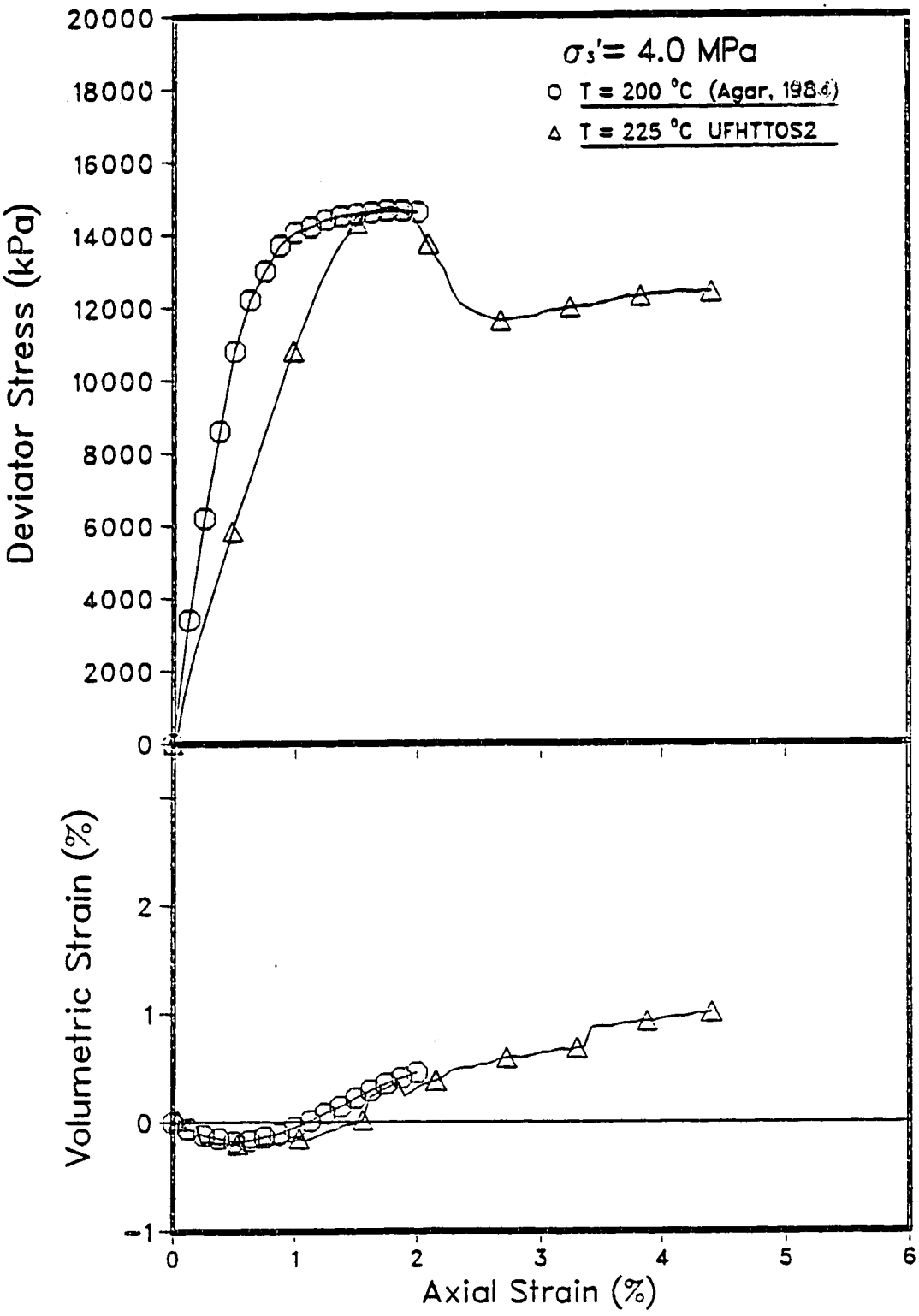

Figure 7.25 Drained Passive Compression Test on McMurray Formation Oil Sands at Elevated Temperatures

The shear strength data on low fines and high fines content McMurray Formation oil sands at 20°C and elevated temperatures are summarized in Figure 7.26. Failure envelopes are shown for low fines and high fines oil sands. Although heat consolidation of shale interbedding appears to increase the strength of high fines oil sands, it is still low when compared to low fines, rich oil sands. It is noted that temperature increases also significantly increase the pore fluid pressure and if pore pressure dissipation cannot occur at the same rate as the temperature increase, the drop in effective stress can cause a considerable decrease in the shear strength. Low permeability shale seams may be a significant barrier to pore fluid drainage in highly interbedded oil sands. The available shear strength in this geotechnical facies during in situ production may therefore be critical for the design of well casings, tunnels or shafts passing through or lying in this strata.

Three triaxial shear tests were performed on high fines, low grade McMurray Formation oil sands following the undrained passive compression stress path at 225°C. The fines content of the test specimens averaged about 55% by weight. The stress-strain and pore fluid pressure response relationships for these specimens are shown in Figure 7.27. The results for each phase of testing are summarized in Table 7.8.

Each of the specimens display an increase in pore fluid pressure at the beginning of the test followed by a pore

Table 7.8 Undrained Passive Triaxial Tests - Athabasca McMurray Formation Oil Sands at 225 °C

Initial Conditions at 20 °C

Test Number	Bulk Density (Mg/m3)	Dry Density (Mg/m3)	% water (mass)	% bitumen (mass)	% solids (mass)	% fines	e	Sr (%)	Pore Pressure Parameter B **	Index of Disturbance (%)
UFHTTOS4	2.04	1.77	4.5	8.6	86.9	48.4	0.49	81	0.98	16.0
UFHTTOS5	2.06	1.80	7.2	5.2	87.6	56.7	0.47	80	0.96	17.0
UFHTTOS6	2.04	1.75	7.8	6.3	85.9	65.5	0.51	85	0.98	11.8

** Note: At 0.5 MPa Effective Confining Stress after saturation at 2.5 MPa Back Pressure

Isotropic Consolidation and Drained Heating to 225 °C

Test Number	Volume Change (%) from σ' = 0.2 to (•) MPa at 20 °C	K (MPa) at 20°C Cycled from (• to •) MPa	Total Vol. Ch. (%) 20-225 °C at σ' = (•) MPa	K (MPa) at 225 °C Cycled from (• to •) MPa	Void Ratio e 20°C	Void Ratio e 225°C	Index of Disturbance (%) 20°C	Index of Disturbance (%) 225°C
UFHTTOS4	-3.31 (4.5)	470 (2.5-4.5)	-7.80 (2.5)	1668 (2.5-4.0)	0.45	0.38	7.9	-3.9
UFHTTOS5	-2.97 (6.3)	749 (4.0-6.3)	-8.19 (4.0)	2079 (4.5-5.5)	0.42	0.35	9.3	-5.3
UFHTTOS6	-3.65 (2.5)	165 (1.0-2.5)	-7.95 (1.0)	1362 (1.0-2.0)	0.46	0.39	3.5	-7.1

Undrained Shear Test

Test Number	Effective Confining Stress (MPa)	Back Pressure (MPa)	B	Maximum Shear Strength (MPa)	Axial Strain at Max. Shear Strength (%)	Max Stress Ratio at Strain (%)	Modulus of Elasticity (MPa)	A at Failure
UFHTTOS4	2.4	7.7	0.50	7.95 ***	4.56	3.04 (1.79)	504	-0.66
UFHTTOS5	4.3	7.4	0.56	7.68 ***	4.66	2.86 (1.77)	1232	-0.16
UFHTTOS6	1.0	7.5	0.79	2.68	1.83	2.83 (1.60)	199	-0.12

*** Test Stopped Prior to Peak

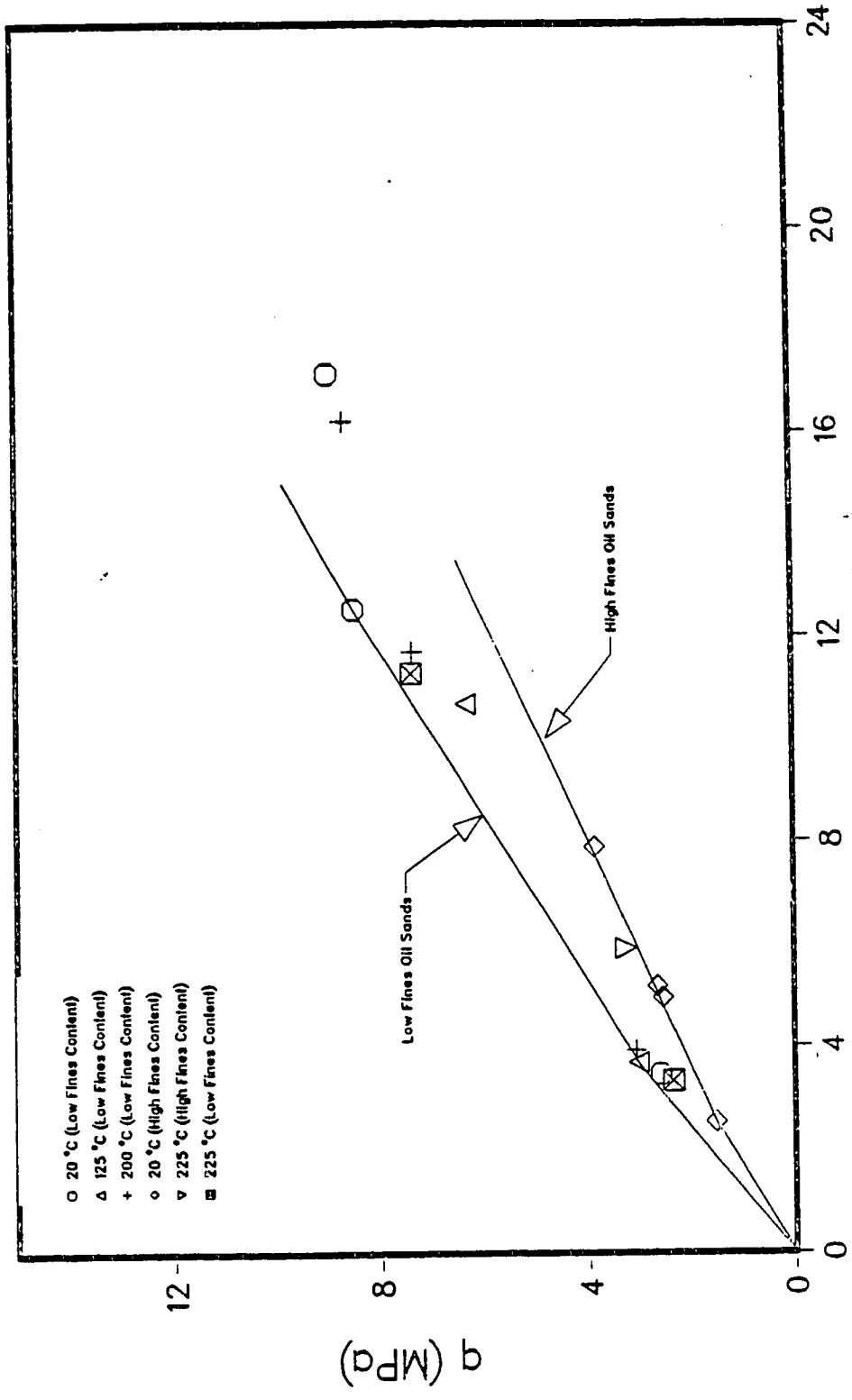

Figure 7.26 Effect of Temperature on Strength of High Fines Oil Sands

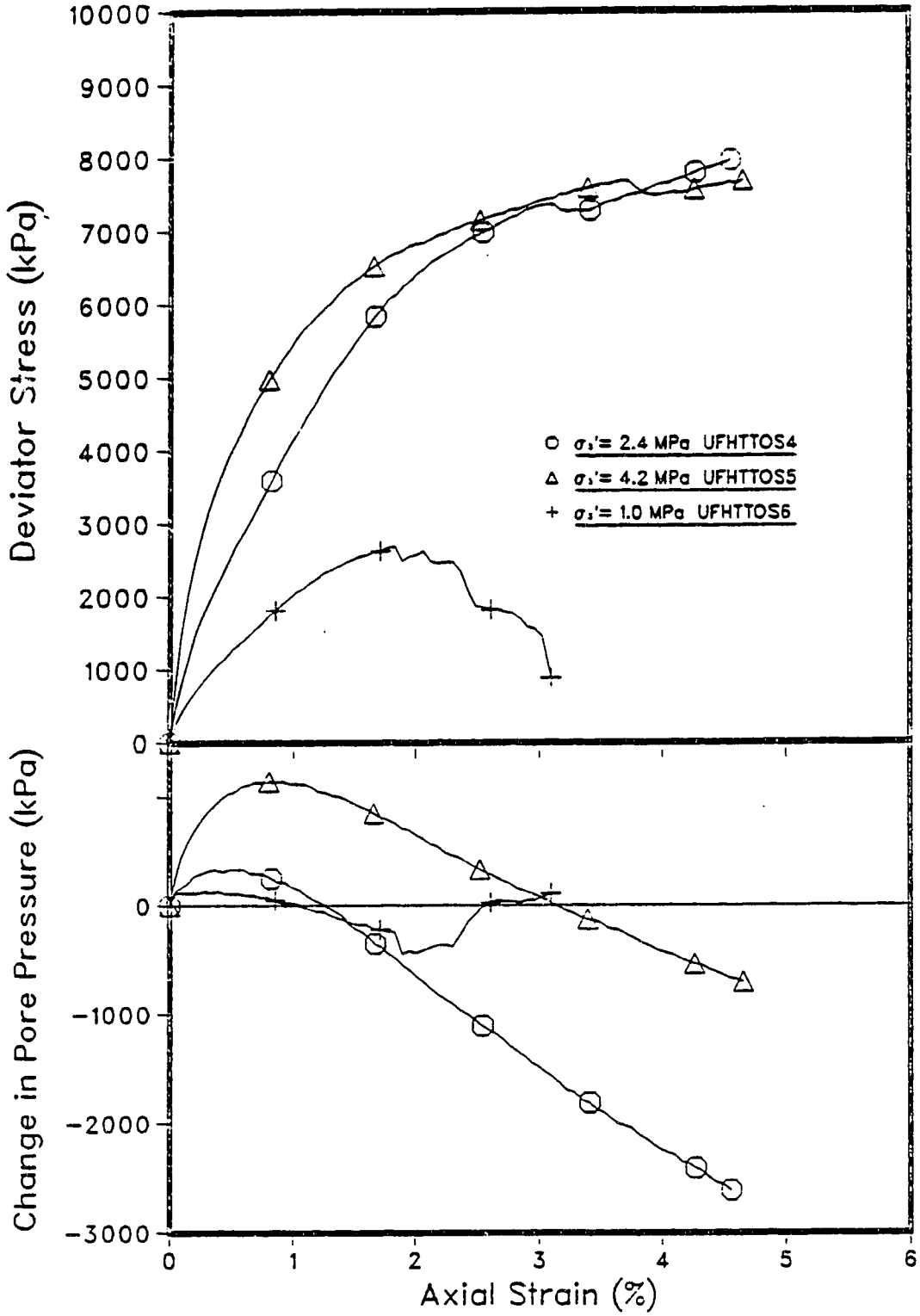

Figure 7.27 Undrained Passive Compression Tests on McMurray Formation Oil Sands at 225 °C

fluid pressure decrease which falls below the initial back pressure in the specimens resulting in a net increase in effective confining pressure on the specimens. It is noted, however, that Specimen UFHTTOS6 displays a rapid increase in pore fluid pressure at 2% axial strain accompanied by a rapid decrease in deviator stress. This behaviour is attributed to a defect in the specimen membrane resulting in communication between the back pressure and confining pressure systems.

The effect of temperature on undrained shear strength in terms of maximum principal stress ratio and ultimate strength is summarized in Figure 7.28. The effective stresses at failure for tests performed at 20°C and tests performed at 225°C are similar. The tests conducted at 225°C had initial void ratios ranging from 0.47 to 0.51 which reduced to 0.42 to 0.46 after isotropic consolidation and stress cycling at 20°C and to 0.35 to 0.39 after drained heating to 225°C. The tests carried out at 20°C had initial void ratios of 0.44 and 0.53 which reduced to 0.38 and 0.47 after isotropic consolidation and stress cycling. Given the variation in the proportion of shale to sand in the specimens (48 to 66% fines by weight) and the rather small variation in void ratio values prior to the shear tests, the similarity in strength values is not unreasonable.

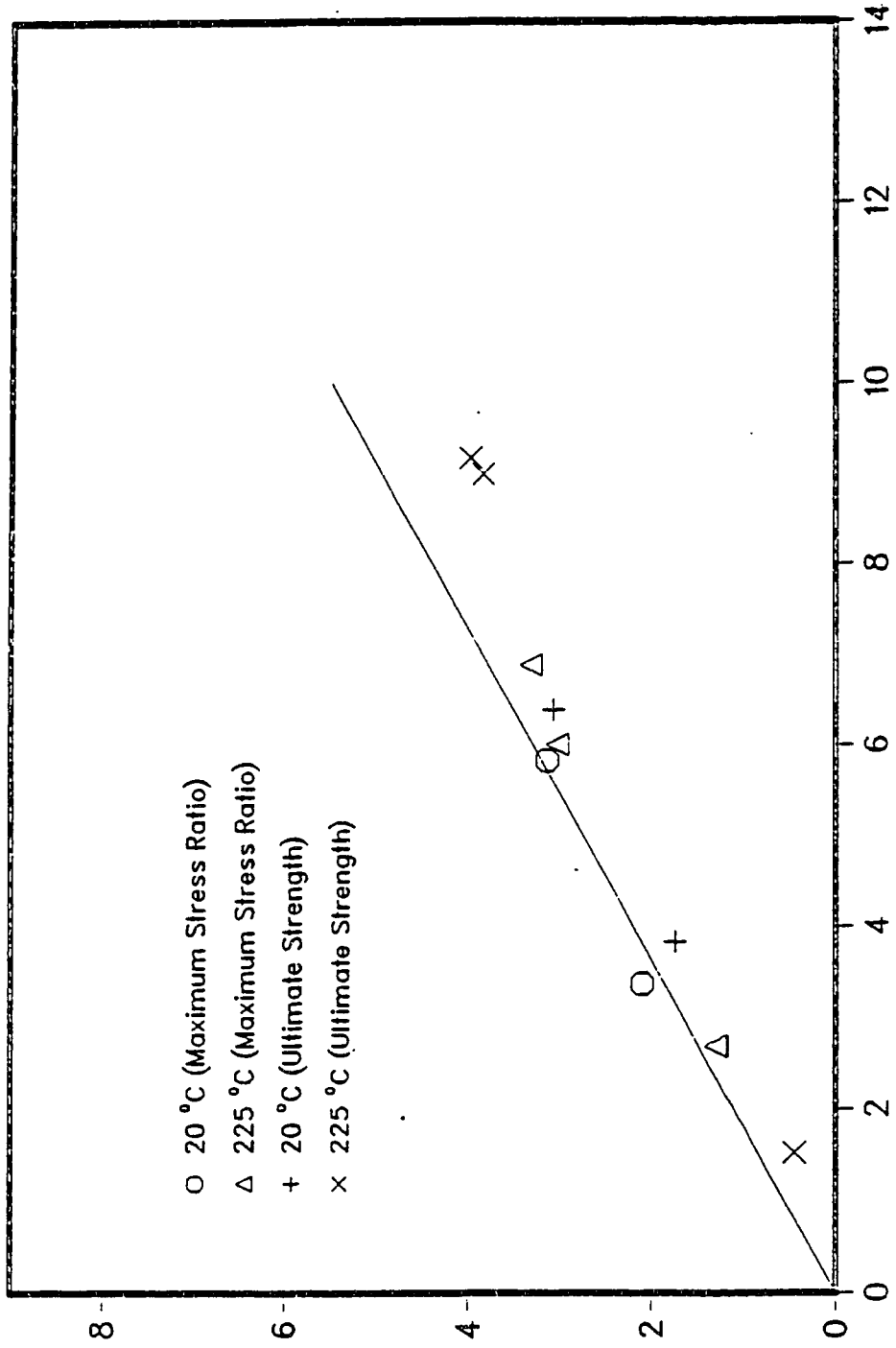

Figure 7.28 Effect of Temperature on Undrained Strength of Interbedded Oil Sands

7.7 Summary

The strength and deformation behaviour of oil bearing sands of the Athabasca Deposit were examined. The oil sands used in the testing program were obtained from three sites and two formations in the deposit at depths ranging from 150 to 300 m. Constitutive behaviour was categorized according to the geological environment of deposition and geological history. McMurray Formation sediments were divided into two major geotechnical facies; high grade, low fines oil sands and low grade, high fines oil sands. One geotechnical facies from the Wabiskaw Member of the Clearwater Formation was studied, a medium grained, medium rich, glauconitic oil sands.

The strength-deformation characteristics of disturbed oil sands of the Wabiskaw Member within the Athabasca Deposit were found to be very similar to disturbed McMurray Formation oil sands from similar depths. Any influence of geological environment of deposition and geological history (such as mineralogy and grain structure) was obscured by excessive sample damage during coring, handling and storage.

The presence of shale interbedding results in a significant decrease in the maximum shear strength of McMurray Formation oil sands as compared to high quality, low fines oil sands. The presence of fines also reduces the initial stiffness of oil sands and the oil sands' tendency to dilate at higher confining stresses. Shale interbedded oil sands may experience a significant reduction from peak

to residual strength if deformation is dominated by failure through the heavily overconsolidated shale strata. The weaker, more compressible shale strata interbedded in the oil sands has a significant effect on overall stress-strain characteristics of the formation regardless of stress path followed.

The stress-strain relationships of Athabasca McMurray Formation oil sands shows a strong stress path dependency. The standard passive drained compression tests exhibit smaller moduli of deformation than did the unloading stress paths (J_1 constant compression, active compression and J_1 constant extension). The results from the passive drained and passive undrained compression tests, however, gave similar results. The strains to failure varied with the stress path indicating that depending on the stress path followed, the strain at which mobilization of shear strength occurs can be significantly different from the conventional passive drained test. Since the oil sands in the field rarely follow a passive drained stress path during the bitumen recovery process, use of results obtained from the standard test in numerical simulations would likely over-predict the deformations occurring in the field.

The shear strength and deformation behaviour of rich, low fines oil sands is not significantly influenced at elevated temperatures. The shear strength and stress-strain modulus of high fines content McMurray Formation oil sands may increase at elevated temperatures if significant heat

consolidation of the thin, discontinuous shale seams occurs. Temperature increases also significantly increase the pore fluid pressure and if pore pressure dissipation cannot occur at the same rate as the temperature increase, the drop in effective stress can cause a decrease in the shear strength. Low permeability shale seams may be a significant barrier to pore fluid drainage in highly interbedded oil sands. The available shear strength in this geotechnical facies during in situ production may therefore be critical for the design of well casings, tunnels or shafts passing through or lying in this strata.

8. SHEAR STRENGTH OF ATHABASCA RELATED STRATA

8.1 General

In the Athabasca Deposit the McMurray Formation overlies limestones of the Devonian Waterways Formation. Lying conformably over the McMurray Formation are the laterally extensive, flat lying marine shales of the Clearwater Formation. Separating McMurray Formation from the Clearwater shale is the Wabiskaw Member of the Clearwater Formation. At the Underground Test Facility site the Wabiskaw consists of a glauconitic sand containing water and some gas (Edmunds et al, 1987). In other areas of the Athabasca Deposit, however, the Wabiskaw Member may be oil saturated (Carrigy and Kramers, 1974) or may consist of oil free sand with high percentages of silt and clay (Issac et al, 1982; Issac and Dusseault, 1984; Carrigy and Kramers, 1974).

The design of well casings and of underground openings such as tunnels and shafts passing through or lying in strata bounding the oil sands production zone must take into account the interaction between the constitutive behaviour of the strata and in situ stress changes and ground deformations arising from the thermal bitumen recovery process. Anderson and Hollingsworth (1982) describe several vertical well casing failures which occurred at Gregoire Lake Block 1 Pilot located approximately 30 km southeast of Fort McMurray. The vast majority of failures in the form of

deformed or bent casing were identified through downhole surveys as occurring at the top of the Upper McMurray Formation at the oil sands-shale interface.

The in situ recovery process was planned to consist of four distinct phases:

1. Stimulation: During this phase wells immediately adjacent to production wells were used to heat the oil sands in the lower portion of the reservoir around the producing wells.

2. Preheat: This phase involved injecting heated air into a row of wells in the center of the nine inverted 5-spot well patterns. The purpose of this phase was to heat the oil sands reservoir to an average temperature of 100°C and establish injector-producer well communication.

3. Blowdown: During this phase producing wells would be pumped to reduce the pore fluid pressure in the reservoir and to create a more homogeneous temperature distribution in the reservoir prior to ignition and injection of air into the central injector wells.

4. Combination of Forward Combustion and Water Flooding (COFCAW): This phase entailed pumping air and water at the central injection wells to displace bitumen to the producing wells.

Due to the lack of flow between wells during the blowdown period pore fluid pressures remained high in the reservoir. Pore fluid pressures continued to build in the reservoir during COFCAW as injection rates far exceeded withdrawal rates. Directional surveys of wellbore casings indicated that the direction of lateral displacement was away from the source of the pressure (air injection wells) and that the most extensive deformation occurred at the top of the McMurray Formation at the shale-oil sands interface. Finite element studies by Smith and Pattillo (1980) concluded that casing failure was due to non-uniform cross-sectional loading or shear failure. Formation movements were attributed to:

1. Expansion of the formation from temperature and pore fluid pressure increases.

2. A reduction in the shear strength of the oil sands due to a decrease in effective stresses from the increase in pore fluid pressure.

In the analyses the shale was assumed to be stiffer and stronger than the underlying oil sands and, therefore, non-uniform loading on the casing resulted at the oil sand-shale interface.

A number of well casing failures at several in situ thermal recovery projects were examined by Chhina and Agar (1984). They suggest that a portion of these failures may have been due to shear deformations in the shale strata overlying the oil sands reservoir. Reduced shearing resistance of the shales from the development of thermally generated pore fluid pressures due to undrained heating after the initiation of steam stimulation combined with formation deformation from temperature and fluid pressure increases were cited as a possible cause of casing failure at these projects.

The mechanisms contributing to thermally induced shear failure in shale strata bounding oil sands reservoirs may be outlined as follows:

1. As discussed in Section 5.2, rich, low fines oil sands subjected to an increase in temperature from 20°C to 300°C under fully drained conditions will increase in volume by approximately 1%. The magnitude of the mineral solids thermal expansion did not vary significantly under high effective confining stresses such as those existing at depths of 100 to 500 m. Due to the high modulus of elasticity of oil sands at

these depths (Chapter 7) thermal expansion will cause a large increase in horizontal stress.

2. Outside the zone of bitumen production where the bitumen is not mobile, in the overlying Clearwater shales and in the clay seams and joints in the underlying Devonian limestone, pore fluid pressure increases occur. These thermally induced pore fluid pressure increases cause a proportional decrease in vertical and horizontal stresses. At depths less than 400 m where the vertical stress is less than the minimum horizontal stress (Chhina and Agar, 1985), the effective stress ratio will increase. Horizontal shear deformations will take place as this ratio increases.

Shear deformations are likely to be concentrated in high plastic, weak horizontal shale seams of high water content and low permeability. Clearwater shale strata would affect vertical wells drilled from the surface while Upper Devonian limestones with clay laminations may be the major source of shear problems affecting wells installed from underground drilling chambers.

Shale free, intact rock may experience some degree of thermal cracking during heating. The differential rates of

heat transfer through the mineral solids in the rock matrix cause the development of shearing and tensile stresses which result in micro-cracks forming. As a result of thermal cracking, the strength and stiffness of the intact rock decreases with increasing temperature. This may affect the anchoring of thermal recovery wells in underground drilling chambers.

8.2 Materials Studied

The Clearwater Formation at the Underground Test Facility site is found to be at a depth of approximately 125 m. The units within this zone, based on characteristic geophysical log responses (Chapter 4), are k_{cc} (100 to 116 m), k_{cb} (116 to 121 m) and k_{ca} (121 to 125 m). The amount of sample disturbance during the coring process was high in units k_{cb} and k_{ca}. The core was highly fractured and no representative specimens for strength determinations were obtained from these zones. Eight specimens suitable for triaxial strength testing were obtained from core samples taken in the k_{cc} unit. The depths of these specimens ranged from 100 to 112 m. The test specimens consisted of high plastic shale of very stiff to hard consistency. Is colour ranged from dark grey to black.

Data describing the shale test specimens are summarized in Table 8.1. The specimens appeared uniform and consistent. Index properties are consistent with those given by Issac et al (1982) for the k_{cc} unit at the Syncrude Canada Ltd.

Table 8.1 Athabasca Clearwater kcc Shale - Initial Conditions

Test Number	Depth (m)	Bulk Density (Mg/m3)	Dry Density (Mg/m3)	Water Content (%)	Liquid Limit (%)	Plastic Limit (%)	Void Ratio	Sr (%)	B
UFTCS1	106.3	2.167	1.89	14.69	64.4	25.4	0.43	92.5	0.98
UFTCS2	106.4	2.143	1.87	14.34			0.44	87.9	----
UFTCS3	106.2	2.168	1.88	15.45			0.44	95.3	0.97
UFTCS4	106.0	2.179	1.89	15.02			0.43	95.4	0.97
UFTCS5	111.7	2.200	1.96	12.25	50.0	23.2	0.38	87.6	0.97
UFHTTCS1	100.2	2.109	1.85	13.73	50.0	23.3	0.46	81.3	----
UFHTTCS2	100.6	2.046	1.72	18.93			0.57	89.8	1.00
UFHTTCS3	100.8	2.028	1.72	18.12			0.57	85.4	0.98

leases east of the Underground Test Facility. Issac et al (1982) report the mean k_{cc} unit clay fraction mineralogy as 15% chlorite, 50% illite, 15% kaoline and 20% smectite.

Three 1.5 m core samples of Devonian limestone were obtained from the Underground Test Facility site. The depth of the coring interval was 151.6 m (top of limestone surface) to 155.6 m. The core consisted of microcrystalline limestone with thinly interbedded shale with the interbedding becoming less frequent and continuous with depth. The limestone core was taken by triple tube core barrel and was frozen on site. Due to the high shale content in the upper 3 m, the freezing process caused the majority of this core to break up. Two specimens of sufficient size for shear strength determinations by triaxial compression were obtained from the bottom 0.5 m of core at a depth of approximately 155 m. The test specimens contained about 10% shale (determined visually) in discontinuous seams and clasts. The shale was light brown, silty and low plastic. The water content was 15% and the liquid and plastic limits were 28% and 18%, respectively.

8.3 Methods and Procedures

The stress-strain and strength behaviour of Clearwater k_{cc} shale was investigated following several different stress paths:

1. Passive drained compression at 20°C.
2. Passive undrained compression at 20°C.
3. Passive drained compression at 225°C.
4. Passive undrained compression at 225°C.

Each shale specimen was placed in the triaxial cell under a small confining stress of 0.2 to 0.5 MPa. The confining stress and back pressure were then increased in equal increments of 0.2 MPa, thereby maintaining the same effective confining stress on the specimen. The back pressure was increased to at least 2.5 MPa to ensure the pore fluid pressure in the specimen was above the pore fluid saturation pressure. A back pore pressure of at least 7.5 MPa was used for specimens tested at 225°C to prevent pore liquid vapourization. The specimens were then allowed to saturate for several hours and a B test was carried out prior to the isotropic consolidation pressure being applied. The confining stress was then increased to give the effective confining stress for the shear test and the volume change was monitored. The volume change and void ratio after isotropic consolidation at 20°C is summarized in Table 8.2.

With the exception of Specimen UFHTTCS1, specimens sheared at 225°C were heated under fully drained conditions after the completion of isotropic consolidation at 20°C and the volume change or heat consolidation was monitored. Specimen UFHTTCS1 was heated immediately after the

Table 8.2 Athabasca Clearwater kcc Shale - After Isotropic Consolidation and Drained Heating

Test Number	Seating Pressure (MPa)	Isotropic Consolidation Stress (MPa)	Volume Change (%)	e after Consolidation	Test Temperature (°C)	Volume Change During Heating (%)	e after Heating
UFTCS1	0.5	1.5	-2.63	0.39	20.0		
UFTCS2	0.5	4.0	-3.73	0.39	20.0		
UFTCS3	0.5	0.5	0.00	0.44	20.0		
UFTCS4	0.5	2.0	-4.14	0.37	20.0		
UFTCS5	0.2	2.5	-6.35	0.29	20.0		
UFHTTCS1	0.5	2.5	----	----	225.0	-6.56	0.36
UFHTTCS2	0.5	1.0	-1.15	0.55	225.0	-11.57	0.37
UFHTTCS3	0.5	2.5	-1.87	0.54	225.0	-8.45	0.41

application of the isotropic consolidation stress and the volume change due to combined mechanical and thermal loading was measured. The volume change and void ratio after drained heating to 225°C is given in Table 8.2. An additional B test was performed on all specimens, both at 20°C and 225°C, prior to shear at the effective confining stress used in the shear test.

Due to the low number of test specimens, a multi-stage test following the drained passive compression stress path was carried out on Specimen UFHTTCS2 at 225°C. This test was performed to determine shear strength and stress-strain behaviour at several effective confining stress levels from a single test. In this test, the specimen was initially sheared under an effective confining stress of 1.0 MPa. As the specimen reached its peak deviator stress, as signified by a levelling of the stress-strain curve, the effective confining pressure was increased to 2.5 MPa and axial straining continued. Passive compression was continued until a second peak deviator stress level was reached, then the effective confining stress was again increased to 4 MPa. Passive compression was continued and the specimen was strained to complete failure. Back pressure was maintained constant at 7.5 MPa throughout the three stages of passive drained compression. The temperature of the specimen was constant at 225°C throughout the test.

The stress-strain and strength behaviour of Devonian limestone was studied during unconfined passive compression

at 20°C, passive drained compression at 20°C and passive drained compression at 225°C.

The first limestone specimen was taken to failure in an unconfined passive compression test at 20°C. The second specimen was placed in the high temperature triaxial cell under an effective confining stress of 0.5 MPa. The confining pressure and back pressure were increased in equal increments until a back pressure of 7.5 MPa was reached. The effective confining stress was then increased to 2.5 MPa and the specimen was allowed to saturate for several hours. The deviator stress was then applied to the specimen and the modulus of deformation was determined over the axial strain range of 0 to 0.17%. The specimen was then unloaded to isotropic stress conditions and the effective confining stress was reduced to 1.0 MPa. The specimen was then heated under fully drained conditions to 225°C with the back pressure maintained at 7.5 MPa.

After the temperature reached 225°C the specimen was allowed to stabilize for several hours. A multi-stage passive drained loading test was then performed at 1.0 MPa and 2.5 MPa effective confining stress.

8.4 Shear Strength and Stress-Strain Behaviour of Clearwater k_{cc} Shale

The effect of temperature on shear strength and stress-strain behaviour of Clearwater k_{cc} shale was studied by performing drained and undrained passive compression

tests at 20°C and 225°C. Results of eight triaxial tests are summarized in Table 8.3. The stress-strain and volume/pore pressure change relationships are shown in Figures 8.1 to 8.3.

The behaviour of Clearwater k_{cc} shale is characteristic of a heavily overconsolidated clay:

1. The material displays strain softening behaviour in the post-peak region during drained loading with a reduction in strength from peak to residual of approximately 35%.

2. Each specimen tested under drained conditions displays a volume decrease during the onset of shear followed by a volume increase as the specimen approaches its peak deviator stress.

3. During undrained loading each specimen displays a pore fluid pressure increase at the onset of shear followed by a pore pressure decrease.

Shear strength and stiffness of k_{cc} shale both increase with increasing effective normal stress and dilatancy is suppressed at elevated confining stresses.

Table 8.3 Athabasca Clearwater kcc Shale - Consolidated Passive Triaxial Tests

Drained Shear Tests

Test Number	Effective Confining Stress (MPa)	Back Pressure (MPa)	B	Deviator Stress at failure (MPa)	Axial Strain at failure (%)	Volumetric Strain at failure (%)	Modulus of Elasticity (MPa)	Poisson's Ratio
UFTCS1	1.5	3.0	0.98	4.90	3.39	-1.38	180	0.28
UFTCS2	4.0	3.0	----	7.18	2.79	-0.52	275	0.38
UFTCS3	0.5	3.0	0.97	1.91	3.10	-0.41	57	0.21
UFTCS5	2.5	2.5	0.97	5.19	2.57	-0.96	222	0.16
UFHTTCS1	2.5	2.5	0.82	6.47	2.53	-1.10	272	0.22
UFHTTCS2-1	1.0	7.5	0.91	3.40	3.18	-1.54	89	0.21
UFHTTCS2-2	2.5	7.5	----	6.93	4.98	-2.90	212	0.12
UFHTTCS2-3	4.0	7.5	----	10.09	6.02	-3.70	327	0.08

Undrained Shear Tests

Test Number	Effective Confining Stress (MPa)	Back Pressure (MPa)	B	Maximum Shear Strength (MPa)	Axial Strain at Max. Shear Strength (%)	Max. Stress Ratio at (% Strain)	Modulus of Elasticity (MPa)	A at Failure
UFTCS4	1.8	10.0	0.97	4.29	2.25	4.60 (2.02)	243	0.16
UFHTTCS3	2.5	7.5	0.97	3.55	2.10	5.75 (1.91)	350	0.48

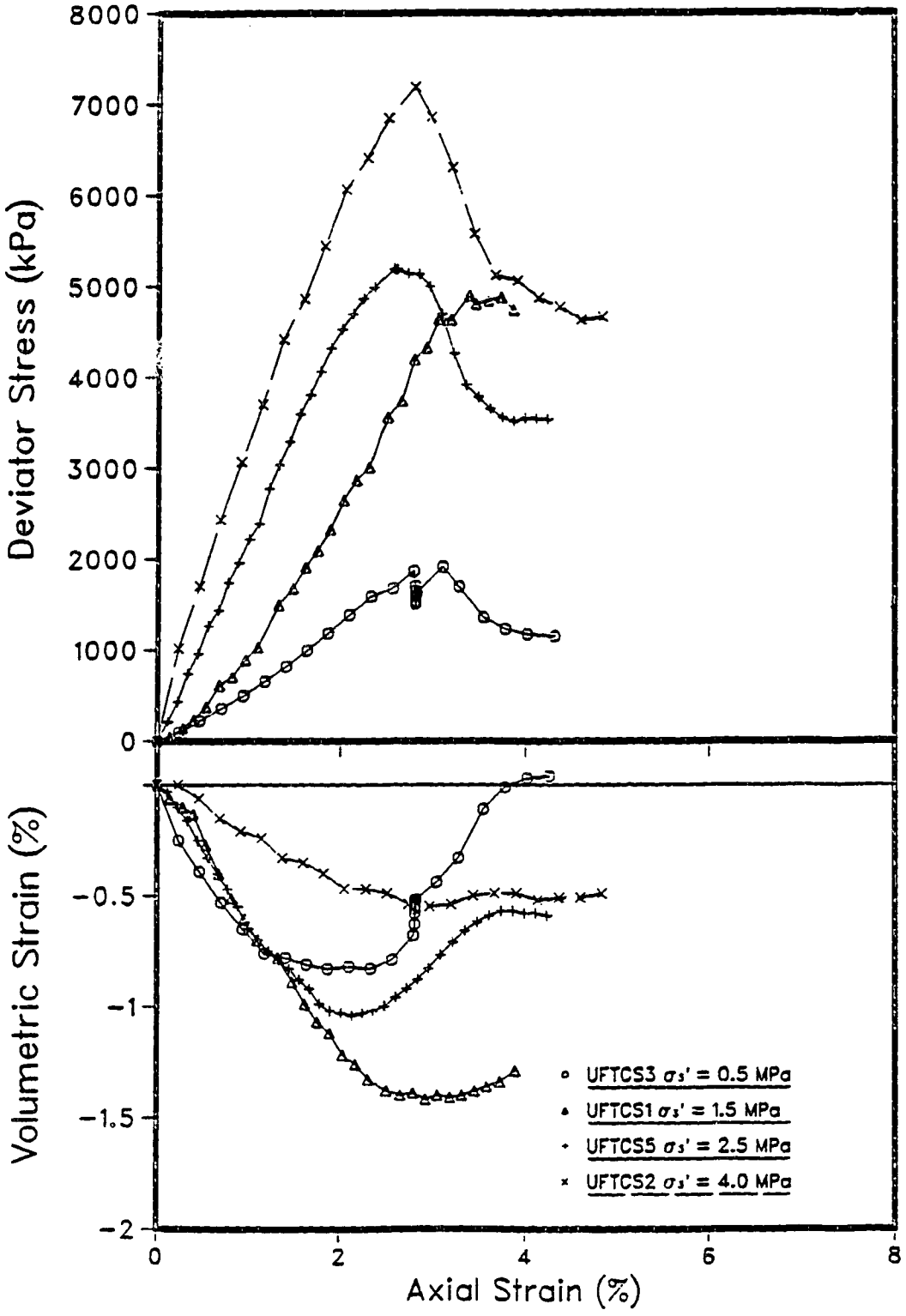

Figure 8.1 Drained Passive Compression Tests on Clearwater kcc Shale at 20 °C

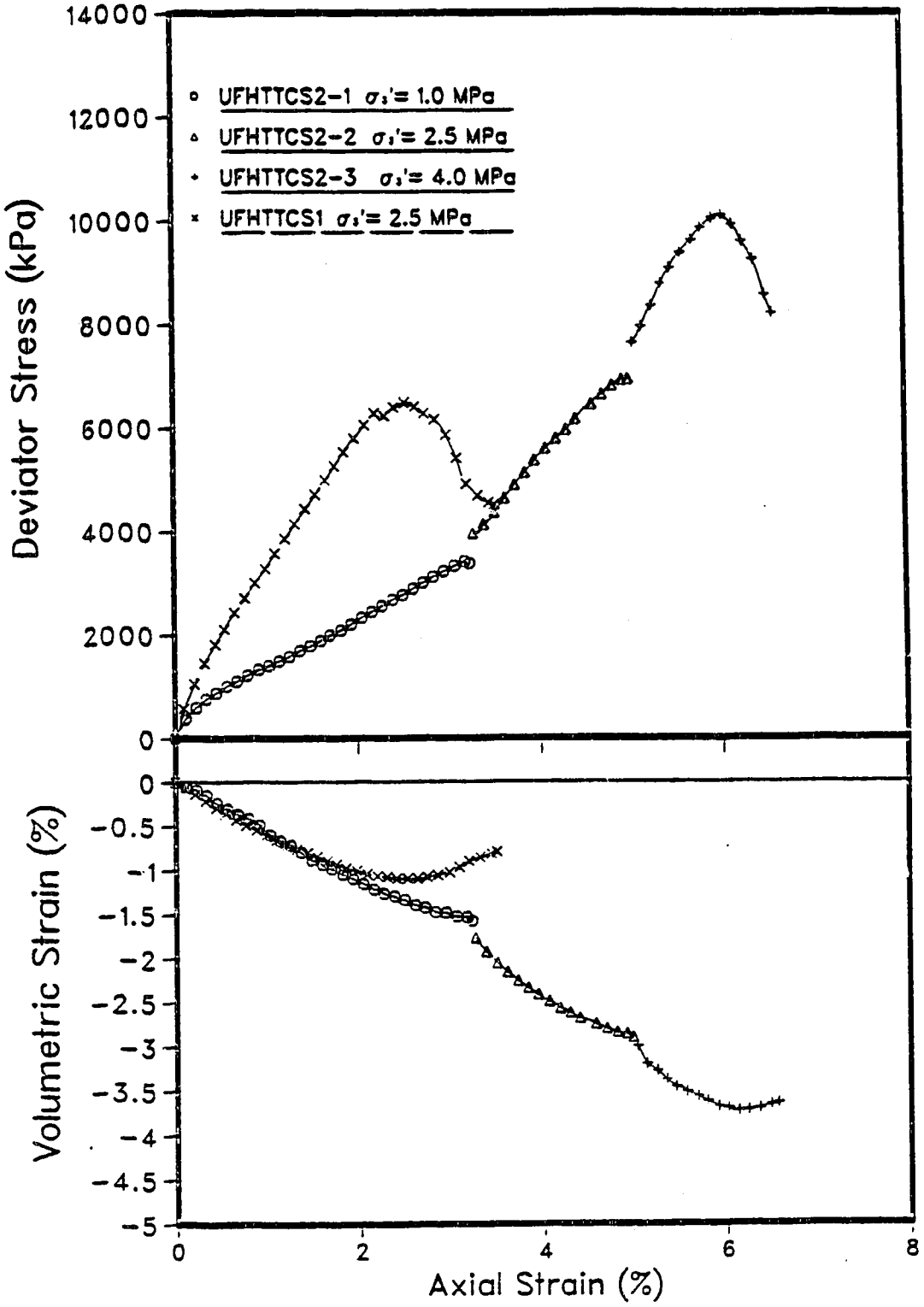

Figure 8.2 Drained Passive Compression Tests on Clearwater kcc Shale at 225 °C

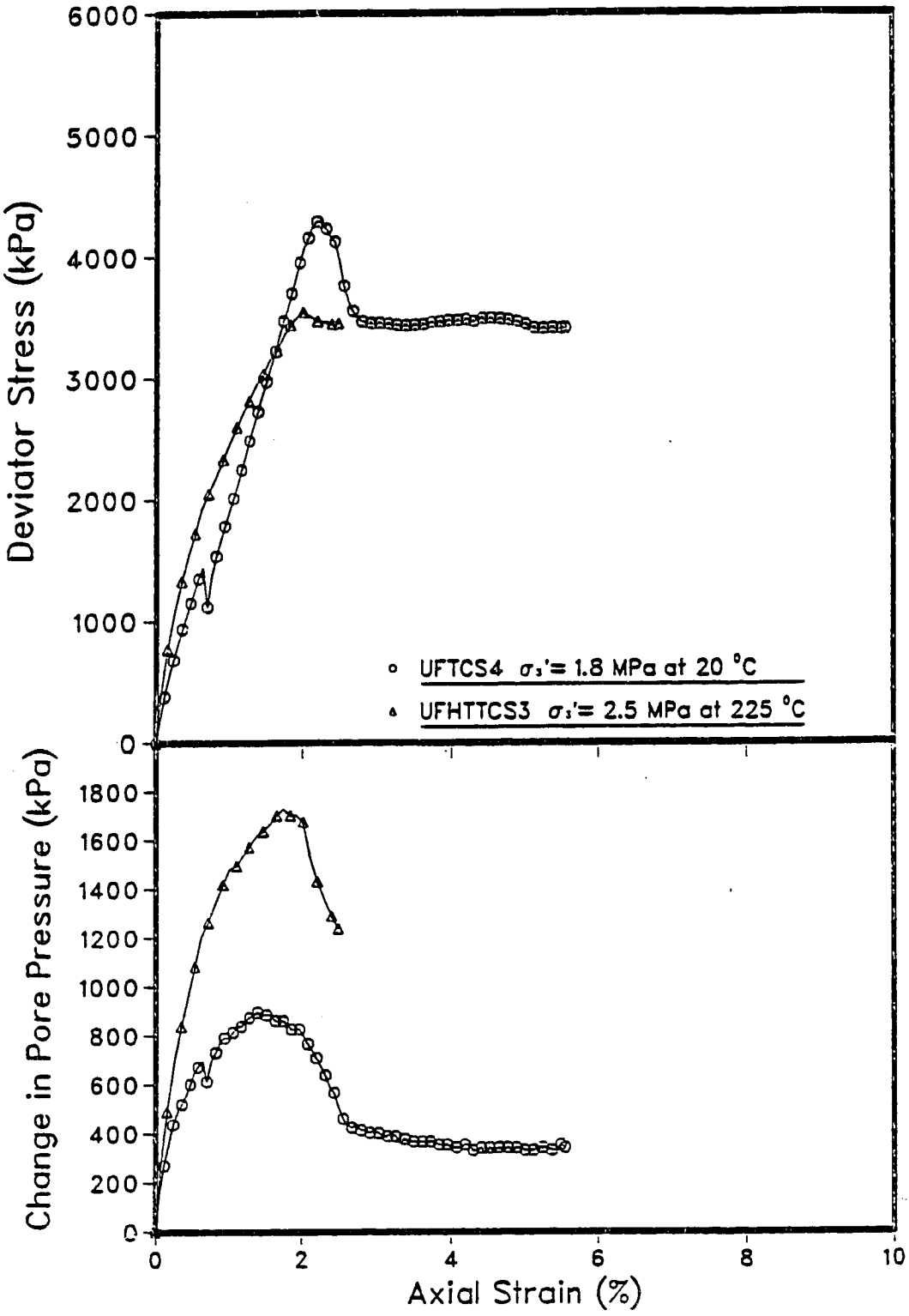

Figure 8.3 Undrained Passive Compression Tests on Clearwater kcc Shale

The shear strength data are plotted in Figure 8.4 in terms of water content at failure for triaxial tests carried out at 20°C and 225°C. Values of p' and q corresponding to the peak points of the stress-strain curves are plotted separately. The p_f'-w_f plot also includes values of p' and w representing conditions after isotropic consolidation and after drained heating to 225°C. Lines connecting points of a particular test indicate the magnitude of volume change during the test. Two important observations concerning shear strength behaviour of k_{cc} shale may be derived from these test results:

1. An increase in temperature under fully drained conditions can cause a significant reduction in water content. Even though the initial water contents of the specimens heated to 225°C were considerably higher than those for the 20°C specimens, after isotropic consolidation and heat consolidation water contents are similar to those obtained for the 20°C specimens after consolidation.

2. The specimens tested at 225°C correlate well with the 20°C specimens in terms of p'-w and q'-w at failure.

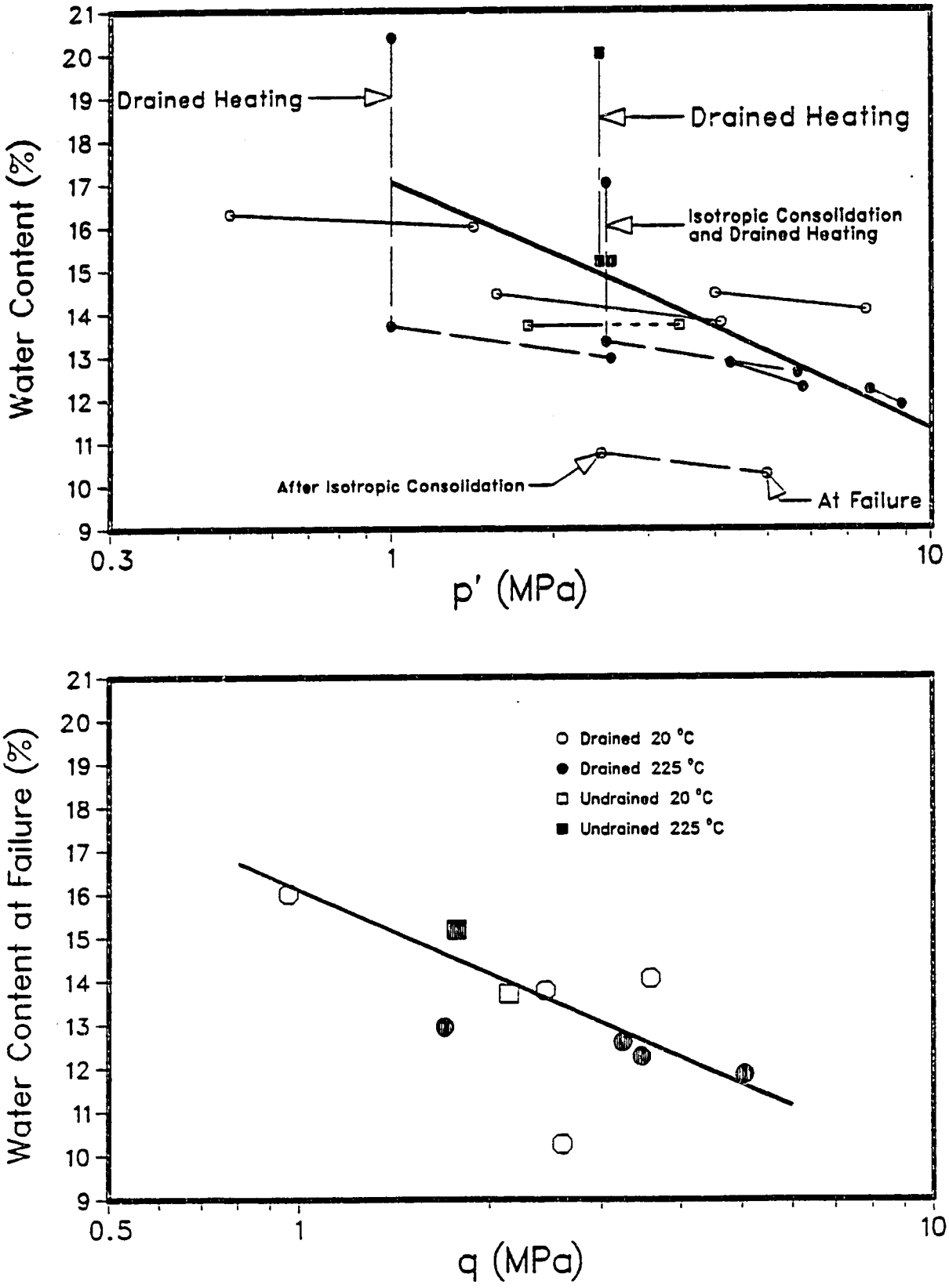

Figure 8.4 Triaxial Test Results on Clearwater kcc Shale

The limited number of triaxial compression tests performed on k_{cc} shale show that shear strength may increase with temperature. Although the water content values after isotropic consolidation at 20°C are higher for specimens subjected to drained heating to 225°C, the water contents prior to shear, water content at failure and p' and q' values at failure are similar for specimens tested at 20°C and 225°C. These similar values may be attributed to heat induced compaction of the shale.

The drained shear strength data are plotted in terms of a p'-q diagram in Figure 8.5. A linear failure line can be drawn through the test values. The k_f-line intercepts the q-axis resulting in an "a" value of 0.27 MPa. The angle of the k_f-line, α, with respect to the horizontal is 28.0°. The failure line is defined by the Mohr-Coulomb parameters c' = 0.32 MPa and ϕ = 32.1°. Figure 8.5 also compares drained and undrained effective stress paths for tests performed at 20°C and 225°C which had similar isotropic stress conditions existing before shear. Figure 8.5 illustrates several important points concerning the stress-strain and strength behaviour of k_{cc} shale:

1. Results of both drained one-dimensional thermal volume change testing (Section 5.2.2) and drained isotropic heating (Figure 8.4) have shown that the cumulative volume change of the soil structure with increasing temperature decreases (heat induced

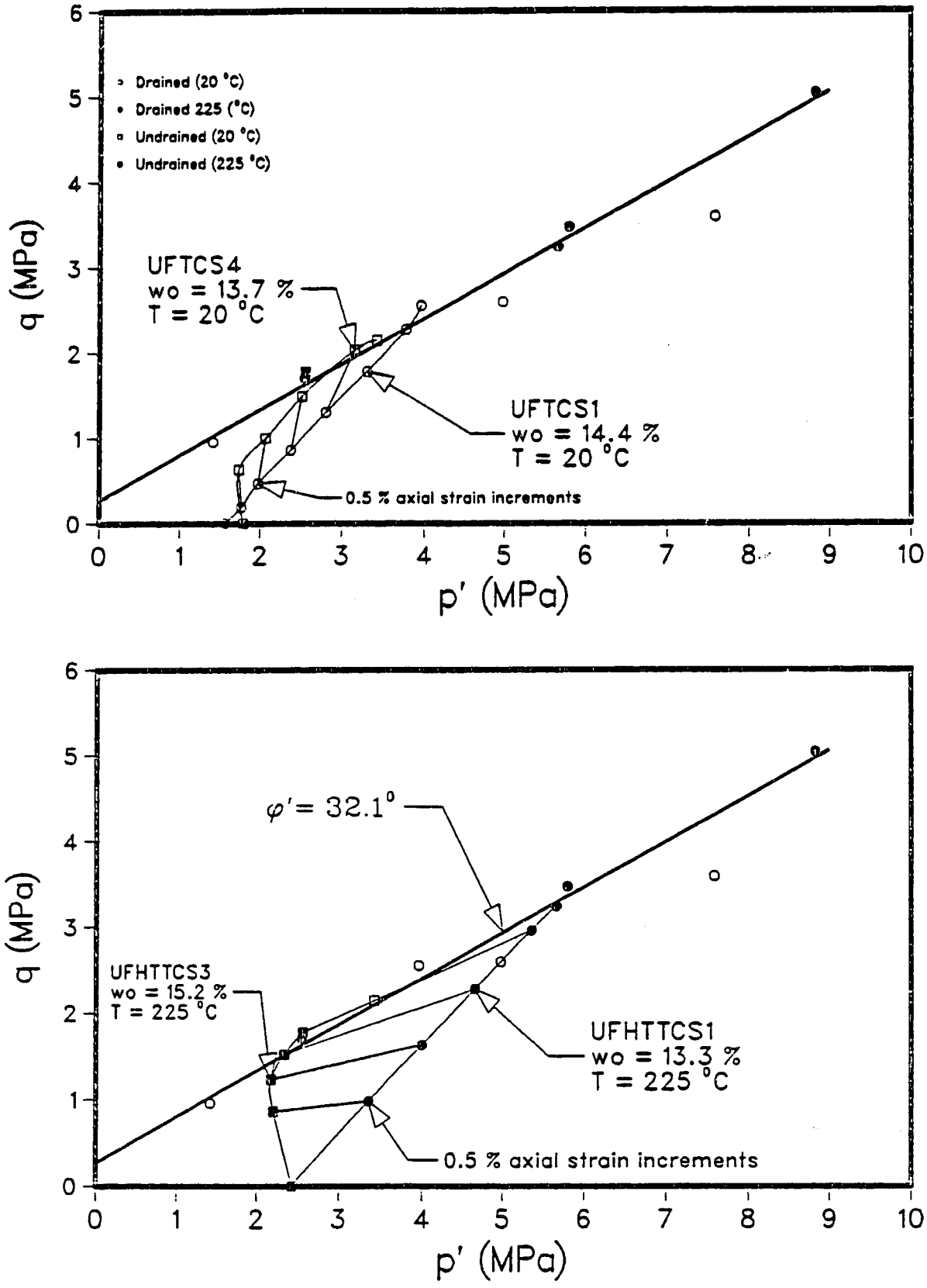

Figure 8.5 Drained Strength of Clearwater kcc Shale

consolidation). Comparing tests performed on Specimen UFTCS1 at 20°C (w_o = 14.4%) and on Specimen UFHTTCS1 at 225°C (w_o = 13.3%) in Figure 8.5, however, indicates that given a similar pre-shear water content (or degree of consolidation) strength under drained conditions of this shale is not significantly affected by the test temperature. This would tend to suggest that the drained strength of k_{cc} shale is dominated by the density or soil fabric which exists just before shear. Whether the soil fabric is attained by mechanical or thermal loading appears to be of little consequence with respect to drained strength.

2. The undrained strength test results show good agreement with the drained test results in terms of effective stress conditions at failure. These results are consistent with Henkel (1959) who demonstrated that for a given saturated clay with a given stress history unique relationships exist at failure between the water content, the strength and the average principal effective stress which is independent of loading and the degree of drainage during shear.

3. Comparing undrained passive compression tests UFTCS4 at 20°C (w_o = 13.7%) and UFHTTCS3 at 225°C (w_o = 15.2%) demonstrates that again given a similar pre-shear water content strength under undrained conditions is not significantly influenced at elevated temperature. Effective stress path, however, is markedly affected by the slight difference in the degree of consolidation (Δw_o of about 1%). The more sustained decrease in p' or average effective confining stress for Test UFHTTCS3 reflects a slightly more compressible soil structure which results in a greater pore fluid pressure response during undrained loading. Deformation properties of k_{cc} shale are more sensitive to the degree of consolidation than is strength.

4. Clearwater k_{cc} shale displays stress path dependency when comparing drained and undrained passive compression stress paths at both 20°C and 225°C. Given the same initial effective confining stress prior to shear, the axial strain to failure is less and the initial tangent modulus is greater during undrained passive compression. This reflects the smaller strain required to mobilize shear strength under the lower effective confining stress.

The variation of initial tangent modulus (at 0.25% axial strain) with effective confining pressure derived from consolidated-drained triaxial tests on Athabasca Clearwater k_{cc} shale is shown in Figure 8.6. The drained modulus increases with effective confining pressure. Also shown in Figure 8.6 are results obtained from the consolidated-undrained triaxial tests carried out at 20°C and 225°C. As discussed previously, undrained moduli values are larger because the axial strain during undrained loading is less than the equivalent loading under drained conditions due to the development of positive excess pore fluid pressures.

Researchers at the University of Berkley have also shown that the mechanical properties of clay are dependent on the amount of heat consolidation clay experiences prior to shear testing. For example, Green (1984) conducted a series of geomechanical tests on undisturbed illite and smectite-rich saturated clays obtained from deep ocean core samples over the temperature range of 4°C to 200°C. The results of the study showed that the soil specimens that were consolidated to test temperatures under drained conditions display an increase in peak shear strength and stiffness with increasing temperatures. The amount of heat consolidation was found to increase with increasing temperature and was attributed to a decrease in attractive forces between clay particles with increased temperature which caused a reduction in interparticle resistance and

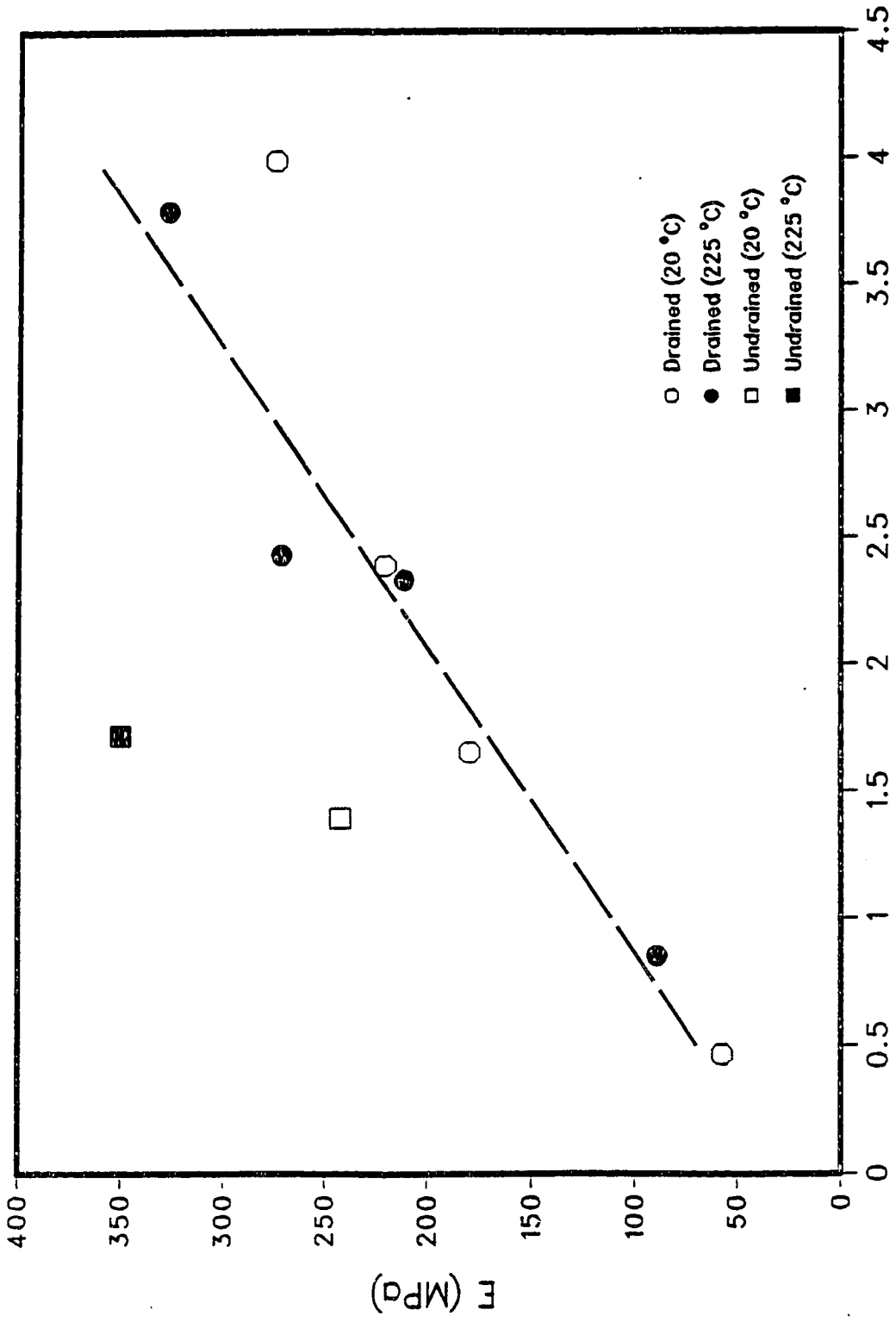

Figure 8.6 Variation of Drained Modulus – Clearwater kcc Shale

allowed the clay to become denser. Similar results are reported by Williams (1982) for remoulded illite specimens. Williams found that the shear strength and stiffness increased with increasing temperatures and attributes the increase in the reduction in void ratio which occurs during the heat consolidation process. Williams also found a unique relationship between peak shear strength and volumetric strain for soils with the same structure and initially at the same void ratio. The volumetric strain is the total decrease in void ratio resulting from volume changes due to thermal loading, mechanical loading or a combination of both. The relationship was not found to be dependent on the consolidation temperature.

8.5 Shear Strength and Stress-Strain Behaviour of Devonian Limestone

Figure 8.7 shows the general stratigraphy and location of access tunnels at the Underground Test Facility. The 5 m wide and 4 m high tunnels are situated approximately 12 m below the Pre-Cretaceous surface in the Waterways Formation of the Devonian Group. These tunnels provide a location from which horizontal wells can be placed in the overlying oil sands reservoir.

To evaluate the effectiveness of using horizontal wells for the recovery of bitumen by steaming (Phase A development), three pairs of horizontal wells spaced 24 m apart with a total length of 160 m and a completed length of

(After Edmunds et al, 1987)

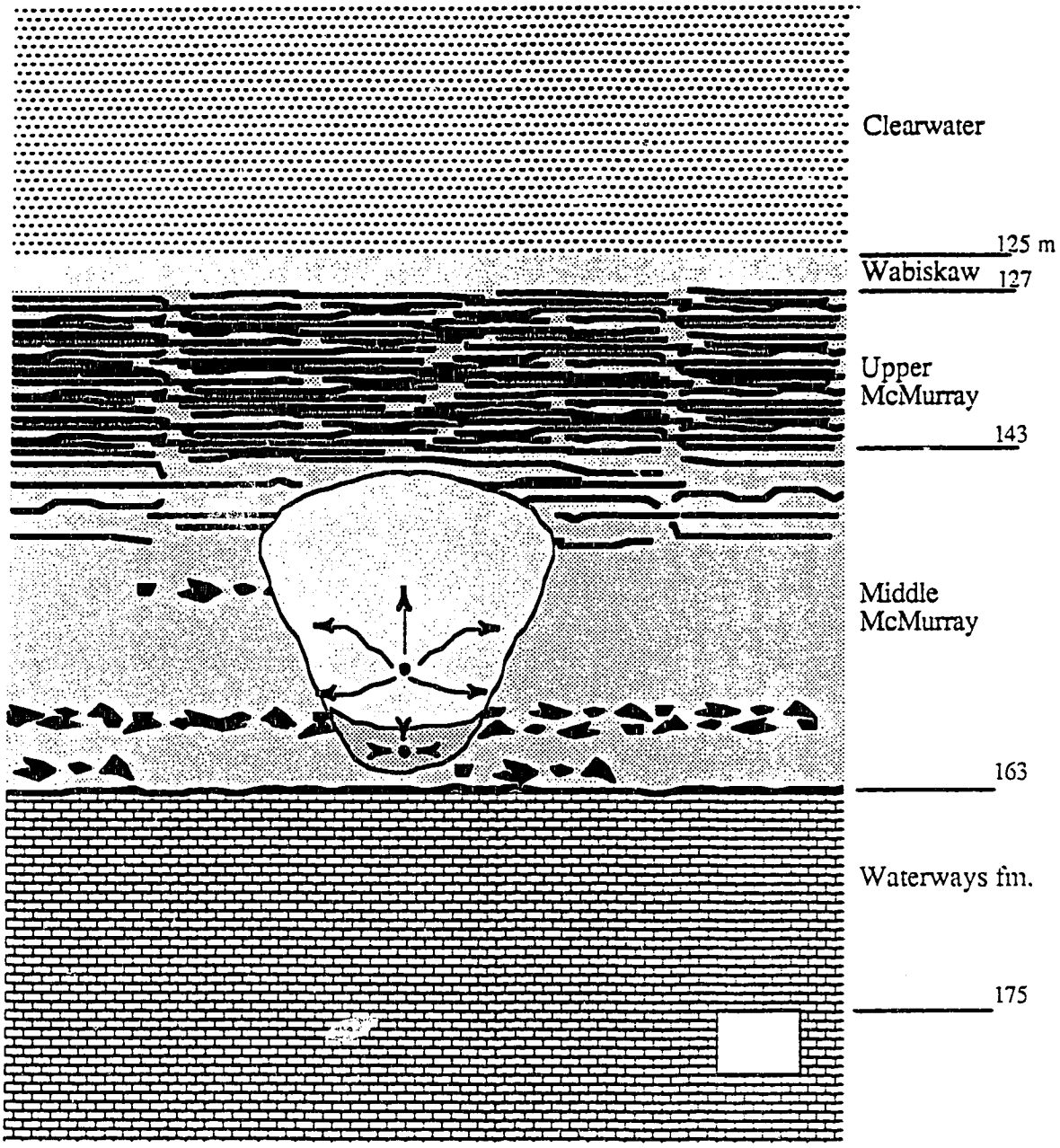

Figure 8.7 Generalized Geological Cross-Section at UTF Site

60 m were installed at the base of the McMurray Formation oil sands (Edmunds et al, 1987). Each well pair consisted of a production well located near the base of the reservoir and a steam injection well approximately 5 m above the producer. During Phase A development it was planned to inject steam at 1.5 MPa pressure at a temperature of about 215°C above the initial reservoir temperature.

AOSTRA (1986) conducted a limited geotechnical study of the Devonian limestone strata at the Underground Test Facility site. Laboratory test specimens were obtained from core samples taken in the Moberly and Christina Members of the Waterways Formation. As a result of this investigation, the limestone strata was divided into four groups (geotechnical facies) based on similar geotechnical properties. These geotechnical rock groups are summarized in Table 8.4 and consist of:

1. Massive Limestones
2. Argillaceous Limestones
3. Limestone/Shale
4. Calcareous Shale

The tunnels were located in the Massive Limestone and Argillaceous Limestone facies while the well pairs encountered the full range of facies described in Table 8.4.

Table 8.4 Summary of Geotechnical Properties of Devonian Limestone at UTF Site

Rock Unit	Moisture Content %	Unit Weight KN/m3	Slake Durability %	Seismic Velocity Ui/T 10^3/m/s	Point Load Strength ⊥ to bedding MPa	Point Load Strength ∥ to bedding MPa	Tensile Strength MPa	Schmidt Hammer MPa	Compressive Strength MPa	Elastic Modulus	Poissons Ratio	MOHS Hardness	Rock Classification Ratings CSIR Rock Mass Rating	Rock Classification Ratings NGI Tunnelling Quality Index
Massive Limestones (R4-R5)														
Recrystallized, lgt. brown to grey. Clay content ranges from 0 - 10%. Horizontal fractures 5-10 cm spcd. Abundant fossils. Porosity and permeability are low.	9 Samples $\bar{x}$ = 1.0 0.4 to 1.6	7 Samples $\bar{x}$ = 26.0 24.2 to 26.0	2 Samples $\bar{x}$ = 99.1 99.0 to 99.2	9 Samples 4770 ∥ to bedding 4770 ⊥ to bedding	16 Samples $\bar{x}$ = 2.9 0.25 to 6.3	16 Samples $\bar{x}$ = 5.3 0.66 to 0.96	4 Samples $\bar{x}$ = 9.1 7.3 to 11.5	4 Samples $\bar{x}$ = 52±35 34±30 to 120±47	5 Samples $\bar{x}$ = 46.9 19.3 to 64.0	5 Samples $\bar{x}$ = 16.3 9.8 to 28.2	5 Samples $\bar{x}$ = 0.06 0.07 to 0.08	2 Samples 4 to 5	Ranges from fair to good Class - 3 to 2	Ranges from fair to extremely good Q - 1.4 to <30
Argillaceous Limestones														
Lgt. brown micritic limestone with boundage structure. Occasional zones of nodular limestone. Clay content ranges from 20 - 50%. Abundant random fractures. Porosity and permeability are low.	13 Samples $\bar{x}$ = 2.3 1.2 to 5.9	3 Samples $\bar{x}$ = 26.2 25.0 to 26.5	2 Samples $\bar{x}$ = 88.4 77.6 to 99.2	6 Samples 4700 ∥ to bedding 4360 ⊥ to bedding	16 Samples $\bar{x}$ = 0.93 0.03 to 3.7	16 Samples $\bar{x}$ = 2.6 0.08 to 8.5	5 Samples $\bar{x}$ = 3.1 1.8 to 6.2	3 Samples $\bar{x}$ = 97±42 28±15 to 140±60	3 Samples $\bar{x}$ = 31.0 27.9 to 34.0	3 Samples $\bar{x}$ = 13.3 10.6 to 17.5	High Variable $\bar{x}$ = 0.06	Scratch Test Medium 1-2 (Incl.) Matrix 3-4 (Sig.R.)	Ranges from poor to good Class - 4 to 2	Ranges from extremely poor to fair Q - 0.08 to 0.9
Limestone/Shale														
Hard, regular limestone nodules and lenses interbedded with med. grey calcareous shale beds. 1-4 cm thick; fractures along sub-horizontal bedding planes.	9 Samples $\bar{x}$ = 4.4 1.3 to 7.3	5 Samples $\bar{x}$ = 25.7 24.5 to 26.4	2 Samples $\bar{x}$ = 70.8 45.2 to 96.3	6 Samples 2860 ∥ to bedding 3590 ⊥ to bedding	1 Sample $\bar{x}$ = 1.1	1 Sample $\bar{x}$ = 6.4	N.A.	6 Samples $\bar{x}$ = 52±23 19±10 to 144±60	3 Samples $\bar{x}$ = 32.6 23.6 to 45.5	3 Samples $\bar{x}$ = 10.8 6.2 to 15.2	N.A. Class - 4 to 2	N.A. Class - 4 to 2	Ranges from poor to good Q - 0.16 to 13.5	Ranges from very poor to good
Calcareous Shale (R3)														
Blue. greenish grey, very thinly bedded to massive frequent dark laminae, sub-horizontal bedding.	7 Samples $\bar{x}$ = 3.8 1.4 to 5.7	4 Samples $\bar{x}$ = 25.1 24.7 to 25.3	2 Samples $\bar{x}$ = 92.8 91.2 to 94.4	7 Samples 3460 ∥ to bedding 3020 ⊥ to bedding	17 Samples $\bar{x}$ = 0.13 0.03 to 0.31	178 Samples $\bar{x}$ = 0.46 0.06 to 1.5	3 Samples $\bar{x}$ = 1.4 0.7 to 2.1	3 Samples $\bar{x}$ = 22±10 21±10 to 22±10	4 Samples $\bar{x}$ = 17.4 12.5 to 20.6	4 Samples $\bar{x}$ = 2.7 1.3 to 4.2	3 Samples $\bar{x}$ = 0.17 0.15 to 0.19	2 Samples 1 to 2	Not Relevant to Tunnel Design	

(After AOSTRA, 1986)

The Devonian limestone specimens tested in this study belong to the Massive Limestone facies described in Table 8.4. Based on the CSIR Geomechanics Rock Mass Classification Scheme, AOSTRA (1986) classify this group of limestone as fair to good rock with an average unconfined compressive strength of 46.9 MPa and elastic modulus of 18.3 GPa. This unit is generally 5.5 m thick and has sub-vertical joints which are tight with a measured spacing of between 0.3 and 3 m (AOSTRA, 1986). As the competency of limestone is generally governed by the proportion of shale to intact rock the specimens studied here which contained about 10% shale by volume are the most competent of the limestone facies encountered at the Underground Test Facility site.

The results of an unconfined passive compression test at 20°C are shown in Figure 8.8. The uni-axial compressive strength was 16.3 MPa. The tangent modulus ranged from an initial value of 398 measured at 0.25% axial strain to 1400 MPa measured at 1.9% axial strain. The rapid increase in stiffness is attributed to the presence of micro-fissures which are closed by the increasing deviatoric stress resulting in more rock to rock contacts.

The results of the multi-stage drained passive compression test carried out at 20°C and 225°C are also shown in Figure 8.8. The initial tangent modulus (determined over the axial strain range of 0 to 0.17%) under an effective confining stress of 2.5 MPa at 20°C was 2320 MPa. The initial tangent modulus over a similar range of strain

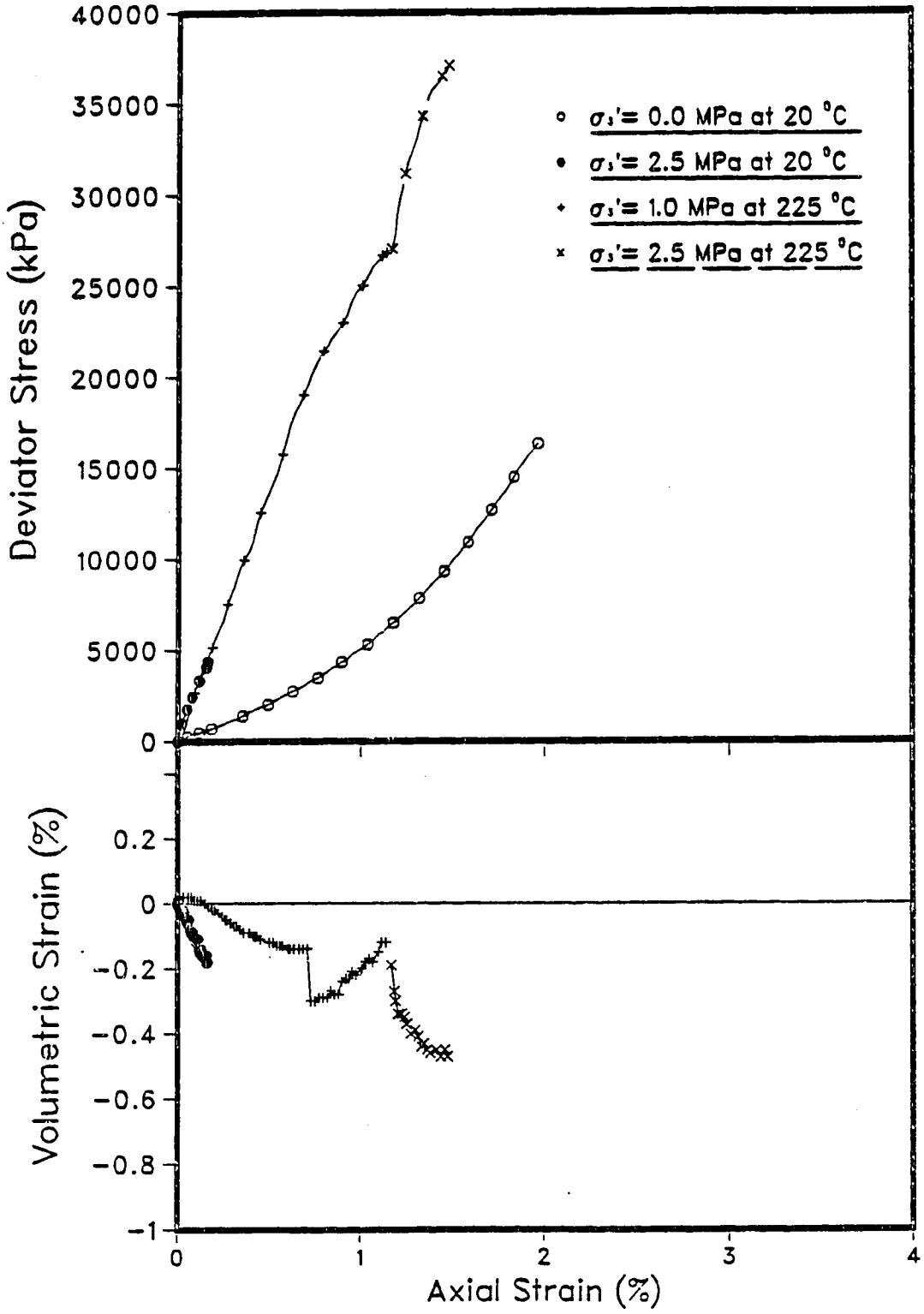

Figure 8.8 Passive Compression Tests on Devonian Limestone

under 1.0 MPa at 225°C was 2720 MPa. The modulus under 2.5 MPa confining stress at the onset of second stage loading at 225°C was 5530 MPa. The shear strength data are plotted in terms of a p'-q diagram in Figure 8.9. A linear k_f line can be drawn through the test values resulting in an α value of 38.9° and a q axis intercept of 1.60 MPa. These values correspond to Mohr-Coulomb strength parameters ϕ = 53.7° and c' = 2.7 MPa.

Mathews, Rawlings and Bharti (1980) carried out a limited number of triaxial compression tests on Devonian limestone in the Fort McMurray area over a confining pressure range of 3.5 to 13 MPa. The investigation was part of a CANMET/EMR sponsored study to assess the tunnelling characteristics of Devonian limestone as it would apply to the Shaft and Tunnel Access Concept (SATAC). Laboratory test specimens were obtained from core samples taken in the Grosmont and Waterways Formations to a limestone depth of 20 m. The limestone strata was divided into four geotechnical facies similar to those described by AOSTRA (1986); that is, massive limestones with occasional stringers of shale, argillaceous limestones with numerous random shale stringers, thinly interbedded limestones and shales, and thinly bedded shale or limey shale. Based on the CSIR Geomechanics Rock Mass Classification Scheme, Mathews, Rawlings and Bharti classify the Massive Limestone Group as fair rock with a friction angle of 35 to 50° and an apparent cohesion of 150 to 200 kPa.

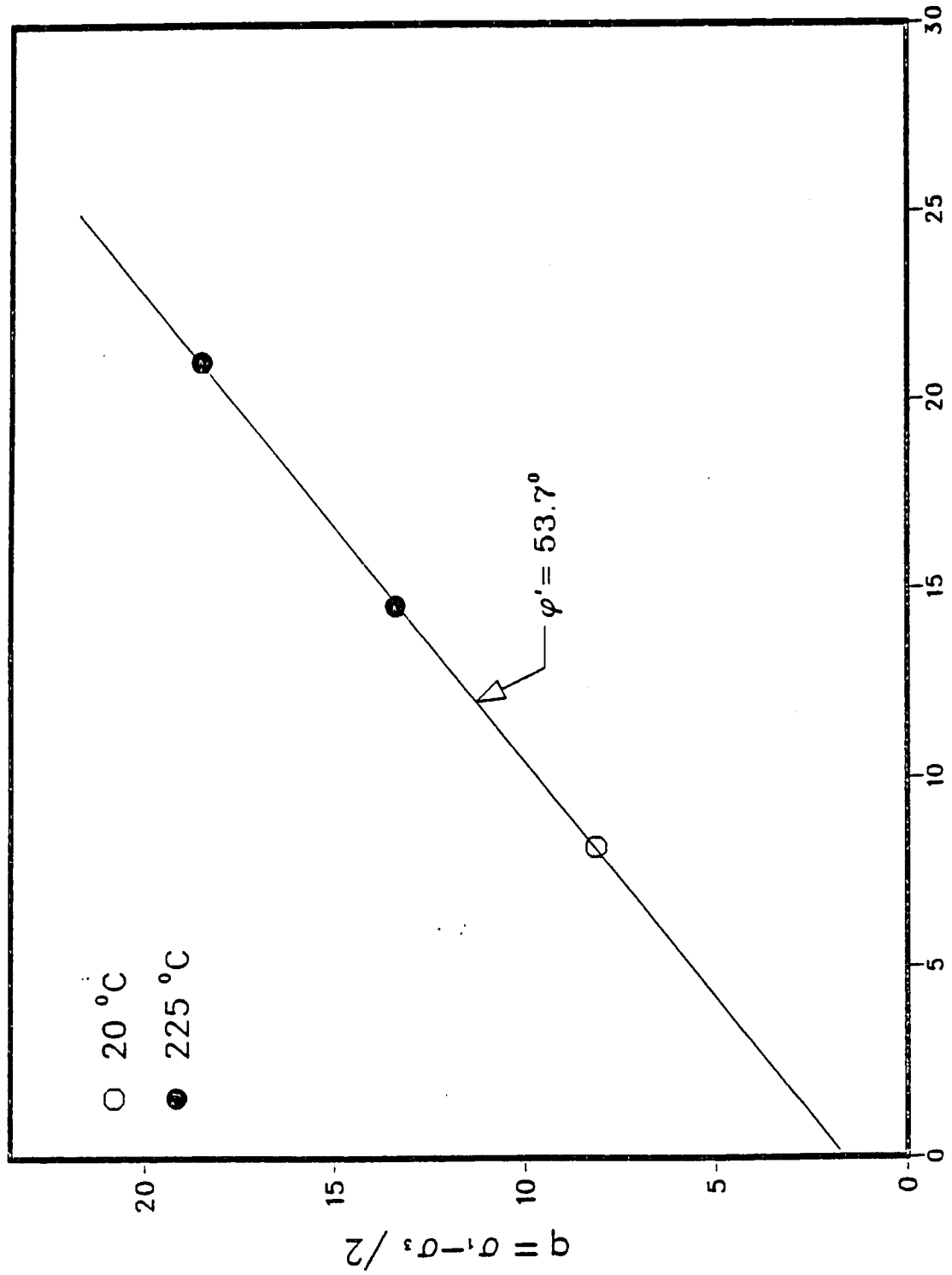

Figure 8.9 Triaxial Compression Tests on Devonian Limestone

Comparing the 225°C test results to those determined by Mathews, Rawlings and Bharti and considering no visual evidence of thermal cracking was found after either the high temperature triaxial test or the one-dimensional thermal volume change test (see Section 5.2.3) may suggest the shear strength of intact, low shale content limestone is not adversely affected at 225°C. This conclusion appears to contradict other studies in the literature which have demonstrated that intact rock specimens usually experience some degree of thermal cracking during heating (eg. Lo and Wai, 1982; Richter and Simmons, 1974; and Cooper and Simmons, 1977). It is noted, however, that the test procedures employed by these investigators differed significantly from those employed in this study. For example, the test procedure adopted by Lo and Wai (1982) for tests conducted on Darlington limestone differed in two important aspects:

1. Specimens were heated at a rate of 120°C per hour as compared to a rate of 25°C per hour used in this study.

2. Specimens were heated unconfined in an electric furnace and were, therefore, susceptible to pore fluid vapourization and drying. In contrast, the limestone in this study was heated with a back fluid

pressure of 7.5 MPa, sufficient to preclude phase change of the pore water. A constant effective confining stress of 1.0 MPa was applied to the specimen prior to heating.

Lo and Wai report that thermal cracking of Darlington limestone following the above procedure occurs at approximately 200°C. They attribute the formation of micro-cracks to differential rates of heat transfer through the mineral solids in the rock matrix which leads to the development of shearing and tensile stresses. They note, as a result of thermal cracking, the strength and stiffness of the intact rock decreases at elevated temperatures.

Athabasca Devonian strata near the unconformable surface has a complex geology with the material ranging from relatively weak, limey shale to relatively strong, massive limestone. Four major geotechnical facies have been identified. This phase of the experimental testing has dealt with the strength and deformation behaviour of fairly competent limestone. This strata is representative of only one geotechnical facies encountered in the SATAC recovery process. As the limestone itself is a strong and stiff material, the mechanical behaviour of the other geotechnical facies which contain appreciable amounts of shale are likely to govern the stability of tunnels, shafts and well casings passing through or near the unconformable surface. It is,

therefore, necessary to sample and test materials representative of each geotechnical facies in order to develop an accurate and reliable constitutive model for numerical or analytical analyses.

8.6 Summary and Conclusions

The shear strength and stress-strain behaviour of Athabasca oil sands related strata obtained from the Underground Test Facility site were examined. The materials studied included one shale facies from the overlying Clearwater Formation (high plastic k_{cc} shale) and one limestone facies from the underlying Waterways Formation (massive microcrystalline limestone containing 10% calcareous shale by volume in thin, discontinuous seams and clasts). The influence of temperature, pressure and stress path on the strength and deformation constitutive behaviour of these materials was investigated.

The fully drained thermal volume change characteristics of Clearwater k_{cc} shale and Devonian intact limestone are significantly different. The volume of the limestone increases with temperature while the shale displays a volume decrease. These results indicate that the volume change of the soil structure dominates that of the mineral grains in shale while the opposite is true for the limestone where the volume change of the mineral grains dominates the total volume change. In other words, heat consolidation is significant for Clearwater k_{cc} shale. A review of the

literature has indicated that the rate and the magnitude of thermal volume change during drained heating is the mechanism controlling the strength and deformation behaviour of these materials at elevated temperatures. The strength and stiffness of shale will increase if appreciable densification occurs during the heat induced compaction process. In contrast, these mechanical properties of intact crystalline rock will decrease if separation along grain boundaries occurs due either to rapid heating or to fluid volumetric expansion and/or fluid pressure increase which cannot be controlled.

The k_{cc} shale specimens tested in this study displayed a significant volume reduction, up to 11.6%, during drained heating. The magnitude of the volume decrease was higher in specimens whose initial void ratios were higher. The amount of heat induced consolidation, therefore, is dependent on the degree to which the shale has been pre-consolidated.

Despite the decrease in void ratio for specimens subjected to heat consolidation, data relating shear strength, effective stress at failure and water content at failure fell within a narrow band. These results suggest that although slow heating of k_{cc} shale, so that drainage of water can occur, will result in densifying the shale, the overall increase in strength and stiffness may not be significant. The medium to high plastic shales of the k_{ca} unit would be expected to behave in a manner similar to the shales of the k_{cc} unit. However, drained heating may cause

much more dramatic changes in the strength and deformation behaviour of the relatively weak, low density, smectite-rich shales of the k_{cb} unit.

Athabasca Deposit formation strata has a complex geology. Figure 8.10 is a summary plot showing k_f envelopes at failure for four major geotechnical facies examined in this study. It is evident that wells placed in an oil sands reservoir either by drilling from the ground surface or by drilling from an underground tunnel will intersect a wide range of materials each displaying significantly different mechanical behaviour. Figure 8.10 illustrates that the strength and stress-strain behaviour of a particular geotechnical facies is controlled by the relative proportion of weaker shale strata. This would imply that the overall constitutive behaviour of the Devonian group strata is governed by the limey shale and shale interbedded limestone facies which exist near the unconformable surface at the base of the McMurray Formation.

The effect of temperature on the mechanical behaviour of these materials is mainly to increase the pore fluid pressure from expansion of the pore fluids. If these pore fluid pressures cannot dissipate, effective stresses and, therefore, the shear strength will decrease. The rate of pore fluid dissipation is controlled by such factors as the dynamic viscosity of the pore fluid, the absolute permeability (a coefficient dependent on the properties of the soil skeleton only) and the density of the pore fluid.

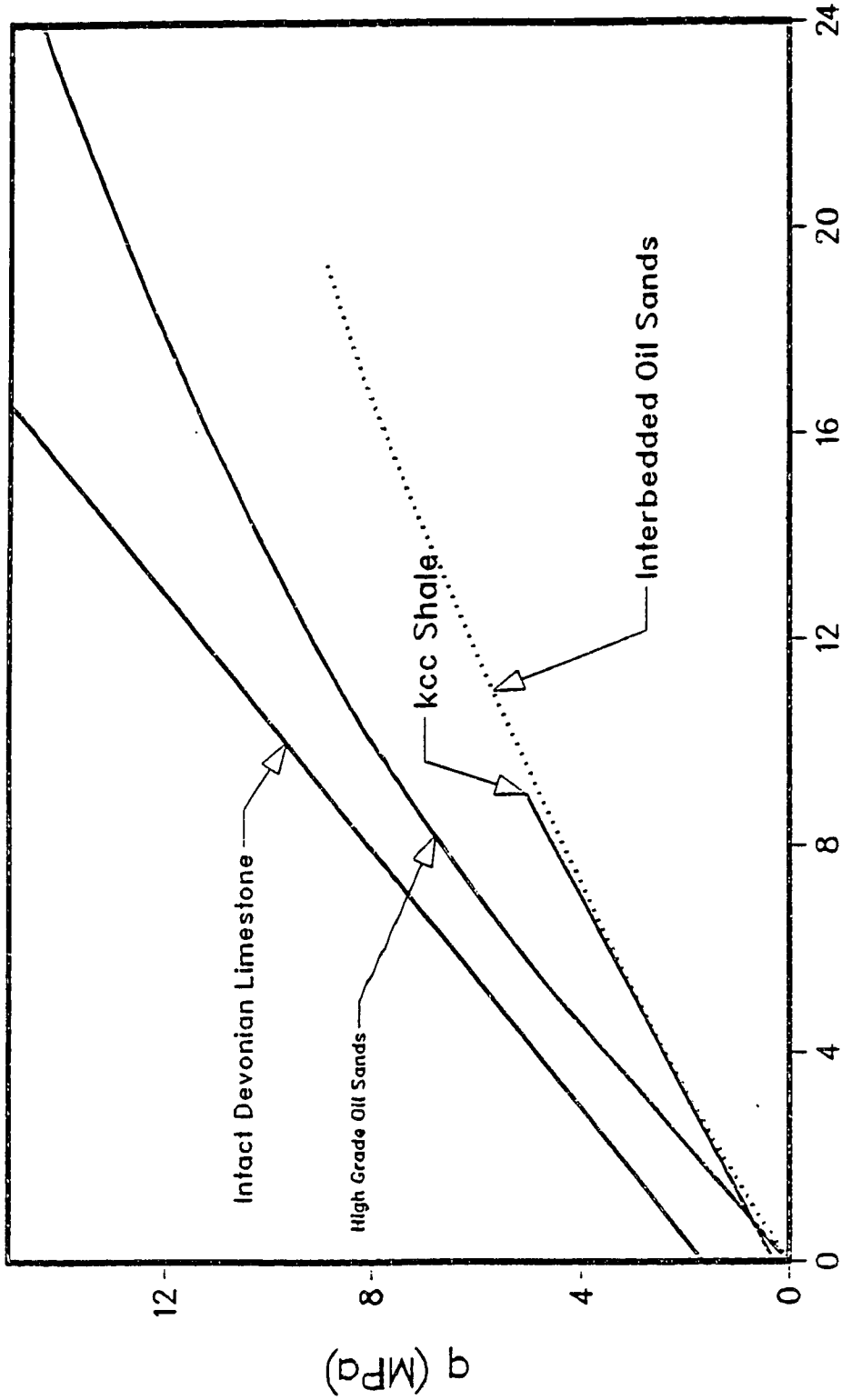

Figure 8.10 Shear Strength of Athabasca Oil Sands and Related Strata

Zones susceptible to large sustained pore fluid pressure increases are oil sands where the bitumen is not mobile, high water content shale Clearwater facies, and the limey shale and interebedded shale and limestone facies of the Devonian Group. Since horizontal stresses are higher than vertical stresses at depths less than 250 m in the Athabasca Deposit (Chhina and Agar, 1985), thermally induced pore fluid pressures will cause shear deformations. Shear deformations will also arise from the large horizontal stress increases caused by mineral grain expansion in the stiff, low fines oil sands facies in the oil sands production zones. The most probable location of shearing problems would be the lower Clearwater shale, oil sands containing high percentages of shale seams and upper Devonian limestone with clay laminations.

The results of tests performed on oil sands related strata serve to illustrate the limitations associated with simple idealized representation of geotechnically complex formation strata in analysis of such problems as formation shearing, hydraulic fracture propagation, well casing performance and the stability of underground openings (uncased wells, tunnels and shafts). Over-simplification will invariably lead to incorrect results.

9. THERMAL VOLUME CHANGE OF COLD LAKE MATERIALS

9.1 Materials Studied

As discussed in Chapter 2, Section 2.1.5, the Clearwater Formation in the northern part of the Cold Lake Deposit consists of a complex sequence of marine sands, silts and shales. Specimens used in the laboratory program were taken from four separate well locations northwest of Cold Lake. The geological detail of these core samples is outlined in Chapter 4, Section 4.2.

Location No. 2 oil sands consisted of homogeneous, high bitumen content, fine grained sand. Oil sands core samples from Locations 1, 3 and 4 were also fine grained but contained frequent interbedded shale seams ranging in thickness from 1 mm to a few cm. Two geotechnical facies from strata adjacent to Location No. 1 and Location No. 4 oil sands were also tested. Each of these facies had a thickness of about 1 m and consisted of a ferron calcite cemented sand and a hard, highly fissile, highly plastic shale. Data describing thermal volume change test specimens are summarized in Table 9.1.

9.2 Oil Sands

A series of one-dimensional thermal volume change tests were carried out on Cold Lake Clearwater Formation oil sands under fully drained and fully undrained conditions. A constant back fluid pressure sufficient to prevent gas

Table 9.1 Cold Lake Clearwater Formation Volume Change Specimens

Test Number	Depth (m)	Lithology	% water (mass)	% bitumen (mass)	% solids (mass)	% fines (<0.074 mm)	liquid limit (%)	plastic limit (%)
CL1COS1	442.7	Oil Sands	8.2	7.3	84.5	22.4		
CL1COS2	442.7	Oil Sands	8.2	7.3	84.5	5.4		
CL1COS3	445.8	Oil Sands	9.9	6.1	84.0	19.4		
CL1CCS1	449.5	Shale	14.4	0	85.6	----	82.6	36.5
CL1CCS2	449.6	Shale	16.5	0	83.5	----	82.6	36.5
CL2COS1	460.5	Oil Sands	7.8	11.1	81.1	10.0		
CL3COS1	487.2	Oil Sands	8.9	6.0	85.1	10.0		
CL3COS2	487.0	Oil Sands	6.4	9.0	84.6	19.7		
CL3COS3	487.3	Oil Sands	11.7	3.9	84.4	27.1		
CL4COS1	474.6	Oil Sands	8.6	9.4	82.0	26.0		
CL4COS2	474.6	Oil Sands	12.4	2.8	84.8	43.3		
CL4COS3	474.6	Oil Sands	11.4	3.2	85.4	41.1		
CL4COS4	474.6	Oil Sands	11.4	3.2	85.4	41.1		
CL4CL1	466.2	Carbonate Rock	--	---	----	----		

evolution (normally 7.5 MPa or 10.0 MPa) was maintained during the tests. Drained thermal volume change was measured at a vertical effective confining stress of 7.0 MPa (the approximate in situ average effective stress) and at a nominal stress of 0.5 MPa. The procedures employed in the testing program were developed recognizing the difference in sand grain mineralogy, geological environment of deposition and geological history between the Athabasca and Cold Lake Deposit sands. As outlined and discussed in Chapter 2, Athabasca oil sands consist of a uniformly graded, predominantly quartz sand whereas Cold Lake oil sands contain several minerals which may be much weaker. In order to evaluate the influence this geological variability has on structural changes in the sand structure of Cold Lake oil sands during heating, the stress path prior to heating and the rate of temperature loading was varied in a number of tests. In all cases, however, to ensure structural changes could be related directly to stress and temperature history, the rate of temperature increase was always slow enough to ensure that a constant uniform pore fluid pressure was maintained throughout the entire test specimen. Sample and test data for the thermal volume change tests are summarized in Table 9.2.

Table 9.2 Cold Lake Oil Sands Thermal Volume Change Test and Specimen Data

Test Number	Location Number	Effective Confining Stress (MPa)	% water (mass)	% bitumen (mass)	% solids (mass)	Bulk Density (Mg/m3)	Void Ratio init.	Void Ratio pre-test	Index of Disturbance (%)
CL1COS1	1	7.0	8.2	7.3	84.5	1.78	0.76	0.49	32.2
CL1COS2	1	7.0	8.2	7.3	84.5	1.82	0.72	0.53	28.3
CL1COS3	1	7.0	9.9	6.1	84.0	1.88	0.68	0.48	20.4
CL2COS1	2	7.0	7.8	11.1	81.1	1.78	0.84	0.53	19.2
CL3COS1	3	0.0	8.9	6.0	85.1	1.94	0.61	0.45	18.9
CL3COS2	3	7.0	6.4	9.0	84.6	1.93	0.62	0.43	17.9
CL3COS3	3	7.0	11.7	3.9	84.4	2.11	0.49	0.33	0.0
CL4COS1	4	0.0	8.6	9.4	82.0	1.87	0.73	0.48	14.6
CL4COS2	4	0.0	12.4	2.8	84.8	1.86	0.68	0.46	25.7
CL4COS3	4	0.5	11.4	3.2	85.4	1.88	0.65	0.65	26.4
CL4COS4	4	0.5	11.4	3.2	85.4	1.87	0.66	0.42	27.4

Location No. 1 Oil Sands

The results of three fully drained volumetric thermal volume change tests carried out on Cold Lake oil sands from Location No. 1 are shown in Figure 9.1. Each specimen was heated under a vertical effective confining stress of 7 MPa; however, the respective stress histories and temperature loading paths were varied in each test. Specimen CL1COS1 was compressed one-dimensionally to 12 MPa and cycled over the vertical effective stress range of 4 MPa to 12 MPa prior to heating. Specimens CL1COS2 and CL1COS3 were each compressed to 7 MPa prior to heating. Each specimen was heated at a rate of 25°C per hour with the exception of Specimen CL1COS2 which was held at 150°C for 17 hours.

Several important conclusions concerning the influence of stress history and temperature loading path on the drained thermal volume change behaviour of Clearwater Formation oil sands may be derived from these test results:

1. Specimen CL1COS1 displays a cumulative volume increase throughout the test. In contrast, the other two specimens show an initial volume increase to about 50°C followed by a volume decrease. Both specimens show a net volume decrease at 225°C. Since all specimens had approximately the same void ratio prior to heating, the difference in drained thermal volume change behaviour may be due to the history of stress applied to the specimens prior to heating.

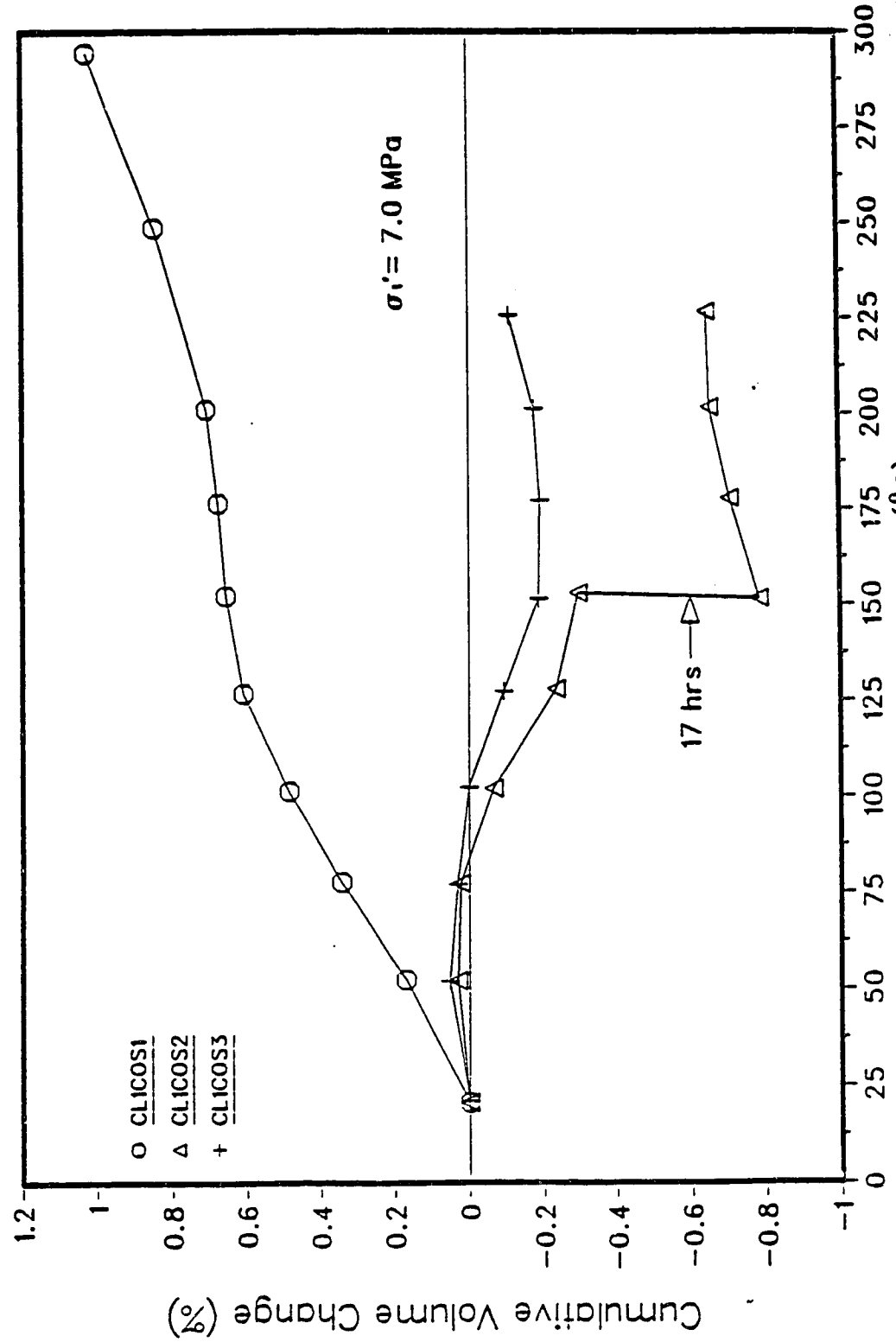

Figure 9.1 Drained Thermal Volume Change of Cold Lake Oil Sands (Location No. 1)

Rearrangement of the sand matrix resulting from thermal shear stresses developed due to lateral constraint in the oedometer is less significant for the specimen subjected to a vertical effective stress of 12 MPa followed by cycling of stress prior to heating. The shearing resistance of the sand grain contacts is greater in the cycled specimen. A significant rearrangement of the sand matrix is required for the non-cycled specimens to carry the 7 MPa vertical effective confining stress at higher temperatures.

2. There is an abrupt reduction in the rate of thermal volume change of Specimen CL1COS1 at 125°C. This indicates either a significant amount of temperature induced grain breakage or a major rearrangement of the sand structure.

3. Specimen CL1COS2 displays a volume reduction of 0.5% during thermal creep after 17 hours at 150°C. The weakening of interparticle shearing resistance at elevated temperatures which allows rearrangement of the sand matrix to occur is, therefore, a time dependent process.

4. Specimens CL1COS2 and CL1COS3 both show a volume increase above 150°C. The specimen which experienced the greater volume decrease up to 150°C also shows a greater thermal volume increase above 150°C. This is attributed to the higher interparticle shearing resistance of the thermally densified sand structure.

Location No. 2 Oil Sands

Drained thermal volume change of Location No. 2 oil sands is shown in Figure 9.2. Prior to the drained thermal expansion test, the specimen was compressed to 12.5 MPa and cycled over the vertical effective confining stress range of 7 MPa to 12.5 MPa. The specimen was subsequently heated under a vertical effective confining stress of 7.0 MPa. A heating rate of 25°C per hour was employed in the test.

The results from this test are similar to those observed for Specimen CL1COS1 which was subjected to a similar history of stress prior to heating. There is an abrupt decrease in the rate of volume change at 75°C indicating structural collapse of the sand matrix or thermal grain crushing.

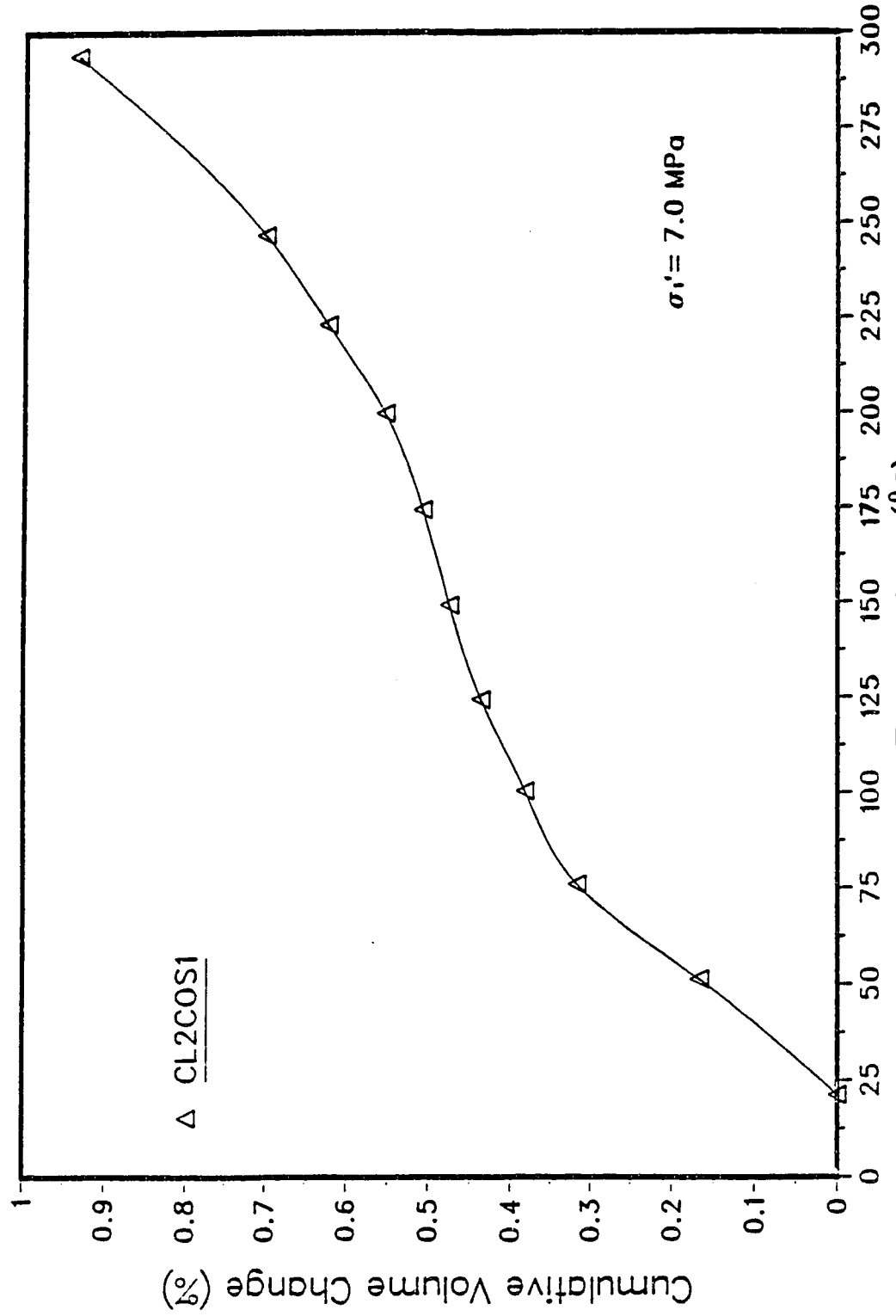

Figure 9.2 Drained Thermal Volume Change of Cold Lake Oil Sands (Location No. 2)

Location No. 3 Oil Sands

The results of two fully drained thermal volume change tests carried out on Location No. 3 oil sands are shown in Figure 9.3. The stress history was the same for each test, both specimens were compressed to 7.0 MPa effective confining stress prior to heating. Each specimen was heated at a rate of 25°C per hour, thermal creep tests were performed at 150°C (CL3COS2) and at 175°C (CL3COS3).

The rate and magnitude of thermal volume change, as well as the magnitude of thermal creep was found to be dependent on the degree of particle packing prior to heating; that is:

1. Specimen CL3COS2, which had a void ratio of 0.43 prior to heating, displayed negligible volume change over the temperature range of 20°C to 150°C. A volume decrease of 0.3% was measured during 15 hours of thermal creep at 150°C. Over the temperature range of 150°C to 225°C the specimen shows a steady volume increase.

2. Specimen CL3COS3, which had a void ratio of 0.33 prior to heating, showed a steady volume increase from 20°C to 225°C. Negligible thermal creep was

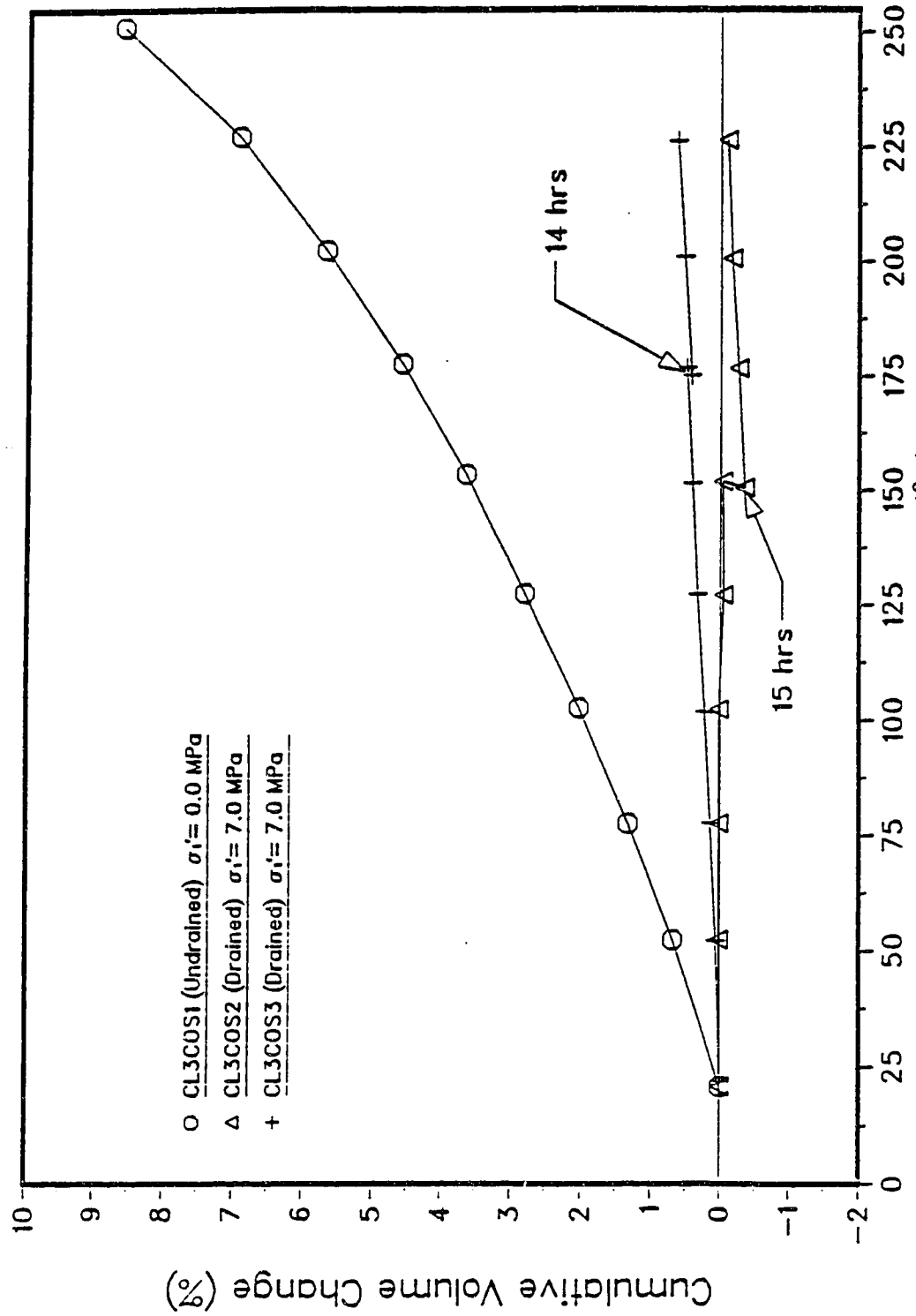

Figure 9.3 Thermal Volume Change of Cold Lake Oil Sands (Location No. 3)

observed after 14 hours at 175°C.

The results of an undrained thermal volume change test are also shown in Figure 9.3. The test was carried out under zero vertical effective confining stress (that is, a free expansion test) at a pore fluid pressure of 10.0 MPa. The specimen was heated at a rate of 25°C per hour. As discussed in Chapter 5, Section 5.3, thermal expansion tests performed on oil sands under fully undrained conditions generate volume increases of mineral grains and pore liquids. Based on the undrained test results, thermal increases of approximately 9% would be expected when Cold Lake Location No. 3 oil sands are heated to 250°C, provided the back fluid pressure is sufficient to keep gases in solution.

Location No. 4 Oil Sands

Drained thermal volume change results for Location No. 4 oil sands are given in Figure 9.4. Both tests were performed at a nominal effective confining stress of 0.5 MPa. Specimen CL4COS4 was compressed to 7 MPa prior to testing while Specimen CL4COS3 was tested in the disturbed state. Each specimen was heated at a rate of 25°C per hour. Specimen CL4COS4 was held at 75°C for 12 hours. The void ratio of Specimen CL4COS4 was slightly smaller, 0.42 as

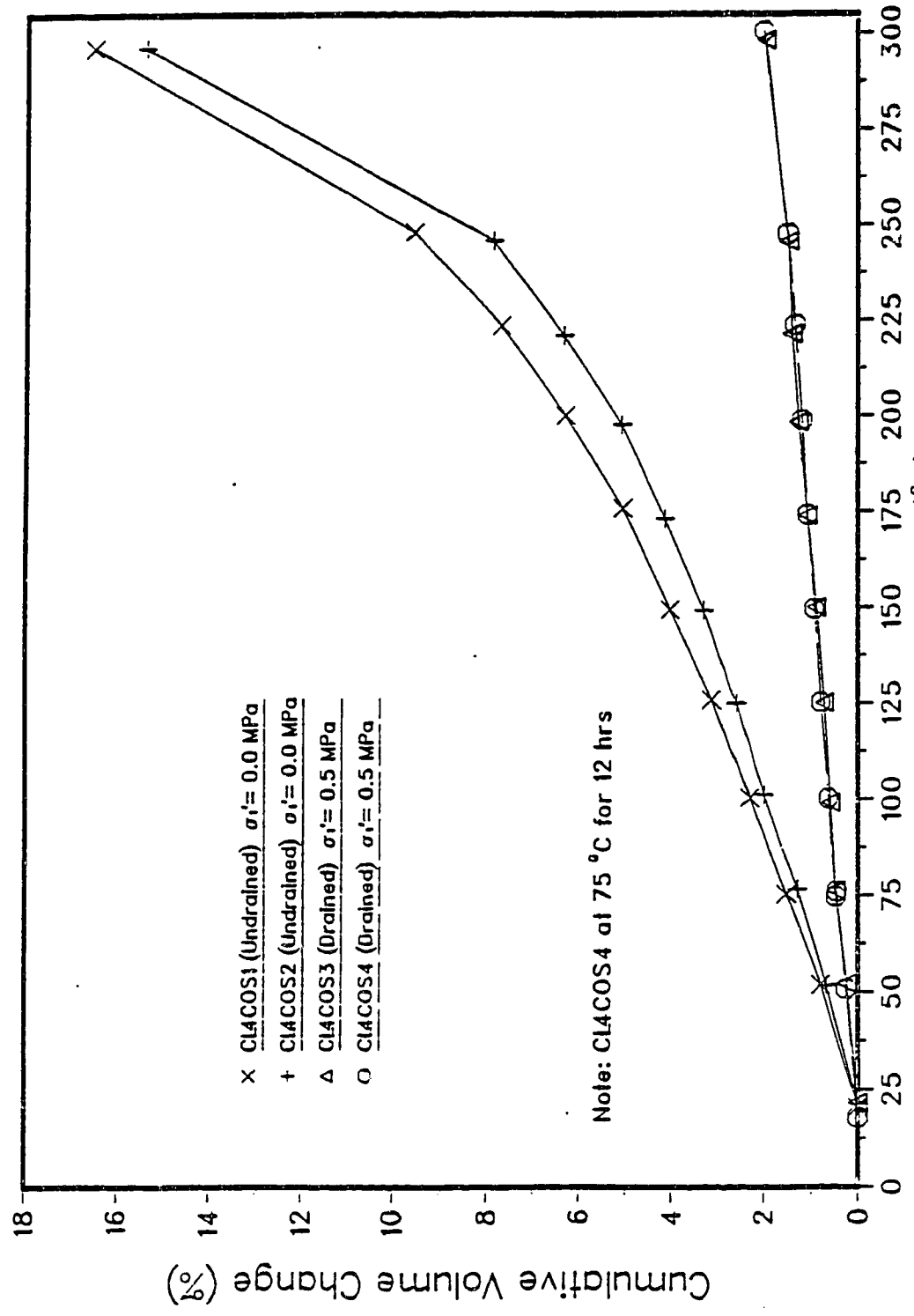

Figure 9.4 Thermal Volume Change of Cold Lake Oil Sands (Location No. 4)

compared to 0.65, reflecting the irreversible strain due to prestressing. The thermal volume change behaviour of these two specimens are virtually identical with each specimen displaying a volume increase of 2% over the temperature range of 20°C to 300°C.

Undrained thermal expansion tests performed on Cold Lake Location No. 4 oil sands are also shown in Figure 9.4. The specimens were heated at a rate of 25°C per hour at a back pore pressure of 10.0 MPa. Small differences in the undrained thermal volume change behaviour are attributed to variations in the proportion of mineral solid to pore liquid in each test specimen. The undrained test results are consistant with those determined for Location No. 3 oil sands.

Discussion

Under fully drained conditions the volume change of oil sands subjected to increases in temperature arises from the expansion of the individual sand grains and structural changes in the sand skeleton. Figure 9.5 illustrates the volume change with temperature of quartz grains (the predominant mineral in Cold Lake oil sands, see Chapter 2) alone and the sand grains and sand skeleton from the drained thermal expansion tests. The volumetric coefficient of thermal expansion of quartz ranges from 3.4×10^{-5} $°C^{-1}$ to

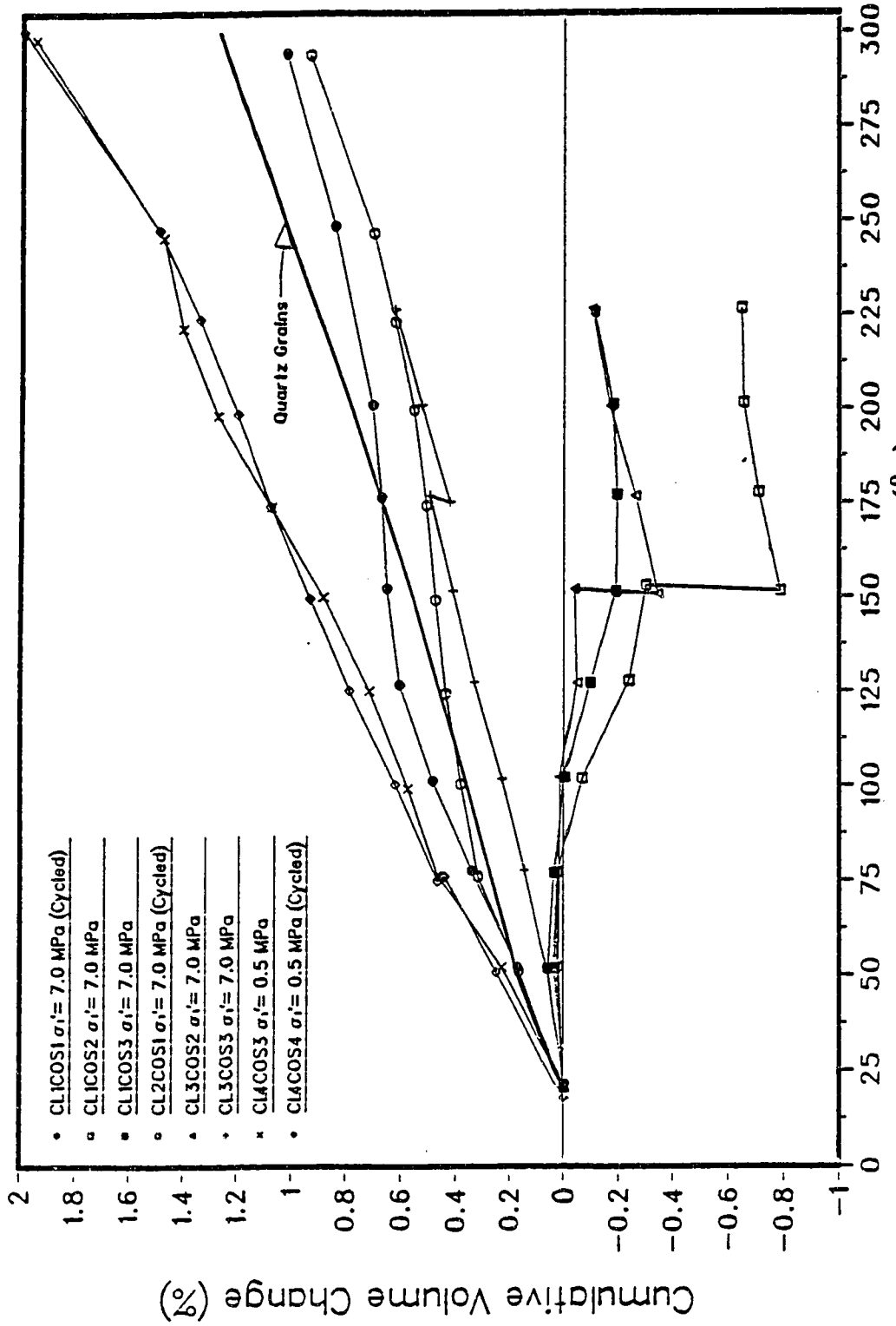

Figure 9.5 Drained Thermal Volume Change of Cold Lake Oil Sands

20°C to 6.9 x 10^{-5} $°C^{-1}$ at 400°C (Clark, 1966). The secondary constitutive mineral solids have similar volumetric thermal expansion coefficients. For example, the coefficient for feldspar ranges from 1.2 x 10^{-5} $°C^{-1}$ at 20°C to 2.7 x 10^{-5} $°C^{-1}$ at 400°C. The volumetric coefficients for volcanic, shale, sandstone, siltstone, metamorphic and plutonic rock fragments vary from 1.6 x 10^{-5} $°C^{-1}$ to 3.3 x 10^{-5} $°C^{-1}$ over the temperature range of 20°C to 100°C (Clark, 1966). For purposes of this discussion, the volume change with temperature of quartz, shown in Figure 9.5, will be assumed to be representative of the mineral solids in Cold Lake oil sands.

The difference between the temperature-volume change curve for quartz grains and the drained thermal expansion curves represent the volume change of the sand structure. The specimens heated at an effective confining stress of 0.5 MPa show the greatest sand grain matrix expansion. The non-cycled specimens tested at an effective confining stress of 7 MPa display the greatest structural collapse during heating.

The magnitude of drained thermal expansion depends on structural changes which occur in the sand grain matrix during heating. Structural changes are in turn dependent on the frictional resistance of individual interparticle contacts, the strength of the individual sand grains and the magnitude of thermally induced interparticle forces. The relative contribution each of these factors makes to the

thermal volume change of the sand matrix depends on the effective confining stress and the history of stress experienced by the oil sands.

Specimens after being cycled above in situ stresses develop a soil structure which is much stiffer than that attained during initial loading as much of the potential slip between sand grains has previously taken place during the initial loading cycle. Under these conditions the overall frictional resistance of the sand grain contacts are high. The development of thermally induced shear stresses as a result of lateral constraint during heating in the oedometer are also high. The sand matrix can expand during the onset of heating but, as thermally induced shear stresses increase, some weakening and crushing of the sand grains occurs. As some sand grains crush, the sand grains must move and reorientate themselves to permit the structure to carry the same effective stress as shown in Figure 9.6. The amount of structural collapse decreases as the sand structure densifies. The above mechanisms result in S-shaped thermal expansion curves as shown in Figure 9.5.

Specimens recompressed to approximate in situ stresses and not cycled attain soil structures which may be significantly more compressible than the dense sand structure found in situ. In this case, the overall frictional resistance of the sand grain contacts is lower than for cycled samples. As a result, as thermally induced shear stresses develop, the shearing resistance is overcome

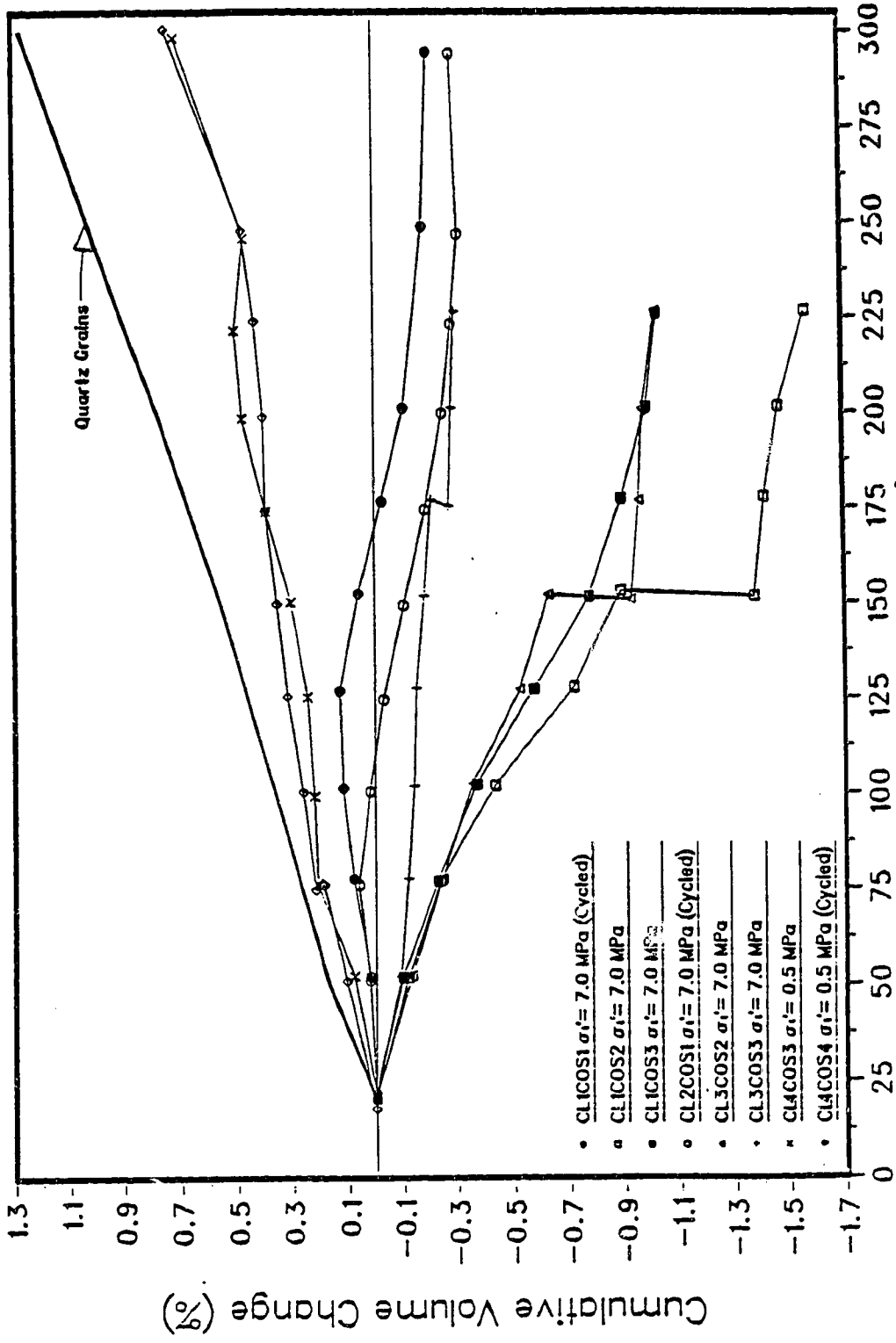

Figure 9.6 Thermal Volume Change of Sand Structure of Cold Lake Oil Sands

and the sand grains must slide over each other and reorientate into a denser configuration to carry the effective stress. This is a time dependent process, as evidenced by the thermal creep experienced by Specimens CL1COS2, CL1COS3 and CL3COS3 (Figure 9.5). Eventually, the sand matrix attains a dense structure and thermal volume increases occur as shown in Figure 9.5. Whether or not the sand matrix expands or contracts after a dense packing is achieved depends on the strength of the sand grains and the amount of thermal grain crushing which occurs.

The sand structure of specimens heated under an effective confining stress of 0.5 MPa expands regardless of the history of stress applied to the specimens prior to heating. In this case, although the overall frictional resistance is low, thermally induced shear stresses are also low and little grain movement is required to carry the effective stress during heating. The drained thermal expansion curves are fairly linear (Figure 9.5) because the shear stressses are not high enough to cause significant grain crushing.

The maximum amount of drained thermal expansion occurs at low effective confining stresses because the amount of temperature induced grain breakage and rearrangement of the sand structure is least. A drained thermal volume increase of Cold Lake oil sands of about 2% can be expected over the temperature range of 20°C to 300°C. The minimum amount of drained thermal expansion occurs at in situ stresses and the

rate of volumetric increase is non-linear due to grain breakage and structural collapse. Under these conditions a thermal volume increase of about 1% can be expected over the temperature range of 20°C to 300°C.

For fully undrained conditions the volume change of oil sands subjected to increases in temperature occurs from expansion of the individual mineral grains and pore liquids. Structural changes in the soil skeleton do not occur during undrained heating. The amount of thermal expansion depends on the proportion of mineral solids to pore liquid. A thermal volume increase of about 17% can be expected during undrained heating to 300°C.

During in situ production, if pore fluid drainage occurs at a rate greater than or equal to that of heat flow, the excess pore pressures will be fully dissipated. Volume changes will be due to the sum of the thermal expansion of the sand grains and the expansion or consolidation of the sand structure. The sand structure may increase or decrease in volume depending on its initial density, compressibility and effective stress and stress path followed during heating. If drainage occurs at a rate slower than that of heat flow, the oil sands mass will be partially drained and additional soil deformations to those above will be caused by pore fluid expansion and by shear strains resulting from the decrease in effective stress.

9.3 Clearwater Shale

Thermal volume change of a Clearwater Formation shale facies from Cold Lake Location No. 1 was measured in tests CL1CCS1 and CL1CCS2. Prior to thermal volume change testing the test specimens were consolidated one-dimensionally at a vertical effective confining stress of 6.5 MPa. The results of a fully drained and a fully undrained volumetric thermal expansion test are shown in Figure 9.7. The drained test was carried out at the effective confining stress of 6.5 MPa while the undrained test was performed under an effective confining stress of 0.0 MPa. A back fluid pressure of 10 MPa was maintained during the tests to prevent gas evolution. The test results shown in Figure 9.7 represent volume change as a percentage of the original sample volume at 1 hour heating increments of 25°C.

The thermal expansion test carried out on shale under undrained conditions generates volume increases of clay particles and pore liquids. Since the thermal volume change of water is well established over a range of pressures in the literature and the water content and volume of the specimen were measured prior to testing, it is possible to back calculate the thermal expansion behaviour of the clay particles. The thermal volume change of the mineral solids is shown in Figure 9.7. For comparative purposes, the volume change with temperature of illite clay particles is also shown. The volumetric coefficient of thermal expansion of illite was estimated to be 0.35×10^{-4} °C^{-1} (Mitchell and

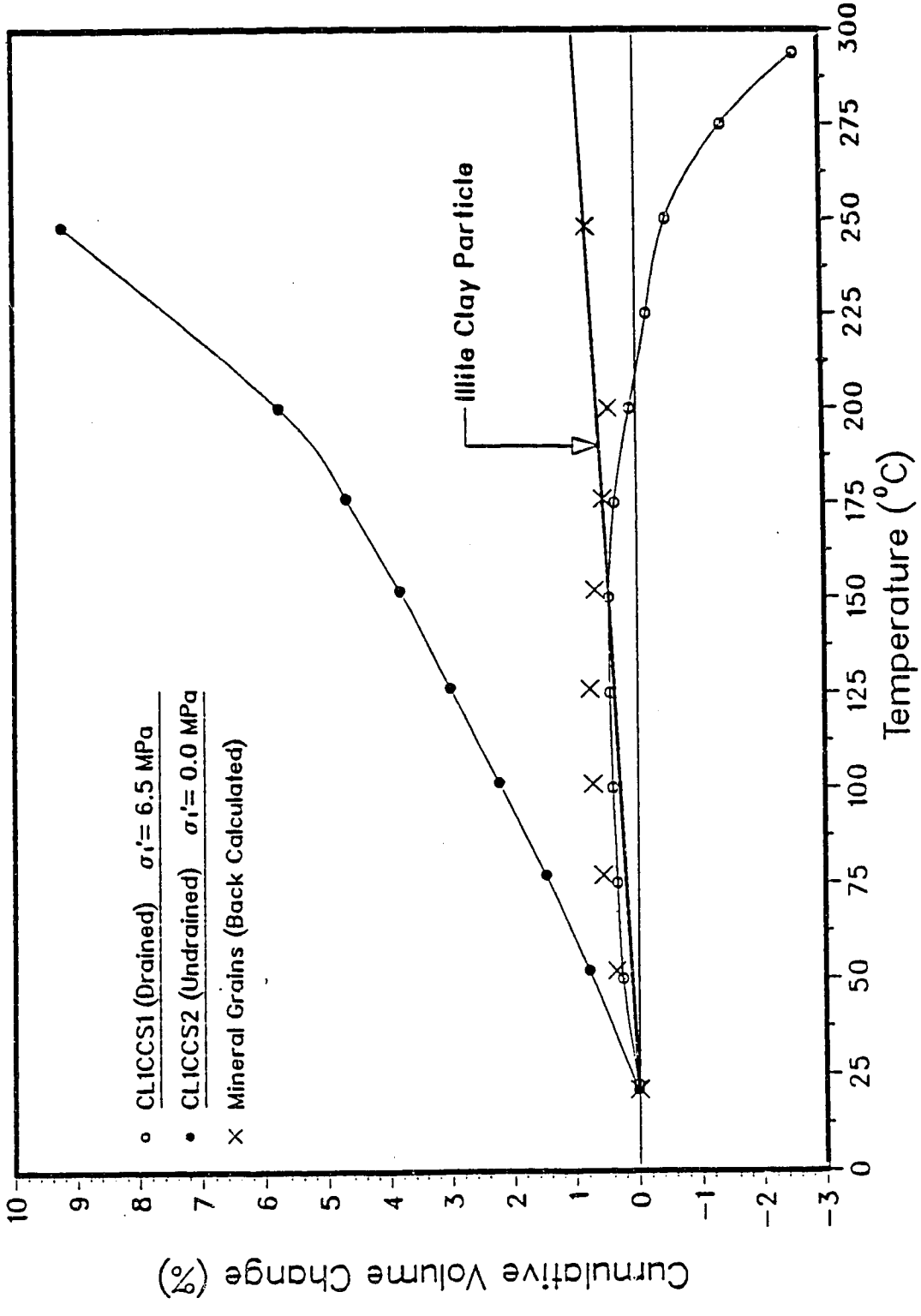

Figure 9.7 Thermal Volume Change of Cold Lake Clearwater Shale

Campanella, 1968). The volumetric expansion of the clay particles determined from the undrained test are highly non-linear and greater than illite below 150°C and approximately the same above 150°C. Illite is the principal clay found in Clearwater Formation shale in the Athabasca Deposit (Issac et al, 1982).

The undrained thermal expansion test shows a volume increase of about 9% over the temperature range of 20°C to 250°C, whereas the drained test shows a thermal volume decrease of about 0.4% over the same temperature range. Since the drained thermal expansion test is a measure of the volume change of the clay particles and soil structure, a significant amount of heat induced consolidation is occurring. Comparing the drained thermal volume change with back calculated mineral grain expansion shows some structural collapse occurs at the onset of the temperature increase. Structural collapse becomes significant at about 100°C and, therefore, a temperature increase to about 100°C is required to overcome the mechanical pre-consolidation pressure of 6.5 MPa.

As previously discussed, structural changes in a soil matrix during drained heating are dependent on interparticle forces, frictional resistance and cohesion. The mechanisms in shales differ slightly from those of sands and are similar to secondary compression under a stress increase (Mitchell, 1976). As the temperature is increased thermally induced shear stresses develop and if the shear strength of

individual interparticle contacts is exceeded the soil structure contracts until enough bonds are formed to allow the shale to carry the same effective stress at higher temperatures. Green (1984) suggests that the attractive forces between clay particles decreases as the temperature increases which causes the interparticle shearing resistance to be reduced.

The drained thermal volume change results were based on 1 hour heating increments of 25°C. The effect of time on the volume change behaviour at constant temperature was not addressed. From the results obtained on Athabasca Clearwater shale and those reported by Green (1984), Williams (1982), Campanella and Mitchell (1968) and others, heat consolidation is a time dependent process. It is probable that structural collapse of the soil structure in situ during slow and prolonged heating would be more severe than the short term results shown in Figure 9.7.

9.4 Clearwater Carbonate Rock

The drained thermal expansion of a highly competent calcite cemented sand facies from Cold Lake Location No. 4 was measured at an effective confining stress of 7.0 MPa. Volumetric thermal expansion results over the temperature range of 20°C to 300°C are shown in Figure 9.8. The specimen was heated at a rate of 25°C per hour and a back pressure of 10 MPa was maintained during the test to prevent gas evolution.

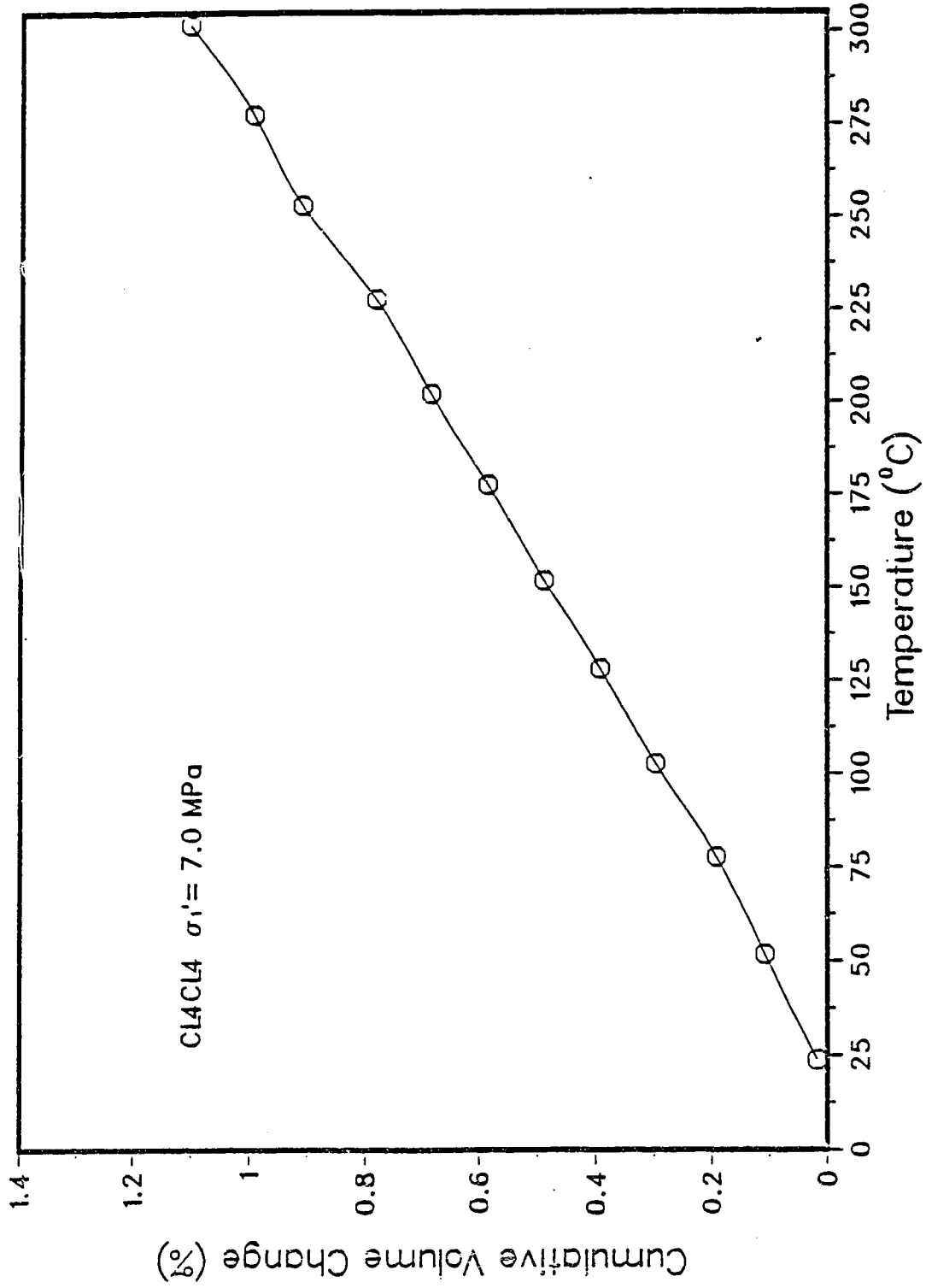

Figure 9.8 Drained Thermal Expansion of Cold Lake Clearwater Carbonate Rock

The volumetric thermal expansion is almost linear to 300°C. The volumetric coefficient of thermal expansion of this carbonate cemented rock is approximately 4.0×10^{-5} °C^{-1}. The cumulative volume increase at 300°C was approximately 1%.

The thermal expansion test carried out on cemented sand generates volume increases of the mineral solids only provided thermal cracking does not occur. Differential heat transfer through mineral solids in the rock matrix can cause the development of shearing and tensile stresses which result in micro-cracks forming. Although there were no visual signs of thermal cracking after the test, the sample displayed a net volume increase of 0.1% after cooling to 20°C. The specimen, therefore, experienced a small degree of thermal cracking during heating.

9.5 Summary and Conclusions

The thermal volume change constitutive behaviour of several Cold Lake Clearwater Formation geotechnical facies was examined. The mechanisms contributing to the thermal volume change of each material have been identified and documented.

Numerical methods used to calculate thermally induced ground deformations and stress changes during in situ production require as input the coefficient of thermal expansion. The coefficient of thermal expansion is maximum during undrained heating where volume change of the mineral

solids and pore liquids occur. The incremental coefficient of thermal expansion of liquid water varies from 2×10^{-4} °C^{-1} at 20°C to 1×10^{-3} °C^{-1} at 200°C and does not vary significantly with pore pressures up to 10 MPa. Kosar (1983) found Athabasca bitumen expanded slightly more than water. The incremental coefficient of thermal expansion of mineral solids such as quartz, feldspar, rock fragments and illite are in the order of 4×10^{-5} °C^{-1} over the same temperature range. The undrained coefficient is, therefore, dominated by the expansion of the pore liquids. The coefficient of thermal expansion is least during drained heating when the pore liquids drain as they expand. Volume change is due to expansion of the mineral grains and expansion or contraction of the soil structure.

Structural changes during drained heating have an important role in the thermal volume change behaviour of each material tested. Structural changes are dependent on the frictional resistance and/or cohesion of the individual interparticle contacts, the strength of the individual sand grains and the magnitude of thermally induced interparticle forces. Each of these components in turn depend on the effective confining stress and the history of stress experienced by the material.

Thermal strains, $\alpha\Delta T$, and compressive stress required to suppress thermal strain, $\alpha E\Delta T$, are large and relatively insensitive to stress history and effective stress for undrained conditions (provided pore fluids can expand

against the confining stress). During in situ production as flow takes place partial drainage occurs and eventually the fully drained condition may be attained. Under these conditions as the influence of pore liquids on the coefficient of thermal expansion decreases the effects of structural changes increase. The coefficient changes as the effective stress and stress history (or stress path) change.

Thermal stresses and strains during undrained heating of shale and oil sands and drained heating of cemented sand beds always increase in situ. Drained heating of oil sands and shale in situ will cause an initial increase in stresses and strains during the early stages of production when temperature increases are small. As temperature increases become large, the increase in thermal stresses and strain will level off in the oil sands as the coefficient of thermal expansion levels off due to structural collapse caused by grain crushing and rearrangement. For shale the thermal stresses and strains will decrease at higher temperatures as the soil matrix consolidates and the coefficient of thermal expansion becomes negative.

10. COMPRESSIBILITY OF COLD LAKE MATERIALS

10.1 Materials Studied

A series of one-dimensional and isotropic tests were conducted to assess the influence stress path and temperature have on the compressibility of Cold Lake Clearwater Formation oil sands. Oil sands from four separate locations in the Cold Lake Deposit were examined to evaluate the effect of spacial variations in mineralogy, geological environment of deposition and geological history on compressibility constitutive behaviour. The geological detail of the oil sands core samples is contained in Chapter 4, Section 4.2.

Oil sands core samples from Cold Lake Locations 1, 3 and 4 were comprised of fine grained sand and contained frequent interbedded shale seams ranging in thickness from 1 mm to a few cm. Specimen bitumen contents varied between 3 and 11% by weight. Location No. 2 oil sands consisted of homogeneous, high bitumen content (10 to 12% by weight), fine grained sand. One related geotechnical facies from strata adjacent to Location No. 1 oil sands was also tested. This facies consisted of a hard, highly fissile, highly plastic shale and had an overall thickness of about 1 m.

10.2 Oil Sands

The results of one-dimensional and isotropic compressibility tests performed on Cold Lake Clearwater Formation oil sands are summarized in Tables 10.1 through 10.6. Individual stress-volume change plots are given in Appendix E. Volumetric changes in mineral structure associated with deviatoric stress changes are presented and discussed separately in subsequent chapters.

A rich, homogeneous oil sands specimen from Cold Lake Location No. 2 experiencing four cycles of one-dimensional loading at 20°C is shown in Figure 10.1. The compressibility is high upon initial loading but reduces to lower values after the first stage of stress cycling. Two stress cycles over the range of 4 to 10 MPa result in approximately 0.4% of permanent or plastic strain. Two additional stress cycles over the range of 7 to 13 MPa result in 0.3% of plastic strain. The development of non-recoverable strain during stress cycling is indicative of grain breakage or crushing. Figure 10.2 is a plot of the grain size distribution of Specimen CL2COS1 before and after testing. The grain size distribution before the test was derived from oil sands taken from the core sample immediately adjacent to the test specimen. The effects of grain breakage can be observed from the grain size distribution curves shown in Figure 10.2. It is noted that this specimen, subsequent to the compressibility test, was subjected to drained heating at 7.0 MPa effective confining stress to 300°C (see Figure 9.2,

Table 10.1 One Dimensional Compressibility of Cold Lake Clearwater Formation Oil Sands (Location No. 1)

Initial Conditions

Test Number	Bulk Density (Mg/m3)	Dry Density (Mg/m3)	% water (mass)	% bitumen (mass)	% solids (mass)	% fines (<0.074 mm)	Void Ratio e	Sr (%)	Index of Disturbance (%)
CL1COS1	1.79	1.51	8.2	7.3	84.5	22.4	0.75	65	31
CL1COS2	1.82	1.54	8.2	7.3	84.5	22.4	0.72	67	28
CL1COS3	1.89	1.59	9.9	6.1	84.0	19.4	0.67	75	19

One Dimensional Compressibility

Test Number	Temp. (°C)	Measured							Calculated (assuming Poisson's ratio = 0.3)						
		Vertical Effective Stress Range (MPa)	Constrained Modulus D (MPa)						Average Principal Effective Stress Range (MPa)	Bulk Modulus K (MPa)					
			First Cycle		Second Cycle		Third Cycle			First Cycle		Second Cycle		Third Cycle	
			Load	Unload	Load	Unload	Load	Unload		Load	Unload	Load	Unload	Load	Unload
CL1COS1	20	4.0 - 12.0	149	1373	813	1366	1140	2074	2.5 - 7.4		850	503	846	706	1284
CL1COS2	225	7.0 - 9.0	412	594	476	596			4.3 - 5.6		368	295	369		
CL1COS3	225	7.0 - 9.0	495	559	547	598			4.3 - 5.6		346	339	370		

Table 10.2 Isotropic Compressiblity of Cold Lake Clearwater Formation Oil Sands (Location No. 1) at 20 °C

Initial Conditions

Test Number	Bulk Density (Mg/m3)	Dry Density (Mg/m3)	% water (mass)	% bitumen (mass)	% solids (mass)	% fines (<0.074 mm)	Void Ratio e	Sr (%)	Index of Disturbance (%)
CL1TOS1	1.89	1.58	10.0	6.5	83.5	20.0	0.68	77	18
CL1TOS2	1.89	1.56	12.9	4.5	82.6	20.0	0.70	80	15
CL1TOS3	1.90	1.59	7.3	9.2	83.5	29.0	0.67	78	17
CL1TOS4	1.82	1.49	8.9	9.4	81.7	17.0	0.78	76	18
CL1TOS5	1.83	1.51	7.2	10.2	82.6	17.0	0.75	74	20
CL1TOS6	1.83	1.49	12.6	5.9	81.5	33.2	0.77	78	16
CL1TOS7	1.85	1.50	9.3	9.3	81.4	9.4	0.76	79	15
CL1TOS8	1.84	1.51	12.8	5.2	82.0	48.5	0.75	77	17
CL1TOS9	1.83	1.48	8.2	10.7	81.1	18.7	0.79	78	16
CL1TOS10	1.87	1.55	9.9	7.2	82.9	20.4	0.71	77	17

Isotropic Compressibility

Test Number	Temp. (°C)	Calculated (assuming Poisson's ratio = 0.3)							Measured					
		Vertical Effective Stress Range (MPa)	Constrained Modulus D (MPa)						Average Principal Effective Stress Range (MPa)	Bulk Modulus K (MPa)				
			First Cycle		Second Cycle		Third Cycle			First Cycle		Second Cycle		Third Cycle	
			Load	Unload	Load	Unload	Load	Unload		Load	Unload	Load	Unload	Load	Unload
CL1TOS1	20	8.1 - 14.5		2706	1854				5.0 - 9.0	147	1675	1148			
CL1TOS2	20	8.1 - 14.5		2601	2460				5.0 - 9.0	457	1610	1523			
CL1TOS3	20	8.1 - 14.5		1822	1187				5.0 - 9.0	364	1128	735			
CL1TOS4	20	8.1 - 14.5		32[illegible]	2035	1640	1795	3040	5.0 - 9.0	334	1981	1260	1015	1111	1882
CL1TOS5	20	8.1 - 14.5		1[illegible]	2279				5.0 - 9.0	323	1169	1411			
CL1TOS6	20	8.1 - 14.5		17[illegible]	1733	1791	1832		5.0 - 9.0	175	1073	1109	1134		
CL1TOS7	20	8.1 - 14.5							5.0 - 9.0	288					
CL1TOS8	20	8.1 - 14.5		1413	1347				5.0 - 9.0	130	875	834			
CL1TOS9	20	8.1 - 14.5		2400	1909				5.0 - 9.0	---	1486	1182			
CL1TOS10	20	8.1 - 14.5		2499	2410	1628			5.0 - 9.0	480	1547	1492	1008		

Table 10.3 Isotropic Compressibility of Cold Lake Clearwater Formation Oil Sands (Location No. 1) at 225 °C

Initial Conditions

Test Number	Bulk Density (Mg/m3)	Dry Density (Mg/m3)	% water (mass)	% bitumen (mass)	% solids (mass)	% fines (<0.074 mm)	Void Ratio e	Sr (%)	Index of Disturbance (%)
CL1TOS11	1.84	1.52	7.4	9.9	82.7	14.0	0.74	75	19
CL1TOS12	1.84	1.52	7.8	9.7	82.6	12.8	0.74	76	18
CL1TOS13	1.94	1.62	10.2	6.2	83.6	21.1	0.63	82	13
CL1TOS14	1.73	1.40	8.3	10.4	81.2	10.4	0.89	68	24
CL1TOS15	1.93	1.60	8.9	7.8	83.3	30.5	0.65	81	14

Isotropic Compressibility

Test Number	Calculated (assuming Poisson's ratio = 0.3)			Measured		
	Vertical Effective Stress Range (MPa)	Constrained Modulus D (MPa)		Average Principal Effective Stress Range (MPa)	Bulk Modulus K (MPa)	
		20 °C	225 °C		20 °C	225 °C
CL1TOS11	7.4 - 12.0	1443	2441 **	4.6 - 7.4	893	1511 **
CL1TOS12	1.6 - 11.6	1191	1254	1.0 - 7.2	737	776
CL1TOS13	4.0 - 11.5	2229	2672	2.5 - 7.1	1442	1654
CL1TOS14	4.4 - 11.6	----	1898	2.7 - 7.2	----	1175
CL1TOS15	11.5 - 14.5	3673	7691	7.1 - 9.0	2274	4761

** Test Performed at 125 °C

Table 10.4 Compressiblity of Cold Lake Clearwater Formation Oil Sands (Location No. 2)

Initial Conditions

Test Number	Bulk Density (Mg/m3)	Dry Density (Mg/m3)	% water (mass)	% bitumen (mass)	% solids (mass)	% fines (<0.074 mm)	Void Ratio e	Sr (%)	Index of Disturbance (%)
CL2COS1	1.78	1.44	7.8	11.1	81.1	10.0	0.84	74	19
CL2TOS1	1.67	1.37	8.4	9.7	81.9	10.6	0.94	62	31
CL2TOS2	1.78	1.46	8.4	9.7	81.9	10.6	0.82	72	22
CL2TOS3	1.66	1.35	6.7	12.3	81.0	5.8	0.97	64	28
CL2TOS4	1.79	1.45	8.2	10.7	81.1	8.3	0.82	75	18

One Dimensional Compressibility

Test Number	Temp. (°C)	Measured: Vertical Effective Stress Range (MPa)	Measured: Constrained Modulus D (MPa)						Calculated (assuming Poisson's ratio =0.3): Average Principal Effective Stress Range (MPa)	Calculated: Bulk Modulus K (MPa)					
			First Cycle		Second Cycle		Third Cycle			First Cycle		Second Cycle		Third Cycle	
			Load	Unload	Load	Unload	Load	Unload		Load	Unload	Load	Unload	Load	Unload
CL2COS1	20	4.0 - 10.0	136	1569	1018	1530	1265		2.5 - 6.2		971	630	947	783	
	20	7.0 - 13.0	163	2386	1253	1983			4.3 - 8.0		1477	776	1228		

Isotropic Compressibility

Test Number	Temp. (°C)	Calculated (assuming Poisson's ratio = 0.3): Vertical Effective Stress Range (MPa)	Calculated: Constrained Modulus D (MPa)						Measured: Average Principal Effective Stress Range (MPa)	Measured: Bulk Modulus K (MPa)					
			First Cycle		Second Cycle		Third Cycle			First Cycle		Second Cycle		Third Cycle	
			Load	Unload	Load	Unload	Load	Unload		Load	Unload	Load	Unload	Load	Unload
CL2TOS1	20	8.1 - 14.5		1972	1443	1908			5.0 - 9.0	229	1221	893	1181		
CL2TOS2	20	8.1 - 14.5		2098	1615	2197			5.0 - 9.0	278	1299	1000	1360		
CL2TOS3	20	8.1 - 14.5		1709	1129	1439	1801	2481	5.0 - 9.0	183	1058	699	891	1115	1536
CL2TOS4	225	8.1 - 14.5		4846	1102	4602			5.0 - 9.0	154	3000	682	2849		

Table 10.5 Compressiblity of Cold Lake Clearwater Formation Oil Sands (Location No. 3)

Initial Conditions

Test Number	Bulk Density (Mg/m3)	Dry Density (Mg/m3)	% water (mass)	% bitumen (mass)	% solids (mass)	% fines (<0.074 mm)	Void Ratio e	Sr (%)	Index of Disturbance (%)
CL3COS1	1.94	1.65	8.9	6.0	85.1	15.0	0.61	76	19
CL3COS2	1.93	1.63	6.4	9.0	84.6	19.7	0.62	77	18
CL3COS3	2.11	1.78	11.7	3.9	84.4	27.1	0.49	100	0
CL3COS4	1.93	1.63	12.3	3.2	84.5	29.5	0.62	78	18
CL3TOS1	1.87	1.55	8.9	8.0	83.1	14.2	0.70	76	18
CL3TOS2	1.90	1.56	10.4	7.9	81.8	16.7	0.70	84	11

One Dimensional Compressibility

Test Number	Temp. (°C)	Measured: Vertical Effective Stress Range (MPa)	Measured: Constrained Modulus D (MPa)						Calculated (assuming Poisson's ratio =0.3): Average Principal Effective Stress Range (MPa)	Calculated: Bulk Modulus K (MPa)					
			First Cycle		Second Cycle		Third Cycle			First Cycle		Second Cycle		Third Cycle	
			Load	Unload	Load	Unload	Load	Unload		Load	Unload	Load	Unload	Load	Unload
CL3COS1	20	2.0 - 7.5	262	1241					1.2 - 4.6		768				
CL3COS2	20	4.5 - 7.5	180						2.8 - 4.6						
	225	7.5 - 9.5	459	627					4.6 - 5.9		382				
CL3COS3	225	7.0 - 9.0	509	578	527	584			4.3 - 5.6		358	326	362		
CL3COS4	20	6.0 - 15.0	253	1713	1085	1703			3.7 - 9.3		1060	672	1054		

Isotropic Compressibility

Test Number	Temp. (°C)	Calculated (assuming Poisson's ratio = 0.3): Vertical Effective Stress Range (MPa)	Calculated: Constrained Modulus D (MPa)						Measured: Average Principal Effective Stress Range (MPa)	Measured: Bulk Modulus K (MPa)					
			First Cycle		Second Cycle		Third Cycle			First Cycle		Second Cycle		Third Cycle	
			Load	Unload	Load	Unload	Load	Unload		Load	Unload	Load	Unload	Load	Unload
CL3TOS1	20	8.1 - 14.5		2262	1787	2362	1945		5.0 - 9.0	457	1400	1106	1462	1204	
CL3TOS2	225	8.1 - 14.5		1821	2344	1793			5.0 - 9.0	392	1127	1451	1110		

Table 10.6 Compressibility of Cold Lake Clearwater Formation Oil Sands (Location No.4)

Initial Conditions

Test Number	Bulk Density (Mg/m3)	Dry Density (Mg/m3)	% water (mass)	% bitumen (mass)	% solids (mass)	% fines (<0.074 mm)	Void Ratio e	Sr (%)	Index of Disturbance (%)
CL4COS1	1.87	1.53	8.6	9.4	82.0	26.0	0.73	80	15
CL4COS2	1.86	1.58	12.4	2.8	84.8	43.3	0.68	70	26
CL4COS3	1.88	1.61	11.4	3.2	85.4	41.1	0.65	70	26
CL4COS4	1.87	1.60	11.4	3.2	85.4	41.1	0.66	69	27
CL4TOS1	1.94	1.60	9.5	7.8	82.6	22.0	0.66	85	11
CL4TOS2	1.89	1.55	10.7	7.3	82.0	34.7	0.71	82	13
CL4TOS3	1.85	1.53	9.0	8.2	82.8	30.0	0.73	75	19

One Dimensional Compressibility

Test Number	Temp. (°C)	Measured: Vertical Effective Stress Range (MPa)	Measured: Constrained Modulus D (MPa) First Cycle Load	First Cycle Unload	Second Cycle Load	Second Cycle Unload	Third Cycle Load	Third Cycle Unload	Calculated (assuming Poisson's ratio = 0.3): Average Principal Effective Stress Range (MPa)	Bulk Modulus K (MPa) First Cycle Load	First Cycle Unload	Second Cycle Load	Second Cycle Unload	Third Cycle Load	Third Cycle Unload
CL4COS1	250	4.0 - 17.0	139	2089	971	2080	1203		2.5 - 10.5		1293	601	1288	745	
CL4COS2	20	10.0 - 18.0	204	2103	610	1899	872	2156	6.2 - 11.1		1302	378	1176	540	1335
	100	10.0 - 18.0	1338	1999					6.2 - 11.1		1237				
	200	10.0 - 15.0	536	2264	1210				6.2 - 9.3		1402	749			
	200	10.0 - 18.0	1018	1912					6.2 - 11.1		1184				
CL4C[illegible]3	200	10.0 - 17.5	180	2877	811	2569	1077	2518	6.2 - 10.8		1781	502	1590	667	1559
CL4C[illegible]4	20	10.0 - 17.5	177	1960	650	2130	894	2378	6.2 - 10.8		1213	402	1319	553	1472

Isotropic Compressibility

Test Number	Temp. (°C)	Calculated (assuming Poisson's ratio = 0.3): Vertical Effective Stress Range (MPa)	Constrained Modulus D (MPa) First Cycle Load	First Cycle Unload	Second Cycle Load	Second Cycle Unload	Third Cycle Load	Third Cycle Unload	Measured: Average Principal Effective Stress Range (MPa)	Bulk Modulus K (MPa) First Cycle Load	First Cycle Unload	Second Cycle Load	Second Cycle Unload	Third Cycle Load	Third Cycle Unload
CL4TOS1	20	9.7 - 16.2		1961	1892	2184	1738	2386	6.0 - 10.0	755	1214	1171	1352	1076	1477
CL4TOS2	20	8.1 - 14.5		2541	1917				5.0 - 9.0	238	1573	1187			
CL4TOS4	225	8.1 - 16.2		4389	1273	3554			5.0 - 10.0	279	2717	788	2200		

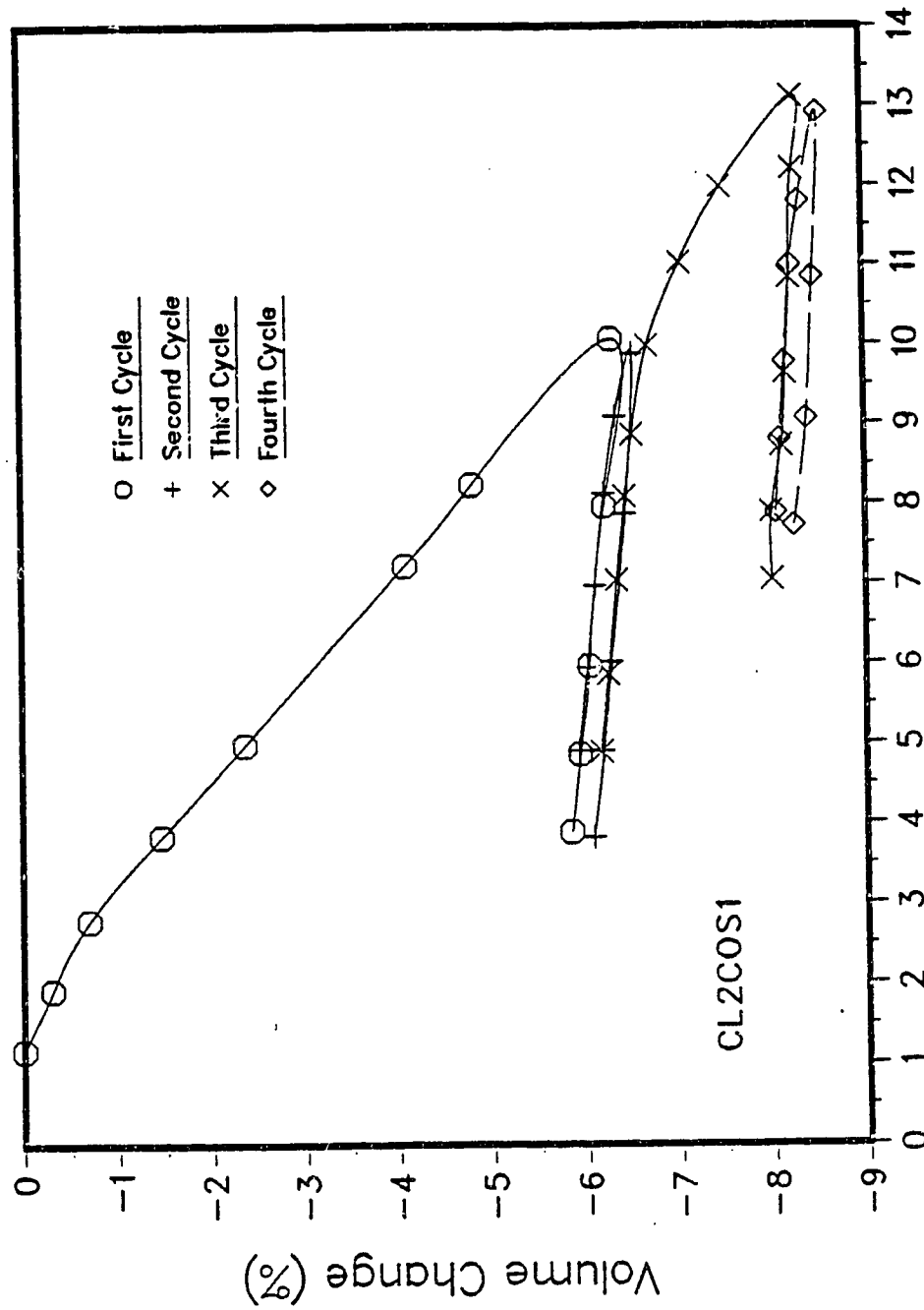

Figure 10.1 One Dimensional Compressibility of Cold Lake Oil Sands

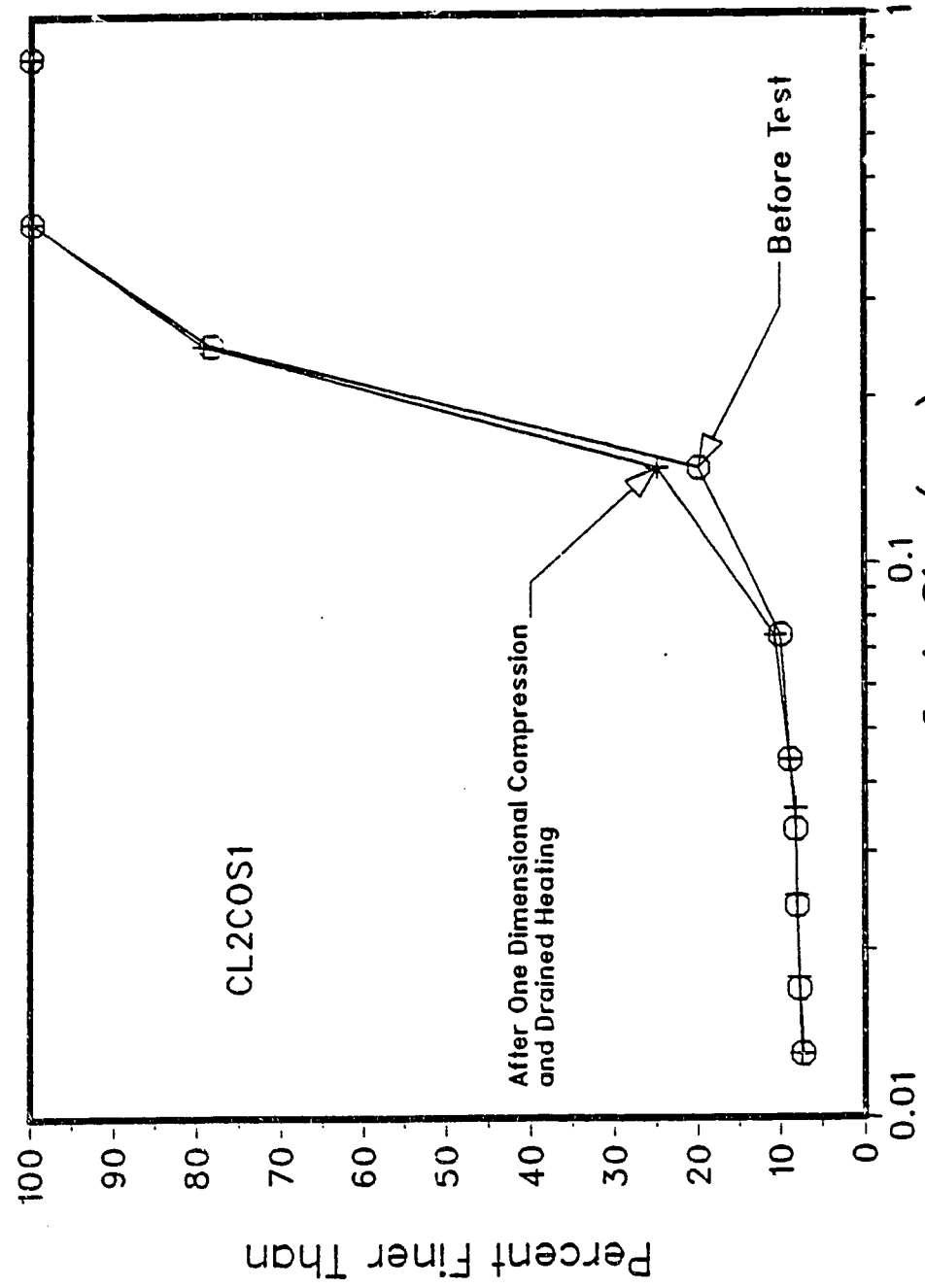

Figure 10.2 Grain Size Distribution Before and After One-Dimensional Loading and Drained Heating

Chapter 9). The grain size distribution curve in Figure 10.2 therefore also reflects temperature induced grain breakage due to thermal loading.

Oil sands from all locations exhibit some degree of grain crushing during one-dimensional stress cycling at 20°C (Appendix E). The amount of plastic strain increased with increasing vertical effective confining stress, from about 0.4% at 10 MPa to about 1.2% at 18 MPa. For specimens subjected to more than two stress cycles, non-recoverable strain was associated with each cycle.

Grain crushing during stress cycling has a marked effect on constrained modulus values. The unloading modulus is typically twice the reloading modulus. The constrained modulus was approximately 2000 MPa during unloading and reduced to about 1000 MPa during reloading. The constrained modulus varied somewhat with effective confining stress range and no appreciable difference in compressibility was observed between oil sands from the different locations.

One-dimensional compressibility tests were performed at temperatures up to 250°C. The history of stress and method of heating was varied prior to compressibility determinations to evaluate the effect of stress path on high temperature compressibility. Location No. 1 and Location No. 3 oil sands were subjected to a vertical effective confining stress of 7 MPa prior to drained heating to 225°C. Oil sands specimens from Location No. 4 were subjected to the following stress and temperature histories prior to

compressibility tests:

1. Specimen CL4COS1 was heated in the disturbed state under fully undrained conditions. Structural changes to the sand matrix during heating were inhibited because the effective stress during free expansion is zero.

2. Specimen CL4COS2 was cycled over the vertical effective stress range of 1 MPa to 18 MPa prior to undrained heating. Compressibility determinations were made at 200°C and subsequently after unloading and cooling to 100°C.

3. Specimen CL4COS3 was heated under fully drained conditions in the disturbed state. The vertical effective confining stress during heating was less than 0.5 MPa.

Two important observations concerning the influence of stress path on compressibility of Clearwater oil sands at elevated temperatures may be derived from these test results:

1. The stress-volume change relationship for specimens heated under drained conditions to 225°C under 7 MPa confining stress is distinctly bi-linear, with concave curvature, as shown in Figures E2, E3, E26 and E27. The constrained modulus is approximately 2500 MPa over the stress range of 5 to 7 MPa but is reduced to approximately 600 MPa over the stress range of 7 to 9 MPa.

2. Compressibility results for Location No. 4 oil sands (heated under nominal or zero effective stress) are given in Figures E31 and E33 through to E36. Constrained modulus values at 100, 200 and 250°C are very similar to the 20°C results (Table 10.6). Non-recoverable strain during stress cycling resulted in unloading moduli which were roughly twice the reloading moduli. Constrained modulus values were very similar to the 20°C values.

One-dimensional compressibility results at elevated temperatures illustrate the profound effect stress history and heating method have on the compressibility of Clearwater oil sands. As previously discussed, volume change during compression is accommodated through sliding between mineral grains and deforming or crushing of individual particles.

During heating under low effective confining stress, volume change occurs primarily through a small amount of relative movement of sand grains (as discussed in Chapter 9). As a result, the compression characteristics at elevated temperatures are similar to the 20°C results. The compressibility is high upon initial loading, reduces to lower values upon unloading and subsequent cycling, and non-recoverable strain occurs during cycling reflecting grain breakage or crushing. During heating under 7 MPa confining stress some grain breakage occurs, as evidenced by the thermal volume change results (Chapter 9). The concave curvature of the stress-volume change curves reflects the grain breakage which occurs above 7 MPa which allows significant relative movement of sand grains.

The results of several isotropic compressibility tests carried out at 20°C are summarized in Tables 10.2 through 10.6. Stress-volume change plots are included in Appendix E. A typical triaxial specimen undergoing three cycles of stress is shown in Figure 10.3. As in the case of the one-dimensional tests, non-linear inelastic behaviour is prominent during initial loading but, unlike the oedometer tests, essentially elastic behaviour is observed during stress cycling (Figure 10.3, also see Appendix E).

Conventional elasticity has been used to compare the results of the isotropic compression stress path and the confined compression stress path. Bulk and constrained moduli were calculated assuming a constant Poisson's ratio

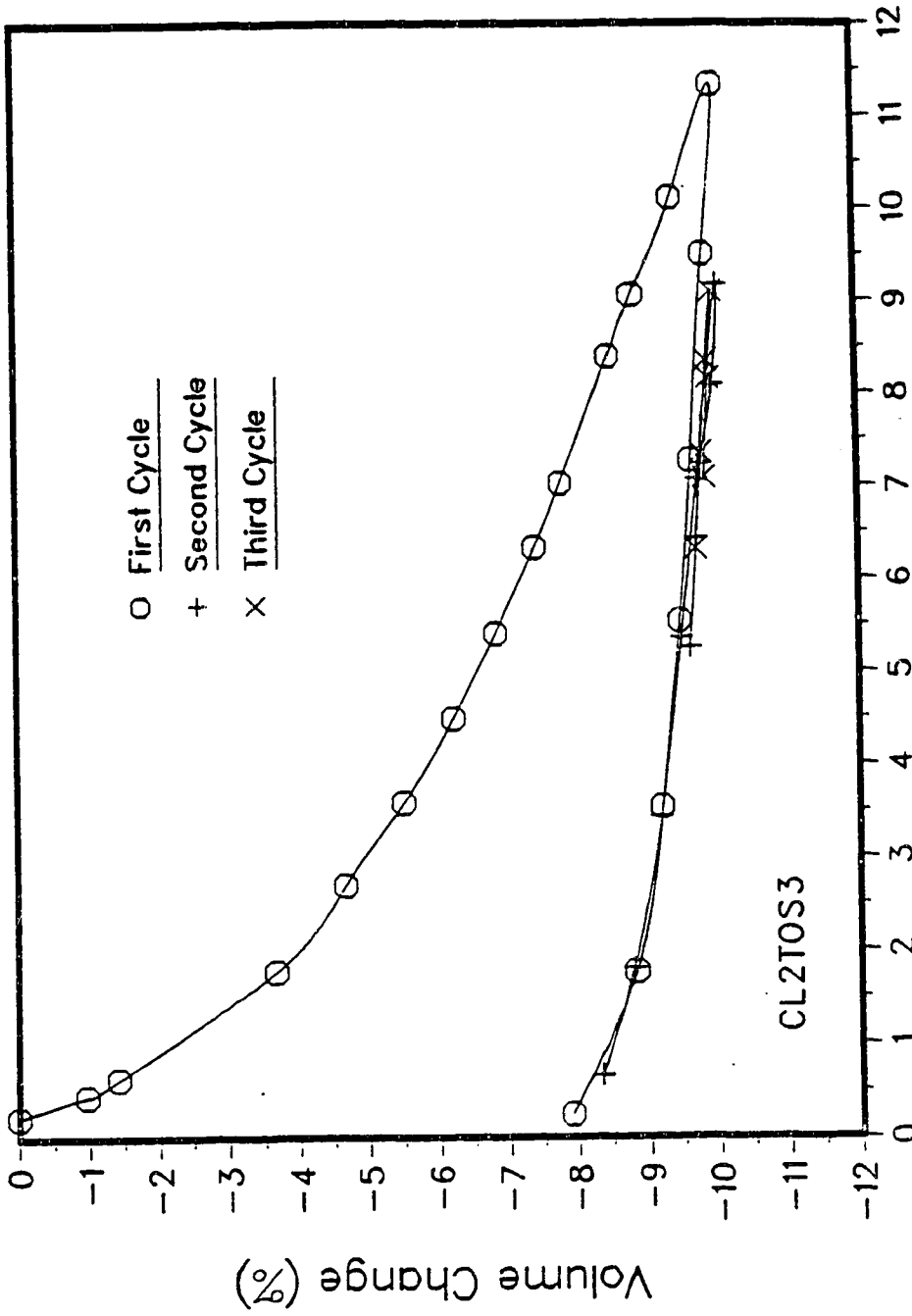

Figure 10.3 Isotropic Compressibility of Cold Lake Oil Sands

of 0.3. Good agreement exists between measured and calculated values during isotropic cycling and one-dimensional unloading. This indicates the oil sands are behaving in an elastic manner during isotropic compression and, unlike one-dimensional compression, significant grain crushing is not occurring. In confined compression the specimen experiences both shear strain and volume change, whereas during isotropic compression the specimen does not undergo shear straining. Therefore, compression involving increases in shear stress (or deviatoric stress) will cause a greater volume reduction than an equivalent increase in all-round stress due to grain crushing.

The results of isotropic compression tests performed at 225°C are also summarized in Tables 10.2 through 10.6. The bulk moduli at 225°C are generally greater than at 20°C. This difference in bulk modulus reflects sand matrix densification observed during drained heating and may be attributed in part to temperature dependent grain breakage. The calculated constrained moduli from the high temperature tests are comparable to the portions of the one-dimensional tests in which significant grain crushing is not occurring. That is, the vertical stress range of 5 to 7 MPa for specimens heated under 7 MPa confining stress and the unloading moduli for specimens heated under a nominal effective stress. Calculated moduli are significantly greater in instances where significant grain crushing has been identified.

10.3 Clearwater Shale

A one-dimensional and an isotropic compressibility test were carried out on Clearwater Formation shale at 20°C. Laboratory specimens were obtained from a core sample taken to a depth of approximately 450 m. The average liquid limit, plastic limit and water content of the shale were 78%, 33% and 17%, respectively, and the initial void ratio was 0.48.

The results of the one-dimensional compression test are shown in Figure 10.4. The constrained modulus is 6.3 MPa during initial loading and is 1590 MPa after unloading and cycling over the vertical effective stress range of 7.5 to 9 MPa. The effect of stress path on compressibility is observed when the initial load constrained modulus is compared to the initial loading bulk modulus shown in Figure 10.5.

The constrained modulus of this heavily over-consolidated shale is comparable to oil sands over the same vertical effective stress range. Thermal volume change results (Chapter 9) have shown a significant amount of heat induced consolidation of Clearwater shale occurs during drained heating.

10.4 Summary and Conclusions

During in situ thermal recovery formation strata is subjected to changes in effective stress caused by thermal volume change of mineral solids and by injection, expansion or withdrawal of pore fluids. Volume changes associated with

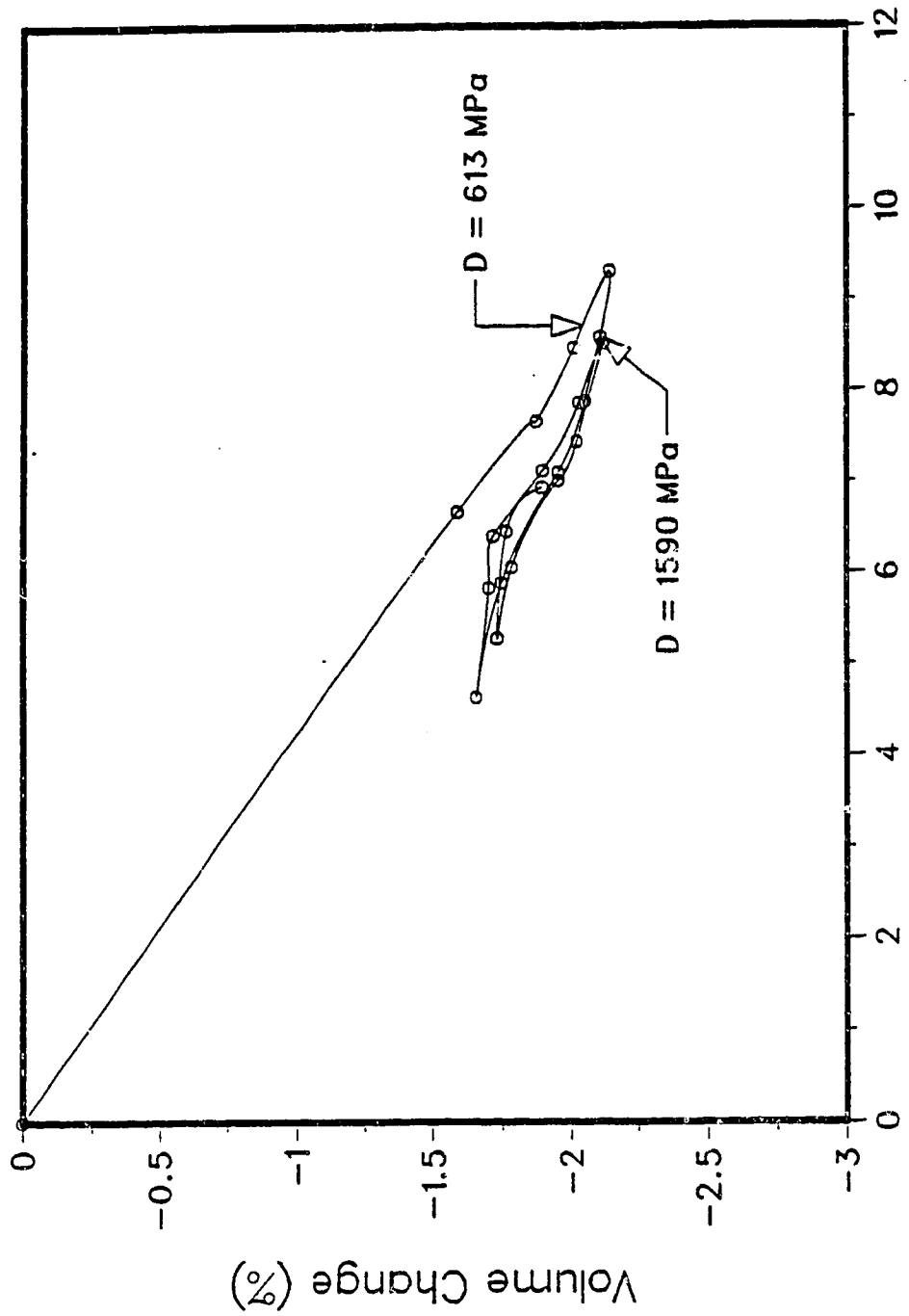

Figure 10.4 One Dimensional Compressibility of Cold Lake Clearwater Shale

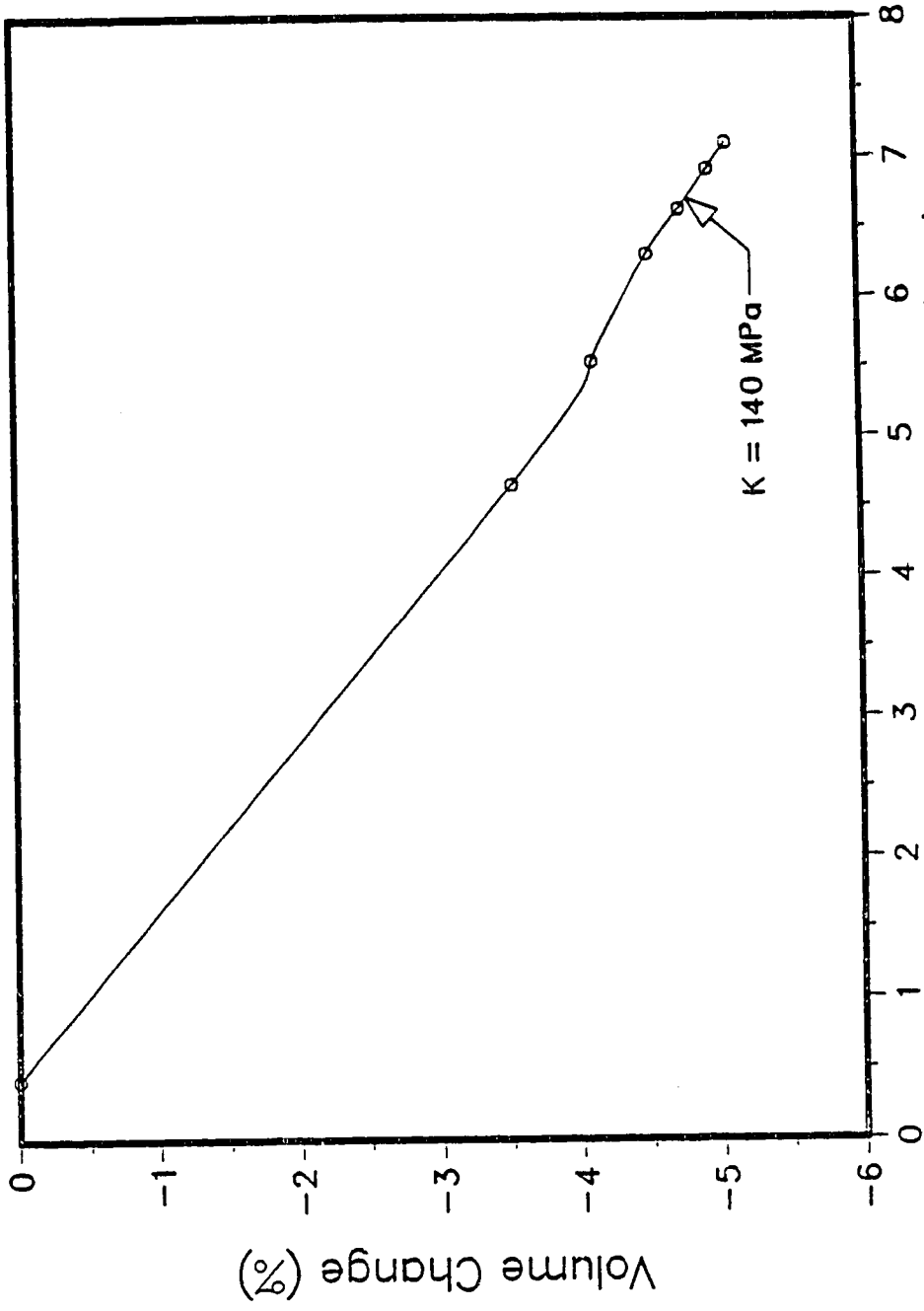

Figure 10.5 Isotropic Compressibility of Cold Lake Clearwater Shale

changes in effective stress occur through sliding between mineral grains and deforming or crushing of individual particles. Volume change is resisted by friction between soil particles, interparticle bonding and particle strength and is dependent on void ratio and the size, shape and gradation of mineral particles.

The compressibility of Cold Lake Clearwater oil sands has been examined following the one-dimensional (or confined compression) stress path and the isotropic compression stress path under stresses and temperatures associated with in situ thermal recovery. Compressibility parameters were found to be highly influenced by stress history, stress path and temperature. Non-linear, inelastic behaviour is attributed to weak minerals in the sand matrix which are susceptible to physical breakdown during shear straining and heating. Since the factors which govern the compressibility of oil sands also govern strength and deformation properties during application of a deviatoric stress, shear strength parameters may be significantly affected by grain crushing. Further, changes in temperature and effective stress may cause significant changes in void ratio and mineral grain gradation which will also affect strength parameters and permeability.

Spacial variations in mineralogy, geological environment of deposition and geological history between the four oil sands tested have little influence on measured compressibility parameters. The effect of geological

processes on compressibility may be overshadowed by sample disturbance during coring.

The compressibility of Athabasca McMurray Formation and Cold Lake Clearwater Formation oil sands is similar when cycled over the same effective stress range. However, the net volume change during initial compression, especially at higher temperatures, is greater for Cold Lake oil sands due to grain breakage. Athabasca oil sands which consist of predominantly quartz sand are essentially elastic during stress cycling in both one-dimensional and isotropic compression.

The compressibility of the heavily over-consolidated Clearwater shale is comparable to that of oil sands. Thermal volume change results indicate a significant amount of heat reduced consolidation occurs during drained heating. Improvements in strength and deformation properties associated with the non-recoverable volume reductions caused by heat consolidation are likely to be retained after the initial in situ heat injection cycle.

11. SHEAR STRENGTH OF COLD LAKE OIL SANDS

11.1 Materials Studied

The shear strength behaviour of oil sands from four separate locations in the Cold Lake Deposit were studied. The oil sands specimens were obtained from core samples taken in the Clearwater Formation at depths ranging from 440 to 490 m. The geological detail of the oil sands core samples is outlined in Chapter 4, Section 4.2 and may be summarized as follows:

1. Location No. 1. The oil sands specimens from Location No. 1 were obtained from a core sample taken northwest of Cold Lake at a depth of approximately 445 m. The test specimens were composed of fine grained sand of low bitumen content (4.5 to 10% by weight) with frequent discontinuous shale seams. The fines content (less than 0.074 mm) of the grain size distribution ranged from 9 to 49%.

2. Location No. 2. The oil bearing sands from Cold Lake Location No. 2 were obtained from a core sample taken northwest of Cold Lake at a depth of about 460 m. The test specimens consisted of homogeneous, fine grained sand with a bitumen content of 10 to 12% by weight and a fines content ranging from 6 to 10% by weight.

3. Location No. 3. The oil sands specimens from Cold Lake Location No. 3 were obtained from a core sample taken northwest of Cold Lake at a depth of approximately 490 m. Test specimens were composed of fine grained sand and contained discontinuous shale seams and clasts. The fines content (less than 0.074 mm) of the grain size distribution was approximately 15% by weight. The majority of fines were concentrated in seams and clasts.

4. Location No. 4. The oil sands test specimens from Cold Lake Location No. 4 were obtained from a core sample taken northwest of Cold Lake at a depth of approximately 475 m. The test specimens were lean, silty, fine grained oil sands with bitumen contents of about 8% by weight. Each specimen contained thin, discontinuous shale seams and clasts. The fines contents were fairly consistent at about 30% by weight.

11.2 Methods and Procedures

A total of 23 triaxial tests were performed on Cold Lake Clearwater Formation oil sands over a range of temperatures from 20°C to 225°C. The stress paths studied during triaxial strength testing are summarized as follows:

1. Location No. 1. Passive drained compression at 20°C, passive undrained compression at 20°C, and passive drained compression at 225°C. Five separate triaxial tests were carried out following each of the above stress paths under an effective confining stress ranging from 1.0 to 7.0 MPa.

2. Location No. 2. Passive drained compression at 20°C and passive drained compression at 225°C. Due to the limited amount of core available for testing only four tests were performed, three at 20°C and one at 225°C. The effective confining stresses applied to the specimens ranged from 1.0 to 7.0 MPa.

3. Location No. 3. Passive drained compression at 20°C and passive drained compression at 225°C. The effective confining stress used for both paths was 7.0 MPa.

4. Location No. 4. Passive drained compression at 20°C under an effective confining stress of 7.0 MPa and passive undrained compression at 20°C under an effective confining stress of 7.0 MPa.

11.3 Cold Lake Location No. 1 Oil Sands

Passive Drained Compression at 20°C

The stress-strain and volume change relationships for Cold Lake Location No. 1 oil sands tested following passive drained compression stress paths at 20°C are shown in Figure 11.1. Each specimen was compressed isotropically to 9 MPa, approximately 2 MPa above the in situ average effective stress. A cyclic stress compressibility test was performed over the stress range of 5 to 9 MPa on each specimen prior to the drained shear test. Results for each phase of each test - initial conditions, isotropic compression and drained shear tests - are summarized in Table 11.1.

The stress-strain-volume change behaviour of Cold Lake Clearwater Formation oil sands is significantly different from that exhibited by Athabasca McMurray Formation oil sands. Cold Lake oil sands display contractive behaviour during shear over the effective stress range encountered in the deposit but a dilatant behaviour at low effective confining stresses. As shown in Chapter 7, Athabasca oil sands display dilatant behaviour during shear over a similar effective confining stress range. This increase in volume change during shear straining accompanied by strain softening behaviour in the post-peak region illustrates the strength of the quartz sand grains. The grains during shear tend to ride up on each other whereas Cold Lake oil sands

Table 11.1 Consolidated Drained Triaxial Tests - Cold Lake Clearwater Formation Oil Sands (Location No. 1)

Initial Conditions

Test Number	Bulk Density (Mg/m3)	Dry Density (Mg/m3)	% water (mass)	% bitumen (mass)	% sand (mass)	Void Ratio e	Sr (%)	Pore Pressure Parameter B **	Index of Disturbance (%)
CL1TOS1	1.89	1.58	10.0	6.5	83.5	0.68	77	Not Performed	17.7
CL1TOS2	1.89	1.56	12.9	4.5	82.6	0.70	80	0.95	14.7
CL1TOS3	1.90	1.59	7.3	9.2	83.5	0.67	78	0.98	16.6
CL1TOS4	1.82	1.49	8.9	9.4	81.7	0.78	76	0.95	17.8
CL1TOS5	1.83	1.51	7.2	10.2	82.6	0.75	74	0.98	19.9

** Note: At 0.2 MPa Effective Confining Stress after saturation at 2.5 MPa Back Pressure

Isotropic Consolidation

Test Number	Volume Change (%) from σ = 0.2 to 9 MPa	Bulk Density (Mg/m3) σ = 9 MPa	Dry Density (Mg/m3) at σ = 9 MPa	K (MPa) Cycled from 5 to 9 MPa	Void Ratio e	Index of Disturbance (%)
CL1TOS1	-5.43	2.04	1.67	1250	0.59	7.7
CL1TOS2	-4.90	2.02	1.64	1520	0.61	6.2
CL1TOS3	-5.87	2.05	1.69	871	0.57	5.9
CL1TOS4	-6.18	1.98	1.58	1070	0.67	7.8
CL1TOS5	-6.53	2.01	1.62	1160	0.64	8.8

Drained Shear Test

Test Number	Effective Confining Stress (MPa)	Back Pressure (MPa)	B	Deviator Stress at failure (MPa)	Axial Strain at failure (%)	Volumetric Strain at failure (%)	Modulus of Elasticity (MPa)	Poisson's Ratio
CL1TOS1	1.0	2.5	0.86	5.85	1.01	-0.14	777	0.34
CL1TOS2	4.0	2.5	0.67	9.85	1.04	-0.29	1404	0.33
CL1TOS3	5.5	2.5	0.71	8.00	2.29	-1.43	1024	0.04
CL1TOS4	7.0	3.1	0.46	8.00	2.06	-1.29	723	0.21
CL1TOS5	7.0	2.5	0.64	8.00	1.68	-1.10	711	0.16

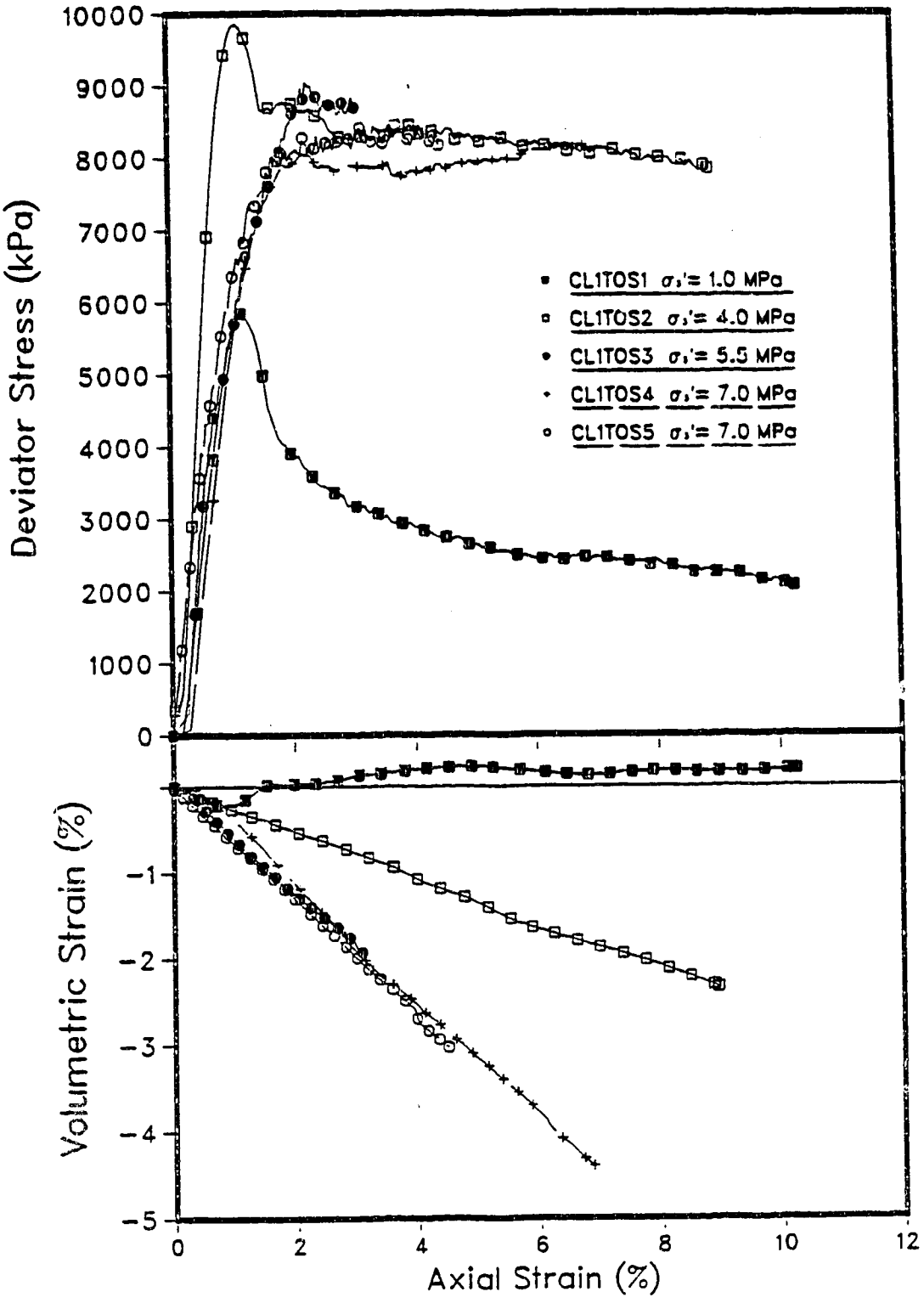

Figure 11.1 Passive Drained Compression of Cold Lake Clearwater Oil Sands (Location No. 1)

tend to shear through sand grains.

A scanning electron micrograph of Specimen CL1TOS4 before and after drained shear under an effective confining stress of 7.0 MPa is shown in Figure 11.2. Prior to testing (Figure 11.2a) the sand grains contacts are comprised of tangential and long contacts. The interlocking contacts associated with pressure solution and authigenic crystal overgrowth, largely found in Athabasca McMurray Formation oil sands, are not evident here. The sand grains appear competent and the sand grain contacts are free of any degradation. Figure 11.2b illustrates the degree of crushing which occurred during shear under high effective confining stress. Crushing is apparent at several grain contacts and crushing of entire grains is evident.

It appears from Figure 11.2b that sand grain breakage during shear is selective; that is, while some grains are almost totally destroyed, some others show no evidence of breakage even at contact points. An Energy Dispersive X-ray analysis was performed on one of the heavily damaged grains and a second on the entire sample. The analysis carried out on the crushed grain is shown in Figure 11.3. The three major elements present in this grain (elements whose atomic numbers are greater than that of sodium) are silicone, aluminum and potassium. This chemical composition suggests that this is a K-feldspar sand grain whose chemical formula is $K(AlSi_3O_8)$.

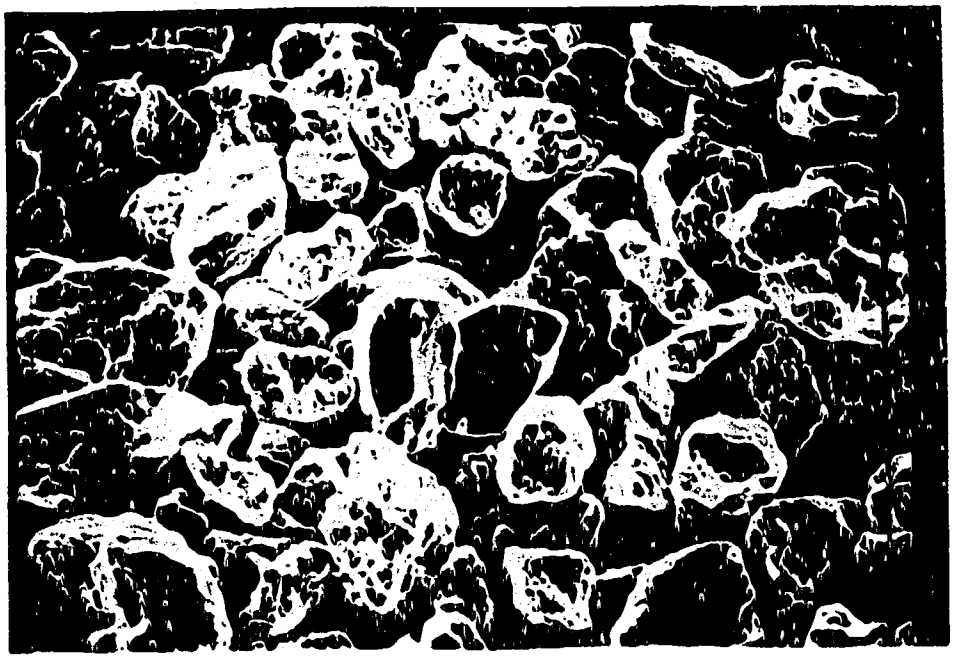

a) Before Test

b) After Drained Shear (σ_3' = 7 MPa)

Figure 11.2 Scanning Electron Micrograph of Specimen CL1TOS4 (Magnification 55X)

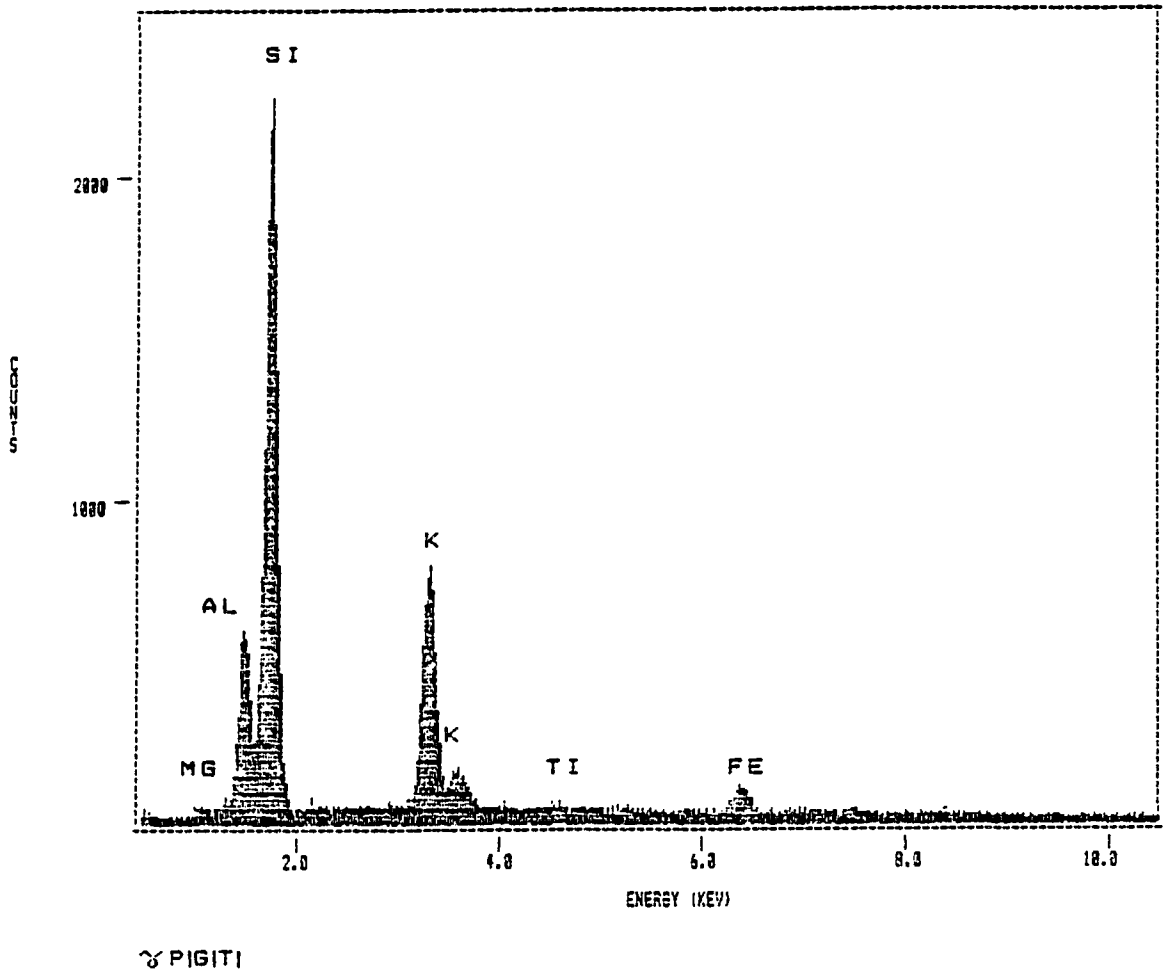

Figure 11.3 Energy Dispersive X-ray Analysis of Crushed Grain in Specimen CL1TOS4

An Energy Dispersive X-ray analysis carried out on the entire specimen (Figure 11.4) illustrates that silicone is the dominant element with relatively small amounts of aluminum, potassium, calcium and iron present. This suggests that quartz (SiO_2) is the dominant mineral grain in the sample. Since quartz is stronger and harder than feldspar, this may explain why some grains after the shear test show significant breakage and others do not. It may also explain how a grain can penetrate and crush an adjacent grain and show no evidence of breakage itself, as shown in Figure 11.2b.

A grain size analysis was performed on each of the test specimens after the shear test and was compared to the grain size distribution of the core directly adjacent to where the test specimen was taken. The purpose of this comparison was to assess the amount of particle degradation during each shear test. Figure 11.5 shows the initial grain size curve and the grain size curve after drained shear at 7.0 MPa effective confining stress for Specimen CL1TOS4. The propensity of Cold Lake Clearwater Formation oil sands to crush during shear at elevated confining stress is clearly demonstrated. Also included in Figure 11.5 is a plot of the grain crushing data expressed in terms of the ratio of the initial 50% size of the sand, D_{50i}, to the 50% size after the shear test, D_{50a}, against effective confining stress. The amount of grain breakage increases with increasing effective confining stress.

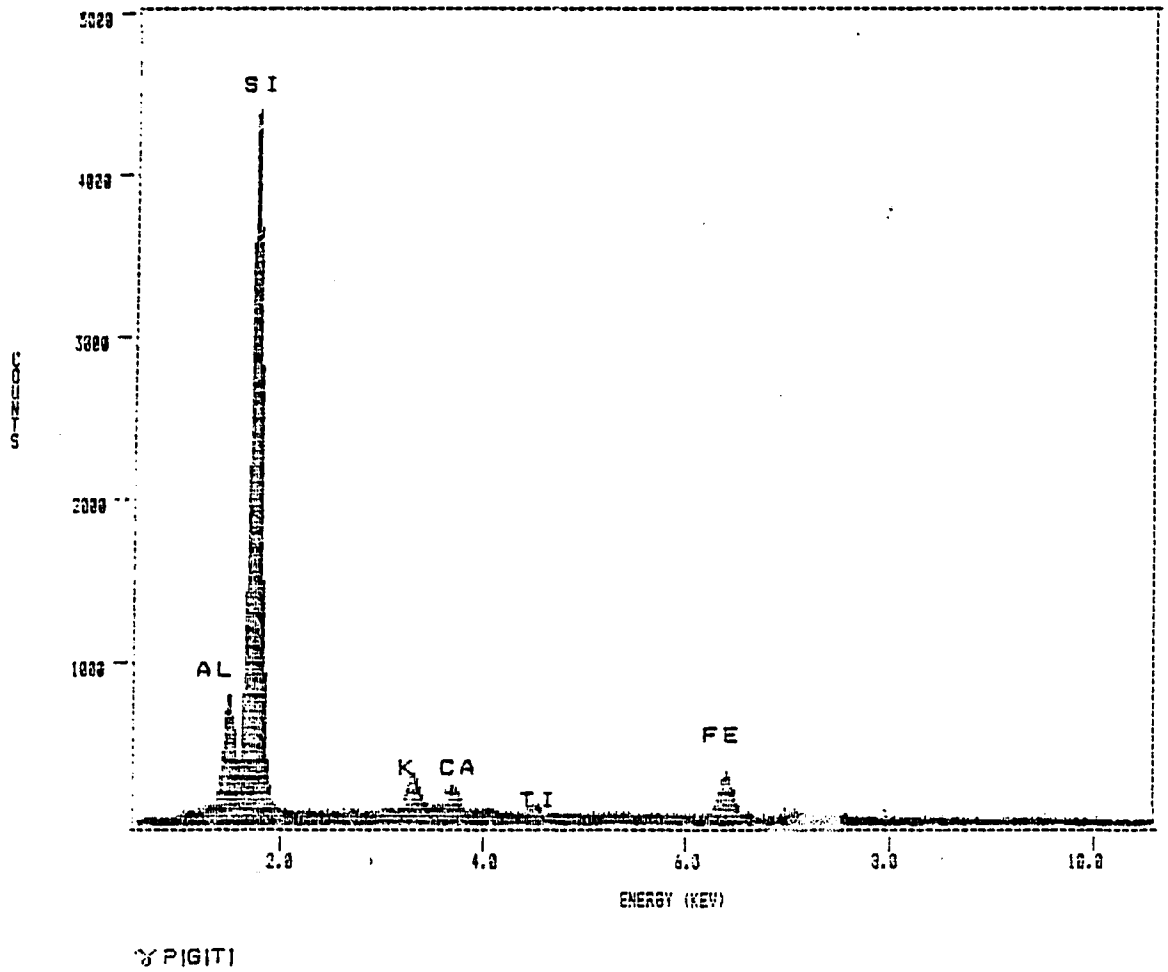

Figure 11.4 Energy Dispersive X-ray Analysis of Specimen CL1TOS4

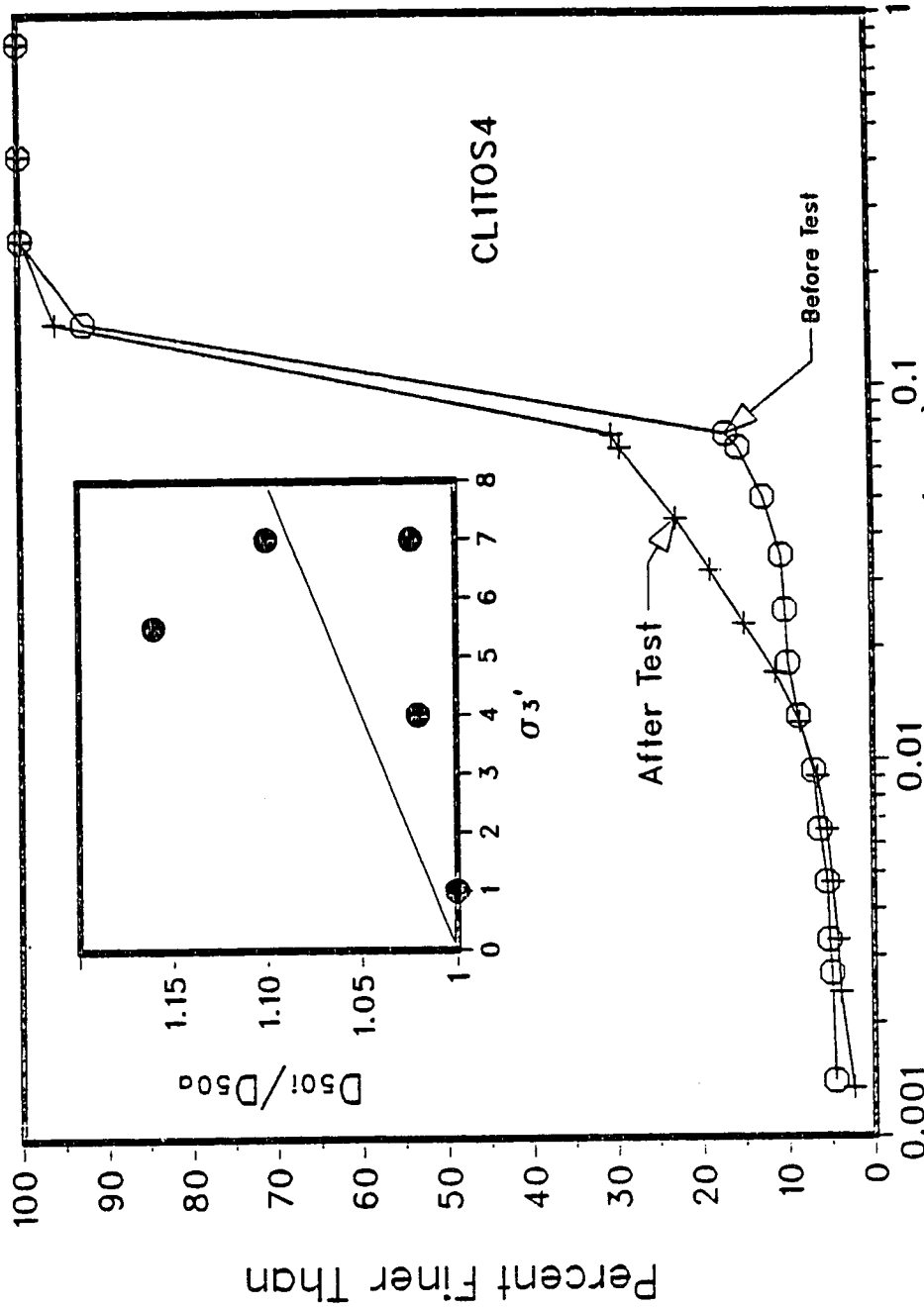

Figure 11.5 Relative Crushing of Cold Lake Location No. 1 Oil Sands

Several investigators have studied the strength deformation behaviour of dense sands over the pressure range employed in this study of Cold Lake Clearwater Formation oil sands (see Chapter 2). Bishop (1966), based on tests performed on Ham River sand, concluded that the curvature in the failure envelope with increasing confining pressure for dense sands was due primarily to the decrease in the rate of dilatancy with increasing pressure. This reduced rate of volume increase at failure at higher confining stresses results from crushing of sand grains which begins locally at grain contacts and may result in crushing of entire grains. This, in turn, results in a significant reduction in the overall effective angle of friction at failure.

The shear strength data obtained from the passive drained compression tests are plotted in the form of a p'-q diagram in Figure 11.6. The shear strength of these oil sands specimens increases with increasing effective confining stress to 4.0 MPa. Above 4.0 MPa effective confining stress, the strength decreases with increasing confining stress. This negative slope of the failure envelope above 4.0 MPa is attributed to the manner in which the maximum shear strength was defined. For specimens tested at 1.0 and 4.0 MPa, the maximum shear strength was determined by a drop in strength during shear (strain softening behaviour). For specimens tested above 4.0 MPa confining pressure, however, no distinct peak shear strength was evident. In other words, these specimens display strain

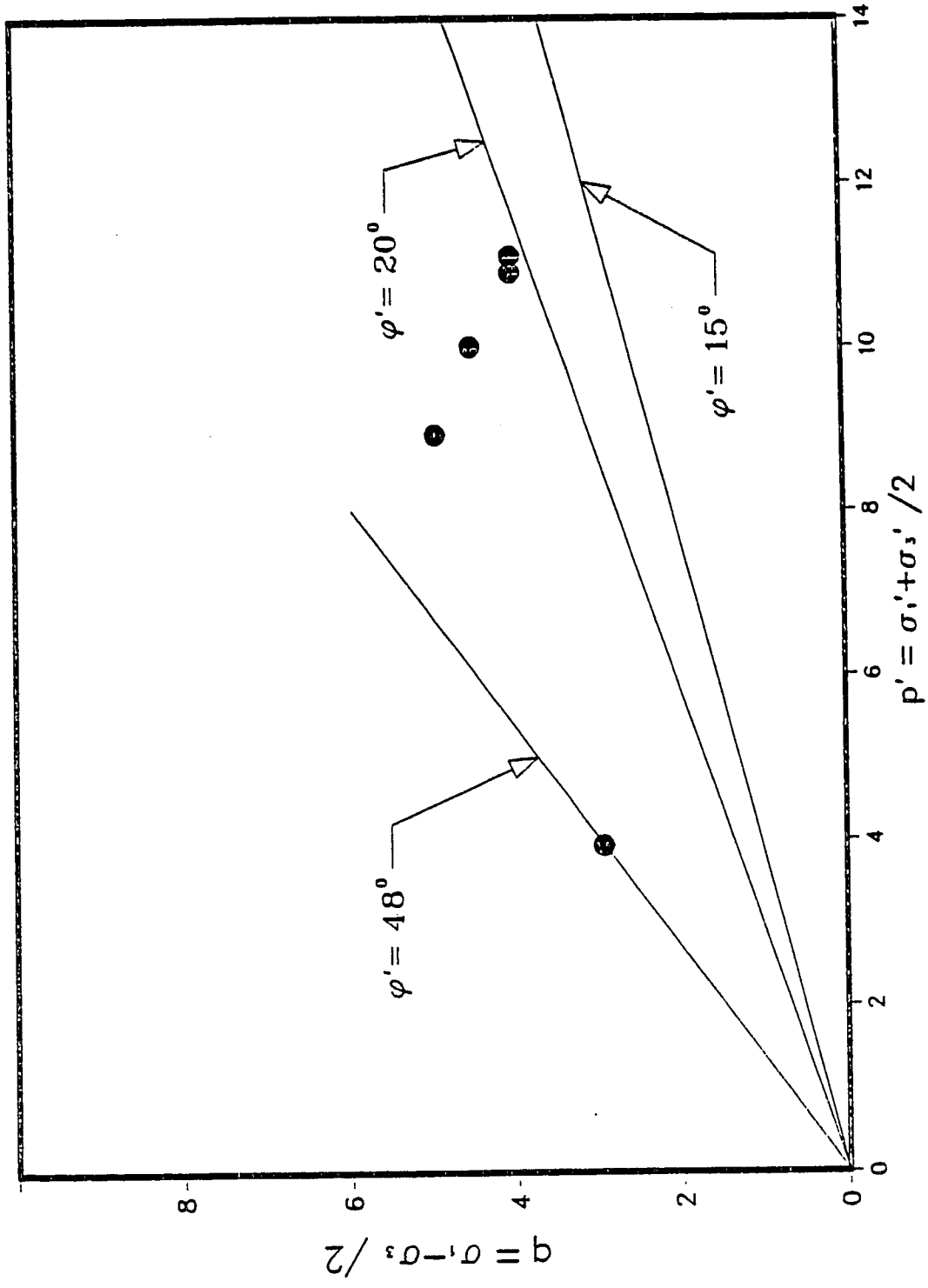

Figure 11.6 Passive Drained Compression Tests on Cold Lake Clearwater Oil Sands (Location No. 1)

hardening behaviour with the shear strength slowly and continuously increasing with increasing axial strain. The maximum shear strength above 4.0 MPa, therefore, was determined as the maximum shear strength obtained during the test which was generally less than 7% axial strain.

Passive drained compression tests on dense sand available in the literature indicate that very large axial strains are required to reach the maximum shear strength under high effective confining pressures. For example, Bishop (1966) found that axial strains in the order of 20% were required to achieve the maximum shear strength of dense, fine to medium grained quartz sand at 7 MPa effective confining pressure. The results of these confined drained tests performed on Ham River sand are shown in Figure 2.16. Vesic and Clough (1968) conducted a series of drained triaxial compression tests on dense Chattahoochee River sand (a medium grained, uniform quartz sand) and found the failure strain increased from approximately 7% at cell pressures of 0.1 MPa to about 26% at cell pressures of 3 MPa. Lo and Roy (1973) performed drained triaxial tests on artificially prepared quartz and limestone sands and found axial strains to failure of over 30% were required for these materials at confining stresses exceeding 3 MPa. Since the axial strains used to define the maximum shear strength for the Clearwater Formation oil sands were relatively small, the negative curvature above 4.0 MPa of the p'-q diagram is, therefore, not representative of the actual shear strength

at failure. The actual failure envelope is distinctly curved, as evident from tests performed at 1.0 and 4.0 MPa, and is likely to retain a net positive slope above 4.0 MPa.

The variation of initial tangent modulus with effective confining pressure for Clearwater Formation oil sands is shown in Figure 11.7. The drained elastic modulus increases with increasing confining pressure to 4 MPa and decreases with increasing confining pressure from 4 MPa to 7 MPa. The decreasing modulus with increasing confining stress above 4 MPa confining stress is unusual and not common during triaxial compression of uncemented sands. As discussed previously in Chapter 7, the drained modulus of elasticity of oil sands is very sensitive to sample disturbance. Considerable scatter was obtained when comparing the modulus of elasticity from several investigations for Athabasca McMurray Formation oil sands. Since the initial index of disturbance of these samples was high, varying from 14 to 20%, the variability in the tangent modulus is probably due to microfabric disturbance during core sampling and transport.

Passive Undrained Compression at 20°C

The stress-strain and pore pressure response for Clearwater Formation oil sands tested following passive undrained compression stress paths at 20°C are shown in

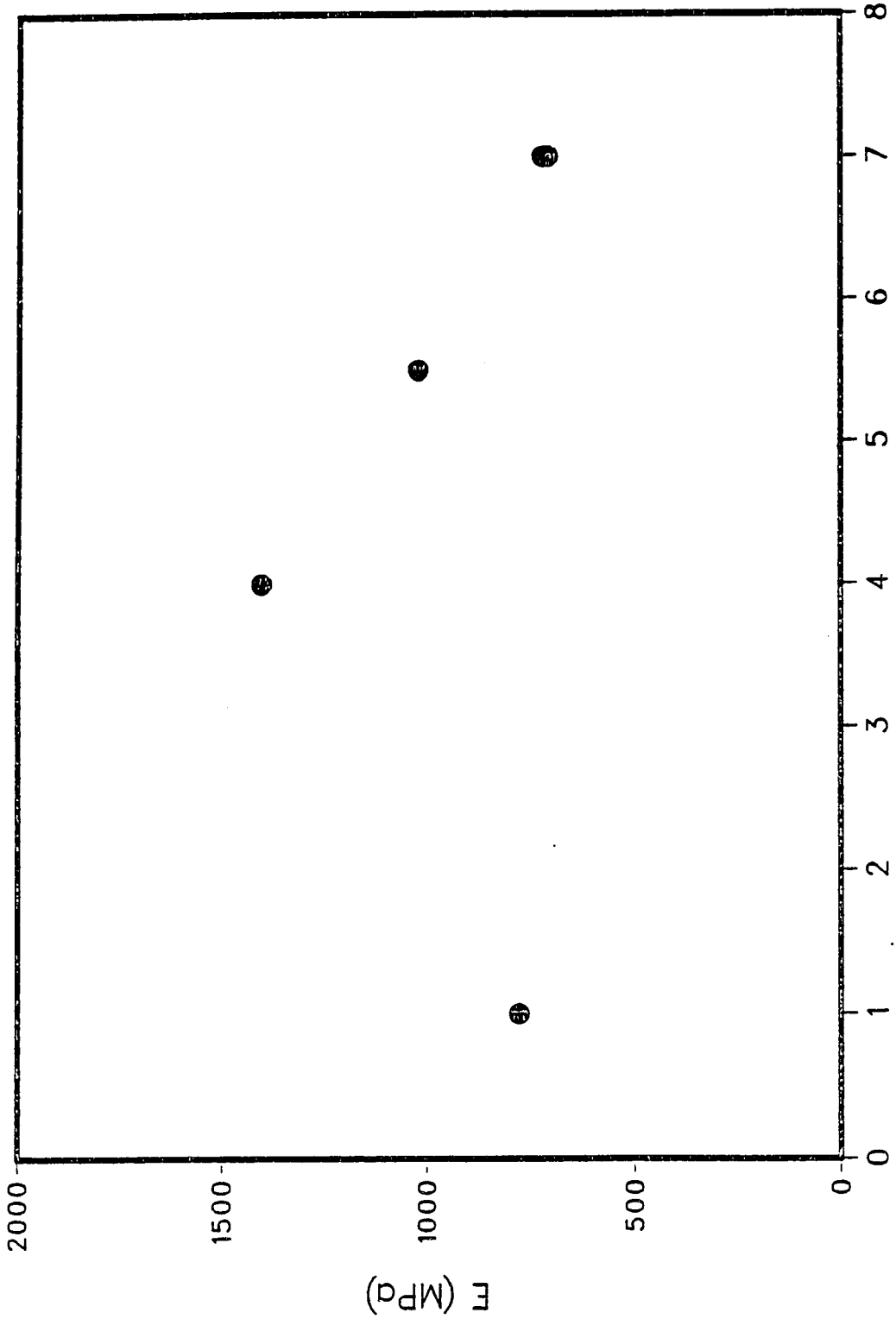

Figure 11.7 Variation of Drained Modulus – Cold Lake Clearwater Oil Sands (Location No. 1)

Figure 11.8. As in the tests performed on this oil sands following the passive drained compression stress path, each sample was compressed isotropically to 9 MPa and cycled over the stress range of 5 to 9 MPa prior to the shear test. Results for each phase of each test are summarized in Table 11.2.

The behaviour of this Clearwater Formation oil sands during undrained shear changes as the initial effective confining stress is increased. At low initial effective confining stresses the oil sands specimens show an increase in pore pressure at the beginning of the test due to compression of the sand matrix during the onset of the stress increase. The volume reduction of the sand matrix results in the pore liquids taking more of the load due to their inability to drain. As the specimen reaches its peak strength, the pore fluid pressure decreases as the sand matrix tendency to dilate under the shear strain is suppressed.

At high initial effective confining stresses the oil sands also show an increase in pore pressure at the beginning of the test due to compression of the sand matrix during the onset of the stress increase. As shear straining takes place, however, particle crushing occurs which tends to compress the sand structure and increase the pore fluid pressures. Therefore, at high initial confining stresses the behaviour of this oil sands is similar to that of a loose sand with positive pore pressures induced due to the sands'

Table 11.2 Consolidated Undrained Triaxial Tests - Cold Lake Clearwater Formation Oil Sands (Location No. 1)

Initial Conditions

Test Number	Bulk Density (Mg/m3)	Dry Density (Mg/m3)	% water (mass)	% bitumen (mass)	% sand (mass)	Void Ratio e	Sr (%)	Pore Pressure Parameter B **	Index of Disturbance (%)
CL1TOS6	1.83	1.49	12.6	5.9	81.5	0.77	78	0.97	16.1
CL1TOS7	1.85	1.50	9.3	9.3	81.4	0.76	79	0.85	14.8
CL1TOS8	1.84	1.51	12.8	5.2	82.0	0.75	77	0.99	16.8
CL1TOS9	1.83	1.48	8.2	10.7	81.1	0.79	70	0.86	15.6
CL1TOS10	1.87	1.55	9.8	7.2	82.9	0.71	77	0.89	17.4

** Note: At 0.2 MPa Effective Confining Stress after saturation at 2.5 MPa Back Pressure

Isotropic Consolidation

Test Number	Volume Change (%) from σ = 0.2 to 9 MPa	Bulk Density (Mg/m3) σ = 9 MPa	Dry Density (Mg/m3) at σ = 9 MPa	K (MPa) Cycled from 5 to 9 MPa	Void Ratio e	Index of Disturbance (%)
CL1TOS6	-4.86	1.98	1.57	1113	0.69	8.4
CL1TOS7	-5.48	1.99	1.59	Not Performed	0.67	6.1
CL1TOS8	-6.66	2.01	1.62	834	0.64	5.7
CL1TOS9	-6.54	1.99	1.58	1182	0.67	6.4
CL1TOS10	-4.31	2.01	1.62	1529	0.64	10.0

Undrained Shear Test

Test Number	Effective Confining Stress (MPa)	Back Pressure (MPa)	B	Maximum Shear Strength (MPa)	Axial Strain at Max. Shear Strength (%)	Max. Stress Ratio at (% Strain)	Modulus of Elasticity (MPa)	A at Failure
CL1TOS6	1.3	4.7	0.87	3.78	1.54	5.04 (0.90)	470	0.04
CL1TOS7	2.0	4.9	0.79	6.26	1.36	5.48 (1.05)	703	0.13
CL1TOS8	4.0	5.0	0.76	4.94	2.85	5.48 (2.85)	744	0.68
CL1TOS9	5.8	6.3	0.65	4.63	1.06	3.42 (5.01)	708	1.07
CL1TOS10	6.9	5.3	0.67	9.89	1.25	4.32 (7.42)	1514	0.48

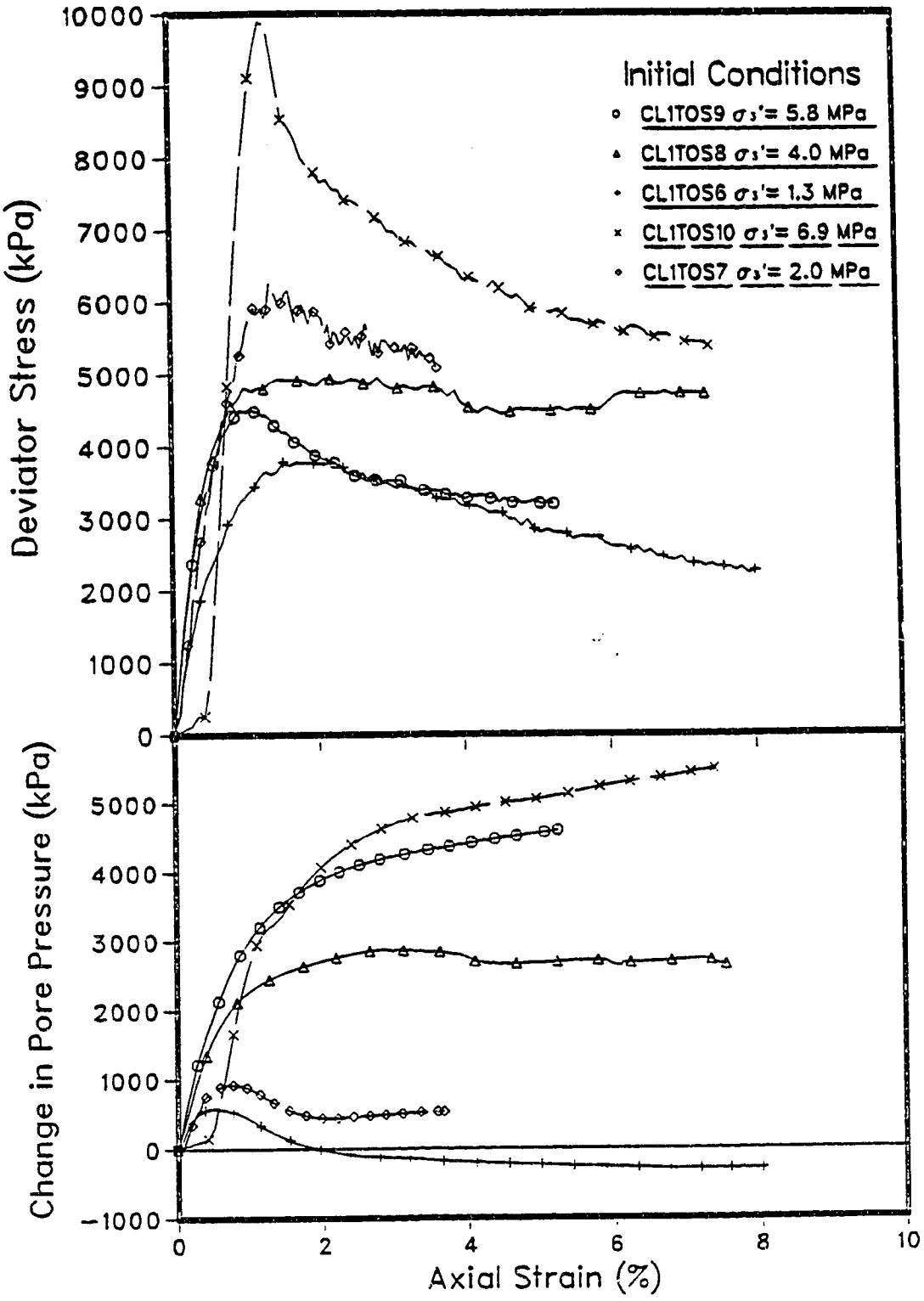

Figure 11.8 Passive Undrained Compression of Cold Lake Clearwater Oil Sands (Location No. 1)

tendency to decrease in volume as shown during the drained shear tests. It would appear from Figure 11.8 that the tendency toward expansion during shear due to dilation dominates below an initial effective confining stress of 4.0 MPa and the tendency toward contraction during shear due to grain crushing dominates above 4.0 MPa.

The results of the passive undrained compression tests performed on Cold Lake Clearwater Formation oil sands are very different from those obtained from similar tests carried out on Athabasca McMurray Formation oil sands. McMurray oil sands require very large strains to achieve the maximum strength failure condition. In order to suppress Athabasca oil sands' high tendency to dilate under shear straining, the pore fluid pressure decreases and, in most cases, falls well below the initial back pore fluid pressure applied to the specimen. This results in a net increase in effective confining pressure on the specimen during the test. Athabasca oil sands, therefore, reach maximum strength when the pore fluid pressure levels out, which generally occurs at large axial strains. The pore fluid pressure for Cold Lake specimens levels out during undrained shear at low confining stresses at much smaller axial strains and remains constant with either a net pore pressure increase or a small pressure decrease. At high confining pressures Cold Lake oil sands require small strains to achieve the maximum strength failure condition due to grain crushing and the pore fluid pressure increases continuously throughout the test due to

the tendency for matrix contraction caused by crushing and rearrangement of grains.

The shear strength data obtained from the passive undrained compression tests carried out on Cold Lake oil sands are plotted in the form of a p'-q diagram in Figure 11.9. The undrained triaxial test results at maximum deviator stress shown in Figure 11.9 are very similar to the failure envelope for the drained tests shown in Figure 11.6. Plewes (1987) found for Athabasca McMurray Formation oil sands the failure envelope for undrained compression at maximum strength was considerably lower when compared to drained tests. The difference in the undrained behaviour of the two oil sands requires some discussion.

During undrained triaxial compression no volume change of the specimen is permitted. There exists for every sand an effective confining pressure at which zero volumetric strain occurs at failure for a given void ratio. This confining pressure is referred to as the critical confining pressure and if an undrained test was performed at this confining stress there would be no tendency for volume change at failure and, therefore, no excess pore pressure will develop. If the effective confining stress is above the critical confining stress for a given void ratio (after consolidation) then a volume reduction would occur under drained conditions. If this test was conducted under undrained conditions, this tendency for volume reduction during shear would result in a positive pore pressure being

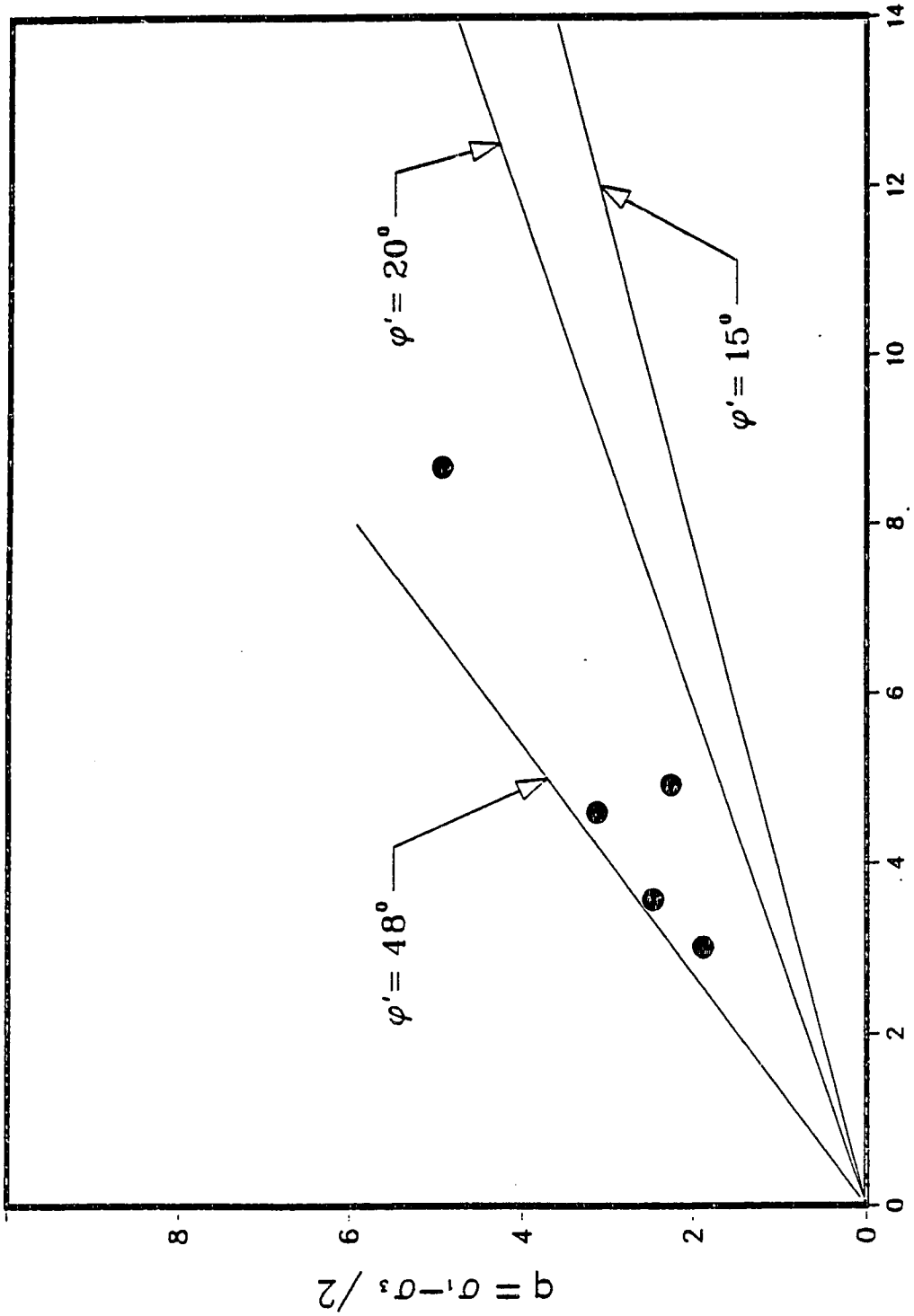

Figure 11.9 Undrained Compression Tests on Cold Lake Clearwater Oil Sands (Location No. 1)

induced which causes a decrease in the effective stress in the specimen. The maximum pore fluid pressures that could develop would be the difference between the initial effective confining stress and the critical effective confining stress. If the effective confining stress is below the critical confining stress for a given void ratio (after consolidation), then a volume increase would occur as the specimen dilates under drained conditions. If this test was conducted under undrained conditions this tendency to dilate would result in a negative pore pressure being developed which increases the effective stress in the specimen. The maximum effective stress which the sample can obtain is the critical confining pressure and the pore pressure decrease is again equal to the difference between the initial effective confining stress and the critical confining stress.

Athabasca McMurray Formation oil sands have a high tendency to dilate under shear straining and require large axial strains to reach the critical confining pressure. These large axial strains result in a decrease in strength of this oil sands and may be enough to cause the strength to approach the residual strength. As a result, the failure envelope, in terms of maximum strength, is much lower than the one obtained for fully drained conditions. If, on the other hand, the failure envelope for the undrained tests is plotted in terms of maximum stress ratio and compared to drained tests corrected for volume change due to dilatancy

effects, the results are very similar (Plewes, 1987). Since the specimen reaches failure conditions at the maximum stress ratio during the initial straining of the specimen, as the tendency to dilate begins to dominate, the angle of shearing resistance is higher and should be similar to the drained compression results.

Clearwater Formation oil sands do not show the high tendency to dilate under shear straining which is associated with McMurray Formation oil sands. Grain crushing becomes more dominant with increasing confining pressure. At confining pressures above 2 MPa this dense sand shows the characteristics of a loose sand by exhibiting a decrease in volume with axial strain. Since the effective confining stress above 2 MPa is above the critical confining stress, a positive pore pressure response occurs which causes a reduction in effective stress. Due to the relatively small strains required to obtain the maximum deviator stress in this material, the effective angle of shearing resistance and maximum strength under undrained conditions are similar to the drained test results.

Above 4 MPa initial effective confining stress the magnitude of grain crushing is very large. For example, the test performed at an initial effective confining stress of 6.9 MPa reaches its maximum deviator stress of 9.89 MPa at 1.25% axial strain corresponding to an effective angle of shearing resistance of 34.7°. This specimen ultimately reaches its maximum stress ratio of 4.32 at 7.4% axial

strain corresponding to an effective angle of shearing resistance of 38.6°. The stress path followed at this initial effective confining stress is very similar to that followed by a normally consolidated sensitive clay during undrained shear. During passive undrained compression a normally consolidated sensitive clay will reach its peak deviator stress at small axial strain and decrease with continued strain. The pore fluid pressure will continue to rise even after the deviator stress has reached its maximum value. This behaviour arises from the loose metastable soil matrix of sensitive clays. The clay undergoes a large decrease in volume in drained shear and as a result large pore pressures develop during undrained shear. As shearing progresses the effective stresses decrease as more available friction is mobilized. As a result, the overall shearing resistance reaches its maximum value prior to full frictional resistance being mobilized. At large strains when all the friction is mobilized, the overall shearing resistance is smaller because the effective stress is smaller.

The initial undrained tangent modulus values for Clearwater Formation oil sands are shown in Figure 11.10. The undrained modulus increases with effective confining pressure. However, the rate of increase decreases with increasing confining pressure. The variability of modulus values again reflects the amount of sample disturbance each specimen has undergone. Comparing Figures 11.10 and 11.7

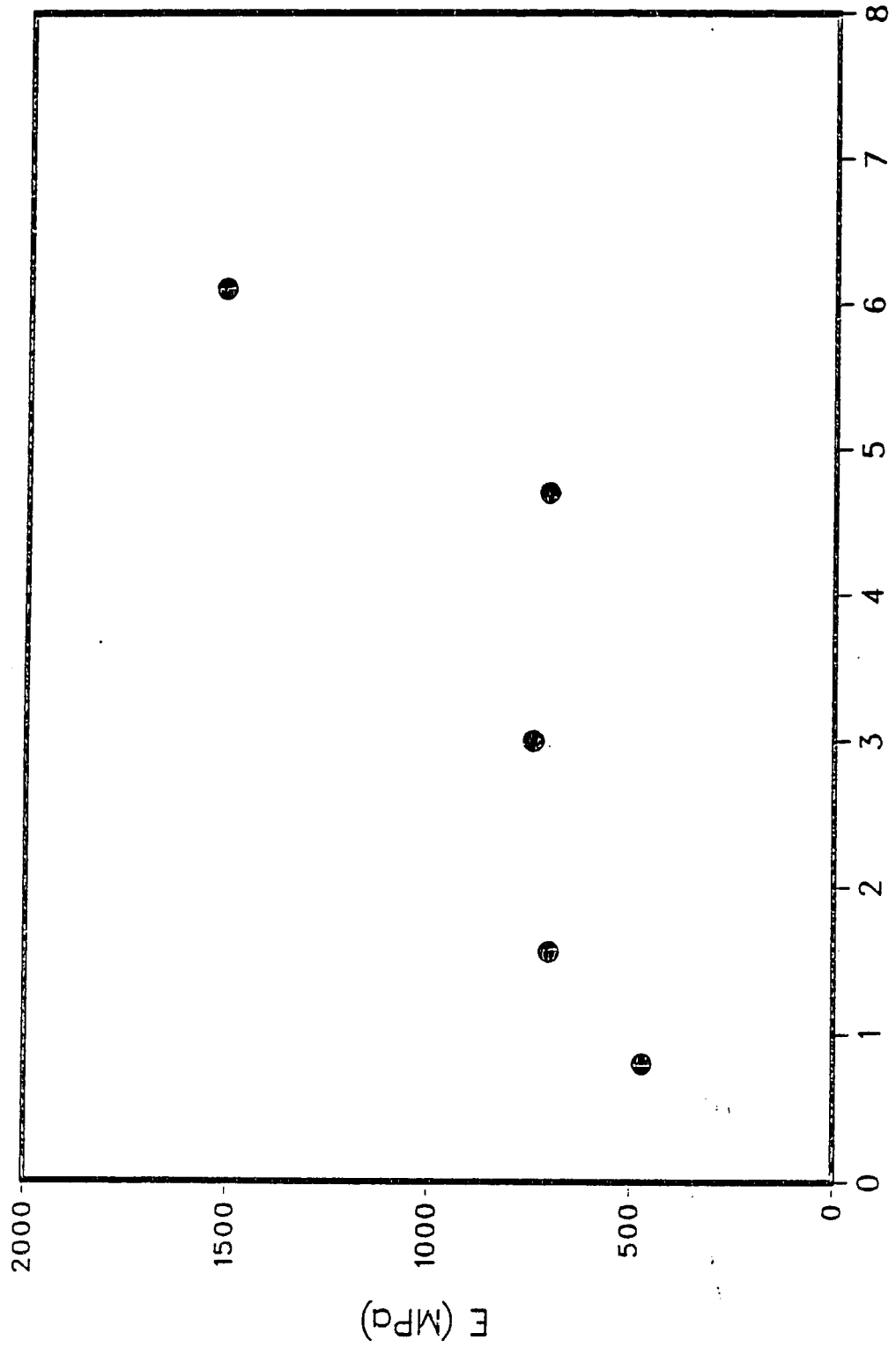

Figure 11.10 Variation of Undrained Modulus – Cold Lake Clearwater Oil Sands (Location No. 1)

shows the initial tangent moduli are similar for drained and undrained compression.

Passive Drained Compression at Elevated Temperatures

To study the effect temperature has on the shear strength of this Clearwater Formation oil sands a series of triaxial tests were performed following the passive drained compression stress path at elevated temperatures. Four triaxial tests were performed at 225°C and one was carried out at an intermediate temperature of 125°C. The procedures used in these tests were the same as those used at 20°C up to and including the cyclic compressibility test. After isotropic consolidation the test specimen was heated slowly under fully drained conditions to the required test temperature under the effective confining stress to be employed in the shear test. During the heating period the volume of fluid leaving the specimen (heat consolidation) was monitored. After the specimen had reached the test temperature, it was allowed to stabilize. The specimen was considered stable when the temperature within the cell was constant and no volume change was observed. A cyclic compressibility test was then performed at test temperature to assess any changes in the sand matrix compressibility caused by the heat consolidation. As in the case of the tests performed at 20°C, the pore pressure parameter B was

measured prior to the shear test. The results of each phase of these tests are summarized in Table 11.3.

Figure 11.11 is a plot of stress-strain and volume change curves comparing triaxial compression tests following passive drained stress path under 4.0 MPa effective confining stress at temperatures of 20°C and 125°C. The major observations arising from these tests may be summarized as follows:

1. Each specimen had the same solids content of 82.7% by mass although the specimen tested at 20°C had a slightly larger fines content, 20% as compared to 14% for the high temperature specimen.

2. The index of disturbance of the high temperature specimen was larger, 19% as compared to 15%.

3. The bulk modulus of the high temperature specimen was lower at 20°C but was equivalent to the room temperature specimen after heat consolidation.

4. The void ratios prior to shear for both specimens were approximately the same, slightly greater than 0.6.

Table 11.3 Consolidated Drained Triaxial Tests - Cold Lake Clearwater Formation Oil Sands at 225 °C (Location No. 1)

Initial Conditions at 20 °C

Test Number	Bulk Density (Mg/m3)	Dry Density (Mg/m3)	% water (mass)	% bitumen (mass)	% solids (mass)	Void Ratio e	Sr (%)	Pore Pressure Parameter B **	Index of Disturbance (%)
CL1TOS11 *	1.84	1.52	7.4	9.9	82.7	0.74	75	0.85	19.0
CL1TOS12	1.84	1.52	7.8	9.7	82.6	0.74	76	0.83	18.4
CL1TOS13	1.94	1.62	10.2	6.2	83.6	0.63	82	0.95	13.4
CL1TOS14	1.73	1.40	8.3	10.4	81.2	0.89	68	1.00	24.4
CL1TOS15	1.93	1.60	8.9	7.8	83.3	0.65	81	0.95	13.8

* Note: Test Performed at 125°C

** Note: At 0.5 MPa Effective Confining Stress after saturation at 2.5 MPa Back Pressure

Isotropic Consolidation and Drained Heating to 225 ° C

Test Number	Volume Change (%) from σ = 0.5 to (•) MPa at 20 °C	K (MPa) at 20°C Cycled from (• to •) MPa	Total Vol. Ch. (%) 20-225 °C at σ = (•) MPa	K (MPa) at 225 °C Cycled from (• to •) MPa	Void Ratio e 20°C	Void Ratio e 225°C	Index of Disturbance (%) 20°C	Index of Disturbance (%) 225°C
CL1TOS11	-5.83 (7.4)	893 (4.6-7.4)	-6.08 (4.0)	1511 (4.6-7.4)	0.64	0.63	9.0	8.6
CL1TOS12	-3.95 (7.3)	737 (1.0-7.3)	-9.08 (1.0)	776 (1.0-7.1)	0.67	0.58	11.9	2.5
CL1TOS13	-1.91 (7.0)	1442 (2.6-7.0)	-8.59 (2.5)	1654 (2.4-7.1)	0.60	0.49	9.9	-3.4
CL1TOS14	-5.45 (7.0)	----------	-10.20 (6.5)	1175 (2.7-7.2)	0.79	0.70	16.4	8.5
CL1TOS15	-4.22 (9.1)	2274 (7.2-9.1)	-10.12 (7.0)	4761 (7.1-8.2)	0.58	0.49	6.1	-5.8

Drained Shear Test

Test Number	Effective Confining Stress (MPa)	Back Pressure (MPa)	B	Deviator Stress at failure (MPa)	Axial Strain at failure (%)	Volumetric Strain at failure (%)	Modulus of Elasticity (MPa)	Poisson's Ratio
CL1TOS11	4.0	7.7	0.68	8.04	1.95	-0.991	1320	0.16
CL1TOS12	1.2	7.4	0.32	3.29	0.89	0.328	502	----
CL1TOS13	2.5	7.5	0.41	7.57	1.07	-0.254	861	0.39
CL1TOS14	5.5	7.4	0.30	9.83	1.19	-0.296	2181	0.11
CL1TOS15	7.0	7.6	----	12.18	1.88	-0.637	2740	0.39

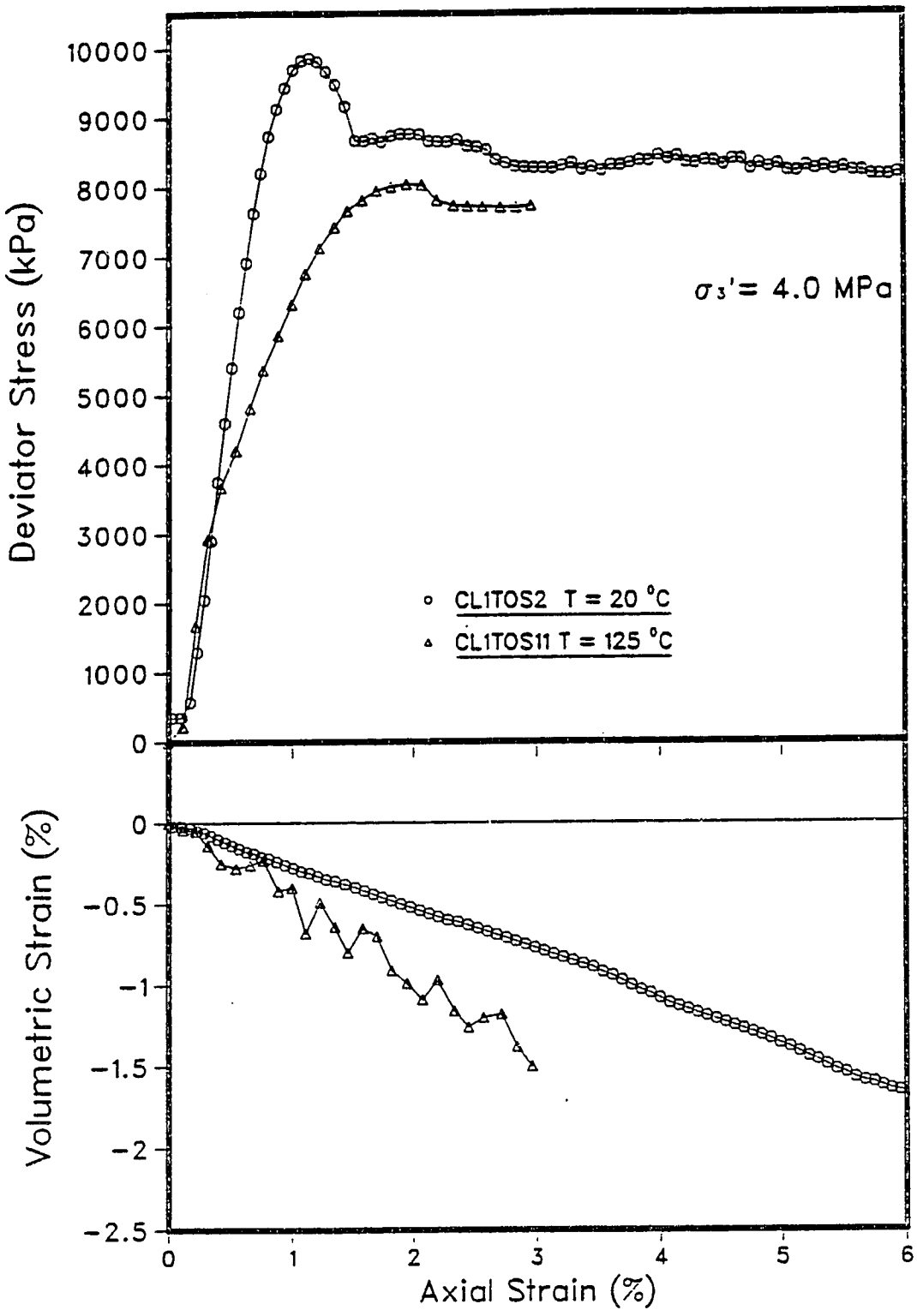

Figure 11.11 Passive Drained Compression at 125 °C
(Location No. 1)

5. The peak deviator stress during shear for the 20°C specimen was larger, 9.85 MPa as compared to 8.04 MPa. The axial strain to failure was larger for the 125°C specimen, 1.95 as compared to 1.04%.

6. Each specimen displayed a net volume decrease at failure. The volume reduction for the 125°C specimen was three times that of the 20°C specimen.

7. The initial tangent modulus measured at 20°C was slightly larger, 1404 MPa as compared to 1320 MPa.

8. Each specimen shows weak strain softening behaviour in the post-peak region and sand matrix contraction throughout the entire shear test.

Based on these observations, it appears that a temperature increase of 105°C has only a slight effect on the mechanical properties of this Cold Lake oil sands. Only a small amount of volume reduction occurs during heat consolidation to 125°C. The index of disturbance is somewhat higher for the specimen heated to 125°C and this difference in sample disturbance alone may account for the reduction in

strength and stiffness at 125°C. In other words, compressing the 20°C specimen to 9 MPa and cycling over the stress range of 5 to 9 MPa improves the quality of the specimen greater than compressing the specimen to 7.4 MPa, cycling from 4.6 to 7.4 MPa and heat consolidation to 125°C.

The results of passive drained triaxial compression tests carried out at 225°C (Specimens CL1TOS12 to CL1TOS14) are shown in Figure 11.12. As indicated in Table 11.3, each specimen displayed a significant amount of heat consolidation, ranging from 8.6 to 10.2%, during drained heating to 225°C. The stress-strain curves obtained from each of these specimens were similar. Each specimen reached its peak strength at about 1% axial strain and had a slight strength decrease followed by a slow continuous strength increase with continued straining. The specimen tested at the low effective confining stress of 1.2 MPa displayed dilatant behaviour during shear while specimens tested under greater confining stresses displayed contractive behaviour.

A scanning electron micrograph of Specimen CL1TOS14 before and after drained shear under an effective confining stress of 5.5 MPa at 225°C is shown in Figure 11.13. Comparing the grain fabric before and after testing illustrates the high degree of grain crushing and rearrangement which has occurred with the crushed fragments occupying the pore space between larger grains. In the bottom right hand portion of Figure 11.13b evidence of a shear plane is seen displacing some grains and shearing

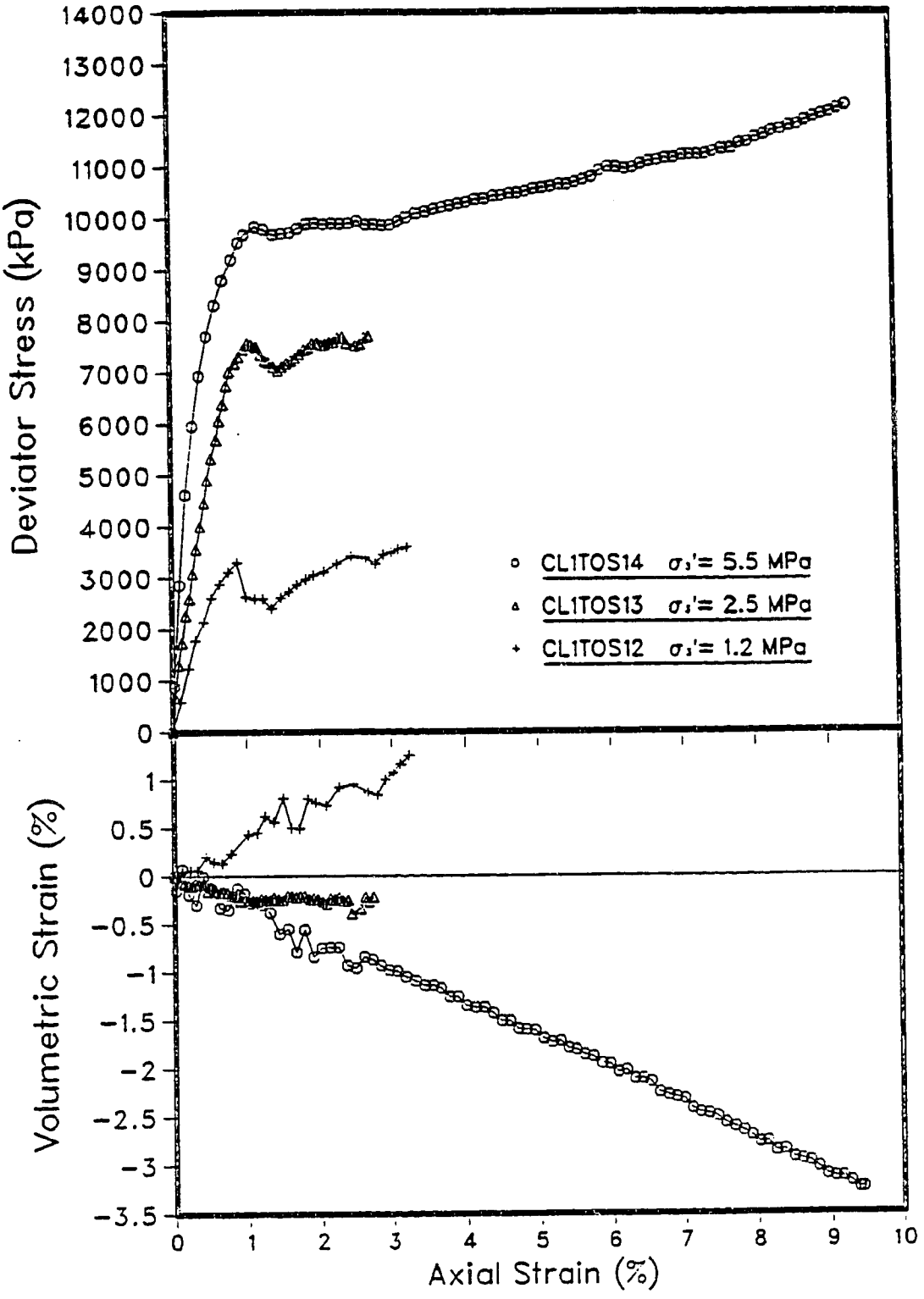

Figure 11.12 Passive Drained Compression at 225 °C
(Location No. 1)

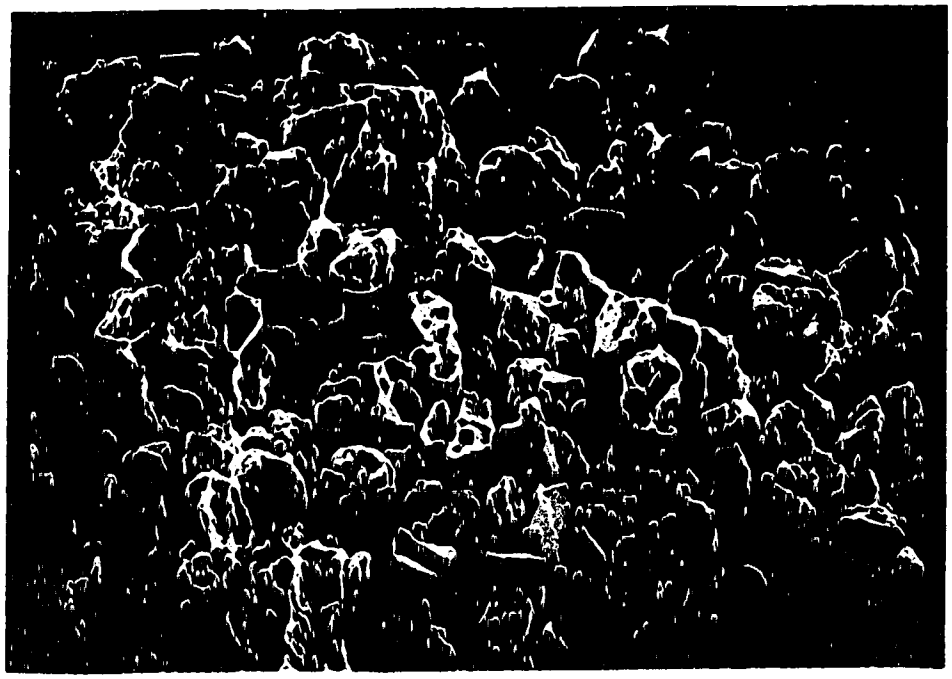

a) Before Test

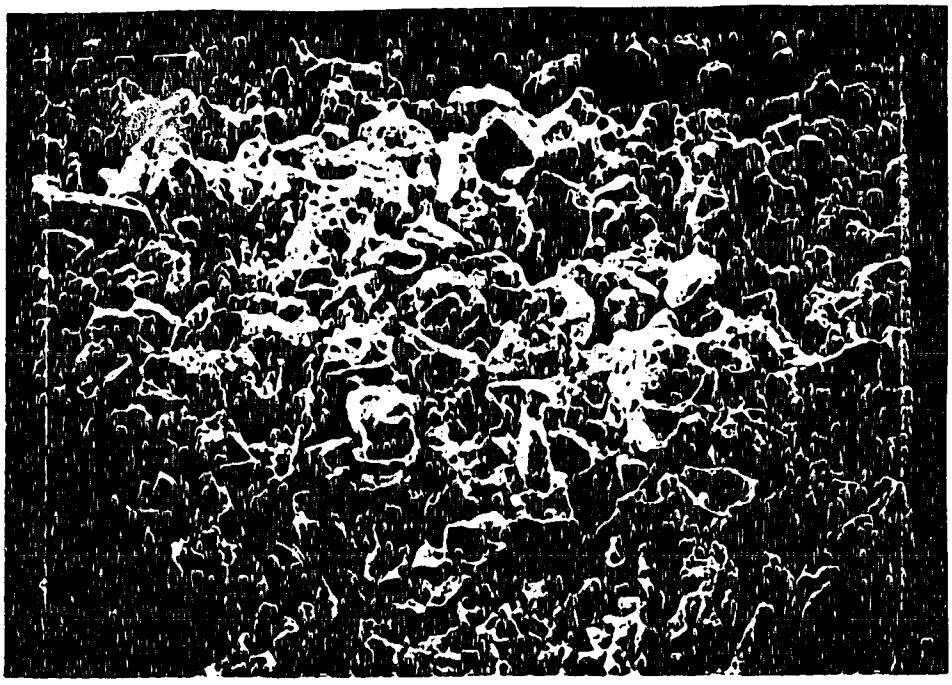

b) After Drained Shear (σ_3' = 5.5 MPa, T = 225°C)

Figure 11.13 Scanning Electron Micrograph of Specimen CL1TOS14 (Magnification 55X)

through others. The amount of grain crushing appears more severe at 225°C than at 20°C (as shown in Figure 11.2b). At 20°C the grain crushing was selective with the weaker grains showing the greater damage. In contrast, at 225°C it appears that few grains survive the heating and shearing process without crushing.

The remaining oil sands specimen (CL1TOS15) from Cold Lake Location No. 1 tested at 225°C was subjected to a number of unloading-reloading cycles during passive drained compression. The history of stress applied during this test may be summarized as follows:

1. The deviator stress was increased to approximately 8 MPa under the effective confining stress of 7 MPa. The specimen was then unloaded to isotropic conditions.

2. The effective confining pressure on the specimen was reduced to 4 MPa. The deviator stress was increased to 10 MPa. The specimen was then unloaded to isotropic conditions.

3. The effective confining pressure on the specimen was reduced to 1.0 MPa. The deviator stress was increased to about 6 MPa. The specimen was then unloaded to isotropic conditions.

4. The original 7 MPa effective confining stress was restored to the specimen and the deviatoric stress was increased to specimen failure.

The stress-strain and volume change relationships for each stage of this test are shown in Figure 11.14. The amount of non-recoverable axial strain during the initial loading and unloading cycle at 7 MPa confining stress was approximately 0.30%. The unloading modulus was greater than the initial modulus, 5506 MPa as compared to 2154 MPa. The loading modulus at 4 MPa confining pressure was 3806 MPa and at 1.0 MPa confining stress was 1504 MPa. The unloading modulus at 1.0 MPa confining stress was 2975 MPa. During the final stage of the test under an effective confining stress of 7.0 MPa, the initial tangent modulus was 2740 MPa. The specimen reached its maximum shear strength of 12.18 MPa at 1.9% axial strain and displayed a volumetric strain at failure of -0.64%.

The results of this test illustrate the stress path dependency of this oil sands at elevated temperatures.

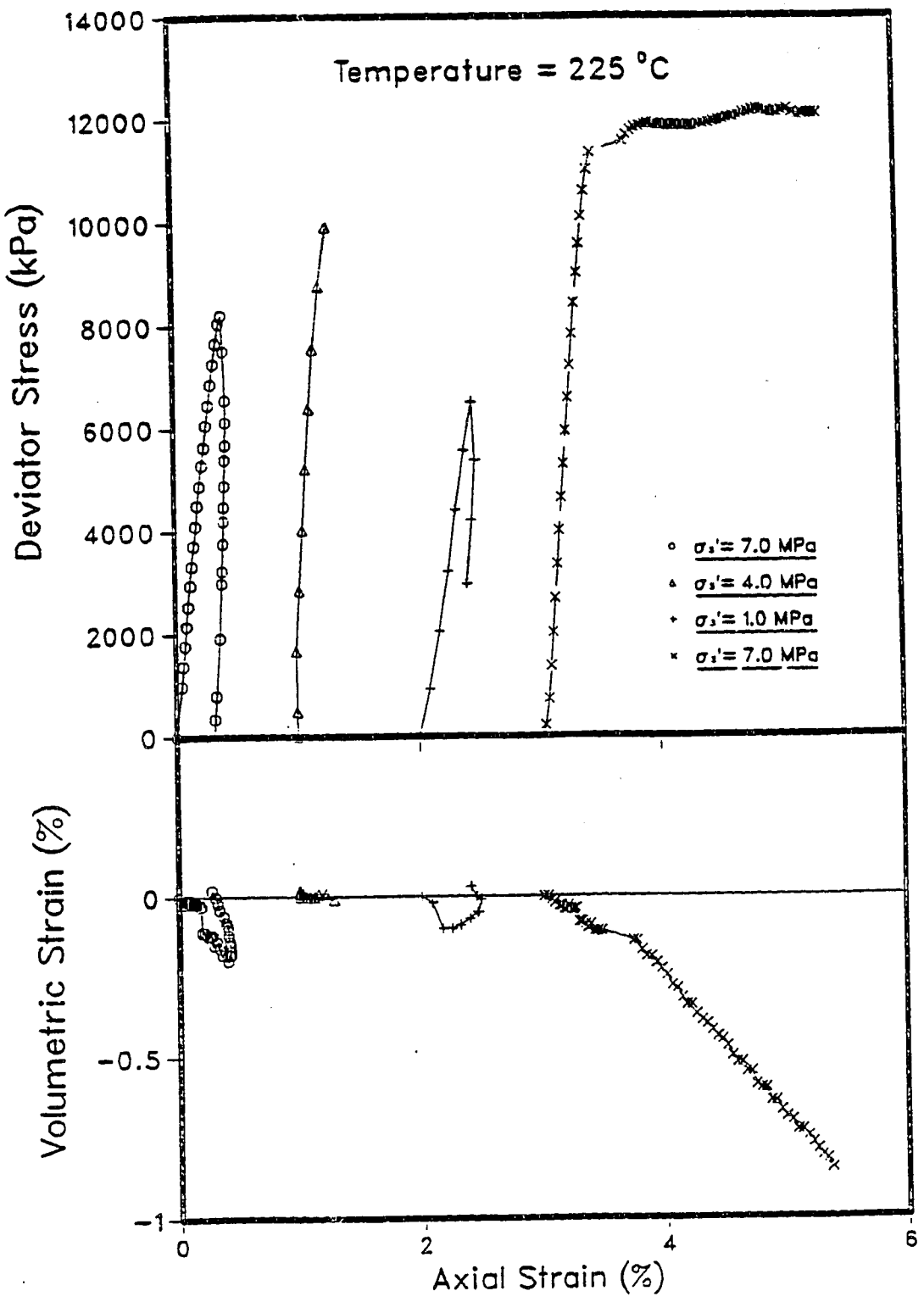

Figure 11.14 Passive Drained Compression Test on Specimen CL1TOS15

Subjecting the oil sands to small axial strains (less than 0.4%) at 7 MPa results in a stronger and stiffer material at lower effective confining stresses. For example, Specimen CL1TOS12 tested at 1.2 MPa effective confining stress had an initial tangent modulus of 503 MPa and a maximum shear strength of 3.29 MPa. Specimen CL1TOS15 after being subjected to the stress history shown in Figure 11.14, had a modulus of 1504 MPa and was essentially elastic to a deviator stress increase of 6 MPa. As a result, drained heating under a high confining stress and deviatoric cycling results in a denser sand matrix not attainable by heating under a low confining stress followed by isotropic cycling of stress.

The sand fabric of Specimen CL1TOS15 after testing is shown in Figure 11.15. The sand matrix shows several features associated with the grain crushing process. A large number of long grain contacts are visible and the amount of pore space appears small. Small grain fragments, probably originating from the crushing of larger grains, occupy the space between larger grains. Some of the larger grains themselves show evidence of fracturing.

The shear strength data from the high temperature triaxial tests, plotted in the form of a p'-q diagram, are shown in Figure 11.16. For comparative purposes, the results of the tests performed at 20°C are also shown in the figure. In general, the failure envelope at 225°C shows significantly less curvature than the envelope obtained for

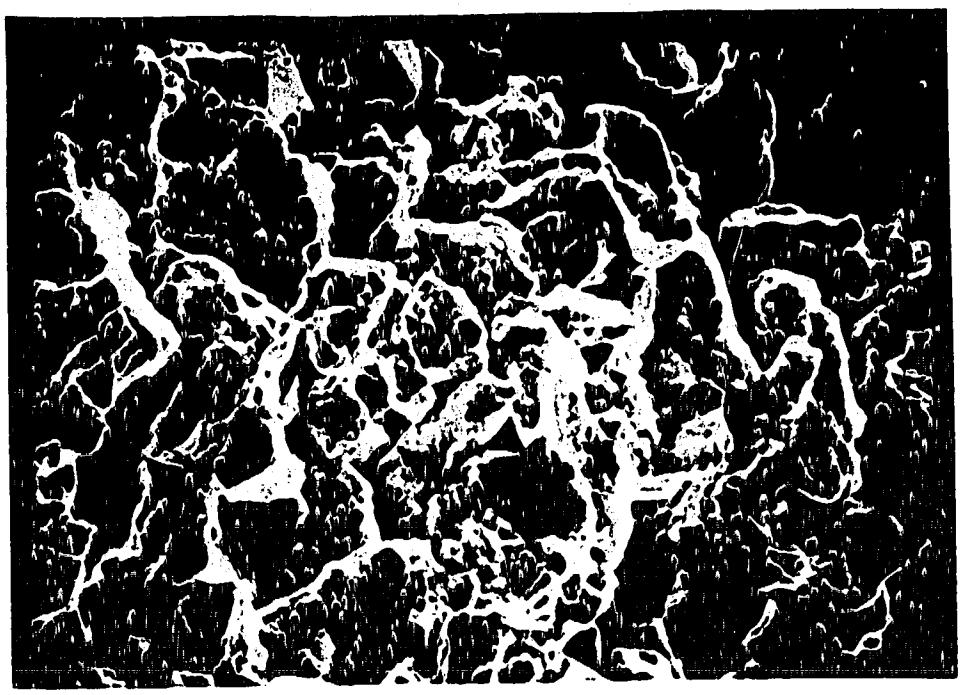

Figure 11.15 Scanning Electron Micrograph of Specimen CL1TOS15 (Magnification 110X)

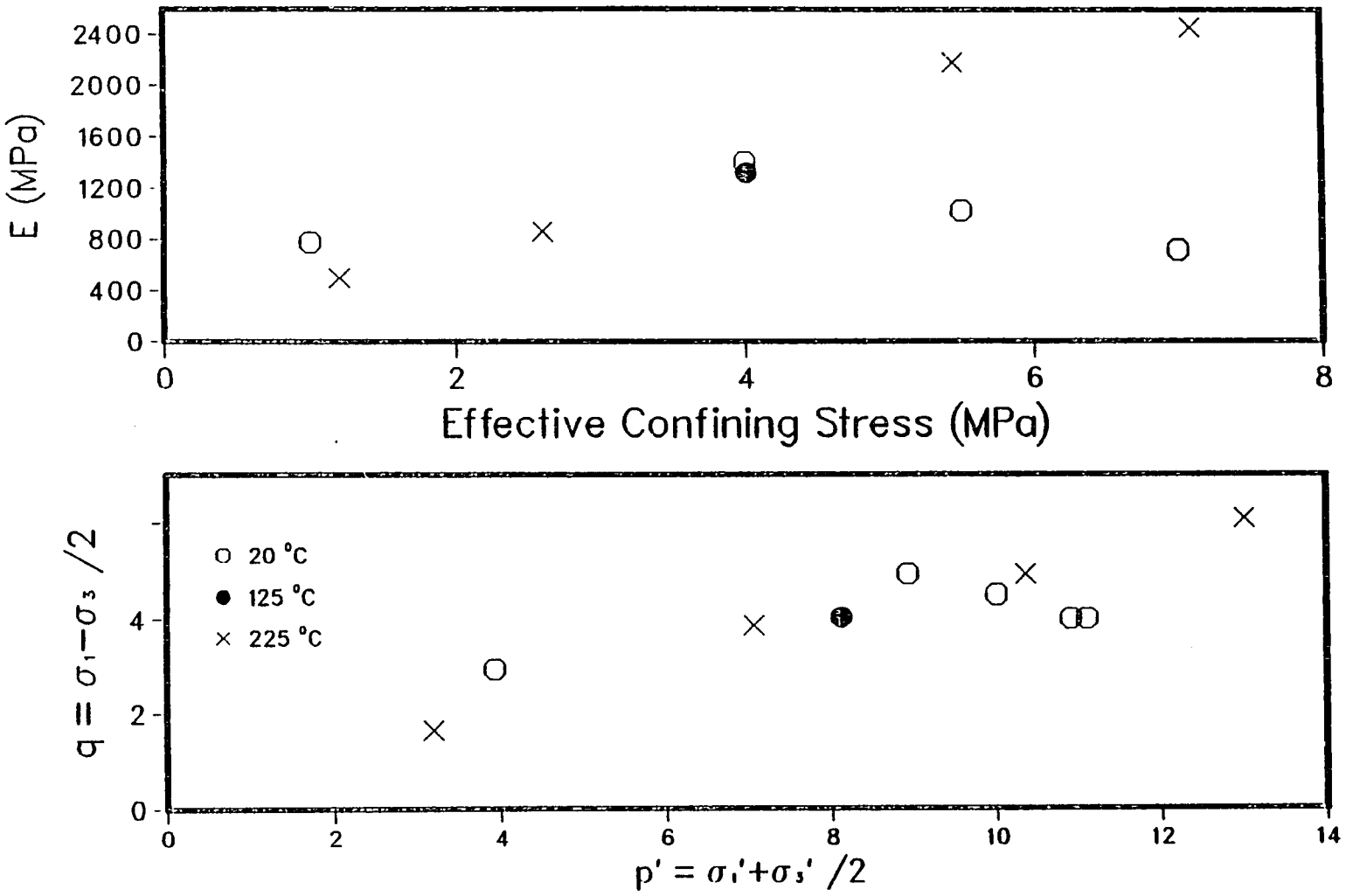

Figure 11.16 Summary of Passive Drained Compression Tests on Cold Lake Oil Sands (Location No. 1)

the tests performed at 20°C. The differences in the failure envelopes may reflect the amount of grain crushing which occurs during the heat consolidation phase of the test. Each specimen heated to 225°C experienced a significant void ratio decrease due to heating. This thermal grain crushing may alter the fabric from a uniform sand to a better graded, silty sand, as shown in Figure 11.13b and 11.15. The decrease in average particle size, the better grading and the greater angularity due to thermal grain crushing may result in greater shearing resistance. The more uniform, coarser graded oil sands at 20°C compress more than the better graded material at 225°C and results in a more curved failure envelope at high confining stresses than at 20°C, as illustrated in Figure 11.16. This is illustrated by comparing the two tests performed at 5.5 MPa effective confining stress. The test performed at 225°C is stronger and stiffer than the test performed at 20°C even though the void ratio of the specimen tested at 225°C is much larger (0.70 as compared to 0.57). The test performed at 20°C displays a greater volume decrease during shear than the specimen tested at 225°C.

The variation of the initial tangent modulus with effective confining stress is also shown in Figure 11.16. The modulus increases with increasing confining stress. At high effective confining stress the modulus is significantly larger than the modulus at 20°C, reflecting the much denser sand structure arising from thermal grain crushing during

the heat consolidation process.

11.4 Cold Lake Location No. 2 Oil Sands

Passive Drained Compression at 20°C

The stress-strain and volume change relationships for Cold Lake Location No. 2 Clearwater Formation oil sands at 20°C are shown in Figure 11.17 and the results for each phase of testing are summarized in Table 11.4.

Initial index of disturbance values show these samples experienced a large amount of expansion during the core sampling process. Although significant improvement in matrix density is shown after isotropic consolidation and cyclic compression, they are well above the limit considered adequate for obtaining representative geomechanical properties. The initial indices of disturbance ranged from 22 to 31% and after compression and cycling they ranged from 12 to 20%.

Even though the strength and deformation results obtained from the laboratory testing may under estimate in situ values due to microfabric disturbance, several important conclusions concerning the characteristic behaviour of this oil sands is apparent. As the effective confining pressure applied to the specimen increases, the

Table 11.4 Consolidated Drained Triaxial Tests - Cold Lake Clearwater Formation Oil Sands (Location No. 2)

Initial Conditions

Test Number	Bulk Density (Mg/m3)	Dry Density (Mg/m3)	% water (mass)	% bitumen (mass)	% sand (mass)	Void Ratio e	Sr (%)	Pore Pressure Parameter B **	Index of Disturbance (%)
CL2TOS1	1.67	1.37	8.4	9.7	81.9	0.84	62	0.99	31.2
CL2IOS2	1.78	1.46	8.4	9.7	81.9	0.82	72	0.89	21.8
CL2IOS3	1.66	1.35	6.7	12.3	81.0	0.97	64	0.92	28.3

** Note: At 0.2 MPa Effective Confining Stress after saturation at 2.5 MPa Back Pressure

Isotropic Consolidation

Test Number	Volume Change (%) from σ = 0.2 to (•) MPa	Bulk Density (Mg/m3) σ = (•) MPa	Dry Density (Mg/m3) at σ = (•) MPa	K (MPa) Cycled from 5 to 9 MPa	Void Ratio e	Index of Disturbance (%)
CL2TOS1	-7.16 (9.0)	1.92 (9.0)	1.47 (9.0)	893	0.80	20.4
CL2IOS2	-6.29 (9.0)	1.97 (9.0)	1.56 (9.0)	1268	0.70	11.8
CL2IOS3	-10.00 (11.3)	1.93 (11.3)	1.50 (11.3)	1100	0.77	13.5

Drained Shear Test

Test Number	Effective Confining Stress (MPa)	Back Pressure (MPa)	B	Deviator Stress at failure (MPa)	Axial Strain at failure (%)	Volumetric Strain at failure (%)	Modulus of Elasticity (MPa)	Poisson's Ratio
CL2TOS1	1.0	3.0	0.89	3.19	2.03	0.14	311	0.40
CL2IOS2	4.0	3.0	0.78	7.00	2.66	-1.12	677	0.27
CL2IOS3	7.0	3.0	0.57	10.80	9.02	-5.03	695	0.20

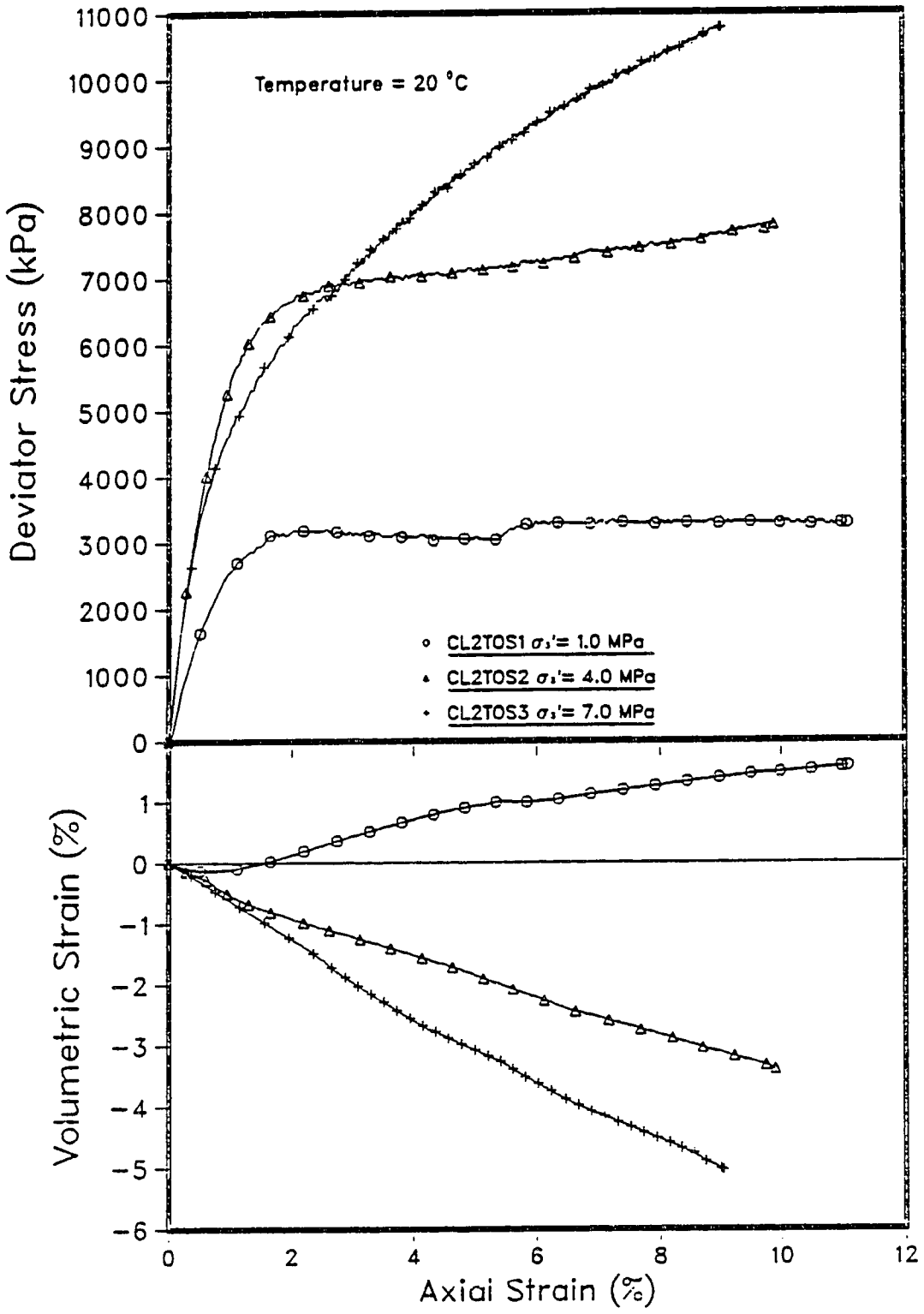

Figure 11.17 Passive Drained Compression Tests on Cold Lake Oil Sands (Location No. 2)

strain to failure increases and the tendency to dilate decreases. The stress-strain curve shows significant strain hardening behaviour at high effective confining stresses. This behaviour is very similar to that observed for Clearwater oil sands from Location No. 1. At low confining stresses, little grain crushing occurs and the sand grains slide over each other and the matrix dilates against the confining stress. At high confining stresses, grain crushing dominates and volume changes are entirely compressive. The net effect of this difference in behaviour at low and high effective confining stresses is a failure envelope which is highly curved.

Passive Drained Compression at 225°C

To investigate the effect temperature has on the strength-deformation properties of Location No. 2 oil sands, a triaxial test was performed following the passive drained compression stress path at 225°C. The test procedure followed during this test varied significantly from that followed for Location No. 1 oil sands. In this test, the specimen (CL2TOS4) was not compressed nor cycled at 20°C and was heat drained under a nominal effective confining stress of 1.0 MPa. During the heating period the volume of fluid leaving the specimen was monitored. After the specimen reached 225°C, a cyclic stress compressibility test was

performed. The effective confining stress was increased to 4 MPa and the drained shear test was carried out. The results for each phase of this test are given in Table 11.4.

The stress-strain and volume change relationships obtained from this test are given in Figure 11.18.

Although the stress path and stress history of this specimen is different from the test performed at 20°C, at the same effective confining stress, the results are very similar. Each of these specimens had a solids content of approximately 81% by mass and each specimen obtained the same void ratio prior to shear of approximately 0.7. This suggests that subjecting a highly disturbed oil sands specimen to isotropic stress cycling produces the same fabric as drained heating the same specimen under low effective confining stresses. In other words, heating a highly disturbed specimen under low confining stress results in rearrangement of the sand particles into a dense packing, whereas heating a dense sample under high confining stresses results in a significant amount of grain crushing as found in the Location No. 1 specimens.

11.5 Cold Lake Location No. 3 Oil Sands

The stress-strain and volume change relationships for Cold Lake Location No. 3 oil sands at 20°C and 225°C are shown in Figure 11.19. The effective confining stress used in both tests was 7.0 MPa. The results for each phase of the tests are summarized in Table 11.5 (CL3TOS2 at 225°C) and

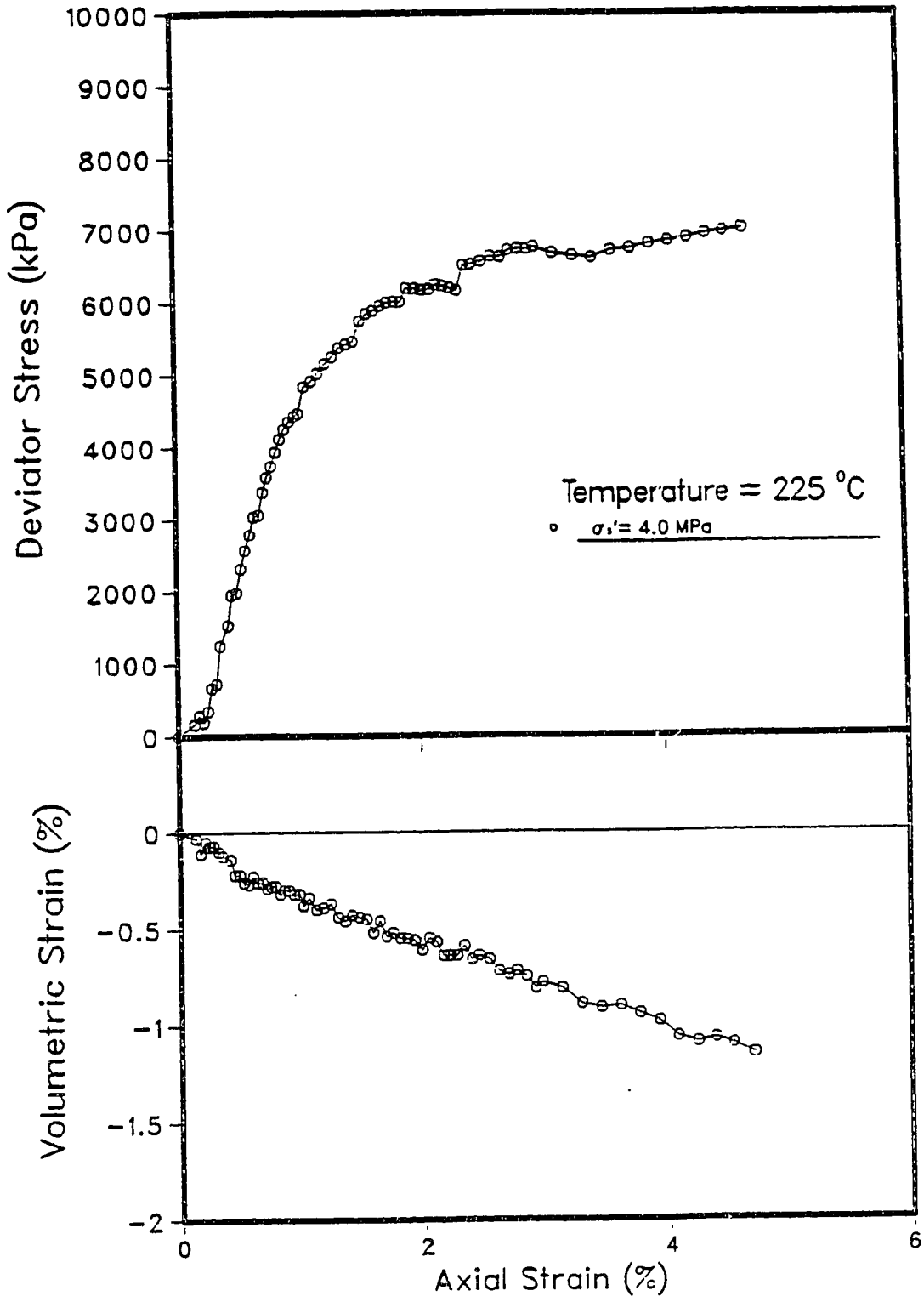

Figure 11.18 Passive Drained Compression Test on Specimen CL2TOS4

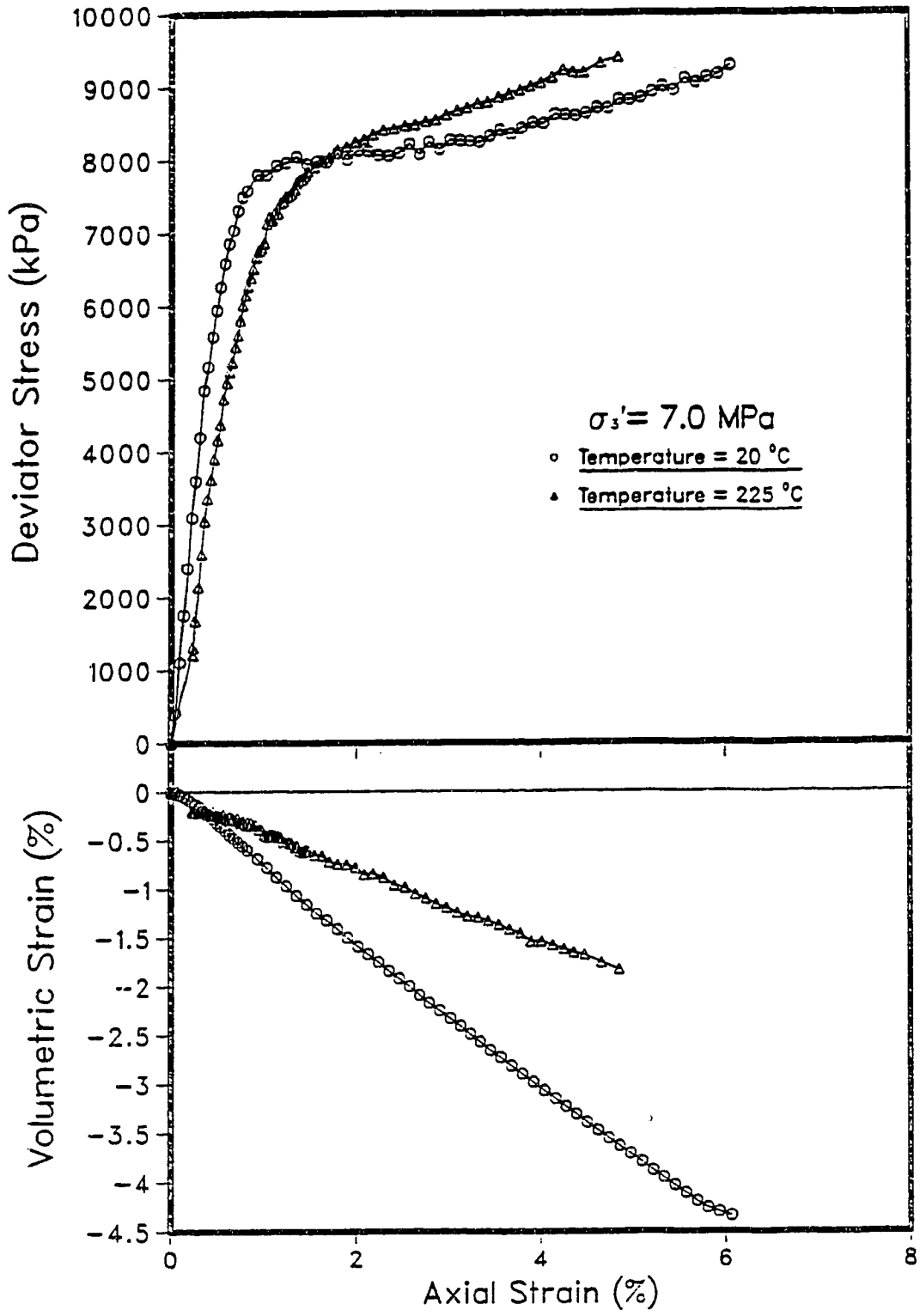

Figure 11.19 Passive Drained Compression Tests on Cold Lake Oil Sands (Location No. 3)

Table 11.6 (CL3TOS1 at 20°C). Each specimen had an initial void ratio of 0.70. Specimen CL3TOS1 underwent a volume reduction of 4.3% during isotropic compression at 9 MPa effective confining stress and had a bulk modulus of 1170 MPa, cycled over the stress range of 5 to 9 MPa. The void ratio prior to drained shear was 0.63. Specimen CL3TOS2 underwent a volume reduction of 7.2% during drained heating to 225°C under a nominal effective confining stress of 1.0 MPa. The specimen was heated in the disturbed state; that is, a compressibility test was not performed prior to heating. The bulk modulus measured at 225°C, cycled over the stress range of 5 to 9 MPa, was 995 MPa. The void ratio after heat consolidation was 0.58. Each test gave very similar stress-strain curves as shown in Figure 11.19.

A scanning electron micrograph of this specimen after shear at 225°C is shown in Figure 11.20. Several grains are broken or fractured and there is evidence of crushing at several contact points. The amount of grain crushing, however, appears less severe in this specimen as compared to Specimen CL1TOS14 (Figure 11.13) which was heated in a dense state under a high effective confining stress. This may suggest that the lower void ratio of the specimen heated to 225°C and the similarity of the stress-strain curves may be due to heat consolidation of the discontinuous shale seams and clasts. Due to the disturbed nature of the oil sands and the low effective confining stress during heating, it seems unlikely that the reduction in void ratio is due entirely to

Table 11.5 Consolidated Drained Triaxial Tests - Cold Lake Clearwater Formation Oil Sands at 225 °C
(Locations No. 2 and No. 3)

Initial Conditions at 20 °C

Test Number	Bulk Density (Mg/m3)	Dry Density (Mg/m3)	% water (mass)	% bitumen (mass)	% solids (mass)	Void Ratio e	Sr (%)	Pore Pressure Parameter B **	Index of Disturbance (%)
CL2TOS4	1.79	1.45	8.2	10.7	81.1	0.82	75	0.99	18.1
CL3IOS2	1.90	1.56	10.4	7.9	81.8	0.70	84	0.92	10.9

** Note: At 0.5 MPa Effective Confining Stress after saturation at 2.5 MPa Back Pressure

Isotropic Consolidation and Drained Heating to 225 C

Test Number	Volume Change (%) from σ = 0.5 to (•) MPa at 20 °C	K (MPa) at 20°C Cycled from (• to •) MPa	Total Vol. Ch. (%) 20-225 °C at σ = (•) MPa	K (MPa) at 225 °C Cycled from 5 to 9 MPa	Void Ratio e 20°C	Void Ratio e 225°C	Index of Disturbance (%) 20°C	Index of Disturbance (%) 225°C
CL2TOS4	Not Done	Not Done	-8.08 (1.0)	882	----	0.67	---	5.5
CL3IOS2	Not Done	Not Done	-7.16 (1.0)	995	----	0.58	---	-1.2

Drained Shear Test

Test Number	Effective Confining Stress (MPa)	Back Pressure (MPa)	B	Deviator Stress at failure (MPa)	Axial Strain at failure (%)	Volumetric Strain at failure (%)	Modulus of Elasticity (MPa)	Poisson's Ratio
CL2TOS4	4.0	7.5	0.76	6.76	2.97	-0.783	630	0.25
CL3IOS2	7.0	7.5	0.48	9.39	4.86	-1.834	912	0.38

Table 11.6 Consolidated Drained Triaxial Tests - Cold Lake Clearwater Formation Oil Sands
(Locations No.3 and No. 4)

Initial Conditions

Test Number	Bulk Density (Mg/m3)	Dry Density (Mg/m3)	% water (mass)	% bitumen (mass)	% sand (mass)	Void Ratio e	Sr (%)	Pore Pressure Parameter B **	Index of Disturbance (%)
CL3TOS1	1.87	1.55	8.9	8.0	83.1	0.70	76	0.93	18.0
CL4TOS1	1.94	1.60	9.5	7.9	82.6	0.66	85	0.92	10.7

** Note: At 0.2 MPa Effective Confining Stress after saturation at 2.5 MPa Back Pressure

Isotropic Consolidation

Test Number	Volume Change (%) from σ = 0.2 to (*) MPa	Bulk Density (Mg/m3) σ = (*) MPa	Dry Density (Mg/m3) at σ = (*) MPa	K (MPa) Cycled from 5 to 9 MPa	Void Ratio e	Index of Disturbance (%)
CL3TOS1	-4.30 (9.0)	2.01 (9.0)	1.62 (9.0)	1170	0.63	10.5
CL4TOS1	-3.36 (10.0)	2.03 (10.0)	1.65 (10.0)	1136	0.60	4.8

Drained Shear Test

Test Number	Effective Confining Stress (MPa)	Back Pressure (MPa)	B	Deviator Stress at failure (MPa)	Axial Strain at failure (%)	Volumetric Strain at failure (%)	Modulus of Elasticity (MPa)	Poisson's Ratio
CL3TOS1	7.0	2.0	0.65	8.04	1.36	-1.07	1390	0.13
CL4TOS1	7.0	6.0	----	9.07	1.24	-0.74	1339	0.27

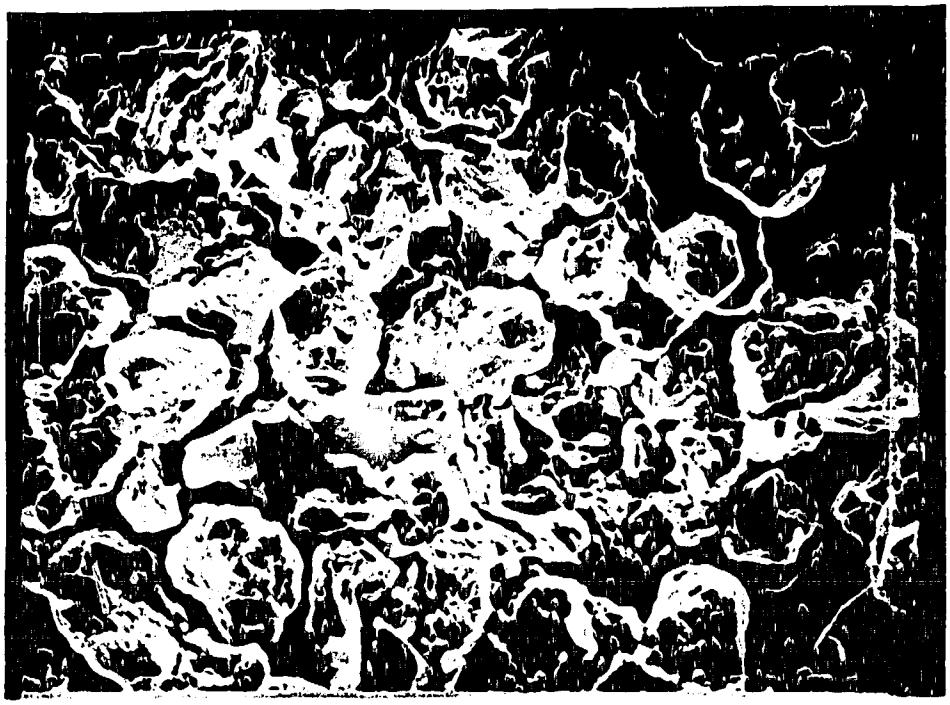

Figure 11.20 Scanning Electron Micrograph of Specimen CL3TOS2 (Magnification 72X)

thermal grain crushing. The heat consolidation of the shale interbedding may also account for the greater volume reduction of the 20°C specimen during drained shear.

11.6 Cold Lake Location No. 4 Oil Sands

Passive Drained Compression at 20°C

Figure 11.21 is a stress-strain and volume change plot for Cold Lake Location No. 4 oil sands subjected to passive drained compression with 7.0 MPa effective confining stress at 20°C. The results for this specimen (CL4TOS1) are summarized in Table 11.6. The index of disturbance of the specimen prior to testing was 10.7%.

Specimen CL4TOS1 reached a maximum shear strength of 9.07 MPa at 1.2% axial strain and displayed a volume reduction of 0.7% at failure. The stress-strain curve showed strain hardening behaviour in the post-peak region and the soil matrix contracted continually during shear. The initial tangent modulus and Poisson's ratio were 1339 MPa and 0.27, respectively. The results of this drained shear test are consistent with previous tests performed on Clearwater oil sands from the other locations.

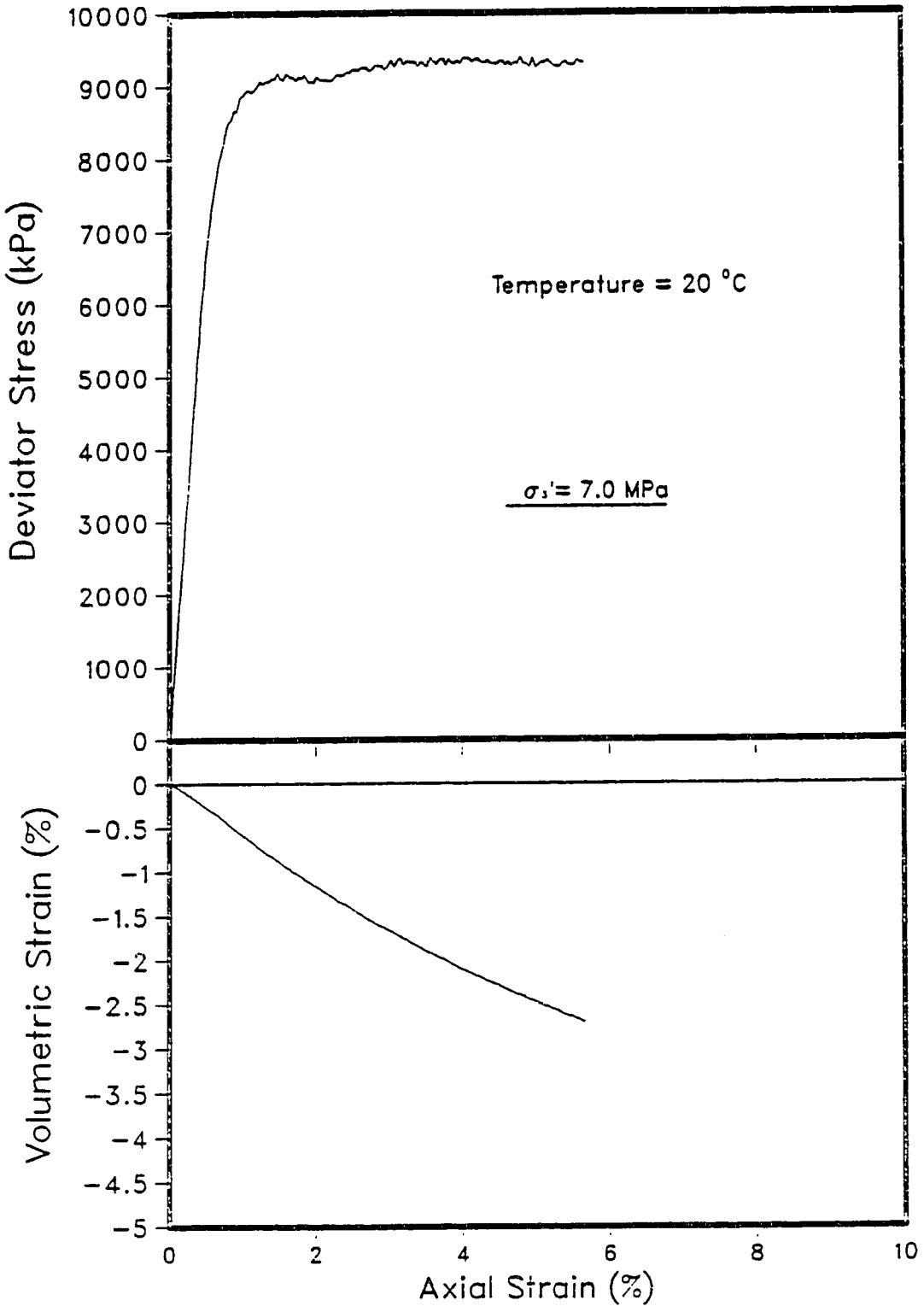

Figure 11.21 Passive Drained Compression Test on Specimen CL4TOS1

Passive Undrained Compression at 20°C

The stress-strain and pore pressure response of Specimen CL4TOS2 following the passive undrained compression stress path at 20°C is shown in Figure 11.22. The results for each phase of testing are summarized in Table 11.7. The initial index of disturbance of this specimen was 12.9%.

Specimen CL4TOS2 was tested under an initial effective confining stress of 7 MPa and reached its maximum shear strength of 7.39 MPa at 0.74% axial strain corresponding to an effective angle of shearing resistance of 29.1°. The specimen obtained its maximum stress ratio of 3.65 at 4.1% axial strain corresponding to an effective angle of shearing resistance of 34.8°. As previously discussed, during undrained compression under a high initial effective confining stress Clearwater Formation oil sands reach peak deviator stress at small axial strain and then decreases with continued strain. The pore fluid pressure continues to rise after the deviator stress has reached its maximum value. This type of behaviour arises from collapse of the sand matrix due to the large amount of grain crushing which occurs during shear at high effective confining pressures. Figure 11.23 compares the grain size distribution of Specimen CL4TOS2 after the shear test with the grain size distribution of core directly adjacent to where the test specimen was taken. A significant amount of grain breakage

Table 11.7 Consolidated Undrained Triaxial Tests - Cold Lake Clearwater Formation Oil Sands (Location No. 4)

Initial Conditions

Test Number	Bulk Density (Mg/m3)	Dry Density (Mg/m3)	% water (mass)	% bitumen (mass)	% sand (mass)	Void Ratio e	Sr (%)	Pore Pressure Parameter B **	Index of Disturbance (%)
CL4TOS2	1.89	1.55	10.7	7.3	82.0	0.71	82	1.00	12.9

** Note: At 0.2 MPa Effective Confining Stress after saturation at 2.5 MPa Back Pressure

Isotropic Consolidation

Test Number	Volume Change (%) from σ = 0.2 to 3.3 MPa	Bulk Density (Mg/m3) σ = 3.3 MPa	Dry Density (Mg/m3) at σ = 3.3 MPa	K (MPa) Cycled from 5 to 9 MPa	Void Ratio e	Index of Disturbance (%)
CL4TOS2	-6.46	2.03	1.66	1187	0.60	1.90

Undrained Shear Test

Test Number	Effective Confining Stress (MPa)	Back Pressure (MPa)	B	Maximum Shear Strength (MPa)	Axial Strain at Max. Shear Strength (%)	Max. Stress Ratio at (% Strain)	Modulus of Elasticity (MPa)	A at Failure
CL4TOS2	7.0	5.0	0.69	7.39	0.74	3.65 (4.06)	1598	0.58

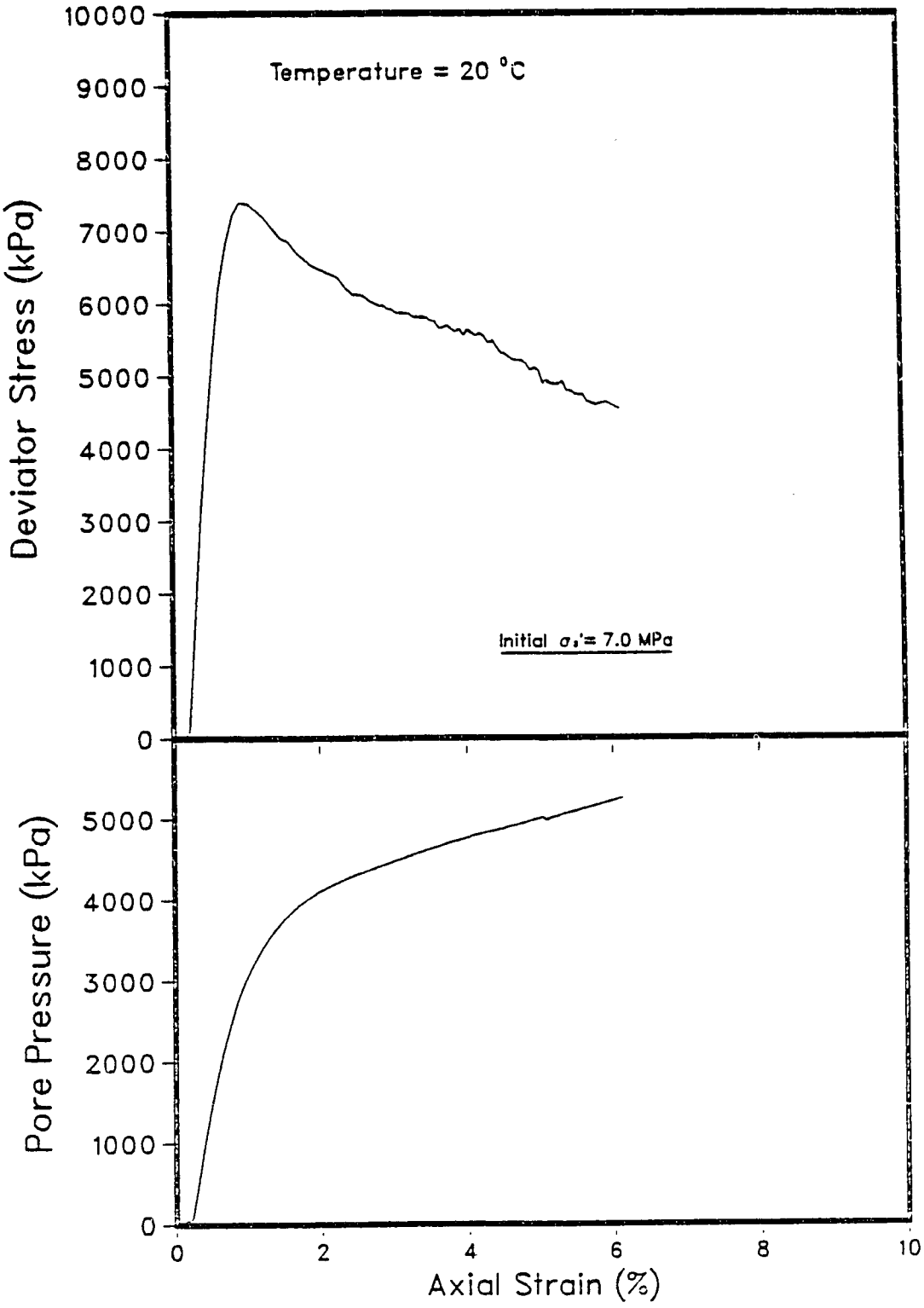

Figure 11.22 Passive Undrained Compression Test on Specimen CL4TOS2

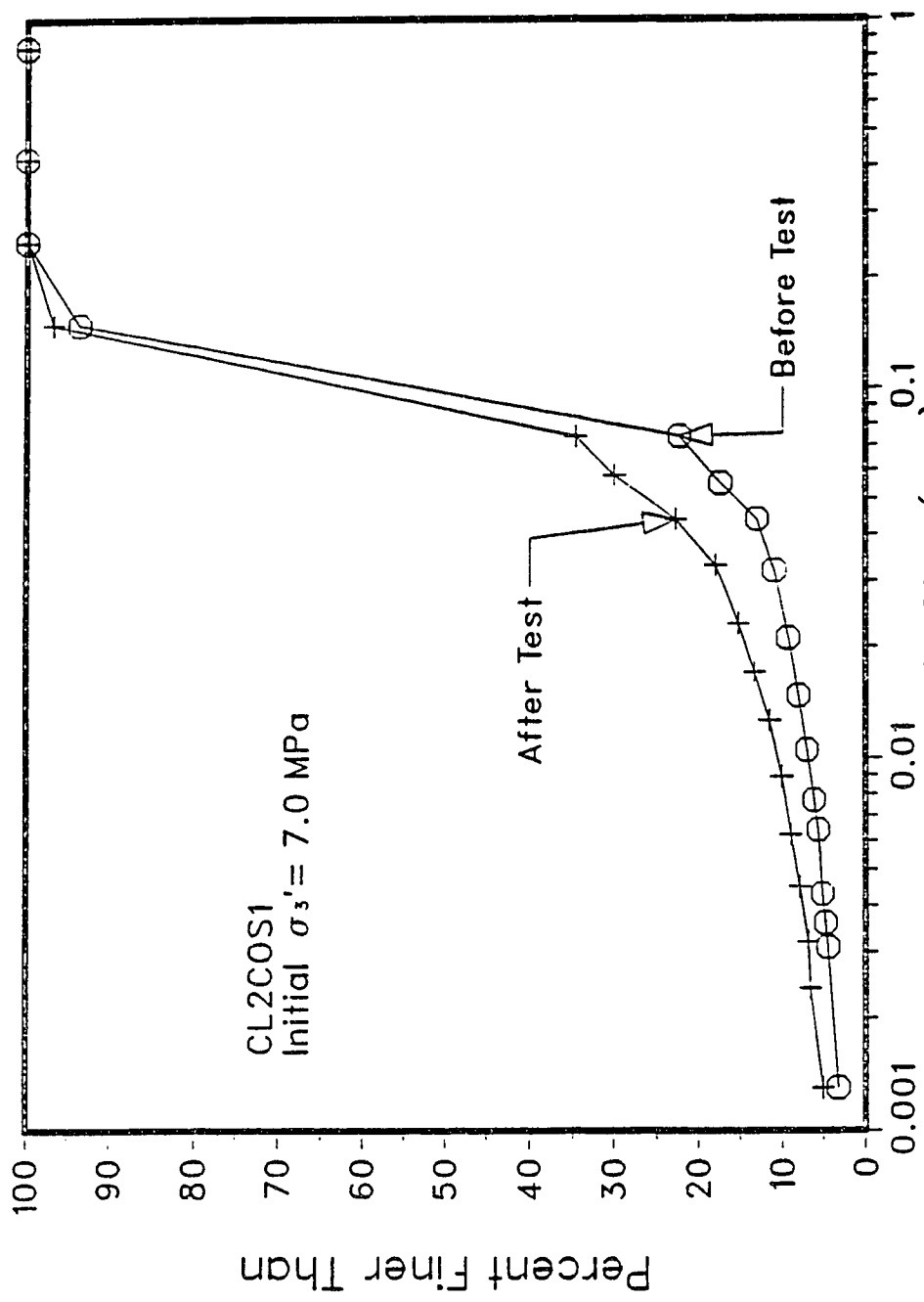

Figure 11.23 Grain Size Distribution Before and After Undrained Shear at 20 °C

is evident.

11.7 Summary and Conclusions

The shear strength behaviour of Clearwater Formation oil sands obtained from four separate locations in The Cold Lake Deposit was studied. The oil sands specimens were from core samples taken at depths ranging from 440 to 490 m using conventional core sampling procedures. The influence of temperature, pressure and stress path on the strength and deformation properties of this oil sands was examined. The major conclusions made during this phase of the experimental research may be summarized as follows:

1. The shear strength properties of Cold Lake Clearwater Formation oil sands are significantly different from those of Athabasca McMurray Formation oil sands, reflecting the difference in sand grain mineralogy, geological environment of deposition and geological history. Athabasca McMurray Formation oil sands consist of a uniformly graded, predominantly quartz sand, whereas Cold Lake Clearwater Formation oil sands contain additional minerals which are much weaker.

2. Clearwater Formation oil sands display significant grain crushing during drained shear at high effective

confining stresses at 20°C. Grain crushing begins at the sand grain contacts and eventually leads to crushing of entire grains. The weaker sand grains, such as feldspar, are very susceptible to crushing during shear.

3. The amount of grain crushing increases at high effective confining stresses as evidenced by a reduced tendency to dilate, greater strains to failure and stronger strain hardening behaviour. Grain crushing results in a significant reduction in the overall effective angle of friction at failure. The decrease in the rate of dilatancy with increasing confining pressure results in significant curvature in the failure envelope.

4. During undrained shear at low initial effective confining stresses the oil sands specimens show an increase in pore pressure at the beginning of the test due to compression of the sand matrix during the onset of the stress increase. The volume reduction of the sand matrix results in the pore fluids taking more of the load due to their inability to drain. As the specimen reaches its peak strength, the pore fluid pressure decreases as the sand matrix tendency

to dilate and the shear strain is suppressed.

5. During undrained shear at high initial effective confining stresses this oil sands reaches peak deviator stress at small axial strains and decreases with continued strain. The pore fluid pressure rises even after the deviator stress has reached its maximum value. The behaviour results from the high amount of grain crushing which the sand matrix undergoes during drained shear and as a result of large pore pressures developed during undrained shear. As shearing progresses, the effective stresses decrease as more available friction is mobilized. As a result, the overall shearing resistance reaches its maximum value prior to full frictional resistance being mobilized. At large strains when all the friction is mobilized, the overall shearing stress is smaller. This type of undrained behaviour is analagous to the behaviour of a normally consolidated sensitive clay.

6. The shear strength of Clearwater Formation oil sands at elevated temperatures depends not only on the strength of the mineral grains at higher temperatures, but also on the amount of grain

crushing and particle rearrangement which occurs during heating. This oil sands contains minerals which are highly susceptible to physical breakdown during heating at elevated temperatures and pressures.

7. The mechanical properties of Cold Lake Clearwater Formation oil sands are dependent on the temperature, pressure and stress path followed during the test. Analytical procedures used to model the stresses and deformations of formation strata must, therefore, utilize geomechanical properties representative of the actual formation response.

Cold Lake Clearwater Formation oil sands form a distinct class of materials dissimilar from Athabasca McMurray Formation oil sands. McMurray Formation oil sands display dilatative volume change behaviour over the in situ effective confining stress range encountered in the Athabasca deposit. This behaviour illustrates the strength of the quartz sand grains. In contrast, Clearwater Formation oil sands are strongly strain hardening and continue to contract with increasing shear strain at the in situ confining stresses found in the Cold Lake deposit. Cold Lake Clearwater Formation oil sands contain a predominance of

minerals which are much weaker than quartz. The stresses and deformations that occur in the respective formations caused by changes in stress, pore fluid pressure and temperature during in situ thermal recovery would, therefore, be vastly different. The dense interpenetrative fabric of McMurray oil sands develop substantially higher stresses with smaller deformations.

The highly compressible, strain hardening behaviour of Cold Lake Clearwater Formation oil sands is similar to that of broken ice in its granular state. Numerical techniques developed for predicting the behaviour of broken ice can aid in the analysis of the behaviour of oil sands. Such techniques are outlined in Wong et al (1988). It is noted, however, the processes contributing to the behaviour are quite different. Gale et al (1987) conclude that broken ice specimens are ductile due to the grain's ability to creep, while for sand ductility was promoted by grain crushing.

12. SHEAR STRENGTH OF COLD LAKE RELATED STRATA

12.1 Materials Studied

The strata studied in this phase of the research program were obtained from the offshore-transitional sedimentary facies of the Upper Clearwater Formation in the northern part of the Cold Lake Deposit. This facies consists of interbedded sands, silts and shales. Two geotechnical facies from strata adjacent to Location No. 1 and Location No. 4 oil sands were tested.

In the 15 m of core obtained for geomechanical testing from Cold Lake Location No. 1, the thickness of the shale beds varied from a few mm to 1 m. The associated sand was comprised of lean to medium rich oil sands to oil free sand. The specimens for triaxial shear strength determinations were taken from a 1 m thick shale bed at a depth of approximately 450 m. The geotechnical facies consisted of dark grey, highly fissile, hard shale. The initial index properties are summarized in Table 12.1. The bulk density and initial water contents were 2.15 Mg/m^3 and 16%, respectively. The shale had a liquid limit of 70% and a plastic limit of 28%. The initial void ratio of these specimens was about 0.4 with an initial saturation of 95%.

The stress-strain characteristics of the shale were investigated following three different stress paths: passive drained compression at 20°C, passive undrained compression at 20°C and passive undrained compression at 225°C. Each

Table 12.1 Cold Lake Clearwater Formation Shale - Initial Conditions

Test Number	Bulk Density (Mg/m3)	Dry Density (Mg/m3)	Water Content (%)	Liquid Limit (%)	Plastic Limit (%)	Void Ratio	Sr (%)	B
CL1TCS1	2.148	1.847	16.33			0.46	95	----
CL1TCS2	2.142	1.842	16.33	72.4	29.8	0.47	95	----
CL1TCS3	2.159	1.861	15.99	68.2	27.0	0.45	96	0.96

triaxial test was carried out under an effective confining stress of approximately 7.0 MPa.

The 18 m core length of Clearwater Formation strata from Cold Lake Location No. 4 contained a 0.9 m thick carbonate rock bed at a depth of 466 m. This geotechnical facies (often referred to in petroleum engineering as a "no permeability barrier" or "tight streak") consisted of a grey, very fine grained, strong, massive, ferron calcite cemented sand. Cemented sandstone streaks are an important facies in in situ thermal bitumen recovery strategies as they are commonly considered to inhibit vertical migration of steam and impede vertical fracture growth out of the oil sands pay zone to adjacent strata.

A multi-stage drained passive compression test was carried out on a specimen from the calcite cemented sand facies in order to examine stress-strain and strength behaviour at different effective confining stress levels from one test. The specimen was subjected to passive compression at both 20°C and 225°C.

12.2 Clearwater Shale

Passive Drained Compression at 20°C

The stress-strain and volume change relationships for Clearwater Formation shale tested following the passive drained compression stress path at 20°C are shown in Figure 12.1. Prior to shear, the specimen (CL1TCS1) was placed in the triaxial cell under a small effective confining stress of 0.2 MPa (Table 12.2). The confining stress and back pressure were then increased in equal increments of 0.2 MPa, thereby maintaining the same effective confining stress on the specimen. When the back pressure reached 2.5 MPa (above the pore fluid saturation pressure) the specimen was allowed to saturate for several hours. The confining stress was then increased to give an effective confining stress of 7.0 MPa and the volume change of the specimen was monitored. This specimen experienced a volume reduction of 5.5% during isotropic consolidation resulting in a void ratio of 0.38 (Table 12.2). A B test was then performed prior to the drained shear test. The B value at 7.0 MPa effective confining stress was 0.84.

The results of the drained triaxial shear test are given in Table 12.3. The shale specimen shows significant strain softening behaviour in the post-peak region. The

Table 12.2 Cold Lake Clearwater Shale - After Isotropic Consolidation and Drained Heating

Test Number	Seating Pressure (MPa)	Isotropic Consolidation Stress (MPa)	Volume Change (%)	e after Consolidation	Test Temperature (°C)	Volume Change During Heating (%)	e after Heating
CL1TCS1	0.2	7.0	-5.47	0.38	20.0		
CL1TCS2	0.2	7.0	-5.08	0.39	20.0		
CL1TCS3	0.5	7.0	-4.52	0.39	225.0	-4.37	0.32

Table 12.3 Consolidated Triaxial Tests - Cold Lake Clearwater Shale

Drained Shear Test

Test Number	Effective Confining Stress (MPa)	Back Pressure (MPa)	B	Deviator Stress at failure (MPa)	Axial Strain at failure (%)	Volumetric Strain at failure (%)	Modulus of Elasticity (MPa)	Poisson's Ratio
CL1TCS1	7.0	2.5	0.84	14.25	1.32	-0.81	1456	0.08

Undrained Shear Tests

Test Number	Effective Confining Stress (MPa)	Back Pressure (MPa)	B	Maximum Shear Strength (MPa)	Axial Strain at Max. Shear Strength (%)	Max. Stress Ratio at (% Strain)	Modulus of Elasticity (MPa)	A at Failure
CL1TCS2	6.7	5.2	0.87	9.39	0.80	3.76 (0.80)	1578	0.36
CL1TCS3	7.3	7.3	0.50	13.94	1.25	4.44 (1.12)	3137	0.47

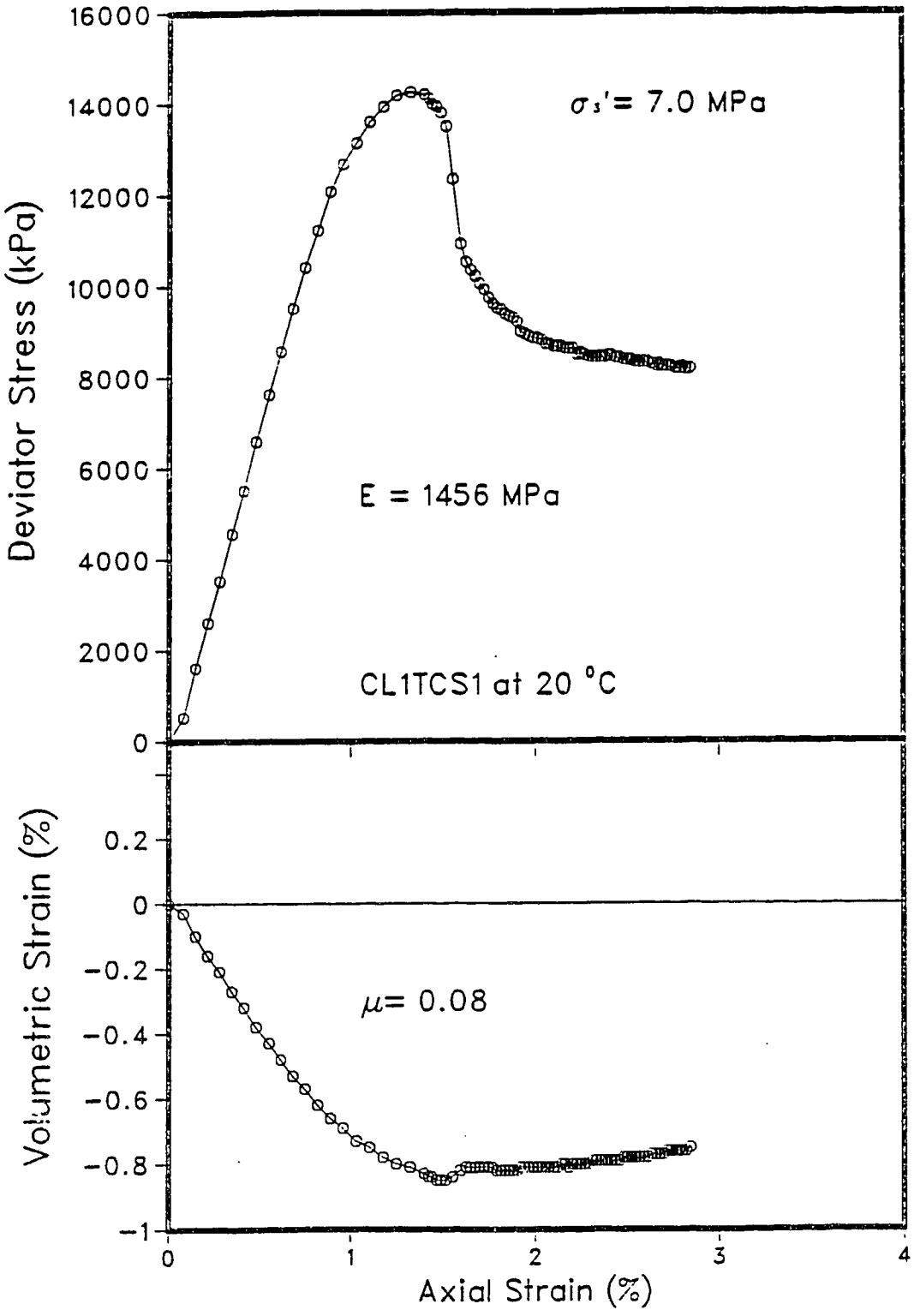

Figure 12.1 Passive Drained Compression Test on Cold Lake Clearwater Shale

strength reduction from peak to residual was approximately 40%. The soil matrix displayed contractive behaviour during the shear test and levelled out at a net volume reduction of about 0.8%.

Passive Undrained Compression at 20°C

The stress-strain and pore pressure response for Clearwater shale tested following the passive undrained compression stress path at 20°C is shown in Figure 12.2. Specimen CL1TCS2 was saturated in the triaxial cell under an effective confining stress of 0.2 MPa at 5.0 MPa back pressure. The confining stress was increased to give an effective confining stress of 7.0 MPa. The specimen underwent a volume decrease of 5.1% during isotropic consolidation, resulting in a void ratio of 0.39 (Table 12.2). The B value prior to the undrained shear stress was 0.87.

The results of the undrained shear test are summarized in Table 12.3. The specimen displays a strain softening behaviour in the post-peak region. The strength reduction from peak to residual was approximately 35%. The pore fluid pressure increased rapidly at the beginning of the test to a maximum of 3.34 MPa at 0.8% axial strain. The pore fluid pressure then decreased with continued straining and levelled off at about 6% strain with a net pore pressure

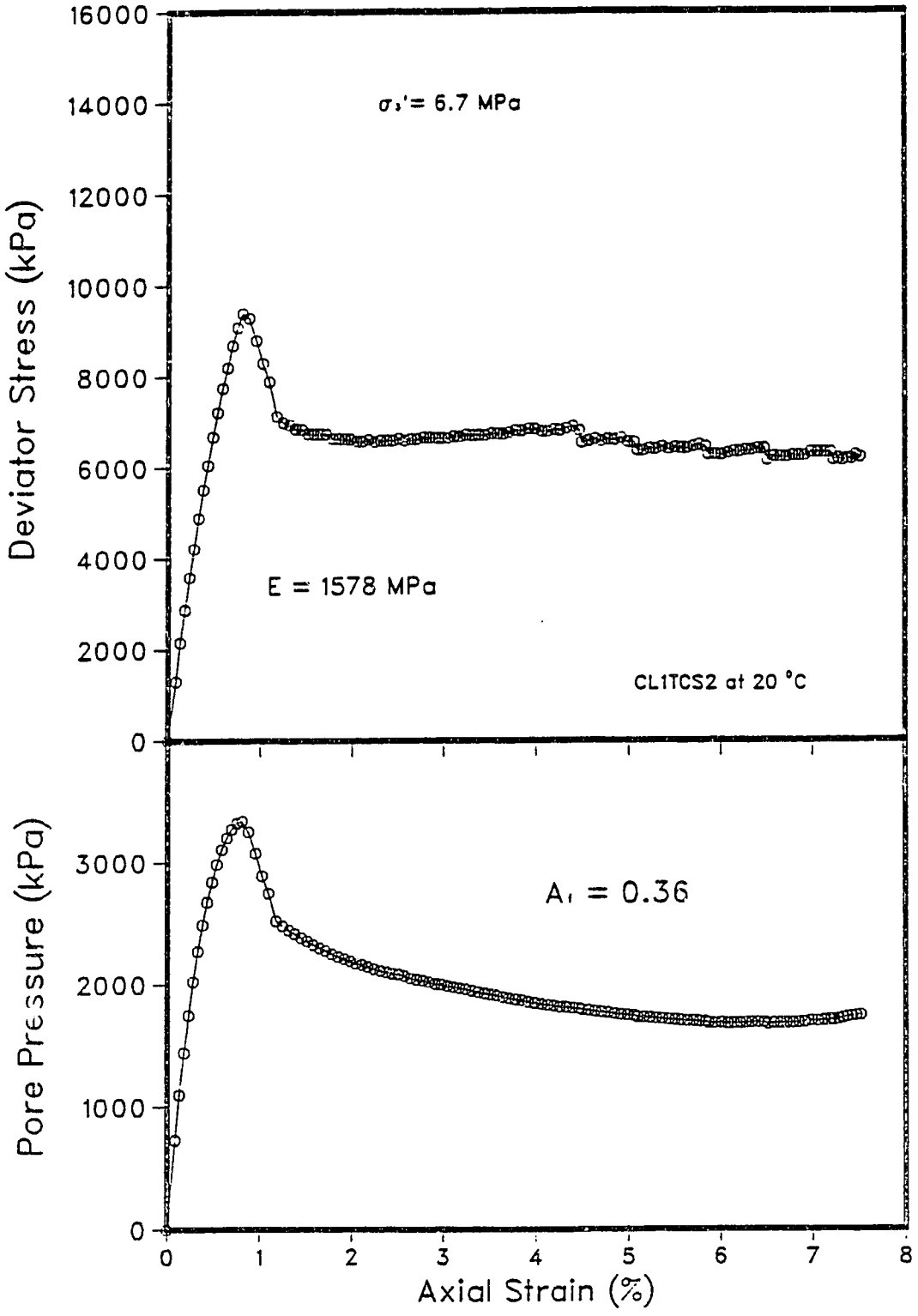

Figure 12.2 Passive Undrained Compression Test on Cold Lake Clearwater Shale

increase of 1.7 MPa.

Passive Undrained Compression at 225°C

Specimen CL1TCS3 underwent a volume decrease of 4.52% during isotropic consolidation under an effective confining stress of 7.0 MPa at 20°C. The void ratio after consolidation was 0.39 (Table 12.2). During drained heating to 225°C the specimen experienced a further volume reduction of 4.37%, resulting in a void ratio prior to undrained shear at 225°C of 0.32. The pore pressure parameter B prior to shear was 0.50. The results of the undrained shear test carried out under an initial effective confining stress of 7.3 MPa are shown in Figure 12.3 and summarized in Table 12.3.

The specimen shows strain softening behaviour in the post-peak region. The strength decrease from peak to residual was about 32%. As in the test performed at 20°C, the pore fluid pressure increased rapidly at the onset of shear straining and reached a maximum of 3.4 MPa at 0.9% axial strain. The pore fluid pressure then decreased with continued straining and levelled off at about 1.5% strain with a net pore pressure increase of 2.2 MPa.

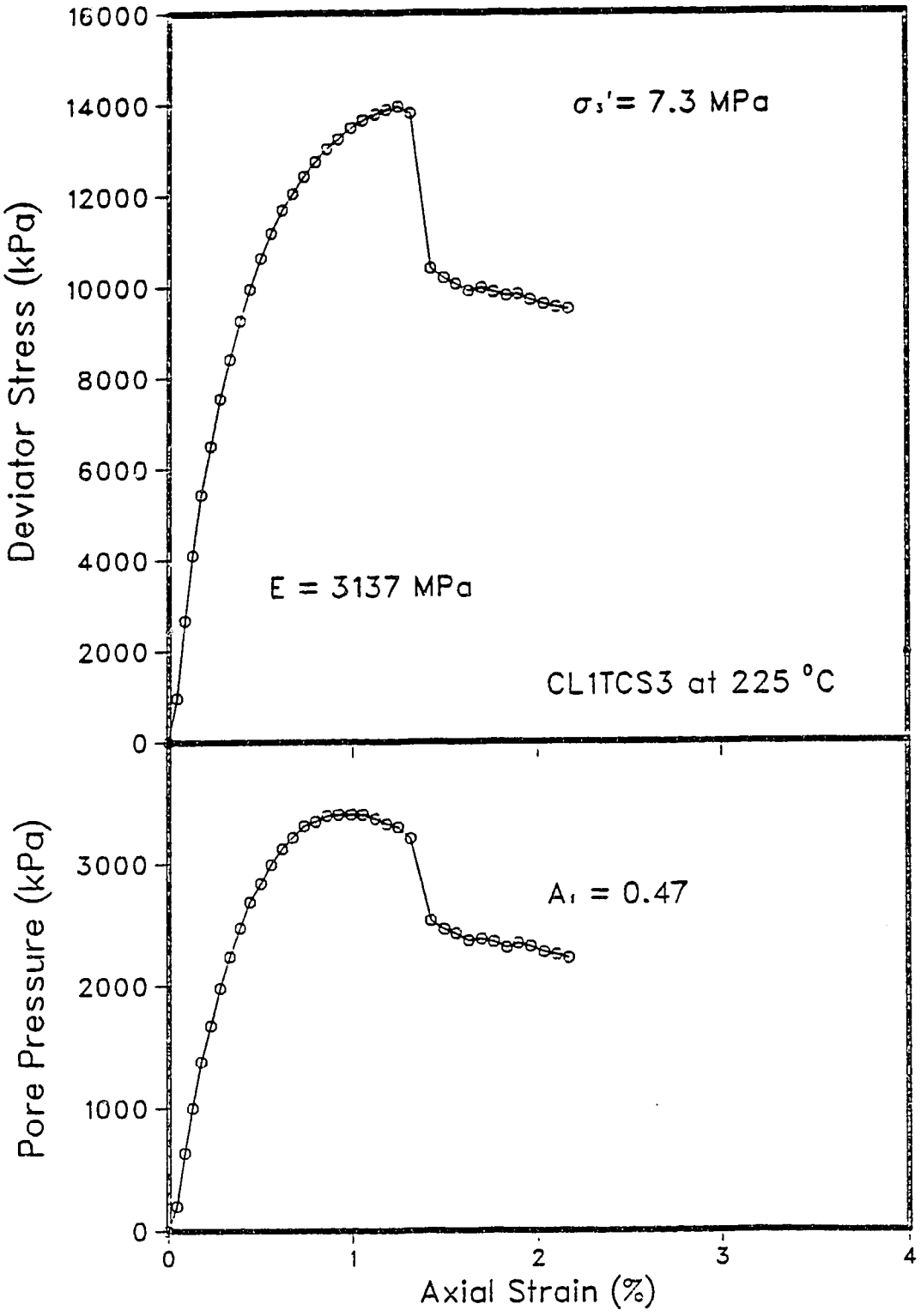

Figure 12.3 Passive Undrained Compression Test on Cold Lake Clearwater Shale at 225 °C

Discussion

The shear strength test results are plotted in terms of a p'-q diagram in Figure 12.4. The tests conducted at 20°C had approximately the same void ratio at failure. A linear failure line drawn through these test values gives a q-axis intercept or "a" value of 1.5 MPa. The angle of the k_f-line, α, with respect to the horizontal is 21.7°. The failure line is defined by the Mohr-Coulomb parameters c' = 1.6 MPa and ϕ' = 23.4°. The results of the undrained test performed at 225°C plot above this k_f-line. The void ratio of this specimen, as a result of heat consolidation, was 0.32 as compared to 0.38 for the 20°C specimens.

Temperature has major effect on the geomechanical properties of Clearwater Formation shale. Heat consolidation causes a reduction in void ratio and as a result the strength and stiffness of the material increase. For the Cold Lake Clearwater Formation shale tested here, a 16% decrease in void ratio during drained heating results in a 50% increase in the undrained shear strength and a 100% increase in the undrained stress-strain modulus.

Cold Lake Clearwater shale displays path dependency when comparing the confined drained and confined undrained stress paths. The strength variation with axial strain for both stress paths is illustrated in Figure 12.4. The strain at which mobilization of shear strength occurs is

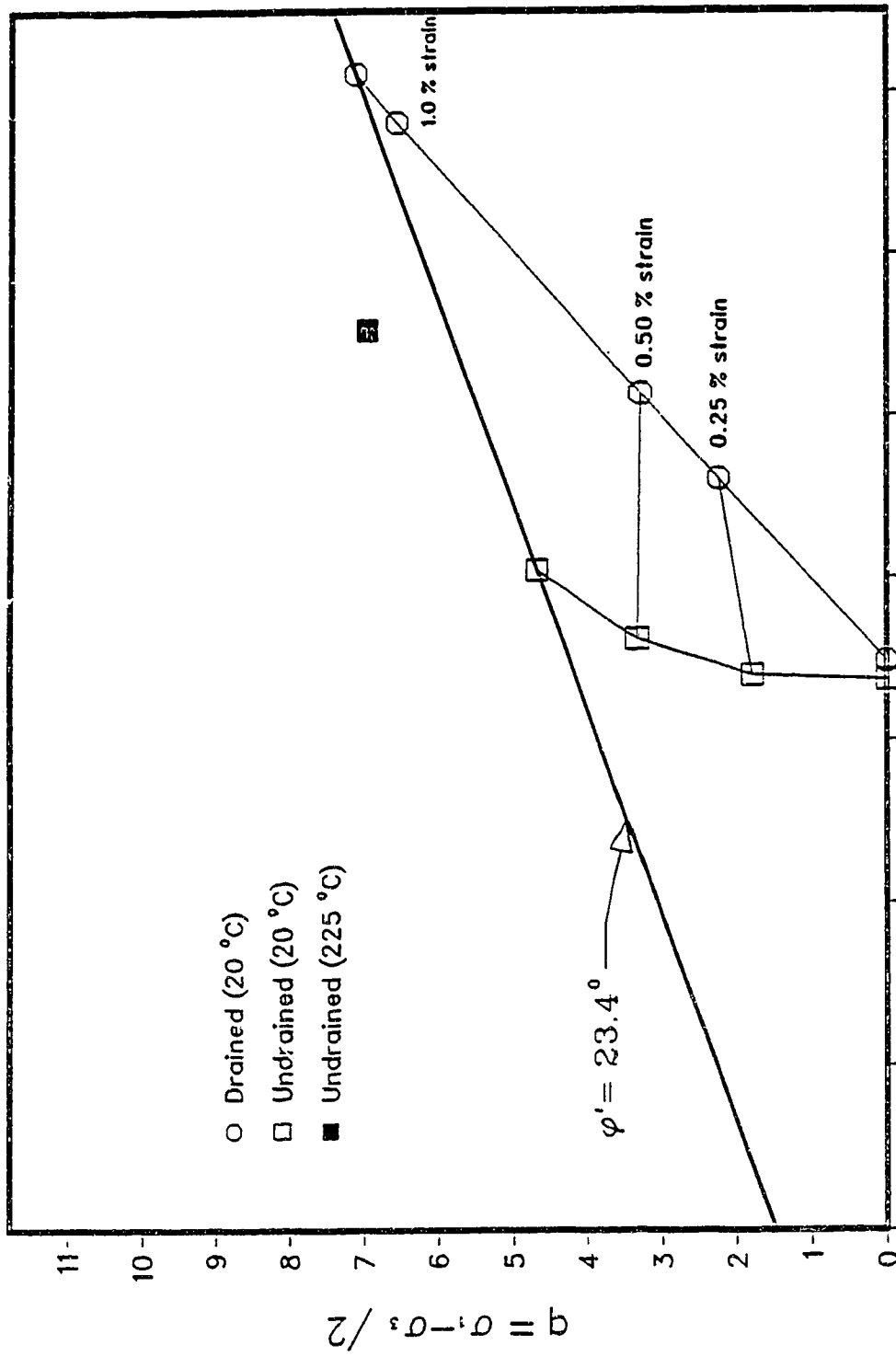

Figure 12.4 Passive Compression Tests on Cold Lake Clearwater Shale

significantly different. The undrained modulus is larger even though the initial effective confining stress is slightly lower. The axial strain to failure for the undrained specimen is 40% smaller than the strain to failure for the drained specimen.

12.3 Carbonate Cemented Sand

A specimen from the cemented sand streak from Cold Lake cation No. 4 was placed in the high temperature triaxial cell under a confining stress of 1.0 MPa. A deviator stress was applied to the specimen and the stress-strain characteristics were measured over the axial strain range of 0 to 0.2%, as shown in Figure 12.5. The modulus of deformation was 6415 MPa measured over the axial strain range of 0.16 and 0.20%. The test specimen was then unloaded to isotropic conditions.

The carbonate rock specimen was heated to 225°C at a rate of 25° per hour. When the specimen reached 225°C it was allowed to stabilize for several hours. The specimen was considered to be stable when the temperature of the confining fluid remained constant at 225°C for 3 to 4 hours. The deviator stress was increased maintaining the confining stress of 1.0 MPa. As the specimen approached its peak shear stress of 68.6 MPa at 0.37% axial strain, indicated by a curvature in the stress-strain curve (Figure 12.6), the cell pressure was increased to 4.0 MPa and the axial straining continued. When the deviator stress reached 112 MPa

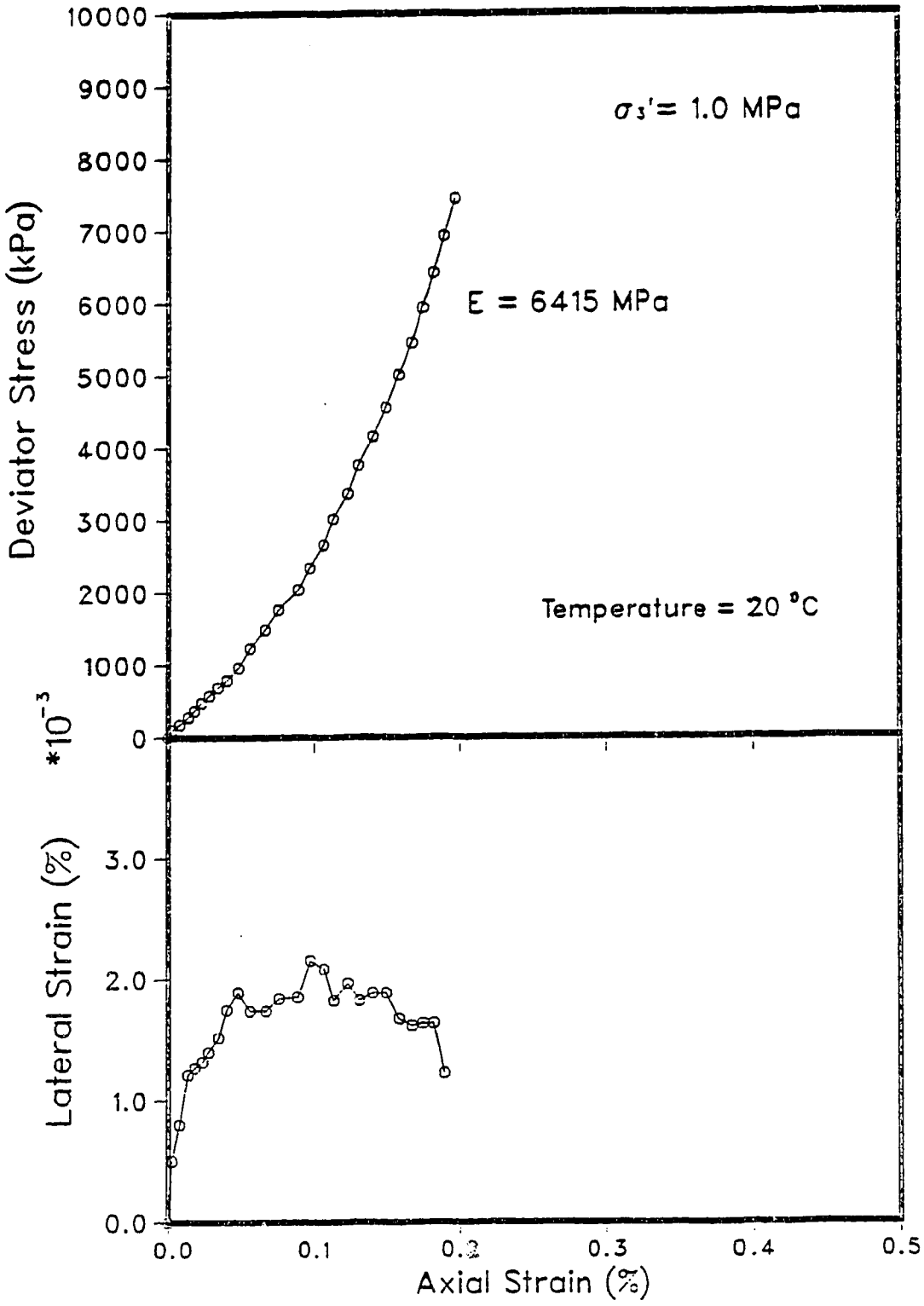

Figure 12.5 Passive Drained Compression Test on Cold Lake Cemented Sand

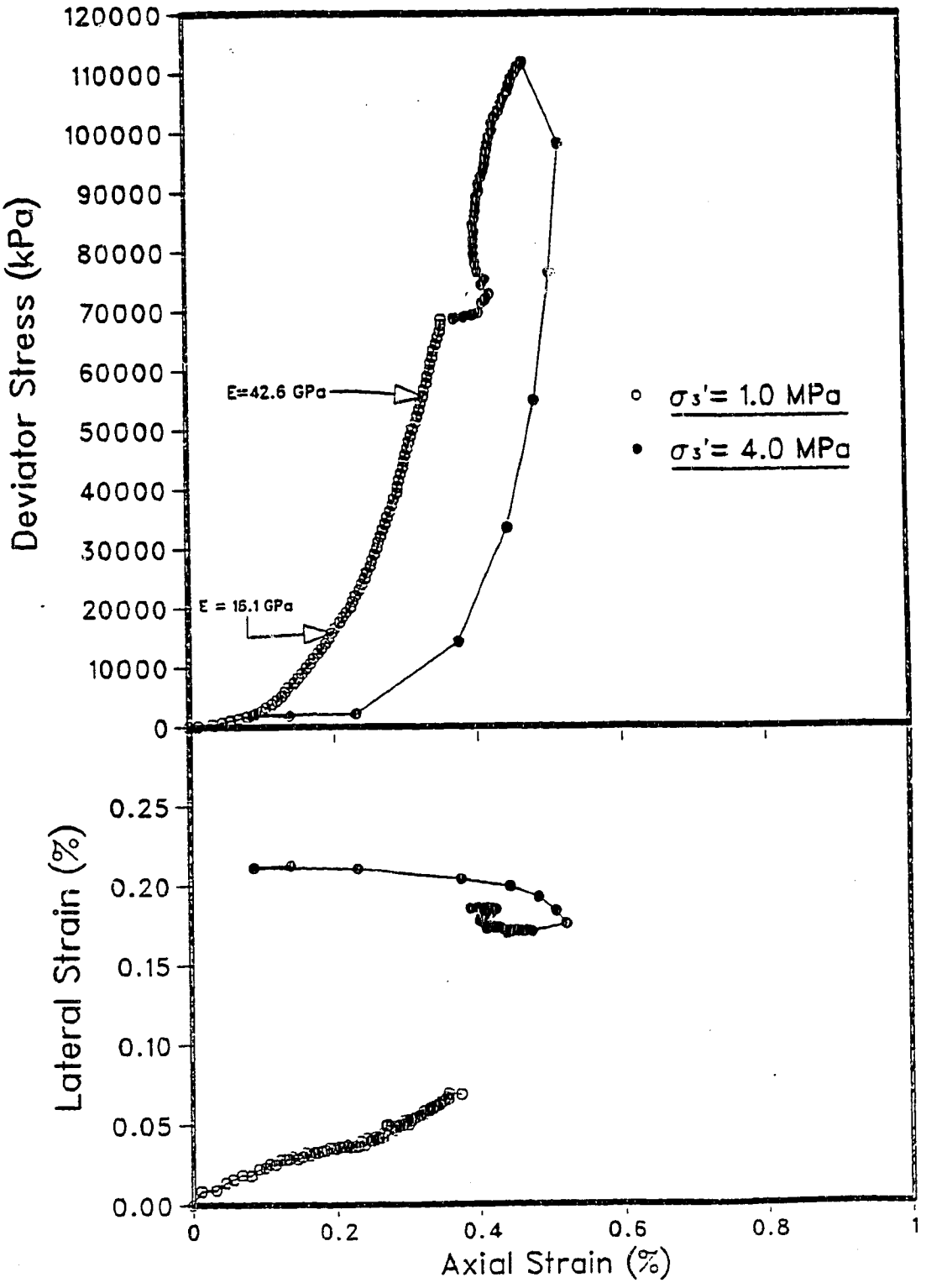

Figure 12.6 Passive Drained Compression Test on Cold Lake Cemented Sand at 225 °C

(approximately 250 kN), the capacity of the internal load cell, axial loading was stopped. The specimen was unloaded to isotropic conditions as shown in Figure 12.6.

Visual inspection of the test specimen after the high temperature shear test did not reveal any evidence of thermal cracking. It is noted, however, that material from the same geotechnical facies subjected to the same rate of temperature increase during a drained heating experiment in the oedometer (Chapter 9, Section 4) did experience a small degree of thermal cracking (0.1% volume increase after cooling to 20°C). The modulus value measured under 1.0 MPa effective confining stress over the axial strain range of 0.16 to 0.20% at 225°C was 16.1 GPa as compared to 6.4 GPa measured over the same range of strain at 20°C. The majority of this difference is undoubtedly due to seating of the loading platens on initial loading. The effect of temperature on the strength and stiffness of intact cemented sandstone streak material could not be evaluated based on these tests.

12.4 Summary and Conclusions

The shear strength behaviour of two geotechnical facies associated with oil sands strata obtained from the Cold Lake Deposit were studied. The strata examined included Clearwater Formation shale and a ferron calcite cemented sand. The influence of temperature, pressure and stress path on the strength and deformation properties of these

materials were investigated. The major conclusions made during this phase of the experimental research may be summarized as follows:

1. The geomechanical properties of Clearwater shale from the Cold Lake Deposit are affected by an increase in temperature. Heat consolidation causes a reduction in void ratio and, as a result, the shear strength and stiffness of the material increase.

2. Cold Lake shale displays path dependency when comparing the passive drained and passive undrained stress paths at 20°C. The undrained specimen is stiffer and requires a smaller axial strain to reach failure.

3. More testing is needed to determine, in quantitative terms, the effect of temperature on the strength and deformation behaviour of carbonate cemented sand streaks which are commonly found adjacent to Cold Lake reservoir oil sands.

13. CONCLUSIONS AND RECOMMENDATIONS

13.1 General

The prediction of stresses and deformations that occur in formation strata during in situ thermal bitumen recovery requires complex computational methods which simulate fully-coupled thermal-mechanical-fluid flow behaviour. The development of constitutive models - that is, mathematical descriptions of material behaviour representing the coupling effects between each of the three pairs of coupling processes (thermal-mechanical, hydro-thermal and hydro-mechanical) is contingent upon our ability to understand and evaluate the fundamental influences of stress, pore fluid pressure and temperature on geotechnical behaviour of oil sands and related strata. Quantitative evaluation of constitutive behaviour of oil sands sediments is difficult for several reasons:

1. Geotechnical behaviour of porous sediments is significantly influenced by geological agents. Mineralogy, fabric and structure of reservoir and confining strata are controlled by the depositional environment. Subsequent geological activity which cause changes in formation temperature, pressure and pore fluid composition may significantly alter fabric and structure (eg. interparticle contacts, bonding and forces). In situ clastic deposits therefore exist

under the influence of many geological factors which may vary from deposit to deposit and may vary through the vertical and lateral extent of a particular deposit.

2. Constitutive behaviour of deeply buried strata must be characterized on the basis of a small amount of sample taken from a limited number of coreholes. Due to the complex and variable nature of reservoir materials, geological and geotechnical facies analyses must be employed to provide interpretive and predictive capability beyond the borehole.

3. Oil sands are very sensitive to sample disturbance. During core sampling from boreholes in situ confining stresses and pore fluid pressures are reduced rapidly and gas evolution from the bitumen and water may occur. This formation of gas bubbles combined with the lack of cementation and, therefore, cohesive strength between sand grains results in expansion of the oil sands fabric. If the amount of sample disturbance caused by core expansion is significant, the interlocking contacts at grain boundaries are lost and the overall grain surface contact area reduced as grain movement and rotation occur. As a

result, during compression of highly disturbed oil sands specimens the ability of sand grains to slide and rotate during shear deformation is increased resulting in reduced shearing resistance and, in most cases, contractive rather than dilatant behaviour.

4. Constitutive behaviour depends on pressure, temperature, time, stress and temperature path, and history of stress. A reliable assessment of in situ behaviour necessitates testing specimens in the laboratory under conditions representative of those prevailing in the field. This requires the development of relatively complex laboratory equipment and the formation of specialized sample preparation and testing techniques.

5. The constitutive behaviour representing a particular interaction between heat flow, pore fluid pressure changes and mechanical deformation are complex due to the individual response of the soil or rock constituents: particulate, mineral structure and pore fluids (liquids and gases). In general, processes contributing to a physical, chemical or mechanical change to a material constituent result in non-linear and irreversible behaviour of the overall geological

material.

The influence of the above factors must be considered in laboratory testing in order that realistic and meaningful results may be obtained and used in the development of constitutive models for oil sands and adjacent or interbedded strata.

A geotechnical oil sands research laboratory was developed to carry out tests to determine the geotechnical behaviour of oil sands and associated strata under high temperature and pressure. The test facility consists of two triaxial cells, two oedometers and a hot water or steam injection system. The systems were designed to operate at confining pressures up to 30 MPa, back pressures up to 27 MPa and temperatures up to 325°C.

A laboratory testing program was carried out to investigate and identify the major factors governing the constitutive behaviour of oil sands and related strata associated with the heat consolidation process. The bulk of the experimental work on each set of materials is separated into three broad categories of constitutive behaviour:

1. Triaxial compression tests were carried out to measure the stress-strain behaviour and strength of strata over a range of temperatures from 20°C to 225°C and effective confining stresses to 7 MPa.

Several stress paths indicative of actual field conditions were investigated.

2. Compression behaviour in response to both one-dimensional and triaxial loading conditions was measured over the temperature range of 20°C to 300°C.

3. Thermal volume change behaviour under various loading conditions and stress histories was measured over the temperature range of 20°C to 300°C.

Physical properties such as density, porosity, water and bitumen saturation, grain size distribution, specific gravity and mineral composition were measured for each test to assess the quality and homogeneity of the test specimen and to aid in the interpretation of the experimental results. The fabric and structure of oil sands specimens were examined using scanning electron microscopy. Mineralogy of sand specimens was studied through energy dispersive X-ray analyses. Mineralogical data for shale samples were obtained by X-ray diffraction analyses.

The geotechnical behaviour of McMurray oil sands, Clearwater oil sands, as well as that of overlying, underlying and interbedded strata occurring with these

formations, was studied. Experimental assessment of constitutive behaviour of oil sands and related strata required recognition of the processes contributing to in situ composition, shape and orientation of mineral particles and mineral structure. The materials comprising both the Athabasca and Cold Lake Deposits are geologically complex and extremely variable in place. Geological complexity is characterized primarily by rapid changes in grain size, material structure and mineralogy and reflects the non-uniform manner in which the sediments were deposited. Facies models applied to depositional and epigenetic processes were found to be useful to organize and analyze the characterization of these geotechnically complex materials. The procedure involves developing geotechnical facies (zones of strata which display common constitutive response) by superimposing epigenetic facies on the various sedimentary facies.

13.2 Athabasca Materials

Materials Studied

The formation strata studied in this phase of the research program were collected from three separate well locations in the Athabasca Deposit. The depths of the oil sands reservoirs at these locations ranged from 150 to 300 m. Geological facies interpretation was based on geophysical data, core examination and local or regional experience. The geotechnical facies examined included:

AOSTRA UNDERGROUND TEST FACILITY SITE

Reservoir Cap Rock

1. **Clearwater k_{cc} Shale.** A medium plastic, silty shale of very stiff to hard consistency. Its colour varied from dark grey to black.
2. **Clearwater k_{cb} Shale.** A medium plastic, silty shale of very stiff to hard consistency. Its colour ranged from dark grey to black.
3. **Clearwater k_{cb} Shale.** A high plastic shale of very stiff consistency. Its colour varied from dark grey to black with frequent brownish smectite-rich bands. The bands are essentially horizontal with thicknesses ranging from 1 mm to several mm.

Reservoir

1. **McMurray Oil Sands.** A fine to medium grained, lean oil sands. Brownish grey to black in colour. Pockets and lenses of silty shale were encountered randomly throughout the specimens. Shale interbedding ranged from 1 mm to several mm thick.

Underlying Strata

1. **Waterways Limestone.** A microcrystalline limestone. The specimen was uniform and massive. Its colour varied from light to medium grey.

SOUTHERN ATHABASCA

Reservoir

1. **McMurray Oil Sands.** A medium grained, uniformly graded, rich oil sands. Dark grey to black in colour. Bitumen content of about 15% by weight. A fines content of approximately 5% by weight. The depth of the core sample was about 295 m.

NORTHERN ATHABASCA

Reservoir

1. **Clearwater Oil Sands (Wabiskaw Member).** A medium grained, medium rich oil sands. Dark grey to black in colour. Bitumen content of about 12% by weight and a fines content ranging from 5 to 21%. The depth of the core sample was about 220 m.

Athabasca oil sands materials considered in this study were formed under several different depositional environments. Clearwater Formation shale was deposited in a regionally extensive marine environment and contains significant variations in clay mineralogy as well as localized siltstone layers. South Athabasca McMurray Formation oil sands consist of a uniformly graded, low fines, quartz sand which is indicative of a moderately strong and prolonged depositing current. These sands are similar in mineralogy and fabric to estuarine channel, mid-channel and point bar sands encountered over much of the area occupied by the Underground Test Facility, surface mining projects and portions of the Saline Creek valley. These sands form the main reservoir unit in the Athabasca Deposit and are the most commonly studied geotechnical facies. Clearwater Formation (Wabiskaw Member) sands obtained from North Athabasca were deposited in a shallow-water marine environment. These sands, although similar in appearance to the bitumen rich, low fines estuarine sands of the McMurray Formation, are less uniformly graded with fines contents up to 21% by weight and slightly low bitumen contents. This glauconitic sand is considered as a separate geotechnical facies in this study. Shaley oil sands obtained from the Underground Test Facility are indicative of estuarine channel margin sedimentation. Although these sands contain from 36% to 72% shale in the form of discontinuous seams and clasts, on a macroscopic

scale they are considered in this study to be of sufficient homogeneity to be classed as one geotechnical facies.

Thermal Volume Change Behaviour

Numerical methods used to calculate thermally induced ground deformations and stress changes during in situ production require as input the coefficient of thermal expansion. The coefficient of thermal expansion is maximum during undrained heating where volume change of the mineral solids and pore liquids occurs. The coefficient of thermal expansion is least during fully drained heating when the pore liquids drain as they expand. Volume change is due to expansion of the mineral grains and expansion or contraction of the soil structure.

Structural changes during drained heating have an important role in the thermal volume change behaviour of shale and interbedded oil sands. Structural changes are dependent primarily on the frictional resistance and cohesion of the individual interparticle contacts and the magnitude of thermally induced interparticle forces. These components are, in turn, dependent on the rate of heating, effective confining stresses and the history of stress experienced by the material. In other words, structural changes are stress and temperature path dependent.

During undrained heating against the confining stress, thermal strains, $\alpha\Delta T$, and compressive stresses required to suppress thermal strains, $\alpha E\Delta T$, are maximum. During in situ production, as flow takes place partial drainage occurs and

eventually the fully drained condition may be attained. During the transition from undrained to drained conditions, the influence of pore liquids on the coefficient of thermal volume change decreases and the effects of structural changes increase. The coefficient also develops a stress and temperature path dependency.

Thermal stresses and strains during undrained heating of interbedded oil sands and shale always increase in situ due to thermal expansion of the mineral grains. The impact mineral grain expansion has on the in situ stress and strain field, however, is overshadowed by the response of the pore fluids during undrained heating. When the pore fluids can expand the thermal stresses and strains are much larger because the thermal expansion coefficient of the pore fluids is large compared to that of the mineral solids. If the pore fluids cannot expand the pore fluid pressure increases and will result in decreasing the vertical and horizontal effective stresses. This effect is also comparatively large since the pore fluids expand more rapidly than the solids.

Thermal stresses and strains during drained heating of rich Athabasca oil sands always increase in situ because the coefficient of thermal expansion is positive (Agar, 1984; Kosar, 1983). Drained heating of interbedded oil sands and shale may cause an increase or decrease in stresses and strains depending on the in situ effective stress field and the rate of heating due to the time and pressure dependent thermal consolidation characteristics of the shale.

Compressibility Behaviour

The isotropic compressibility of McMurray Formation and Clearwater Formation oil sands obtained from depths of 300 m and 220 m, respectively, were examined. These core samples were obtained using conventional coring techniques and resulted in laboratory specimens which were highly disturbed (i.e., indices of disturbance, I_D, ranging from 11 to 21%). The cyclic compressibility values of these specimens were significantly lower than those reported by Agar (1984) for high quality (I_D less than 20%) oil sands obtained from the Saline Creek surface exposure. The cyclic compressibility values were, however, similar to the lower range of values reported by Plewes (1987) for Saline Creek oil sands. The initial indices of disturbance for these specimens ranged from 2.7 to 24% and generally higher compressibility values were associated with the more initially disturbed specimens.

The compressibility of oil sands depends on the physiochemical characteristics of the sand structure such as frictional resistance between sand grains, particle strength, void ratio and the size, shape and gradation of the mineral particles. These factors are, in turn, dependent on the sand grain mineralogy, geological environment of deposition and geological history. The similarity of compressibility results between the McMurray and Clearwater oil sands tested here and between the more disturbed Saline Creek oil sands suggests that excessive sample disturbance (I_D greater than 10%) from coring causes a sufficient amount

of microfabric disturbance which is not recoverable during the stress cycling process. While cyclic compressibility tests performed on high quality oil sands specimens provide a good indication of the in situ compressibility, excessive disturbance may reduce the compressibility of oil sands of similar mineralogy and may eradicate the influence of geological processes between different oil sands.

It should be noted that factors which govern the compressibility of oil sands also govern the strength and deformation properties during shear. As a consequence, although stress cycling prior to shear generally produces specimen densities comparable to in situ densities, the shear strength parameters may be significantly affected.

The presence of shale interbedding has a major influence on the compressibility of McMurray Formation oil sands. Discontinuous seams and clasts of more compressible shale interspersed in the oil sands matrix increases the overall compressibility of the oil sands. After drained heating, the compressibility of interbedded oil sands is reduced. The influence of shale interbedding on the compressibility of oil sands, therefore, decreases with the amount of consolidation experienced by the shale inclusions. In fact, if enough heat consolidation of the shale interbedding occurs, the compressibility of the oil sands becomes comparable to rich oil sands.

Generally volumetric strains associated with thermal consolidation of shale during first time heating are not

recoverable (Green, 1984; Williams, 1982; Campanella and Mitchell, 1968). Improvements in strength and deformation properties associated with volume reductions caused by heat consolidation are likely to be retained after the initial in situ steam injection cycle. The gain in strength parameters is, however, at the expense of losses in porosity-dependent permeability. Temperature increase also significantly increases the pore fluid pressure and if pore pressure dissipation cannot occur at the same rate as the temperature increase, the drop in effective stress can cause a considerable decrease in the shear strength.

The volumetric compressibility of high plastic, smectite-rich Clearwater k_{cb} shale due to thermal loading is time dependent. The time required to complete heat consolidation under temperatures and pressures associated with in situ recovery is relatively small (about 12 hours) when compared to the steam injection phase of the in situ recovery cycle which is generally a month or more.

Intact, relatively shale-free limestone is about one-half as compressible as high quality, rich oil sands and approximately one-tenth as compressible as Clearwater shale. Based on observations on the effects of shale interbedding on the compressibility of oil sands, the shaley limestone near the unconformable surface which separates McMurray and Devonian sediments are likely to be governed by the more compressible shale interbedding.

The compressibility of oil sands and shale is dependent on the temperature, pressure and stress path followed during the test. Analytical procedures used to model the stresses and deformations of formation strata must, therefore, utilize compressibility values representative of the actual formation response.

Shear Strength Behaviour

The strength-deformation characteristics of disturbed oil sands of the Wabiskaw Member within the Athabasca Deposit were found to be very similar to disturbed McMurray Formation oil sands from similar depths. Any influence of geological environment of deposition and geological history (such as mineralogy and grain structure) were obscured by excessive sample damage during coring, handling and storage.

The presence of shale interbedding results in a significant decrease in the maximum shear strength of McMurray Formation oil sands as compared to high quality, low fines oil sands. The presence of fines also reduces the initial stiffness of oil sands and the oil sands' tendency to dilate at higher confining stresses. Shale interbedded oil sands may experience a significant reduction from peak to residual strength if deformation is dominated by failure through the heavily overconsolidated shale strata. The weaker, more compressible shale strata interbedded in the oil sands has a significant effect on overall stress-strain characteristics of the formation regardless of stress path followed.

The stress-strain relationships of Athabasca McMurray Formation oil sands show a strong stress path dependency. The standard passive drained compression tests exhibit smaller moduli of deformation than did the unloading stress paths (J_1 constant compression, active compression and J_1 constant extension). The results from the passive drained and passive undrained compression tests, however, gave similar results. The strains to failure varied with the stress path indicating that, depending on the stress path followed, the strain at which mobilization of shear strength occurs can be significantly different from the conventional passive drained test. Since the oil sands in the field rarely follow a passive drained stress path during the bitumen recovery process, use of results obtained from the standard test in numerical simulations would likely over-predict the deformations occurring in the field.

The shear strength and deformation behaviour of rich, low fines oil sands is not significantly influenced at elevated temperatures. The shear strength and stress-strain modulus of high fines content McMurray Formation oil sands may increase at elevated temperatures if significant heat consolidation of the thin, discontinuous shale seams occurs. Temperature increases also significantly increase the pore fluid pressure and if pore pressure dissipation cannot occur at the same rate as the temperature increase the drop in effective stress can cause a decrease in the shear strength. Low permeability shale seams may be a significant barrier to

pore fluid drainage in highly interbedded oil sands. The available shear strength in this geotechnical facies during in situ production may therefore be critical for the design of well casings, tunnels or shafts passing through or lying in this strata.

The fully drained thermal volume change characteristics of Clearwater k_{cc} shale and Devonian intact limestone are significantly different. The volume of the limestone increases with temperature while the shale displays a volume decrease. These results indicate that the volume change of the soil structure dominates that of the mineral grains in shale while the opposite is true for the limestone where the volume change of the mineral grains dominates the total volume change. In other words, heat consolidation is significant for Clearwater k_{cc} shale. A review of the literature has indicated that the rate and the magnitude of thermal volume change during drained heating is the mechanism controlling the strength and deformation behaviour of these materials at elevated temperatures. The strength and stiffness of shale will increase if appreciable densification occurs during the heat induced compaction process. In contrast, these mechanical properties of intact crystalline rock will decrease if separation along grain boundaries occurs due either to rapid heating or to fluid volumetric expansion and/or fluid pressure increase which cannot be controlled.

The k_{cc} shale specimens tested in this study displayed a significant volume reduction, up to 11.6%, during drained heating. The magnitude of the volume decrease was higher in specimens whose initial void ratios were higher. The amount of heat induced consolidation, therefore, is dependent on the degree to which the shale has been pre-consolidated.

Despite the decrease in void ratio for specimens subjected to heat consolidation, data relating shear strength, effective stress at failure and water content at failure fell within a narrow band. These results suggest that although slow heating of k_{cc} shale so that drainage of water can occur will result in densifying the shale, the overall increase in strength and stiffness may not be significant. The medium to high plastic shales of the k_{ca} unit would be expected to behave in a manner similar to the shales of the k_{cc} unit. However, drained heating may cause much more dramatic changes in the strength and deformation behaviour of the relatively weak, low density, smectite-rich shales of the k_{cb} unit.

Athabasca Deposit formation strata has a complex geology. Figure 8.10 is a summary plot showing k_f envelopes at failure for four major geotechnical facies examined in this study. It is evident that wells placed in an oil sands reservoir either by drilling from the ground surface or by drilling from an underground tunnel will intersect a wide range of materials, each displaying significantly different mechanical behaviour. Figure 8.10 illustrates that the

strength and stress-strain behaviour of a particular geotechnical facies is controlled by the relative proportion of weaker shale strata. This would imply that the overall constitutive behaviour of the Devonian group strata is governed by the limey shale and shale interbedded limestone facies which exist near the unconformable surface at the base of the McMurray Formation.

The effect of temperature on the mechanical behaviour of these materials is mainly to increase the pore fluid pressure from expansion of the pore fluids. If these pore fluid pressures cannot dissipate, effective stresses and, therefore, the shear strength will decrease. The rate of pore fluid dissipation is controlled by such factors as the dynamic viscosity of the pore fluid, the absolute permeability (a coefficient dependent on the properties of the soil skeleton only) and the density of the pore fluid. Zones susceptible to large sustained pore fluid pressure increases are oil sands where bitumen is not mobile, high water content shale Clearwater facies, and the limey shale and interbedded shale and limestone facies of the Devonian group. Since horizontal stresses are higher than vertical stresses at depths less than 250 m in Athabasca Deposit (Chhina and Agar, 1985), thermally induced pore fluid pressures will cause shear deformations. Shear deformations will also arise from the large horizontal stress increases caused by mineral grain expansion in the stiff, low fines oil sands facies in the oil sands' production zones. The

most probable location of shearing problems would be the lower Clearwater shale, oil sands containing high percentages of shale seams and upper Devonian limestone with clay laminations.

The results of tests performed on oil sands related strata serve to illustrate the limitations associated with simple idealized representation of geotechnically complex formation strata in analysis of such problems as formation shearing, hydraulic fracture propagation, well casing performance and the stability of underground openings (uncased wells, tunnels and shafts). Over-simplification will invariably lead to incorrect results.

13.3 Cold Lake Materials

Materials Studied

The majority of bitumen production in the Northern Cold Lake Deposit is obtained from the Clearwater Formation. The Clearwater Formation contains three vertically stacked reservoir units designated as C-1, C-2 and C-3 sands. Cold Lake Deposit specimens used for laboratory testing were taken from four separate well locations northwest of Cold Lake. The core includes both the C-2 and C-3 reservoir oil sands as well as the intervening formation strata (typically interbedded sands, silts and shales). The Location No. 2 oil sands consisted of homogeneous, high bitumen content, fine grained sand. Oil sands core samples from Locations 1, 3 and 4 were also fine grained but contained frequent interbedded

shale seams ranging in thickness from 1 mm to a few cm. Two geotechnical facies from strata adjacent to Location No. 1 and Location No. 4 oil sands were also tested. Each of these facies had a thickness of about 1 m and consisted of a ferroan calcite cemented sand (tight streak) and a hard, highly fissile, highly plastic shale.

Thermal Volume Change Behaviour

Structural changes during drained heating have an important role in the thermal volume change behaviour of each material tested. Structural changes are dependent on the frictional resistance and/or cohesion of the individual interparticle contacts, the strength of the individual sand grains and the magnitude of thermally induced interparticle forces. Each of these components in turn depend on the effective confining stress and the history of stress experienced by the material.

Thermal strains, $\alpha\Delta T$, and compressive stress required to suppress thermal strain, $\alpha E\Delta T$, are large and relatively insensitive to stress history and effective stress for undrained conditions (provided pore fluids can expand against the confining stress). During in situ production as flow takes place partial drainage occurs and eventually the fully drained condition may be attained. Under these conditions as the influence of pore liquids on the coefficient of thermal expansion decreases the effects of structural changes increase. The coefficient changes as the effective stress and stress history (or stress path)

changes.

Thermal stresses and strains during undrained heating of shale and oil sands and drained heating of cemented sand beds always increase in situ. Drained heating of oil sands and shale in situ will cause an initial increase in stresses and strains during the early stages of production when temperature increases are small. As temperature increases become large, the increase in thermal stresses and strain will level off in the oil sands as the coefficient of thermal expansion levels off due to structural collapse caused by grain crushing and rearrangement. For shale the thermal stresses and strains will decrease at higher temperatures as the soil matrix consolidates and the coefficient of thermal expansion becomes negative.

Compressibility Behaviour

During in situ thermal recovery formation strata is subjected to changes in effective stress caused by thermal volume change of mineral solids and by injection, expansion or withdrawal of pore fluids. Volume changes associated with changes in effective stress occur through sliding between mineral grains and deforming or crushing of individual particles. Volume change is resisted by friction between soil particles, interparticle bonding and particle strength and is dependent on void ratio and the size, shape and gradation of mineral particles.

The compressibility of Cold Lake Clearwater oil sands has been examined following the one-dimensional (or confined

compression) stress path and the isotropic compression stress path under stresses and temperatures associated with in situ thermal recovery. Compressibility parameters were found to be highly influenced by stress history, stress path and temperature. Non-linear, inelastic behaviour is attributed to weak minerals in the sand matrix which are susceptible to physical breakdown during shear straining and heating. Since the factors which govern the compressibility of oil sands also govern strength and deformation properties during application of a deviatoric stress, shear strength parameters may be significantly affected by grain crushing. Further, changes in temperature and effective stress may cause significant changes in void ratio and mineral grain gradation which will also affect strength parameters and permeability.

Spacial variations in mineralogy, geological environment of deposition and geological history between the four oil sands tested have little influence on measured compressibility parameters. The effect of geological processes on compressibility may be overshadowed by sample disturbance during coring.

The compressibility of Athabasca McMurray Formation and Cold Lake Clearwater Formation oil sands is similar when cycled over the same effective stress range. However, the net volume change during initial compression, especially at higher temperatures, is greater for Cold Lake oil sands due to grain breakage. Athabasca oil sands which consist of

predominantly quartz sand are essentially elastic during stress cycling in both one-dimensional and isotropic compression.

The compressibility of the heavily over-consolidated Clearwater shale is comparable to that of oil sands. Thermal volume change results indicate a significant amount of heat reduced consolidation occurs during drained heating. Improvements in strength and deformation properties associated with the non-recoverable volume reductions caused by heat consolidation are likely to be retained after the initial in situ heat injection cycle.

Shear Strength Behaviour

The influence of temperature, pressure and stress path on the strength and deformation properties of Cold Lake oil sands was examined. The major conclusions made during this phase of the experimental research may be summarized as follows:

1. The shear strength properties of Cold Lake Clearwater Formation oil sands are significantly different from those of Athabasca McMurray Formation oil sands, reflecting the difference in sand grain mineralogy, geological environment of deposition and geological history. Athabasca McMurray Formation oil sands consist of a uniformly graded, predominantly quartz sand, whereas Cold Lake Clearwater Formation oil sands contain additional minerals which are much

weaker.

2. Clearwater Formation oil sands display significant grain crushing during drained shear at high effective confining stresses at 20°C. Grain crushing begins at the sand grain contacts and eventually leads to crushing of entire grains. The weaker sand grains, such as feldspar, are very susceptible to crushing during shear.

3. The amount of grain crushing increases at high effective confining stresses as evidenced by a reduced tendency to dilate, greater strains to failure and stronger strain hardening behaviour. Grain crushing results in a significant reduction in the overall effective angle of friction at failure. The decrease in the rate of dilatancy with increasing confining pressure results in significant curvature in the failure envelope.

4. During undrained shear at low initial effective confining stresses the oil sands specimens show an increase in pore pressure at the beginning of the test due to compression of the sand matrix during the

onset of the stress increase. The volume reduction of the sand matrix results in the pore fluids taking more of the load due to their inability to drain. As the specimen reaches its peak strength, the pore fluid pressure decreases as the sand matrix tendency to dilate and the shear strain is suppressed.

5. During undrained shear at high initial effective confining stresses this oil sands reaches peak deviator stress at small axial strains and decreases with continued strain. The pore fluid pressure rises even after the deviator stress has reached its maximum value. The behaviour results from the high amount of grain crushing which the sand matrix undergoes during drained shear and as a result of large pore pressures developed during undrained shear. As shearing progresses, the effective stresses decrease as more available friction is mobilized. As a result, the overall shearing resistance reaches its maximum value prior to full frictional resistance being mobilized. At large strains when all the friction is mobilized, the overall shearing stress is smaller. This type of undrained behaviour is analagous to the behaviour of a normally consolidated sensitive clay.

6. The shear strength of Clearwater Formation oil sands at elevated temperatures depends not only on the strength of the mineral grains at higher temperatures, but also on the amount of grain crushing and particle rearrangement which occurs during heating. This oil sands contains minerals which are highly susceptible to physical breakdown during heating at elevated temperatures and pressures.

7. The mechanical properties of Cold Lake Clearwater Formation oil sands are dependent on the temperature, pressure and stress path followed during the test. Analytical procedures used to model the stresses and deformations of formation strata must, therefore, utilize geomechanical properties representative of the actual formation response.

Cold Lake Clearwater Formation oil sands form a distinct class of materials dissimilar from Athabasca McMurray Formation oil sands. McMurray Formation oil sands display dilatative volume change behaviour over the in situ effective confining stress range encountered in the Athabasca deposit. This behaviour illustrates the strength of the quartz sand grains. In contrast, Clearwater Formation

oil sands are strongly strain hardening and continue to contract with increasing shear strain at the in situ confining stresses found in the Cold Lake deposit. Cold Lake Clearwater Formation oil sands contain a predominance of minerals which are much weaker than quartz. The stresses and deformations that occur in the respective formations caused by changes in stress, pore fluid pressure and temperature during in situ thermal recovery would, therefore, be vastly different. The dense interpenetrative fabric of McMurray oil sands develop substantially higher stresses with smaller deformations.

The highly compressible, strain hardening behaviour of Cold Lake Clearwater Formation oil sands is similar to that of broken ice in its granular state. Numerical techniques developed for predicting the behaviour of broken ice can aid in the analysis of the behaviour of oil sands. Such techniques are outlined in Wong et al (1988). It is noted, however, the processes contributing to the behaviour are quite different. Gale et al (1987) conclude that broken ice specimens are ductile due to the grain's ability to creep, while for sand ductility was promoted by grain crushing.

The geomechanical properties of Clearwater shale from the Cold Lake Deposit are affected by an increase in temperature. Heat consolidation causes a reduction in void ratio and, as a result, the shear strength and stiffness of the material increase. Cold Lake shale displays path dependency when comparing the passive drained and passive

undrained stress paths at 20°C. The undrained specimen is stiffer and requires a smaller axial strain to reach failure. More testing is needed to determine, in quantitative terms, the effect of temperature on the strength and deformation behaviour of carbonate cemented sand streaks which are commonly found adjacent to Cold Lake reservoir oil sands.

13.4 Comparison of Athabasca and Cold Lake Materials

Some of the major conclusions reached from the geotechnical testing of oil sands and related strata are discussed below:

1. The mechanical properties of Athabasca and Cold Lake materials are dependent on the temperature, pressures and stress paths followed during the test. Analytical procedures used to model the stresses and deformations of formation strata must therefore utilize geomechanical properties representative of the actual formation response.

2. X-ray diffraction analyses carried out by the Alberta Research Council on the fine fraction (less than 2 μm) of shale facies from Athabasca and Cold Lake Deposits are given in Table 13.1. Test procedures are outlined in Appendix B. The results indicate no

Table 13.1 Results of X-Ray Diffraction Analyses

Before Test

Test Number	Location	Test Temperature (°C)	Illite (%)	Montmorillonite (%)	Chlorite (%)	Kaolinite (%)	Other ** Minerals
UFCCS4	Athabasca	225	65	15	10	10	Q, PF
UFTCS1	Athabasca	20					
UFTCS4	Athabasca	20					
UFHTTCS3	Athabasca	225	55	5	10	30	Q
BPCCS2	Cold Lake	300	50	30	15	5	Q, PF
BPHTTCS1	Cold Lake	225	50	20	15	15	Q, PF

Q = Quartz PF = Plagioclase Feldspar

After Test

Test Number	Location	Test Temperature (°C)	Illite (%)	Montmorillonite (%)	Chlorite (%)	Kaolinite (%)	Other ** Minerals
UFCCS4	Athabasca	225	60	25	10	5	Q
UFTCS1	Athabasca	20	65	15	10	10	Q, PF
UFTCS4	Athabasca	20	55	15	15	15	Q
UFHTTCS3	Athabasca	225	55	15	15	15	Q, PF
BPCCS2	Cold Lake	300	50	30	15	5	Q, PF
BPHTTCS1	Cold Lake	225	50	25	15	10	Q

** Note: Semi-quantative analysis assumes 100 % clay, "other minerals" refers to non-clay minerals present quantity of non-clay minerals is not determined in the analysis

significant mineral alteration under test temperatures to 300°C. The mechanical behaviour of particular shale strata at elevated temperatures is therefore dependent on the water content, fabric, structure and mineralogy prior to testing.

3. The maximum shear strengths and stress-strain moduli of Athabasca oil sands are much greater than those of Cold Lake oil sands, reflecting the difference in sand grain mineralogy, geological environment of deposition and geological history. Athabasca oil sands consist of a uniformly graded, predominantly quartz sand whereas Cold Lake oil sands contain several additional minerals which are much weaker.

4. Athabasca oil sands display dilatant behaviour during shear over the effective confining stress range encountered in the deposit. This increase in volume change during shear straining accompanied by strain softening behaviour in the post-peak region illustrates the strength of the quartz sand grains. The grains during shear tend to ride up on each other whereas Cold Lake oil sands tend to shear through sand grains. Cold Lake oil sands do, however, display a dilatant behaviour at low effective confining

stresses (generally less than 2.5 MPa).

5. Athabasca oil sands also have an undrained shear strength similar to Cold Lake oil sands but require very large strains to achieve the maximum strength failure condition. This higher undrained strength also reflects the strength of Athabasca's quartz mineralogy. In order to suppress Athabasca oil sands high tendency to dilate under shear straining, the pore fluid pressure decreases and in most cases falls well below the initial back pore fluid pressure applied to the specimen. This results in a net increase in effective confining pressure on the sample during the test. Athabasca oil sands therefore reach maximum strength when the pore fluid pressure levels out, which generally occurs at large axial strains. The pore fluid pressures for Cold Lake specimens usually level out during undrained shear at much smaller axial strains and remain constant with a net pore pressure increase (a net decrease in effective confining stress).

6. The shear strength of oil sands at elevated temperatures depends not only on the strength of the mineral grains at higher temperatures but also on the

amount of grain crushing and particle rearrangement which occurs during heating. Cold Lake oil sands contain minerals more susceptible to physical breakdown during heating at elevated temperatures and pressures resulting in a more densely packed sand structure after heating which exhibits a higher resistance to shear. Athabasca oil sands, on the other hand, may or may not show a significant change in shear strength at high temperatures depending on the amount of fines present in the specimen.

7. The compressibility of Athabasca and Cold Lake oil sands is similar when cycled over the same effective stress range. However, the net volume change during initial compression, especially at higher temperatures, is greater for Cold Lake oil sands due to grain breakage.

8. Fully drained thermal expansion tests carried out on both Athabasca and Cold Lake oil sands show Cold Lake oil sands are much more susceptible to temperature induced grain breakage which is evident at temperatures as low as 75°C. Undrained thermal volume change measurements of both oil sands are similar since volume increases under this condition are due

to volume increases of the pore liquids and individual sand grains. The thermal volume change of the pore liquids, approximately the same for both deposits, accounts for over 90% of the expansion over the temperature range of 20 to 300°C.

In general, the experimental results show that the geotechnical properties of the Cold Lake Deposit differ significantly from those of the oil sands of the Athabasca Deposit. Cold Lake oil sands are generally weaker and contain minerals which are more susceptible to physical breakdown at elevated temperatures and pressures. The majority of the geotechnical properties of oil sands and associated strata vary non-linearly with pressure and temperature.

13.5 Recommended Future Research

A laboratory testing program has been carried out to investigate and identify the major factors governing the constitutive behaviour of oil sands and related strata through representative laboratory testing. Many of the behavioural characteristics and material properties of several geotechnical facies from both the Athabasca and Cold Lake oil sands deposits which may be subjected to either direct or peripheral heating have been documented over the temperature range of 20°C to 300°C.

The following recommendations may prove valuable in future studies:

1. The present research has concentrated on constitutive behaviour associated with thermal-mechanical and hydro-mechanical processes. It is noted, however, that to properly ascertain the effect of temperature, the rate of temperature change of the oil sands formation strata must be coupled to the rate of pore fluid dissipation in the analysis of this class of problem.

Thermal properties required for geotechnical and reservoir modeling should be evaluated over the temperature range of 20°C to 300°C for oil sands and related strata. A transient line heat source technique has been used successfully with the present equipment by Seto (1985) to determine the thermal conductivity of rich, undisturbed Athabasca oil sands core samples at elevated temperature and pressure. The transient state heat transfer test apparatus was designed to fit inside the high temperature and pressure triaxial cell and operate at temperatures ranging from 20°C to 300°C. Pore fluid pressures up to 27 MPa can be applied through top and/or bottom drainage ports in the sample and platens and measurements are possible at top and bottom and at mid-height of the specimen. Vertical confining loads up to 440 kN can be applied to the sample by the top loading piston. Thermal testing includes direct

measurement of thermal conductivity and thermal diffusivity utilizing the transient thermal testing procedure. The specific heat of the specimen is then calculated from the experimentally derived thermal conductivity and diffusivity values using specimen density measured during the test. A single specimen of oil sands from Cold Lake Location No. 2 was tested for general comparison to high grade Athabasca McMurray Formation oil sands. The thermal conductivity of Athabasca oil sands is approximately 2.0 W/m°C at 20°C (Seto, 1985) as compared to 1.2 W/m°C for rich Cold Lake oil sands. This difference reflects the differences in sand grain mineralogy. Tests should be carried out on other oil sands and related geotechnical facies from both deposits in order to obtain reliable constitutive behaviour characterization of these materials.

Permeability testing of oil sands as well as interbedded and adjacent strata should be measured both in the oedometer and triaxial cell of the present equipment under pressures and temperatures appropriate to the in situ production conditions. Effective (or relative) permeability of oil, water and gas are essential for the determination of the rate of pore pressure dissipation and, therefore, two phase flow permeability parameters for undisturbed

oil sands specimens are recommended at elevated temperatures and pressures and for various representative fluid saturations.

2. Low effective confining stress levels are expected to be reached in oil sands reservoir strata arising from pore fluid pressure increases due to heating and injection during thermal recovery. A rapid reduction in effective stress will result in large ground deformations and a significant reduction in shear strength. As a consequence, there is a need to study the stress-strain and strength behaviour both following the proportional unloading stress path and for subsequent appropriate loading or unloading stress paths at these low effective stresses.

3. Long term heat consolidation tests would be useful in evaluating whether mineralogical changes in shale strata occur during sustained and prolonged heating associated with in situ bitumen recovery methods. Mineral alteration may have a significant effect on the mechanical behaviour of these geotechnical facies at elevated temperatures.

4. Laboratory shear strength testing at temperatures between 225°C and 300°C would fill in gaps in the existing data for Athabasca and Cold Lake materials. Geotechnical testing of geotechnical facies from other parts of the Athabasca and Cold Lake Deposits is warranted due to the geological complexity inherent in each deposit. Geotechnical characterization of Peace River Deposit materials is also desirable.

5. Constitutive models derived from mathematical formulation of laboratory behaviour must be verified by comparison of the model to reliable field measurements. As a consequence, there is a need to incorporate geotechnical instrumentation and field testing equipment in the design of in situ pilot or commercial developments.

BIBLIOGRAPHY

Abrams, A., 1975. "The influence of Fluid Viscosity, Interfacial Tension and Flow Velocity on Residual Oil Saturation Left by Waterflood". Society of Petroleum Engineers of AIME, Vol. 15, pp. 437-447.

Afinogenov, Y.A., 1970. "How the Liquid Permeability of Rocks is Affected by Pressure and Temperature". Consultants Bureau, Plenum Publishing Corporation, New York, Translated from Russian Publication SN11G1MS, No. 6, pp. 34-42.

Agar, J.G., 1984. "Geotechnical Behaviour of Oil Sands at Elevated Temperatures and Pressures". Ph.D. Thesis, University of Alberta, 906 p.

Agar, J.G., Morgenstern, N.R. and Scott, J.D., 1987. "Shear Strength and Stress-Strain Behaviour of Athabasca Oil Sand at Elevated Temperatures and Confining Pressures". Accepted for Publication by the Canadian Geotechnical Journal. Tentative Publication Issue: Vol. 24, No. 1, Feb. 1987.

Agar, J.G., Morgenstern, N.R. and Scott, J.D., 1986. "Thermal Expansion and Pore Pressure Generation in Oil Sands". Canadian Geotechnical Journal, Vol. 23, No. 3, Aug., pp. 327-333.

Agar, J.G., Morgenstern, N.R. and Scott, J.D., 1983. "Geotechnical Testing of Alberta Oil Sands at Elevated Temperatures and Pressures". Proceedings of the 24th U.S. Symposium on Rock Mechanics, Texas A & M University, June, pp. 795-806.

Alberta Energy and Natural Resources, 1979. "Alberta Oil Sands Facts and Figures". ENR Report No. 110, 67 p.

Aldea, G.N. and Sandru, L.T., 1985. "Oil Production by Mining Methods in the Socialist Republic of Romania". Proceedings of the Sixth Annual Advances in Petroleum Recovery and Upgrading Technology Conference, Alberta Oil Sands Technology and Research Authority, Edmonton, June 6-7, 26 p.

Alheid, H.J., Moehring-Erdmann, G. and Rummel, F., 1983. "Experimental and Theoretical Approach to Friction in Rocks at High Pressure and Temperature". In Proceedings of the 24th U.S. Symposium on Rock Mechanics, Texas A & M University, pp. 481-488.

Alsands Project Group, 1978. Application to the Alberta Energy Resources Conservation Board for an Oil Sands Mining Project, 240 p.

American Society of Mechanical Engineers, 1977. "ASME Steam Tables - Thermodynamic and Transport Properties of Steam". ASME, New York, 3rd Edition, 1977, 329 p.

American Society for Testing and Materials, 1963. "Symposium on X-ray and Electron Probe Analysis". Sixty-sixth Annual Meeting of ASTM, Atlantic City, N.J., June 27, 1963, ASTM Special Technical Publication No. 349, 209 p.

Amyx, J.A., Bass, D.M. Jr. and Whiting, R.L., 1960. "Petroleum Reservoir Engineering". McGraw-Hill Book Company, New York, 610 p.

Anand, J., Somerton, W.H. and Gomaa, E., 1973. "Predicting Thermal Conductivities of Formations from Other Known Properties". Society of Petroleum Engineers Journal, Vol. 13, pp. 267-273.

Anderson, D.R. (ed.), 1981. Proceedings of the Sixth Annual NEA-Seabed Working Group Meeting, Paris, France, Published by Scandia National Laboratories, Albuquerque, New Mexico, 220 p.

Anderson, P.D. and Hollingsworth, F.H., 1982. "Casing Damage at the AMOCO-AOSTRA Athabasca In Situ Combustion Pilot". UNITAR Conference, Caracus, Venezuela, pp. 828-835.

Annor, A., Miles, P., Kapeller, F. and Larocque, G., 1981. "High Temperature and Pressure Triaxial Compression Tests on Rock Samples from Pinawa and the Creighton Mine". Atomic Energy of Canada Limited, Technical Record TR-158, 32 p.

AOSTRA, 1986. "An Experimental In Situ Recovery Scheme in Oil Sands Using Shaft and Tunnel Access". Application to Amend Approval #4198, Submitted to Alberta Energy Resources Conservation Board, 97 p.

AOSTRA, 1978. "Saline Creek Tunnel: Research Observations". Alberta Oil Sands Technology and Research Authority, 159 p.

Atwater, G.I. and Miller, E.E., 1965. "The Effect of Decrease in Porosity with Depth on Future Development of Oil and Gas Reservoirs in South Louisianna". Amerc. Assn. Pet. Geol. Prog. Ann. Mtg., New Orleans, p. 48.

Au, K.S., 1984. "The Strength-Deformation Properties of Alberta Oil Sands". M.Eng. Report, University of Alberta, 135 p.

Austin, R.S. and Droullard, R.F., 1979. "Effects of Heating on Radon-222 Emanation from Domestic Uranium Ores". U.S. Department of the Interior, Bureau of Mines, Report of Investigations, #R1 8361, 46 p.

Babcock, E.A., 1975. "Fracture Phenomena in the Waterways and McMurray Formation, Athabasca Oil Sands Region, Northeastern Alberta". Bulletin of Canadian Petroleum Geology, Vol. 23, No. 4, pp. 810-826.

Barden, L. and Proctor, D.C., 1971. "The Drained Strength of Granular Materials". Canadian Geotechnical Journal, Vol. 8, pp. 372-383.

Barnes, D.J., 1980. "Micro-fabric and Strength Studies of Oil Sands". M.Sc. Thesis, University of Alberta, Edmonton, Alberta, 244 p.

Barnes, D.J. and Dusseault, M.B., 1982. "The Influence of Diagenetic Microfabric on Oil Sands Behavior". Canadian Journal of Earth Sciences, Vol. 19, No. 4, pp. 804-818.

Barnes, D.J. and Dusseault, M.B., 1980. "The Influence of Diagenesis on the Behavior of Oil Sands". In Proceedings of Applied Oilsands Geoscience, edited by M.B. Dusseault, Edmonton, Alberta, 32 p.

Barton, C.M., 1975. "A Geotechnical Facies Analysis of Some Quarternary Sediments Beneath Westernport Bay". Proc. R. Soc. Vict., Vol. 87, Parts 1 and 2, pp. 139-148.

Bauer, A. and Crosby, W.A., 1979." The Effect of Blasting on the Stability of Tar Sand Slopes". Canadian Institute of Mining and Metallurgy, Bulletin, Vol. 72, No. 812, pp. 43-49.

Bauer, S.J. and Johnson, B., 1979. "Effects of Slow Uniform Heating in the Physical Properties of the Westerly and Charcoal Granites". Proceedings of the 20th Symposium on Rock Mechanics, pp. 7-18.

Bawden, W.F., 1981. "Hydraulic Fracturing in Alberta Tar Sands Formations - A Unique Material for In-situ Stress Management". Proceedings of the Workshop on Hydraulic Fracturing, Monterey, CA, pp. 91-103.

Bawden, W.F. and McCreath, D.R., 1979. "Geotechnical Study for an Abandoned Limestone Mine for Crude Oil Storage". Canadian Geotechnical Journal, Vol. 16, No. 3, pp. 577-590.

Beiser, A., 1975. "The Origin of Rocks". In Theory and Problems of the Earth Sciences, McGraw-Hill Book Company, New York, 1975, 129 p.

Bell, J.S. and Babcock, E.A., 1986. "The Stress Regime of the Western Canadian Basin and Implications for Hydrocarbon Production". Bulletin of Canadian Petroleum Geology, Vol. 34, No. 3, pp. 364-378.

Bell, M.L. and Nur, A., 1978. "Strength Changes Due to Reservoir-Induced Pore Pressure and Stresses with Application to Lake Oroville". Journal of Geophysical Research, Vol. 83, No. B9, pp. 4469-4483.

Bennion, D.W., Vorndran, L., Donnelly, J.K. and Moore, R.G., 1977. "Fire Flooding Changes in Athabasca Bitumen". Oil Sand and Oil Shale Chemistry, Edited by Otto P. Strausz and Elizabeth M. Lown, Montreal, Canada, pp. 186-197.

Berthomieu, G. and Jouanna, P., 1984. "Stability of Rock Faces Subjected to Temperature Changes - Application to Hot Dry Granite". Int. J. Rock Mechanics, Mineral Science and Geomechanical Abstracts, Vol. 21, No. 5, pp. 277-287.

Billam, J., 1972. "Some Aspects of the Behaviour of Granular Materials at High Pressures". In Stress-Strain Behaviour of Soils, pp. 69-80.

Biot, M.A., 1959. "Stability Problems of Inhomogeneous Visoelastic Media". Non-Homogeneity in Elasticity and Plasticity, Proceedings of IUTAM, New York, Pergamon Press, 26 p.

Biot, M.A., 1955. "Theory of Elasticity and Consolidation for a Porous Anisotropic Solid". Journal of Applied Physics, Vol. 25, No. 2, February 1955, pp. 182-185.

Biot, M.A., 1941. "General Theory of Three-Dimensional Consolidation". Journal of Applied Physics, Vol. 12, February 1941, pp. 155-164.

Biot, M.A., 1941. "Consolidation Settlement Under a Rectangular Load Distribution". Journal of Applied Physics, Vol. 12, May 1941, pp. 426-431.

Biot, M.A., 1941. "Consolidation Settlement of a Soil with an Impervious Top Surface". Journal of Applied Physics, Vol. 12, July 1941, pp. 578-581.

Bishop, A.W., 1973. "The Influence of an Undrained Change in Stress on the Pore Pressure in Porous Media of Low Compressibility". Geotechnique, Vol. 23, No. 3, pp. 435-442.

Bishop, A.W., 1972. "Shear Strength Parameters for Undisturbed and Remoulded Soils Specimens". In Stress-Strain Behaviour of Soils, pp. 3-58.

Bishop, A.W., 1966. "Soils and Soft Rocks as Engineering Materials". Inaugural Lecture, Imperial College of Science and Technology, 6, pp. 289-313.

Bishop. A.W., 1966. "The Strength of Soils as Engineering Materials". Geotechnique, Vol. 16, pp. 89-130.

Bishop, A.W., 1965. "Contribution to Panel Discussion, Division 2". Proceedings of 6th International Conference on Soil Mechanics and Foundation Engineering, Vol. 3.

Bishop, A.W., 1959. "The Principle of Effective Stress". Teknisk Ukeblad, 106: No. 39, pp. 859-863.

Bishop, A.W. and Eldin, A.K.G., 1950. "Undrained Triaxial Tests on Saturated Sands and Their Significance in the General Theory of Shear Strength". Geotechnique, Vol. 1, No. 2, pp. 13-32.

Bishop, A.W. and Green, G.E., 1965. "The Influence of End Restraint on the Compression Strength of a Cohesionless Soil". Geotechnique 15, No. 3, pp. 243-266.

Bishop, A.W. and Henkel, D.J., 1962. "The Measurement of Soil Properties in the Triaxial Test". Second Edition, Edward Arnold (Publishers) Ltd., London, U.K., 227 p.

Bishop, A.W., Webb, D.L. and Skinner, A.E., 1965. "Triaxial Tests on Soils at Elevated Cell Pressures". Proceedings of 6th International Conference on Soil Mechanics and Foundation Engineering, Montreal, pp. 170-174.

Bjerrum, L., 1961. "The Effective Shear Strength Parameter of Sensitive Clays". Proceedings of 5th International Conference on Soil Mechanics and Foundation Engineering, Vol. 1, pp. 23-28.

Black, D.K. and Lee, K.L., 1973. "Saturating Laboratory Samples by Back Pressure". Journal of Soil Mechanics and Foundation Division, ASCE, Vol. 99, No. SM1, pp. 75-93.

Blatt, H., Middleton, G. and Murray, R., 1972. "Origin of Sedimentary Rocks". Prentice-Hall Inc., Englewood Cliffs, New Jersey, 634 p.

Boade, R.R., 1980. "True In-situ Bed Preparation: Oil Shale and Tar Sand". Technical Information, U.S. Department of Energy, Rept. SAND-80-1203C, 25 p.

Boga, S.K., Hwang, C.T. and Krishnayya, A.V.G., 1980. "Thermal Foundation Design for Syncrude's Hot-Bitumen Tanks". Applied Oilsands Geoscience, Edmonton, Alberta, 41 p.

Boley, B.A. and Weiner, J.H., 1960. "Theory of Thermal Stresses". John Wiley & Sons, Inc., New York, 470 p.

Bolton, M.D., 1986. "The Strength and Dilatency of Sands". Geotechnique, Vol. 36, No. 1, pp. 65-78.

Bonnet, G. and Jouanna, P., 1980. "Thermomechanical Friction Tests on Artificial Joints". International Journal of Rock Mechanics, Mineral Science and Geomechanics Abstract, Vol. 17, pp. 209-217.

Boon, J.A., Hamilton, T., Holloway, L. and Wiwchar, B., 1982. "Reaction Between Rock Matrix and Injected Fluids in Cold Lake Oil Sands - Potential for Formation Damage". Petroleum Society of CIM, 6th Symposium on Engineering Applications of Mechanics, Calgary, Alberta, June 6-9, 1982, CIM Paper No. 82-33-37.

Borg, I., Friedman, J., Handin, J. and Higgs, D.V., 1960. "Experimental Deformation of St. Peter Sand: A Study of Cataclastic Flow, Rock Deformation". Geological Society of America, Memoir 79, pp. 133-192.

Bowman, C.W., Humphreys, R.D. and Mossop, G.D., 1983. "Oil Sands Technology and Economics". Short Course Sponsored by the Alberta Research Council, 287 p.

Brace, W.F., 1980. "Permeability of Crystalline and Argillanceous Rocks". International Journal of Rock Mechanics, Mining Sciences and Geomechanical Abstracts, 18, pp. 241-251.

Branco, P., 1988. "Isothermal Behaviour of Gassy Soils". Ph.D. Thesis, University of Alberta, 723 p.

Bratli, R.K. and Risnes, R., 1981. "Stability and Failure of Sand Arches". Society of Petroleum Engineers Journal, April, pp. 236-248.

Braun, R.L. and Chin, R.C.Y., 1977. "Research and Development on Rubble In Situ Extraction of Oil Shale (RISE) at Lawrence Livermore Laboratory". In Proceedings of the 10th Oil Shale Symposium, Edited by J.H. Gary, Colorado School of Mines, 166 p.

Brooker, E.W., 1980. "Geotechnical Frontiers in Oilsand Mining". Proceedings of the International Mining Exposition and Conference, Calgary, Aug. 26, 30 p.

Brooker, E.W., 1975. "Tarsand Mechanics and Slope Evaluation". 10th Canadian Rock Mechanics Symposium, Kingston, Ontario, September 1975, Vol. 1, pp. 409-446.

Brooker, E.W., 1974. "Geotechnical Design Problems in Tar Sand Development". Proceedings of the Athabasca Oil Sands Conference, Engineering Institute of Canada, Edmonton, April, pp. 71-97.

Brooker, E.W., Devenny, D.W. and McRae, A.M., 1978. "Deep Excavation in Oil Sand - Why, Where, How?" AOSTRA Seminar on Underground Excavation in Oil Sands, Edmonton, Alberta, Paper No. 12, 27 p.

Brooker, E.W. and Khan, F.Z., 1980. "Design and Performance of Oil Sand Surface Mine Slopes". Applied Oil Sands Geoscience 1980, Edited by M.B. Dusseault, University of Alberta, Edmonton, 18 p.

Brown, E.T., Bray, J.W., Ladanyi, B. and Hoek, E., 1983. "Ground Response Curves for Rock Tunnels". American Society of Civil Engineers, Journal of Geotechnical Engineering, Vol. 109, No. 1, January, 1983, pp. 15-39.

Burcik, E.J., 1957. "Properties of Petroleum Reservoir Fluids". International Human Resources Development Corporation, Boston, Ma., 190 p.

Burnham, C.W., Holloway, J.R. and Davis, N.F., 1969. "Thermodynamic Properties of Water to 1000°C and 10,000 bars". Geological Society of America, Spec. Paper 132, Boulder, Colorado, 96 p.

Burst, J.F., 1969. "Diagenesis of Gulf Coast Clayey Sediments and Its Possible Relation to Petroleum Migration". Amer. Assn. Pet. Geol. Bull., 53, pp. 73-93.

Butler, R.M., 1986. "The Expansion of Tar Sands During Thermal Recovery". Journal of Petroleum Technology, Sept.-Oct., pp. 51-56.

Butler, R.M. and Stephens, D.J., 1981. "The Gravity Drainage of Steam-Heated Heavy Oil to Parallel Horizontal Wells". Journal of Canadian Petroleum Technology, April-June 1981, pp. 90-96.

Byrne, P.M. and Eldridge, T.L., 1982. "A Three Parameter Dilatant Elastic Stress-Strain Model for Sand". International Symposium on Numerical Methods in Geomechanics, Zurich, Switzerland, September 13-17, 1982, pp. 73-80.

Byrne, P.M., Janzen, W.F. and Mittal, H.K., 1982. "Finite Element Analysis of Excavation in Oil Sands". Proceedings of the 33rd Annual Technical Meeting of the Canadian Institute of Mining and Metallurgy, Calgary, Alberta, June, Preprint, Paper 82-33-10, 7 p.

Byrne, P.M., Smith, B.L., Grigg, R.F. and Stewart, W.P., 1980. "A Computer Model for Stress-Strain and Deformation Analysis of Oilsands". Proceedings of Applied Oilsands Geoscience '80 Conference, Edmonton, Alberta, June 11 to 13, 38 p.

Camp, F.W., 1970. "The Tar Sands of Alberta, Canada". Manuscript Published by Cameron Eng. Inc., Denver, Colorado, 82 p.

Campanella, R.G. and Mitchell, J.K., 1968. "Influence of Temperature Variations on Soil Behaviour". Journal of Geotechnical Engineering, ASCE, Vol. 94, SM3, May 1968, pp. 709-734.

Campbell, J.H. and Burnham, A.K., 1980. "Reaction Kinetics for Modelling Oil Shale Retoring". In Situ, 4(1), pp. 1-37.

Canadian Institute of Steel Construction, 1970. "Handbook of Steel Construction". Second Edition, Published by the Canadian Institute of Steel Construction, Toronto, Ontario, 720 p.

Carpenter, H.C., Jensen, H.B. and Decora, A.W., 1977. "Potential Shale Oil Production Processes". Symposium on Oil Sand and Oil Shale, Montreal, CIM, pp. 48-65.

Carrier, W.D. III and Bromwell, L.G., 1983. "Disposal and Reclamation of Mining and Dredging Wastes". Proceedings of the Seventh PanAmerican Conference on Soil Mechanics and Foundation Engineering, Vancouver, Canada, June, Vol. 2, pp. 727-738.

Carrigy, M.A., 1967. "The Physical and Chemical Nature of a Typical Tar Sand: Bulk Properties and Behaviour". Proc. of the 7th World Petroleum Congress, Mexico City, Vol. 3, Tar Sands Section, pp. 573-581.

Carrigy, M.A. and Kramers, J.W., 1974. "Geology of the Alberta Oil Sands". In Athabasca Oil Sands, Conference Proceedings, 1974, EIC, Western Region, pp. 13-24.

Carrigy, M.A. and Kramers, J.W., 1973. "Guide to the Athabasca Oil Sands Area". Published by Alberta Research Council, Information Series 65, 215 p.

Carslaw, H.S. and Jaeger, J.C., 1959. "Conduction of Heat in Solids". 2nd Edition, Oxford University Press, London, 1959, 510 p.

Carter, C., 1951. "Soil Temperature, Moisture Content and Thermal Properties". University of Tennessee, Engineering Experiment Station, Bulletin 15, 32 p.

Carter, W.J., 1978. "Permeability Enhancement Using Explosive Techniques". Technical Information, U.S. Department of Energy, Rept. LA-UR-78-1418, 6 p.

Cassagrande, A., 1936. "Characteristics of Cohesionless Soils Affecting the Stability of Slopes and Earth Fills", Journal of Boston Society of Civil Engineers, Vol. 23, No. 1, pp. 13-32.

Casse, F.J. and Ramey, H.J., 1979. "The Effect of Temperature and Confining Pressure on Single-Phase Flow in Consolidated Rocks". Journal of Petroleum Technology, August, 1979, pp. 1051-1059.

Cassis, R., Fuller, N., Hepler, L.G., McLean, R.J.C., Skauge, A., Srinivasan, N.S. and Yan, H.K., 1985. "Specific Heat Capacities of Bitumens and Heavy Oils, Reservoir Minerals, Clays, Dehydrated Clays, Asphaltenes, and Cokes". AOSTRA Journal of Research, Vol. 1, No. 3, pp. 163-173.

Cedergren, H.R., 1977. "Seepage, Drainage and Flow Nets". John Wiley & Sons, Inc., New York, 534 p.

Cervenan, M.R., Vermeulen, F.E. and Chute, F.S., 1981. "Thermal Conductivity and Specific Heat of Oil Sand Samples". Applied Oilsands Geoscience 1980, Edited by M.B. Dusseault, University of Alberta, Edmonton, Alberta, 26 p.

Chan, T. and Jeffrey, J.A., 1983. "Scale and Water Saturation Effects for Thermal Properties of Low-Porosity Rock". Proceedings of the 24th U.S. Symposium on Rock Mechanics, Texas A & M University, pp. 287-302.

Charlwood, R.G., 1981. "Thermal-Geomechanical Analyses for the Design of a Mine Assisted Heavy Oil Recovery Facility". AOSTRA Workshop on Computer Modelling, University of Alberta, January, 1981.

Charlwood, R.G., Byrne, P.M., McKinlay, D.W. and Varoglu, E., 1980. "Thermal Geomechanical Analyses and Criteria for the Design of a Mine Assisted Heavy Oil Recovery Facility". In Applied Oilsands Geoscience, M. Dusseault (Editor), University of Alberta, Edmonton, Alberta, 57 p.

Chatterji, P.K., Smith, L.B., Insley, A.E. and Sharma, L., 1979. "Construction of Saline Creek Tunnel in Athabasca Oil Sand". Canadian Geotechnical Journal, Vol. 16, No. 1, pp. 90-107.

Chen, Chia-Shyum and Reddell, D.L., 1983. "Temperature Distribution Around a Well During Thermal Injection and a Graphical Technique for Evaluating Aquifer Thermal Properties". Water Resources Research, Vol. 19, No. 2, pp. 351-363.

Chhina, H.S. and Agar, J.G., 1985. "Potential Use of Fracture Technology for Recovery of Bitumen from Oil Sands". Proceedings of the Third International Conference on Heavy Crude and Tar Sands, Sponsored by: UNITAR/UNDP Information Centre, Long Beach, California, July 22-30, 32 p.

Chu, M.S. and Chang, N.Y., 1980. "Uniaxial Creep of Oil Shale Under Elevated Temperatures". In Rock Mechanics, A State of the Art, Proceedings of the 21st Symposium on Rock Mechanics, University of Missouri, Rolla, pp. 207-216.

Chute, F.S., Vermeulen, F.E., Cervenan, M.R. and McVea, F.J., 1979. "Electrical Properties of Athabasca Oil Sands". Canadian Journal of Earth Sciences, Vol. 16, No. 10, pp. 2009-2021.

Clark, K.A., 1960. "Permeabilities of the Athabasca Oil Sands". Transactions, Canadian Institute of Mining and Metallurgy (CIM), Vol. 63, pp. 151-156.

Clark, K.A., 1957. "Bulk Densities, Porosities and Liquid Saturations of Good Grade Athabasca Oil Sands". Edmonton, Research Council of Alberta, Mimeo., Circ. 22, 22 p.

Clark, K.A., 1944. "Some Physical Properties of a Sample of Alberta Bitumenous Sand". Canadian Journal of Research, 22F, pp. 174-180.

Clark, S.P., 1966. "Handbook of Physical Constants". The Geological Society of America, Memoir 97, 175 p.

Closmann, P.J. and Bradley, W.B., 1979. "The Effect of Temperature on Tensile and Compressive Strengths and Young's Modulus of Oil Shale". Society of Petroleum Engineers, Journal, 19, pp. 301-312.

Closmann, P.J. and Phocas, D.M., 1978. "Thermal Stresses near a Heated Fracture in Transversely Isotropic Oil Shale". Society of Petroleum Engineers Journal, AIME, February, 1978, pp. 59-74.

Coates, D.F., 1981. "Rock Mechanics Principles". Published by Canadian Centre for Mineral and Energy Technology, Energy, Mines and Resources Canada, Monograph 874.

Collins, H.N., 1974. "Log-Core Correlations in the Athabasca Oil Sands". Proceedings of the Annual Fall Meeting of the Society of Petroleum Engineers, American Institute of Mining, Metallurgical and Petroleum Engineers, Paper SPE 5037, 18 p.

Cominco Engineering Services Ltd. and Norwest Resources Consultants Ltd., 1985. "Application of Conventional Mining Techniques to Underground Oil Sands Mining". Prepared for the Department of Supply and Services, Canada Centre for Mineral and Energy Technology, Energy, Mines and Resources, Canada, Aug., Report No. 84-473/1, 233 p.

Cook, N.G.W., 1983. "Effects of Joints on Thermally Induced Displacements and Stresses". Proceedings of the 24th U.S. Symposium on Rock Mechanics, Texas A & M University, pp. 303-308.

Cooper, H.W. and Simmons, G., 1977. "The Effects of Cracks on Thermal Expansion of Rocks". Earth Planetary and Scientific Letters, 36, pp. 404-413.

Cornforth, D.H., 1964. "Some Experiments on the Influence of Strain Conditions on the Strength of Sand". Geotechnique, Vol. 14, No. 2, pp. 143-167.

Cowell, M.J. and Thrall, F.G., 1983. "The Influence of Processing on the Planning of Tar Sand Waste Disposal Facilities". Proceedings of the National Meeting of the American Institute of Chemical Engineers, Denver, Aug., 23 p.

Cox, D.O., 1978. "Generalizations of the Heat Balance for Thermal Recovery Projects". Proceedings of the Fifth Symposium on Improved Methods for Oil Recovery, Society of Petroleum Engineers of AIME, Tulsa, Oaklahoma, pp. 451-458.

Cramer, M.L., Cunningham, J.P. and Kim, K., 1983. "Rock Mass Deformational Properties from a Large Scale Block Test". Proceedings of the 24th U.S. Symposium on Rock Mechanics, Texas A & M University, pp. 267-270.

Cryer, C.W., 1963. "A Comparison of the Three-Dimensional Consolidation Theories of Biot and Terzaghi". Quarterly Journal of Mechanics and Applied Mathematics, Vol. 16, No. 4, pp. 401-412.

Cuderman, J.F., 1984. "Rock Mechanics Effects Observed Subsequent to Multiple Fracturing of Wellbores". Proceedings of the 25th U.S. Symposium on Rock Mechanics, Evanston, Ill.

Cullity, B.D., 1956. "Elements of X-Ray Diffraction". Addison-Wesley Publishing Co., Inc., Reading, Massachusetts, 1956, 514 p.

Cummins, A.B. and Given, I.A. (Editors), 1973. "SME Mining Engineering Handbook (Volumes I and II)". Society of Mining Engineers of the American Institute of Mining, Metallurgical, and Petroleum Engineers, Inc., New York, 2615 p.

Curry, D.M. and Cox, J.E., 1971. "Two-Dimensional Analysis of Heat and Mass Transfer in Porous Media". Environmental and Geophysical Heat Transfer, Vol. 4, American Society of Mechanical Engineers (ASME), Heat Transfer Division, pp. 9-19.

Daniel, D.E., 1983. Shallow Land Burial of Low-Level Radioactive Waste. American Society of Civil Engineers, Journal of Geotechnical Engineering, Vol. 109, No. 1, January 1983, pp. 40-55.

Datta, M., Gulhati, S.K. and Rao, G.V., 1980. "Crushing of Calcareous Sands During Drained Shear". Journal of SPE, Vol. 20, pp. 77-85.

Davidson, L.B., 1969. "The Effect of Temperature on the Permeability Ratio of Different Fluid Paris in Two-Phase Systems". Journal of Petroleum Technology, August 1969, pp. 1037-1046.

Davis, S.N., 1982. "Hydrogeology of Radioactive Waste Isolation". Geological Society of America, Special Paper 189, 1982, pp. 389-395.

Dealy, J.M., 1979. "Viscosity of Oil Sands Liquids". Progress Report to AOSTRA, 1979, Department of Chemical Engineering, McGill University, Montreal, Quebec.

Dealy, J.M., 1979. "Rheological Properties of Oil Sand Bitumens". Canadian Journal of Chemical Engineering, Vol. 57(6), 677 p.

Delaney, P.T., 1982. "Rapid Intrusion of Magma into Wet Rock: Groundwater Flow Due to Pore Pressure Increases". Journal of Geophysical Research, Vol. 87, No. B9, September 10, 1982, pp. 7739-7756.

Demaison, G.J., 1977. "Tar Sands and Supergiant Oil Fields". In The Oil Sands of Canada-Venezuala. Edited by D.A. Redford and A.G. Winestock, CIM Special Volume 17, pp. 9-16.

Devenny, D.W., 1977. "Oil Sand Tailings Integrated Planning to Provide Long-Term Stabilization". Proceedings of the Annual General Meeting of the Canadian Land Reclamation Association, Edmonton, Alberta, Aug., 18 p.

Devenny, D.W., 1975. "Subsidence Problems Associated with Reclamation at Oil Sands Mines". Proceedings of the Tenth Canadian Rock Mechanics Symposium, Queen's University, Kingston, Ontario, Sept., pp. 161-180.

Devenny, D.W. and Raisbeck, J.M., 1980. "Rock Mechanics Considerations for In-situ Development of Oil Sands". In CIM Special Volume 22, Underground Rock Engineering, 13th Canadian Rock Mechanics Symposium, Toronto, 1980, pp. 90-95.

Doucet, R., 1984. "Drilling and Blasting in Tarsand". Presented by Suncor Inc. Oil Sands Group, Proceedings of the Blasting Seminar, San Diego, CA.

Duncan, J.M., Bryne, P., Wong, K.S. and Mabry, P., 1980. "Strength, Stress-Strain and Bulk Modulus Parameters for Finite Element Analyses of Stresses and Movements in Soil Masses". Report No. UCB/GT/80-01, College of Engineering, Office of Research Services, University of California, Berkley, 80 p.

Duncan, J.M. and Chang, C.Y., 1970. "Non-linear Analysis of Stress and Strain in Soils". Proceedings, Journal of Geotechnical Engineers, American Society of Civil Engineers, Vol. 96, pp. 1629-1654.

Durham, W.B. and Abey, A.E., 1981. "Thermal Conductivity and Diffusivity of Climax Stock Quartz Monzonite at High Pressure and Temperature". Proc. of the 17th Int. Conf. on Thermal Conductivity, ed. by J.G. Hust, Plenum Press, N.Y., pp. 459-468.

Dusseault, M.B., 1985. "Fluid Injection Design to Preclude Induced Shear Failure of Formations". Proceedings of the 36th Annual Technical Meeting, Petroleum Society of the Canadian Institute of Mining and Metallurgy, pp. 77-83.

Dusseault, M.B., 1984. "Determination of Geomechanical Parameters from Geophysical Logs". AAPG Research Conference on Exploration for Heavy Crude Oil and Bitumen, Santa Maria, California, Nov. 1984, 13 p.

Dusseault, M.B., 1983. Personal Communication.

Dusseault, M.B., 1982. "Identifying Reservoirs Susceptible to Subsidence due to Fluid Withdrawal". Proceedings of the Forum on Subsidence due to Fluid Withdrawal, U.S. Department of Energy and Republic of Venezuela Ministry of Energy and Mines, Oklahoma, U.S.A., Nov. 14-17, Nov., pp. 6-14.

Dusseault, M.B., 1981. "Liquefaction of Low-Permeability Cohesionless Sand-stones by Gas Expansion". Seminar on Liquefaction of Soils, INTEVEP S.A. Caracas, Venezuela, 15 p.

Dusseault, M.B., 1980. "Sample Disturbance in Athabasca Oil Sands". Journal of Canadian Petroleum Technology, Vol. 19, No. 2, pp. 85-92.

Dusseault, M.B., 1980. "The Behavior of Hydraulically Induced Fractures in Oil Sands". Underground Rock Engineering, Canadian Institute of Mining and Metallurgy Special Volume 22, 13th Canadian Rock Mechanics Symposium, Toronto, pp. 36-41.

Dusseault, M.B., 1980. "The Development of Permeability in Cohesionless Bituminous Sands". Proceedings of the Tar Sands Permeability Enhancement Seminar, Sandia National Laboratories, Albuquerque, New Mexico, Proceeding Published 1981, pp. 45-84.

Dusseault, M.B., 1979. "A Conceptual Geomechanical Model for Hydraulic Fracture in the Athabasca Oil Sands". University of Alberta, Preprint, 44 p.

Dusseault, M.B., 1979. "Stress and Volume Changes in Gas-Saturated Very Dense Sands". Proceedings of the First International Conference on the Future of Heavy Crudes and Tar Sands, United Nations Institute for Training and Research, Edmonton, Alberta, June, pp. 312-320.

Dusseault, M.B., 1979. "Undrained Volume and Stress Change Behavior of Unsaturated Very Dense Sands". Canadian Geotechnical Journal, Vol. 16, No. 4, pp. 627-640.

Dusseault, M.B., 1978. "Stress State and Hydraulic Fracturing in the Athabasca Oil Sands". The Oil Sands of Canada-Venezuela 1977, Canadian Institute of Mining and Metallurgy Special Volume 17, D.A. Redford and A.G. Winestock, eds., Edmonton, pp. 27-35.

Dusseault, M.B., 1977. "Stress State and Hydraulic Fracturing in the Athabasca Oil Sands". Journal of Canadian Petroleum Technology, Vol. 16, No. 3, pp. 19-27.

Dusseault, M.B., 1977. "The Geotechnical Characteristics of Athabasca Oil Sands". Ph.D. Thesis, University of Alberta, Edmonton, 1977.

Dusseault, M.B., Cimolini, P., Soderberg, H. and Scafe, D.W., 1983. "Rapid Index Tests for Transitional Material". Geotechnical Testing Journal, American Society for Testing and Materials, Vol. 6, No. 2, pp. 64-72.

Dusseault, M.B. and Morgenstern, N.R., 1979. "Locked Sands". Quarterly Journal of Engineering Geology, Vol. 12, No. 2, pp. 117-131.

Dusseault, M.B. and Morgenstern, N.R., 1978a. "Characteristics of Natural Slopes in the Athabasca Oil Sands". Canadian Geotechnical Journal, Vol. 15, pp. 202-215.

Dusseault, M.B. and Morgenstern, N.R., 1978b. "Shear Strength of Athabasca Oil Sands". Canadian Geotechnical Journal, Vol. 15, pp. 216-238.

Dusseault, M.B. and Morgenstern, N.R., 1978c. "Locked Sands". University of Alberta, Department of Civil Engineering, Internal Memorandum.

Dusseault, M.B. and Morgenstern, N.R., 1977. "Sampling and Testing of Athabasca Oil Sands for Stability Studies". The Oil Sands of Canada-Venezuela 1977, Canadian Institute of Mining and Metallurgy Special Volume 17, D.A. Redford and A.G. Winestock, eds., Edmonton, pp. 260-269.

Dusseault, M.B. and Nyland, E., 1983. "Passive Seismic Monitoring of In Situ Processes for Energy Recovery". Proceedings of the Conference on Field Measurements in Geomechanics, Zurich, Switzerland, 15 p.

Dusseault, M.B. and Nyland, E., 1982. "Fireflood Microseismic Monitoring: Rock Mechanics Implications". In Proceedings of the Twenty-third Symposium on Rock Mechanics, Berkley, California, Published by the Society of Mining Engineers of AIME, pp. 1065-1076.

Dusseault, M.B. and Scafe, D.W., 1984. "The Effect of Vermiculitic Mixed-Layer Clays on the Residual Strength of the Clayey Basal Unit of the McMurray Formation". Quarterly Journal of Engineering Geology, Vol.

Dusseault, M.B. and Scafe, D.W., 1979. "Mineralogical and Engineering Index Properties of the Basal McMurray Formation Clay-Shales". Canadian Geotechnical Journal, Vol. 16, pp. 285-294.

Dusseault, M.B. and Scott, J.D., 1984. "Coring and Sampling in Heavy Oil Exploration: Difficulties and Proposed Cures". Proceedings of the American Association of Petroleum Geologists Research Conference on Exploration for Heavy Crude Oil and Bitumen, Santa Maria, California, Oct. 29 to Nov. 2, 16 p.

Dusseault, M.B. and Scott, J.D., 1983. "Tailings Pond Behavior and Characterization of Oil Sand Tailings Sludge". Journal of Particulate Science and Technology, Vol. 1, pp. 295-309.

Dusseault, M.B. and Scott, J.D., 1982. "Characterization of Oil Sand Tailings Sludge". Proceedings of the Short Course on Consolidation Behavior of Fine Grained Waste Materials, Bromwell Engineering, Denver, Colorado, Oct., 35 p.

Dusseault, M.B. and Simmons, J.V., 1982. "Injection Induced Stress and Fracture Orientation Changes". Canadian Geotechnical Journal, Vol. 19, No. 4, November 1982, pp. 483-498.

Dusseault, M.B., Soderberg, H. and Sterne, K., 1984. "Preparation Techniques for Oil Sand Testing". Geotechnical Testing Journal, American Society for Testing and Materials, Vol. 7, No. 1, pp. 3-9.

Dusseault, M.B., Soderberg, H. and Sterne, K., 1981. "Sample Preparation and Testing Techniques for Oil Sands". Proceedings of the 34th Canadian Geotechnical Conference, Fredericton, New Brunswick, Oct., 23 p.

Dusseault, M.B. and Sterne, K.B., 1980. University of Alberta, Department of Civil Engineering, Edmonton, Alberta, Personal Communication.

Dusseault, M.B. and Van Domselaar, H.R., 1982. "Canadian and Venezuelan Oil Sand: Problems and Analysis of Uncemented Gaseous Sand Sampling". Proceedings of the Engineering Foundation Conference on Updating Subsurface Sampling of Soils and Rocks and Their In-Situ Testing, Santa Barbara, California, Jan., 20 p.

Dusseault, M.B. and Van Domselaar, H.R., 1982. "Unconsolidated Sand Sampling in Canadian and Venezuelan Oil Sands". Revista Tecnica Intevep, Vol. 2, No. 2, pp. 165-174.

Dusseault, M.B. and Van Domselaar, H.R., 1982. "Unconsolidated Sand Sampling in Canadian and Venezuelan Oil Sands". Second Unitar Conference on the Future of Heavy Crudes and Tar Sands, Caracas, Venezuela.

Edmonson, T.A., 1965. "Effect of Temperature on Waterflooding". Petroleum Society of CIM, Heavy Oil Seminar, Calgary, Alberta, May 5, 1965, pp. 236-242.

Edmunds, N.R., Wong, A., McCormack, M.E. and Suggett, J.C., 1987. "Design of Horizontal Well Completions, AOSTRA Underground Test Facility". Fourth Annual Heavy Oil and Oil Sands Symposium at the University of Calgary, February 18, 1987, Paper No. 2.

Eisenstein, Z. and Law, S.T.C., 1979. "The Role of Constitutive Laws in Analysis of Embankments". Third International Conference on Numerical Methods in Geomechanics, Edited by W. Wittke, Aachen, April 2-6, 1979, pp. 1413-1430.

Eisenstein, Z. and Medeiros, L.V., 1983. "Deep Retaining Structure in Till and Sand". Canadian Geotechnical Journal, Vol. 20, No. 1, pp. 131-140.

Elliott, G.M. and Brown, E.T., 1985. "Yield of a Soft High Porosity Rock". Geotechnique, Vol. 35, No. 4, pp. 413-423.

Ells, S.C., 1930. "Core Drilling Bituminous Sands of Northern Alberta". Investigations of Mineral Resources and the Mining Industry, pp. 28-46.

Energy Development Consultants Inc., Golden CO., 1983. "Evaluation of Heavy Oil Mining - Final Report, Volume II". Technical Information, U.S. Department of Energy, Rept. DE83011338, 316 p.

Energy Development Consultants Inc., Golden CO., 1983. "Evaluation of Heavy Oil Mining - Final Report, Volume 1". Technical Information, U.S. Department of Energy, Rept. DE83011339, 266 p.

Energy Resources Conservation Board of Alberta, 1976. "Geology and Proved In-Place Reserves of the Wabasca Oil Sands Deposit". Calgary, Alberta, May 1976.

Energy Resources Conservation Board of Alberta, 1974. "Geology and Proved In-Place Reserves of the Peace River Oil Sands Deposits". Calgary, Alberta, October 1974.

Energy Resources Conservation Board of Alberta, 1973. "Geology and Proved In-Place Reserves of the Cold Lake Oil Sands Deposits". Calgary, Alberta, September, 1973.

Enniss, D.O., Butters, S.W., McFarland, C.B. Jr. and Jones, A.H., 1979. "Capabilities to Determine Rock Properties at Simulated Geothermal Conditions". Transactions of the American Society of Mechanical Engineers, Journal of Energy Resources Technology, Volume 101, No. 117, pp. 117-123.

Facca, G., 1980. "Geothermal Energy Development: An Historic Summary". Geothermal Energy, Vol. 8, No. 10 & 11, October-November 1980, 12 p.

Fair, A.E. and Hanford, T.G., 1986. "Overview of the Tailings Dyke Instrumentation Program at Syncrude Canada Ltd.". Proceedings of the International Symposium on Geotechnical Stability in Surface Mining, Calgary, Alberta, Nov. 6-7, pp. 245-253.

Fair, A.E. and Issac, B.A., 1985. "Highwall Stability Monitoring at Syncrude Canada Ltd., Open Pit Mining Operation". Proceedings of the 13th Annual Meeting of the Mining and Metallurgy Industries, Salt Lake City, Utah, U.S.A., May, 10 p.

Fair, A.E. and Lord, E.R.F., 1984. "Methods used to Monitor and Control Block Slides in Oilsands at Syncrude's Dragline Operation in Northern Alberta, Canada". Preprints of the 37th Canadian Geotechnical Conference, Canadian Geotechnical Society, Toronto, Canada, Sept. 17, pp. 103-112.

Farouq-Ali, S.M., 1982. "Integrated Simulation of Oil and Gas Production and the Accompanying Rock Deformations". Proceedings of the Fourth International Conference on Numerical Methods in Geomechanics, Edmonton, Alberta, Volume 3, pp. 1081-1090.

Farouq-Ali, S.M., 1981. "Elements of Reservoir Modelling". Department of Mineral Engineering, University of Alberta, Edmonton, Alberta, 64 p.

Farouq-Ali, S.M., 1974. "Application of In Situ Methods of Oil Recovery from Tar Sands". In Oil Sands Fuel of the Future, Canadian Society of Petroleum Geologists, Calgary, pp. 199-212.

Farouq-Ali, S.M., 1967. "Fluid Viscosity, Its Estimation, Measurement and Role in Thermal Recovery". Producers Monthly, pp. 20-25.

Fertl, W.H., 1979. "Evaluation of Heavy Oil and Tar Sand Deposits using Geophysical Well Logging Techniques in Open and Cased Wellbores". Proceedings of the First International Conference on the Future of Heavy Crudes and Tar Sands, United Nations Institute for Training and Research, Edmonton, Alberta, June, pp. 283-294.

Fertl, W.H. and Chilingarian, G.V., 1978. "Formation Evaluation of Tar Sands using Geophysical Well-Logging Techniques". Bitumens, Asphalts, and Tar Sands, pp. 260-276.

Fertl, W.H. and Chilingarian, G.V., 1978. "Tar Sand Evaluation using Geophysical Well Logs". Energy Sources, Vol. 3, No. 3/4, pp. 375-384.

Fetzner, R.W., Henson, W.L. and Feigl, F.J., 1966. "Athabasca Oil Sand Evaluation using Core and Log Analysis and Geological Data Processing Methods". Proceedings of the Seventh Logging Symposium, Society of Professional Well Log Analyst, Tulsa, May, 13 p.

Finn, F.N., 1951. "The Effect of Temperature on Consolidation Characteristics of Remoulded Clay". ASTM, STP No. 120, pp. 65-71.

Finnie, I., Cooper, G.A. and Berlie, J., 1979. "Fracture Propagation in Rock by Transient Cooling". International Journal of Rock Mechanics, Mining Science and Geomechanics Abstract, Vol. 16, pp. 11-21.

Fisekci, M.Y. and Stuart, N.J., 1985. "Initial Field Application/Tests of Telemetry System to Monitor Stability of Highwall and Tailings Areas at the Syncrude Oil Sands Open Pit Mine". CANMET, Coal Research Laboratories Division Report ERP/CRL 85-96(TR), 17 p.

Fredlund, D.G., 1976. "Density and Compressibility Characteristics of Air-Water Mixtures". Canadian Geotechnical Journal, Vol. 13, pp. 386-396.

Freeze, R.A. and Cherry, J.A., 1979. "Groundwater". Prentice-Hall International, Inc., London, 604 p.

Friedman, G.M., 1964. "Early Diagenesis and Lithification in Carbonate Sediments". Journal Sed. Petrology, 34, pp. 777-813.

Frydman, S., 1972. "An Inquiry into the Stress-Strain Behaviour of Particulate Media". D.Sc. Thesis, Technion-Israel Institute of Technology, Haifa, April 1972, 240 p.

Frydman, S., 1968. "The Effect of Stress History on the Stress Deformation Behaviour of Sand". M.Sc. Thesis, Technion-Israel Institute of Technology, Haifa, 170 p.

Fuel and Mineral Resources, Inc., Reston, Va., 1984. "Detailed Technical and Economic Feasibility of Light Oil Mining in the United States - Final Report". Technical Information, U.S. Department of Energy, Rept. DE84015848, 483 p.

Fung, Y.C., 1965. "Foundations of Solid Mechanics". Prentice-Hall, Inc., Englewood Cliffs, New Jersey, 1965, 525 p.

Gale, A.D., Sego, D.C. and Morgenstern, N.R., 1987. "Geotechnical Properties of Ice Rubble". NSERC Strategic Grant No. G1106, Ice Rubble Mechanics, Report No. 3, 195 pp.

Gallup, W.B., 1960. "Current Exploratory Techniques in the Athabasca Bituminous Sands Area". Transactions of the Canadian Institute of Mining and Metallurgy, Vol. 63, pp. 157-161.

Garg, S.K., Pritchett, J.W., Rice, M.H. and Riney, T.D., 1977. "U.S. Gulf Coast Geopressured Geothermal Reservoir Simulation". Systems, Science and Software Report No. SSS-R-77-3147, University of Texas at Austin and U.S. Energy Research and Development Administration Contract E (40-1)-5040, February 1977, 113 p.

Gates, E.M. and Gilpin, R.R., 1982. "Downhole Jet Piercing of Oil Sands". Proceedings of the 33rd Annual Technical Meeting of the Canadian Institute of Mining and Metallurgy, Calgary, Alberta, June, Preprint, Paper 82-33-13, 7 p.

Gates, E.M. and Gilpin, R.R., 1978. "Jet Cutting of Oil Sand". In AOSTRA Seminar on Underground Excavation in Oil Sand, University of Alberta, Edmonton, Alberta, Paper No. 10, 14 p.

Gates, E.M. and Toogood, R.W., 1984. "A Model for Jet Piercing of Oil Sands". Proceedings of the Energy Sources Technology Conference, American Society of Mechanical Engineers, New Orleans, Feb., Preprint 84-PET-17, 8 p.

Gates, E.M., Toogood, R.W. and Simms, B.W., 1984. "A Model for Drilling by High Pressure Water Jet". Proceedings of the Seventh International Symposium on Jet Cutting Technology, National Research Council of Canada, Ottawa, June, pp. 221-236.

Geertsma, J., 1974. "Estimating the Coefficient of Inertial Resistance in Fluid Flow Through Porous Media". Society of Petroleum Engineers of American Institute of Mining Engineers Journal, Vol. 14, pp. 445-451.

Geertsma, J., 1973a. "Survey of Rock Mechanics Problems Associated with the Extraction of Mineral Fluids from Underground Formations". Proceedings of the Third Congress of the International Society for Rock Mechanics, Vol. 1, Part B, May 1973, pp. 1471-1481.

Geertsma, J., 1973b. "Land Subsidence Above Compacting Oil and Gas Reservoirs". Transactions of the American Institute of Mining Engineers, Vol. 255, 1973, pp. 734-744.

Ghaboussi, J. and Wilson, E.L., 1972. "Variational Formulation of Dynamics of Fluid Saturated Porous Elastic Solids". Journal of Engineering Mechanics Division of ASCE, Vol. 98, No. EM4, pp. 947-963.

Giguere, R.J., 1976. "An In Situ Recovery Process for the Oil Sands of Alberta". 26th Chemical Engineering Conference, Symposium on Tar Sands, Toronto, Ontario, 1976.

Gilpin, R.R. and Gates, E.M., 1981. "Jet Piercing of Oil Sands". Journal of Energy Resources Technology, Vol. 103, No. 4, pp. 330-335.

Gilpin, R.R., Gates, E.M. and Chau, W.T.R., 1980. "Jet Cutting of Oil Sands". Proceedings of the Fifth International Symposium on Jet Cutting Technology, Hanover, Federal Republic of Germany, June, pp. 427-438.

Gobran, B.D., 1981. "Permeability of Unconsolidated Sands and Sandstone with Temperature, Pore Pressure and Confining Pressure". Ph.D. Dissertation, Stanford University, 210 p.

Gobran, B.D., Brigham, W.E. and Ramey, H.J., 1981. "Absolute Permeability as a Function of Confining Pressure, Pore Pressure and Temperature". Society of Petroleum Engineers of the American Institute of Mining Engineers, Proceedings 56th Annual Fall Technical Conference, San Antonio, Texas, October 5-7, 1981.

Goetze, C., 1971. "High Temperature Rheology of Westerly Granite". Journal of Geophysical Research, 76, pp. 1223-1230.

Golder Associates, 1979. "Investigation of Waterways Formation Limestones". Prepared for Canada Department of Energy, Mines and Resources, Contract No. OSQ78-00106, 250 p.

Golder Associates, Inc., Kirkland, WA, 1978. "Oil Mining - A Technical and Economic Feasibility Study of Oil Production by Mining Methods". Technical Information, U.S. Department of Energy, Rept. PB-297134, 293 p.

Golder, H.Q. and Akroyd, T.N., 1959. "An Apparatus for Triaxial Compression Tests at High Pressures". Geotechnique, Vol. 4, pp. 131-136.

Goldstein, J.I. and Yakowitz, H., 1975. "Practical Scanning Electron Microscopy". Plenum Press, New York, 1975, 582 p.

Grandone, P. and Holleyman, J.B., 1949. "Injection Rates and Pressures for Water Flooding Mid-Continent Oil Sands". U.S. Department of the Interior, Bureau of Mines, Report of Investigations 4600, 31 p.

Green, G.E., 1971. "Strength and Deformation of Sand Measured in an Independent Stress Control Cell". Proceedings, Roscoe Memorial Symposium on Stress-Strain Behaviour of Soils, Cambridge, pp. 285-323.

Green, G.E., 1969. "Strength and Compressibility of Granular Materials Under Generalized Strain Conditions". Ph.D., University of London.

Green, S.L., 1984. "The Behaviour of Deep Ocean Sediments in Response to Thermo-Mechanical Loading". Ph.D. Thesis, University of California, Berkley.

Greg, D.W., 1980. "Relative Merits of Alternate Linking Techniques for Underground Coal Gasification and Their System Design Implications". In Situ, 4(3), pp. 207-236.

Greg, D.W., 1977. "Ground Subsidence Resulting from Underground Gasification of Coal". Lawrence Livermore Laboratory, Report UCRL-52255, 42 p.

Greg, D.W., Hill, R.W. and Olness, D.U., 1976. "An Overview of the Soviet Effort in Underground Gasification of Coal". Lawrence Livermore Laboratory, Report UCRL-520004, 66 p.

Greg, D.W. and Olness, D.U., 1976. "Basic Principles of Underground Coal Gasification". Lawrence Livermore Laboratory, Report UCRL-52107, 36 p.

Griffin, T.J. and Bush, D.C., 1985. "Core Analysis in Unconsolidated Reservoirs using an Improved Consolidation Technique". Proceedings of the 36th Annual Meeting of the Petroleum Society, CIM, Edmonton, Alberta, June 2-5, pp. 625-643.

Griggs, D.T. and Handin, J., 1960. "Observations on Fracture and an Hypothesis of Earthquakes". In Rock Deformation, Geol. Soc. Am. Mem. 79, pp. 347-364.

Grim, R.E., 1968. "Clay Mineralogy". McGraw-Hill, Toronto, Ontario, 1968, 596 p.

Hackbarth, D.A., 1978. "Hydrogeological Concerns in Underground Excavation, Athabasca Oil Sands Area". In AOSTRA Seminar on Underground Excavation in Oil Sands, University of Alberta, Edmonton, Paper No. 2, 28 p.

Hackbarth, D.A. and Nastasa, N., 1979. "Hydrogeology of the Athabasca Oil Sands Area, Alberta". Alberta Research Council Bulletin.

Hall, C.D. Jr. and Harrisberger, W.H., 1970. "Stability of Sand Arches: A Key to Sand Control". Journal of Petroleum Technology, July, pp. 821-829.

Hall, E.B. and Gordon, B.B., 1963. "Triaxial Testing with Large-Scale Pressure Equipment". Symposium on Laboratory Shear Testing of Soils, ASTM STP 361, pp. 315-328.

Hall, P.B., 1951. "Coring Bituminous Sands". Oil Canada, Vol. 4, No. 50, pp. 34,50.

Hall, P.B., 1951. "Coring of the Bituminous Sands in the Fort McMurray District of Alberta". Proceedings of the Athabasca Oil Sands Conference, King's Printer, Edmonton, Sept., pp. 101-107.

Hanley, E.J., Dewitt, D.P. and Roy, R.F., 1978. "The Thermal Diffusivity of Eight Well Characterized Rocks for the Temperature Range 300-1000 K". Engineering Geology, 12, pp. 31-47.

Hardin, B.O., 1985. "Crushing of Soil Particles". Journal of Geotechnical Engineering, ASCE, Vol. III, No. 10, pp. 1177-1192.

Hardin, E.L., Voegele, M.D., Board, M.P. and Pratt, H.R., 1983. "Development of a Test Series to Determine In Situ Thermomechanical and Transport Properties". Symposium on Measurement of Rock Properties at Elevated Pressures and Temperatures, College Station, Texas, American Society for Testing and Materials, pp.?

Hardy Associates (1978) Limited, 1979. "Athabasca Oil Sands Tailings Disposal Beyond Surface Mineable Limits". Report for Alberta Energy Resources Conservation Board, Alberta Energy and Natural Resources, and Alberta Environment, 2 Volumes.

Hardy Associates Ltd. and Hatch Associates Ltd., 1977. "Feasibility Study for the Underground Mining of Oil Sand". Prepared for Canada Department of Energy, Mines and Resources, 314 p.

Hardy, R.M., 1980. "Expansive Soils and Overconsolidated Clays". Proceedings of the 28th Annual Soil Mechanics and Foundation Engineering Conference, Continuing Education Division of the University of Minnesota, American Society of Civil Engineers, Minnesota Geotechnical Society, Minnesota, Feb., Preprint, 26 p.

Hardy, R.M., 1980. "Implications of the Peculiar Geotechnical Characteristics of Tar Sand to the Design of Viable Open Pit Mining Plants". Oil Sands Geoscience Conference, Edited by M.B. Dusseault, Edmonton, Alberta, 16 p.

Hardy, R.M. and Hemstock, R.A., 1963. "Shearing Strength Characteristics of Athabasca Oil Sands". In The K.A. Clark Volume on the Athabasca Oil Sands, Edited by M.A. Carrigy, Published by The Research Council of Alberta, Information Series No. 45, pp. 109-122.

Hardy, R.M. and Scott, J.D., 1978. "The 1963 G.C.O.S. Test Shaft". In AOSTRA Seminar on Underground Excavation in Oil Sand, University of Alberta, Edmonton, Paper No. 13, 22 p.

Harris, M.C., Poppen, S.A.G. and Morgenstern, N.R., 1979. "Tunnels in Oil Sand". Journal of Canadian Petroleum Technology, Vol. 18, No. 4, pp. 34-40.

Harris, M.C. and Sobkowicz, J.C., 1978. "Feasibility Study of Underground Mining of Oil Sand". In AOSTRA Seminar on Underground Excavation in Oil Sands, 1978, University of Alberta, Edmonton, Paper No. 5, 23 p.

Harris, M.C. and Sobkowicz, J.C., 1977. "Engineering Behaviour of Oil Sand". The Oil Sands of Canada-Venezuala, CIM Special Volume 17, Edited by D.A. Redford and A.G. Winestock, pp. 270-282.

Hart,R.D., 1980. "A Fully Coupled Thermal-Hydraulic-Mechanical Model for Non-Linear Geologic Systems". Ph.D. Dissertation, University of Minnesota, 327 p.

Harrison, D.B., Glaiste, R.P. and Nelson, H.W., 1981. "Reservoir Description of the Clearwater Oil Sand, Cold Lake, Alberta, Canada". In First International Conference on the Future of Heavy Crude Oils and Tar Sands, UNITAR, Edited by R.F. Meyer and C.T. Steele, Chapter 30, pp. 264-280.

Haston, J.A., 1978. "Mine Assisted In Situ Processing". In AOSTRA Seminar on Underground Excavation in Oil Sands, May 19, 1978, University of Alberta, Edmonton, Paper No. 4, 23 p.

Hay, R.S. and Evans, J.B., 1983. "Grain Boundary Grooving of Calcite Bicrystals". Proceedings of the 24th U.S. Symposium on Rock Mechanics, Texas A & M University, pp. 469-472.

Heald, B.D., 1983. "A Geotechnical Investigation of the Devonian Waterways Formation at the Sandalta Lease". Thesis Presented to the University of Alberta, Edmonton, Alberta, in Partial Fulfillment of the Requirements for the Master Degree, 375 p.

Heard, H.C., 1982. "Mechanical, Thermal and Fluid Transport Properties of Rock at Depth". In Proceedings of the Twenty-Third Symposium on Rock Mechanics, Berkley, California, Published by the Society of Mining Engineers of the American Institute of Mining, Metallurgical and Petroleum Engineers, Inc., New York, pp. 249-260.

Heard, H.C., 1980. "Thermal Expansion and Inferred Permeability of Climax Quartz Monozonite to 300°C and 27.6 MPa". International Journal of Rock Mechanics, Mining Sciences and Geomechanics Abstracts, 17, pp. 289-296.

Heard, H.C., 1960. "Transition from Brittle to Ductile Flow in Solenhofen Limestone as a Function of Temperature, Confining Pressure and Institial Fluid Pressure". In Rock Deformation, Geol. Soc. Amer. Mem. 79, pp. 193-226.

Heard, H.C. and Page, L., 1982. "Elastic Moduli, Thermal Expansion and Inferred Permeability of Two Granites to 350°C and 55 Megapascals". Journal of Geophysical Research, Vol. 87, No. B11, pp. 9340-9348.

Heard, H.C. and Raleigh, C.B., 1971. "Steady-State Flow in Marble at 500°C to 800°C". Geological Society of America Bulletin.

Henkel, D.J., 1959. "The Relationships Between the Strength, Pore Water Pressure and Volume-Change Characteristics of Saturated Clays". Geotechnique 9, pp. 119-135.

Hennig-Michaeli, C. and Siemes, H., 1982. "Compression Experiments on Natural Magnetite Crystals at 200°C and 400°C at 400 MPa Confining Pressure". In Proceedings of the Twenty-Third Symposium on Rock Mechanics, Berkley, California, Published by the Society of Mining Engineers of the American Institute of Mining Engineers, New York, pp. 380-388.

Heuze, F.E., 1983a. "High Temperature Mechanical, Physical and Thermal Properties of Granitic Rocks - A Review". International Journal of Rock Mechanics, Mining Sciences and Geomechanical Abstracts, Vol. 20, No. 1, pp. 3-10.

Heuze, F.E., 1983b. "Thermal and Thermomechanical Calculations of Deep-Rock Nuclear Waste Disposal with the Enhanced SANGRE Code". Lawrence Livermore Laboratory, University of California, Manuscript UCRL-53394, 42 p., Published by

Heuze, F.E., 1981. "On the Geotechnical Modelling of High Level Nuclear Waste Disposal by Rock Melting". Lawrence Livermore Laboratory, University of California, Manuscript UCRL-53183, 53 p., Published by National Technical Information Service, U.S. Department of Commerce, Springfield, VA 22161. National Technical Information Service, U.S. Department of Commerce, Springfield, VA 22161.

Highway Research Board, 1969. "Effects of Temperature and Heat on the Engineering Behavior of Soil". Special Report 103, 225 p.

Hilchie, D.W., 1982. "Applied Openhole Log Interpretation". Douglas H. Hilchie Inc., Golden, Colorado.

Hinga, K.R., 1982. "Ocean Research Conducted for the Subseabed Disposal Program". EOS, Transactions, American Geophysical Union, Vol. 63, No. 40, October 5, 1982, pp. 802-803.

Hinga, K.R., Heath, G.R., Anderson, D.R. and Hollister, C.D., 1982. "Disposal of High-Level Radioactive Wastes by Burial in the Sea Floor". Environment Science Technology, No. 16, pp. 28A-37A.

Hirschfeld, R.C. and Poulos, S.J., 1963. "High Pressure Triaxial Tests on Compacted Sand and Undisturbed Silt". Symposium on Laboratory Shear Testing of Soils, ASTM STP 361, pp. 329-339.

Hoek, E. and Brown, E.T., 1980. "Underground Excavations in Rock". Published by the Institute of Mining and Metallurgy, London, 527 p.

Hoekstra, P., Henderson, J.D. and Kaufman, A.A., 1980. "Geophysical Surveys for Oilsands Exploration". Proceedings of Applied Oilsands Geoscience '80 Conference, Edmonton, Alberta, June 11 to 13, 33 p.

Holman, J.P., 1976. "Heat Transfer". McGraw-Hill Book Company, New York, 4th Edition, 1976, 528 p.

Holzhausen, G.R., Wood, M.D., Raisbeck, J.M. and Card, C.C., 1980. "Results of Deformation Monitoring During Steam Stimulation in a Single Well Test". Applied Oilsands Geoscience, Edited by M.B. Dusseault, University of Alberta, Edmonton, Alberta, June 1980.

Horkoff, C.T., 1982. "Evaluation of Bitumen Resource Development Utilizing Horizontal Wells Drilled from the Surface or from Underground Tunnels". Proceedings of the Second International Conference on the Future of Heavy Crude and Tar Sands, United Nations Institute for Training and Research, Caracas, Venezuela, Feb., pp. 903-906.

Horsrud, P., Risnes, R. and Bratli, R.K., 1982. "Fracture Initiation Pressures in Permeable Poorly Consolidated Sands". International Journal of Rock Mechanics, Mineral Science and Geomechanics Abstract, Vol. 19, pp. 255-266, Dec. 1982.

Hoskins, W.MN., Upadhyay, R.P., Bills, J.B. and Sanberg, C.R., 1977. "A Technical and Economic Study of Candidate Underground Mining Systems for Deep, Thick Oil Shale Deposits". Quarterly of the Colorado School of Mines, pp. 199-234.

Houston, S.L., Houston, W.N. and Williams, N.D., 1985. "Thermal Mechanical Behaviour of Seafloor Sediments". Journal of Geotechnical Engineering, ASCE, Vol. III, No. 11, November 1985, pp. 1249-1263.

Hsu, T.R., Chen, G.G. and Gong, Z.L., 1985. "A Technique for the Measurement of Dynamic Mechanical Properties of Oil Sands". Journal of Petroleum Technology, May-June, pp. 63-68.

Hsu, T.R., Pizey, G. and Ashour, H.A., 1984. "On an Analytical Method for In Situ Fracture of Oil Sands Formation". Proceedings of the 35th Annual Technical Meeting of the Canadian Institute of Mining and Metallurgy, Calgary, Alberta, June, Preprint, Paper 84-35-44, 13 p.

Hsu, T.R., Scott, J.D. and Plewes, H.D., 1985. "Dynamic Fracturing of Oil Sands". Proceedings of the Heavy Oil and Oil Sands Technical Symposium - Challenges and Innovations 1985, University of Calgary, Calgary, Alberta, Feb. 20, 30 p.

Hume, G.S., 1951. "Drilling and Sampling Bituminous Sand Deposits". Proceedings of the Athabasca Oil Sands Conference, King's Printer, Edmonton, Sept., pp. 98-100.

Hume, G.S., 1949. "Drilling and Sampling of Bituminous Sands of Northern Alberta, Volume 1: Results of Investigations 1942-1947; Volume 2: Detailed Drilling and Sampling Reocrds; Volume 3: Cross Sections and Plans of Ores Drilled". Canada Mines Branch Publication 826, Ottawa.

Hume, G.S., 1947. "Results and Significance of Drilling Operations in the Athabasca Bituminous Sands". Transactions of the Canadian Institute of Mining and Metallurgy, Vol. 50, pp. 298-333.

Hungr, O. and Morgenstern, N.R., 1980. "A Numerical Approach to Predicting Stresses and Displacements Around a Three-Dimensional Pressurized Fracture". Internal Report, Department of Civil Engineering, University of Alberta, Edmonton, Alberta, April 1980.

Hutcheon, W.L., 1958. "Moisture Flow Induced by Thermal Gradients within Soils". Special Report No. 40, Highway Research Board, National Research Council, Washington, D.C., pp. 113-133, 1958.

Hutchins, J.S., Bond, E. and Bass, D.M., 1978. "Mining for Petroleum: Feasibility Study". U.S. Department of the Interior, Bureau of Mines, Open File Rept. 56-79, 363 p.

Huygen, H.A. and Lowry, W.E., 1983. "Steamflooding Wabasca Tar Sand Through the Bottomwater Zone-Scaled Model Tests". Society of Petroleum Engineers Journal, Vol. 23, No. 1.

Hwang, C.T., Morgenstern, N.R. and Murray, D.T., 1971. "On Solutions of Plane Strain Consolidation Problems by Finite Element Methods". Canadian Geotechnical Journal, Vol. 8, No. 1, pp. 109-118.

Imperial Oil Limited, 1978. "The Cold Lake Project: A Report to the Energy Resources Conservation Board". Calgary, Alberta, 3 Volumes.

Insley, A.E. and Hillis, S.F., 1965. "Triaxial Shear Characteristics of a Compacted Glacial Till Under Unusually High Confining Pressures". Proceedings of 6th International Conference on Soil Mechanics and Foundation Engineering, Vol. 1, pp. 244-248.

Issac, B.A. "Handbook on Mine Monitoring". Chapter 2, Open Pit Applications, Section 2.3, Oilsands, CANMET, 9 p. (In Press).

Issac, B.A. and Dusseault, M.B., 1984. "Mine Design in a Cretaceous Clay Shale". Proceedings of the International Symposium on Landslides, Canadian Geotechnical Society, Toronto, Ontario, pp. 103-108.

Issac, B.A., Dusseault, M.B., Lobb, G.D. and Root, J.D., 1982. "Characterization of the Lower Cretaceous Overburden for Oil Sands Surface Mining within Syncrude Canada Ltd. Leases, Northeast Alberta, Canada". Proceedings of the Fourth International Congress of the International Association of Engineering Geology, New Delhi, India, Dec. 10-15, Vol. 2, pp. II371-II384.

Ishijima, Y. and Rogiers, J.C., 1983. "Fracture Initiation and Breakdown Pressure - Are They Similar?". Proceedings of the 24th U.S. Symposium on Rock Mechanics, Texas A & M University, pp. 761-772.

Jaeger, J.C. and Cook, N.G.W., 1979. "Fundamentals of Rock Mechanics". Chapman and Hall, London, England, 3rd Edition, 593 p.

Janoo, V., 1986. "Drained and Undrained Behavior of Sands Under High Pressures". Ph.D. Thesis, Dept. of Civil, Environmental and Architectural Engineering, University of Colorado, 586 p.

Japanese Society of Mechanical Engineers, 1968. "JSME Steam Tables, 3rd Edition, JSME, Tokyo, Japan, 1968, 116 p.

Jeremic, M.L., 1975. "Tar Sand Influence of Composition on Behavior". Western Miner, Vol. 48, No. 9, pp. 25-28, 30-31.

Jeremic, M.L. and Ronca, L.B., 1981. "The State of Geological Stresses in the Athabasca Oil Sand Deposits". Modern Geology, Vol. 8, No. 1, pp. 43-50.

Jessberger, H.L., 1979. "Shaft Sinking in Oil Sand Formations". Design Parameters in Geotechnical Engineering, British Geotechnical Society, London, Vol. 1, pp. 189-194.

Johnson, B. and Gangi, A.F., 1980. "Thermal Cracking of Non-Uniformly Heated, Thick-Walled Hollow Cylinders of Westerly Granite". Proceedings of the 21st U.S. Symposium on Rock Mechanics, Rolla, Mo., pp. 197-206.

Johnson, B., Gangi, A.F. and Handin, J., 1978. "Thermal Cracking of Rock Subjected to Slow, Uniform Temperature Changes". Proceedings of the 19th U.S. Symposium on Rock Mechanics, University of Nevado-Reno, 1978, pp. 259-267.

Johnson, H.S., 1981. "Hydraulic Mining of Tar Sands". U.S. Patent 4,437,706, Granted to Gulf Canada Limited, July 30, 1981.

Johnson, L.A. Jr., Marchant, L.C. and Cupps, C.Q., 1975. "Properties of Utah Tar Sands - South Seep Ridge Area, PR Springs Deposit". U.S. Department of the Interior, Bureau of Mines, RI 8003, 17 p.

Jones, A.H., Sinha, K.P. and Abou-Sayed, A.S., 1980. "A Review of a Hydraulic Fracture Test in the Tar Sands at Asphalt Ridge, Utah". Proceedings of the Tar Sands Permeability Enhancement Workshop, Albuquerque, New Mexico, May, 27 p.

Karim, G.A. and Hanafi, A., 1981. "The Thermal Conductivity of Oil Sands". The Canadian Journal of Chemical Engineering, Vol. 59, pp. 461-464.

Kern, L.R., 1980. "Use of Weighted Brines in Recovery of Geothermal Energy from Hot Dry Rock". Geothermal Energy, Vol. 8, No. 2, 12 p.

Kersten, M., 1949. "Thermal Properties of Soils". Bulletin No. 28, Engineering Experiment Station, University of Minnesota Institute of Technology, Vol. 52, No. 21, 262 p.

Kessick, M.A., 1977. "Clay Tailings from Alberta Oil Sands and Other Sources - A Review". Alberta Environment Report 1978/2, 87 p.

Khan, F.Z., Fair, A.E. and Cuddy, G., 1982. "Depressurization and Basal Highwall Stability at Syncrude Mine". Proceedings of the Seminar on Geotechnical Aspects of Mine Design and Tailings Containment, Calgary, Alberta, April 15-16.

Kirk, J.S., 1986. "Laboratory Study of Mineralogical Changes During Steam Condensate Flooding of Cold Lake Oil Sands". M.Sc. Thesis, Department of Geology, University of Alberta, 147 p.

Knapp, R.B. and Knight, J.E., 1977. "Differential Thermal Expansion of Pore Fluids: Fracture Propogation and Microearthquake Production in a Hot Pluton Environment". Journal of Geophysical Research, 82, pp. 2515-2522.

Knapp, R.B. and Norton, D., 1981. "Preliminary Numerical Analysis of Processes Related to Magma Crystallization and Stress Evolution in Cooling Pluton Environments". American Journal of Science, 281, pp. 35-68.

Kokelaar, B.P., 1982. "Fluidization of Wet Sediments During the Emplacement and Cooling of Various Igneous Bodies". Journal of the Geological Society, Vol. 139, Part 1, pp. 21-33.

Kolb, C.R., 1962. "Distribution and Engineering Significance of Sediments Bordering the Mississippi from Donaldsonville to the Gulf". Misc. Paper No. 3-481, U.S. Waterways Experimental Station, Vicksburg, Mississippi.

Kondner, R.L., 1963. "Hyperbolic Stress-Strain Response: Cohesive Soils". Proceedings of the American Society of Civil Engineers, Journal of the Soil Mechanics and Foundations Division, SMI, February 1963, pp. 115-143.

Kosar, K.M., 1983. "The Effect of Heated Foundations on Oil Sand". M.Sc. Thesis, University of Alberta, 248 p.

Kosar, K.M., Scott, J.D. and Morgenstern, N.R., 1987. "Testing to Determine the Geotechnical Properties of Oil Sands". Proceedings of the 38th Annual Technical Meeting of the Petroleum Society of CIM, Calgary, June 7-10, 1987, Paper No. 87-38-59, pp. 995-1010.

Kramers, J.W., 1974. "Geology of the Wabasca A Oil Sand Deposit (Grand Rapids Formation)". In Oil Sands, Fuel of the Future, Edited by L.V. Hills, Canadian Society of Petroleum Geologists Memoir No. 3, pp. 68-83.

Kulhawy, F.H. and Duncan, J.M., 1972. "Stresses and Movements in Oroville Dam". Proceedings of the American Society of Civil Engineers, Journal of the Soil Mechanics and Foundations Division, SM7, July 1972, pp. 653-665.

Lachenbruch, A.H., 1980. "Frictional Heating, Fluid Pressure and the Resistance to Fault Motion". Journal of Geophysical Research, Vol. 85, No. B11, pp. 6097-6112.

Lade, P.V. and Duncan, J.M., 1975. "Elastoplastic Stress-Strain Theory for Cohesionless Soils". Journal of the Geotechnical Engineering Division, ASCE, Vol. 101, No. GT10.

Laguros, J.G., 1969. "Effect of Temperature on Some Engineering Properties of Clay Soils". HRB Spe. Rept. 103, pp. 186-193.

Lambe, T.W. and Whitman, R.V., 1969. "Soil Mechanics". John Wiley & Sons, Inc., New York, 553 p.

Lambrechts, J.R. and Leonards, G.A., 1978. "Effects of Stress History on Deformation of Sand". Journal of the Geotechnical Engineering Division, ASCE, Vol. 104, No. GT11, pp. 1371-1387.

Land, L.S., 1967. "Diagenesis of Skeletal Carbonates". Jour. Sed. Petrology, 37, pp. 914-930.

Lane, S., 1983. "Lime Coagulation and Stabilization of Total Oil Sands Tailings". Proceedings of the 34th Annual Technical Meeting of the Canadian Institute of Mining and Metallurgy, Banff, Alberta, May, Preprint, Paper 83-34-33, 17 p.

Langer, M., 1982. "Geotechnical Investigation Methods for Rock Salt". Bulletin of the International Association of Engineering Geologists, No. 25, June 1982, pp. 155-164.

Larson, G. and Chilingar, G.V. (eds), 1967. "Diagenesis in Sediments". Developments in Sedimentology No. 8, Elsevier, Amsterdam, 551 pp.

Laumbach, D.D., 1975. "A High-Accuracy Finite-Difference Technique for Testing the Convective-Diffusion Equation". Society of Petroleum Engineers Journal, AIME, December 1975, pp. 517-531.

Lauriello, P.J., 1974. "Application of a Convective Heat Source to the Thermal Fracturing of Rock". International Journal of Rock Mechanics, Mining Sciences and Geomechanics Abstracts, Vol. 11, pp. 75-81.

Law, K.T., 1981. "Effect of Stress Path Geometry on Soil Brittleness". Geotechnique, Vol. 31, No. 2, pp. 279-287.

Lee, C.F. and Simmons, G.R., 1981. "Thermal Effects on Rock and Fluid Flow". Proceedings of the 9th Waste Management Information Meeting, AECL, Toronto, Ontario, January 1981.

Lee, K.L., 1970. "Comparison of Plane Strain and Triaxial Tests on Sand". ASCE Journal of the Soil Mechanics and Foundation Engineering Division, 96, SM3, pp. 901-923.

Lee, K.L. and Farhoomand, I., 1967. "Compressibility and Crushing of Granular Soil in Anisotropic Triaxial Compression". Canadian Geotechnical Journal, Vol. 4, No. 1, pp. 68-100.

Lee, K.L., Morrison, R.A. and Haley, S.C., 1969. "A Note on the Pore Pressure Parameter B". Proceedings of the 7th International Conference on Soil Mechanics and Foundation Engineering, pp. 231-237.

Lee, K.L. and Seed, H.B., 1967a. "Drained Strength Characteristics of Sands". Journal of Soil Mechanics and Foundation Engineering, American Society of Civil Engineers, Vol. 93, SM6, pp. 117-141.

Lee, K.L. and Seed, H.B., 1967b. "Undrained Strength Characteristics of Cohesionless Soils". Journal of Soil Mechanics and Foundation Engineering, American Society of Civil Engineers, Vol. 93, SM6, pp. 333-360.

Lee, K.L., Seed, H.B. and Dunlop, P., 1969. "Effect of Transient Loading on the Strength of Sand". Proceedings of 7th International Conference of Soil Mechanics and Foundation Engineering, Vol. 1, pp. 239-247.

Lee, K.L., Seed, H.B. and Dunlop, P., 1967. "Effects of Moisture on the Strength of Clean Sand". Journal of the Soil Mechanics and Foundation Engineering, ASCE, Vol. 93, No. SM6, pp. 17-40.

Lehnoff, T.F. and Scheller, J.D., 1975. "The Influence of Temperature Dependent Properties on Thermal Rock Fragmentation". International Journal of Rock Mechanics, Mining Sciences and Geomechanics Abstracts, Vol. 12, pp. 255-260.

Lewis, A.E. and Rothman, A.J., 1975. "Rubble In Situ Extraction (RISE): A Proposed Program for Recovery of Oil from Oil Shale". National Technical Information Service, U.S. Department of Commerce, 32 p.

Lin, C.J. and Wheeler, J.D., 1978. "Simulation of Permafrost Thaw Behaviour at Prudhoe Bay". Journal of Petroleum Technology, Vol. 30, March 1978, pp. 461-467.

Lindroth, D.P., 1974. "Thermal Diffusivity of Six Igneous Rocks at Elevated Temperatures and Reduced Pressures". U.S. Bureau of Mines, Report of Investigations, R17954, 21 p.

Lo, H.Y. and Mungan, N., 1973. "Temperature Effect on Relative Permeabilities and Residual Saturations". Petroleum Recovery Research Institute, Calgary, Alberta, Research Report RR-19, April 1973, 36 p.

Lo, H.Y. and Roy, M., 1973. "Response of Particulate Materials at High Pressures". Soils and Foundations, JSSMFE, Vol. 13, No. 1, pp. 61-76.

Lo, H.Y. and Wai, R.S.C., 1982. "Thermal Expansion, Diffusivity and Cracking of Rock Cores from Darlington, Ontario". Canadian Geotechnical Journal, Vol. 19, No. 2, May 1982, pp. 154-166.

Lobb, G., 1982. "Lithostratigraphy of the Clearwater Formation Within the Region of Syncrude Canada Leases". Abstracts of Papers, International Association of Sedimentologists 11th International Congress on Sedimentology, p. 87.

Locker, J.G., 1973. "Petrographic and Engineering Properties of Fine-Grained Rocks of Central Alberta". Research Council of Alberta Bulletin 30, Edmonton, 144 p.

Lockner, D.A., Summers, R., Moore, D. and Byerlee, J.D., 1982. "Laboratory Measurements of Reservoir Rock from the Geysers Geothermal Field, California". International Journal of Rock Mechanics, Mining Sciences and Geomechanical Abstracts, Vol. 19, pp. 65-80, 1982.

Loop, R.B., 1981. "Materials Testing at the Vernal, Utah Tar Sands Liquefaction Site". Technical Information, U.S. Department of Energy, Rept. DE 81-028074, 29 p.

Lord, E.R.F. and Cameron, R., 1985. "Compaction Characteristics of Athabasca Tar Sand". Proceedings of the 38th Canadian Geotechnical Conference, Theory and Practice in Foundation Engineering, CGS, Edmonton, Alberta, Sept. 25-27, pp. 359-368.

Lundstrom, L. and Stille, H., 1978. "Large Scale Permeability Tests in the Granite of the Stripa Mine (Sweden)". Lawrence Berkley Laboratory, Research Report #LBL-7052.

Lyness, L.S., Devenny, D.W. and Dabrowski, T.L., 1987. "Views on Sand Control Comparison of Water Well Completions". Fourth Annual Heavy Oil and Oil Sands Technical Symposium, University of Calgary, Calgary, Alberta, Feb. 18, 28 p.

Maini, B. and Sayegh, S., 1983. "Laboratory Techniques for Investigating Recovery in Heavy Oil Reservoirs". Alberta Oil Sands Technology and Research Authority, Proceedings of the 4th Annual Conference on Advances in Petroleum Recovery Technology, Calgary, Alberta, 31 p.

Mainland, G.G., 1983. "The Development of In-situ Recovery Technology at Cold Lake". Alberta Oil Sands Technology and Research Authority, Proceedings of the 4th Annual Conference on Advances in Petroleum Recovery Technology, Calgary, Alberta, 13 p.

Martschuk, J., Chan, W.K. and Slawinski, A., 1985. "Basal Aquifer Dewatering at the Suncor Oil Sands Mine". Proceedings of the Heavy Oil and Oil Sands Technical Symposium - Challenges and Innovations, 1985, University of Calgary, Calgary, Alberta, Feb. 20, 40 p.

Mathews, C.S., Van Meurs, P. and Volek, C.W., 1969. "Process for Horizontally Fracturing Subterranean Earth Formations". U.S. Patent No. 3, 455, 391; July 15, 1969.

Mathews, K.E., 1980. "Potential of the Underground Mining of Oil Sands in Canada". Rockstore '80, Proceedings of the International Symposium on Subsurface Space for Environmental Protection, Low-Cost Storage and Energy Savings, Stockholm, Sweden, June 1980.

Mathews, K.E., Rawlings, G.E. and Bharti, S., 1980. "Investigation of the Geotechnical and Mining Characteristics of the Devonian Limestones Athabasca Oil Sands Area". Applied Oilsands Geoscience Conference, Edited by M. Dusseault, University of Alberta, Edmonton, Alberta, 1980.

Mattison, B.W., 1987. "Ichnology, Paleontology and Depositional History of the Lower Cretaceous McMurray Formation, Athabasca Oil Sands Area, Northeastern Alberta". M.Sc. Thesis, Dept. of Geology, University of Alberta.

Maugh, T.H., 1977. "Underground Gasification: An Alternate Way to Exploit Coal". Science, Vol. 198, December 16, 1977, pp. 1132-1134.

Maxwell, J.C., 1960. "Experiments on Compaction and Cementation of Sand". In Rock Deformation, Edited by Griggs and Handin, pp. 105-132.

McClain, W.C., 1969. "The Mechanics of Hydraulic Fractures in Shales". The Northern Ohio Geological Society Inc., Proceedings of the 3rd Symposium on Salt, Vol. 2, pp. 410-420.

Medeiros, L.V. and Eisenstein, Z., 1983. "A Deep Retaining Structure in Till and Sand: Part I: Stress Path Effects". Canadian Geotechnical Journal, Vol. 20, pp. 120-130.

Medeiros, L.V. and Eisenstein, Z., 1982. "Stress Path Effects in Till and Sand". Canadian Geotechnical Journal, Vol. 20, No. 1, pp. 120-130.

Mercer, J.W., Faust, C.R., Miller, W.J. and Pearson, F.J., Jr., 1982. "Review of Simulation Techniques for Aquifer Thermal Energy Storage (ATES)". In Advances in Hydroscience, Vol. 13, edited by Ven Te Chow, pp. 1-129.

Mesri, G., Adachi, K. and Ulrich, C.R., 1976. "Pore Pressure Response in Rock to Undrained Change in All Round Stress". Geotechnique 26, No. 2, June 1976, pp. 317-330.

Milne, W.E., 1970. "Numerical Solution of Differential Equations". Dover Publications, Inc., New York, 360 p.

Minken, D.F., 1974. "The Cold Lake Oil Sands: Geology and a Reserves Estimate". In Oil Sands, Fuel of the Future. Edited by L.V. Hills, CSPG, Memoir 3, pp. 84-99.

Mitchell, J.K., 1976. "Fundamentals of Soil Behaviour". John Wiley and Sons Inc., 422 p.

Mitchell, J.K., 1969. "Temperature Effects on the Engineering Properties and Behavior of Soils". NRC Highway Research Board, Special Report 103, pp. 3-32.

Mitchell, J.K., 1956. "The Fabric of Natural Clays and its Relation to Engineering Properties". Proc. of the Highway Research Board, Vol. 35, pp. 693-713.

Mitchell, R.F. and Goodman, M.A., 1978. "Permafrost Thaw-Subsidence Casing Design". Journal of Petroleum Technology, Vol. 30, March 1978, pp. 455-460.

Mittal, H.K., 1980. "Tailings Disposal Concepts in Oil Sands Open Pit Mining". Proceedings of a Seminar on Design and Construction of Tailings Dams, Colorado School of Mines, Golden, Colorado, Nov., pp. 207-230.

Mittal, H.K. and Hardy, R.M., 1977. "Geotechnical Aspects of a Tar Sand Tailings Dyke". Proceedings of the Conference on Geotechnical Practice for Disposal of Solid Waste Materials, American Society of Civil Engineering, Ann Arbor, Michigan, June 13-15, pp. 327-347.

Mogi, K., 1972. "Fracture and Flow of Rocks". In The Upper Mantle. Edited by A.R. Ritsema. Tectonophysics, 13 (1-4), pp. 541-568.

Mogi, K., 1966. "Pressure Dependence of Rock Strength and Transition from Brittle Fracture to Ductile Flow". Bull. Earthquake Res. Inst., (Japan), Vol. 44, pp. 215-232.

Moore, D.E., Summers, R. and Byerlee, J.D., 1983. "Strengths of Clay and Non-Clay Fault Gauges at Elevated Temperatures and Pressures". Proceedings of the 24th U.S. Symposium on Rock Mechanics, Texas A & M University, pp. 489-500.

Mordecai, M. and Morris, L.H., 1971. "An Investigation into the Changes of Permeability Occurring in a Sandstone when Failed Under Triaxial Stress Conditions". Proc. 12th Symp., Rock Mechanics, Rolla, AIME, pp. 221-239.

Morgenstern, N.R., 1981. "Geotechnical Engineering and Frontier Resource Development". 21st Rankine Lecture, March 1981, Geotechnique 31, pp. 303-365.

Morgenstern, N.R., 1962. "A Relation Between Hydraulic Fracture Pressure and Tectonic Stresses". Geofisca Pura E Applicate, Volume 52, pp. 104-114.

Morgenstern, N.R. and Cruden, D., 1979. "Description and Classification of Geotechnical Complexities". Proc. Int. Symp. on The Geotechnics of Structurally Complex Formations, Capri, Associazione Geotechnica Italiana, Vol. 2, pp. 195-203.

Morrow, C., Moore, D. and Byerlee, J., 1983. "Permeability and Pore Fluid Chemistry of the Bullfrog Tuff in a Temperature Gradient". Proceedings of the 24th U.S. Symposium on Rock Mechanics, Texas A & M University, pp. 819-828.

Mossop, G.D., 1980. Geology of the Athabasca Oil Sands". Science Vol. 207, No. 11, January 1980, pp. 145-152.

Mossop, G.D., 1978a. "Geological Controls on Reservoir Heterogeneity in Athabasca Oil Sands". In AOSTRA Seminar on Underground Excavation in Oil Sands, University of Alberta, Edmonton, Alberta, Paper No. 1, 27 p.

Mossop, G.D., 1978b. "Facies Control on Bitumen Saturation in the Athabasca Oil Sands". Canadian Society of Petroleum Geologists, Calgary, Alberta, Memoir 6, June 1978.

Mossop, G.D. and Flach, P.D., 1983. "Deep Channel Sedimentation in the Lower Cretaceous McMurray Formation, Athabasca Oil Sands, Alberta". Sedimentology, Vol. 30, pp. 493-509.

Mossop, G.D., Kramers, J.W., Flach, P.D. and Rottenfusser, B.A., 1979. "Geology of Alberta's Oil Sands and Heavy Oil Deposits". In Proceedings of the 1st International Conference on the Future of Heavy Crude and Tar Sands, June 4-12, 1979, McGraw-Hill, New York, pp. 197-207.

Murayama, S., 1969. "Effect of Temperature on the Elasticity of Clays". HRB Spec. Rept. 103, pp. 194-203.

Muskat, M., 1946. "The Flow of Homogeneous Fluids Through Porous Media". J.W. Edwards Inc., 1st Edition, Ann Arbor, Michigan, 1946, 755 p.

Mysen, B.O., 1981. "Melting Curves and Vescosity of Rock Forming Melts". In Physical Properties of Rocks and Minerals, Chapter 11, Edited by Touloukian & Ho, McGraw-Hill, New York, pp. 361-407.

Nakornthap, K. and Evans, R.D., 1982. "Temperature Dependent Relative Permeability and its Effect Upon Oil Displacement by Thermal Methods". Society of Petroleum Engineering of AIME, 57th Annual Fall Technical Conference, New Orleans, LA., September 26-29, 1982.

Nichols, L., et al, 1985. "Application of Geophysical Techniques in Oil Sands". Report Submitted to Energy Mines and Resources Canada, Report No. 05SQ.23440-4-9243, June 27, 132 pp.

Noble, C.A. and Demirel, T., 1969. "Effect of Temperature on Strength Behaviour of Cohesive Soil". HRB Spec. Rpt. 103, p. 204-219.

Norris, A.W., 1973. "Devonian Stratigraphy of Northeastern Alberta and Northwestern Saskatchewan". Geol. Surv. Canada, Mem. 313, pp. 168.

Norwest Resource Consultants, 1983. "Application for Approval of an Experimental Underground Shaft and Tunnel Access Scheme in Oil Sands, Volume 1 of 2". Prepared for AOSTRA.

Nur, A. and Byerlee, J.D., 1971. "An Exact Effective Stress Law for Elastic Deformation of Rock with Fluids". Journal of Geophysical Research, Vol. 76, No. 26, September 1971.

Nyland, E. and Dusseault, M.B., 1983. "Fireflood Microseismic Monitoring: Results and Potential for Process Control". Journal of Canadian Petroleum Technology, March-April 1983, pp. 62-68.

Nyren, R.H., Haakonson, K.A. and Mittal, H.K., 1978. "Disposal of Tar Sand Tailings at Syncrude Canada Limited". Tailings Disposal Today, Vol. 2, Proceedings of the Second International Tailings Symposium, Denver, Colorado, May, pp. 54-74.

O'Donnell, N.D. and Jodrey, J.M., 1984. "Geology of the Syncrude Mine Site and its Application to Sampling and Grade Control". Preprint #84-421, Society of Mining Engineers of AIME, SME-AIME Fall Meeting, Denver, Colorado, Oct. 24-26, 19 p.

Oil and Gas Conservation Board of the Province of Alberta, 1963. "A Description and Reserve Estimate of the Oil Sands of Alberta". Calgary, Alberta, 1963, 124 p.

Olsson, J.T., 1974. "Effects of Temperature, Pressure and Displacement on the Frictional Characteristics of a Limestone". International Journal of Rock Mechanics, Mining Sciences and Geomechanical Abstracts, Vol. 11, pp. 267-281.

Outtrim, C.P. and Evans, R.G., 1978. "Alberta's Oil Sands Reserves and Their Evaluation". In Redford, D.A. and Winestock, A.G. (eds). The Oil Sands of Canada-Venezuela, Canadian Institute of Mining and Metallurgy, Special Volume No. 17, pp. 36-66.

Paaswell, R.E., 1967. "Temperature Effects on Clay Soil Consolidation". ASCE, JSMFD, Vol. 93, SM3, pp. 9-22, May 1967.

Page, L. and Heard, H.C., 1981. "Elastic Moduli, Thermal Expansion and Inferred Permeability of Climax Quartz Monzonite and Sudbury Giabbro to 500°C and 55 MPa". Journal of Geophysical Research, Vol. 4, 1981, pp. 97-103.

Palciauskas, V.V. and Domenica, P.A., 1982. "Characterization of Drained and Undrained Response of Thermally Loaded Repository Rocks". Water Resources Research, Vol. 18, No. 2, pp. 281-290, April 1982.

Pamatmat, M.M., 1982. "Heat Production by Sediment: Ecological Significance". Science, Vol. 215, pp. 395-397, January 22, 1982.

Pantella, E.A. and Caswell, G.R., 1982. "Design and Analysis of Hydraulic Fracture Treatments Using Numerical Simulation Techniques". Proceedings of the Advances in Petroleum Recovery and Upgrading Technology Conference, Calgary, June, Reprints, 19 p.

Paquet, J. and Francois, P., 1980. "Experimental Deformation of Partially Melted Granitic Rocks at 600-900°C and 250 MPa Confining Pressures". Tectonophysics, 68, pp. 131-146.

Parrish, D.K., Krivz, A.L. and Carter, N.L., 1976. "Finite Element Folds of Similar Geometry". Tectonophysics, 32, pp. 183-207.

Parsons, L.J. and Hemstock, J.D., 1983. "Peace River In-situ Project: Current Operations and Future Outlook". Alberta Oil Sands Technology and Research Authority, 4th Annual Conference on Advances in Petroleum Recovery

Patching, T., Jeremic, M. and Stimpson, B., 1978. "On the Possibility of Mining Oil Sand by Underground Methods". In AOSTRA Seminar on Underground Excavation in Oil Sands, University of Alberta, Edmonton, Alberta, Paper No. 3, 17 p.

Patterson, M.A., Cuthbert, L.G. and Trimble, D., 1985. "Blind Boring Through Oil Sands - A Trail Blazer". Proceedings of the Sixth Annual Advances in Petroleum Recovery and Upgrading Technology Conference, Alberta Oil Sands Technology and Research Authority, Edmonton, June 6-7, 50 p.

Patton, F.D., 1980. "The Role of Engineering Geology in Alternative Surface Mining Operations in the Athabasca Oilsands". Proceedings of Applied Oilsands Geoscience '80 Conference, Edmonton, Alberta, June 11 to 13, 31 p. and Research Authority, 4th Annual Conference on Advances in Petroleum Recovery Technology, Calgary, Alberta, 22 p.

Patton, F.D. and Scott, J.D., 1980. "Subsurface Monitoring for Deep In-situ Oil Sand Production". Oilsands Geoscience '80, Edited by M.B. Dusseault, University of Alberta, Edmonton, Alberta, June 1980.

Peaceman, D.W. and Rachford, H.H., 1962. "Numerical Calculation of Multidimensional Miscible Displacement". Society Petroleum Engineers Journal, December 1962, Trans. AIME, Vol. 225, pp. 327-339.

Peacock, D., 1986. "Gas Evolution in Athabasca Oil Sands". M.Sc. Thesis, University of Alberta, Edmonton, Alberta.

Pearson, C., 1981. "The Relationship Between Microseismicity and High Pore Pressures During Hydraulic Stimulation Experiments in Low Permeability Granitic Rocks". Journal of Geophysical Research, 86, pp. 7855-7864.

Perkins, T.K. and Gonzalez, J.A., 1984. "Changes in Earth Stresses Around a Wellbore Caused by Radially Symmetrical Pressure and Temperature Gradients". Society of Petroleum Engineers Journal, Vol. 24, No. 2, pp. 129-140.

Perry, C. and Gillott, J.E., 1982. "Mineralogical Transformations as Indicators of Combustion Zone Temperatures During In-situ Combustion". Bulletin of Canadian Petroleum Geology, Vol. 30, No. 1, March 1982, pp. 34-42.

Pincus, H.J., Handin, J., Judd, W.R. and Engelder, T., 1982. "Rock Mechanics Research Requirements for Resource Recovery, Construction and Earthquake Hazard Reduction". EOS, Transactions, American Geophysical Union, Vol. 23, No. 25, June 22, 1982, pp. 545-547.

Pittman, E.D., 1972. "Diagenesis of Quartz in Sandstones as Revealed by Scanning Electron Microscopy". Jour. Sed. Petrology, Vol. 42, No. 3, pp. 507-519.

Plewes, H.D., 1987. "Undrained Strength of Athabasca Oil Sand". M.Sc. Thesis, University of Alberta, Edmonton, Alberta.

Plum, R.L. and Esrig, M.I., 1969. "Some Temperature Effects on Soil Compressibility and Pore Water Pressure". HRB Special Report 103, pp. 231-242.

Pollard, D.P. and Johnson, A.M., 1973a. "Mechanics of Growth of Some Laccolith Intrusions in the Henry Mountains, Utah, 1: Field Observations, Gilbert's Model, Physical Properties and Flow of the Magma". Tectonophysics, 18, pp. 261-309.

Pollard, D.P. and Johnson, A.M., 1973b. "Mechanics of Growth of Some Laccolith Structures in the Henry Mountains, Utah, II: Bending and Failure of Overburden Layers and Sill Formation". Tectonophysics, 18, pp. 311-354.

Pollard, D.P. and Muller, O.H., 1976. "The Effect of Gradients in Regional Stress and Magma Pressure on the Form of Stress Intrusions in Cross-Sections". Journal of Geophysical Research, Vol. 81, No. 5, pp. 975-984.

Poulos, H.G. and Davis, E.H., 1984. "Elastic Solutions for Soil and Rock Mechanics". John Wiley & Sons, New York, 411 p.

Poulos, S.J., 1981. "The Steady State of Deformation". JGED, Proceedings ASCE, Vol. 107, No. GT5, May 1981, pp. 553-561.

Putnam, P.E. and Pedskalny, M.A., 1983. "Provenance of Clearwater Sandstones, Cold Lake, Alberta with Comments on Feldspar Composition". Bulletin of Canadian Petroleum Geology, 31, pp. 148-160.

Quinn, P.C. and Duncan, G., 1979. "The Mine Assisted In-situ Project". Proceedings of the First International Conference on the Future of Heavy Crudes and Tar Sands, United Nations Institute for Training and Research, Edmonton, Alberta, June, pp. 460-465.

Radhakrishna, H.S., 1968. "Heat Flow and Moisture Migration in Cable Backfills". Ontario Hydro Research Quarterly, 20, No. 2, 16 p.

Radhakrishna, H.S. and Tsui, K.K., 1981. "Thermal Properties of Buffer/Backfill Materials and Their Effects on the Near-Field Thermal Regime in a Nuclear Fuel Waste Disposal Vault". Proceedings of the 9th Waste Management Meeting, AECL, 18 p.

Raisbeck, J.M. and Card, C.C., 1978. "Recovery of Heavy Oil From Oil Sands". Proceedings of the 28th Canadian Chemical Engineering Conference, Halifax, Nova Scotia.

Raisbeck, J.M. and Currie, J.B., 1981. "A Laboratory Investigation of Hydraulic Fracturing in Oil Sands". In Situ, 5 (1), pp. 1-24.

Raisbeck, J.M. and Currie, J.B., 1979. "In-situ Oil Sands Geotechnique". Proceedings of the Fourth Alberta Oil Sands University Seminar, Alberta Oil Sands Technology and Research Authority, Fort McMurray, Sept., Preprint, 27 p.

Ranger, M., 1982. "The Sedimentology of the Wabiskaw Oil Sands, Clearwater Formation, Northeastern Alberta". In Abstracts of Papers, International Association of Sedimentologists 11th International Congress on Sedimentology, p. 87.

Read, H.E. and Hegemier, G.A., 1984. "Strain Softening of Rock Soil and Concrete - A Review Article". Mechanics of Materials, Vol. 3, pp. 271-294.

Readdy, L.A. and Skyllingstad, P., 1982. "Evaluation of the Kern River Oil Field as a Potential Candidate for the Mining of Oil". Proceedings of the Second International Conference on the Future of Heavy Crude and Tar Sands, United Nations Institute for Training and Research, Caracas, Venezuela, Feb., pp. 1069-1075.

Redford, D.A., 1985. "In-situ Recovery from the Athabasca Oil Sands - Past Experience and Future Potential". Journal of Petroleum Technology, May-June, pp. 52-62.

Regier, H.F., 1976. "Oil Sand Overburden Characterization within the Mine Area of Syncrude Lease No. 17 for Reclamation of Spent Oil Sand". Alberta Environment, Environmental Protection Services, June, 35 p.

Reynolds, D.L., 1954. "Fluidization as a Geological Process, and its Bearing on the Problem of Intrusive Granites". American Journal of Science, Volume 252, pp. 577-614.

Richter, D. and Simmons, G., 1974. "Thermal Expansion Behaviour of Igneous Rocks". International Journal of Rock Mechanics, Mineral Science and Geomechanic Abstract, Vol. 11, pp. 403-411, 1974.

Roberts, J.E. and De Souza, J.M., 1958. "The Compressibility of Sand". Proceedings of American Society for Testing and Materials, Vol. 58, pp. 1269-1277.

Roberts, J.O.L., Yong, R.N. and Erskine, H.L., 1980. "Surveys of Some Tar Sand Sludge Ponds: Results and Interpretations". Proceedings of Applied Oilsands Geoscience '80 Conference, Edmonton, Alberta, June 11 to 13, 46 p.

Robinson, D.B. and Sim, S.K., 1981. "The Behavior of Bitumen Mixtures During In-situ Recovery". A Progress Report to Alberta Oil Sands Technology and Research Authority on AOSTRA Agreement 184, 32 p.

Roesner, E.K. and Poppen, S.A., 1978. "Shaft Sinking and Tunnelling in the Oil Sands". In AOSTRA Seminar on Underground Excavation in Oil Sands, University of Alberta, Edmonton, Alberta, Paper No. 11, 36 p.

Rogers, G., 1978. "Geological Aspects of Saline Creek Tunnel". In AOSTRA Seminar on Underground Excavation on Oil Sands, University of Alberta, Edmonton, Alberta, Paper No. 8, 42 p.

Roscoe, K.H., Schofield, A.N. and Wroth, C.P., 1958. "On the Yielding of Soils". Geotechnique, Vol. 8, No. 1, pp. 22-52.

Ross, C.T.F., 1982. "Computational Methods in Soil and Continimum Mechanics". Ellis Horwood Ltd., Chichester, 288 p.

Round, G.F., 1960. "The Shear Strength of McMurray Oil Sands". Transactions of the Canadian Institute of Mining and Metallurgy, Vol. 63, pp. 145-150.

Rowe, P.W., 1971. "Theoretical Meaning and Observed Values of Deformation Parameters for Soil, Stress-Strain Behavior of Soils". Proceedings of the Roscoe Memorial Symposium, Cambridge University, pp. 143-194.

Rowe, P.W., 1969. "The Relation Between the Shear Strength of Sands in Triaxial Compression, Plane Strain and Direct Shear". Geotechnique, Vol. 19, No. 1, pp. 75-86.

Rowe, P.W., 1962. "The Stress Dilatency Relation for Static Equilibrium of an Assembly of Particles in Contact". Royal Society, Series A, Vol. 269, pp. 500-527.

Rowe, P.W., 1955. "A Stress Strain Theory for Cohesionless Soil with Application to Earth Pressures at Rest and Moving Walls". Geotechnique, Vol. 4, pp. 70-88.

Rowe, P.W., Barden, L. and Lee, I.K., 1964. "Energy Components During the Triaxial Cell and Direct Shear Tests". Geotechnique, Vol. 14, No. 3, pp. 247-261.

Rowe, R.K., Lo, K.Y. and Tham, L.G., 1982. "The Analysis of Tunnels and Shaft in Dense (Oil) Sand". Proceedings of the Fourth International Conference on Numerical Methods in Geomechanics, Edmonton, Alberta, Edited by Z. Eisenstein, Volume 2, pp. 587-596.

Ruedrich, R.A., Perkins, T.K., Rochan, J.A. and Christman, S.A., 1978. "Casing Strain Resulting from Thawing of Prudhoe Bay Permafrost". Journal of Petroleum Technology, March 1978, Vol. 30, pp. 468-474.

Sass, J.H., Kennelly, J.P., Wendt, W.E., Moses, T.H. and Ziagos, J.P., 1981. "In-situ Determination of Heat Flow in Unconsolidated Sediments". Geophysics, Vol. 46, No. 1, January 1981, pp. 76-81.

Sauty, J.P., Gringarten, A.C., Menjoz, A. and Landell, P.A., 1982. "Sensible Energy Storage in Aquifers 1. Theoretical Study". Water Resources Research, Vol. 18, No. 2, April 1982, pp. 245-252.

Schamaun, J.T., 1980. "Enhancing Permeability in Oil Shale and Applications to Tar Sand". Proceedings of the Tar Sands Permeability Enhancement Workshop, Alburquerque, New Mexico, May, pp. 85-98.

Schiffman, R.L., 1971. "A Thermoelastic Theory of Consolidation". Environmental and Geophysical Heat Transfer, American Society of Mechanical Engineers (ASME), Heat Transfer Division, Volume 4, pp. 78-84.

Schmidt, R.A., Warpinski, N.R. and Cooper, P.W., 1980. "Enhanced Formation Permeability Through Tailored-Pulse Loading of Wellbores". Proceedings of the Tar Sands Permeability Enhancement Workshop, Albuquerque, New Mexico, May, pp. 123-146.

Schora, F.C., Tarman, P.B. and Feldkirchner, H.L., 1977. "In Situ Shale Processing: State-of-the-Art". Hydrocarbon Processing, Volume 56, No. 3, March 1977, pp. 127-129.

Schrider, L.A. and Fischer, D.D., 1976. "In-situ Coal Gasification, A Unique Means of Energy Recovery". Mechanical Engineering, March 1976.

Schrodt, J.K. and Holder, J.T., 1983. "Temperature and Strain Rate Effects on Micromechanical Behaviour in Triaxially Compressed Marbles". Proceedings of the 24th U.S. Symposium on Rock Mechanics, Texas A & M University, pp. 449-468.

Schultz, E. and Moussa, A., 1961. "Factors Affecting the Compressibility of Sand". Proceedings of 5th International Conference on Soil Mechanics and Foundation Engineering, Paris, pp. 335-340.

Schuyler, J.N. and McLennan, J.D., 1984. "The Injection of Geology, Mechanical Properties and In Situ Stresses in Hydraulic Fracturing". Proc. 25th U.S. Symposium on Rock Mechanics, Northwestern University, Society of Mining Engineers of AIME, pp. 145-156.

Scott, J.D., 1982. "Applications of Geotechnical Mechanics to Oil Sand In Situ Recovery Processes". Proceedings of the Sixth Symposium on Engineering Applications of Mechanics, National Research Council of Canada, Calgary, Alberta, June, pp. 111-115.

Scott, J.D., 1982. "Oil Sands Tailings Disposal". Seminar Proceedings of Geotechnical Aspects of Mine Design and Tailings Containment, University of Calgary, April, 30 p.

Scott, J.D., 1979. "Engineering Constraints on Environmental Enhancement of Oil Sands Tailings Ponds". Proceedings of the Symposium on Biological Issues in Energy Development, Alberta Society of Professional Biologists, Calgary, Alberta, April, pp. 40-52.

Scott, J.D., 1978. "General Report on the AOSTRA Seminar on Underground Excavation in Oil Sands". In Proceedings of the AOSTRA Seminar on Underground Excavation in Oil Sands, Edmonton, Alberta, 27 p.

Scott, J.D. and Cymerman, G.J., 1984. "Prediction of Viable Tailings Disposal Methods". Proceedings of a Symposium: Sedimentation Consolidation Models, American Society of Civil Engineering, San Francisco, CA, Oct. 1, pp. 522-544.

Scott, J.D. and Dusseault, M.B., 1982. "Behavior of Oil Sand Tailings Sludge". Presented at the 33rd Annual Technical Meeting of the Petroleum Society of the Canadian Institute of Mining and Metallurgy, Calgary, Alberta, June, Paper No. 82-33-85, 19 p.

Scott, J.D. and Dusseault, M.B., 1981. "Disposal of Oil Sand Tailings Sludge". Proceedings of the 34th Canadian Geotechnical Conference, Fredericton, New Brunswick, Oct., 19 p.

Scott, J.D. and Dusseault, M.B., 1980. "Behavior of Oil Sand Tailings". Proceedings of the 33rd Canadian Geotechnical Conference, Calgary, Sept., 35 p.

Scott, J.D., Dusseault, M.B. and Carrier, W.D. III, 1986. "Large Scale Self-Weight Consolidation Testing Consolidation of Soils: Testing and Evaluation". ASTM SPT 892, May, pp. 500-515.

Scott, J.D., Dusseault, M.B. and Carrier, W.D. III, 1985. "Behaviour of the Clay/Bitumen/Water Sludge System from Oil Sands Extraction Plants". Journal of Applied Clay Science, Vol. 1, No. 1/2, July, pp. 207-218.

Scott, J.D., Eisenstein, Z. and Branco, P., 1985. "Geotechnical Aspects of Construction and Operation of the Mining Access Concept". Proceedings of the Sixth Annual Advances in Petroleum Recovery and Upgrading Technology Conference, Alberta Oil Sands Technology and Research Authority, Edmonton, June 6-7, 30 p.

Scott, J.D., Eisenstein, Z., Branco, P. and Peacock, D., 1985. "Heave in Foundation Excavations in Oil Sands". Proceedings of the 38th Canadian Geotechnical Conference, Theory and Practice in Foundation Engineering, CGS, Edmonton, Alberta, Sept. 25-27, pp. 123-133.

Scott, J.D. and Hsu, T.R., 1986. "Measurements of Thermophysical and Mechanical Properties of Oil Sands". Tar Sand Symposium Proceedings, U.S. Department of Energy, Jackson, Wyoming, July 7-10, 14 p.

Scott, J.D. and Kosar, K.M., 1985. "Design of Hot Foundations on Oil Sands". Proceedings of the 38th Canadian Geotechnical Conference, Theory and Practice in Foundation Engineering, CGS, Edmonton, Alberta, Sept. 25-27, pp. 111-121.

Scott, J.D. and Kosar, K.M., 1985. "Foundation Movements Beneath Hot Structures". Proceedings of the Eleventh International Conference on Soil Mechanics and Foundation Engineering, San Francisco, California, Aug. 12-16, pp. 653-658.

Scott, J.D. and Kosar, K.M., 1984. "Geotechnical Properties of Athabasca Oil Sands". Proceedings of WRI-DOE Tar Sand Symposium, Western Research Institute and U.S. Department of Energy, Vail, Colorado, June 26-29, Paper No. 2-3, 32 p.

Scott, J.D. and Kosar, K.M., 1982. "Thermal Expansion of Oil Sands". Forum on Subsidence Due to Fluid Withdrawal, U.S. Department of Energy and Republic of Venezuala Minstry of Energy and Mines, Oklahoma, U.S.A., 28 p.

Scott, J.D., Mittal, H.K. and Prasad, B.D., 1980. "Sizing of Oil Sands Tailings Ponds". Proceedings of Applied Oilsands Geoscience '80 Conference, Edmonton, Alberta, June 11 to 13, 30 p.

Scott, J.D. and Seto, A.C., 1986. "Thermal Property Measurements on Oil Sands". Journal of Canadian Petroleum Technology, Vol. 25, No. 6, Nov-Dec, pp. 70-77.

Scott, J.D. and Seto, A.C., 1985. "Thermal Property Measurements on Oil Sands". Proceedings of the 36th Annual Technical Meeting of the Petroleum Society of the Canadian Institute of Mining and Metallurgy, Edmonton, Alberta, June 2-5, Paper No. 85-36-15, pp. 171-187.

Scott, J.D., Taylor, D.E. and Scott, A.M., 1979. "Transportation of Oil Sands Tailings Over Long Distances". Proceedings of the Third International Symposium on Transport and Handling of Minerals, Vancouver, Oct., 23 p.

Sedimentology Research Group, University of Calga 1981. "The Effects of In-Situ Steam Injection on Cold Lake Oil Sands". Bulletin of Canadian Petroleum Geology, Vol. 29, No. 4, December 1981, pp. 447-478.

Seed, H.B. and Lundgren, R., 1954. "Investigation of the Effects of Transient Loading Upon the Strength and Deformation Characteristics of Saturated Sands". Proceedings of American Society for Testing Materials, Vol. 54, p. 1288.

Seki, N., Cheng, K.C. and Fukusako, S., 1981. "Measurements on Thermal Conductivity and Thermal Diffusivity of Alberta Oil Sands". Proc. of the 17th Int. Conf. on Thermal Conductivity, ed. by J.G. Hust, Pleum Press, N.Y., pp. 635-642.

Sensey, P.E., 1983. "Determination of a Constitutive Law for Salt at Elevated Temperature and Pressure". Symposium on Measurement of Rock Properties at Elevated Pressures and Temperatures, College Station, Texas, American Society for Testing and Materials, pp. ?.

Seto, A.C., 1985. "Thermal Testing of Oil Sands". M.Sc. Thesis, University of Alberta, Edmonton, Alberta, 320 p.

Settari, A. and Raisbeck, J.M., 1981. "Analysis and Numerical Modeling of Hydraulic Fracturing During Cyclic Steam Stimulation in Oil Sands".

Settari, A. and Raisbeck, J.M., 1979. "Fracture Mechanics Analysis in In-situ Oil Sands Recovery". Journal of Canadian Petroleum Technology, 18, pp. 85-94. Journal of Petroleum Technology, Vol. 33, No. 11, pp. 2201-2212.

Sharma, H.D., Harris, M.C., Scott, J.D. and McAllister, K.W., 1986. "Bearing Capacity of Bored Cast-in-place Piles on Oil Sand". Journal of Geotechnical Engineering, ASCE, Vol. 112, No. 12, Dec., pp. 1101-1116.

Sherif, M. and Burrous, C.M., 1969. "Temperature Effects on the Unconfined Shear Strength of Saturated Cohesive Soil". HRB Spe. Rept. 103, pp. 267-272.

Shimamoto, T. and Hara, I., 1976. "Geometry and Strain Distribution of Single-Layer Folds". Tectonophysics, 30, pp. 1-34.

Shuster, J.A., 1972. "Controlled Freezing for Temporary Ground Support". RETC Proceedings, Vol. 2, Chapter 49, pp. 863-895.

Sibson, R.H., 1973. "Interactions Between Temperature and Pore Fluid Pressure During Earthquake Faulting and a Mechanism for Partial and Total Stress Relief". NATURE Physical Science, Vol. 243, pp. 66-68.

Simmokrot, A.A., Raney, H.J. and Marsden, S.S., 1971. "Effect of Temperature Level Upon Capillary Pressure Curves". Society of Petroleum Engineers Journal, March 1971, pp. 13-22.

Simmons, G. and Cooper, H.W., 1978. "Thermal Cycling Cracks in Three Igneous Rocks". International Journal of Rock Mechanics, Mineral Science and Geomechanics Abstract, Vol. 15, pp. 145-148.

Sisco, F.T., 1947. "Modern Metallurgy for Engineers". Second Edition, Pitman Publishing Corporation, New York, 499 p.

Skempton, A.W., 1960. "Effective Stress in Soils, Concrete and Rocks". Proceedings of the Conference on Pore Pressure and Suction in Soils, Butterworths, London, England, pp. 4-16.

Skempton, A.W., 1954. "The Pore Pressure Coefficients A and B". Geotechnique, Volume 13, No. 4, pp. 143-147.

Skempton, A.W. and Bishop, A.W., 1954. "Soils". Chapter X of Building Materials, Their Elasticity and Inelasticity. North Holland Publishing Company, Amsterdam, pp. 418-482.

Skinner, B.J., 1966. "Thermal Expansion". In Handbook of Physical Constants, Geological Society of America, New York, Memoir 37, Section 6, pp. 75-96.

Smith, G.E., 1986. "Fluid Flow and Sand Production in Heavy Oil Reservoirs Under Solution Gas Drive". Proc. 56th California Regional Meeting of the Society of Petroleum Engineers, Oakland, California, April 2-4, pp. 29-41.

Smith, G.W. and Butler, R.M., 1979. "Studies on the Use of Tunnels and Horizontal Wells for the Recovery of Heavy Crudes". First International Conference on the Future of Heavy Crude Oils and Tar Sands, edited by R.F. Meyer and C.T. Steele, United Nations for Training and Research, AOSTRA, and the U.S. Department of Energy, Edmonton, Alberta, Chapter 49, pp. 455-459.

Smith, J.B., 1980. "Computer Model for Stress-Strain Analysis of Oil Sand". Thurber Consultants Ltd., Prepared for Canada Department of Energy, Mines and Resources, Contract No. OSQ78-00139, 215 p.

Smith, J.W. and Atwood, M.T. (Editors), 1976. "Oil Shale and Tar Sands". American Institute of Chemical Engineers, Symposium Series, Volume 72, No. 55, 84 p.

Smith, L.B. and Byrne, P.M., 1980. "Convergence-Confinement Method of Design for Shafts and Tunnels in Oilsands". Proceedings of Applied Oilsands Geoscience '80 Conference, Edmonton, Alberta, June 11 to 13, 40 p.

Smith, L.B. and Chapman, D.S., 1983. "On the Effects of Groundwater Flow, Regional Scale Systems". Journal of Geophysical Research, Vol. 88, no. B1, pp. 593-608.

Smith, L.B., Chatterji, P.K., Insley, A.E. and Sharma, L., 1978. "Construction of Saline Creek Tunnel in Athabasca Oil Sand". In AOSTRA Seminar on Underground Excavation in Oil Sand, University of Alberta, Edmonton, Alberta, Paper No. 7, 58 p.

Smith, M.B. and Pattillo, P.D., 1980. "Analysis of Casing Deformations Due to Formation Flow". Oil Sands Geoscience, Edmonton, Alberta, June 1980, 15 p.

Smith-MacGowan, D., Skauge, A. and Hepler, L.G., 1982. "Specific Heats of Athabasca Oil Sands and Components". Journal of Canadian Petroleum Technology, May-June 1982, pp. 28-32.

Sneddon, I.N., 1946. "The Distribution of Stress in the Neighborhood of a Crack in an Elastic Solid". Proceedings of the Royal Society of London, A, 187, pp. 229-260.

Sobkowicz, J.C., 1982. "The Mechanics of Gassy Sediments". Ph.D. Thesis, University of Alberta, Edmonton, Alberta, 531 p.

Sobkowicz, J.C. and Morgenstern, N.R., 1984. "The Undrained Equilibrium Behavior of Gassy Sediments". Canadian Geotechnical Journal, Vol. 21, No. 3, pp. 439-448.

Solberg, P., Lockner, D. and Byerlee, J.D., 1980. "Hydraulic Fracturing in Granite Under Geothermal Conditions". International Journal of Rock Mechanics, Mineral Science and Geomechanics Abstract, Vol. 17, pp. 25-33.

Somerton, W.H., 1982. "Porous Rock-Fluid Systems at Elevated Temperatures and Pressures". Geological Society of America, Special Paper 189, 1982, pp. 183-197.

Somerton, W.H., 1973. "Thermal Properties of Hydrocarbon Bearing Rocks at High at High Temperature and Pressures". Berkley, University of California, American Petroleum Institute, Research Project 117, Final Report, 83 p.

Somerton, W.H., 1958. "Some Thermal Characteristics of Porous Rocks". Petroleum Transactions, AIME, Vol. 213, pp. 375-378.

Somerton, W.H. and Gupta, V.S., 1965. "Role of Fluxing Agents in Thermal Alteration of Sandstones". Journal of Petroleum Technology, May 1965, pp. 585-593.

Somerton, W.H., Keese, J.A. and Chu, S.L., 1974. "Thermal Behavior of Unconsolidated Oil Sands". Society of Petroleum Engineering Journal, Vol. 14, pp. 513-521, 1974.

Somerton, W.H. and Udell, K.S., 1981. "Thermal and High Temperature Properties of Rock-Fluid Systems". Department of Mechanical Engineering, University of California, Berkley Internal Research Report UCB/ME/81-01, College of Engineering, Office of Research Services, 12 p.

Somerton, W.H., Zimmerman, R.W. and Haraden, J.L., 1983. "The Effects of Pore Pressure, Confining Pressure and Temperature on Pore and Bulk Volume Compressibilities of Consolidated Sandstones". Symposium on Measurement of Rock Properties at Elevated Pressures and Temperatures, College Station, Texas, American Society for Testing and Materials, pp.?.

Speight, J.G. and Moschopedis, S.E., 1979. "The Influence of Crude Oil Composition on the Nature of the Upgrading Process: Athabasca Bitumen". Chapter 67 in the First International Conference on the Future of Heavy Crude Oils and Tar Sands, Edited by R.F. Meyers and C.T. Steele, Edmonton, Alberta, June 4-12, 1979, pp. 603-611.

Srajer, V., 1980. "Air Injection Test in Oil Sands". Proceedings of Applied Oilsands Geoscience '80 Conference, Edmonton, Alberta, June 11 to 13, 15 p.

Srajer, V., 1980. "1979 Oil Sands Mining Review". Prepared for Canada Department of Energy, Mines and Resources, Rept. ERP/MRL 80-50 (TR), 24 p.

Srajer, V. and Barron, K., 1978. "Gas Observations in the Saline Creek Tunnel". In AOSTRA Seminar on Underground Excavation in Oil Sand, University of Alberta, Edmonton, Alberta, Paper No. 9, 20 p.

Starr, J. and Prats, J.M., 1979. "Chemical Properties and Reservoir Characteristics of Bitumen and Heavy Oil from Canada and Venezuala". Chapter 21 in the First International Conference on the Future of Heavy Crude Oil and Tar Sands, Edited by R.F. Meyers and C.T. Steele, Edmonton, Alberta, pp. 168-173.

Stephens, G. and Voight, B., 1982. "Hydraulic Fracturing Theory for Conditions of Thermal Stress". International Journal of Rock Mechanics, Mineral Science and Geomechanics Abstract, Vol. 19, pp. 279-284.

Stephenson, H.G., 1978. "An Evaluation of the Underground Approach to Oil Sand Development". In AOSTRA Seminar on Underground Excavation in Oil Sands, University of Alberta, Edmonton, Alberta, Paper No. 6, 18 p.

Stephenson, H.G. andd Owen, H., 1983. "The AOSTRA Underground Test Facility - An Update". Proc. of the 1st District Five Meeting of the Canadian Institute of Mining and Metallurgy, Calgary, Sept., 39 p.

Sterne, K.B., 1981. "Hollow Cylinder Testing of Oil Sands". M.Sc. Thesis, University of Alberta, Edmonton, Alberta, 228 p.

Sternberg, E., 1958. "On Transient Thermal Stresses in Linear Viscoelasticity". Proceedings of Third U.S. National Congress of Applied Mechanics, pp. 96-102.

Stewart, G.A. and MacCallum, G.T., 1978. "Athabasca Oil Sands Guide Book". Canadian Society of Petroleum Geologists, Calgary, Alberta, 33 p.

Stone, R.B., 1977. "Technical and Economic Study of an Underground Mining, Rubblization and in situ Retorting System for Deep Oil Shale Deposits". Quarterly of the Colorado School of Mines, pp. 235-258.

Stout, K.S., 1980. "Mining Methods and Equipment". McGraw-Hill, Inc., New York, 218 p.

Streeter, V.L. and Wylie, E.B., 1979. "Fluid Mechanics". Seventh Edition, McGraw-Hill Book Company, New York, 570 p.

Sufi, A.H., Ramey, H.J. and Brigham, W.E., 1982. "Temperature Effects on Relative Permeabilities of Oil-Water Systems". Society of Petroleum Engineers of AIME, 57th Annual Fall Technical Conference, New Orleans, LA., SPE 11071, 12 p.

Summers, R., Winkler, K. and Byerlee, J.D., 1978. "Permeability Changes During the Flow of Water Through Westerly Granite at Temperatures of 100-400°C". Journal of Geophysical Research, Volume 83, pp. 339-344.

Surguchev, M.L., Vakhitov, G.G., Epik, I.P., Mashin, V.N., Gurov, E.I. and Tabakov, V.P., 1983. "Recovery of Hydrocarbons from Oil Sands and Oil Shales by Mining". Proceedings of the Eleventh World Petroleum Congress, London, Aug. to Sept., pp. 373-381.

Sydansk, R.D., 1980. "Discussion of the Effect of Temperature and Confining Pressure on Single-Phase Flow in Consolidated Rocks". Journal of Petroleum Technology, August 1980, pp. 1329-1330.

Syncrude Canada Limited, 1979. "Syncrude Analytical Methods for Oil Sand and Bitumen Processing". AOSTRA, Edmonton, 173 p.

Takamura, K., 1982. "Microscopic Structure of Athabasca Oil Sand". The Canadian Journal of Chemical Engineering, Vol. 60, pp. 538-545.

Taylor, D.W., 1948. "Fundamentals of Soil Mechanics". John Wiley and Sons Inc., New Yorek, 425 p.

Taylor, J.M., 1950. "Pore Space Reduction in Sandstones". Bulletin Amer. Assoc. Petrol. Geol., Vol. 34, pp. 701-716.

Techman Limited and Rheinbraun - Consulting GmbH, 1979. "Oil Sand Reclamation: A Study Integrating Mining, Tailings Disposal and Reclamation". Prepared for the Alberta Department of the Environment, 3 Volumes.

Terzaghi, K., 1943. "Theoretical Soil Mechanics". John Wiley and Sons, Inc., New York, New York, 510 p.

Terzaghi, K. and Peck, R.B., 1948. "Soil Mechanics in Engineering Practice". New York, John Wiley and Sons, pp. 58-61.

Terzaghi, K. and Richart, F.E., 1952. "Stress in Rock About Cavities". Geotechnique, Vol. 3, 1952, pp. 57-90.

Thomson, A., 1959. "Pressure Solution and Porosity". Proc. Soc. Econ. Paleontologists and Mineralogists, Spec. Publ. 7, pp. 92-109.

Thompson, T.W. and Potts, E.L.J., 1979. "The Influence of Thermal Stresses on the Stability of Underground Storage Cavities". International Journal of Rock Mechanics, Mineral Science and Geomechanics Abstract, Vol. 16, pp. 117-125.

Timoshenko, S.P. and Goodier, J.N., 1934. "Theory of Elasticity". McGraw-Hill Book Company, Third Edition, Engineering Societies Monographs, 567 p.

Toma, P., Livesey, D.B. and Heidrick, T.R., 1986. "A New Sand Control Filter for Thermal Recovery Wells". Proc. 56th California Reginal Meeting of the Society of Petroleum Engineers, Oakland, California, April 2-4, 11 pp.

Towson, D.E., 1984. "The Mine Assisted In-situ Project". Proceedings of the Advances in Petroleum Recovery and Upgrading Technology Conference, Calgary, June, 4 p.

Towson, D., 1979. "The Electrical Preheat Recovery Process". Chapter 45 in the First International Conference on the Future of Heavy Crude Oil and Tar Sands, Edited by R.F. Meyers and C.T. Steele, Edmonton, Alberta, pp. 410-412.

Tsang, C.F. and Hopkins, D.L., 1982. "Aquifer Thermal Energy Storage: A Survey". Geological Society of America, Special Paper 189, 1982, pp. 427-441.

Tsui, K.K., Lee, C.F., Tsai, A. and Harris, N.L., 1982. "Thermo-mechanical Modelling of a Nuclear Waste Disposal Vault in Crystalline Hard Rock". Proceedings of the Fourth International Conference on Numerical Methods in Geomechanics, Edmonton, Alberta, edited by Z. Eisenstein, Vol. 2, pp. 503-512.

Tustin, T.G., 1949. "The Shear and Consolidation Characteristics of the McMurray Tar Sands". M.Sc. Thesis, University of Alberta, Edmonton, Alberta, 102 p.

U.S.S.R. Naval Ministry, 1975. "Recommendations for Thermal Consolidation of Weak Clayey Soils". Draft Translation 630, Translated by U.S. Foreign Sciences and Technology Centre for the U.S. Army Cold Regions Research and Engineering Laboratory, Hanover, New Hampshire, 36 p.

Vaid, Y.P., 1985. "Effect of Consolidation and Stress Path on Hyperbolic Stress-Strain Relations". Canadian Geotechnical Journal, Vol. 22, No. 2, pp. 172-176.

Van Buskirk, R., Enniss, J. and Schatz, J., 1983. "Measurement of Thermal Conductivity and Thermal Expansion at Elevated Temperatures and Pressures". Symposium on Measurement of Rock Properties at Elevated Pressures and Temperatures, College Station, Texas, American Society for Testing and Materials, pp.?.

Van Der Molen, I., 1981. "The Shift of the Alpha-Beta Transition Temperature of Quartz Associated with the Thermal Expansion of Granite at High Pressures". Tectonophysics 73, pp. 323-342.

van Helden, G.L.M., Scott, J.D., Hemstock, R.A. and van Hemert, J., 1980. "Open Pit Mining of Oil Sands using Hydraulic Techniques". Proc. of Applied Oilsands Geoscience '80 Conference, Edmonton, Alberta, June 11 to 13, 23 p.

Vaziri, H.H., 1986. "Finite Element Analysis of Oil Sands Subjected to Thermal Effects". Proc. of the 37th Annual Technical Meeting of the Canadian Institute of Mining and Metallurgy, Calgary, Alberta, June, Preprint, Paper 86-37-74, 11 p.

Vaziri, H.H., 1986. "Mechanics of Fluid and Sand Production from Oil Sand Reservoirs". Proc. 37th Annual Technical Meeting of the Petroleum Society of CIM, Calgary, Alberta, June 8-11, pp. 519-535.

Vesic, A.S. and Barksdale, R.D., 1963. "Discussion on Test Methods and Equipment". ASTM STP 361, pp. 301-305.

Vesic, A.S. and Clough, G.W., 1968. "Behaviour of Granular Materials Under High Pressures". Jour. of the Soil Mechanics and Foundation Division, Amer. Soc. of Civil Engineers, Vol. 94, SM3, pp. 661-688.

Vickers, B., 1978. "Laboratory Work in Soil Mechanics". Second Edition, Granada Publishing Limited, London, 170 p.

Vigrass, L.W., 1968. "Geology of Canadian Heavy Oil Sands". Amer. Assoc. of Petrol. Geologists, Bulletin, Vol. 52, No. 10, 1968, pp. 1984-1999.

Visser, K., Dankers, P.H.M., Leckie, D. and Van Der Marel, A.G.P., 1985. "Mineralogy and Geology of the Clearwater Reservoir Sands in the Wolf Lake Area, Cold Lake, Alberta". Third International Conference on Heavy Crude and Tar Sands, Long Beach California, July 22-31, 1985, Vol. 1, pp. 380-400.

Vladut, T., 1983. "Mining Oil - Considerations for Underground Access". Proceedings of the 1st District Five Meeting of the Canadian Institute of Mining and Metallurgy, Calgary, Sept., 24 p.

Voegele, M.D. and Brace, W.F., 1983. "Measurement of Permeability at Elevated Pressures and Temperatures". Symposium on Measurement of Rock Properties at Elevated Pressures and Temperatures, College Station, Texas, Amer. Soc. for Testing and Materials, pp.?.

Voegele, M., Hardin, E., Lingle, D., Board, M. and Barton, N., 1981. "Site Characterization of Joint Permeability Using the Heated Block Test". Proceedings of the 22nd U.S. Symposium on Rock Mechanics, pp. 120-128.

Voight, B. and Faust, C., 1982. "Frictional Heat and Strength Loss in Some Rapid Landslides". Geotechnique 32, No. 1, pp. 43-54.

Wai, R.S.C. and Lo, K.Y., 1981. "Temperature Effects on Strength and Deformation Behavior of Rocks in Southern Ontario". Research Report GEOT-6-81, University of Western Ontario, London Ontario, 31 p.

Walker, R.G., 1979. "Facies and Facies Models. General Introduction". Facies and Facies Models, Geoscience Canada, Vol. 3, No. 1, pp. 1-8.

Walsh, J.B. and Decker, E.R., 1966. "Effect of Pressure and Saturating Fluid on the Thermal Conductivity of Compact Rock". Journal of Geophysical Research, Vol. 71, No. 12, pp. 3053-3061.

Wang, J.S.Y., Tsang, C.F., Cook, N.G.W. and Witherspoon, P.A., 1981. "A Study of Regional Temperature and Thermohydrologic Effects of an Underground Repository for Nuclear Wastes in Hard Rock". Journal of Geophysical Research, Vol. 86, No. B5, pp. 3759-3770.

Waywanko, A., 1982. "Sedimentology and Shaley Sand Analysis of the Clearwater Formation (Lower Cretaceous Mannville Group), Cold Lake Oil Sands Area, Alberta". Eleventh International Conference on Sedimentology, McMaster University, August 22-27, 1982, p. 87.

Weaver, C.E., 1959. "The Clay Petrology of Sediments: Clays and Clay Minerals". Proc. 6th Natl. Conf., pp. 154-187.

Weaver, C.E. and Pollard, L.D., 1973. "The Chemistry of Clay Minerals". Developments in Sedimentology, 15, Elsevier, Amsterdam, 213 pp.

Weinbrant, R.M., Ramey, H.J. and Casse, F.J., 1975. "The Effect of Temperature on Relative and Absolute Permeability of Sandstones". Society of Petroleum Engineers Journal, October 1975, pp. 376-384.

Weyl, R.G., 1959. "Pressure Solution and the Force of Crystallization - A Phenomenological Theory". Journal of Geophysical Research, Vol. 64, No. 11, pp. 2001-2025.

Wightman, D.M., 1984. "Cold Lake Regional Studies". In Oil Sands Geology Studies of the Alberta Research Council, Compiled by J.W. Kramers Industry AOSTRA/ARC Access Report 8485-30.

Williams, K.A., Stimpson, B., Patching, T.H. and Jeremic, M.L., 1980. "Rock Mechanics Properties of the Waterways Formation". Applied Oilsands Geoscience Conference, Edited by M.B. Dusseault, University of Alberta, Edmonton, Alberta, 24 p.

Williams, N., 1982. "The Effects of Elevated Temperature on the Engineering Properties of Seafloor Sediments". Ph.D. Thesis, University of California, Berkley.

Wilson, J.W., 1956. "Determination of Relative Permeability Under Simulated Reservoir Conditions". A.I.Ch.E. Journal, March 1956, pp. 94-100.

Winestock, A.G., 1974. "Developing a Steam Recovery Process". In Oil Sands Fuel of the Future, Canadian Society of Petroleum Geologists, Calgary, Alberta, pp. 186-198.

Wingquist, C.F., 1970. "Elastic Moduli of Rock at Elevated Temperatures". U.S. Department of the Interior, Bureau of Mines, Rpt. of Investigations #7269, 18 p.

Winterkorn, H., 1954. "Fundamental Similarities Between Electro-osmotic and Thermo-osmotic Phenomena". Highway Research Board Proceedings, Vol. 27, National Research Council, Washington, D.C.

Witherspoon, P.A., Cook, N.G.W. and Gale, J.E., 1981. "Geologic Storage of Radioactive Waste: Field Studies in Sweden". Science, Vol. 211, pp. 894-900.

Wissa, A.E.Z., 1969. "Pore Pressure Measurement in Saturated Stiff Soils". ASCE, JSMFD, SM4, July 1969, pp. 1063-1073.

Wong, A. and McCormack, M.E., 1985. "Operating Experiences with Bottomhole Instrumentation at AOSTRA Pilots". Proceedings of the Heavy Oil and Oil Sands Technical Symposium - Challenges and Innovations 1985, University of Calgary, Calgary, Alberta, Feb. 20, 20 p.

Wong, S.K., 1986. "Analysis and Implications of In-situ Stress Changes During Steam Stimulation of Cold Lake Oil Sands". Rocky Mountain Regional Meeting of the Society of Petroleum Engineers, Billings, Montana, May 19-21, pp. 475-487.

Wong, T.F. and Brace, W.F., 1979. "Thermal Expansion of Rocks: Some Measurements at High Pressure". Tectonophysics, 57, pp. 95-117.

Wong,T.T., Morgenstern, N.R. and Sego, D.C., 1988. "A Plasticity Model for Broken Ice". 41st Canadian Geotechnical Conference, Waterloo, Ontario, October 5 - 7, pp. 114-123.

Wood, M.D. and Holzhausen, G.R., 1980. "Frac-Map Process Monitoring in the Asphalt Ridge Tar Sand, Vernal, Utah". Proceedings of the Tar Sands Permeability Enhancement Workshop, Albuquerque, New Mexico, May, pp. 157-166.

Wood, M.D., Holzhausen, G., Smith, C., Porter, S., Bachmann, W. and Khaw, M., 1979. "A System for Mapping and Monitoring Subsurface Processes in Enhancing Recovery Schemes". Proceedings of the First International Conference on the Future of Heavy Crudes and Tar Sands, United Nations Institute for Training and Research, Edmonton, Alberta, June, pp. 442-454.

Woodhouse, R., 1976. "Athabasca Tar Sand Reservoir Properties Derived from Cores and Logs". Proceedings of the 17th Annual Logging Symposium, Society of Professional Well Log Analysts, Denver, June 9-12, 13 p.

Wyckoff, R.D. and Botset, H.G., 1936. "Flow of Gas-Liquid Mixtures Through Sands". Physics, 1936, 325 p.

Wyllie, P.J., 1971. "The Dynamic Earth". John Wiley and Sons, Inc., New York, 416 p.

Yamaguchi, U. and Miyazaki, M., 1970. "A Study of the Strength at Failure of Rocks Heated to High Temperatures". Journal of the Mining and Metallurgical Institute of Japan, 86, (986), pp. 346-351.

Yong, R.N. and Sethi, A.J., 1978. "Mineral Particle Interaction Control of Tar Sand Sludge Stability". Journal of Canadian Petroleum Technology, Vol. 17, No. 4, pp. 76-83.

Yong, R.N., Sheeran, D.E., Sethi, A.J. and Erskine, H.L., 1982. "The Dynamics of Tar Sand Tailings". Proceedings of the 33rd Annual Technical Meeting of the Canadian Institute of Mining and Metallurgy, Calgary, Alberta, June, Preprint, Paper 82-33-42, 6 p.

Yong, R.N. Siu, S.K.H. and Sheeran, D.E., 1983. "On the Stability and Settling of Suspended Solids in Settling Ponds. Part 1, Piece-Wise Linear Consolidation Analysis of Sediment Layer". Canadian Geotechnical Journal, Vol. 20, No. 4, pp. 817-826.

Zeuch, D.H., 1983. "The Mechanical Behavior of Anvil Points Oil Shale at Elevated Temperatures and Confining Pressures". Canadian Geotechnical Journal, Vol. 20, No. 2, pp. 344-352.

Zienkiewicz, O.C., 1977. "The Finite Element Method". McGraw-Hill Book Company, Third Edition, London, England, 787 p.

Zienkiewicz, O.C., Leung, K.H. and Hinton, E., 1982. "Earthquake Response Behaviour of Soils with Drainage". In Proceedings of the Fourth International Conference on Numerical Methods in Geomechanics, Edited by Z. Eisenstein, Edmonton, Alberta.

Zimmerman, R.W., Somerton, W.H. and King, M.S., 1986. "Compressibility of Porous Rocks". Journal of Geophysical Research, Vol. 91, No. B12, pp. 12765-12777.

Zoback, M.D. and Byerlee, J.D., 1976a. "Effect of High Pressure Deformation on Permeability of Ottawa Sand". The American Association of Petroleum Geologists, Bulletin, Vol. 60, No. 9, pp. 1531-1542.

Zoback, M.D. and Byerlee, J.D., 1976b. "A Note on the Deformational Behaviour and Permeability of Crushed Granite". Int. J. Rock Mech. Min. Sci. and Geomech., Abstr. Vol. 13, pp. 291-294.

Zwicky, R.W. and Eade, J.R., 1977. "The Tar Sands Core Analysis Versus Log Analysis Controversy - Does It Really Matter?". The Oil Sands of Canada-Venezuela, 1977, Canadian Institute of Mining and Metallurgy Special Volume 17, D.A. Redford and A.G. Winestock, eds., Edmonton, pp. 256-259.

A. EQUIPMENT DETAILS

High Temperature Triaxial Cell

The essential features of the high temperature and high pressure triaxial cell are shown in Figure A.1. The cell was designed to operate at confining pressures up to 30 MPa, back pressures up to 27 MPa and temperatures up to 315°C. Loads up to 440 kN can be applied to shear the test specimen. Interchangeable load cap and internal load cell assemblies allow the testing of specimens 54 mm, 63.5 mm and 76 mm diameter by 108 mm, 127 mm and 152 mm in height, respectively.

The triaxial cell is constructed of 316 stainless steel. The cylindrical cell wall houses eight equally spaced 1000 watt (at 240 volts) cartridge heaters 12.7 mm in diameter by 305 mm long. A J-type thermocouple is located at the midpoint between two of the heating rods to monitor temperature and to provide feedback to the controller powering the heaters. Top closure is provided by a threaded and countersunk plate sealed with an O-ring. The loading piston ram accesses the cell through a hole in the center of the top plate and is sealed with two O-rings.

Strain gauge wires for internal instrumentation, ports for application of back and confining pressures and thermocouples for temperature determinations egress the sample chamber through pressure sealed fittings in the threaded pedestal/threaded base plate assembly (Figure A.1). An O-ring is utilized to pressure seal the base plate to the

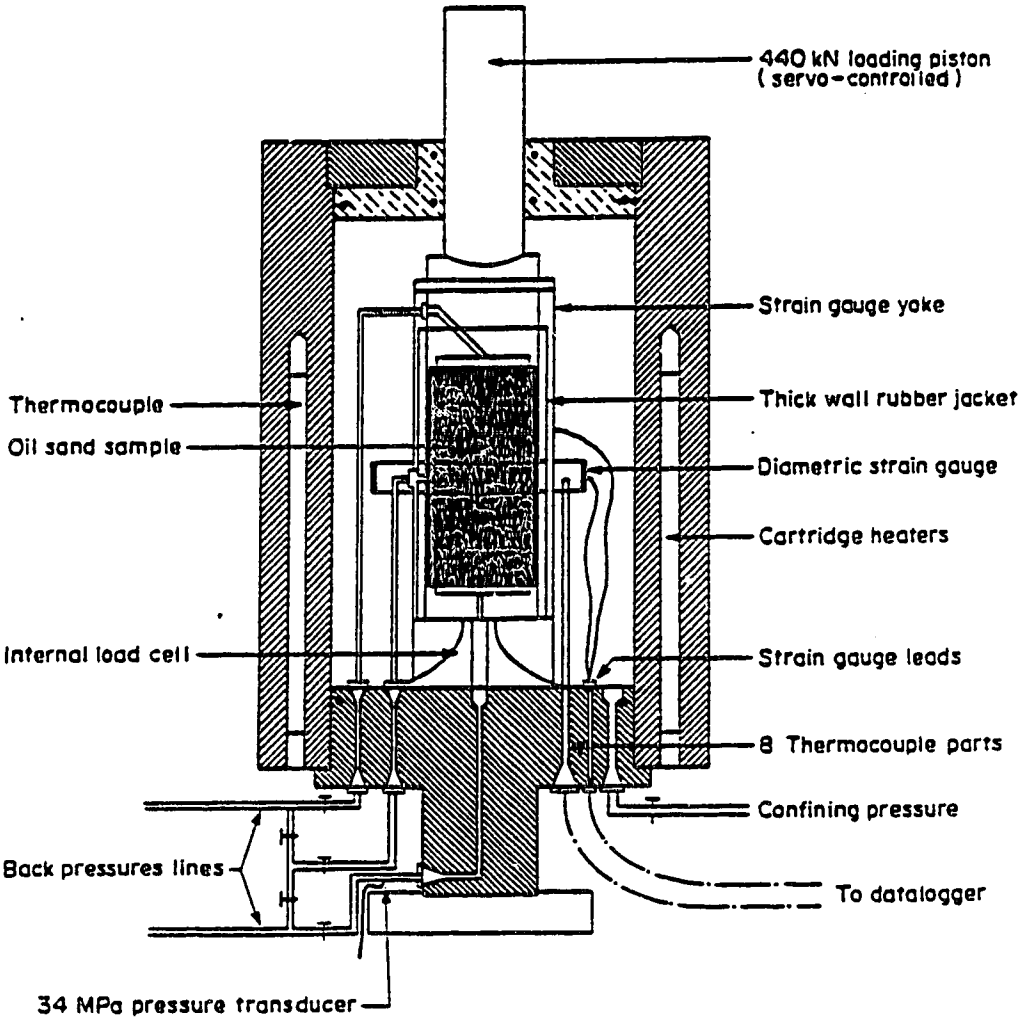

Figure A1: High Temperature Triaxial Compression Cell
With Internal Load Cell.

cell wall. Fusite connectors are used for connecting strain gauge wires from the internal load cell, vertical strain arms and diametric strain device (Figure A.2).

The test specimen rests directly on the internal strain gauge load cell which is bolted to the base plate as shown in Figure A.2. Back pressure drainage ports access the specimen through porous stainless steel discs recessed in the load cell and loading cap. The specimen is isolated from the cell fluid by a flexible teflon or silicone rubber membrane which is sealed to the load cell and loading cap by internal O-rings and external stainless steel adjustable clamps.

Internal axial strains are measured by a yoke and cone assembly attached to the loading cap and internal load cell as shown in Figure A.2. As vertical displacement of the test specimen occurs, the stainless steel strained gauged arms of the yoke (fastened to the loading cap) are displaced laterally by the steel cone fastened to the load cell. Each internal load cell and corresponding loading cap is proportioned in height to enable equivalent positioning of the yoke and cone assembly.

The triaxial cell was also designed to incorporate an additional back pressure drainage port which may be connected to the mid-height of the specimen through the membrane and a lateral strain gauge clamp which may be fastened to stainless steel buttons casted in the membrane wall.

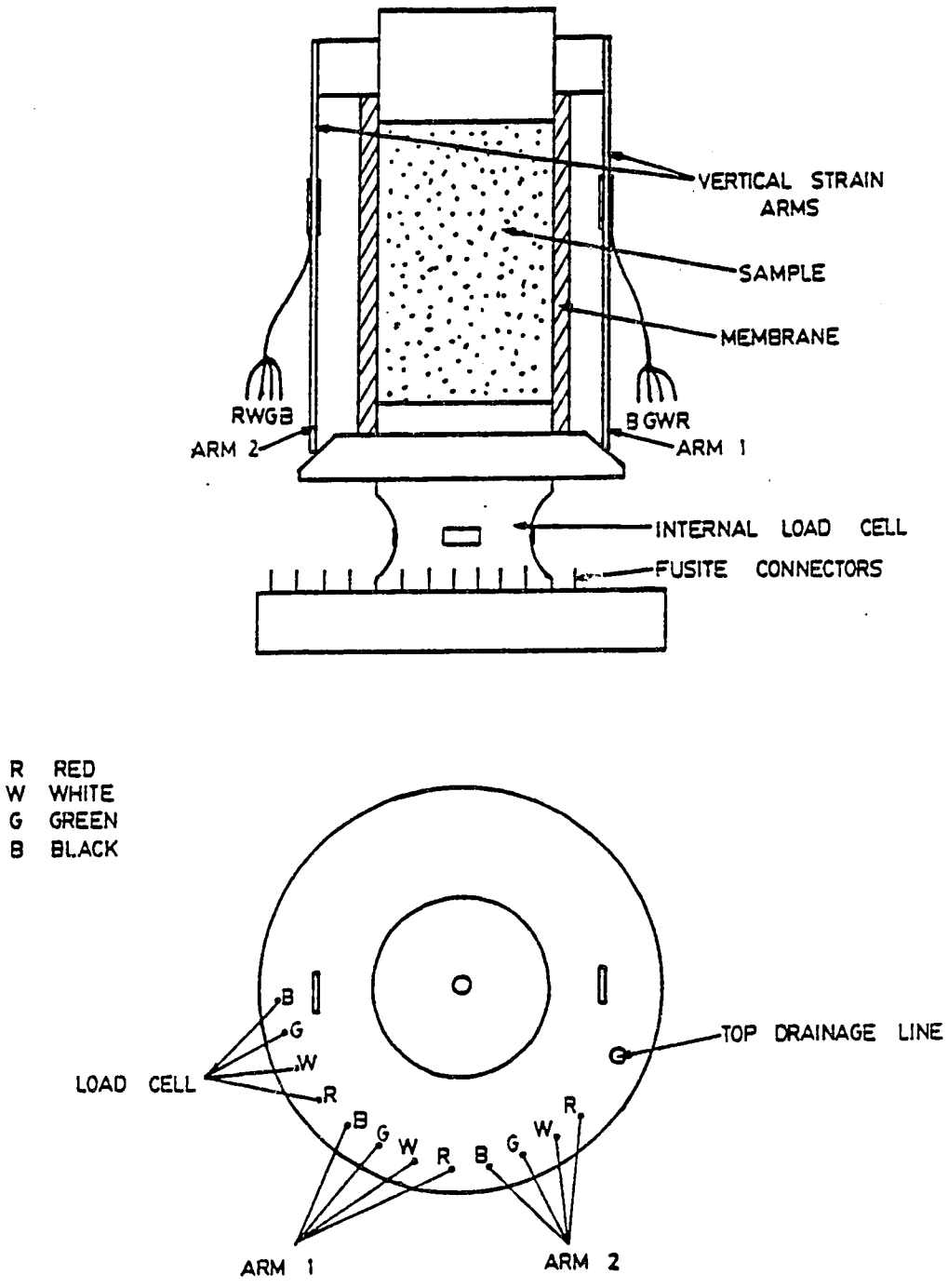

Figure A2: Sketch of Installation and Wiring of the Internal Load Cell and Vertical Strain Arms.

High Temperature Oedometer Cell

The oedometer can measure one-dimensional compressibility under stresses up to 30 MPa and temperatures up to 315°C. Vertical compression, pore fluid pressure, and volume change of the specimen can be measured. The pressure injection system can also be used with the oedometer to measure permeability and to flush out bitumen.

A schematic drawing of the oedometer cell is shown in Figure A.3. Specimens 54 mm and 76 mm in diameter and up to 76 mm in height may be inserted in the cell through interchangeable stainless steel rings. Each specimen ring is equipped with a loading piston and the specimen chamber is sealed by rubber O-rings on the piston and around the bottom of the ring. Vertical stress is applied hydraulically through a ram mounted on top of the cell. A constant pressure air actuated pump is utilized to apply the hydraulic pressure to the ram. An LVDT is mounted on the top of the cell to measure vertical displacement of the ram and sample. Back pressure may be applied to the top or bottom of the specimen through ports located in the side of the cell. To ensure a uniform distribution of pressure across the faces of the specimen back pressure is conveyed through a network of holes in the loading piston and oedometer base to sintered stainless steel discs and glass filter paper placed on the top and bottom of the specimen. This configuration also aids in inhibiting fines from being washed from the specimen during testing.

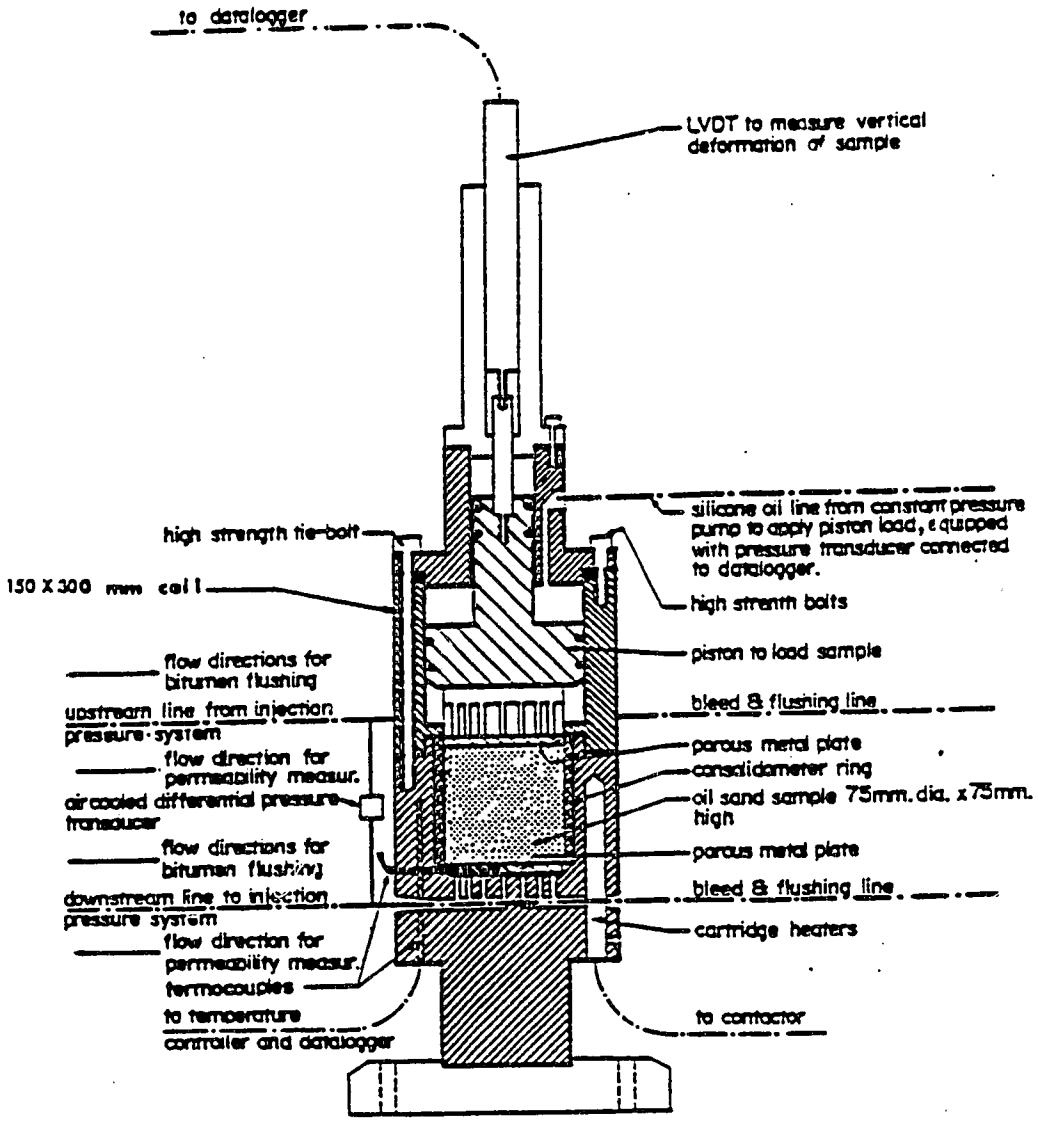

Figure A3: High Temperature Consolidometer.

The oedometer cell wall houses four equally spaced 500 watt (at 240 volts) cartridge heaters 12.7 mm in diameter by 102 mm long. A J-type thermocouple is located at the midpoint between two of the heating rods to monitor temperature and to provide feedback to the controller powering the heaters. An additional thermocouple is located in the bottom stone for monitoring the specimen temperature.

Pressure Systems

Pressure systems used to apply cell pressures, back pressurese and pressure systems for loading the high temperature triaxial cell, high temperature oedometer and room temperature triaxial cell are schematically shown in Figures A.4, A.5 and A.6.

The low pressure system (0 - 1 MPa) is driven by a compressed air system. This pressure system is controlled by Moore Regulators which are self-relieving.

The medium pressure range is to 4 MPa and consists of a series of Circle Seal "Dynareg" regulator relief valves driven by a nitrogen booster pump (Haskel - single acting - single stage). This pump supplies up to 34 MPa pressure. The nitrogen booster is driven by a compressed air system with a nitrogen bottle to supply the nitrogen for the system. A 17 MPa pressure can be maintained on the upstream side of the Dynareg valves with a nitrogen reserve pressure of only 700 kPa.

Additional pumps for use in the mid to high pressure range (4 - 30 MPa) consist of air actuated diaphragm pumps

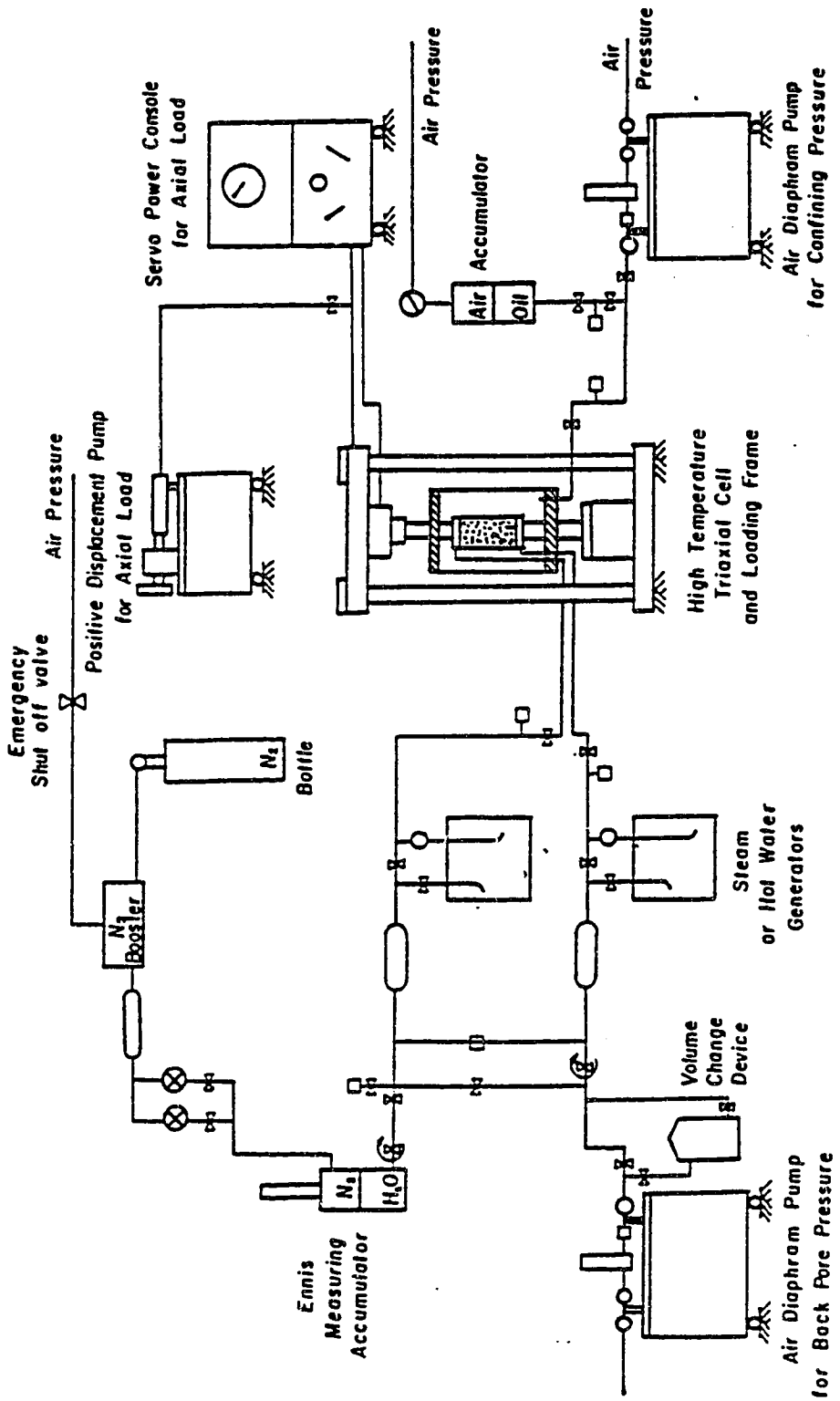

Figure A4: Schematic of High Temperature and High Pressure Triaxial Cell and Pressure Systems.

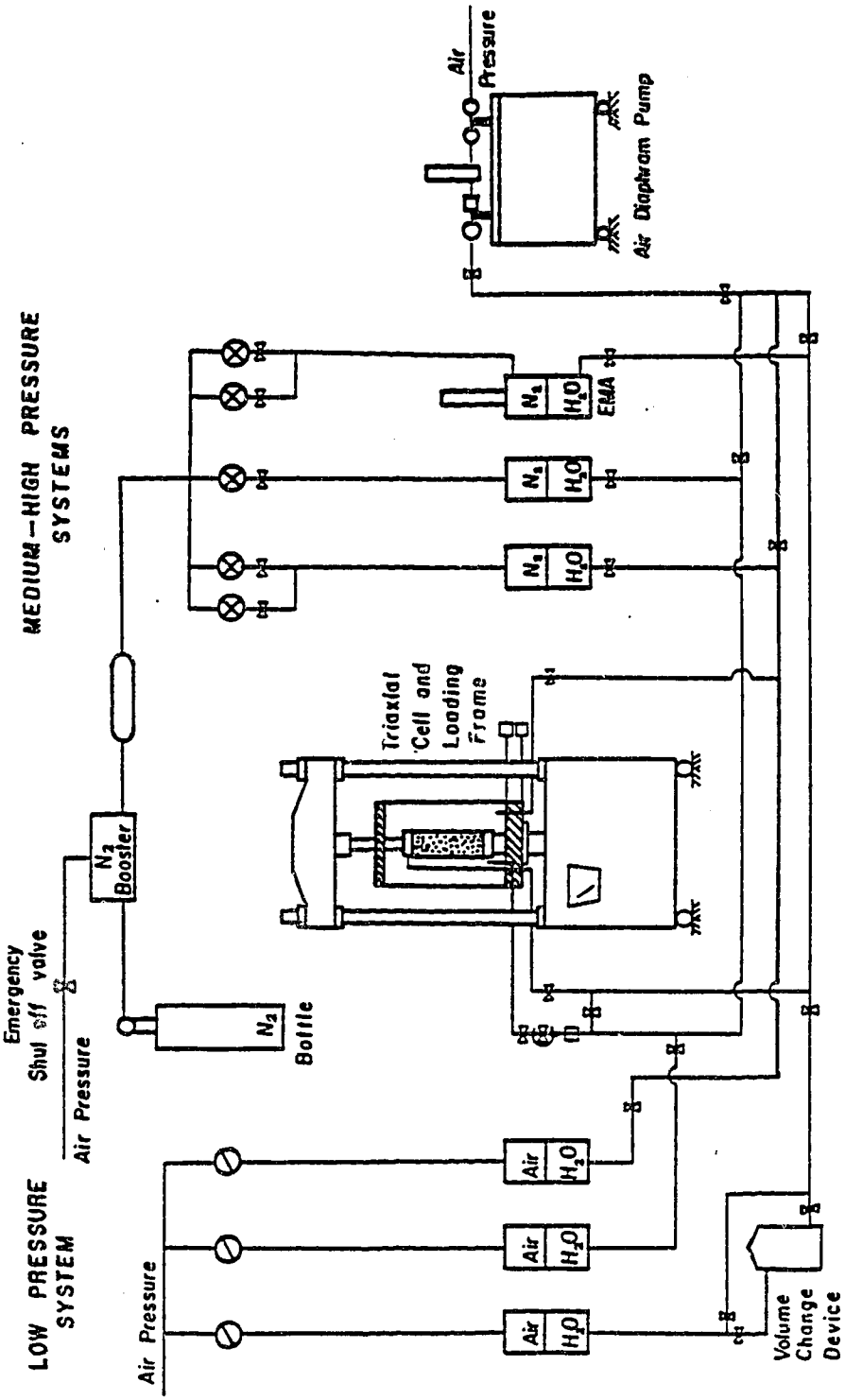

Figure A5: Schematic of Room Temperature Triaxial Cell and Pressure Systems.

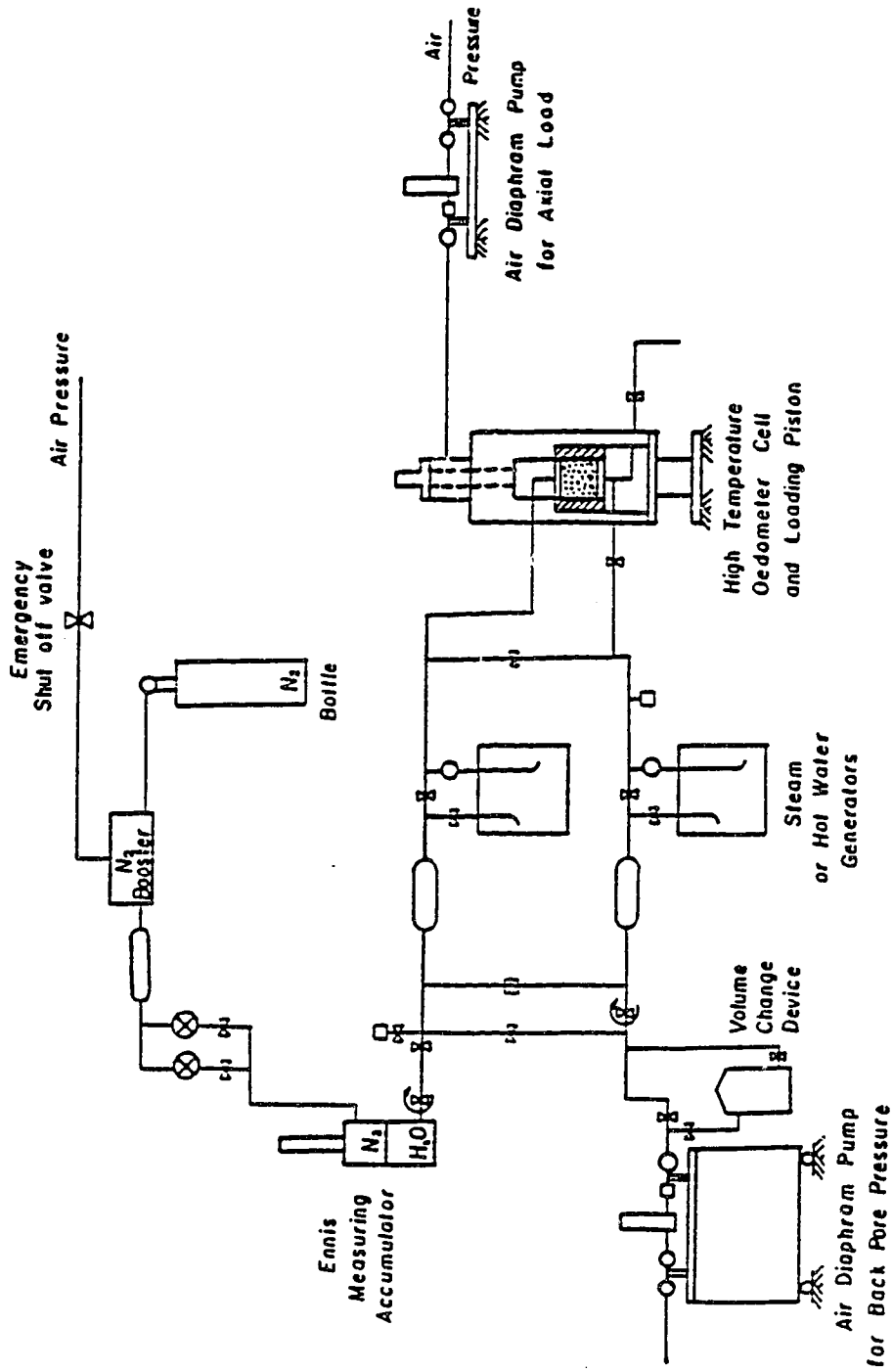

Figure A6: Schematic of High Temperature Consolidometer and Pressure Systems.

(SBEL Model AP-300 and AP-500). These pumps are driven by a 700 kPa compressed air system. A schematic diagram of the pump components and assembly is shown in Figure A.7. For fluid pumping or static pressure applications, the pump diaphragm responds to slight decreases in fluid pressure. These pumps suffer as constant pressure sources since as the diaphragm engages the pressure decreases instantly by about 5% prior to restoring the set point pressure. The system is, however, equipped with an accumulator which aids in damping large fluctuations in pressure during static tests in the 4 to 30 MPa pressure range.

A 440 kN hydraulic jack mounted in the top plate of the triaxial loading frame supplies the vertical load to the triaxial cell. Strain controlled testing is performed utilizing a positive displacement pump ("Jeffri pump"). The pump can operate to 35 MPa and is controlled by a micro processor which can be programmed to supply fluid at a specified constant rate. The micro processor controls a servo motor which drives a piston into a fluid filled cylinder. An LVDT is used to control the rate of volume applied to the loading ram in the high temperature triaxial loading frame. The stress controlled system (block diagram - Figure A.8) utilizes a servo-controlled electric motored powered hydraulic pump which drives the hydraulic jack. The servo controlled system built by SBEL (Model 327 E) uses a load cell as a feedback to control the hydraulic pump; that is, the rate at which the fluid is supplied to the jack.

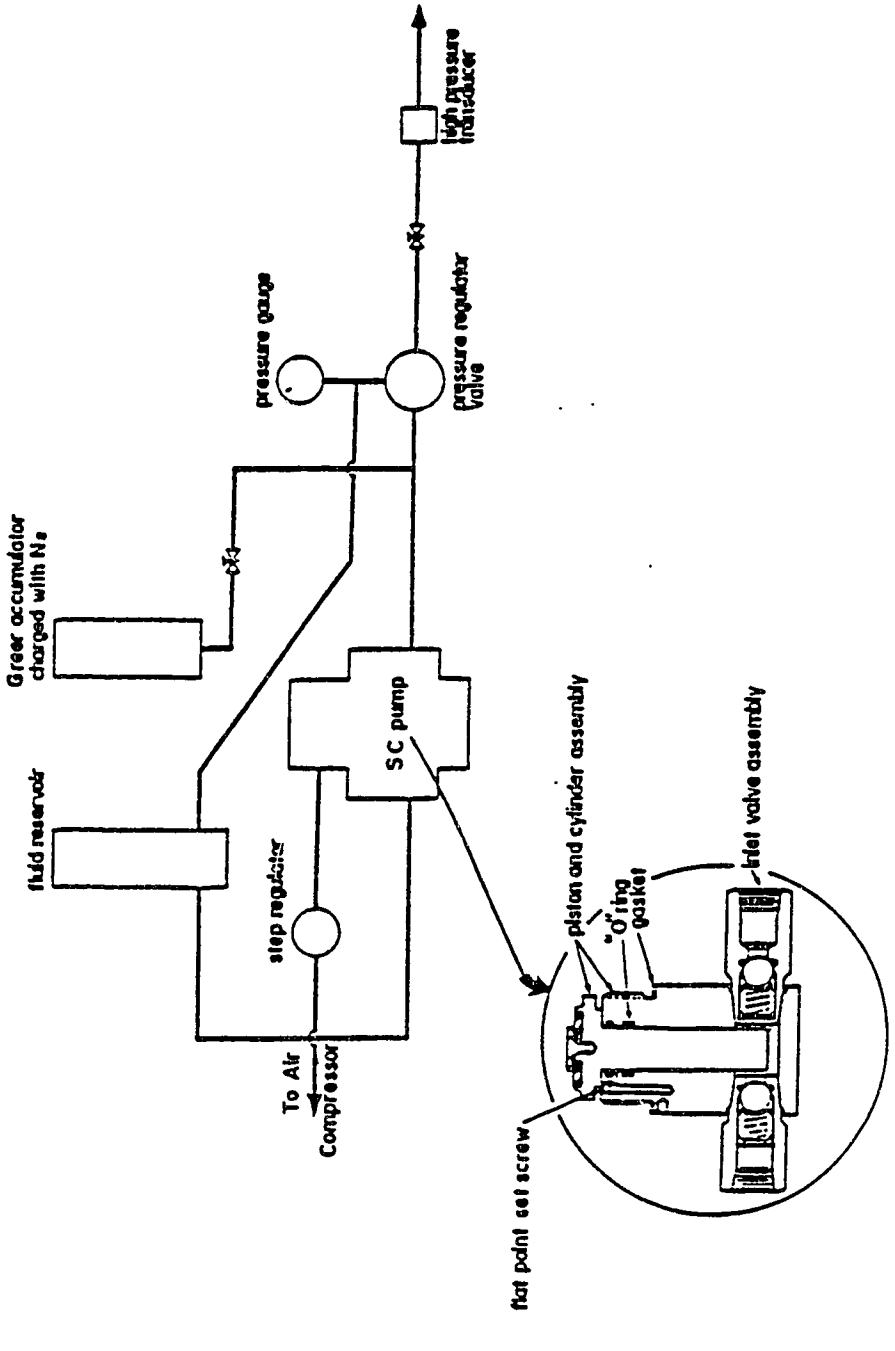

Figure A7: High Pressure Air-Actuated Pump.

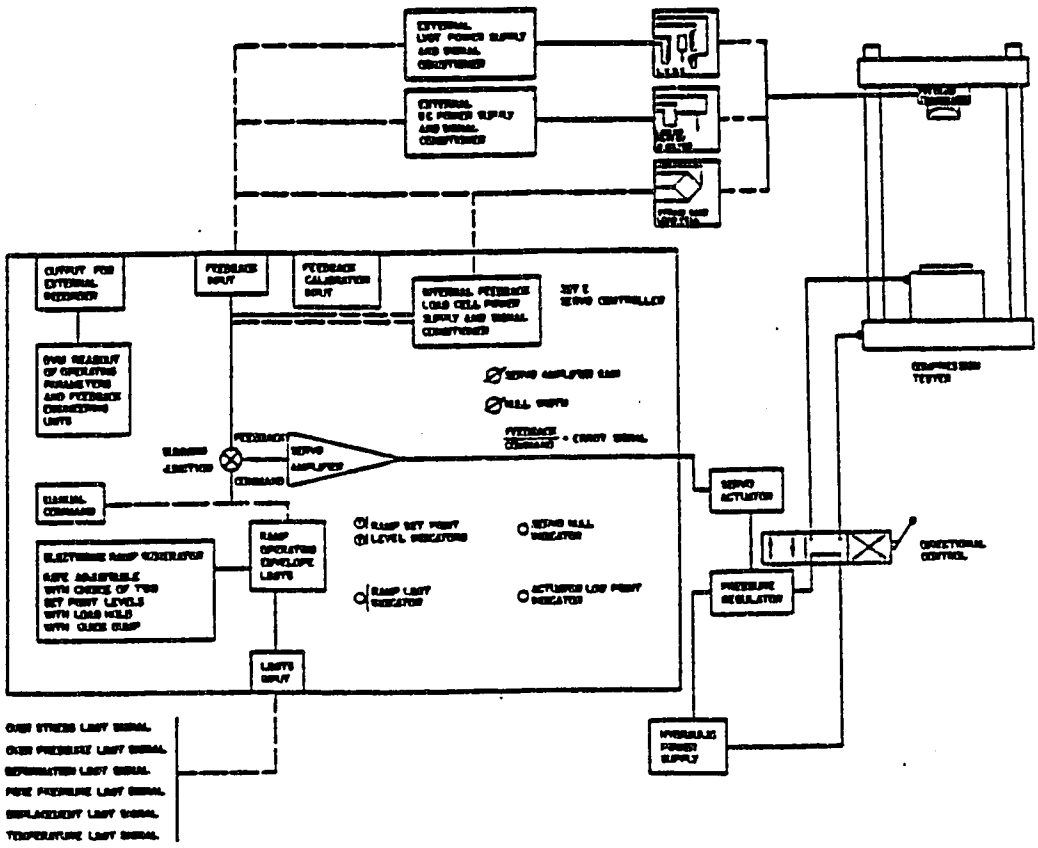

Figure A8: Servo-Controller: Block Function Diagram.

Present limits can be programmed prior to testing. This system can also be used for strain rate testing but it was found that the positive displacement pump gave better control.

The above pressure systems have accumulators plumbed in line for maintaining pressures, dampening pressure spikes, allowing changes from gas to liquid pressure systems. Some accumulators have the ability to measure volume change of the pressurizing fluid. The "Ennis Measuring Accumulator" (EMA) shown in Figure A.9 is constructed of stainless steel and has a capacity of 500 ml. It operates by applying gas pressure (at constant pressure) on the upstream side of a piston which separates the gas from a confining fluid, usually water. The piston is connected to an LVDT which measures the displacement of the piston. Through a calibration, displacements are converted to a volume change measurement.

Volume Change Devices

In addition to measuring accumulators the laboratory equipment is supplied with a bellows volume change device. The bellows volume change device (Figure A.10) consists of a fully enclosed chamber with a metal bellows mounted on the base. The cylindrical bellows expands and contracts vertically under pressure gradients as small as 0.5 kPa. To prevent the bellows from buckling travel is limited by three stainless steel rods inserted in the bottom flange in the middle of the bellows. An LVDT connected to the top of the

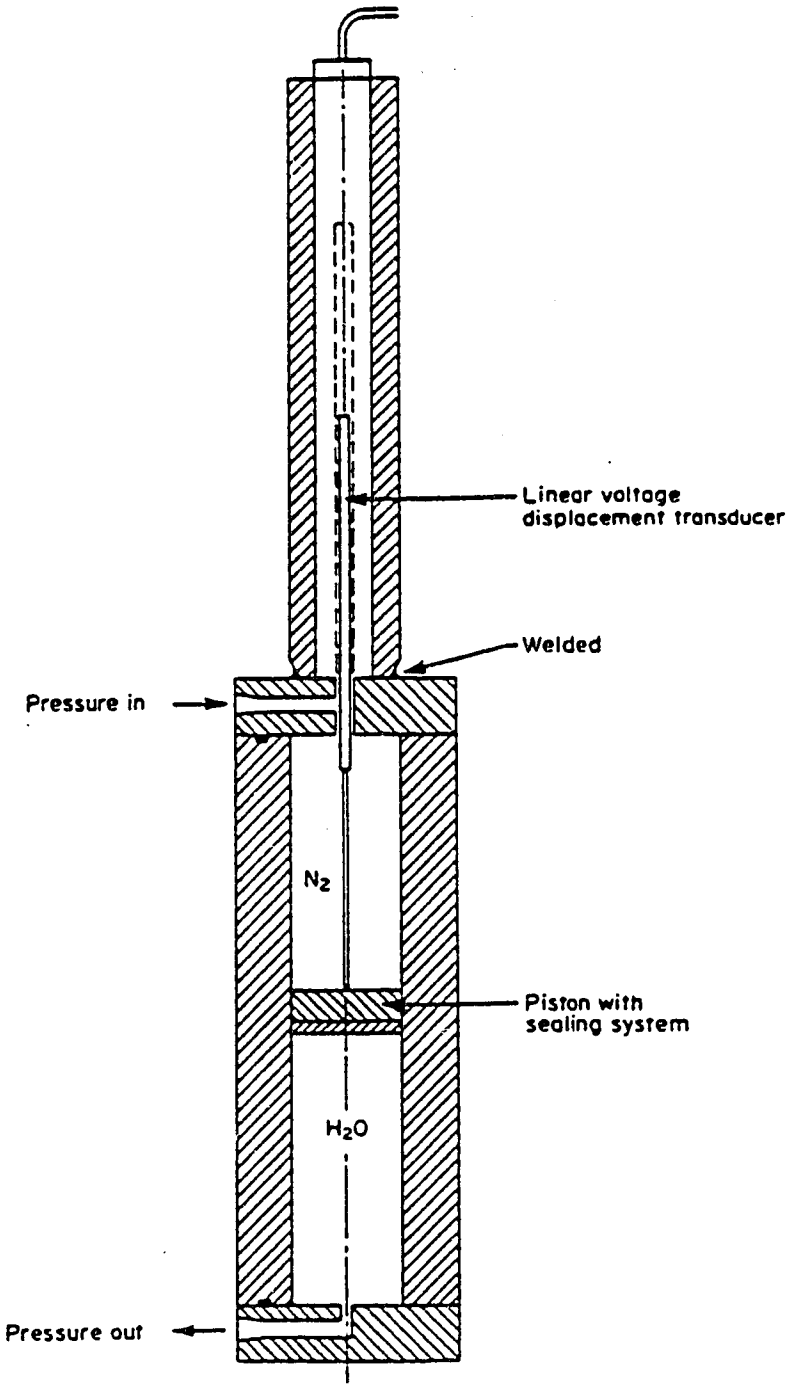

Figure A9: Ennis Measuring Accumulator (EMA).

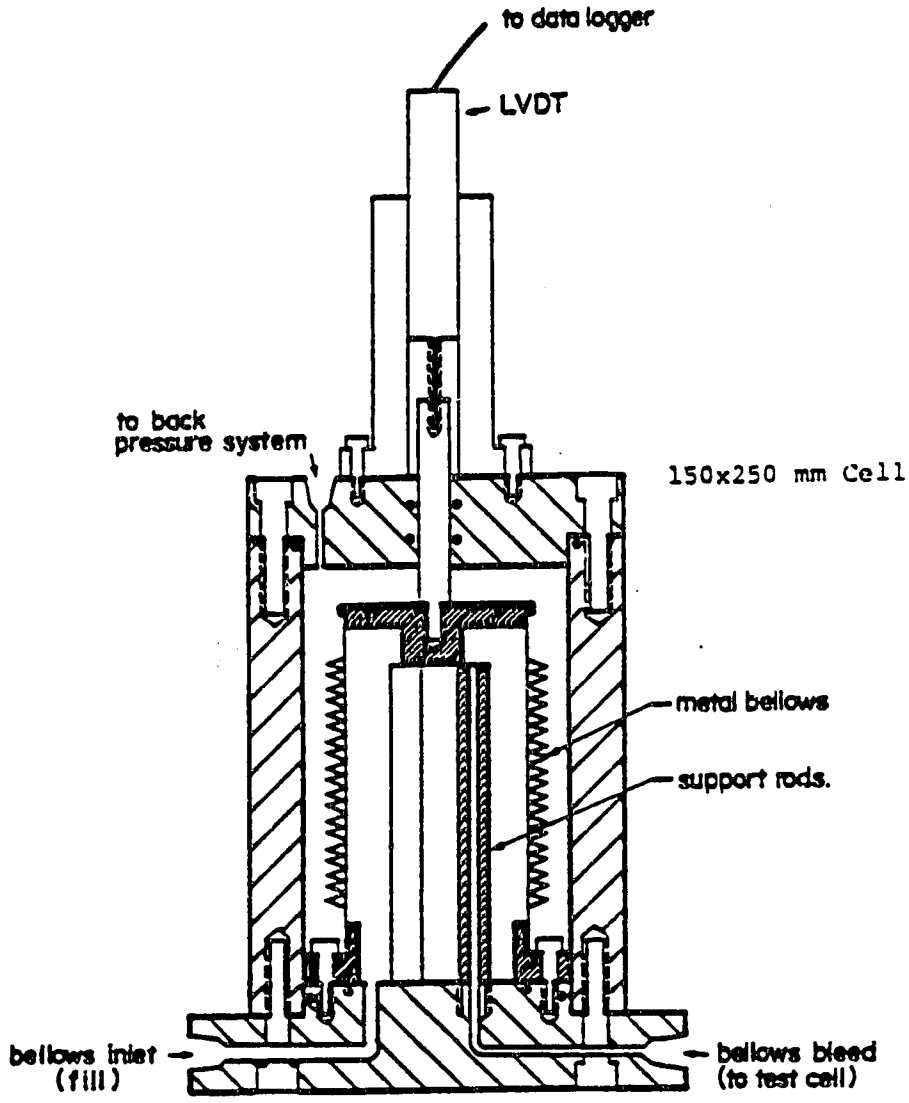

Figure A10: Bellows Volume Change Device.

bellows is used to measure displacements which are converted through a calibration factor to volume change measurements. The volume change device can operate under temperatures to 315°C and a maximum of 100 ml can be displaced. The device is limited to a differential pressure of 450 kPa when it is fully extended or contracted.

High Temperature Cell Loading Frame

The loading frame (Figure A.11) is constructed from 416 stainless steel and has a capacity of 450 kN. The frame consists of a top and bottom plate each 560 mm by 560 mm by 75 mm thick and four threaded rods, each 50 mm in diameter by 1400 mm long. On the outside of these rods a sleeve of 25 mm wall thickness is placed over the rod. This arrangement allows the frame to be prestressed to 440 kN. Strain gauges were mounted on the sleeves to ensure equal stressing was applied to all four rods on the frame. This prestressing allows the measurement of the post-peak stress-strain curve which otherwise would be difficult to measure due to excessive energy release from the test frame.

Internal Strain Gauge Load Cell

Internal mushroomed shaped load cells were designed from 416 stainless steel (tempered above 250°C) were incorporated inside the high temperature triaxial cell. This allows testing without being concerned with calibrating for piston friction. Sketches of the load cell mounting and wiring in the triaxial cell are shown in Figures A.1 and

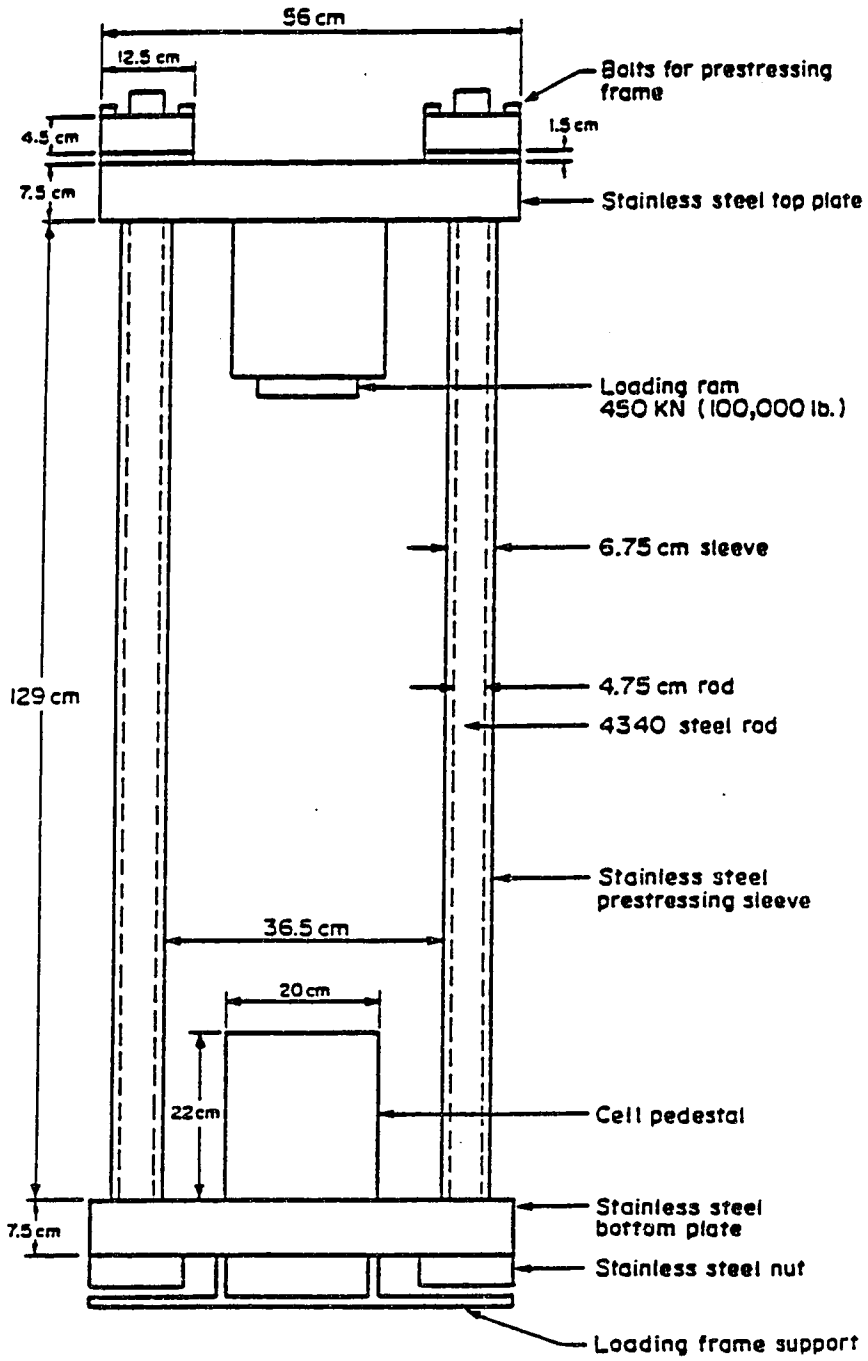

Figure A11: Loading Frame.

A.2.

Hot Water or Steam Generators

Upstream and downstream hot water or steam generators each with a 1900 ml volume capacity act as reservoirs of hot injection fluid and serve as reservoirs for collection of bitumen drained or flushed from the specimen during injection or permeability testing. A steam generator is shown schematically in Figure A.12. The generator chambers are constructed of 316 stainless steel and are heated by electrical steel heating jackets over the surface area of the generators and produce 2.5 watts/cm^2 at 240 volts.

Valves and Lines

High pressure stainless steel Whitey valves are used throughout the system. For safety, air operated valves are used on the steam generators to allow immediate shut down from the main control station. Stainless steel (316) tubing is 6.35 mm outside diameter and is consistent with ASTM Standard A-269. Tubing wall thickness varies from 0.89 mm in the room temperature zone (rated for pressures up to 40 MPa) to 1.24 mm in the heated zone (rated for pressures up to 55 MPa at 300°C). Stainless steel tubing in the heated zone is heated with silicone rubber heat tracing which supplies a wattage density of 2.2 watts/cm^2 at 120 volts.

O-Rings

O-ring seals originally supplied with the equipment by the manufacturer (Kalrez Compound 3018, manufactured by

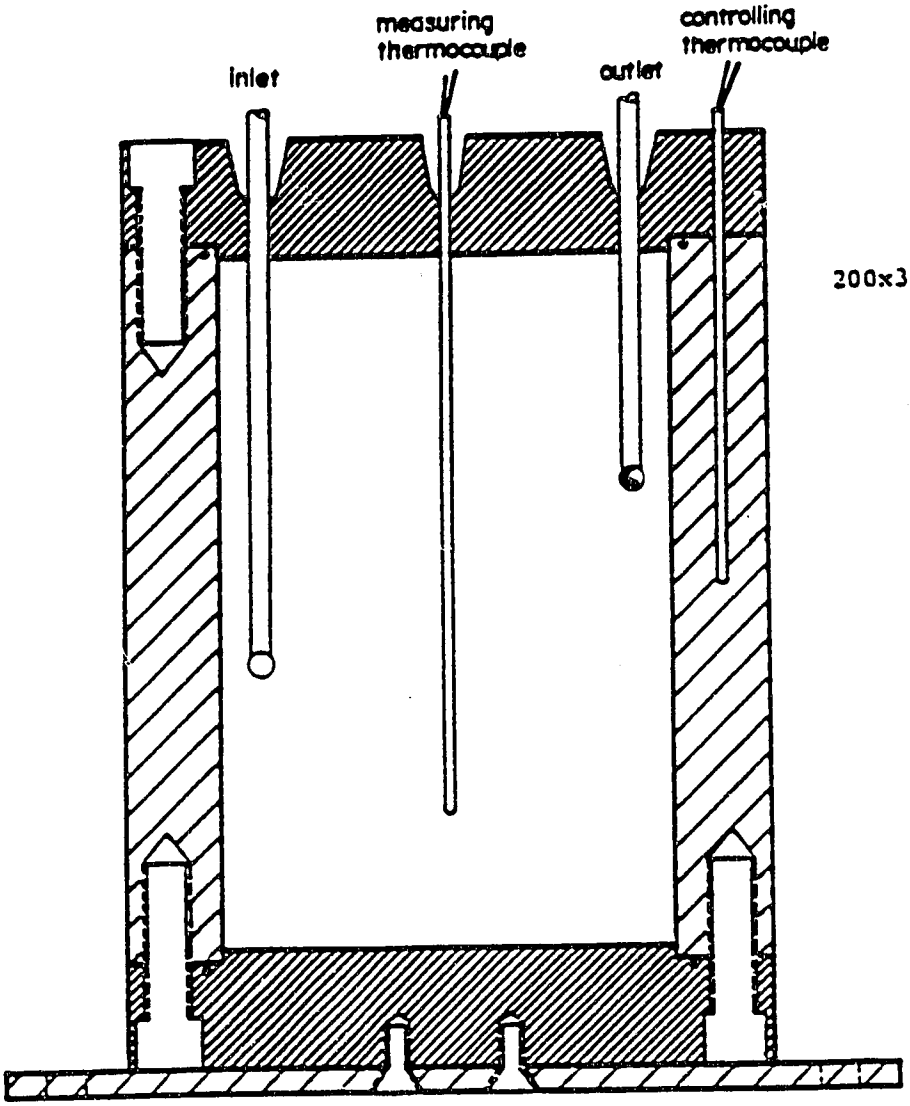

Figure A12: Steam Generator

Dupont) proved susceptible to degradation through thermal cycling. As a consequence, O-rings composed of chemical compounds commercially referred to as Vitan and Kalrez Compounds 1050 and 1018 were adopted for use. These compounds are more resistant to degradation over the operational temperature range of the equipment, are more compatible with petroleum products and are more stable during frequent thermal cycling. Steam generators were equipped with metal O-rings.

Insulation

Heated components of the laboratory equipment are externally insulated with "Fibrefrax Moist-Pack D" manufactured by the Carborundum Company Insulation Division. The material is composed of ceramic fiber and an inorganic binder which is easily workable but cures to a rigid structure. The insulation is composed primarily of alumina-silica with an operational limit of 1260°C. The material has good thermal reflectance, low heat storage and low thermal conductivity.

Electronic Signal Conditioning and Data Acquisition Systems

The majority of transducer circuits are Wheatstone bridge configurations. Constant voltage from the power supply is transmitted by the signal conditioner to each electronic transducer. The signal conditioner receives output voltage signals from the transducers and sends these signals to the data acquisition system. The output voltage

signals are normally adjusted (corrected for electronic zero drift) prior to transmission to the data acquisition system.

The data acquisition unit was manufactured by the Hewlett Packard Company. The unit consists of an "HP-85F Desktop Computer" and an "HP-3497A Data Acquisition Control Unit".

The data logger is programmable to print measurements on paper as well as record on floppy disks. During testing up to three channels can be monitored on the CRT display. The data recorded by the unit on the floppy disk is transferable through a "gandolf" serial interface to the University mainframe "AMDAHL" computer for processing.

The operational use, although not complex, is somewhat involved and will not be discussed here. Procedural instructions and unit specifications are available in the "Operator's Handbook" accompanying the equipment.

Temperature Control Systems

Oedometer and triaxial cell cartridge heaters are controlled by two independent microprocessor-based (Model 580) temperature controllers manufactured by the Barber-Colman Company. The controllers have a rated accuracy of ±(0.5% of reading + 2°C) and a temperature range of 0 to 400°C. The controllers have a temperature sampling time of three per second. Detailed specifications are available from the manufacturer.

Three additional temperature controllers control the temperatures of the steam generator heating jackets and

tubing heat tracing. Two of these controllers were manufactured by Omega Engineer Inc. and the remainder by Chromalox. The control boxes have internal microprocessor based set-point delay time relays rated at 7 amps at 120 volts A.C.

The relays of the control boxes are wired through an external 20 amp circuit breaker. The set-point delay time microprocessor relay responds to feedback from thermocouples and turns the heating elements on and off at a fixed time interval to reach and hold the set-point temperature.

Multiple Range Differential Pressure Transducers

Valedyne transducers consist of a diaphragm mounted between two stainless steel blocks. On each side of the diaphragm is an E-shaped inductance coil. When a pressure is applied to the diaphragm it deflects changing the electrical output.

Differential transducers are useful in measuring the pressure gradient across test specimens and to accurately measure pressures from various pumps and loading systems over a wide range of pressures by inserting the appropriate pressure range diaphragm.

Triaxial Sample Membranes and Cell Fluids

RTV silicone rubber manufactured by Dow Corning and Canadian General Electric were initially used to enclose triaxial specimens. RTV silicone rubber was purchased in liquid form with the accompanying catalyst. A mold and

injection system were constructed for forming 54 mm and 75 mm inside diameter membrane jackets. A schematic diagram of the membrane mold is shown in Figure A.13. RTV silicone rubber was found susceptible to swelling and depolyerization at elevated temperatures. The practical temperature limit was determined to be 200°C. As a consequence, teflon membranes were adopted for triaxial testing at 225°C. "Heat Shrink" teflon tubing 0.5 mm in thickness provided greater reliability due to its compatibility with oil at elevated temperatures.

Copper membranes machined from tubing were developed utilizing a tapered end cap O-ring sealing mechanism. Copper is non-reactive with oil cell fluid and is stable to 1000°C. However, the excessive cost and time required to machine membranes prohibited routine usage.

Silicone oil with graphite additive was initially used as the triaxial cell fluid. Silicone oil, however, resulted in degradation of RTV silicone rubber at elevated temperatures. This oil was replaced by "Essotherm N-69" oil which permitted limited short term usage of silicone rubber at 225°C. Both oils are temperature stable; that is, they possess a high flash point and low vapourization pressure.

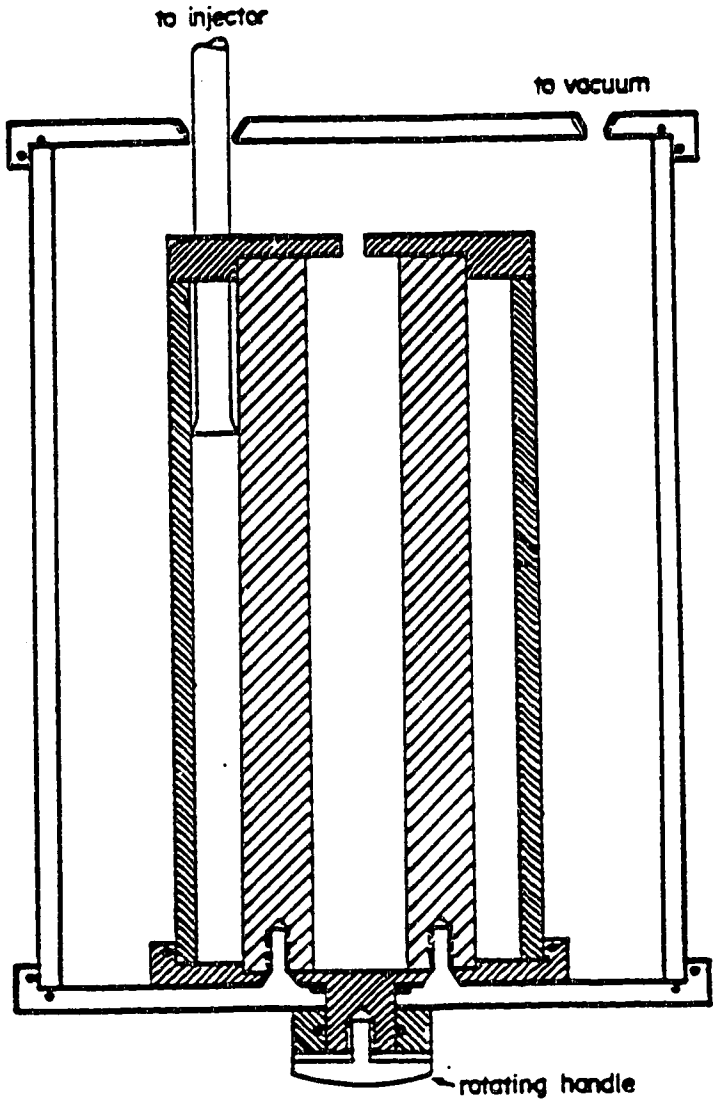

Figure A13: Mould for Forming Rubber Triaxial Membranes.

B. SAMPLE PREPARATION AND TEST PROCEDURES

Sample Preparation

Oil sand and heavy oil cores must be frozen as soon as possible after recovery to minimize gas evolution and volume change in order that the mineral grain structure is undisturbed as little as possible. Valid geomechanical and thermal properties can only be obtained from such undisturbed cores.

The cores are kept frozen during transportation to the laboratory where they are sealed in plastic and stored in a cold room at -20 to -25°C. When an oil sand sample is required for testing a piece of frozen core is taken and sealed in an air-tight metal container. The container is then placed in a styrofoam receptacle and covered with dry ice. Sealing the sample in a metal container prevents disturbance of the sample from carbon dioxide gas emitted from the dry ice. The container is left in the dry ice (at approximately -78°C) for several hours.

To obtain a test sample of the proper dimensions, the piece of highly frozen core is first machined to the correct diameter (using a diamond bit) in a lathe situated in the cold room. To inhibit swelling of the specimen from heat developed during machining, the sample is trimmed in stages, between which the sample is sealed in the metal container and placed in dry ice for several minutes. After the sample is machined to the correct diameter it is cut to the required height using a diamond saw which is also located in

the cold room. The final stage involves machining the ends of the sample flush and smooth. The test sample is also mounted in the required testing apparatus in the cold room prior to transfer to the testing laboratory. Final assemblying of the test apparatus, confining the sample under the required vertical and horizontal stresses, and raising the sample fluid pressure to the desired level is accomplished before the sample thaws.

After thawing and when the sample has reached equilibrium under the applied stresses, the required test is carried out.

Test Procedures

Procedure for Room Temperature Triaxial Test

1) Saturate the sintered stainless steel stones with deaired water. Boil for 15 minutes if necessary.
2) Saturate all lines to and within the cell with water.
3) Machine a sample to a length of 4 inches(10.16 cm) and diameter of 2 inches (5.08 cm). Measure sample and weigh for density calculation. Take sample from dry ice storage. Saturate radial filter paper with distilled water and apply to frozen sample. Roll the sample on the filter paper on a smooth hard surface to remove air bubbles. Trim if required. Wet the top and bottom filter papers and apply to ends of the sample, pressing to remove air bubbles. Place sample

back in freezer for 5 minutes. Note: Prior to mounting, ensure that there is communication between radial strips and the ends of the sample.

4) Mount sample in cell using two rubber membranes. Assemble cell and install in test frame. With loading mechanism in neutral crank up ram until system is tight. Pump cell full of water. Apply a cell pressure of 200 kPa, then apply a back pressure of 100 kPa. Let thaw overnight with drainage ports open. Measure volume change (amount flowing in, which reflects compression of gas bubbles less consolidation of sample under 100 kPa effective stress).

5) Close drainage port to sample. Run B test under constant effective stress of 100 kPa. Raise confining and back pressure in equal increments of 100 to 200 kPa. Perform B test following each increment in pressure and determine the variation of B with pore pressure. The B value will level off when the pore fluid saturation pressure is reached.

6) Once the pore fluid saturation pressure is established, carry out cyclic compression tests. With back pressure maintained slighty above pore fluid saturation pressure, apply effective confining pressure in increments of 1 MPa to required stress level and measure volume change. Perform at least three cycles of stress, and calculate the bulk

modulus for each test.

7) Rerun B test after completion of the cyclic compression test and calculate final B value.

8) Perform drained triaxial compression test:
Back pressure: slighty above saturation.
Cell pressure: 1.5 MPa effective stress/100 m depth.
Strain rate: 5×10^{-7} sec^{-1}
Machine rate: 1.2×10^{-4} in/sec.

9) After the test remove sample and freeze. Measure density and sketch failure mode.

Procedure for Room Temperature Triaxial Cell for Stress Path Testing

For this testing the upper platen has an O-ring in the top so that the cell pressure can be isolated from the loading ram.

1) Assemble specimen as per usual procedure.

2) Assemble triaxial cell, ensure O-ring on top platen is well greased and loading piston is seated on O-ring.

3) Position cell in compression frame, hook up cell pressure line and cell pressure transducer. Hook up pore pressure transducer leaving one side of bottom porous stone blocked and apply vacuum to the other bottom drainage port.

4) Zero internal load cell and apply a vertical stress of 100 kPa.

5) Fill up triaxial cell with water and apply confining

stress of 100 kPa.

6) Readjust the vertical stress to 100 kPa using load cell readings before and after applying the 100 kPa confining stress.

7) Remove vacuum from specimen and first apply a vertical stress of 200 kPa followed by a confining stress of 200 kPa.

8) Apply a back pore fluid pressure of 100 kPa using burrette to record volume. Let thaw and saturate overnight. Increase vertical and confining stress to 300 kPa.

9) Increase the vertical stress and confining stress and the pore fluid pressure in 200 kPa increments until desired levels are obtained. For all stress path tests: back pore fluid pressure of 2500 kPa, vertical and confining stress of 5000 kPa is applied which results in effective vertical and effective lateral confining stresses of 2500 kPa.

10) For the J1 tests, an effective confining stress of 2500 kPa is applied. An average principal effective stress of 2500 or 5000 kPa is maintained throughout the test by increasing the vertical stress at constant strain rate and decreasing the confining stress proportionally. Desired strain rate is 100 kPa/minute

11) Perform B test.

12) Do 3-D cyclic compressibility at 2 MPa above and 1

MPa below test pressure. That is 2000 kPa above 2500 kPa (effective confining stress) and 1000 kPa below 2500 kPa (effective confining stress).

High Temperature and Pressure Triaxial Test Procedure

1) Saturate sintered stainless steel stones. Boil for 15 minutes if necessary.
2) Saturate all lines to and within cell.
3) Cool down partially assembled cell base and platens in the freezer. Leave hydraulic jack and screw assembly outside cold room to transport sample to lab.
4) Preshrink Teflon membrane, allowing for tolerances needed to place membrane over sample and filter paper. Note: oil sand tests will not require filter paper.
5) Precut top, bottom, and radial filter paper (use Whatman Glass Microfibre filters). Saturate these filter papers with water and place on table outside freezer.
6) Take sample from dry ice and apply radial filter paper by rolling it carefully across the filter paper. Care must be taken because the filter paper freezes instantaneously to the sample and cannot be removed easily. Place top and bottom drainage paper on the sample. Return sample to freezer.
7) While in the freezer the teflon membrane and then

the rubber membrane are mounted on the sample. The sample and membranes are mounted on the lower platen. The top platen is put on with axial strain arms attached.

8) Locate silicon rubber rings and hose clamps on top and bottom platen. The internal drainage line is then installed.

9) Move the completely assembled triaxial cell base to the lab.

10) Screw the base into the bottom of cell. Fill the cell with silicone oil to just below the threads on the top of cell. Screw on top plate then push ram into cell (leave vent open so that air and excess oil are removed). Shut in vent.

11) Place cell in frame and align it with loading ram.

12) Connect all lines. Put on LVDT and insulate the cell.

13) Allow the sample to thaw over night under nominal effective stress (1 MPa), measure volume change. Put on a small back pressure of about 500 kPa in sample. This would mean a cell pressure of 1.5 MPa.

14) Do a quick saturation based on previous tests. Apply back pore fluid pressure of 2500 kPa (effective confining stress of 500 kPa)

15) Perform a B test.

16) Continue saturation until the back pore fluid pressure equals 7500 kPa and the effective confining

stress is that required for test.

17) Do a compressibility in increments to 2 MPa above test pressure and to 1 MPa below test pressure.

18) Perform B test.

Drained High Temperature and High Pressure Triaxial Test Procedure

19) Heat drained to test temperature.

20) Measure compressibility of apparatus and water external to triaxial cell by isolating triaxial cell and then increasing pressure and measuring volume change.

21) Perform one cycle of compressibility approx. 1 MPa above and below test effective stress level.

22) Perform B Test.

23) Shear sample (drained). Record strain rate.

Undrained High Temperature and High Pressure Triaxial Test Procedure

Same as drained except step 23 should be undrained shearing. Back pore pressure should be high enough to prevent gas evolution if pore pressure decreases during shear.

Undrained Heating to Failure Test Procedure

Same as high temp.,high press. procedure to step 18.

19) Apply deviator stress to establish in situ K_o,

drained condition.

20) Heating drained to failure in temperature steps of 5 °C.

Oedometer Tests

1) Saturate, sintered stainless steel stones with deaired water. Boil for 15 minutes if necessary.
2) Saturate all lines to and within cell with water.
3) Machine a sample at a length of 1 inch(2.54 cm) and diameter of 2.125 inches (5.4 cm) or 3.0 inches (7.6 cm). Measure sample and weigh for density calculation. It is very important that the sample fits tightly in the oedometer ring so machining of these samples requires low tolerances. Saturate the filter paper and apply to ends of frozen sample.
4) Put the oedometer ring in the cold room before inserting sample.
5) Install ring into oedometer.
6) Bolt cell together and attach pressure lines, transducers and LVDT.
7) Apply a small seating load and take LVDT zero reading.
8) Apply a load of 100 kPa. Leave to thaw and saturate.
9) After thaw: Increase vertical load and pore pressure to saturate maintaining an effective stress of 100 kPa. Do a B test.
10) Carry out a cyclic compression test.

11) Adjust effective stress to the value required for test.

Thermal Expansion Test: Drained

12) Heat up sample in 25 °C increments to 300 °C. Monitor temperature, vertical displacements, pressures and volume change.

Thermal Expansion Test: Undrained

12) Close pore pressure port.
13) Heat sample in 25 °C increments to 300 °C. Monitor temperature, vertical displacements and pressures.

Permeability

12) Do steps 1 to 11.
13) Flow water through the sample using a metering valve to adjust pressure drop across the sample.
14) Monitor temperatures, flow volumes and pressures.
15) Flush specimen with hot water or steam to flush bitumen out as required and repeat permeability test.

X-Ray Diffraction Analysis

Clay Seperation

1. Place approximately 5 grams of sample into a 40 ml centrifuge tube.

2. Add distilled water to half the tube and add a few drops of .05% Sodium Hexa-Meta Phosphate (a dispersant).
3. Mix the sample on a Vortex mixer.
4. Let stand overnight to hydrate.

NEXT MORNING

5. Check if the clays are in suspension or have flocculated* - if the clays have flocculated, add a few drops of dispersant to keep them in suspension. Mix sample again and let stand for a few hours longer. If clays have flocculated again, repeat Step #5.
6. Fill the tube up with distilled water as follows:

   Small 40 ml tubes - fill to 10 cm in height

   For large 250 ml bottles - fill to 11 cm in height
7. Shake the tube on the shaker for 10 minutes.
8. Place the tubes into a centrifuge.
9. Centrifuge the samples at 600 RPM according to the TIME-TEMPERATURE charts (timing the spinning action of the centrifuge at a measured temperature of the samples).
10. After the centrifuging process is done, decant suspended clay portion into a 250 ml centrifuge bottle.
11. Repeat Steps #6 to #10 until a clear solution is left in the suspension.
12. Add a few drops of magnesium chloride solution (a flocculant) to the 250 ml bottle with the clay fraction and add distilled water to the appropriate height.
13. Spin down the clays at 1500 RPM for about 45 min.

14. If the liquid above the clays is not clear, add a few more drops of magnesium chloride solution and repeat Step #13.
15. Decant clean liquid and invert the bottles in the racks until the desired clay consistency is achieved (do not allow clays to dry out).
16. Mix the clay sample thoroughly with a spatula (this ensures the presence of representative amounts of each clay in the sample required for a semi-quantitative clay determination).
17. Remove the sample with the spatula and smear a thin layer on two petrographic slides (strive for an even, one crystal layer clay smear).
18. Let slides dry at room temperature.
19. Diagnostic Treatments:
    a. Ethylene Glycol - spray one slide with ethylene glycol (blot off excess with a tissue) or place slide into a desiccator containing ethylene glycol for several days. Continuous scan from 2 - 35 degrees.
    b. Heated - heat one slide in the muffle furnace at 550 degrees Celsius for 1 hour (collapses the montmorillonite peak - eliminates the water attached to the montmorillonite - therefore allowing the chlorite peak to be seen). Continuous scan from 2 - 15 degrees.
    c. Natural or untreated - slides are untreated. If the ethylene glycol and/or heated X-ray diffractograms

exhibit badly defined reflections and/or irrational sequence of (001) reflections run an untreated slide - may suggest the presence of mixed layer clays (regularly interstratified mineral or random interstratified structure). Continuous scan from 2 - 35 degrees.

* Samples containing a high percentage of carbonates tend to exhibit floculating problems.

CENTRIFUGAL ACCELERATION

SMALL TUBES R =26cm S = 16cm

less than 2 micron 600rpm s.g. = 2.65

Temp °C	Settling time
20	5min 33sec
21	5min 25sec
22	5min 18sec
23	5min 11sec
24	5min 03sec
25	4min 56sec
26	4min 50sec
27	4min 44sec

LARGE TUBES R =24cm S = 13cm

less than 2 micron 600rpm s.g. = 2.65

Temp °C	Settling time
20	7min 01sec
21	6min 51sec
22	6min 42sec
23	6min 33sec
24	6min 23sec
25	6min 14sec
26	6min 07sec
27	5min 58sec

C. COMPLIANCE TESTING

Calibration of Electronic Measuring Devices

To process the data collected by the data acquisition unit it was necessary to calibrate each of the measuring devices independent of the apparatus. To precisely define the calibration functions for each instrument each was taken to capacity.

A dead weight table hydraulic pressure system (Barnet Instruments Ltd. "Calibrator") was used to calibrate the strain gauge pressure transducers. The linear varying displacement transducers (LVDT's) were calibrated with a precision micrometer. Volume change devices were calibrated against a graduated burrette.

External and internal load cells were calibrated against proving rings of similar capacity. To verify the accuracy of these calibrations internal and external load cells were calibrated independently and checked against each other during the compression of aluminum cylinders. Internal load cell calibrations were checked at elevated temperatures and did not vary significantly from room temperature values. Internal load cells were temperature compensated by mounting strain gauges in pairs.

PVC plastic tube spacers, cut to precise tolerances, were used to calibrate the internal strain device for the high temperature and pressure triaxial cell. The internal lateral strain device was calibrated using a precision micrometer. The calibrations of these devices showed little

deviation at elevated temperatures due to strain gauge temperature compensation.

Thermocouples were calibrated by the manufacturer and were verified by placing the thermocouples in constant temperature baths.

All of the above calibrations were checked and verified periodically during the research program to ensure reliable performance.

Calibration factors and instrument tolerances for the electronic measuring devices are summarized in Table C.1.

Compliance of the High Temperature and Pressure Triaxial System

Piston Friction

The high temperature and pressure triaxial system is equipped with internal load cells to measure the axial load applied to the test specimens. The internal load cells are mounted inside the triaxial cell and directly measure the load applied to the test specimen, eliminating the need to compensate for friction between the piston and O-ring seals. During the testing program the strain gauges on the internal load cells failed and required repair. Several tests were performed during the repair period using only the external load cell to measure axial load on the specimen. For these tests it was necessary to correct the external load cell for the influence of piston friction.

Table C.1 Calibration Factors for Electronic Measuring Devices

Device	Apparatus	Function	Calibration	Accuracy +/-
LVDT (1000 HR)	Oedometer	Vertical Displacement	1.956 mm/V	0.001 mm/V
Strain Guage Transducer (35 MPa)	HTP Triaxial	Back Pressure (U/S)	1288.76 kPa/mV	0.05 kPa
Strain Guage Transducer (7 MPa)	Oedometer	Back Pressure	193.72 kPa/mV	0.10 kPa
LVDT (1000 HR)	HTP Triaxial	External Axial Displacement	1.496 mm/V	0.005 mm
Measuring Accumulator LVDT	HTP Triaxial	Volume Change	34.28 ml/V	0.01 ml
Internal Strain Guage Yoke	HTP Triaxial	Axial Displacement Arm #1	1.329 mm/V	0.005 mm
Internal Strain Guage Yoke	HTP Triaxial	Axial Displacement Arm #2	1.330 mm/V	0.005 mm
Measuring Accumulator LVDT	RT Triaxial	Volume Change	17.358 ml/V	0.01 ml
Validyne Transducer (22 MPa Diaphragm)	RT Triaxial	Back Pressure	1754.49 kPa/V	0.50 kPa
Valydyne Transducer (22 MPa Diaphragm)	RT Triaxial	Confining Pressure	1704.82 kPa/V	0.50 kPa
Strain Guage Transducer (35 MPa)	HTP Triaxial	Back Pressure (D/S)	1177.76 kPa/mV	0.50 kPa
Strain Guage Transducer (35 MPa)	Oedometer	Confining Pressure	715.732 kPa/mV	0.50 kPa
Strain Guage Load Cell (440 kN)	HTP Triaxial	External Load Cell	32.079 kN/V	0.01 kN
Strain Guage Transducer (35 MPa)	HTP Triaxial	Confining Pressure	1160.74 kPa/mV	0.50 kPa
Strain Guage Transducer (7 MPa)	HTP Triaxial	Confining Pressure	188.26 kPa/mV	0.10 kPa
Strain Guage Load Cell	RT Triaxial	External Load Cell	9.087 kN/mV	0.01 kN
LVDT (500 HR)	RT Triaxial	Axial Displacement	1.185 mm/V	0.001 mm
LVDT (1000 HR)	Pos. Dis. Pump	Pump Volume Change	21.505 ml/V	0.01 ml
Strain Guage Transducer (7 MPa)	Oedometer	Back Pressure	222.13 kPa/mV	0.10 kPa
LVDT (500 HR)	RT Triaxial	Axial Displacement	1.164 mm/V	0.001 mm
Strain Guage Load Cell	RT Triaxial	Internal Load Cell	17.365 kN/mV	0.01 kN
Strain Guage Load Cell (54 mm)	HTP Triaxial	Internal Load Cell	11.131 kN/mV	0.01 kN
Strain Guage Load Cell (63 mm)	HTP Triaxial	Internal Load Cell	11.192 kN/mV	0.01 kN
Strain Guage Load Cell (76 mm)	HTP Triaxial	Internal Load Cell	32.32 kN/V	0.01 kN
Validyne Differential Transducer (140 kPa)	All Systems	Differential Pressure	11.515 kPa/V	0.01 kPa
J Type Thermocouples (Iron/Constantin)	HTP Triaxial	Temperature	Linearized Circuit	0.5 deg C
J Type Thermocouples (Iron/Constantin)	Oedometer	Temperature	Linearized Circuit	0.5 deg C
Lateral Strain Guage Clamp Device	HTP Triaxial	Radial Deformation	0.500 mm/V	0.01 mm
Bellows Volume Change LVDT (500 HR)	Oedometer	Volume Change	10.0 ml/V	0.01 ml

The evaluation of piston friction is complex since it depends on confining stress, temperature and axial stress employed during the test. It was only necessary to calibrate, however, for specific tests where the internal load cells were not operational. All triaxial tests performed without the use of internal load cells were carried out at 225°C over an effective confining stress range of 1.0 to 7.0 MPa. It was, therefore, only necessary to quantify piston friction for these specific test conditions. The piston friction was measured using two techniques. The first method involved pushing the piston into the triaxial cell at the appropriate confining stress (or cell pressure) at 225°C and recording the external load cell reading. The results of the high temperature and pressure calibration test are shown in Figure C.1. These magnitudes of piston friction were confirmed by a second method which entailed examining tests employing an operational internal load cell. Piston friction was determined as the difference between external and internal load measurements.

The piston friction was found to vary from 0.2 kN (total confining stress of 8.5 MPa) to 0.32 kN (total confining stress of 14.5 MPa). Since the back pressure for all tests was 7.5 MPa, this corresponds to an effective stress range of 1.0 to 7.0 MPa. The relatively small value of piston friction is attributed, in part, to lubrication of the piston O-ring seals with a molybdenum based lubricant.

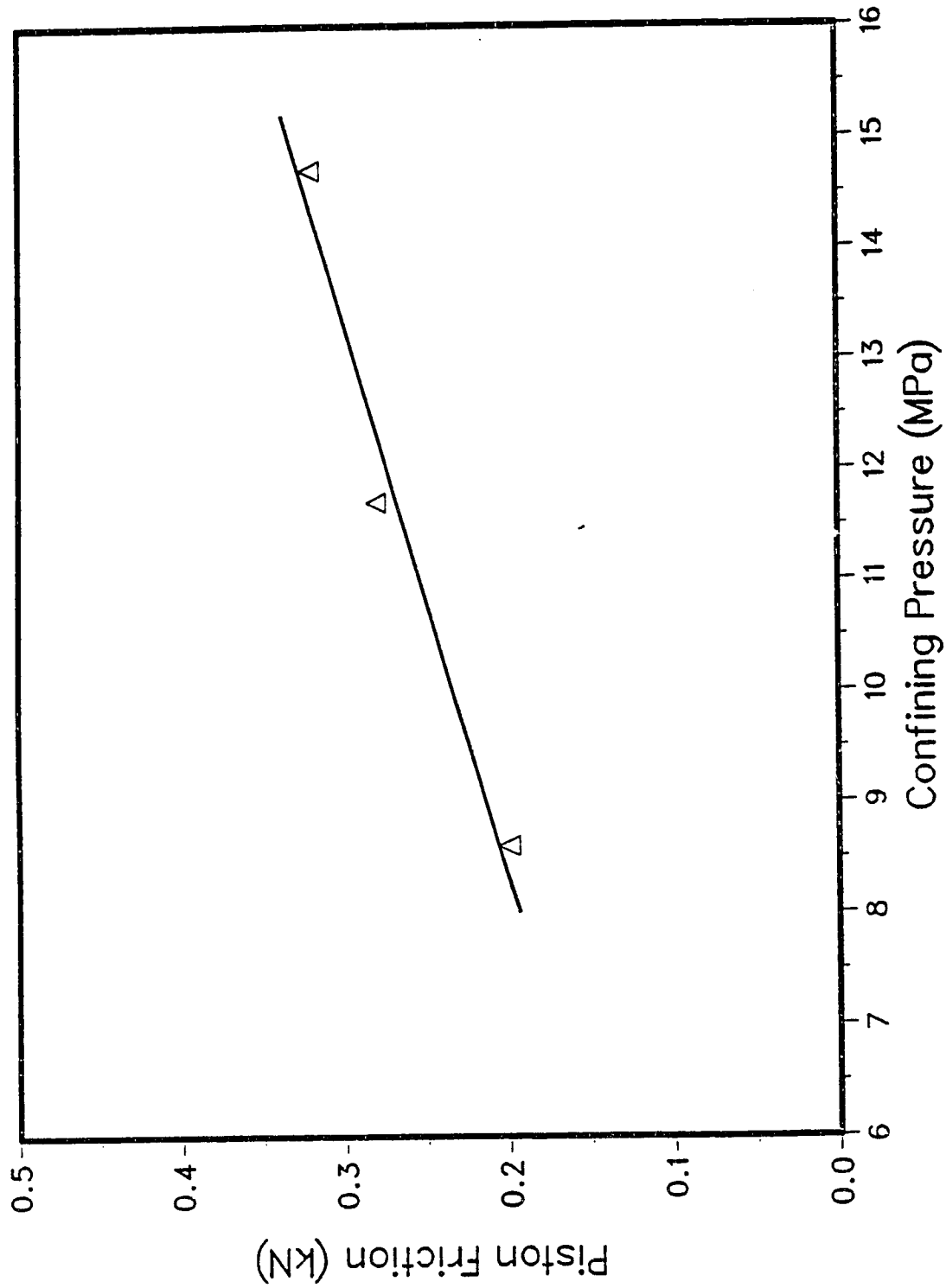

Figure C.1 Variation of Piston Friction with Confining Pressure at 225 °C

Load Frame Stiffness

In order to accurately trace the entire past failure stress-strain curve, the triaxial apparatus is equipped with a stiff loading frame (pre-stressed to 440 kN) with a small energy storage capacity.

Loading system stiffness K_{ls} is defined as:

$$K_{ls} = \Delta P \; / \; \delta_{ls} \qquad (C.1)$$

where:

ΔP = load increment

δ_{ls} = displacement of loading system

and includes contributions of the loading frame as well as the triaxial cell apparatus. The amount of strain energy stored in the loading system during triaxial shear is:

$$E_s = 0.5 \; \Delta P \; \delta_{ls} \qquad (C.2)$$

as shown in Figure C.2. Alternatively, strain energy stored in the testing machine may be written in terms of loading system stiffness:

$$E_{ls} = 0.5 \; \Delta P^2 \; / \; K_{ls} \qquad (C.3)$$

As the loading system is unloaded this strain energy is instantaneously recovered and the test specimen is subjected to the additional deformation δ_{ls}. This deformation of the loading system causes a higher applied strain rate on the

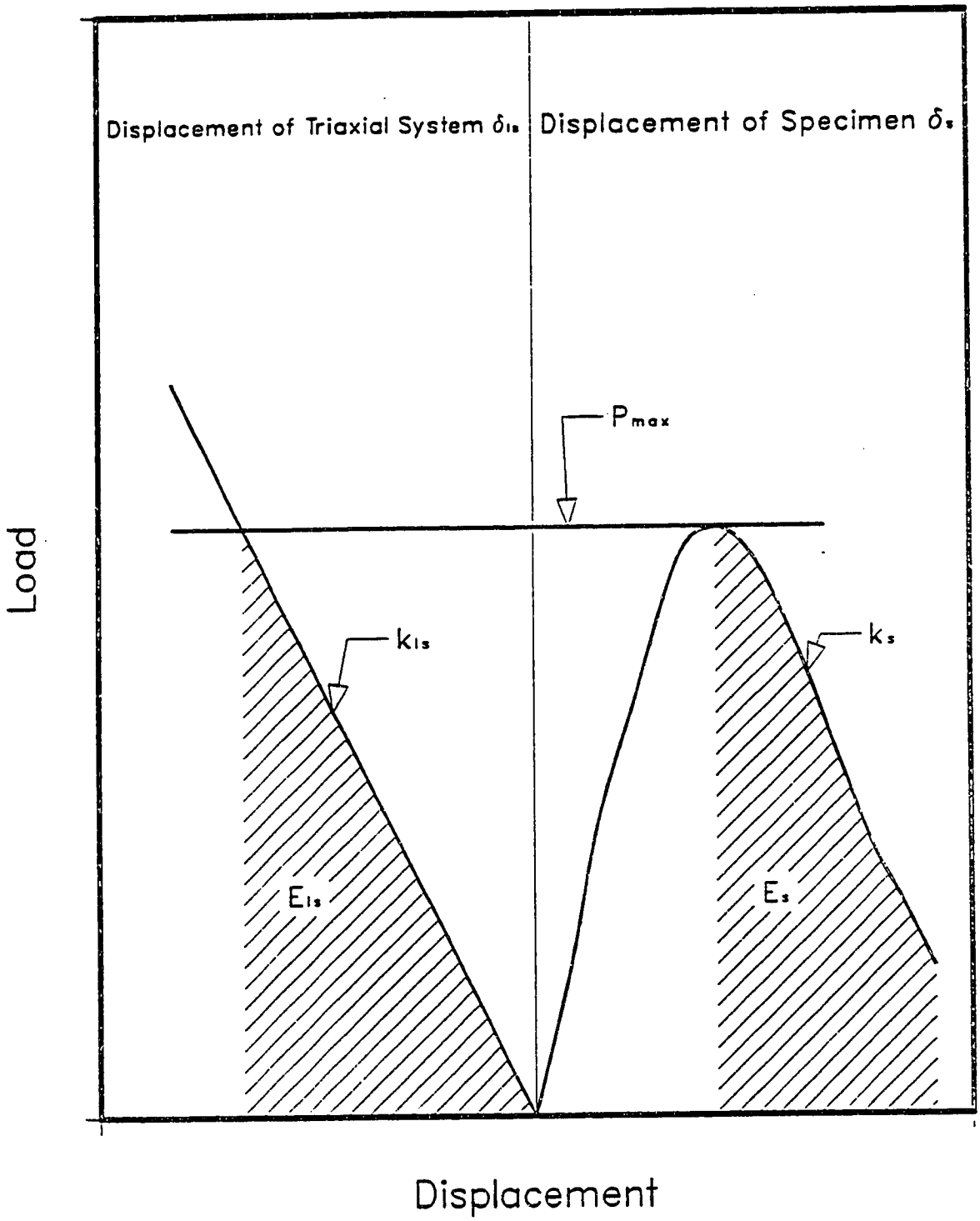

Figure C.2 Loading System Stiffness

sample and, for brittle materials, may result in a rapid reduction in strength. Therefore, to accurately trace the post-peak stress-strain curve, the amount of energy required for straining the test specimen beyond peak deviator stress (E_s) in Figure C.2) must be greater than the strain energy stored in the load system (E_{ls}. In contrast, if E_s is less than E_{ls} uncontrolled rapid failure will occur.

Loading system and specimen strain energy are quantitatively comparable in terms of loading system stiffness K_{ls} and specimen stiffness K_s (Figure C.2). To enable the measurement of the entire post-failure stress-strain curve the incremental loading system stiffness, ΔK_{ls}, must be greater than the incremental specimen stiffness, ΔK_s.

Load system stiffness determinations were carried out at 20°C and 225°C by compressing an aluminum cylinder and measuring the displacement response of the aluminum cylinder, triaxial cell and loading frame. Loading system stiffness K_{ls} may be rewritten as:

$$K_{ls} = \Delta P \; / \; \delta_l - \delta_s \qquad (C.4)$$

where:

δ_l = displacement of loading system and sample

δ_s = displacement of aluminum sample

The displacement of the loading system and sample was measured by an external LVDT mounted on the top plate of the loading frame and connected to the piston. Displacement of

the aluminum cylinder was calculated assuming elastic modulus values of 67 x 10^4 kPa at room temperature and 46.6 x 10^4 kPa at 225°C. The results of the loading system stiffness test conducted at 225°C are shown in Figure C.3.

The stiffness of the loading system was calculated to be 254,000 kN/m at 225°C and 240,000 kN/m at 20°C during axial loading to 95 kN. The overall stiffness of the triaxial system does not appear to be significantly affected over the temperature range of 20°C to 225°C.

Triaxial shear strength testing performed on Athabasca and Cold Lake oil sands and shale indicate specimen stiffness, K_s, ranges up to approximately 11,000 kN/m. This results in a specimen to load system stiffness ratio of about 0.044. In other words, straining an oil sands or shale specimen beyond peak deviator stress causes an additional deformation of about 4% to be applied to the specimen caused by the unloading of the triaxial system. Since the amount of strain energy stored in the loading system is very small compared to energy required to deform the specimen beyond strength, it is possible to measure the entire post-failure stress-strain curve.

Vertical Compression of Loading System with Applied Load

Vertical compression of the loading system with applied load was assessed by conducting compression tests on an aluminum cylinder at various temperatures up to and including 250°C. Compression tests carried out at 20°C and 225°C are shown in Figures C.4 and C.5, respectively.

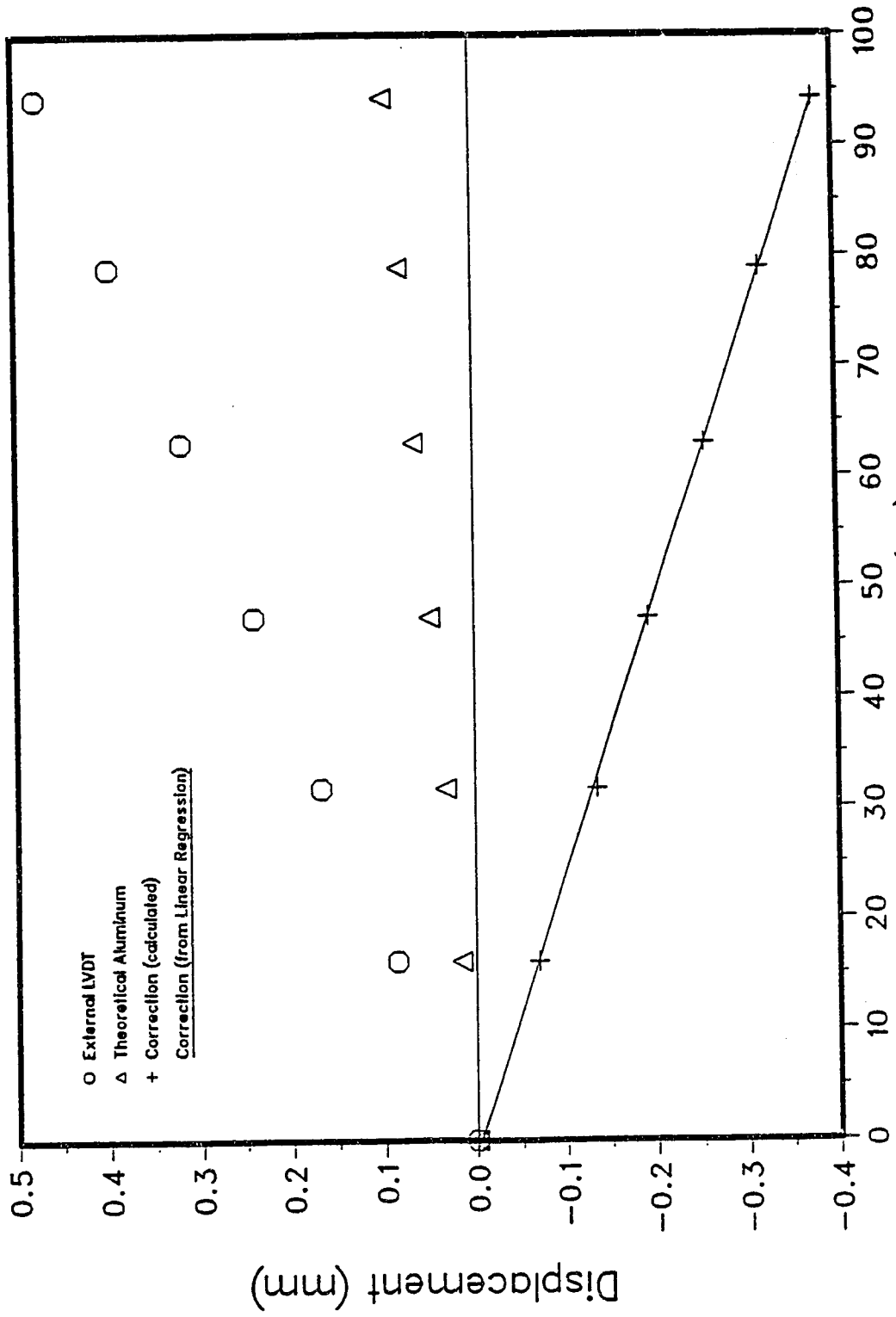

Figure C.3 Loading System Stiffness Test at 225 °C

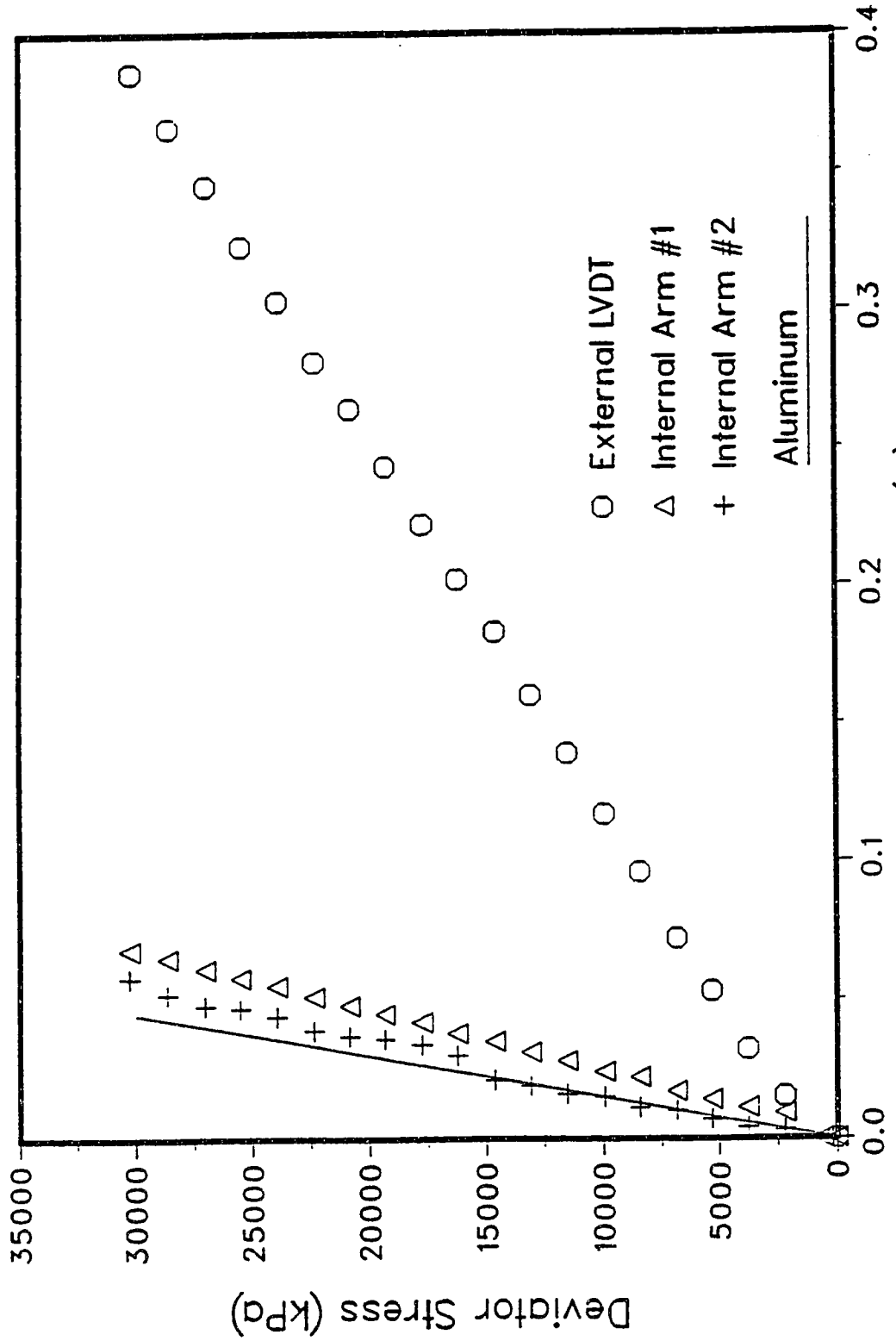

Figure C.4 Vertical Compression of Aluminum Cylinder at 20 °C

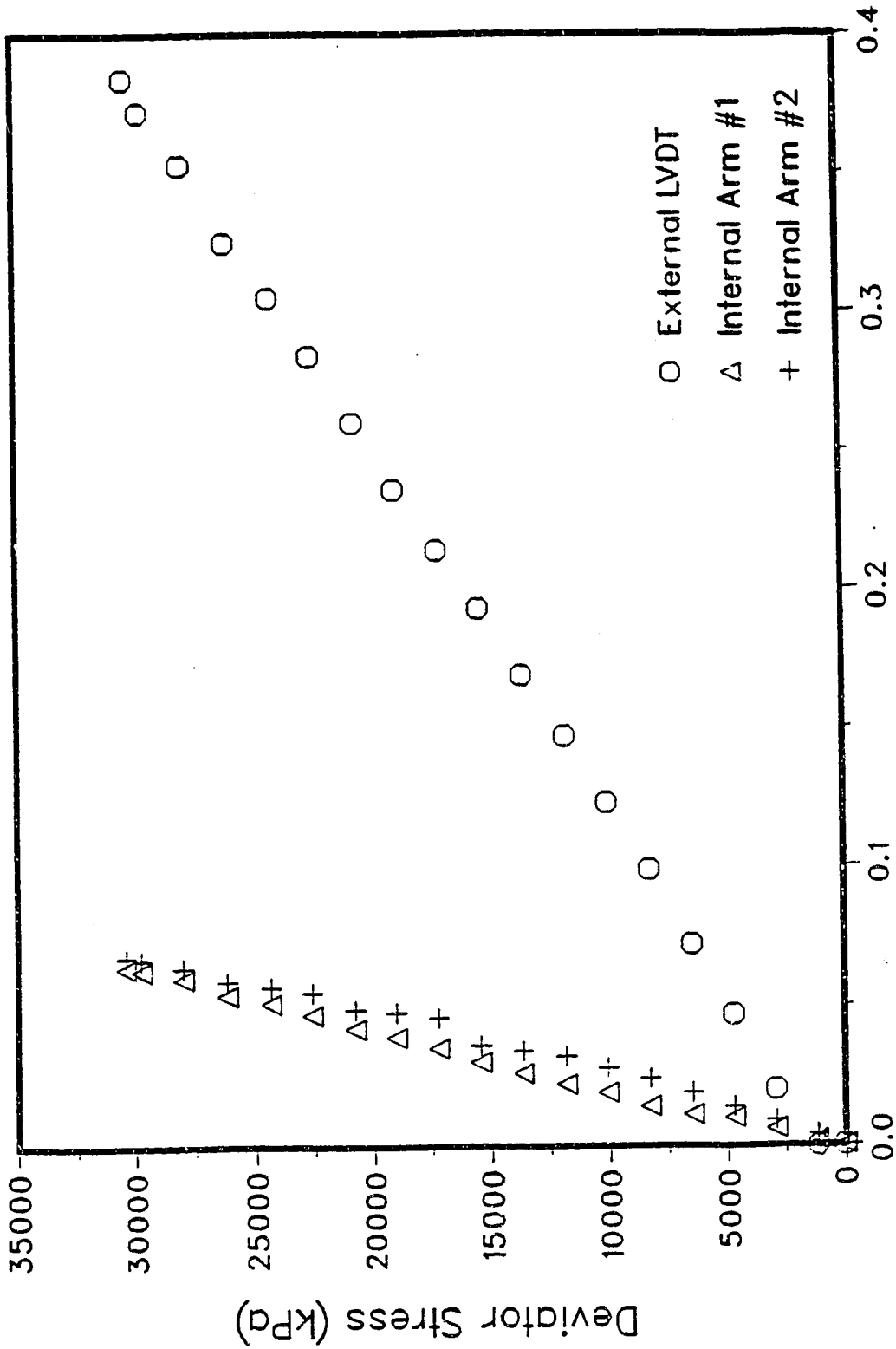

Figure C.5 Vertical Compression of Aluminum Cylinder at 225 °C

Correction factors for the internal and external axial strain measuring devices were calculated by taking the difference between measured values and those predicted assuming modulus values of aluminum at the appropriate temperature. The correction factor for the internal devices at 225°C was 2.5×10^{-4} mm/kN and for the external device was 3.9×10^{-3} mm/kN. The difference in correction factors between internal and external devices reflects the compressibility of the various triaxial system components. Internal devices, in addition to measuring specimen compression, also measure the compressibility of the loading caps and porous stainless steel plates and, accordingly, the correction factor is very small. The external devices measure the vertical deformation of the specimen as well as the triaxial cell apparatus and loading frame and, therefore, is about an order of magnitude larger.

Extraneous Water in Triaxial Cell

The volume of extraneous water in the triaxial cell was quantified as follows:

Load cell and base = 5.00 cm^3

75 cm of 0.635 cm tubing = 6.00 cm^3

Two back pressure transducers = 2.00 cm^3

Tubing coil and port = 4.00 cm^3

Top cap = 0.50 cm^3

Total volume of extraneous water = 17.5 cm^3

Where applicable, volume change measurements were corrected for thermal volume change and compressibility of

extraneous water utilizing published steam table data.

Volume Change Measurements in Room Temperature Zone

The volume change device for measuring the volume of fluid entering or expelled from the heated triaxial cell is located away from the triaxial cell and is maintained at room temperature. The volume change device therefore underestimates the volume of fluid entering the triaxial cell (due to thermal expansion) and leaving the cell (due to thermal contraction). Correction of volume change measurements for thermal volume change was based on the observed thermal gradient in the stainless steel tubing transitional between the heated cell and the room temperature zone, thermal volume change of the steel tubing and the thermal expansion of water as determined from steam table data. To verify the volume change correction method an aluminum cylinder was inserted in the triaxial cell and heated. Thermal volume change of extraneous water in the load cell, base, tubing coil and top cap as measured by the volume change device was corrected and showed excellent agreement with calculated thermal expansion values.

Thermal Expansion of Apparatus During Heating

Compliance testing was conducted to isolate the triaxial system response to increase in temperature. An aluminum sample was placed in the triaxial cell and was heated to 225°C. Figure C.6 shows measured versus theoretical vertical thermal expansion results. This test

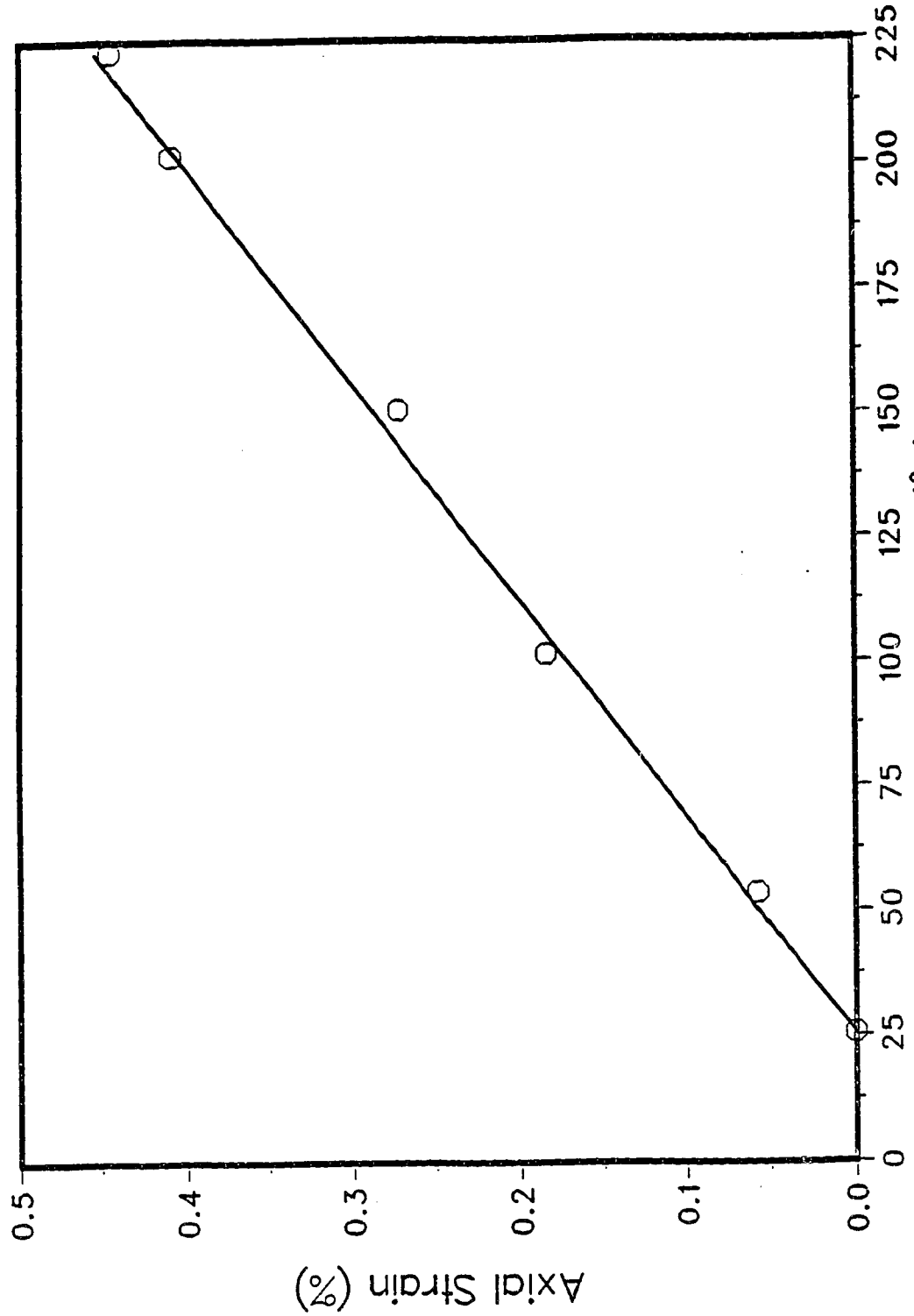

Figure C.6 Vertical Thermal Expansion of Aluminum Cylinder

indicates the internal strain gauge devices are successful in eliminating measurement errors associated with triaxial cell thermal expansion.

Volume Change of Water and Drainage Lines External to Cell

Approximately 75 cm of 0.635 cm diameter stainless steel drainage lines separate the triaxial cell from the upstream and downstream back pressure valves. During undrained tests specimen pore pressure response is affected by the volume increase of the drainage lines and by the compressibility of water contained in the lines. Drainage line compressibility was measured by isolating this section of line and measuring the volume response to change in pressure. Compressibility of the lines was determined to be 0.26 ml/MPa and was essentially linear over the pressure range of 0 to 14 MPa.

Membrane Stiffness

Membrane stiffness may be determined following the procedure outlined in Bishop and Henkel (1957). The procedure was formulated on the following assumptions:

1. The membrane is capable of taking compression when held against the specimen by the cell pressure.
2. The extension modulus is similar to the compression modulus.
3. The specimen deforms as a right cylinder.
4. Since Poisson's ratio for rubber is approximately 0.5, hoop stresses are small.

Agar (1984) conducted membrane extension tests on silicone rubber membranes (wall thickness of 8.3 mm) over the temperature range of 20°C to 205°C. Results indicated that the stiffness of these membranes in extension was about three orders of magnitude smaller than the compressive stiffness of oil sands. The correction factor was therefore considered to be negligible.

The majority of triaxial tests conducted at elevated temperatures utilized teflon membranes with 0.50 mm wall thicknesses. Membrane extension tests were carried out at 20°C and at 61°C to evaluate the extension modulus. The stiffness of the teflon membrane in extension was 149 kN/m at 20°C and 36 kN/m at 61°C. For a 54 mm diameter specimen at 20°C this translates to a correction to the measured compressive strength due to the effect of the membrane of 28 kPa at 0.25% strain and 425 kPa at 4% strain. At 61°C the correction reduces to 7 kPa at 0.25% strain and 102 kPa at 4% strain. With the exception of one test conducted at 125°C, tests employing teflon membranes were performed at 225°C. Considering the marked reduction in the correction due to a 41°C increase in temperature, the corrections at 125°C and 225°C were judged to be negligible.

Membrane Penetration

Volumetric strains in drained tests and pore pressures in undrained tests are affected by the amount of membrane penetration into the triaxial specimen. Membrane penetration is dependent on the effective confining stress, particle

size and gradation and the thickness and rigidity of the membrane.

The volume change correction for membrane penetration effects for oil sands was estimated using the relationship established by Baldi and Nova (1984). The maximum estimated error in volume change measurements computed in this manner ranges from 0.13% to 0.24% for the effective confining stresses utilized in the testing program. It is noted that the estimated volume correction is very small compared to the volume change required to recompress an oil sands specimen due to sample disturbance.

Compliance of High Temperature Oedometer

General

The high temperature oedometer is subject to significant error in measurement in the following areas:

1. Vertical expansion due to heating.
2. Vertical compression due to loading.
3. Radial expansion due to heating.
4. Radial expansion due to increases in back pressure and vertical effective confining stress.
5. Thermal expansion or compression of extraneous water due to heating and loading.
6. Piston friction.

To eliminate the influence of each of these factors from the experimental data a series of tests were conducted

to provide a set of correction curves. Compliance test methods and results used to isolate system response to changes in temperature and stress are detailed in subsequent sections.

To provide an independent check on the derived corrections and to ensure precise and reliable performance required testing of a substance whose characteristics under temperature and pressure are well documented. Water was selected as the testing material owing to the vast amount of information contained in the literature.

Several thermal expansion tests were carried out on water under pressures up to 10 MPa and temperatures up to 300°C at the beginning of the testing program and were repeated periodically during the research. Two typical tests conducted for the 54 mm and 76 mm oedometer rings are shown in Figures C.7 and C.8. For comparative purposes, theoretical curves calculated based on steam table data are also shown. Excellent agreement between theoretical and experimental results indicate the system performance and calibrations are satisfactory.

Vertical Thermal Expansion During Heating

During thermal volume change testing the vertical LVDT measures the combined response of the specimen and oedometer to changes in temperature. Compliance testing was carried out on an aluminum cylinder in order to isolate the vertical thermal expansion of the system. The vertical thermal expansion of the oedometer is the difference between the

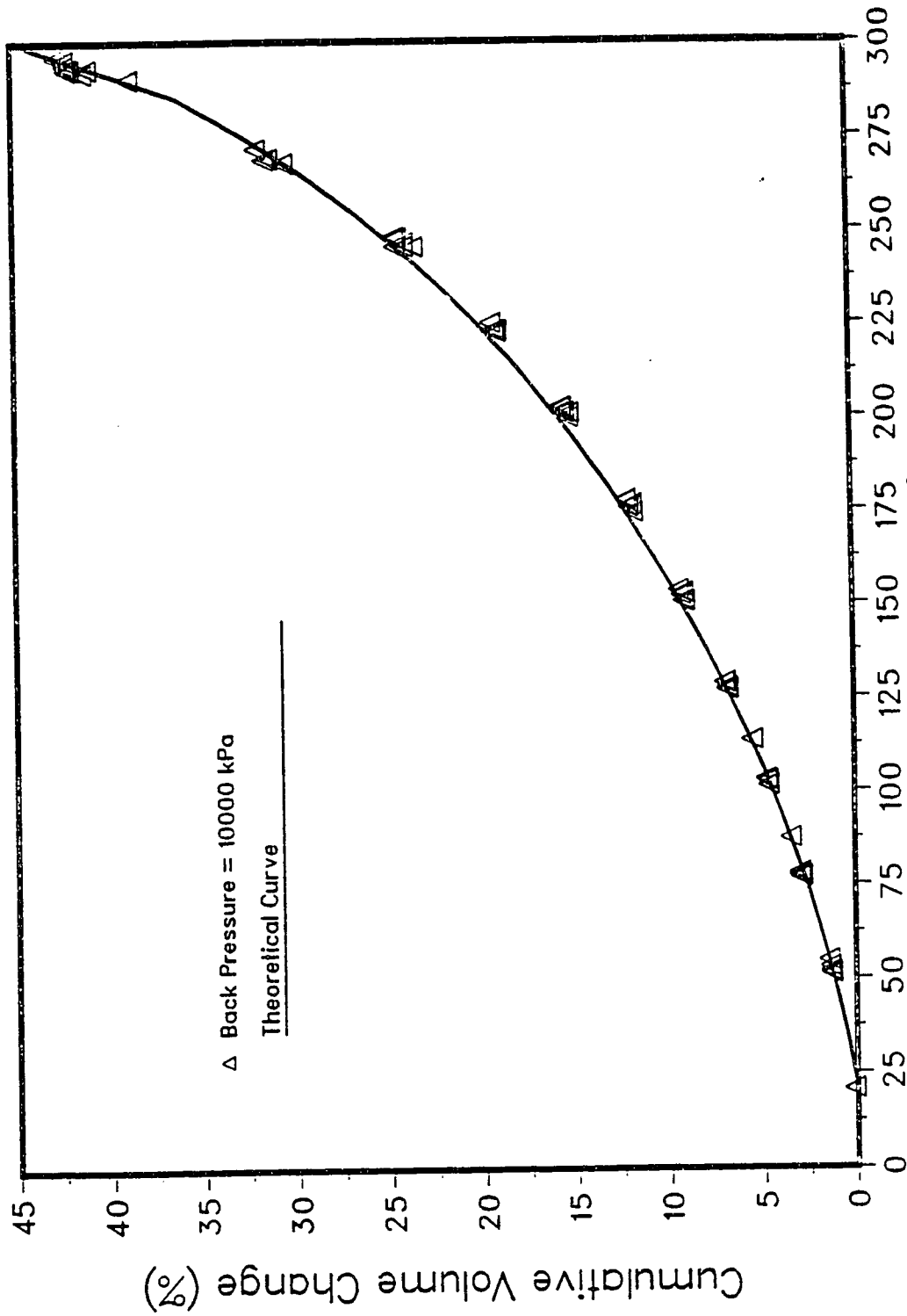

Figure C.7 Thermal Expansion of Water (54 mm Ring)

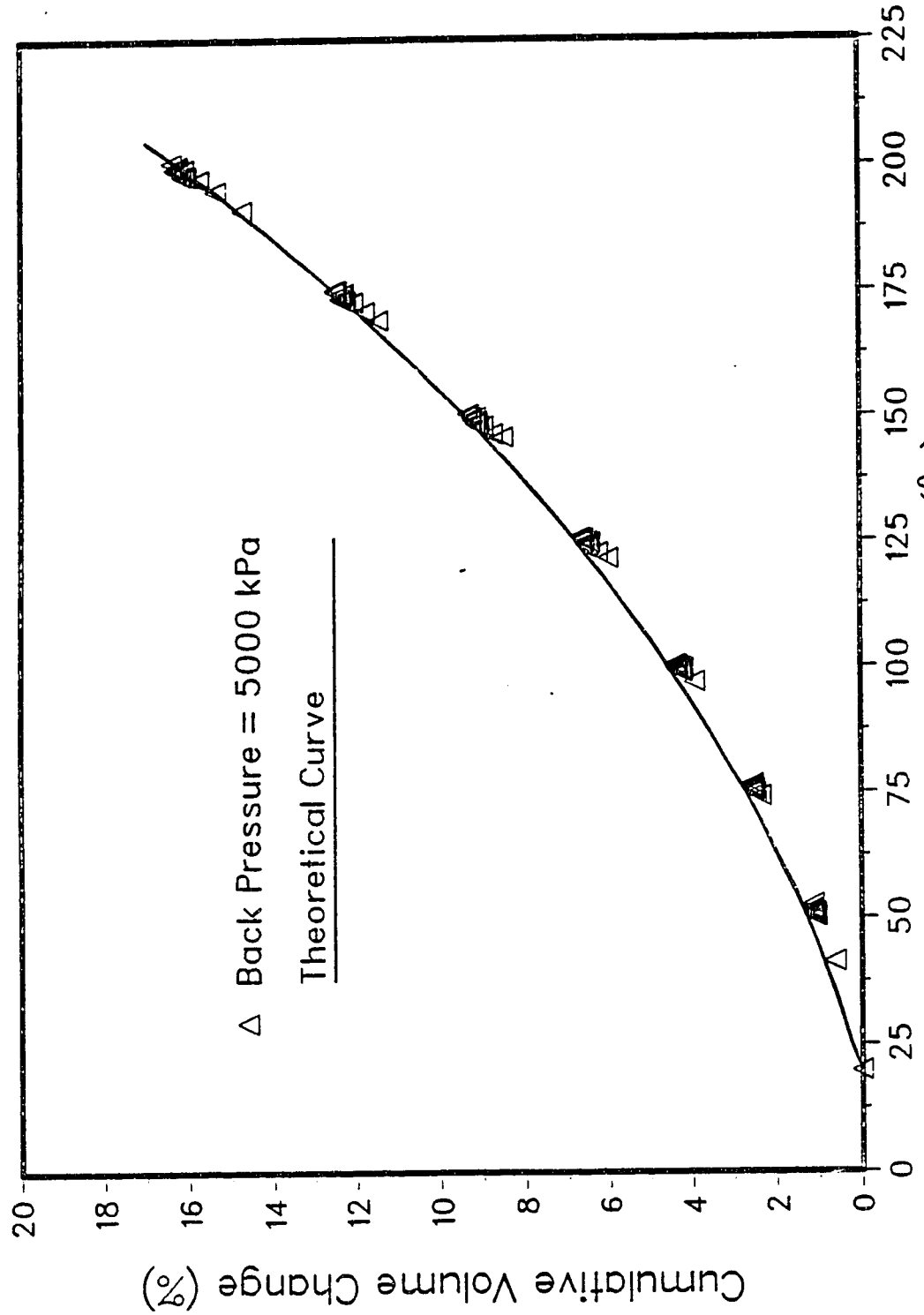

Figure C.8 Thermal Expansion of Water (76 mm Ring)

expansion measured during the test and the theoretical expansion of the aluminum block.

The results of a thermal expansion test performed on aluminum are shown in Figure C.9. The method used to derive the vertical expansion correction curve is specifically shown.

Vertical Compression Due to Loading

A series of tests were carried out to determine the degree of compression the oedometer experiences during loading at different temperature levels. The tests were conducted using an aluminum cylinder machined to the approximate dimensions of an actual soil specimen. To eliminate any influence of induced pressure within the sample chamber water was excluded from the tests and the back pressure drainage ports were kept open to atmospheric pressure. The temperature range for the compliance testing was varied from 20°C to 300°C and vertical confining pressures up to 30 MPa.

The results derived from this series of testing are shown in Figure C.10. To account for compression of the apparatus during actual testing, the vertical displacement as measured by the tests at 100°C and 300°C were averaged. The test performed at 20°C was considered separately due to lack of similarity with respect to the other tests. It is evident from Figure C.10 that influence of temperature on the compression of the oedometer system by the applied loads is not a significant factor above 20°C.

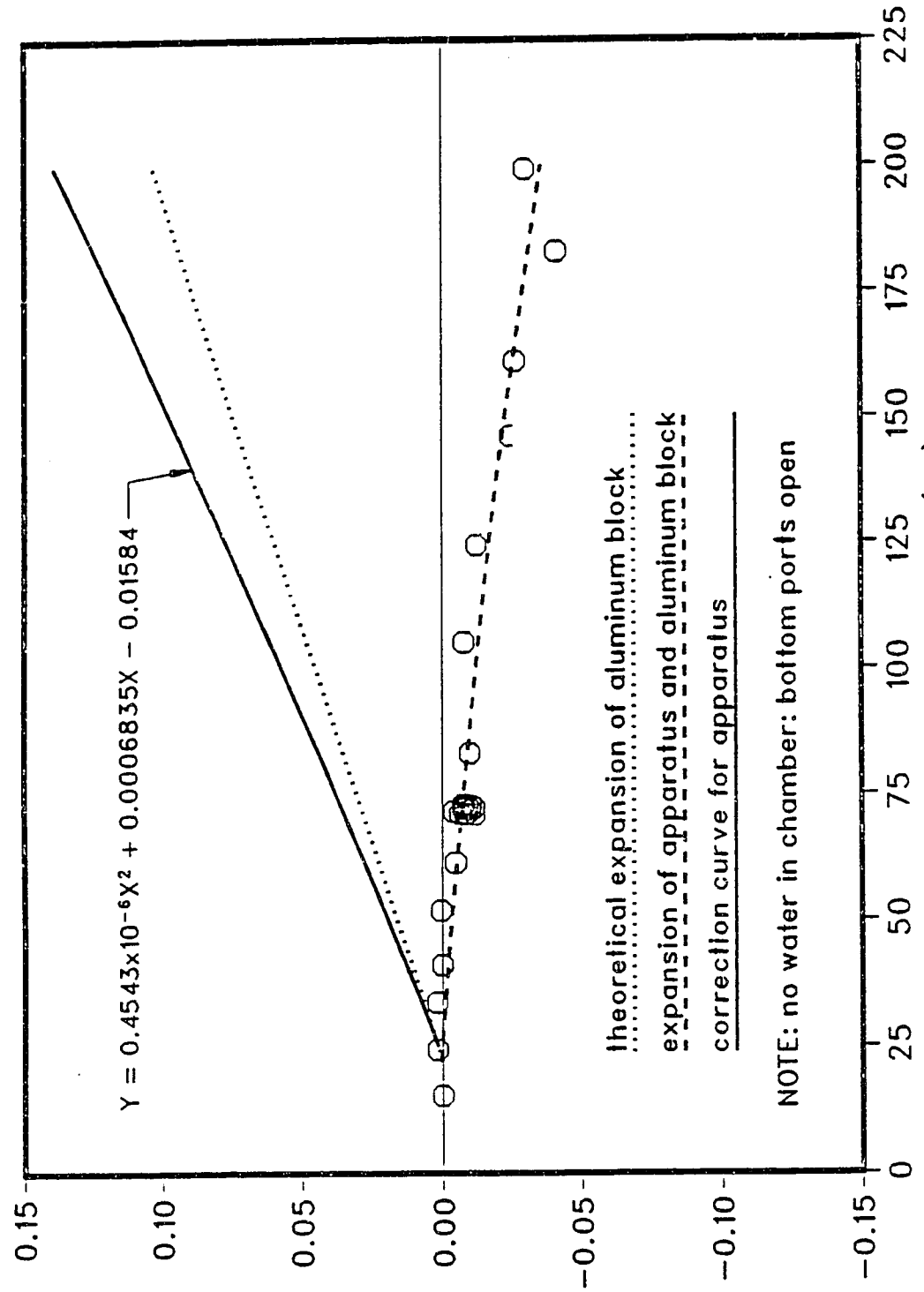

Figure C.9 Vertical Expansion of Oedometer

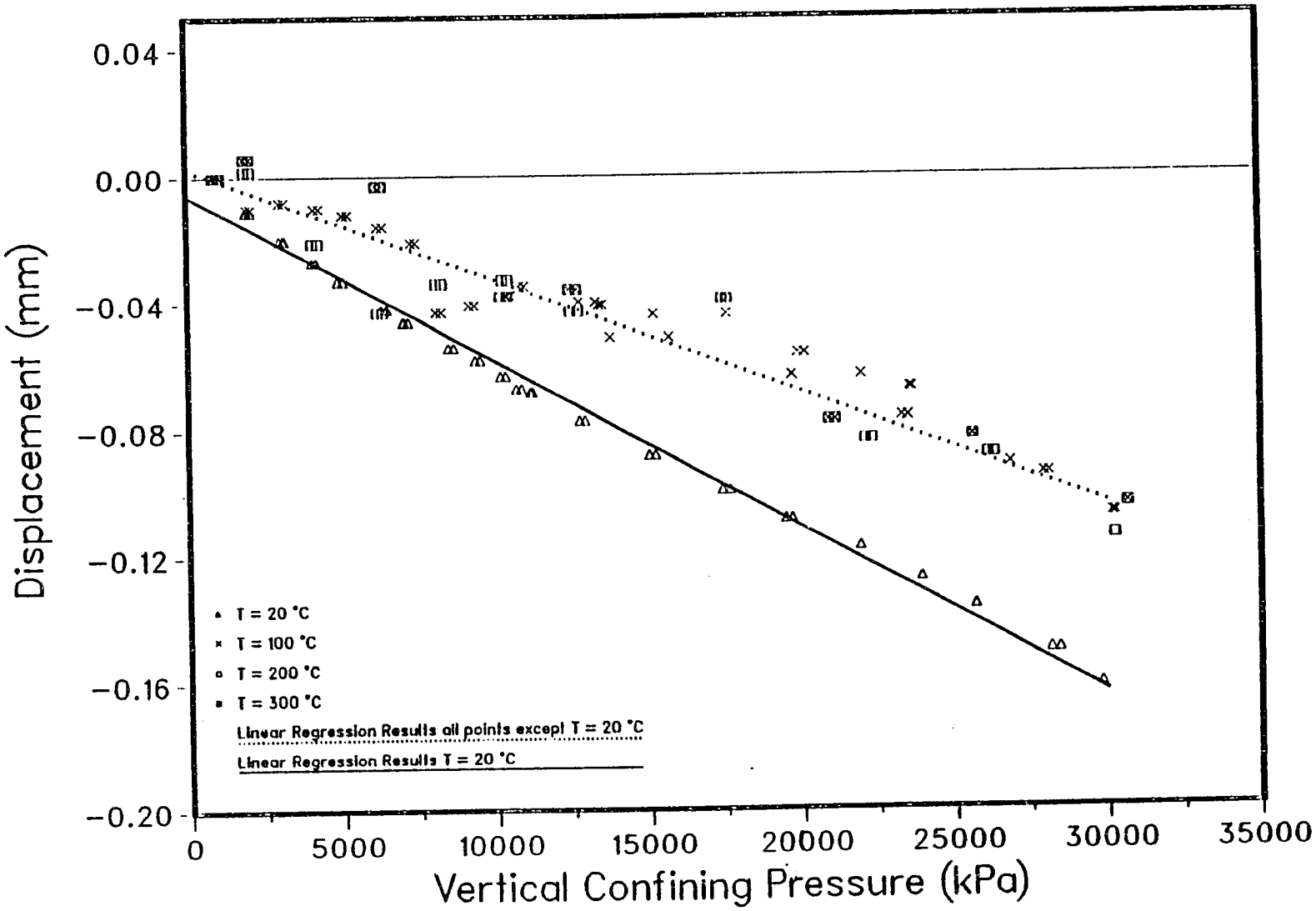

Figure C.10 Oedometer Compression for Different Temperatures

Radial Expansion Due to Heating

The radial expansion of the sample chamber with temperature was taken into account by considering the sample chamber as an isotropic solid. When an isotropic solid is subjected to a temperature change it expands with the distance between any two points increasing in the ratio α (α being the coefficient of linear expansion). This means the inside diameter of the sample ring enlarges in the same ratio as the external dimension.

It can be shown theoretically that the coefficient of area expansion of an isotropic solid is twice the coefficient of linear expansion. Therefore, the change in area of the sample chamber is two times the linear coefficient of linear expansion times the original area (at room temperature) times the change in temperature.

The thermal volume change of the oedometer was taken into account in the measurements by multiplying the change in area of the sample chamber by the specimen height.

Agar (1984) confirmed the validity of this approach by measuring the radial thermal expansion of the oedometer using an external LVDT and comparing the results to predicted thermal expansion of a thick walled stainless steel cylinder. The measured and theoretical deformations were found to be essentially identical.

Radial Expansion Due to Increase in Back Pressure and Vertical Effective Confining Stress

The oedometer sample chamber expands or contracts radially in response to changes in back pressure and vertical effective confining stress. An oil sands specimen was inserted in the sample chamber and radial expansion of the chamber due to changes in confining and back pressure was measured directly using a horizontally mounted LVDT. The correction required to volume measurements varied from 6.31×10^{-3} ml/MPa at 20°C to 6.65×10^{-3} ml/MPa at 300°C for back pressures up to 20 MPa.

The volumetric correction factor for increases in vertical effective confining stress ranged from 4.22×10^{-3} ml/MPa at 20°C to 4.52×10^{-3} ml/MPa at 300°C for effective confining stresses up to 20 MPa. It should be noted, however, that this correction factor depends on the Poisson's ratio of the specimen tested. Since specimen volumes typically range from 70 to 125 ml, the variation in corrected volume changes associated with slight variations in Poisson's ratio is very small.

Extraneous Water

The amount of water in the oedometer cell extraneous to the test specimen (i.e. water contained in ports, stones, etc.) varied slightly from 30.5 ml for the 54 mm diameter ring to 32.0 ml for the 76 mm diameter ring. Volume change measurements were corrected for thermal expansion and compression of extraneous water in accordance with steam table data.

Piston Friction

Piston friction may cause a significant underestimation of the vertical confining stress applied to the test specimen. At the onset of the testing program the sample chamber was filled with water and the oedometer system was totally deaired. Piston friction was measured by holding the temperature constant and by either varying the pressure applied to the piston or varying the back fluid pressure. Piston friction was taken as the difference between the pressure applied to the piston and the pressure in the water as measured by the back pressure transducer.

Piston friction evaluations were made throughout the testing program after each undrained thermal expansion test by determining the difference between confining and pore pressure during each heating increment. Temperature-piston friction relationships for the 54 mm and 76 mm oedometer rings for pore fluid pressures ranging from 5 to 10 MPa compiled from both calibration and actual undrained expansion tests are shown in Figure C.11.

The maximum piston friction for the 76 mm diameter ring was approximately 8.5 kN at 300°C, representing an error in applied pressure of about 770 kPa. Similarly, the maximum piston friction for the 54 mm diameter ring was about 2.5 kN at 300°C, representing an underestimation of applied pressure of about 1000 kPa.

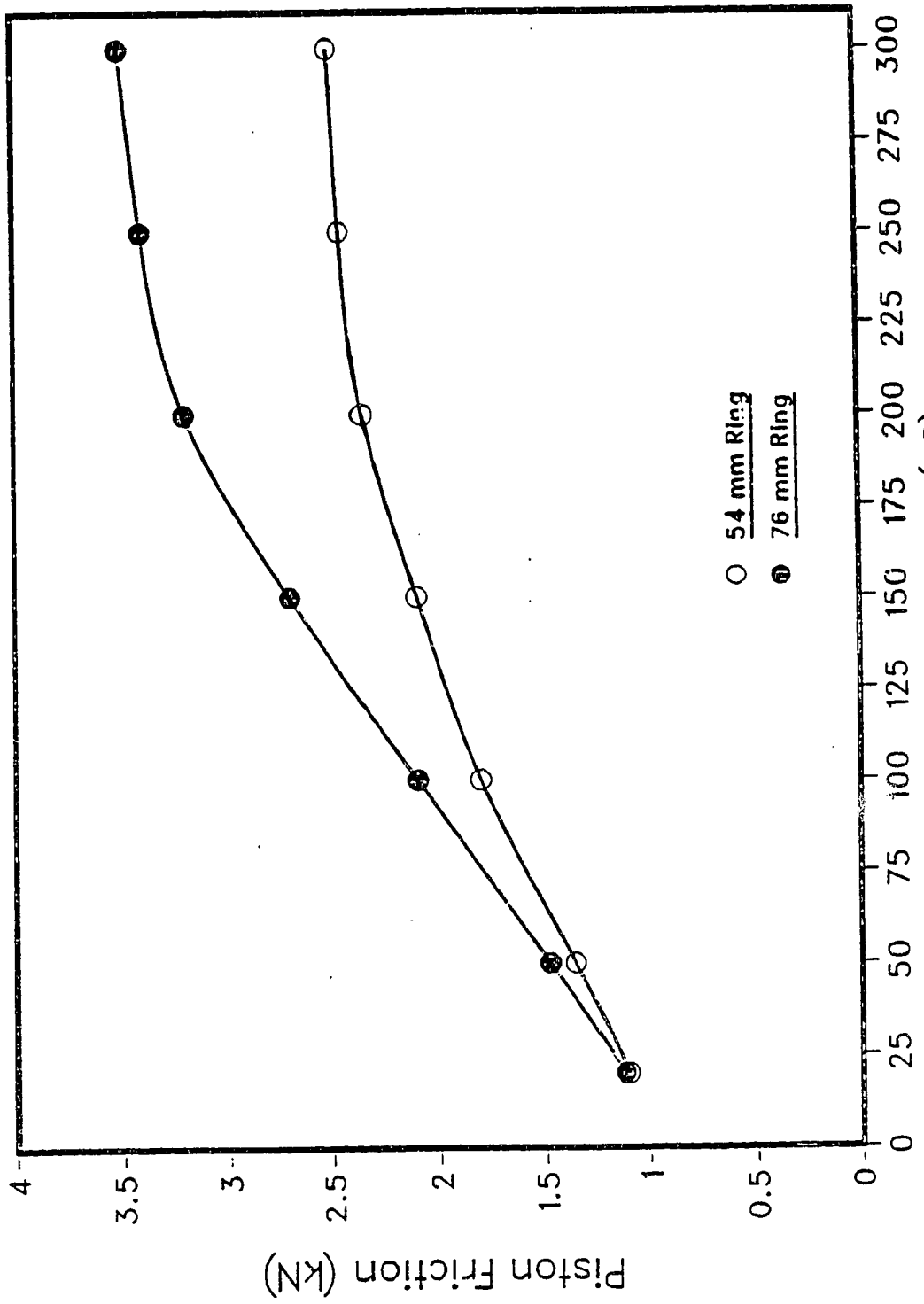

Figure C.11 Odometer Piston Friction

D. ATHABASCA MATERIALS: COMPRESSIBILITY TEST RESULTS

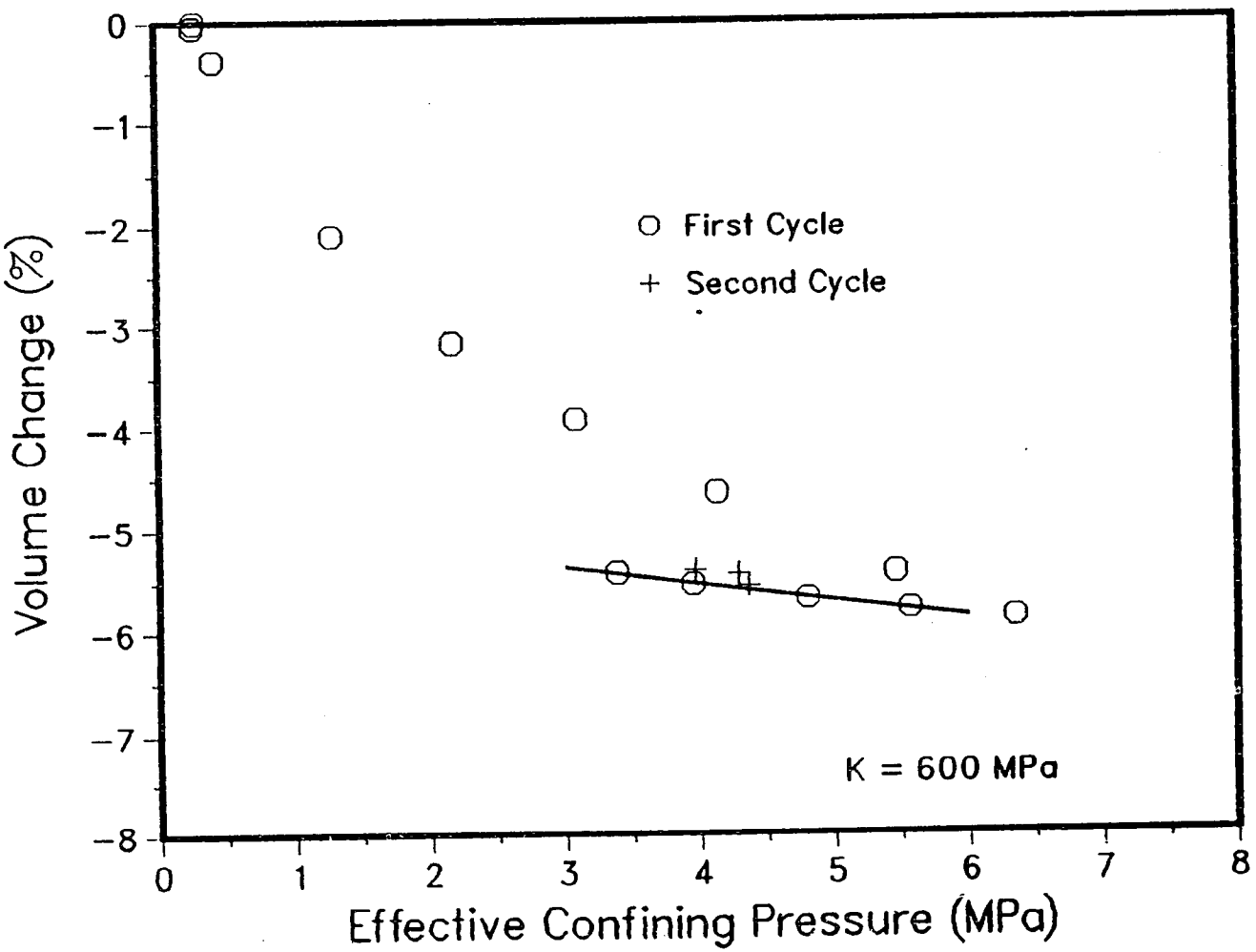

Figure D.1 Isotropic Compressibility Test AMTOS1

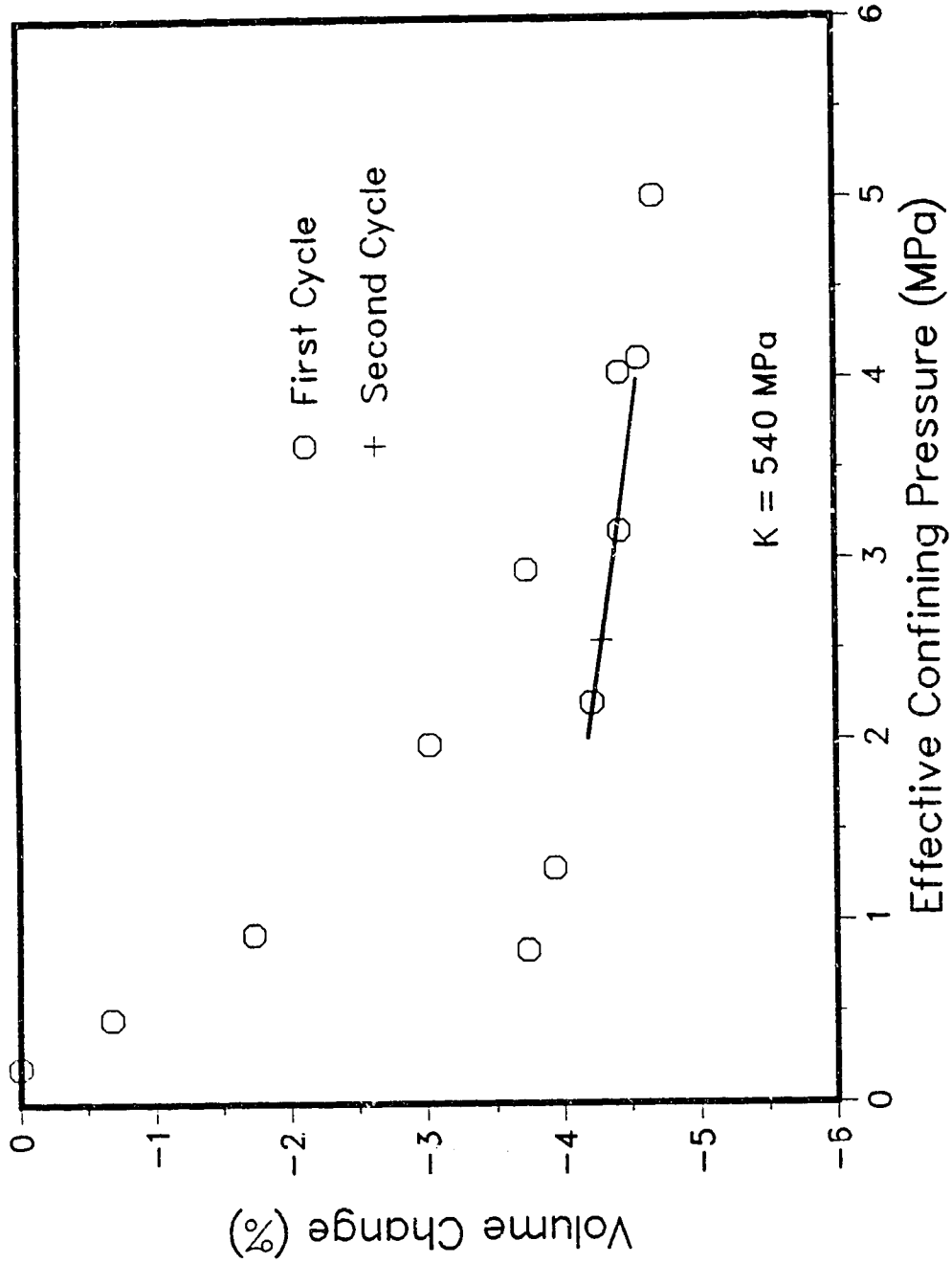

Figure D.2 Isotropic Compressibility Test AMTOS2

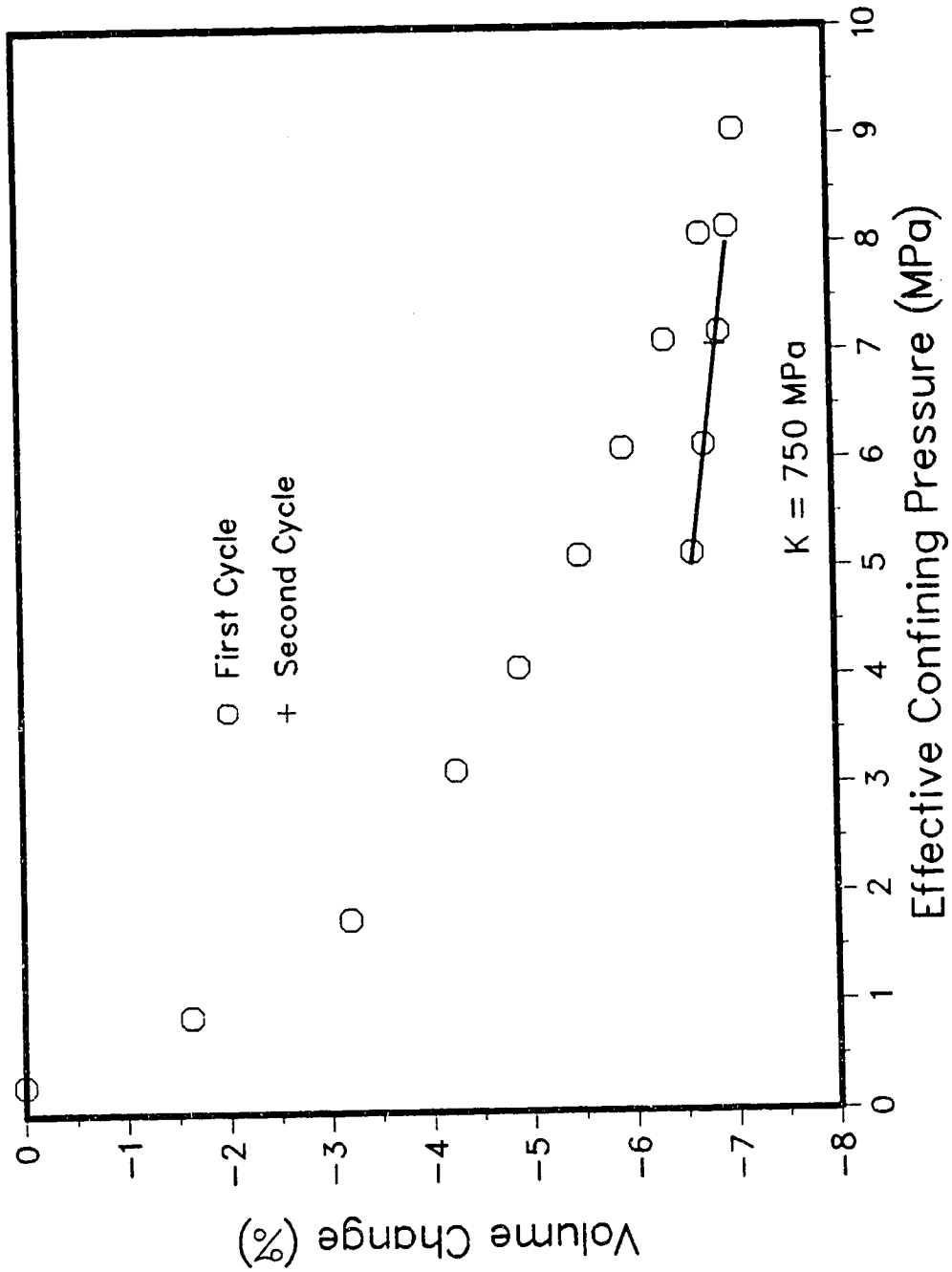

Figure D.3 Isotropic Compressibility Test AMTOS3

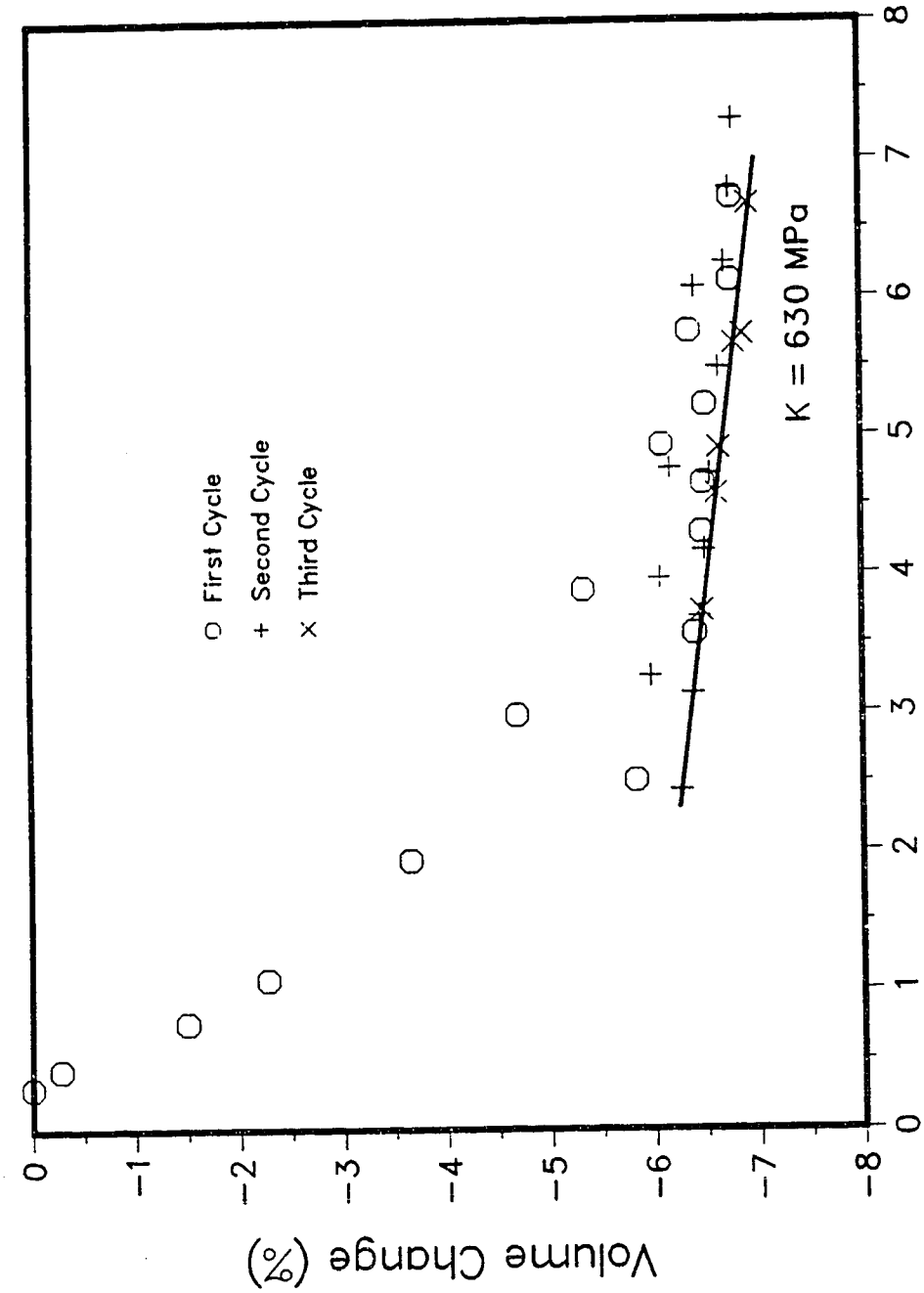

Figure D.4 Isotropic Compressibility Test ACTOS1

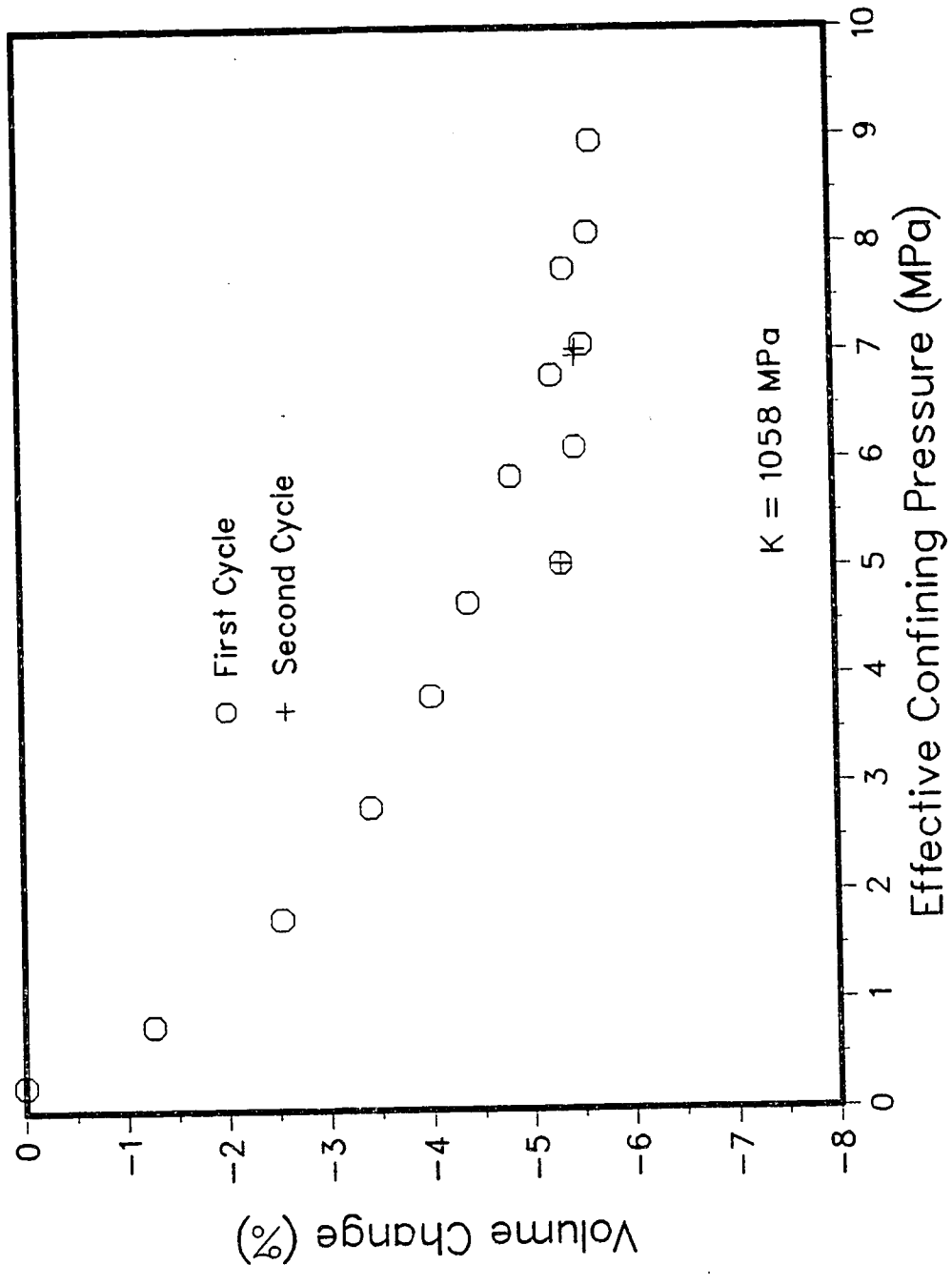

Figure D.5 Isotropic Compressibility Test ACTOS2

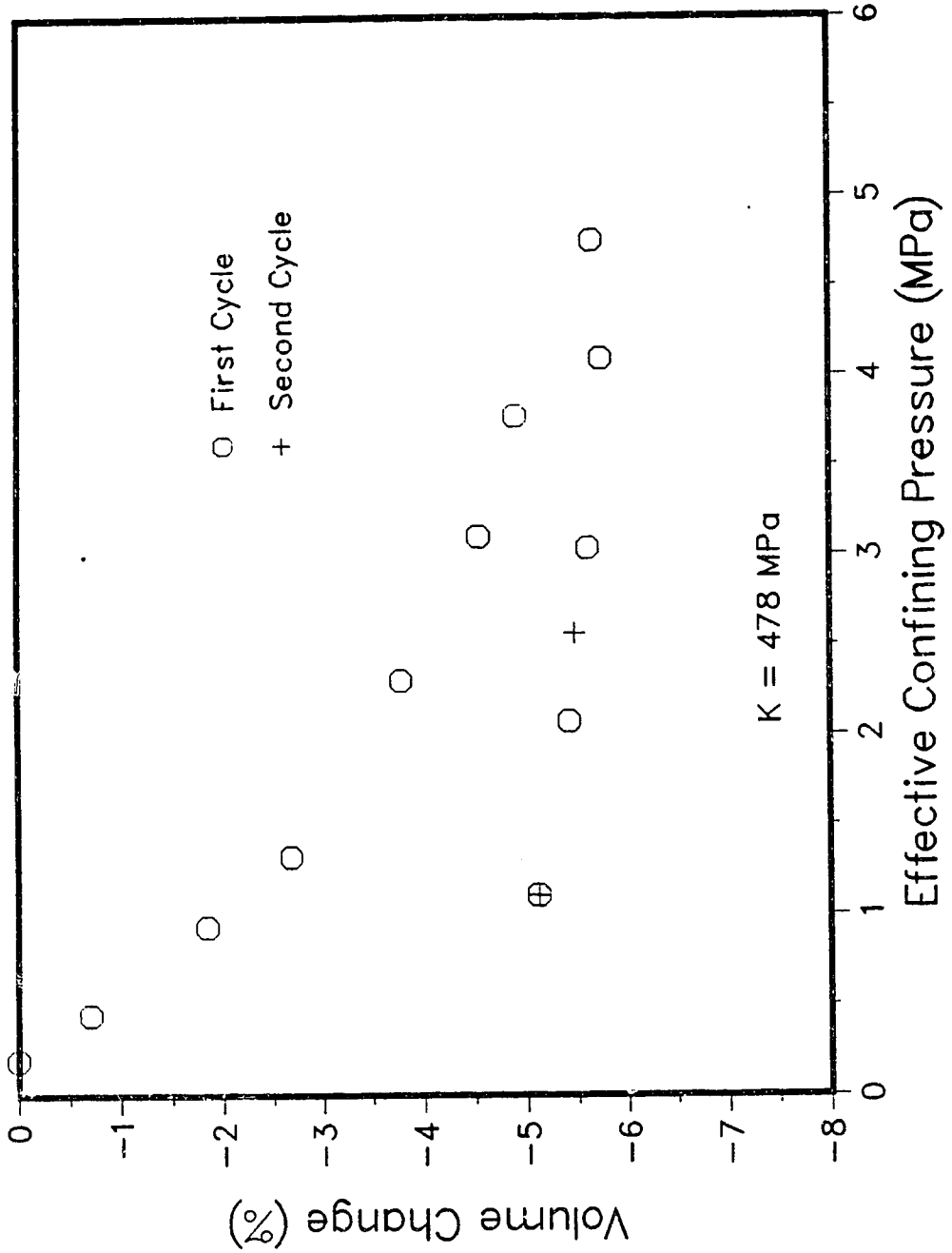

Figure D.6 Isotropic Compressibility Test ACTOS3

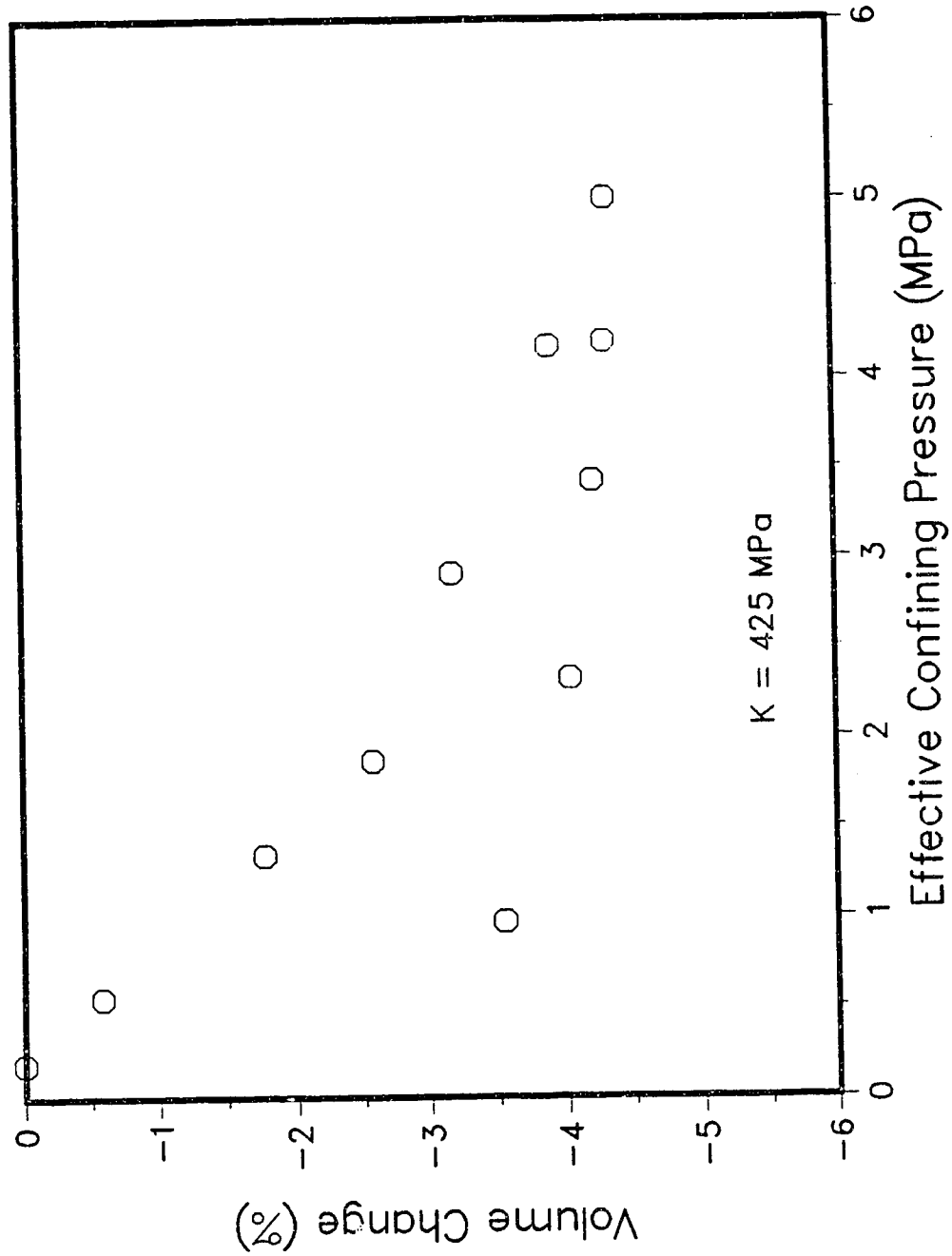

Figure D.7 Isotropic Compressibility Test ACTOS4

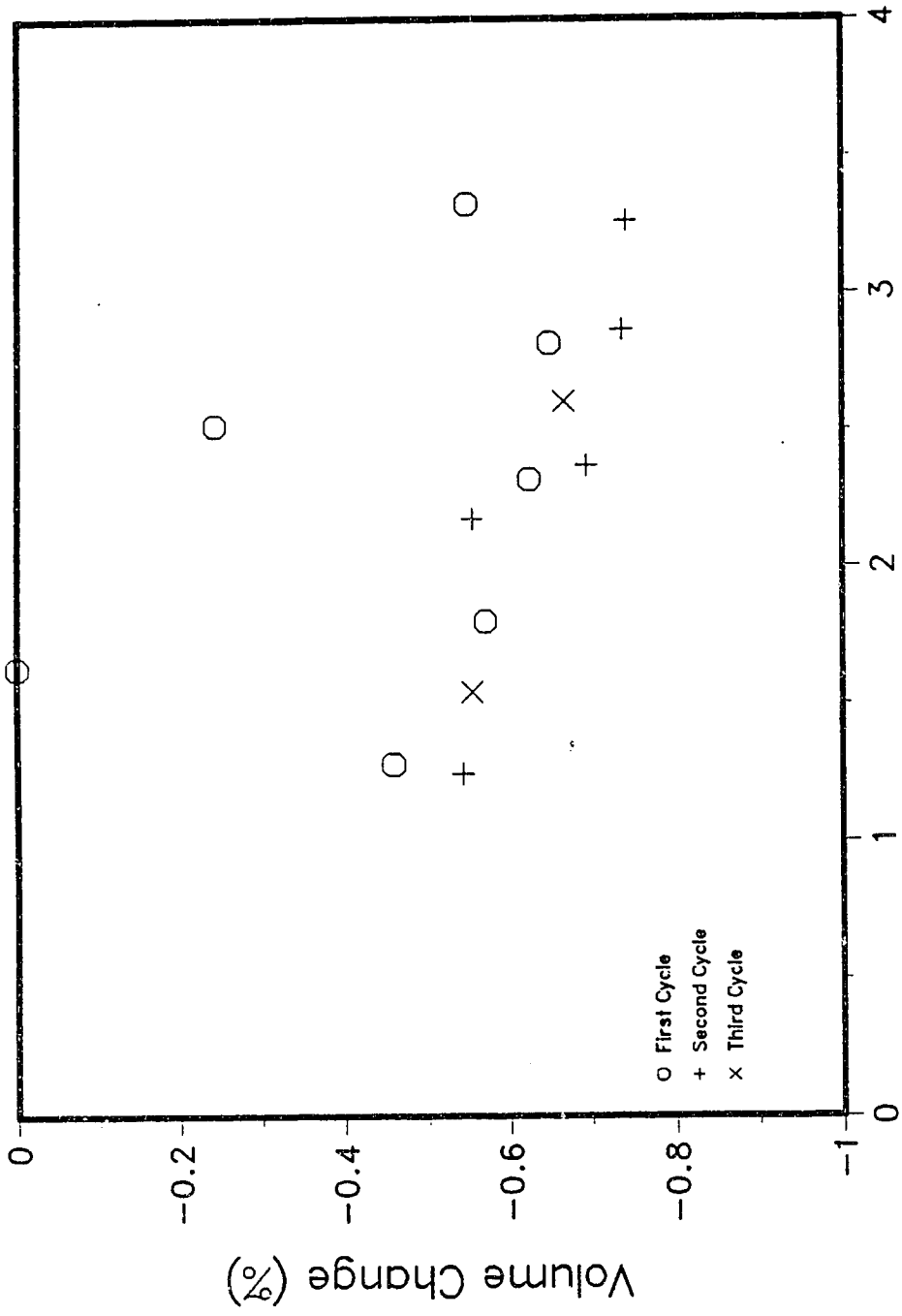

Figure D.8 One Dimensional Compressibility Test UFCOS1

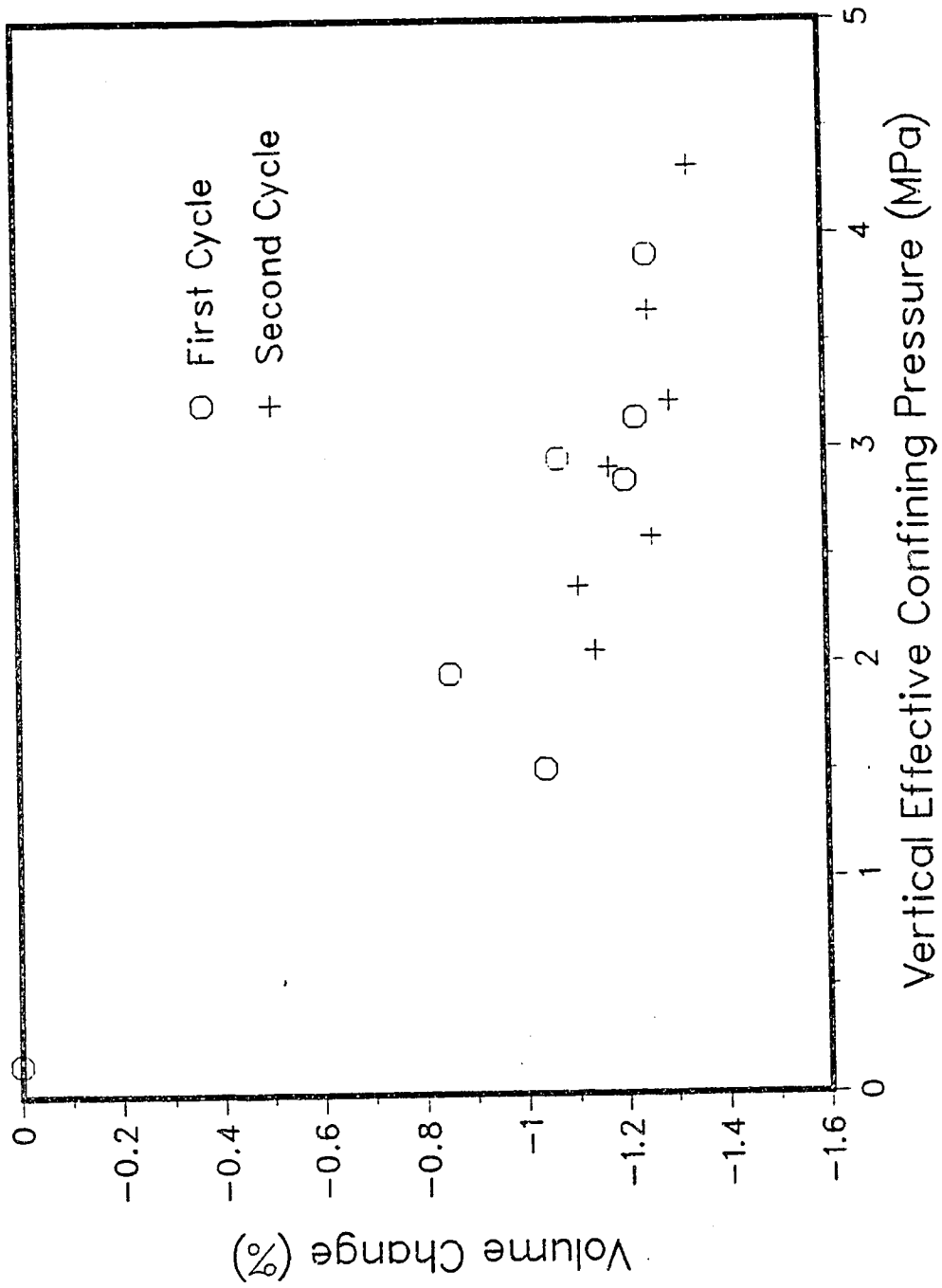

Figure D.9 One Dimensional Compressibility Test UFCOS2

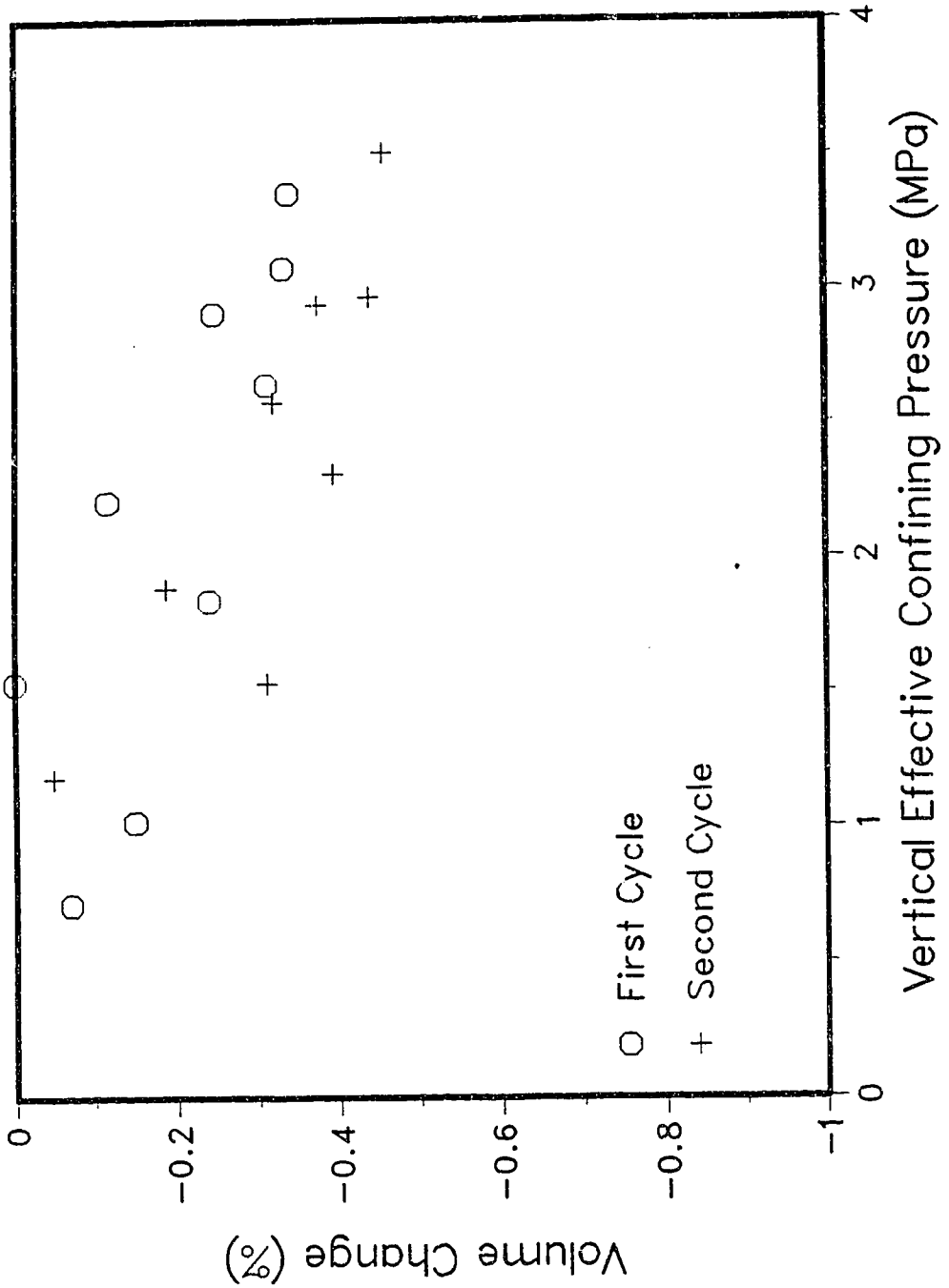

Figure D.10 One Dimensional Compressibility Test UFCOS3

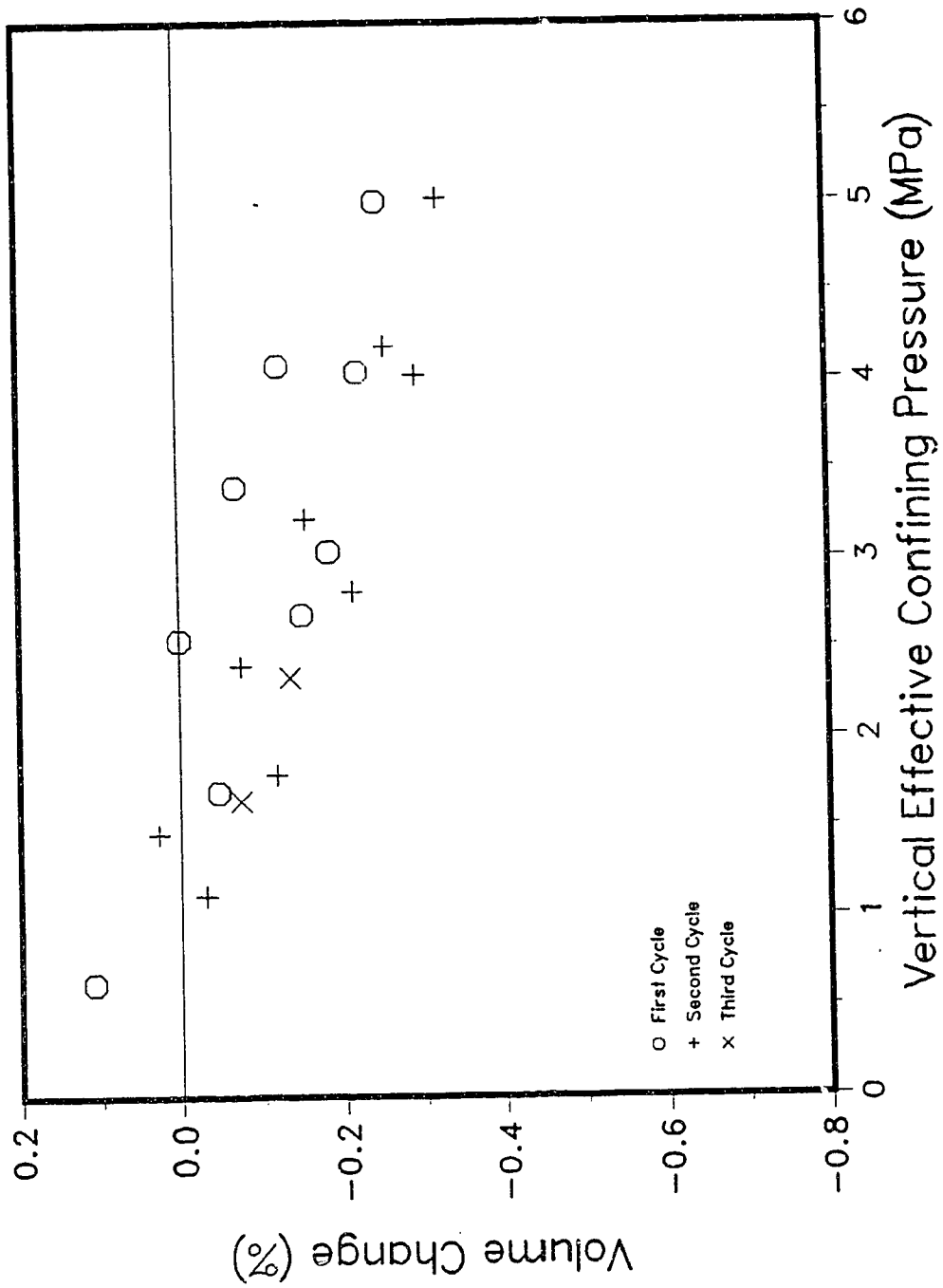

Figure D.11 One Dimensional Compressibility Test UFCOS4

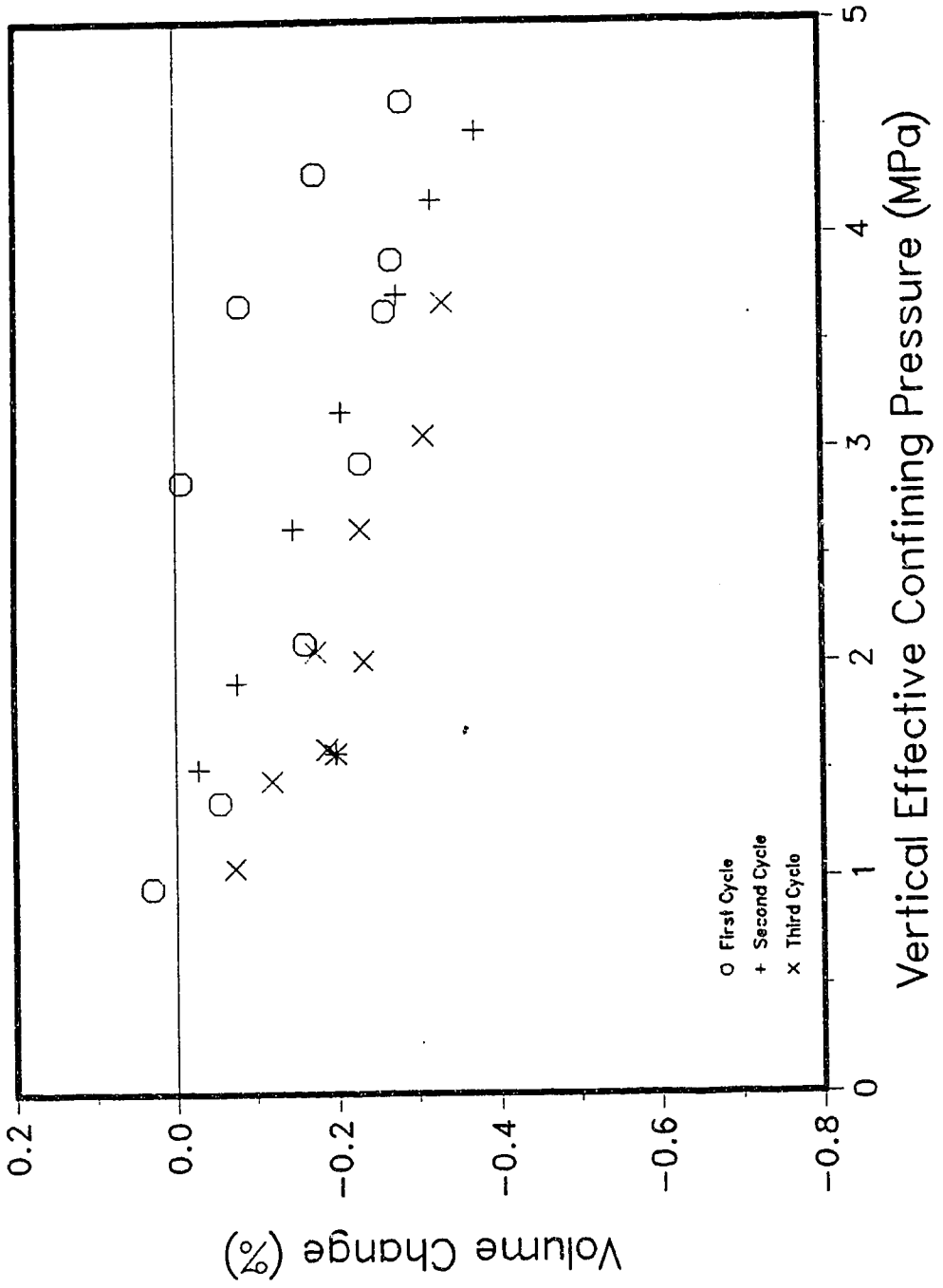

Figure D.12 One Dimensional Compressibility Test UFCOS5

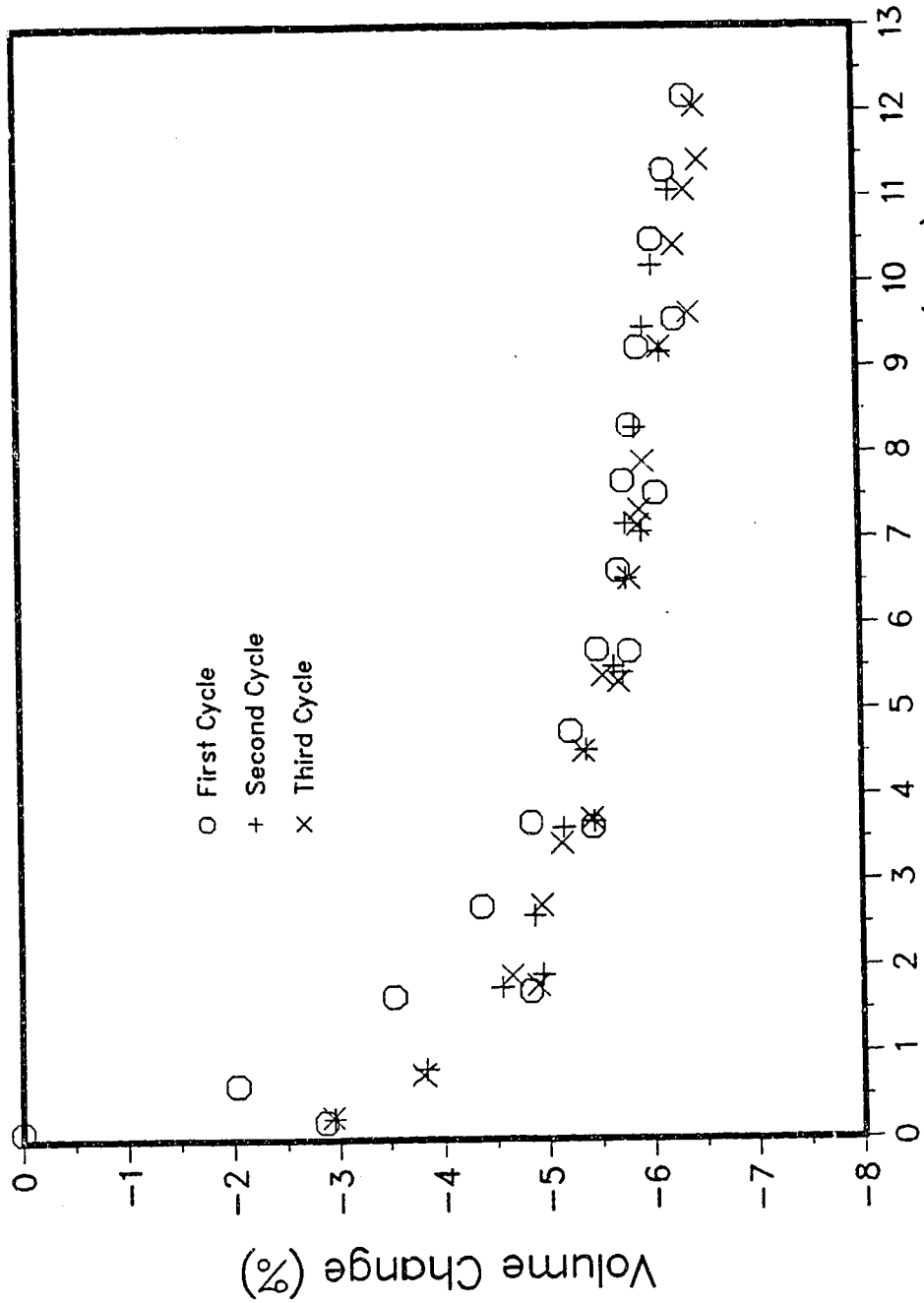

Figure D.13 Isotropic Compressibility Test UFTOS1

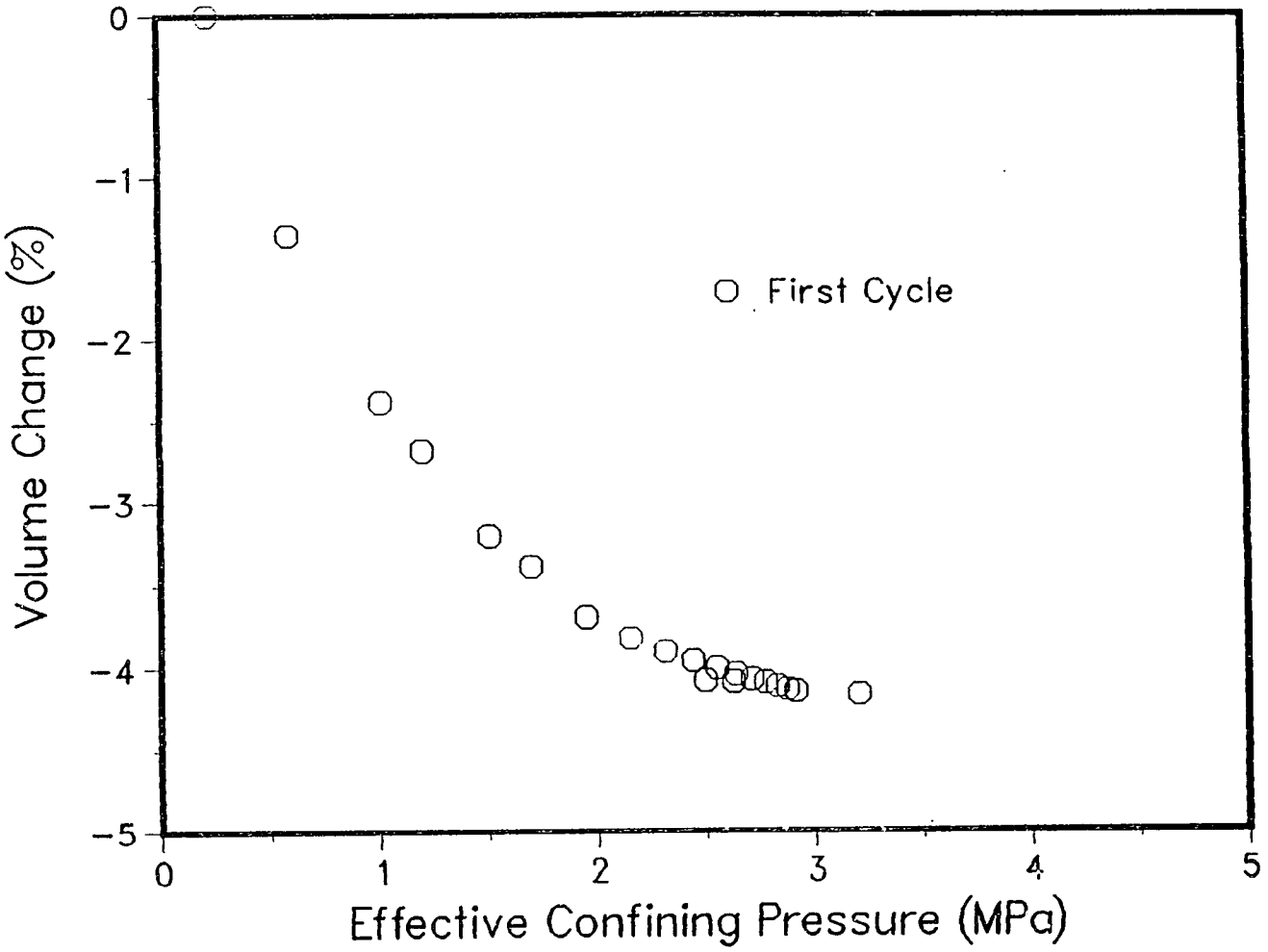

Figure D.14 Isotropic Compressibility Test UFTOS2

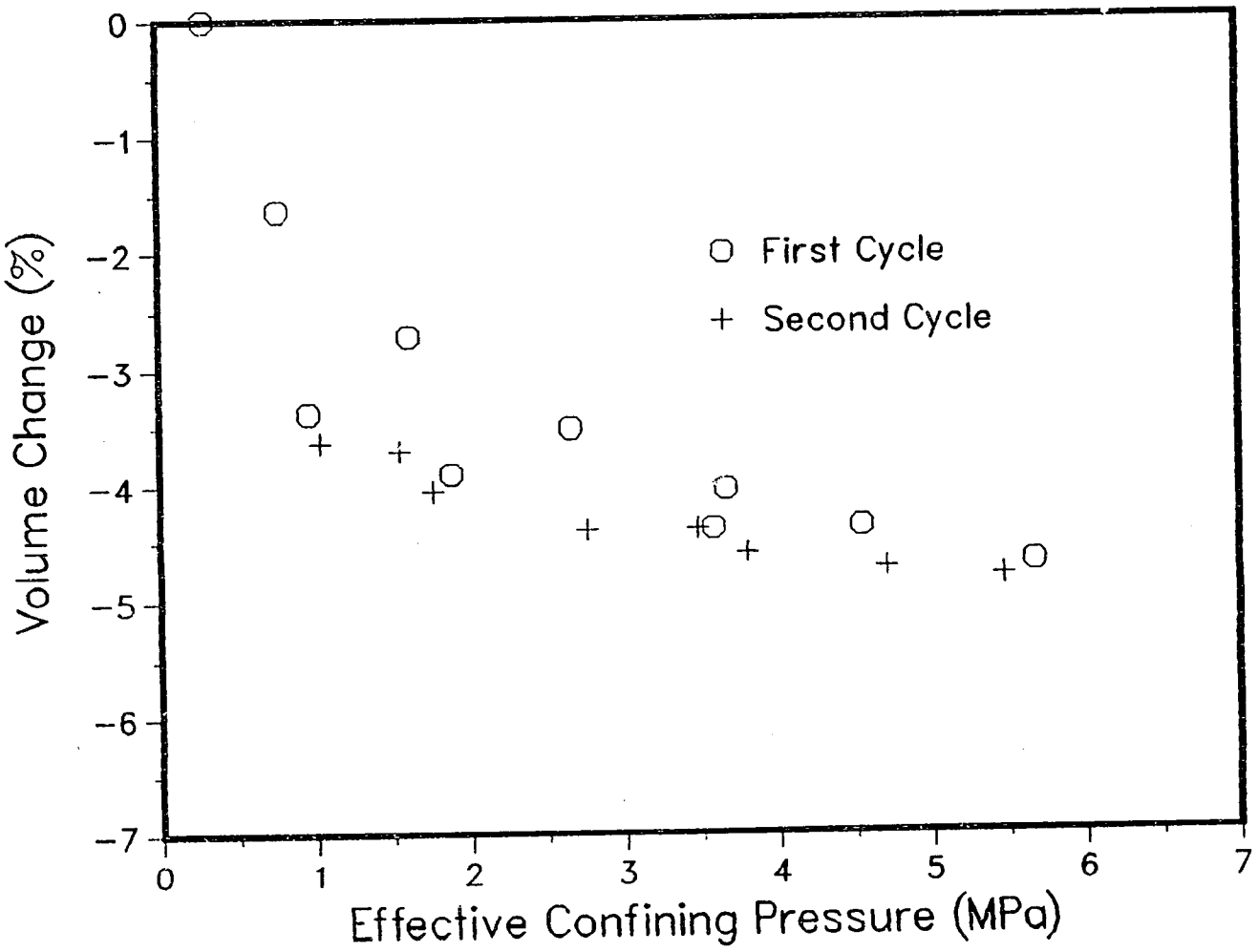

Figure D.15 Isotropic Compressibility Test UFTOS3

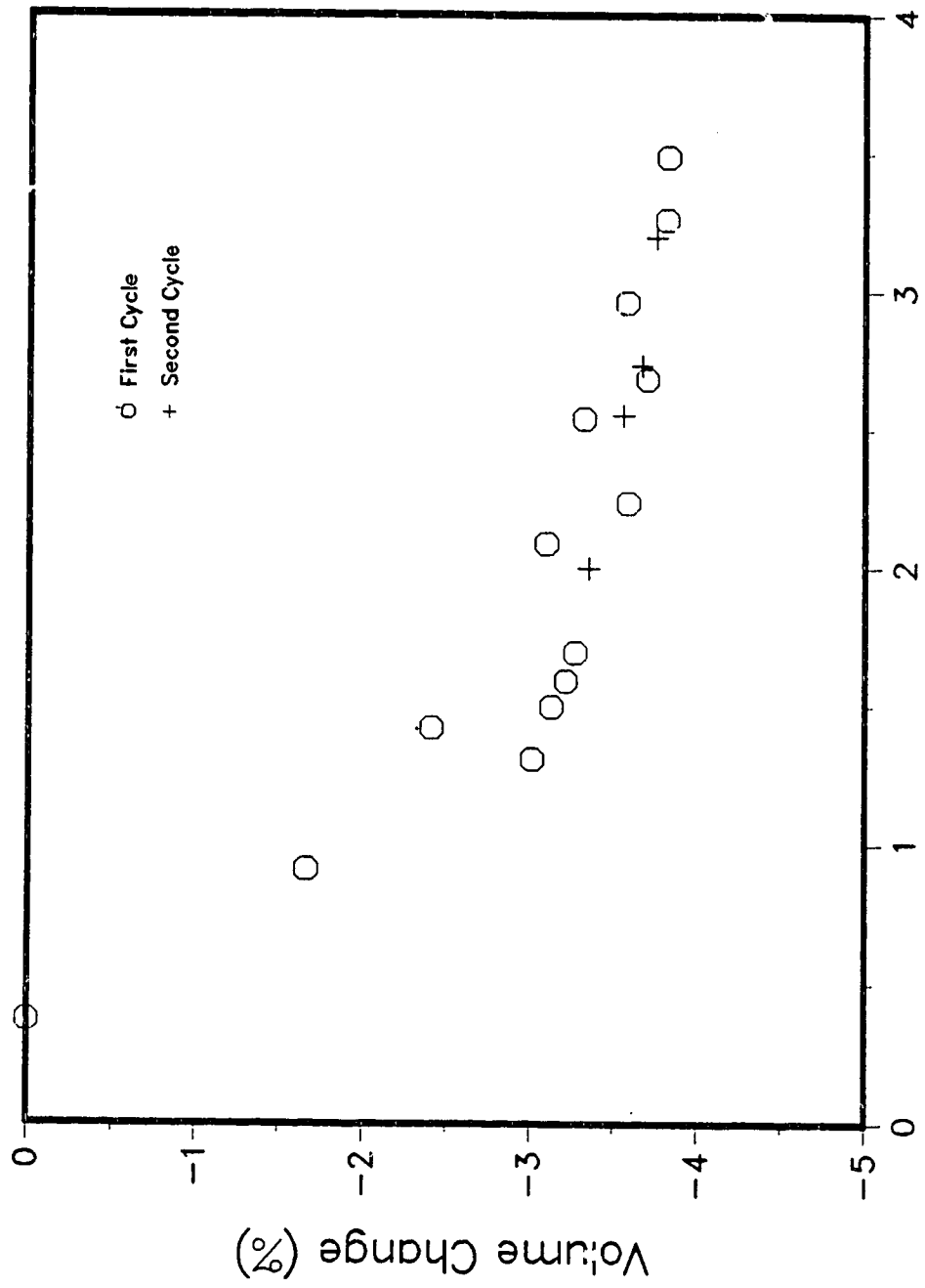

Figure D.16 Isotropic Compressibility Test UFTOS5

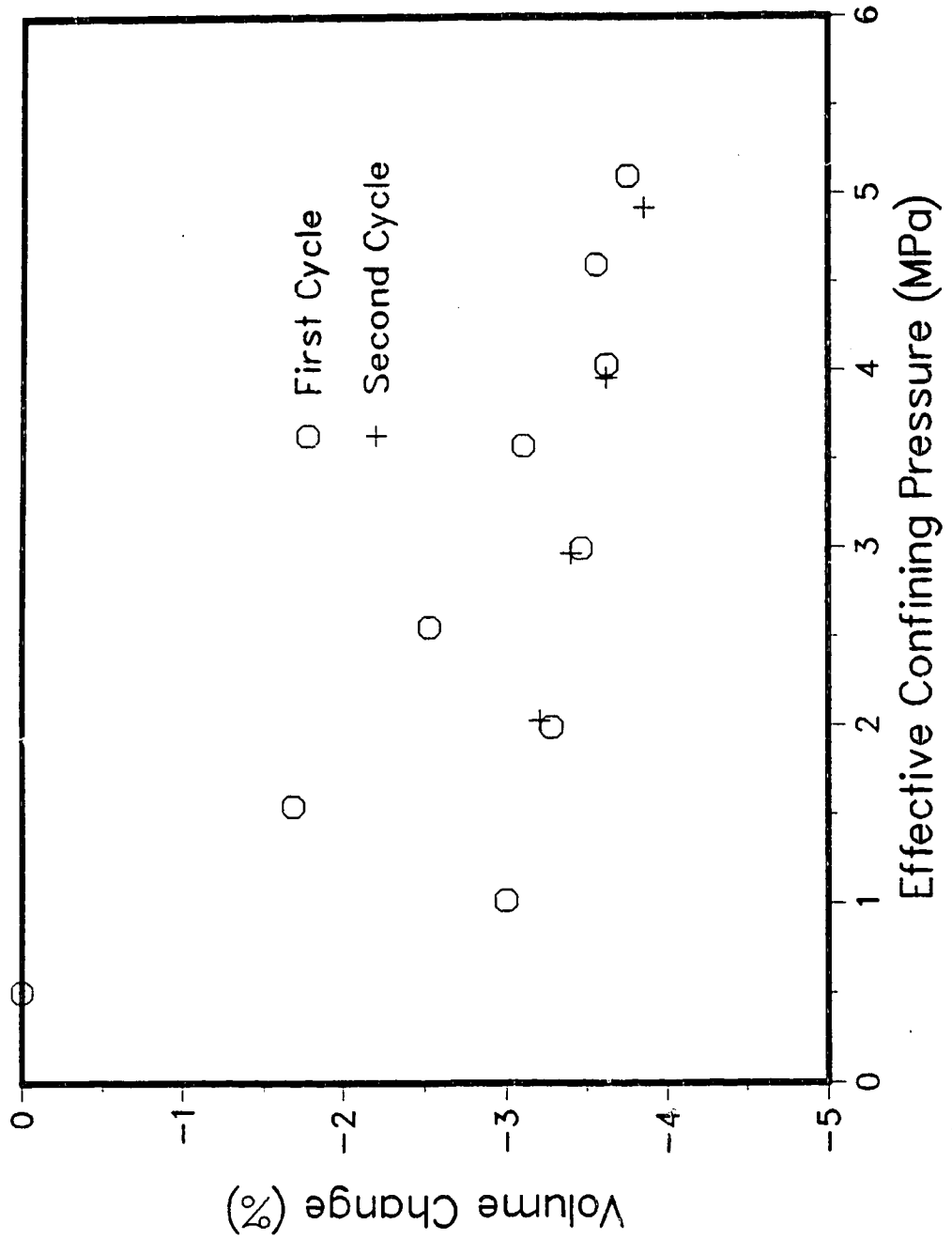

Figure D.17 Isotropic Compressibility Test UFTOS6

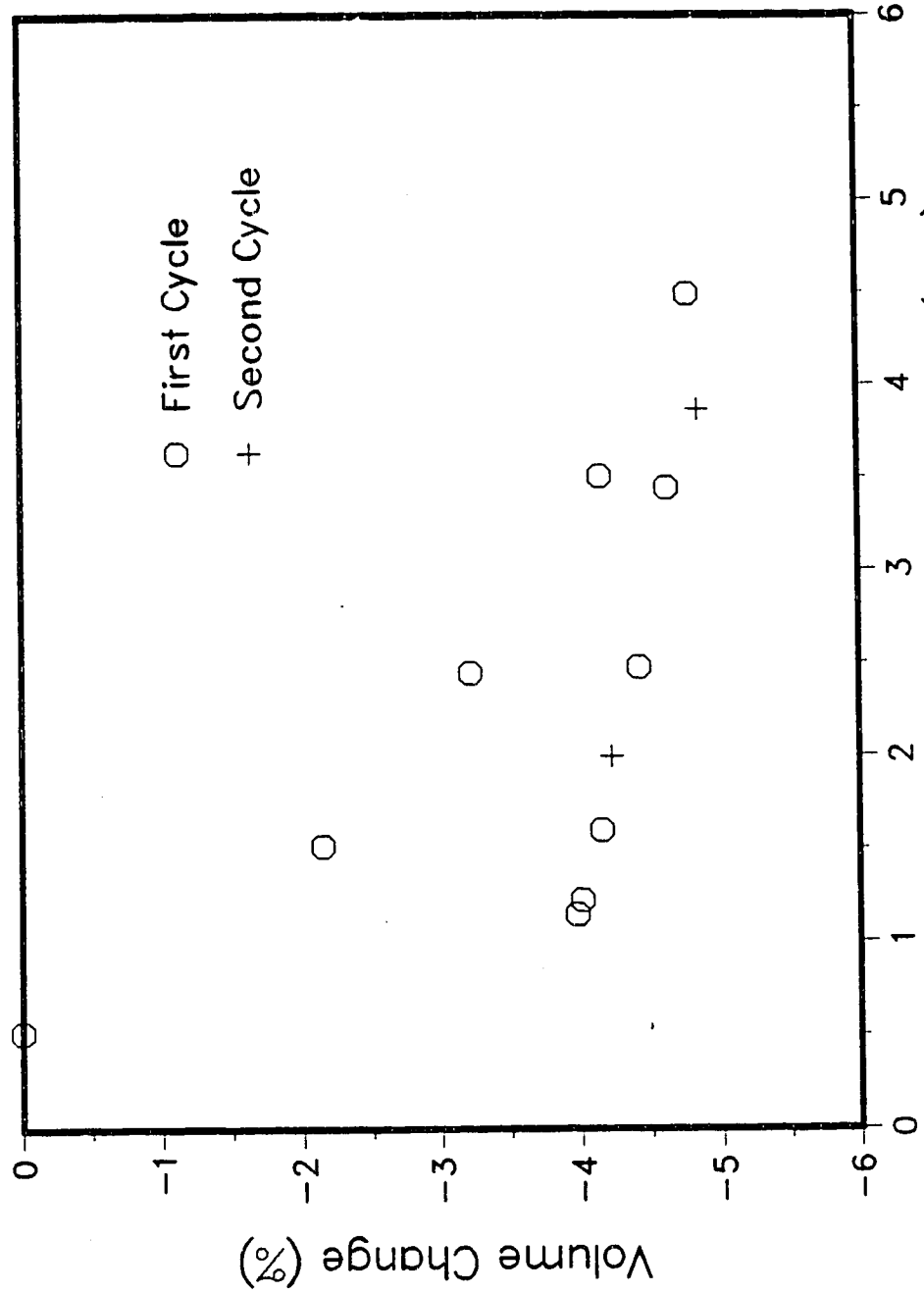

Figure D.18 Isotropic Compressibility Test UFTOS7

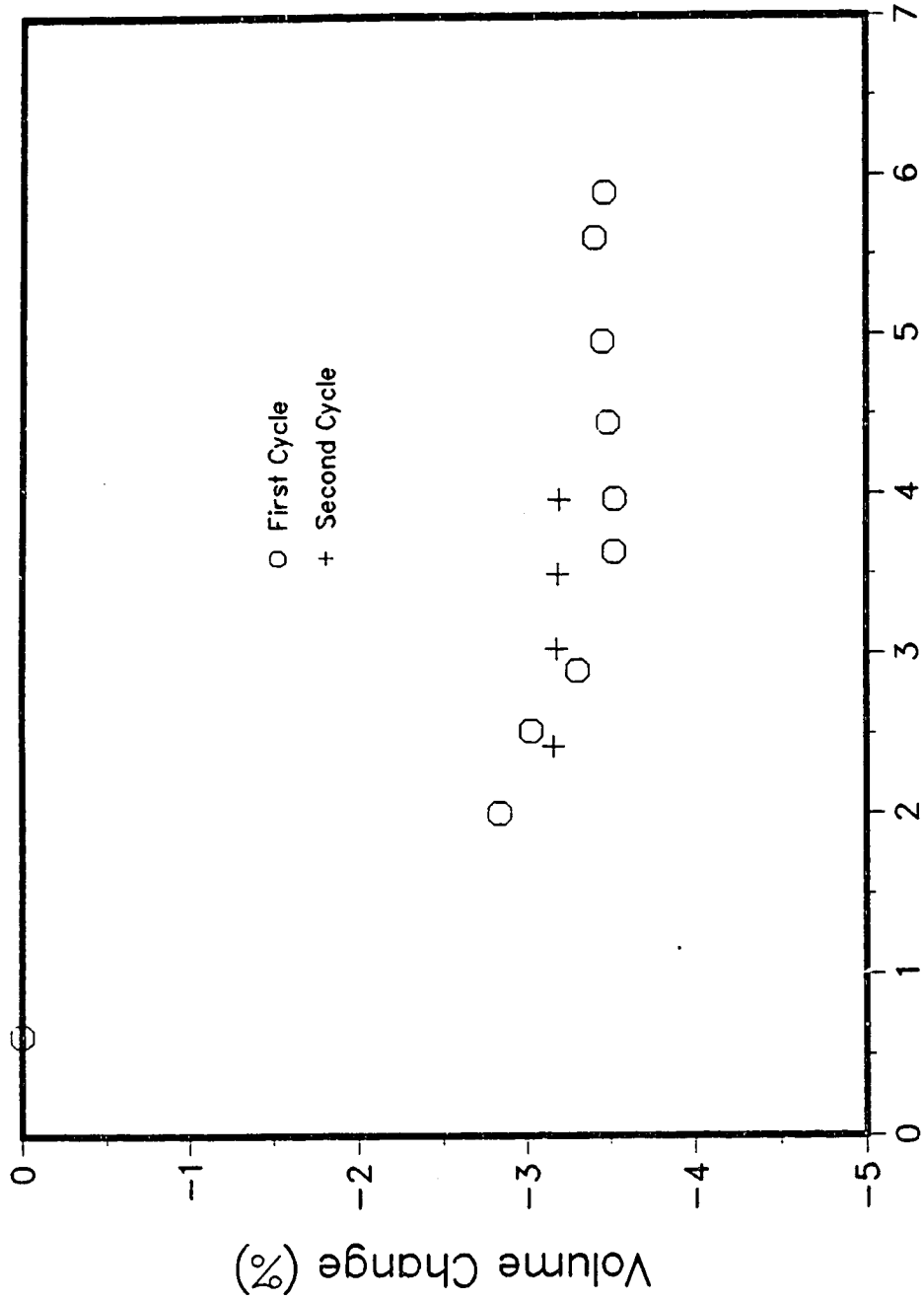

Figure D.19 Isotropic Compressibility Test UFTOS8

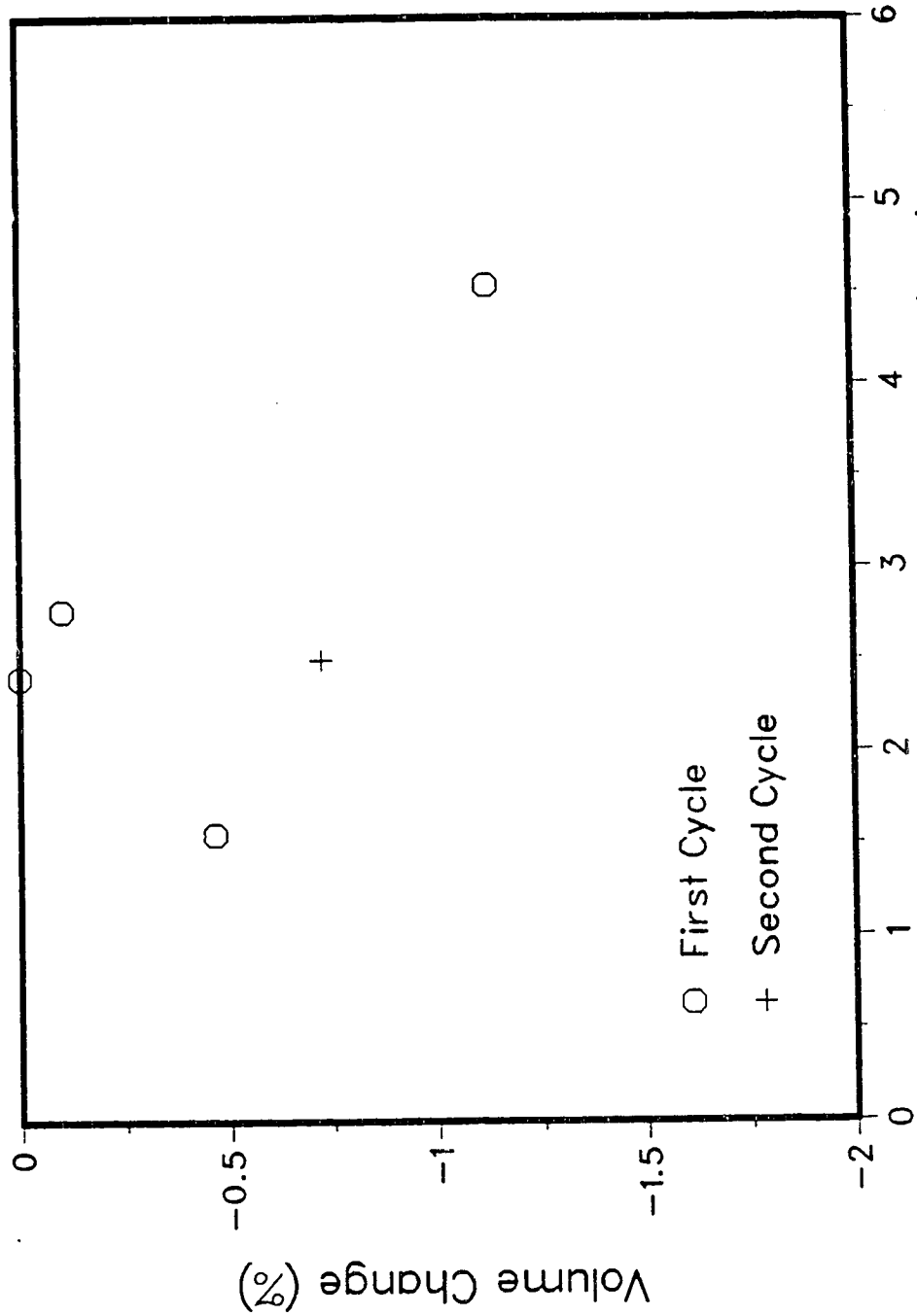

Figure D.20 Isotropic Compressibility Test UFTOS9

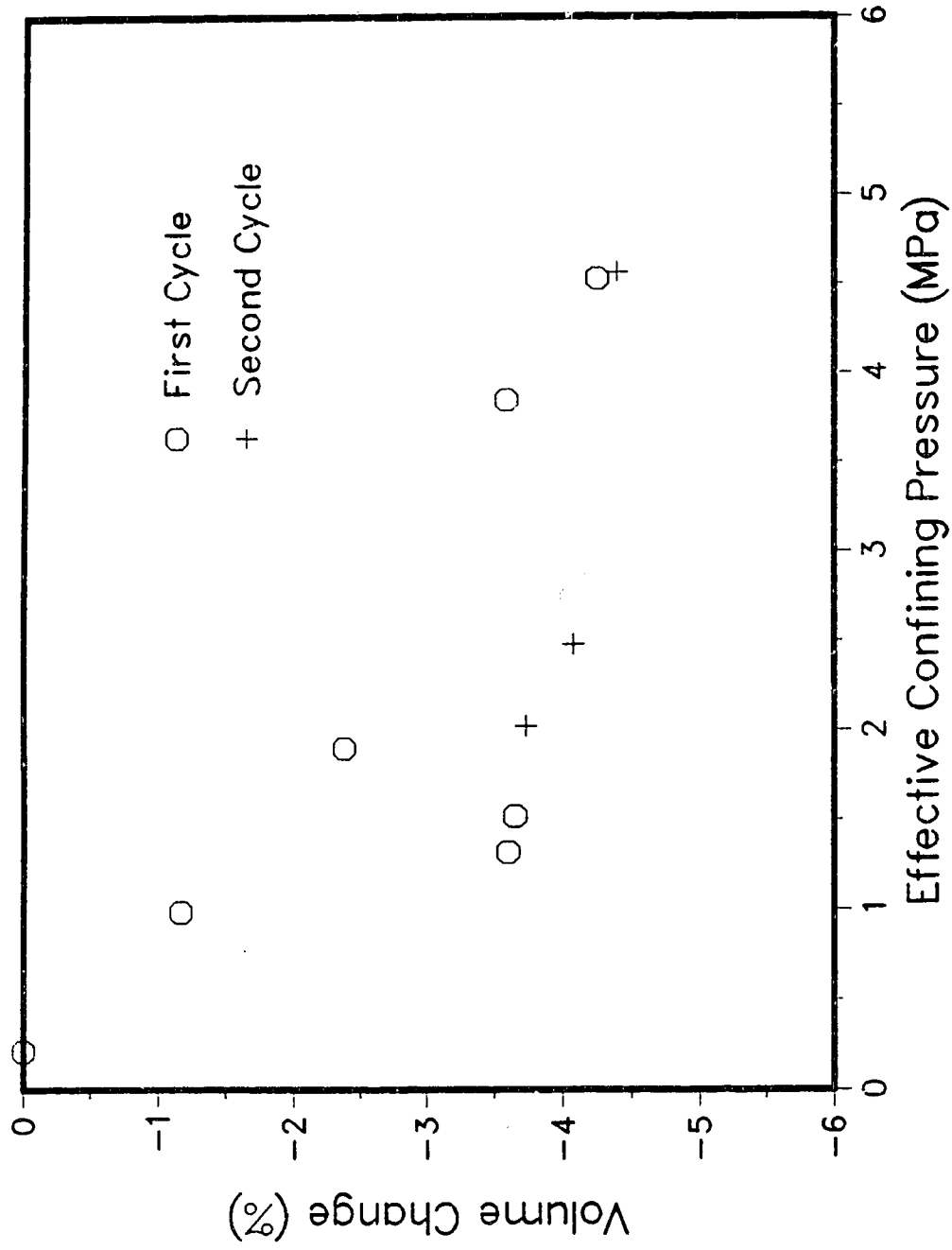

Figure D.21 Isotropic Compressibility Test UFTOS10

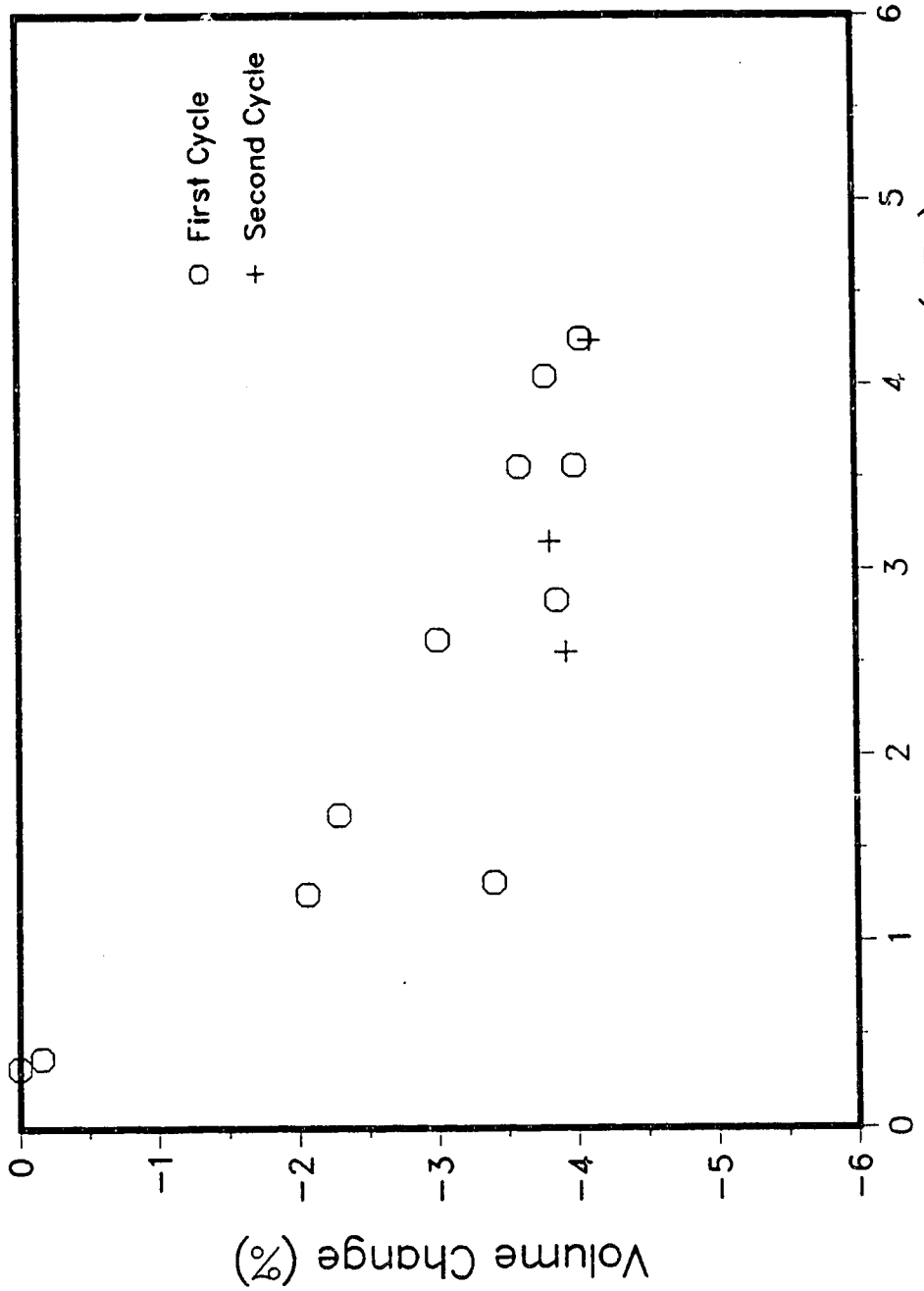

Figure D.22 Isotropic Compressibility Test UFTOS12

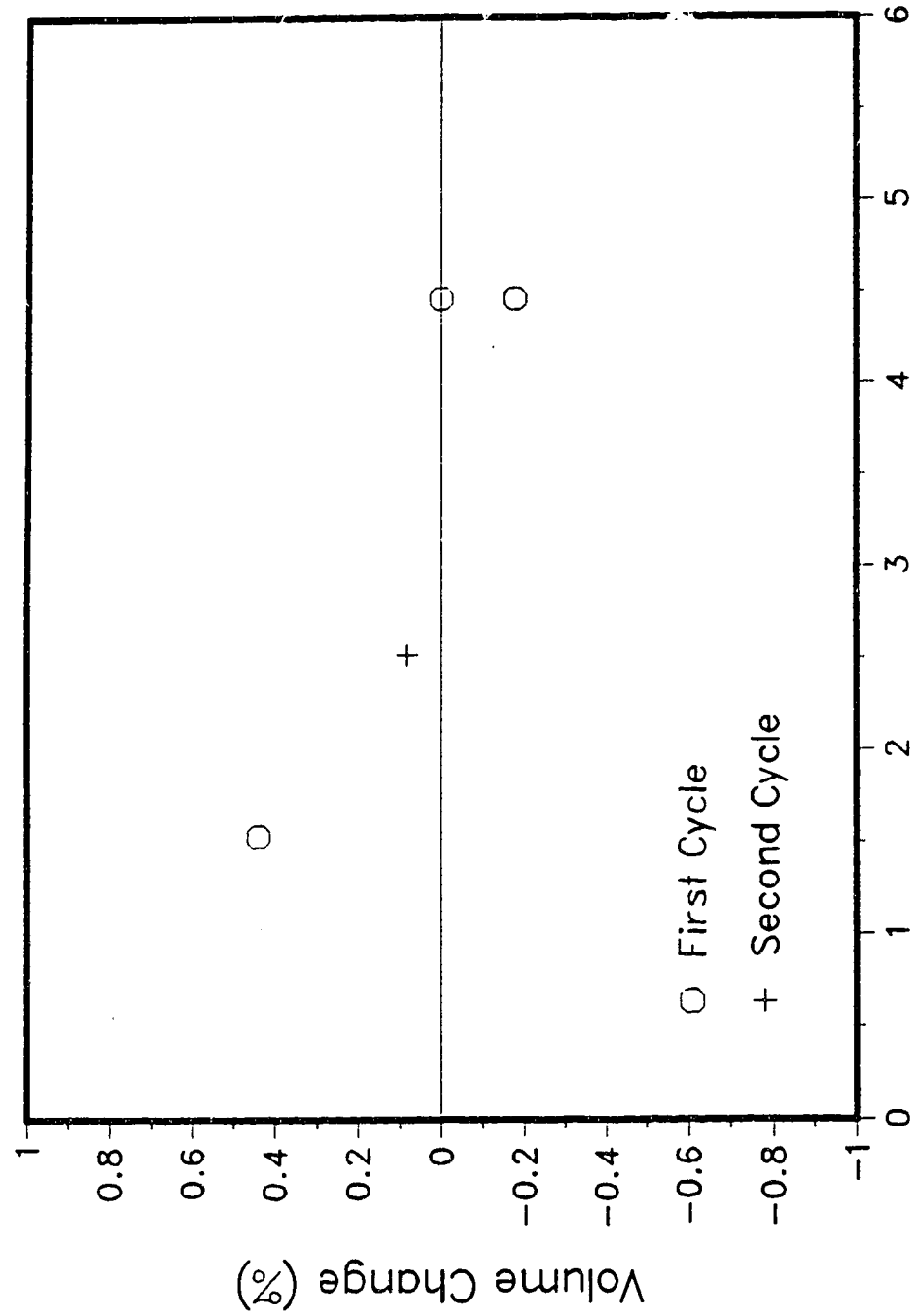

Figure D.23 Isotropic Compressibility Test UFTOS14

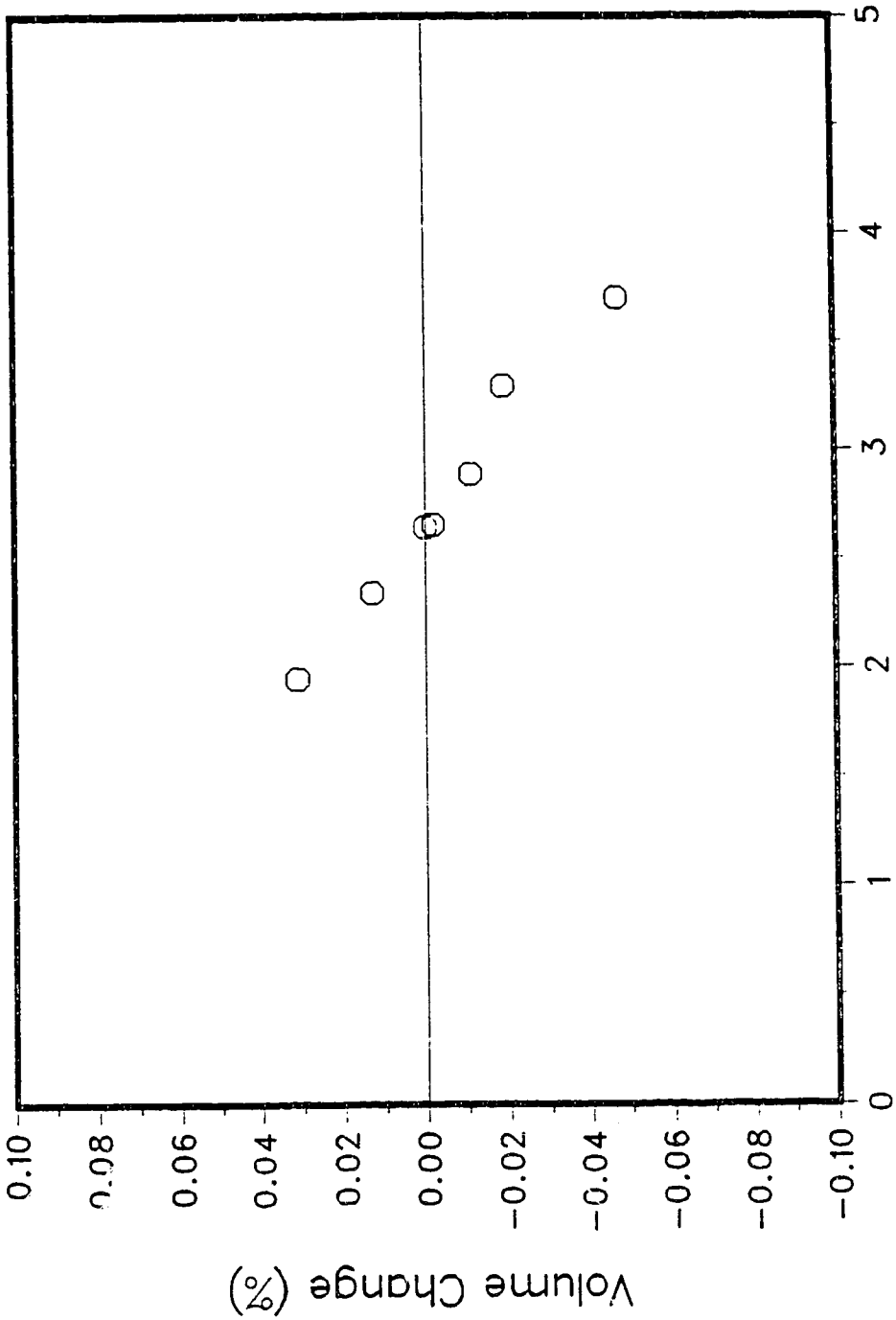

Figure D.24 Isotropic Compressibility Test UFHTTOS1 225 °C

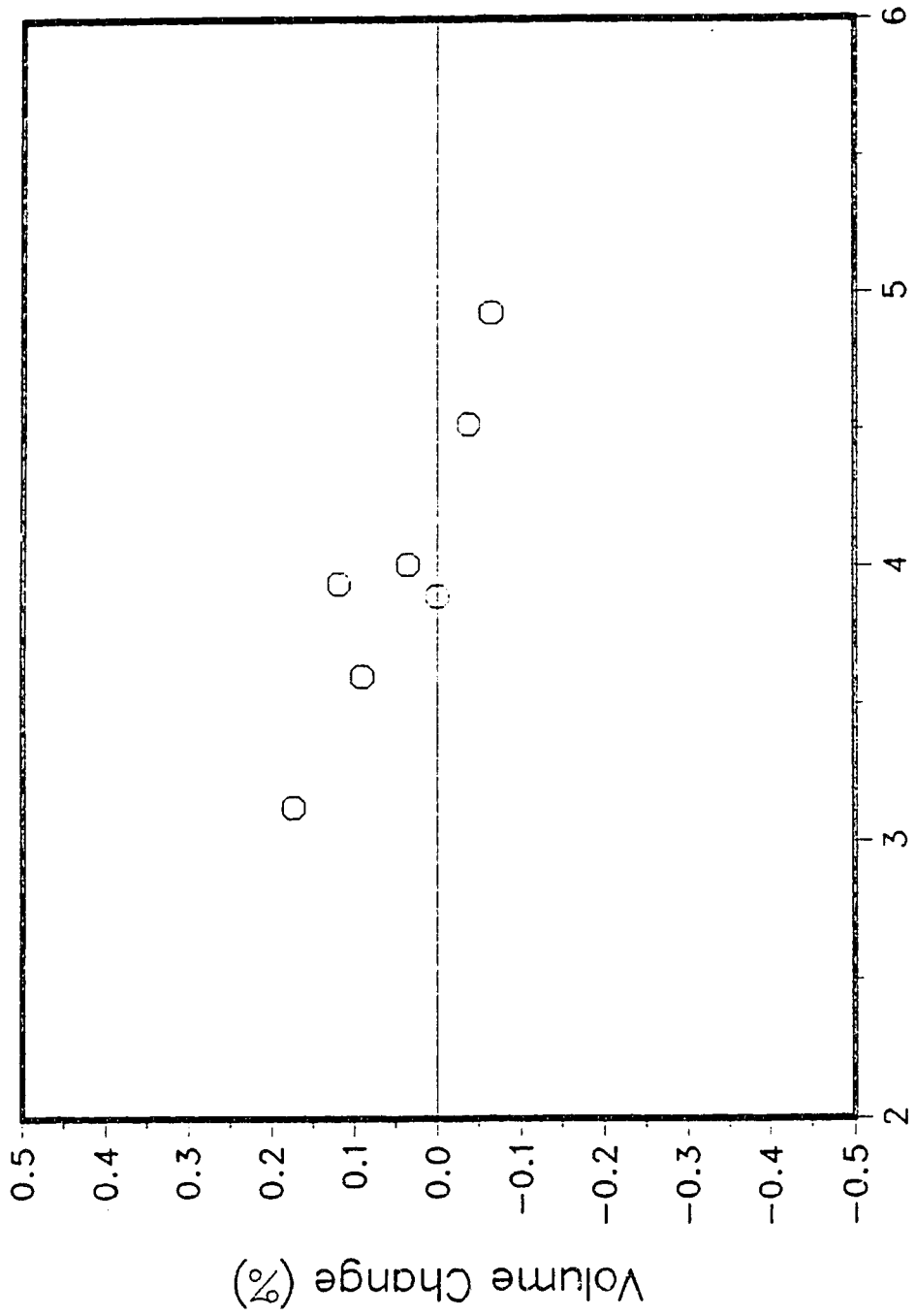

Figure D.25 Isotropic Compressibility Test UFHTTOS2 225 °C

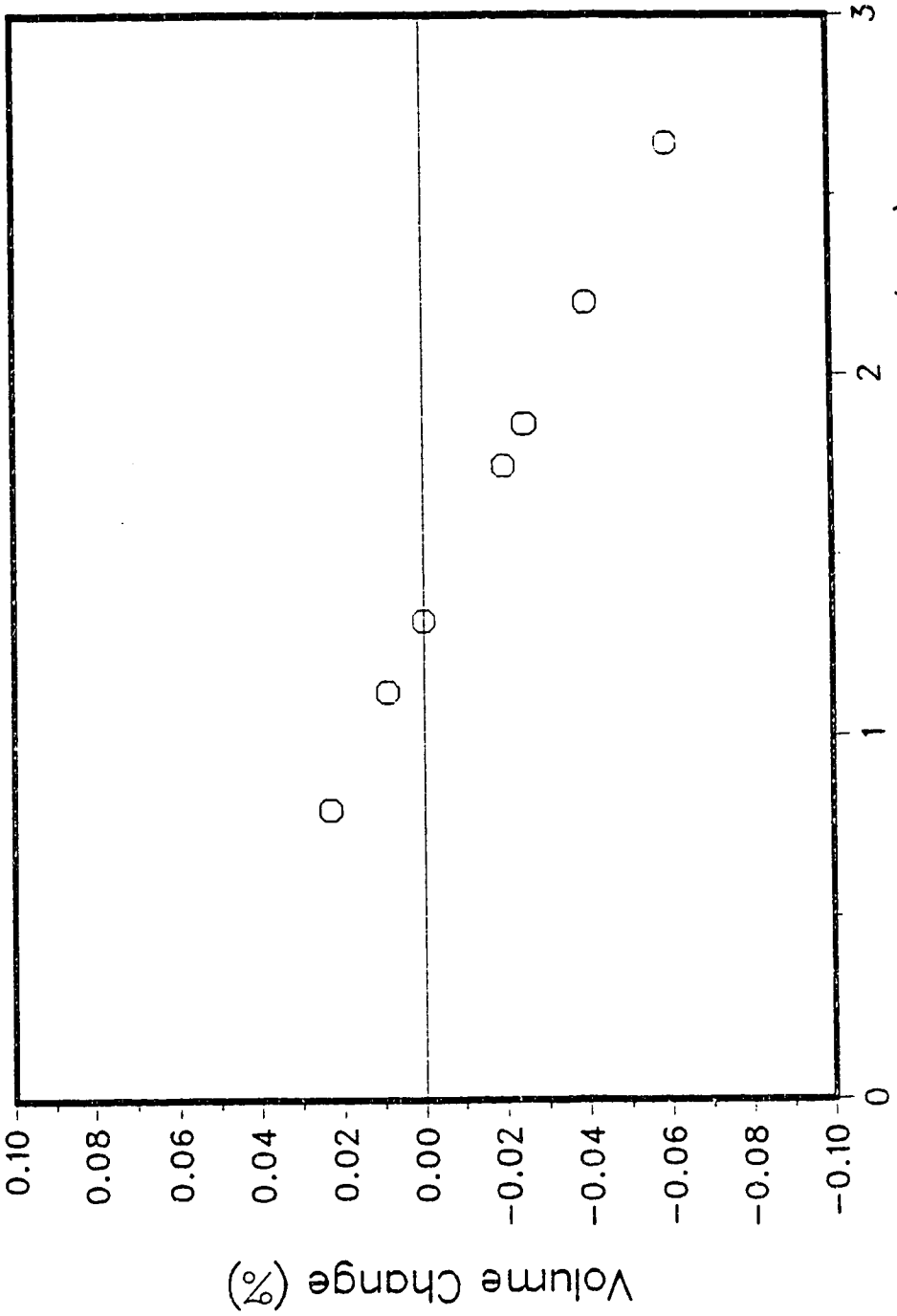

Figure D.26 Isotropic Compressibility Test UFHTTOS3 225 °C

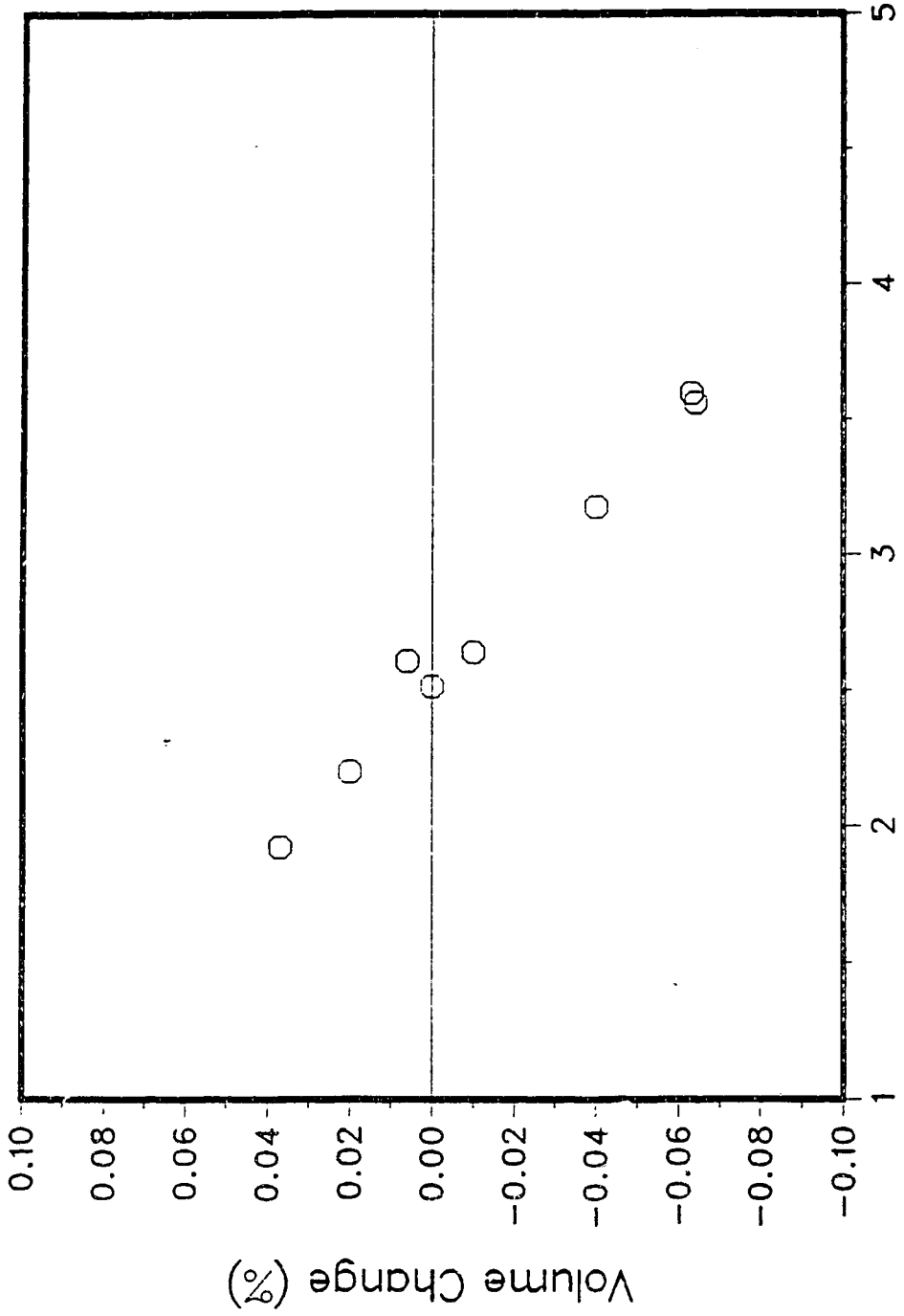

Figure D.27 Isotropic Compressibility Test UFHTTOS4 225 °C

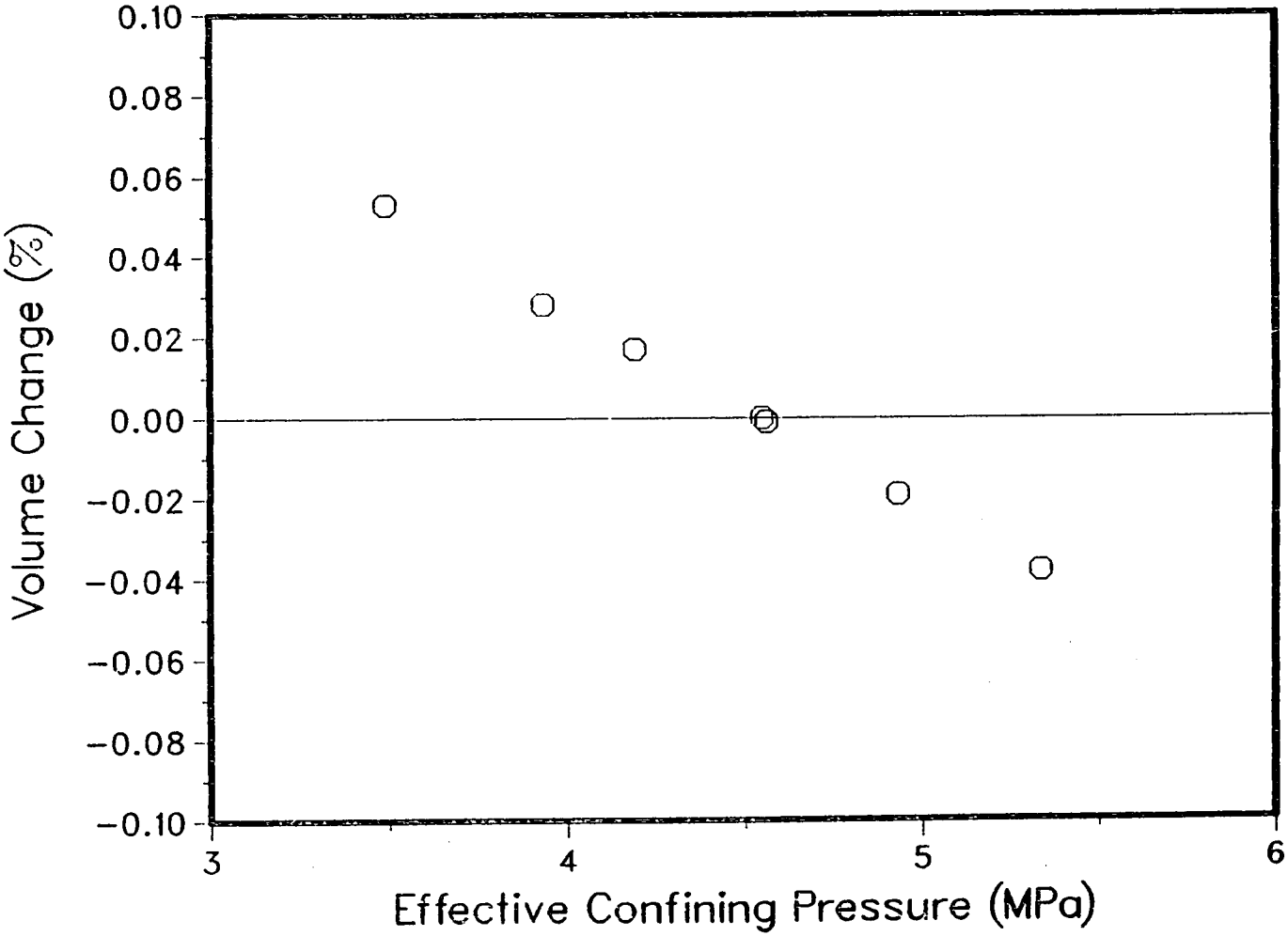

Figure D.28 Isotropic Compressibility Test UFHTTOS5 225 °C

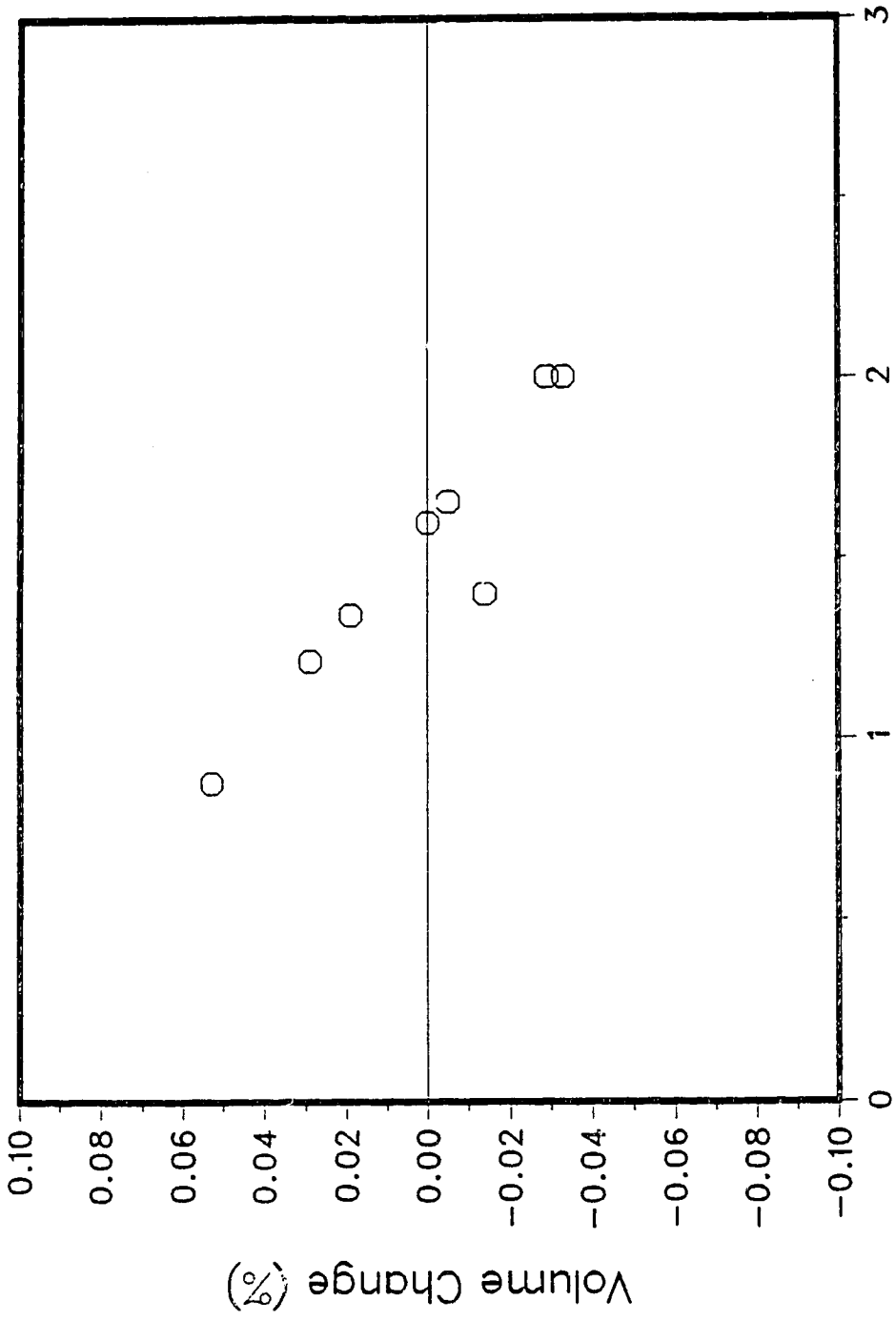

Figure D.29 Isotropic Compressibility Test UFHTTOS6 225 °C

E. COLD LAKE MATERIALS: COMPRESSIBILITY TEST RESULTS

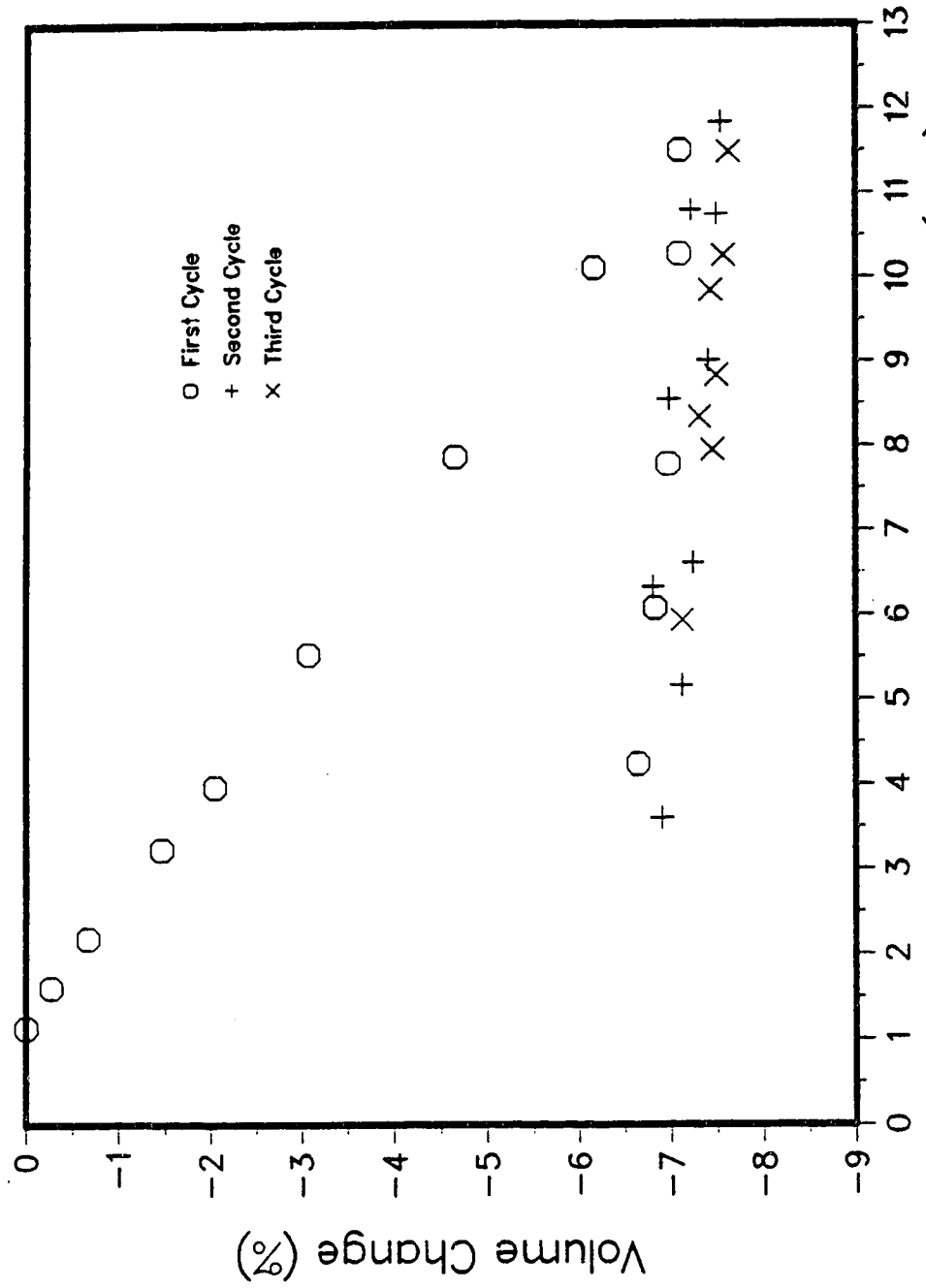

Figure E.1 One Dimensional Compressibility Test CL1C0S1

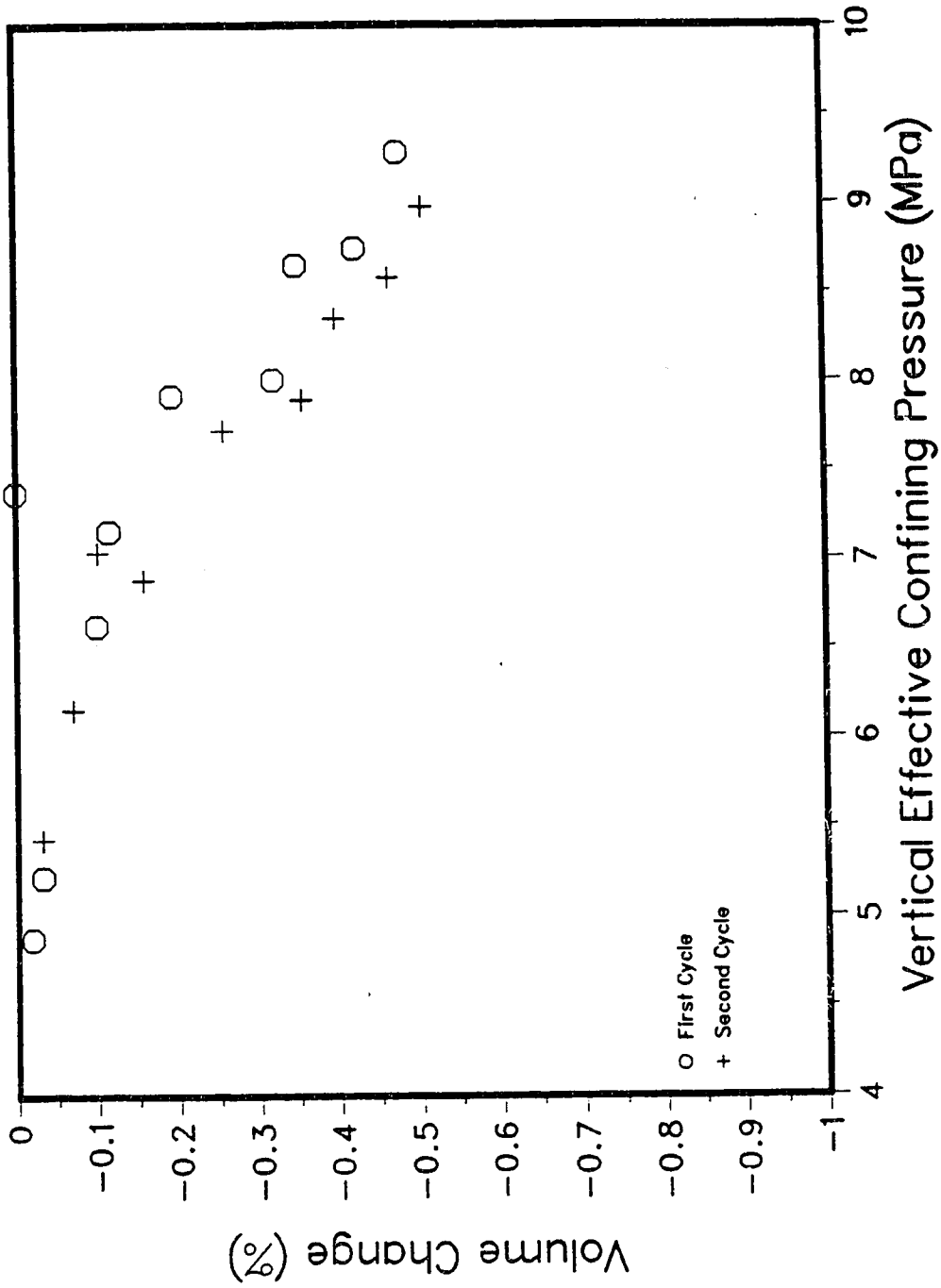

Figure E.2 One Dimensional Compressibility Test CL1C0S2 225 °C

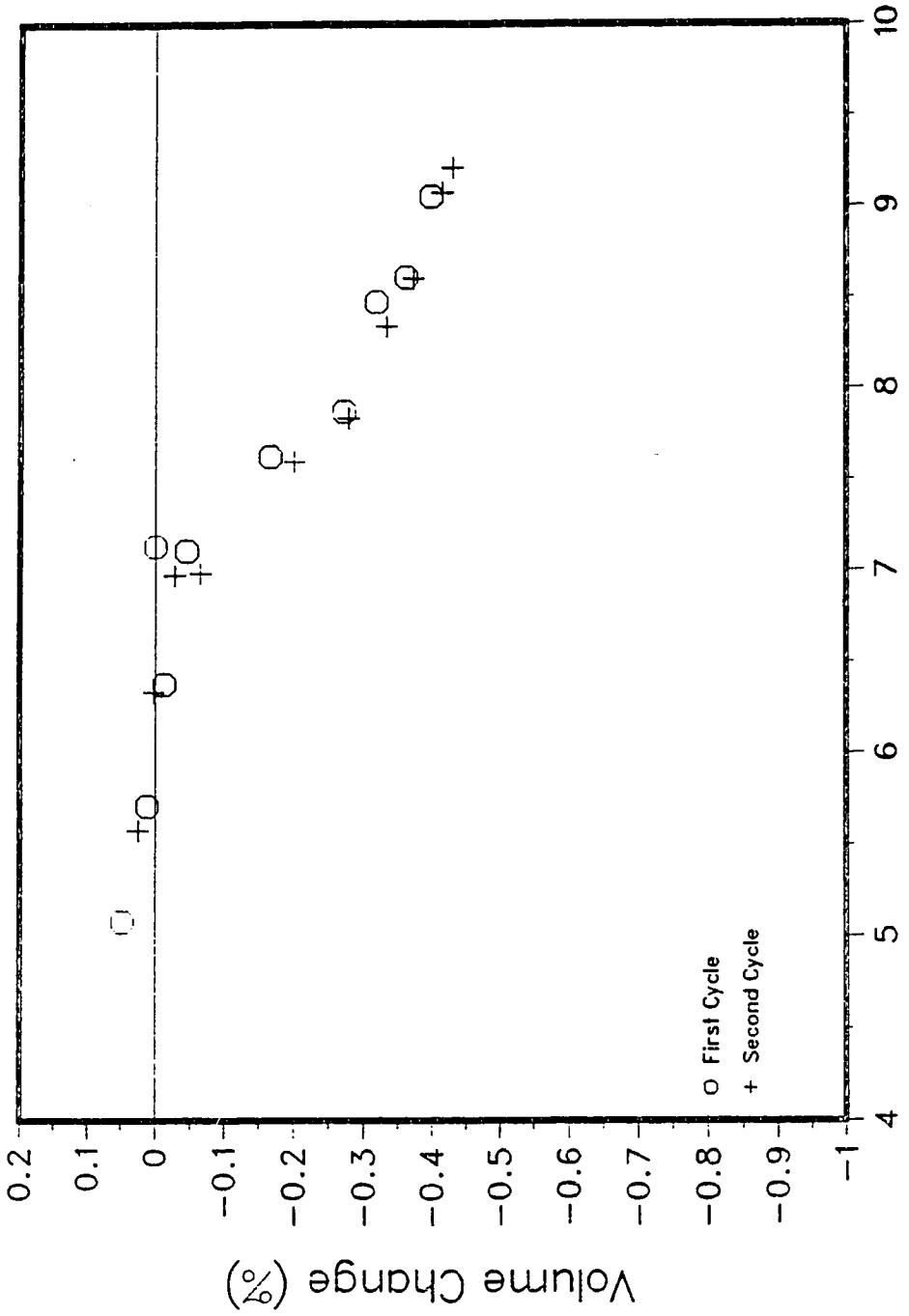

Figure E.3 One Dimensional Compressibility Test CL1COS3 225 °C

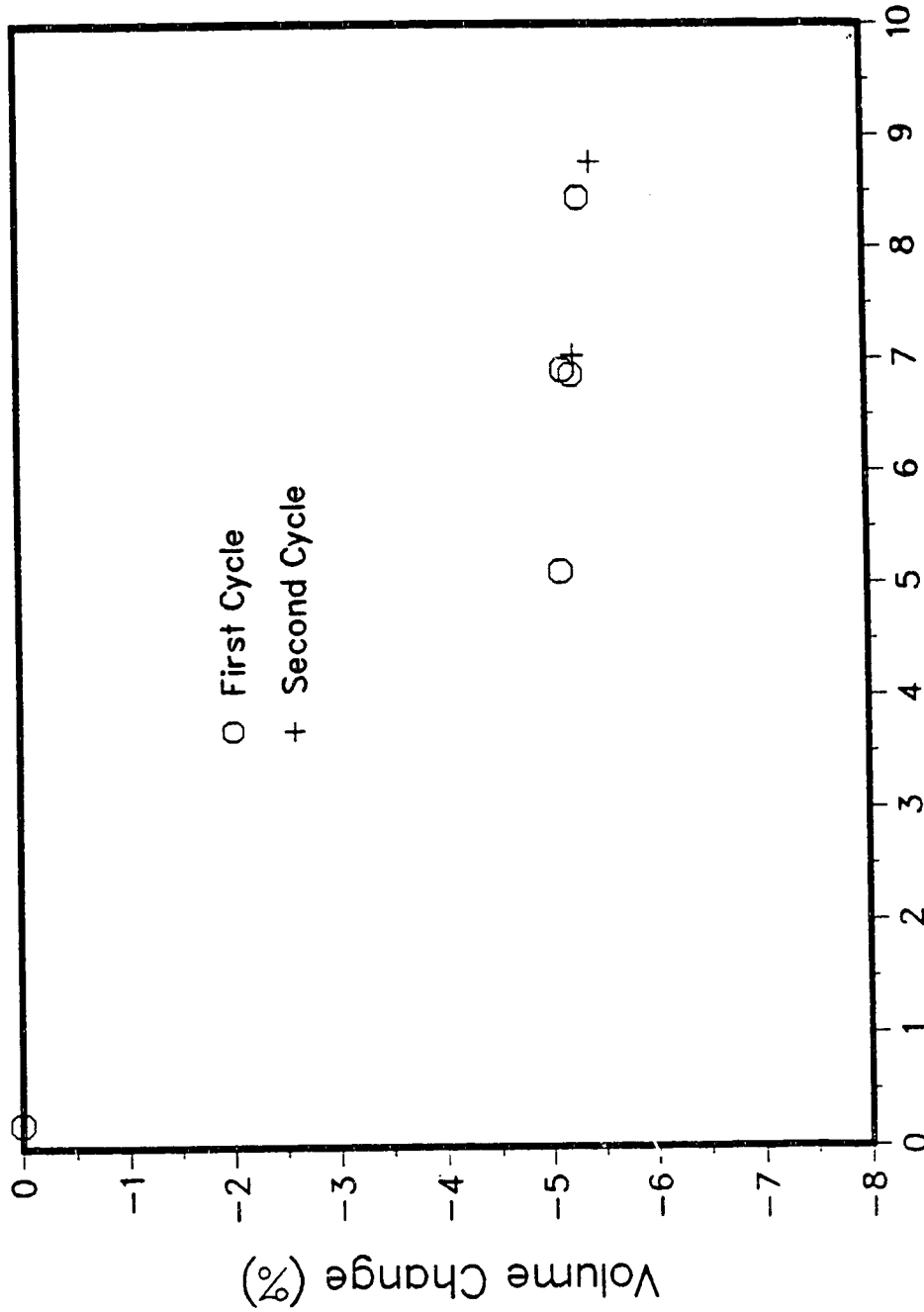

Figure E.4 Isotropic Compressibility Test CL1TOS1

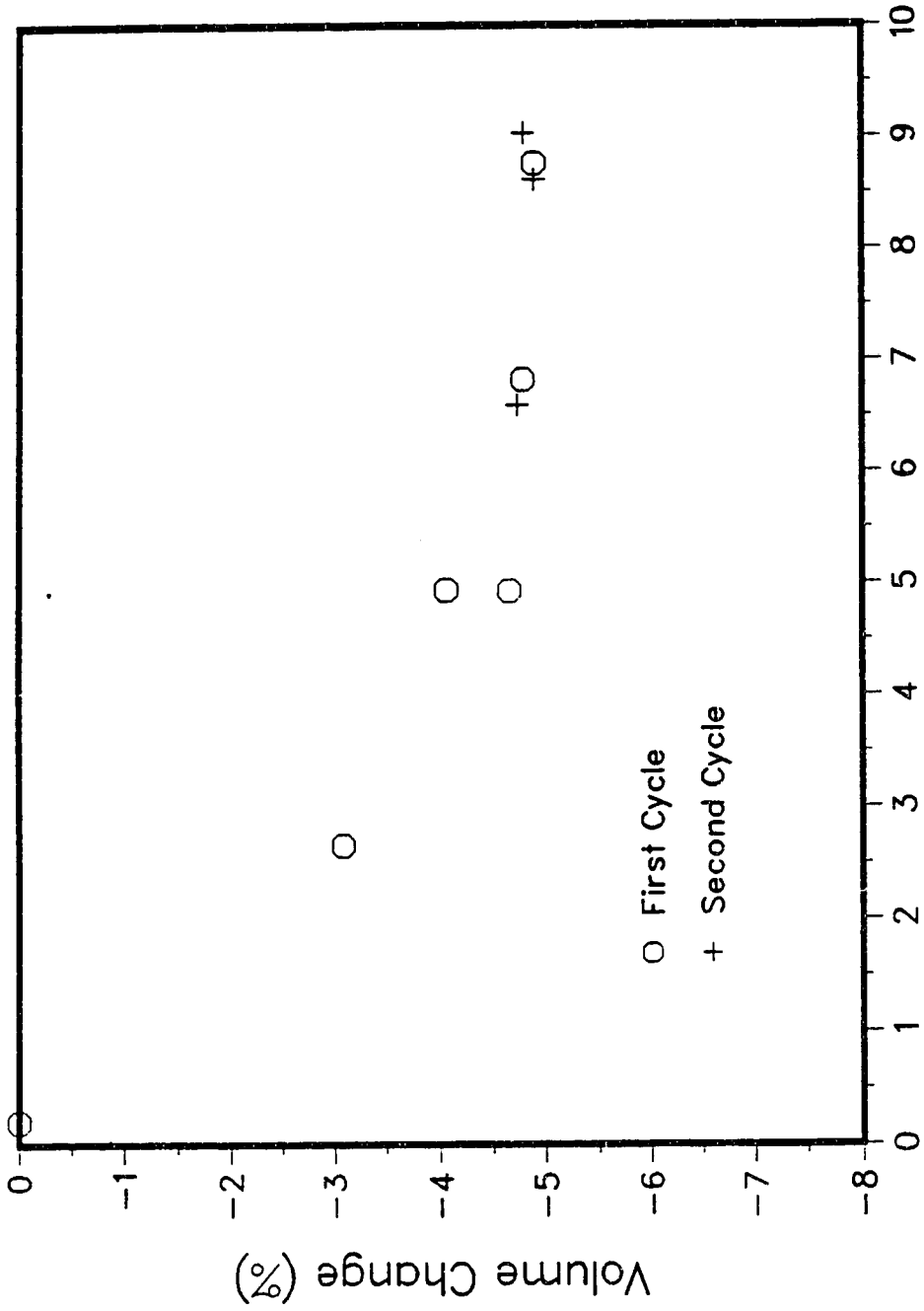

Figure E.5 Isotropic Compressibility Test CL1TOS2

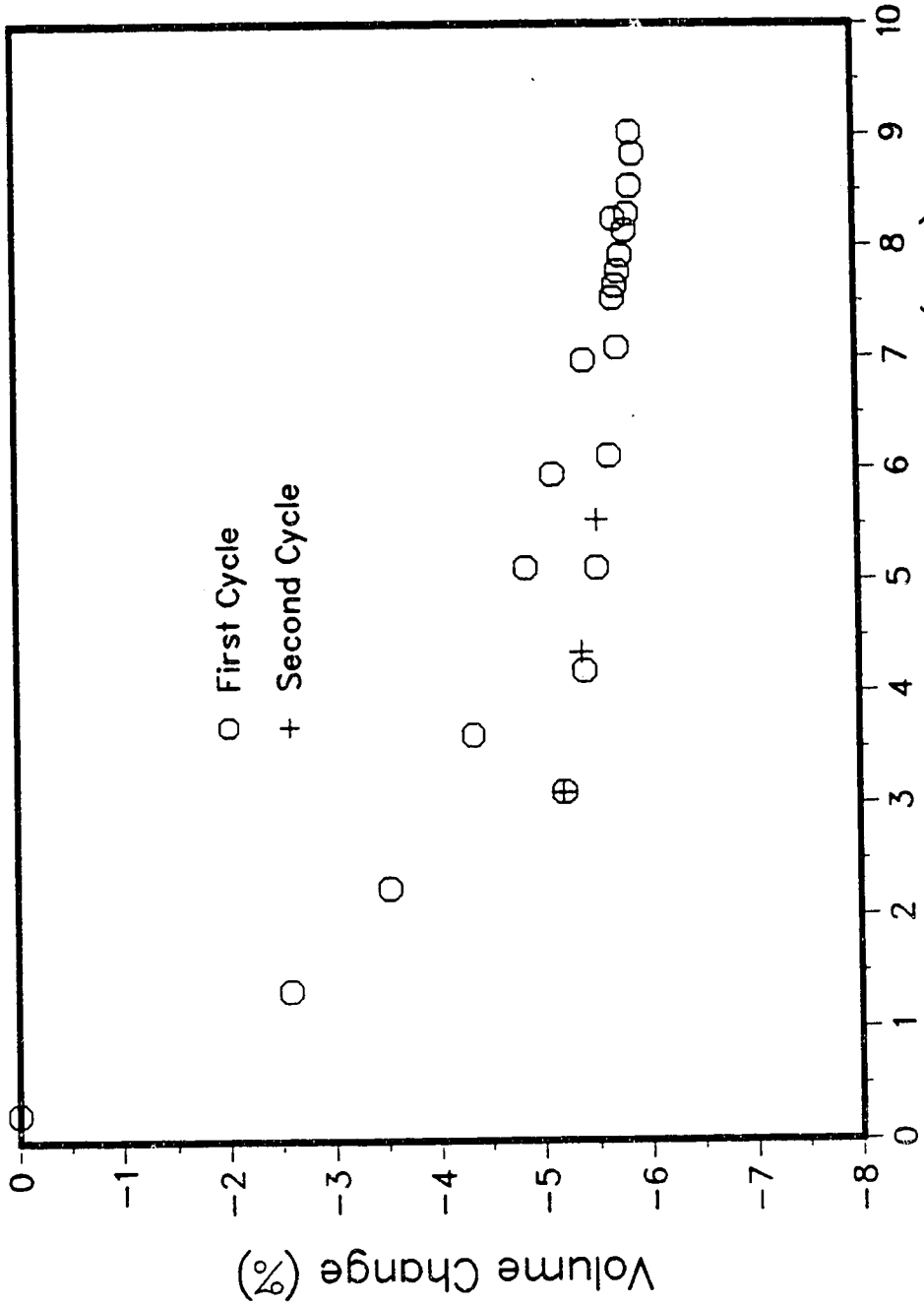

Figure E.6 Isotropic Compressibility Test CL1TOS3

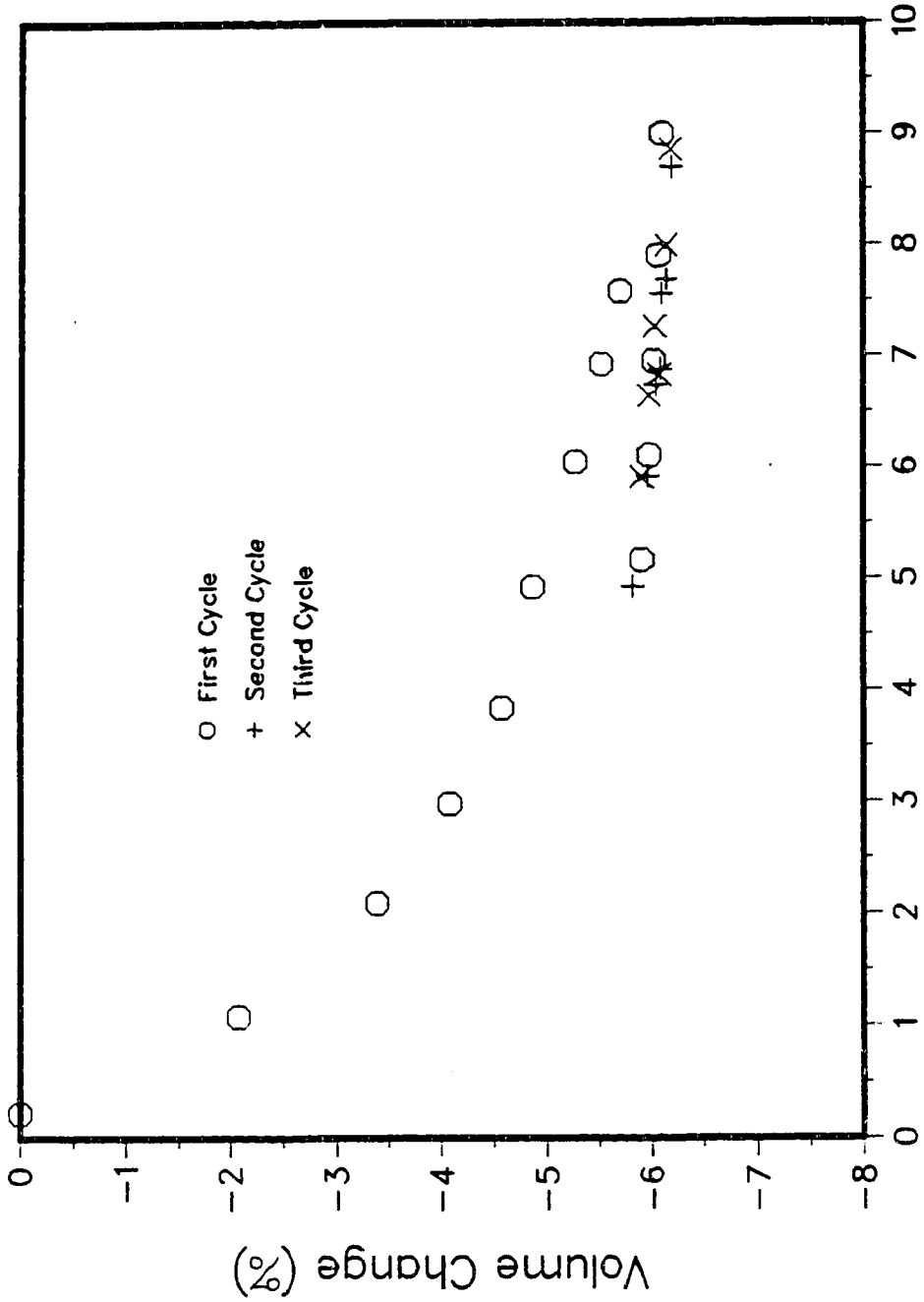

Figure E.7 Isotropic Compressibility Test CL1TOS4

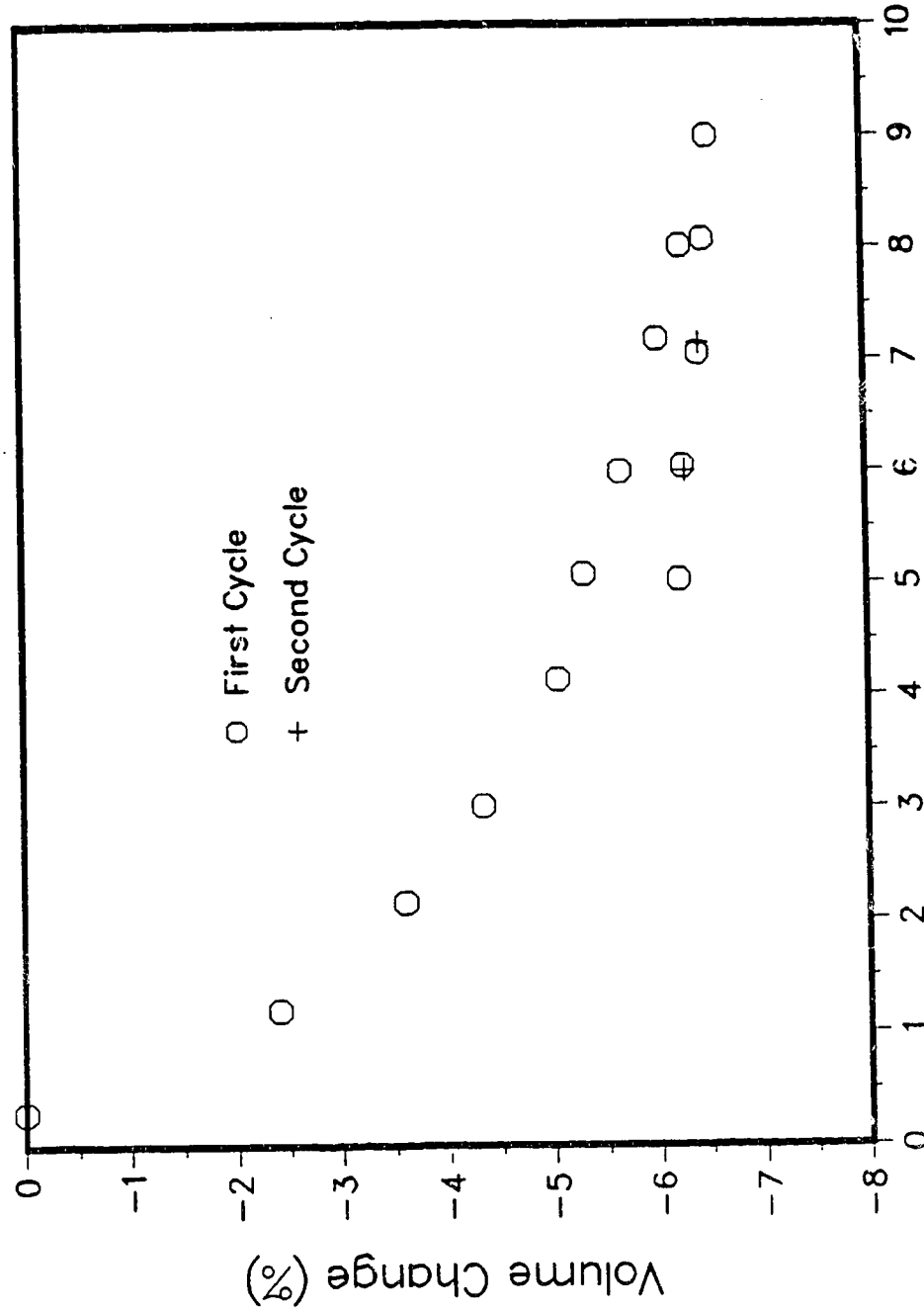

Figure E.8 Isotropic Compressibility Test CL1TOS5

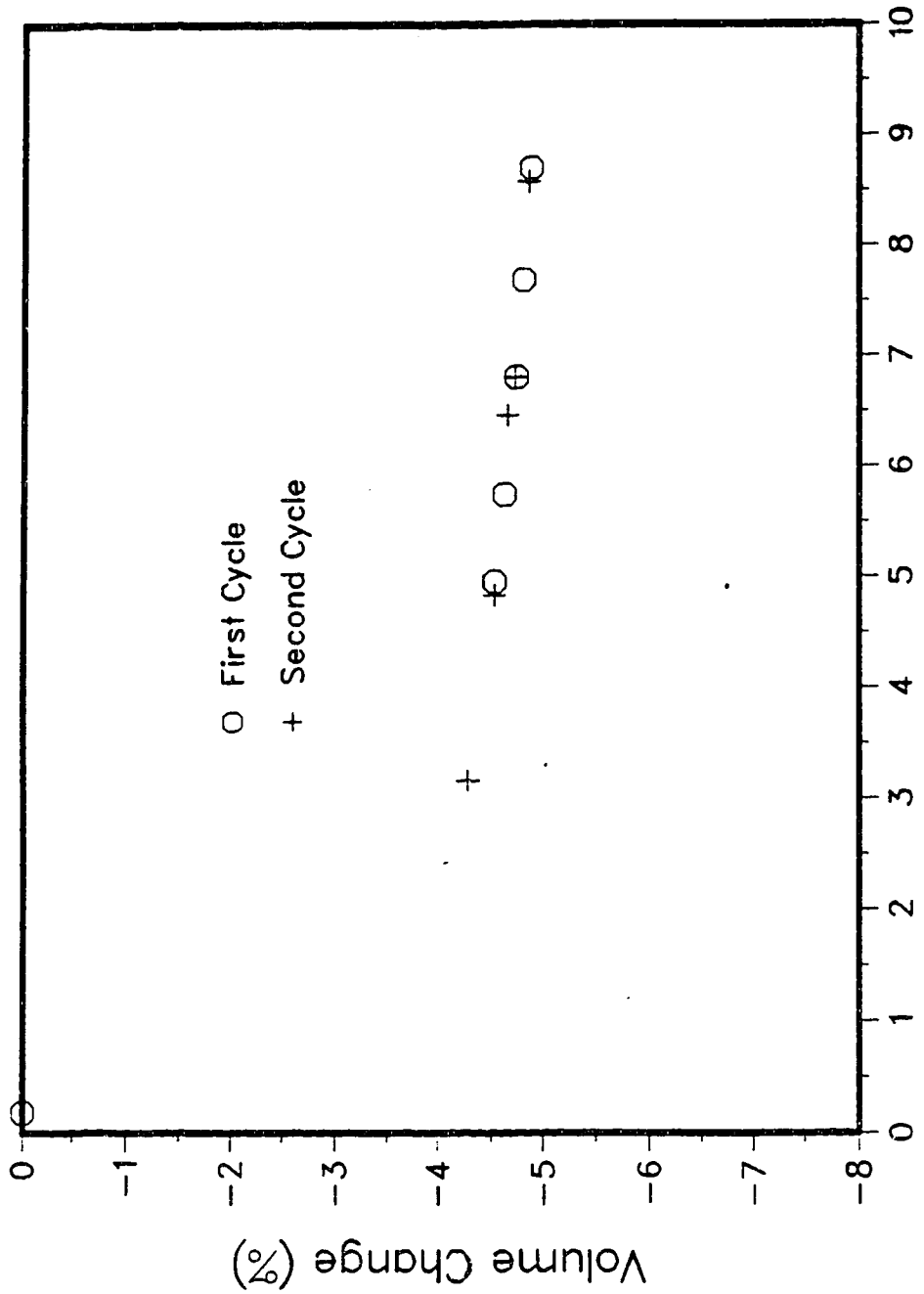

Figure E.9 Isotropic Compressibility Test CL1TOS6

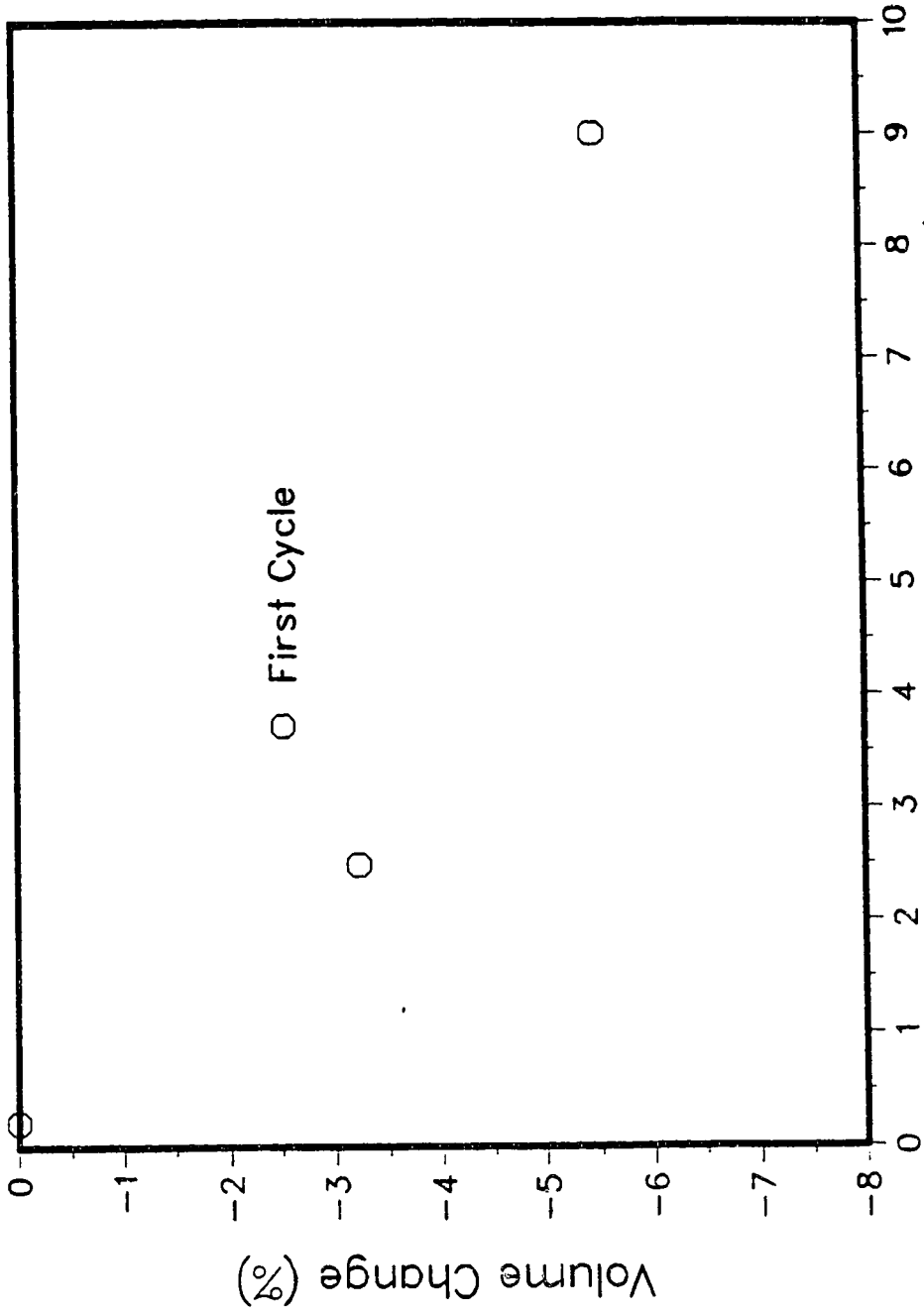

Figure E.10 Isotropic Compressibility Test CL1TOS7

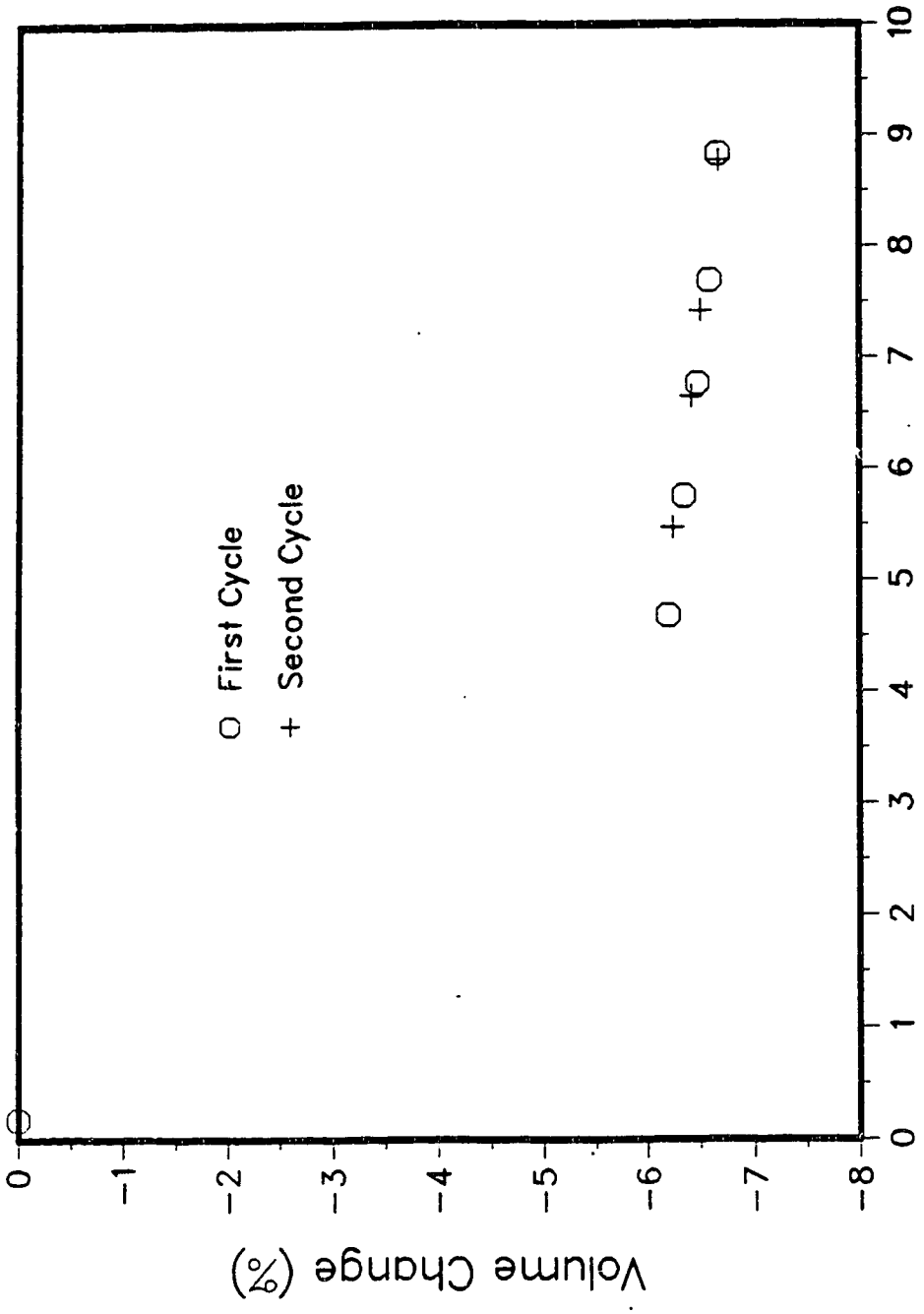

Figure E.11 Isotropic Compressibility Test CL1TOS8

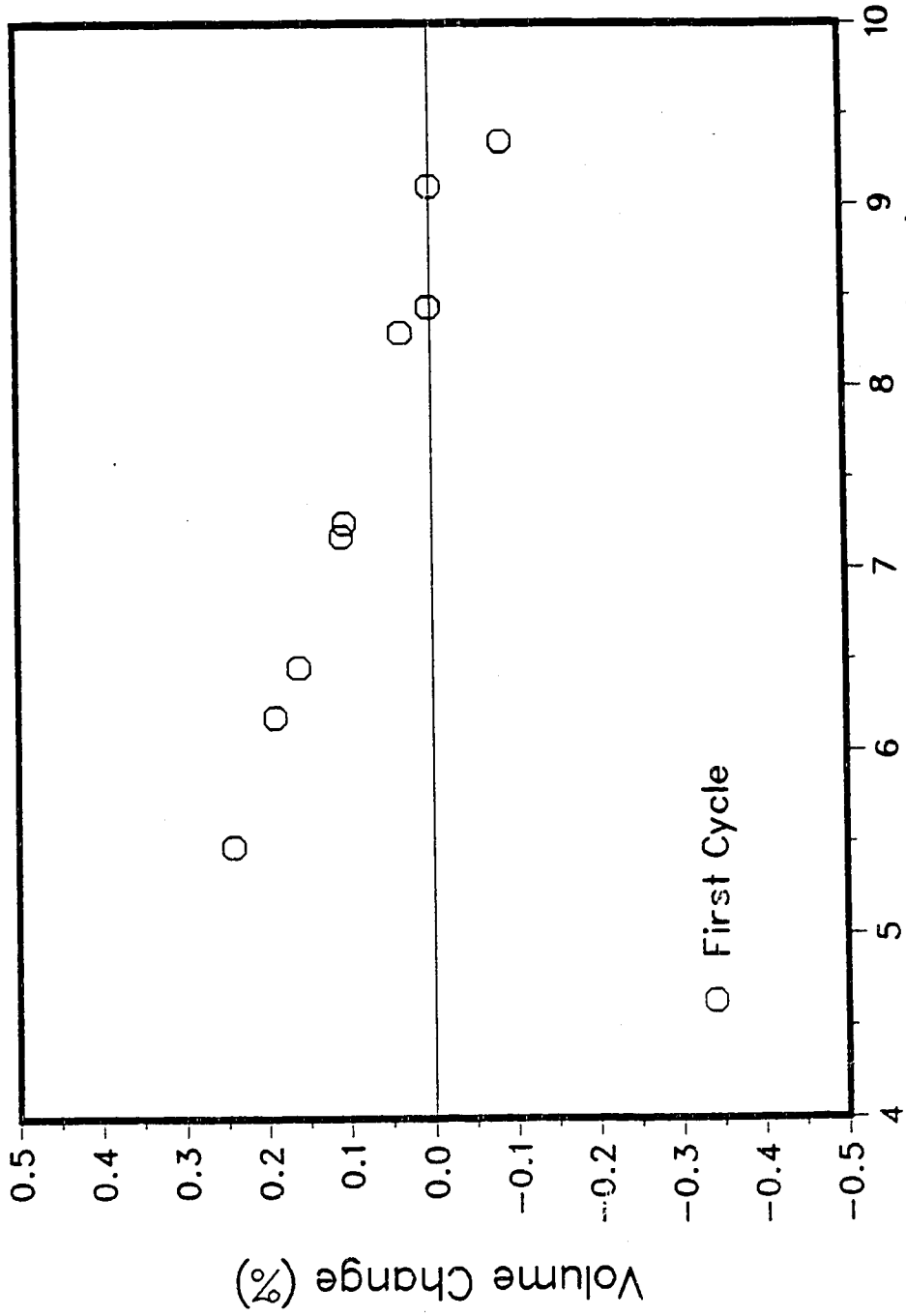

Figure E.12 Isotropic Compressibility Test CL1TOS9

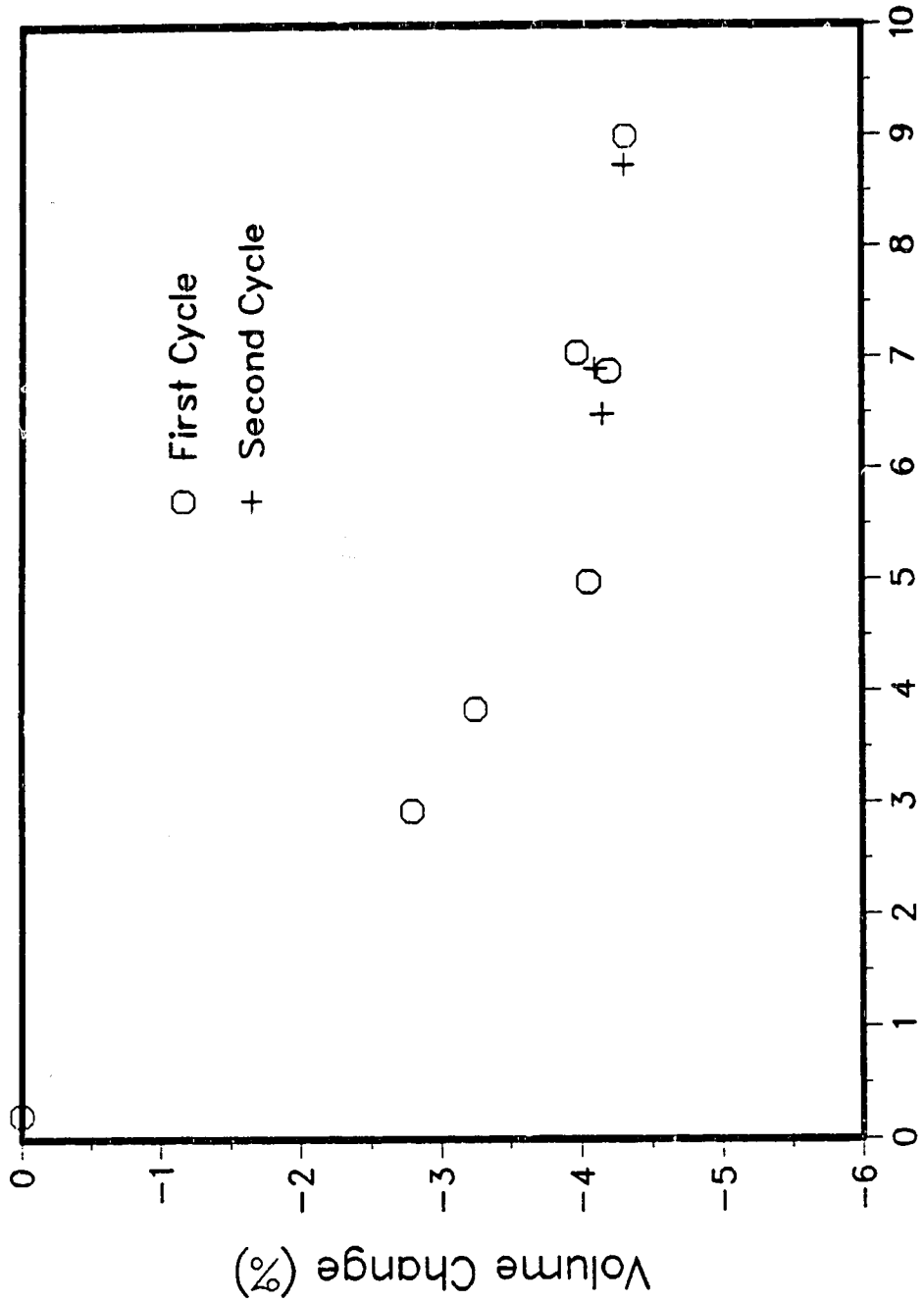

Figure E.13 Isotropic Compressibility Test CL1TOS10

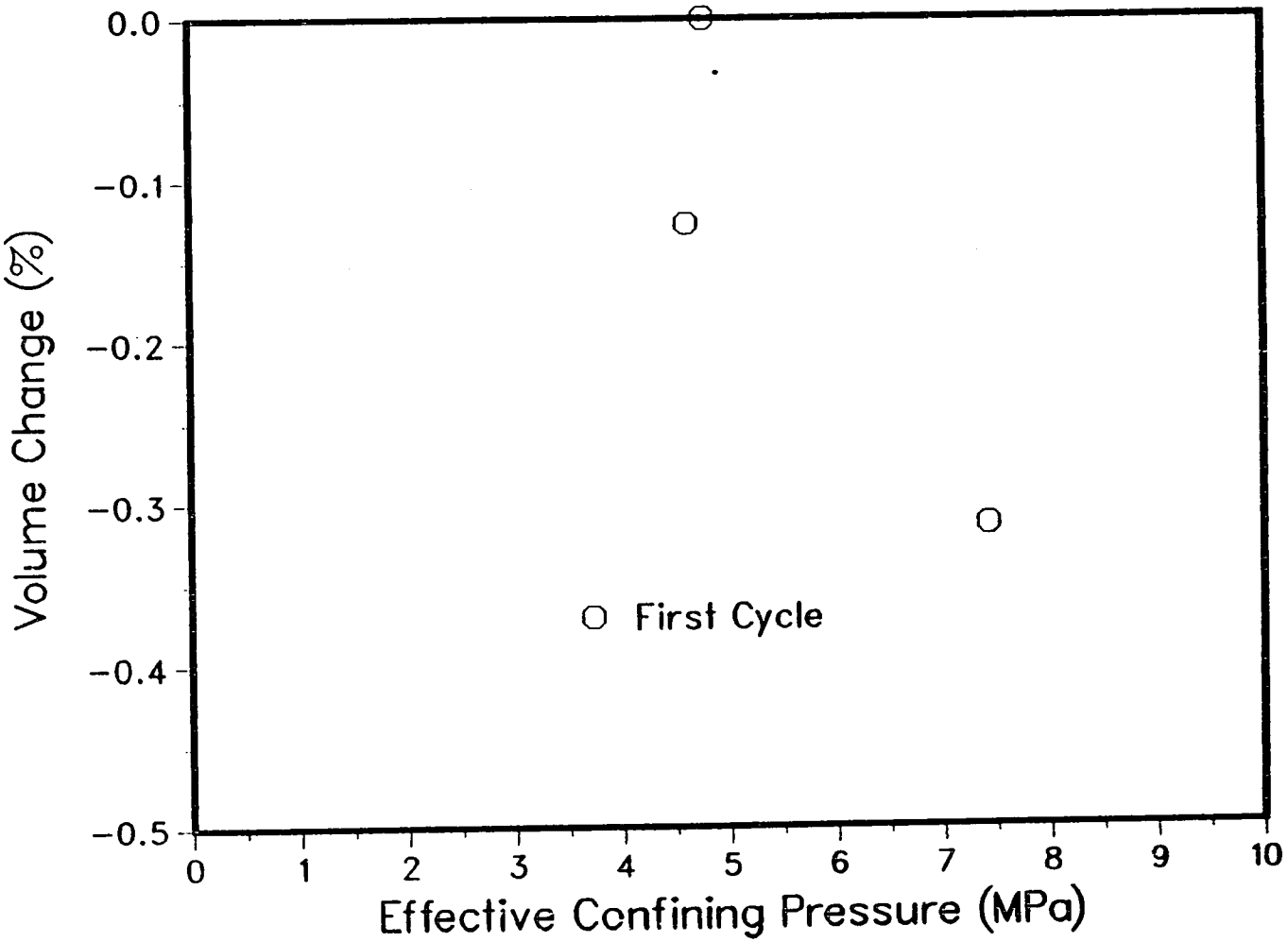

Figure E.14 Isotropic Compressibility Test CLiTOS11 125 °C

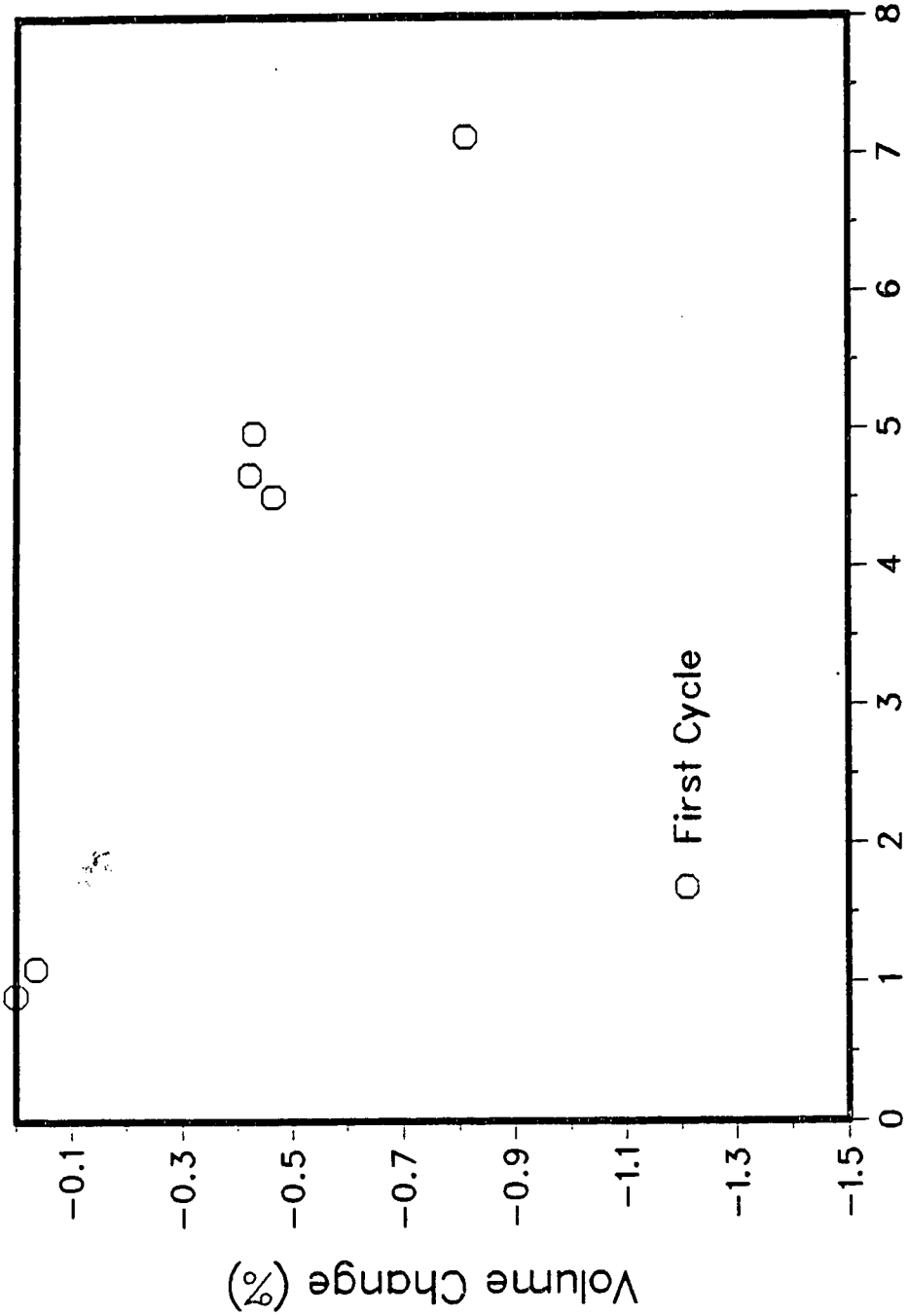

Figure E.15 Isotropic Compressibility Test CL1TOS12 225 °C

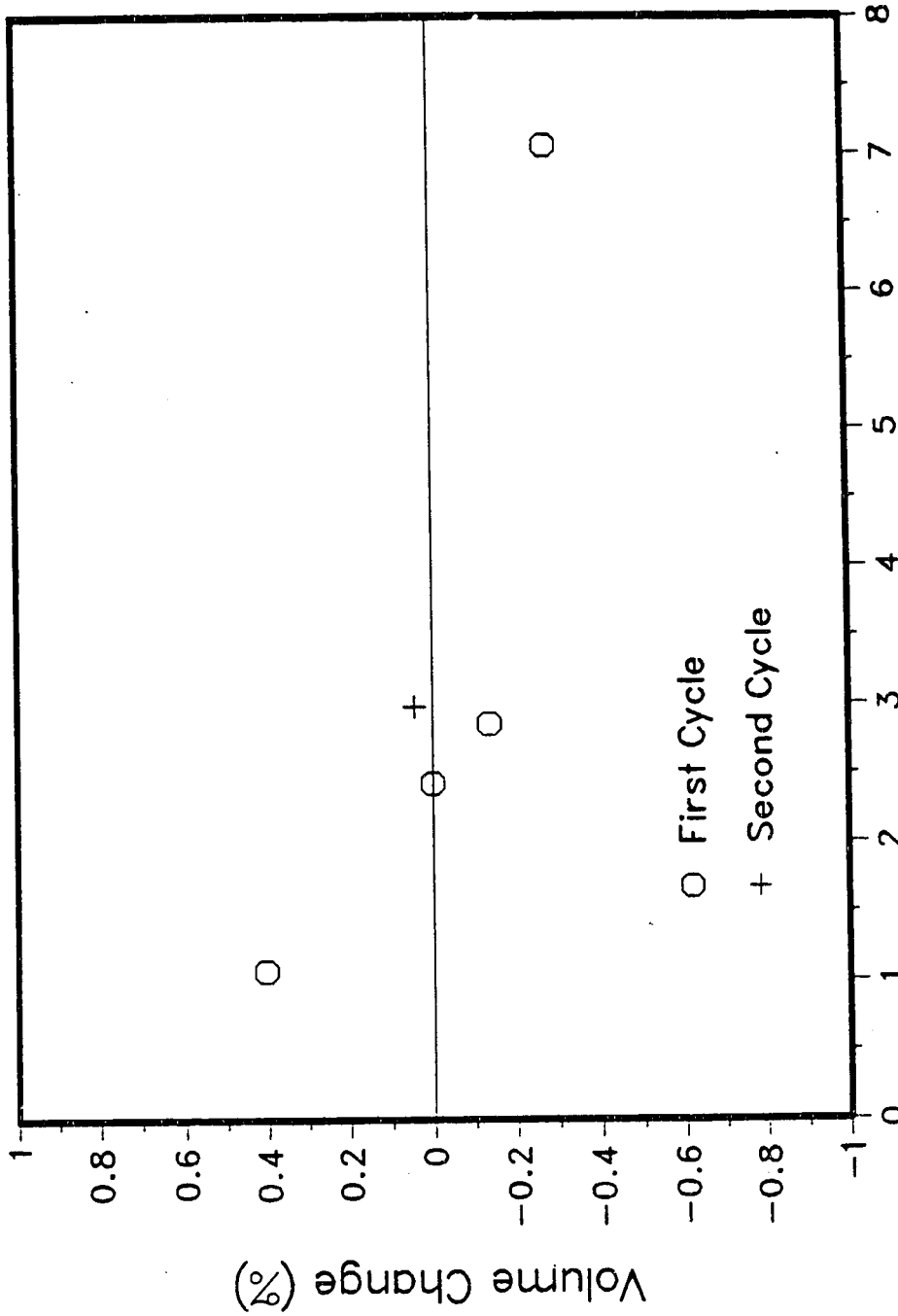

Figure E.16 Isotropic Compressibility Test CL1TOS13 225 °C

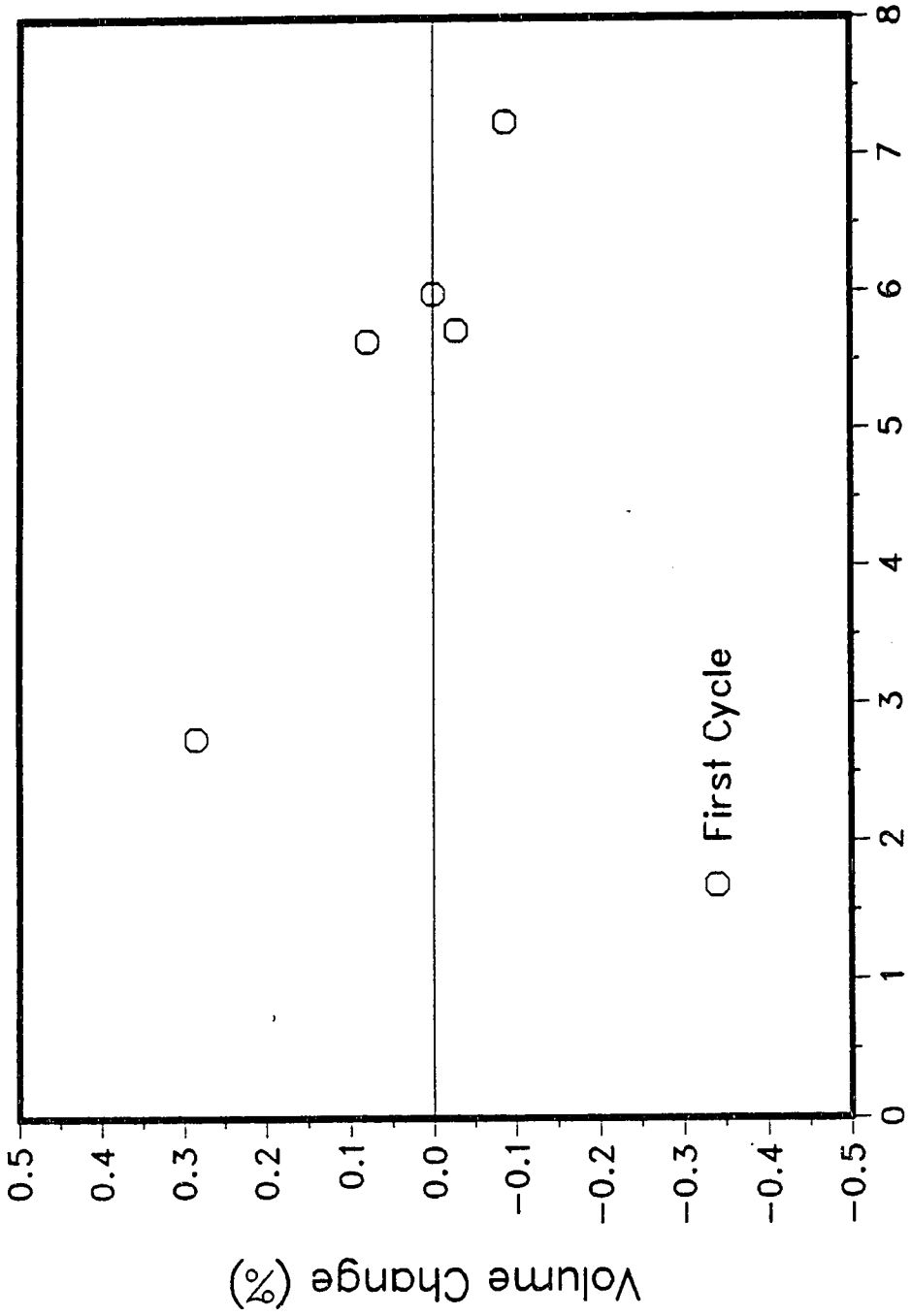

Figure E.17 Isotropic Compressibility Test CL1TOS14 225 °c

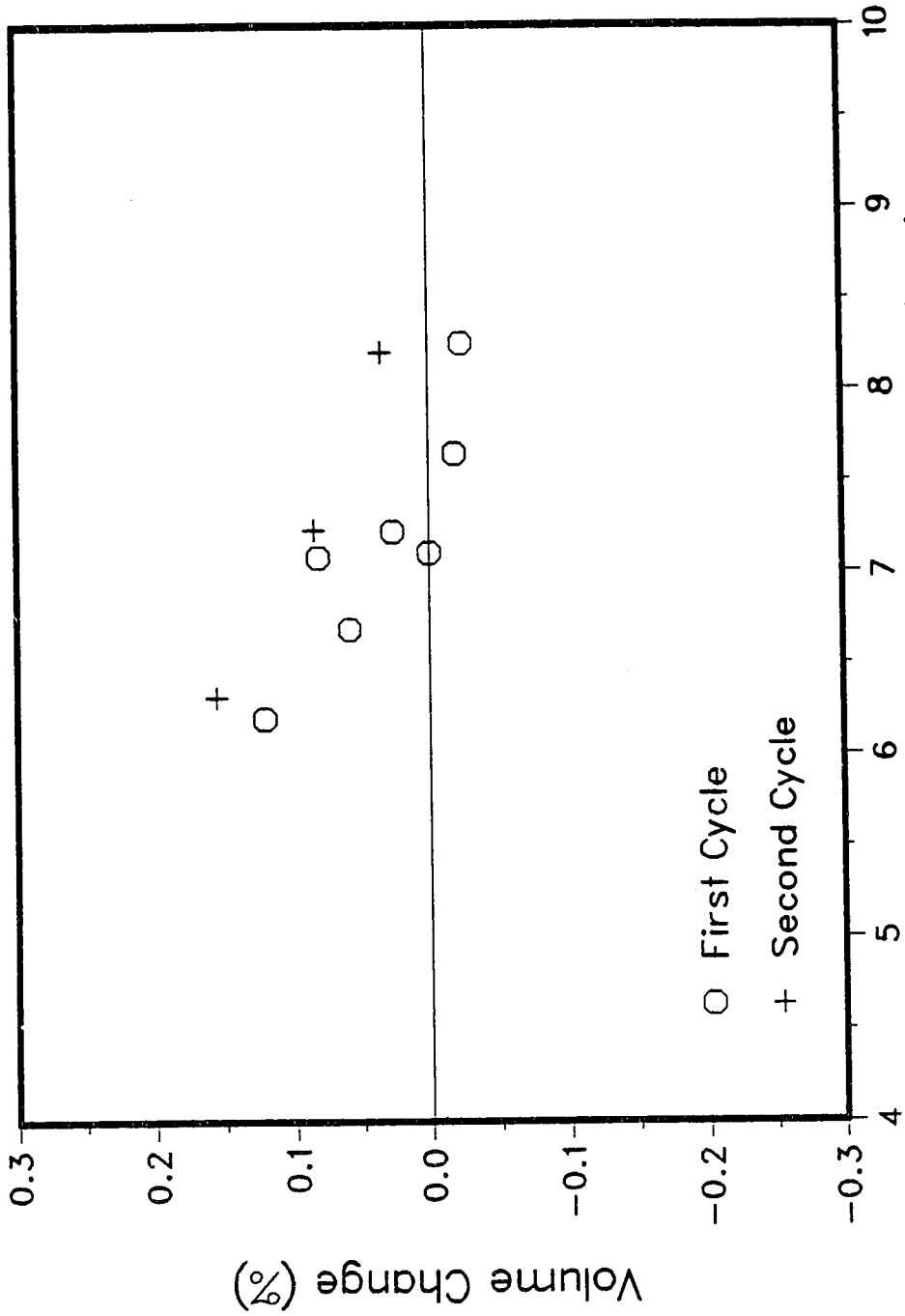

Figure E.18 Isotropic Compressibility Test CL1TOS15 225 °C

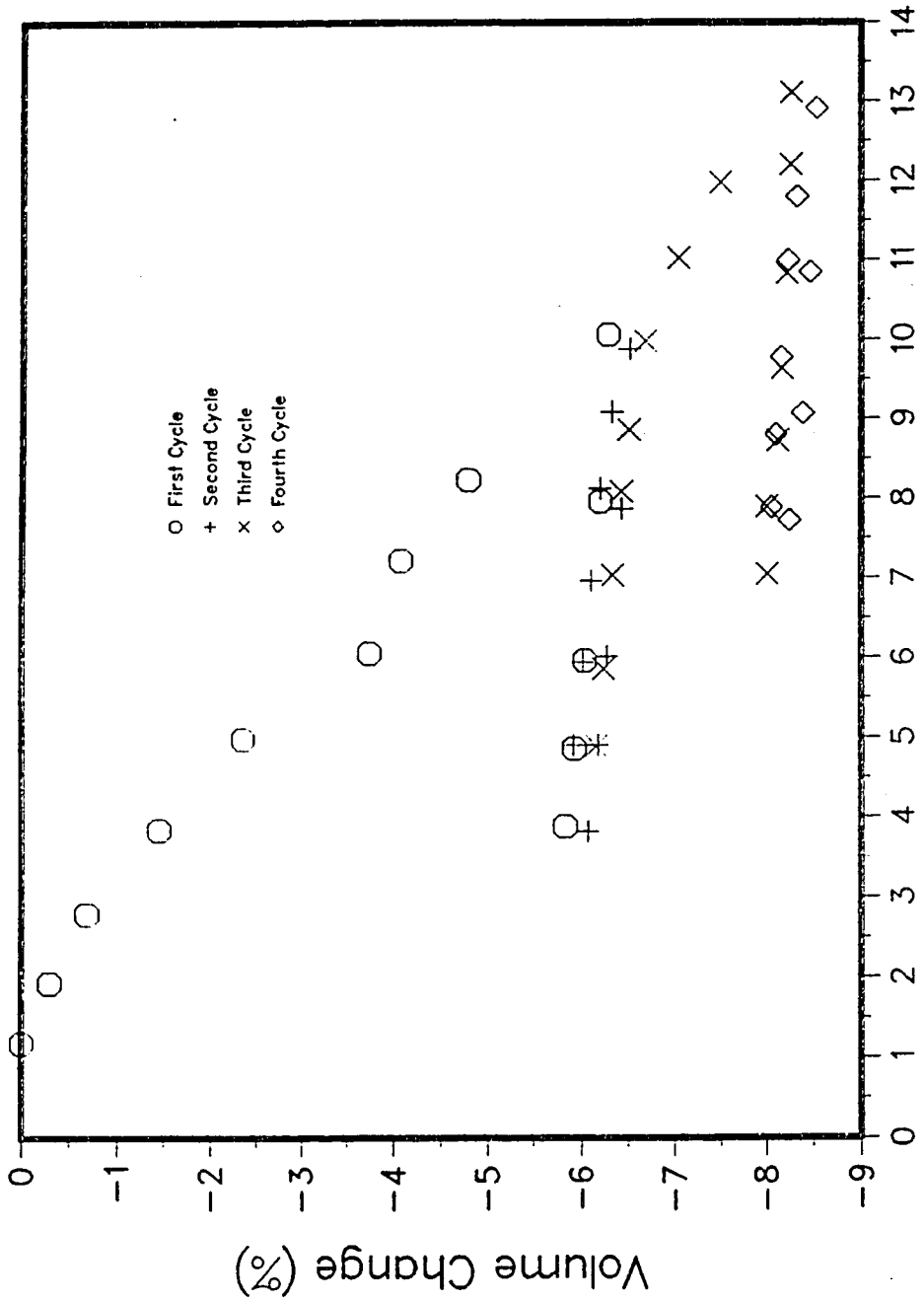

Figure E.19 One Dimensional Compressibility Test CI2COS1

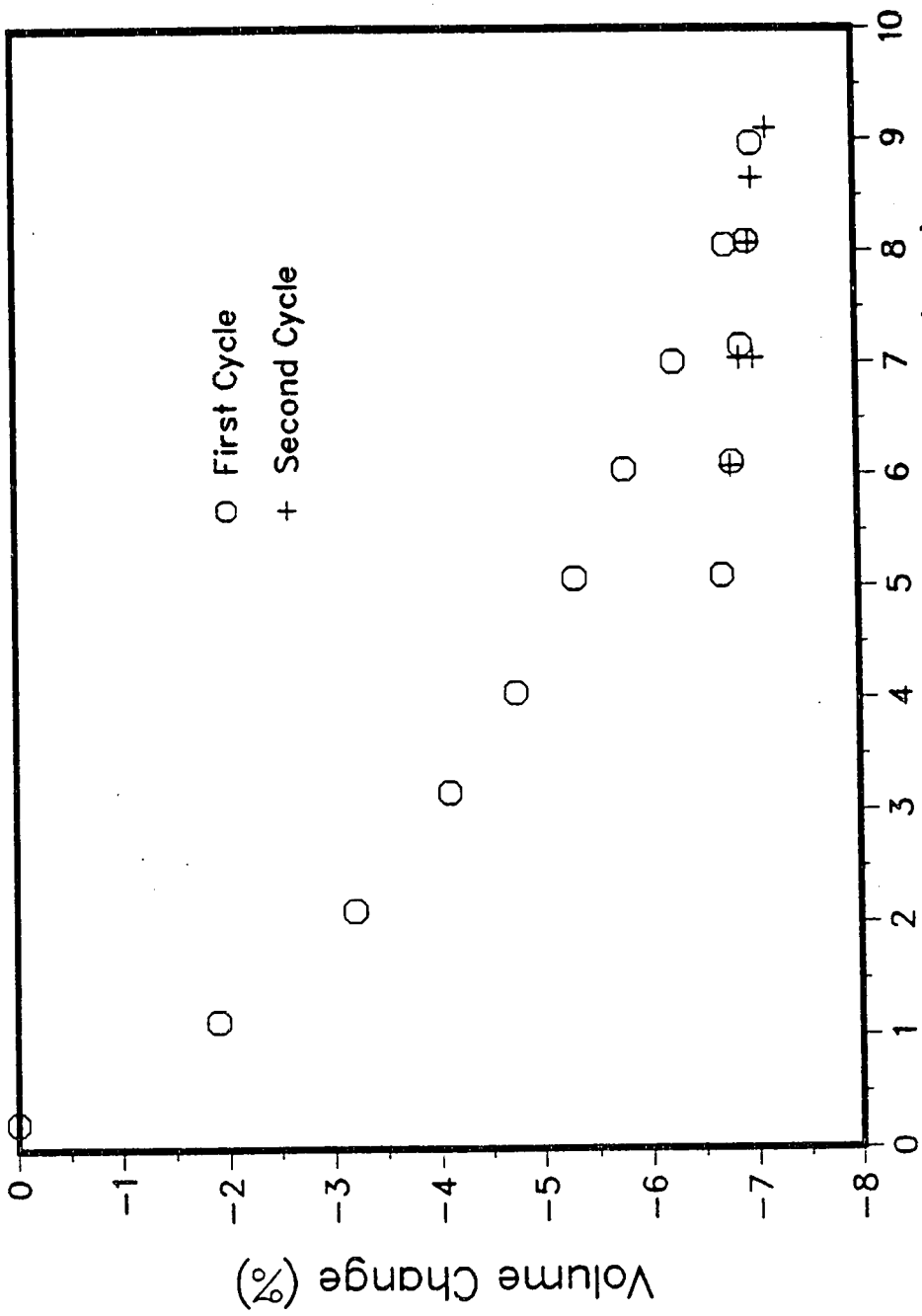

Figure E.20 Isotropic Compressibility Test CL2TOS1

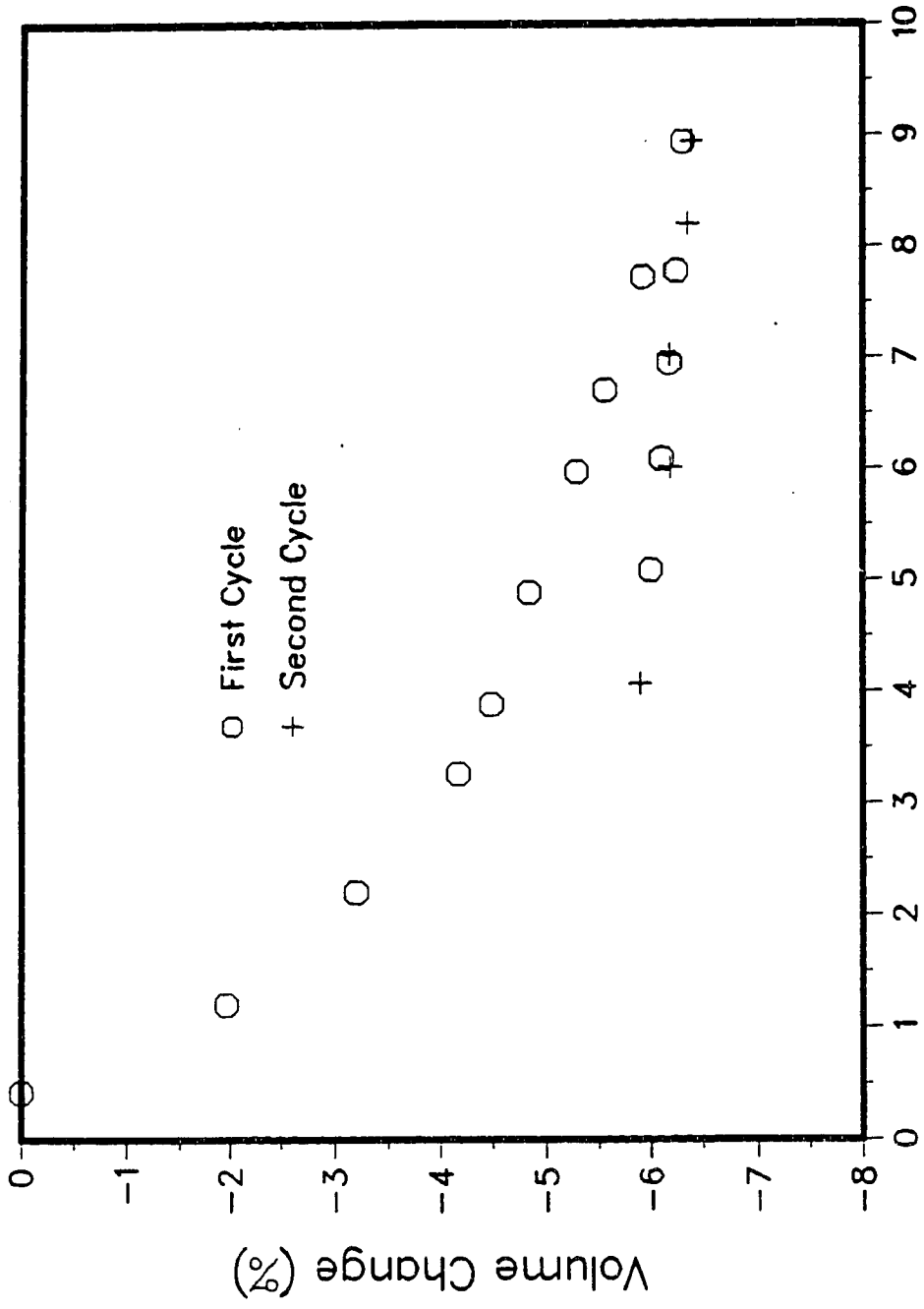

Figure E.21 Isotropic Compressibility Test CL2TOS2

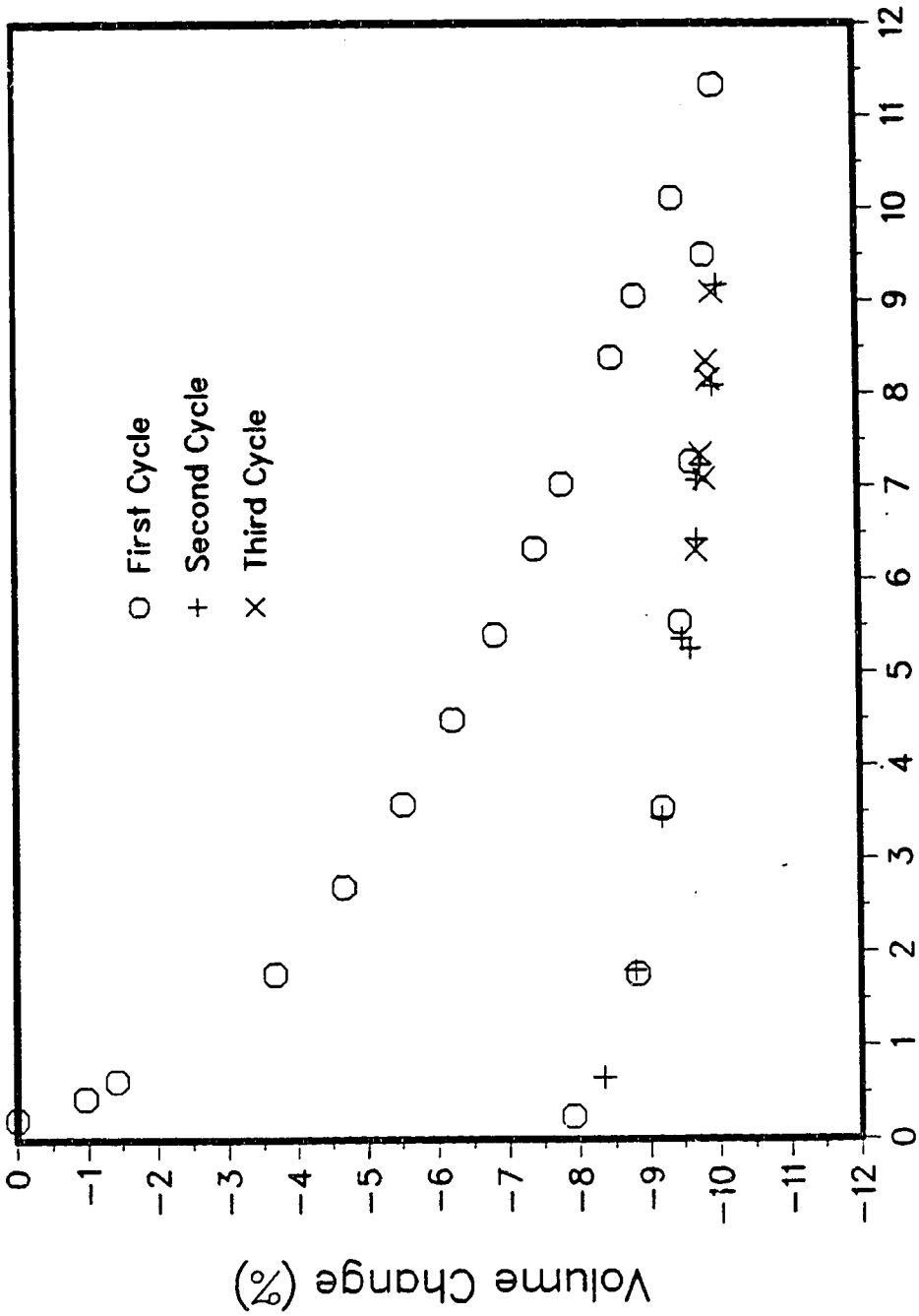

Figure E.22 Isotropic Compressibility Test CL2TOS3

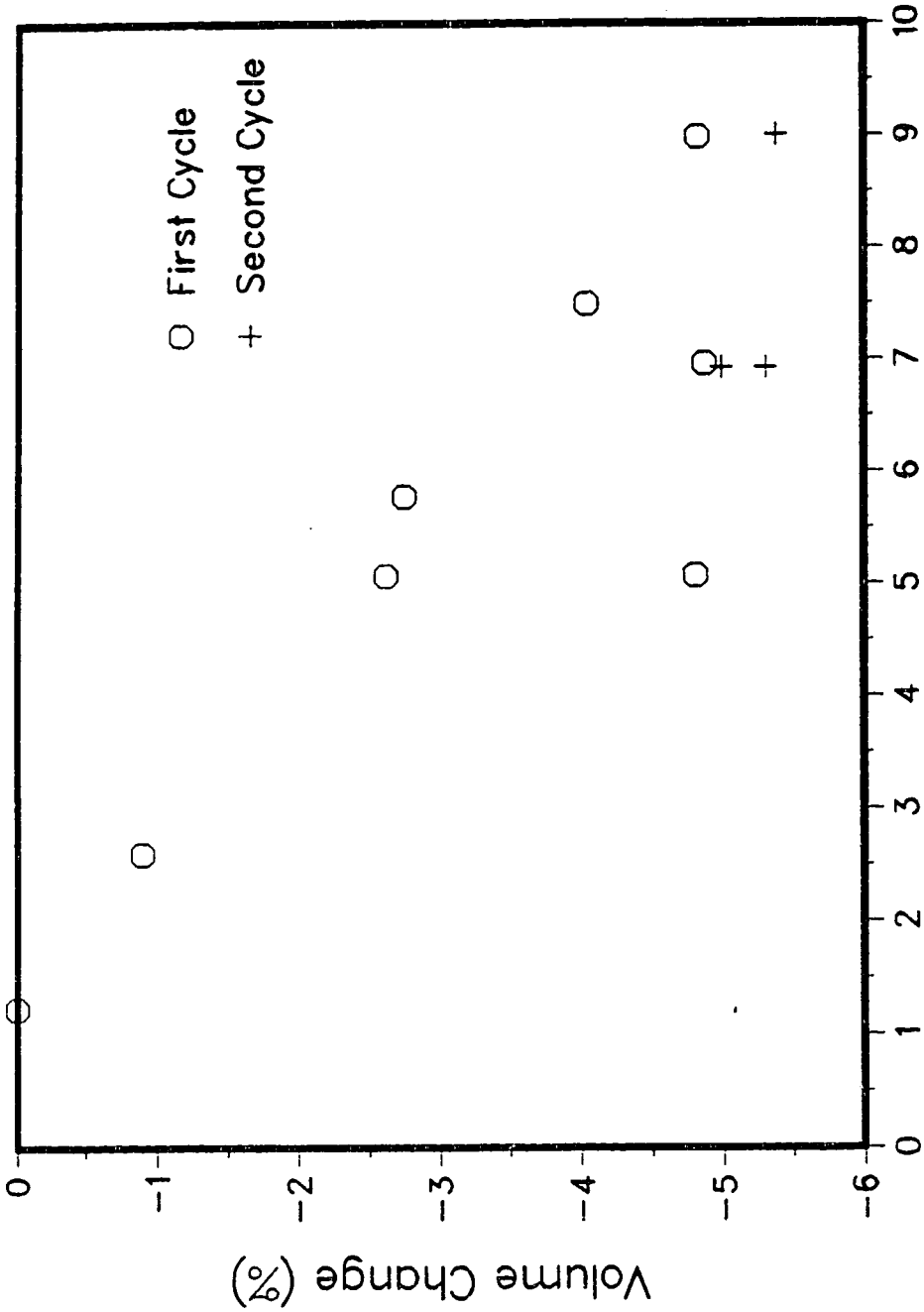

Figure E.23 Isotropic Compressibility Test CL2TOS4 225 °C

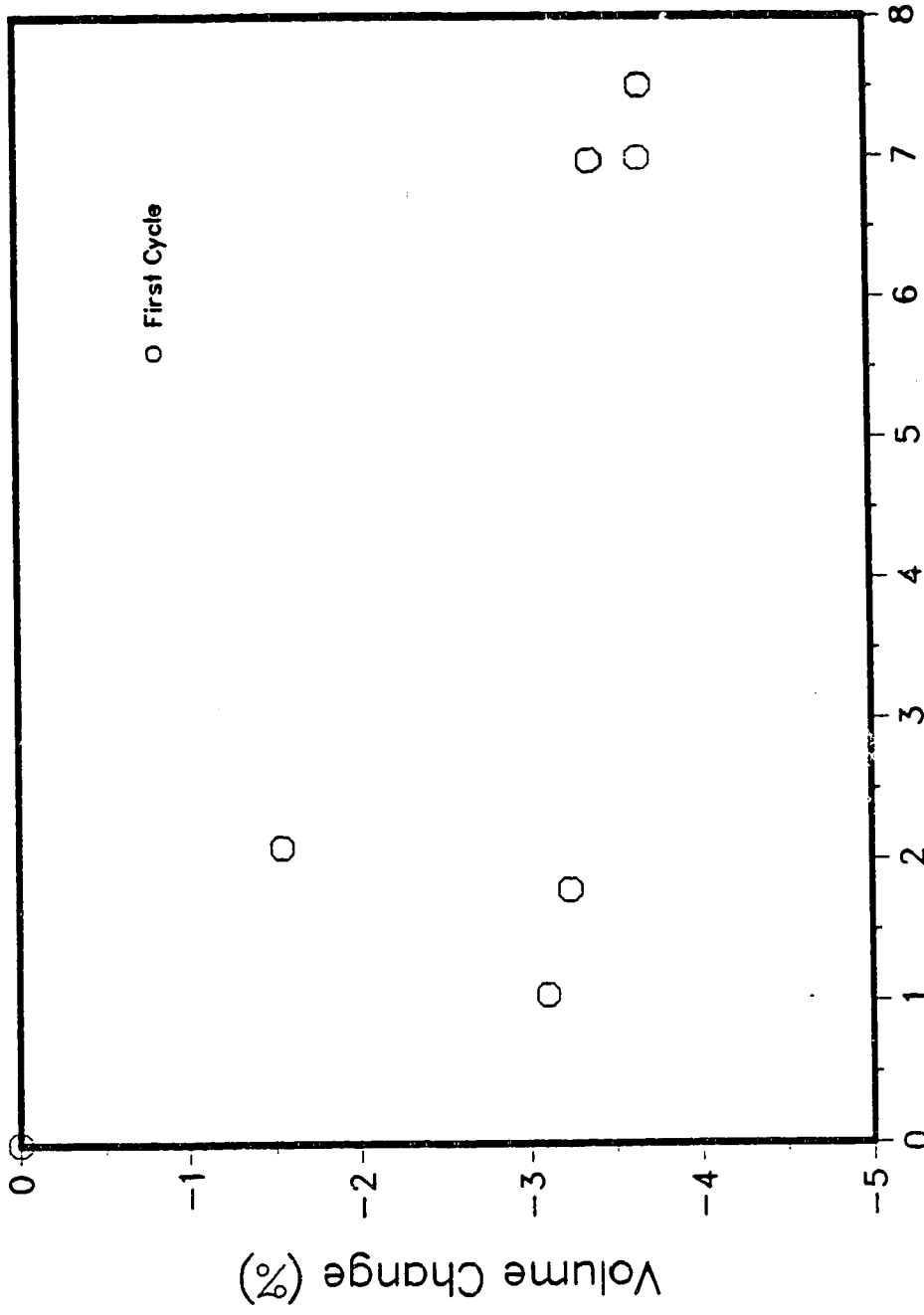

Figure E.24 One Dimensional Compressibility Test CL3C0S1

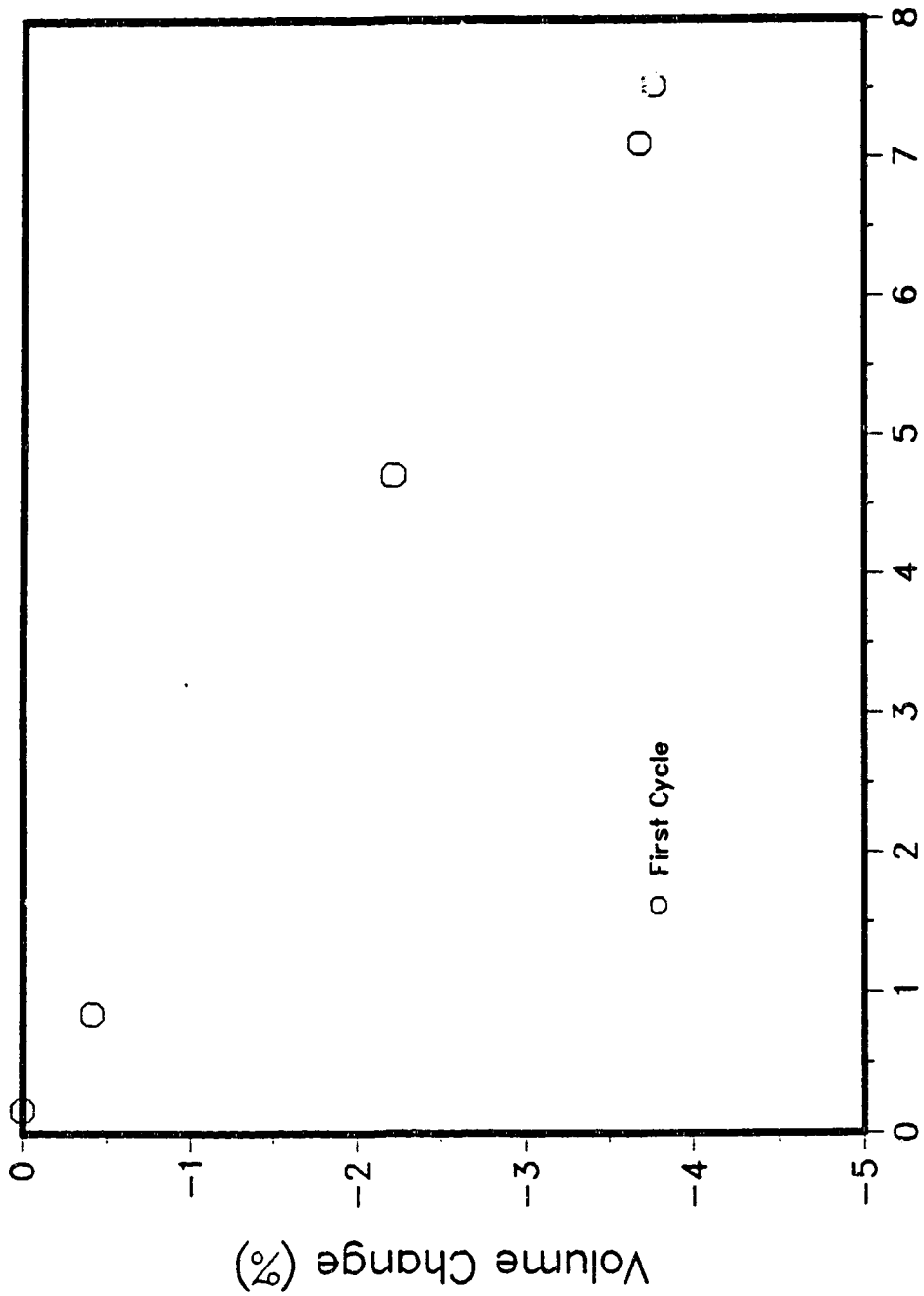

Figure E.25 One Dimensional Compressibility Test CL3C0S2

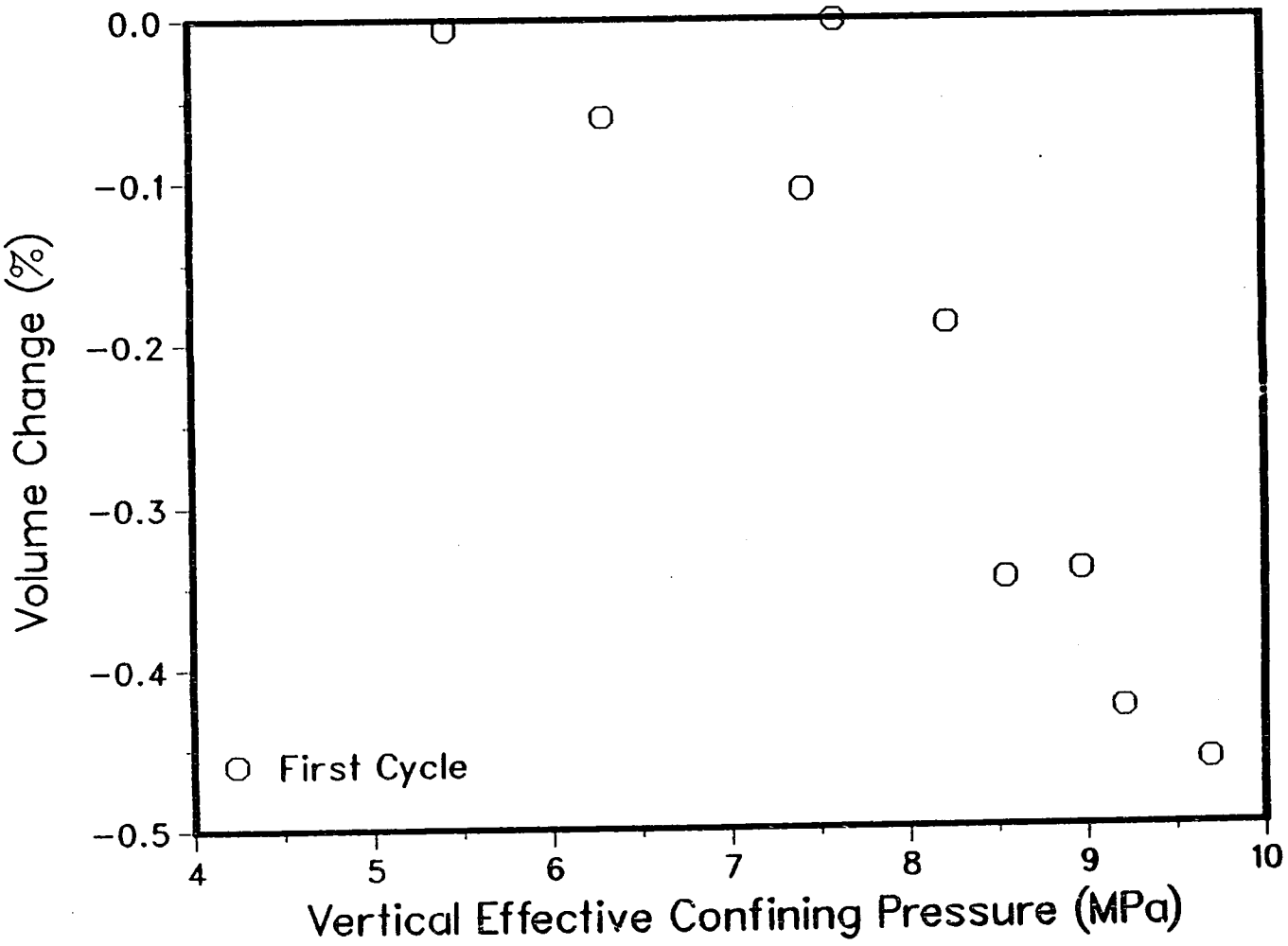

Figure E.26 One Dimensional Compressibility Test CL3COS2 225 °C

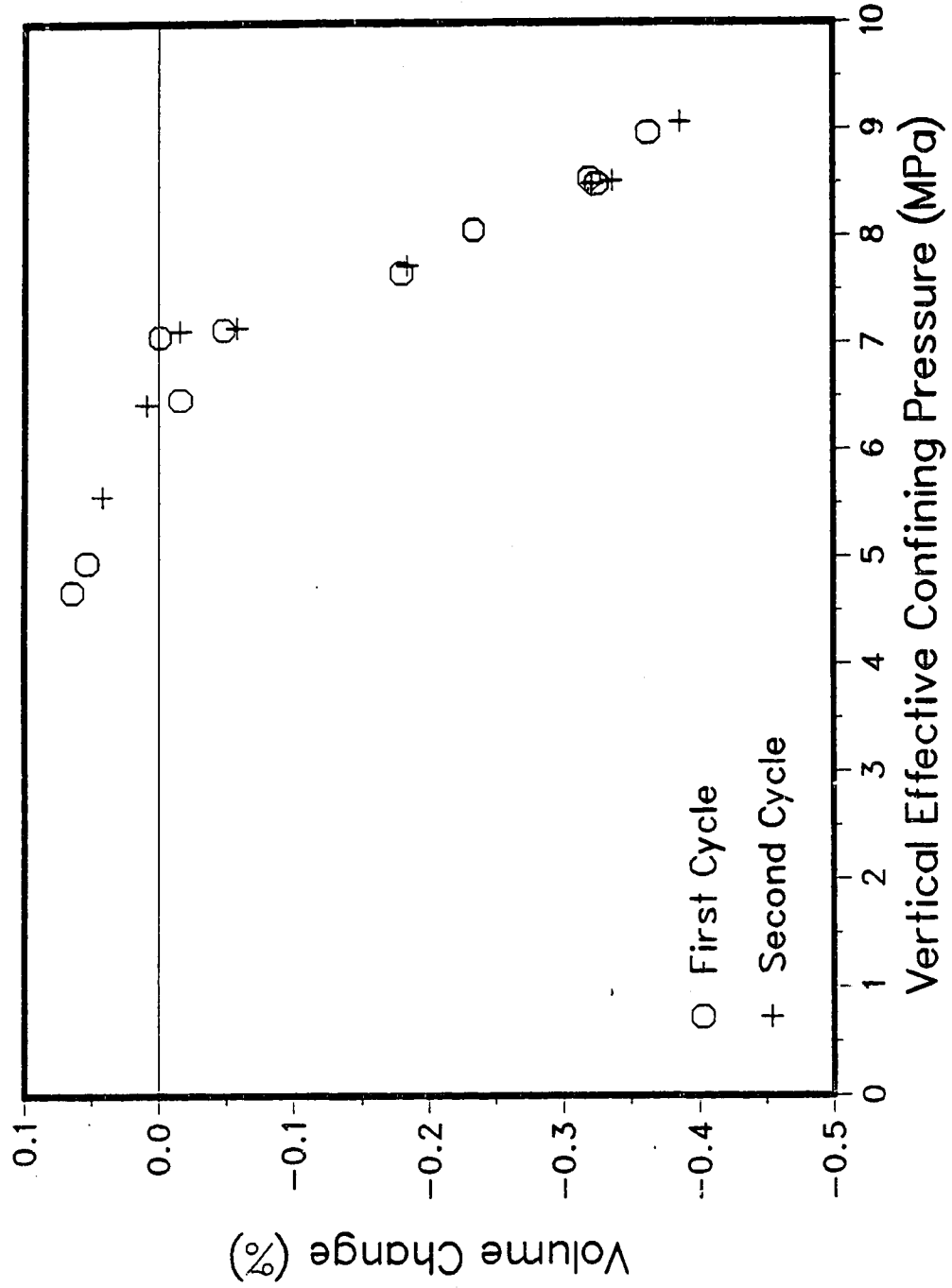

Figure E.27 One Dimensional Compressibility Test CL3COS3 225 °C

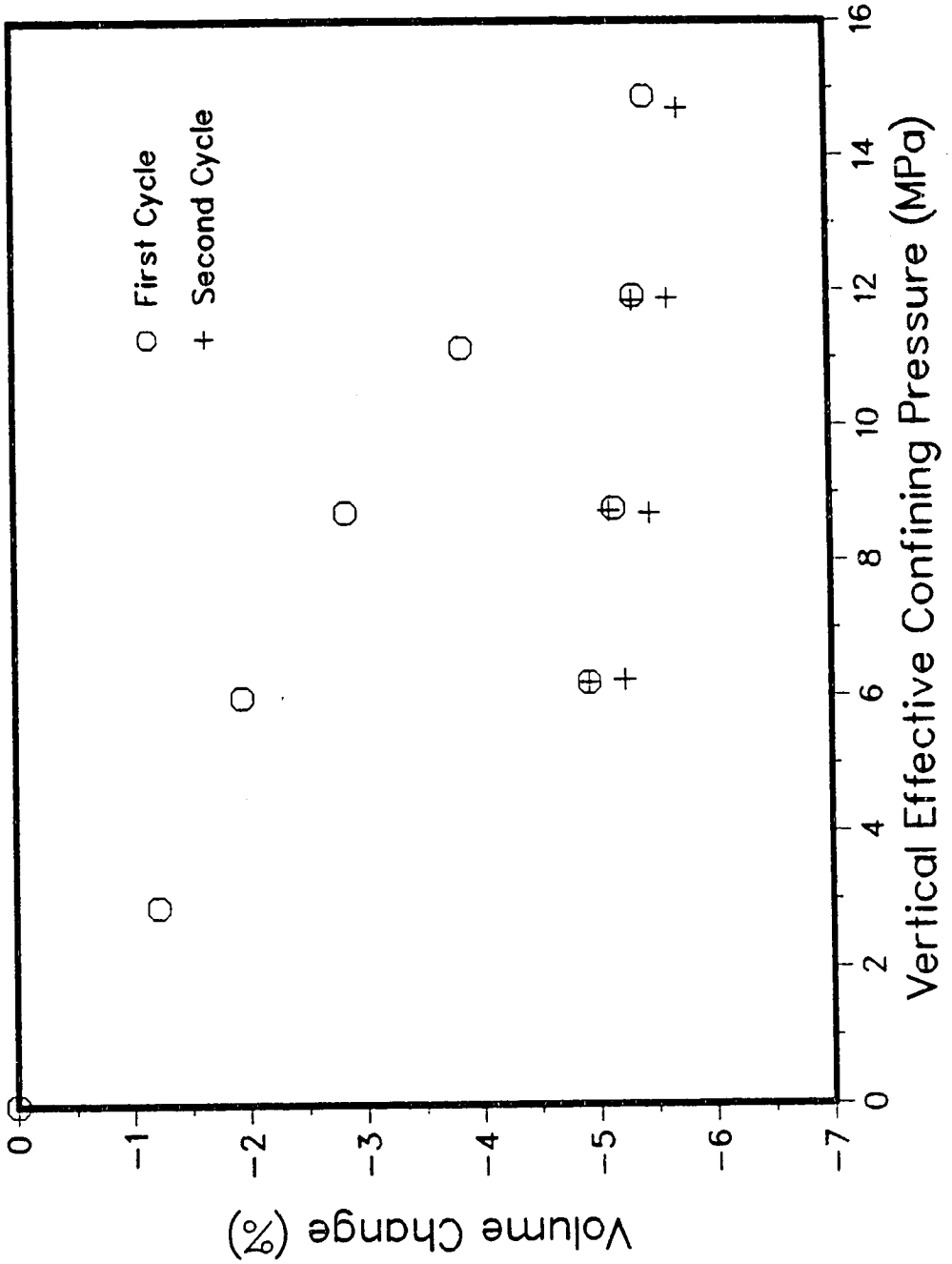

Figure E.28 One Dimensional Compressibility Test CL3C0S4

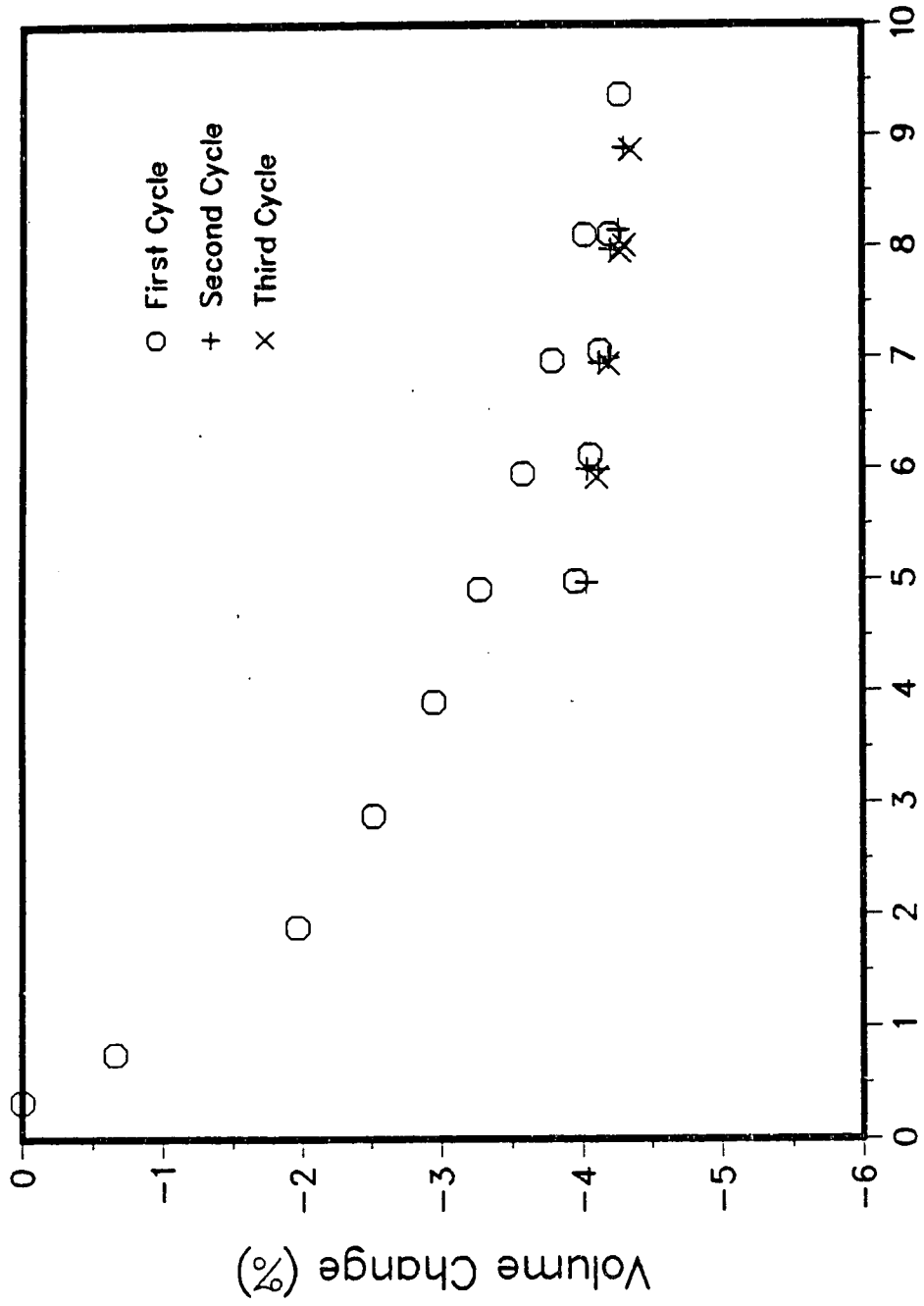

Figure E.29 Isotropic Compressibility Test CL3TOS1

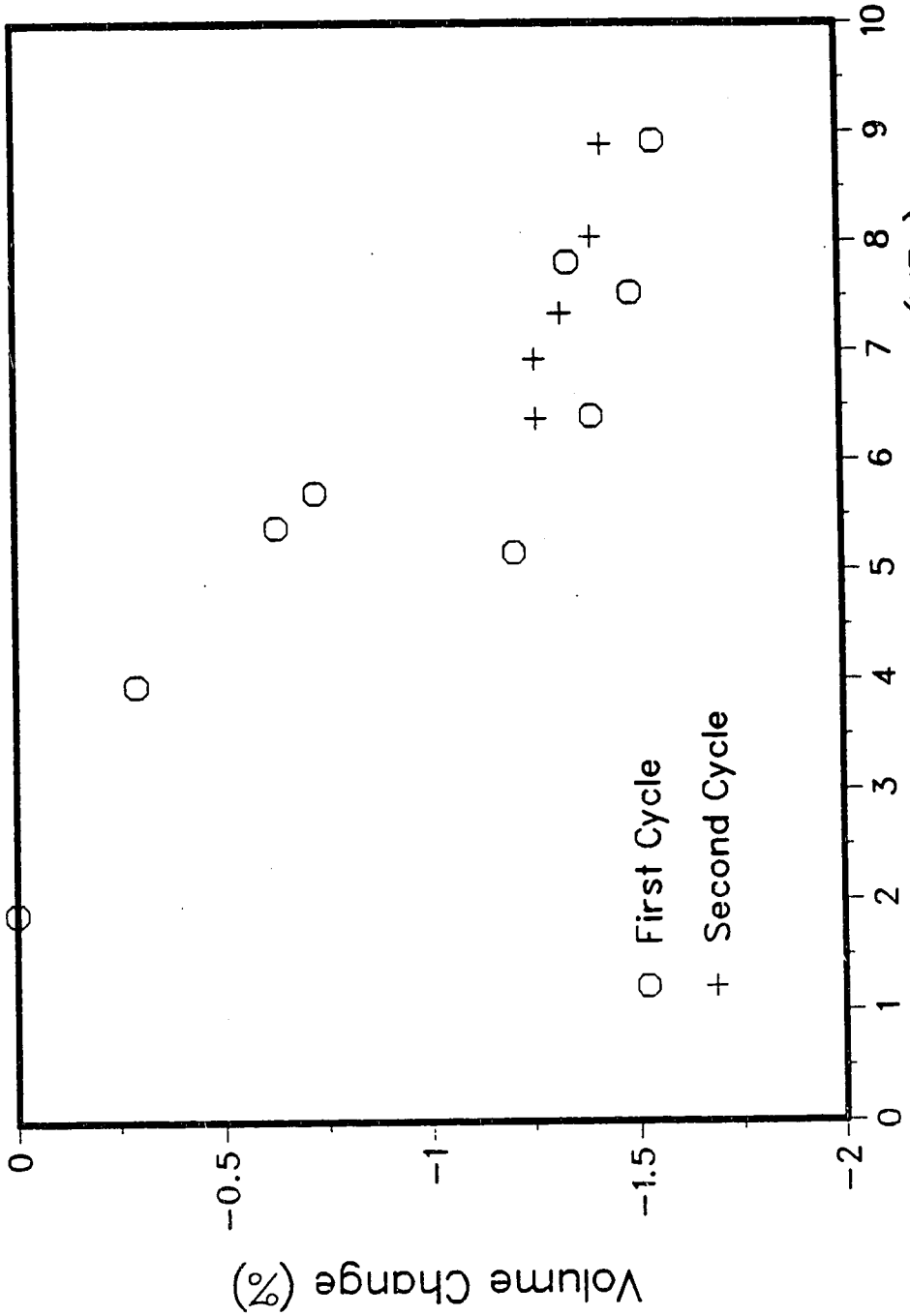

Figure E.30 Isotropic Compressibility Test CL3TOS2 225 °C

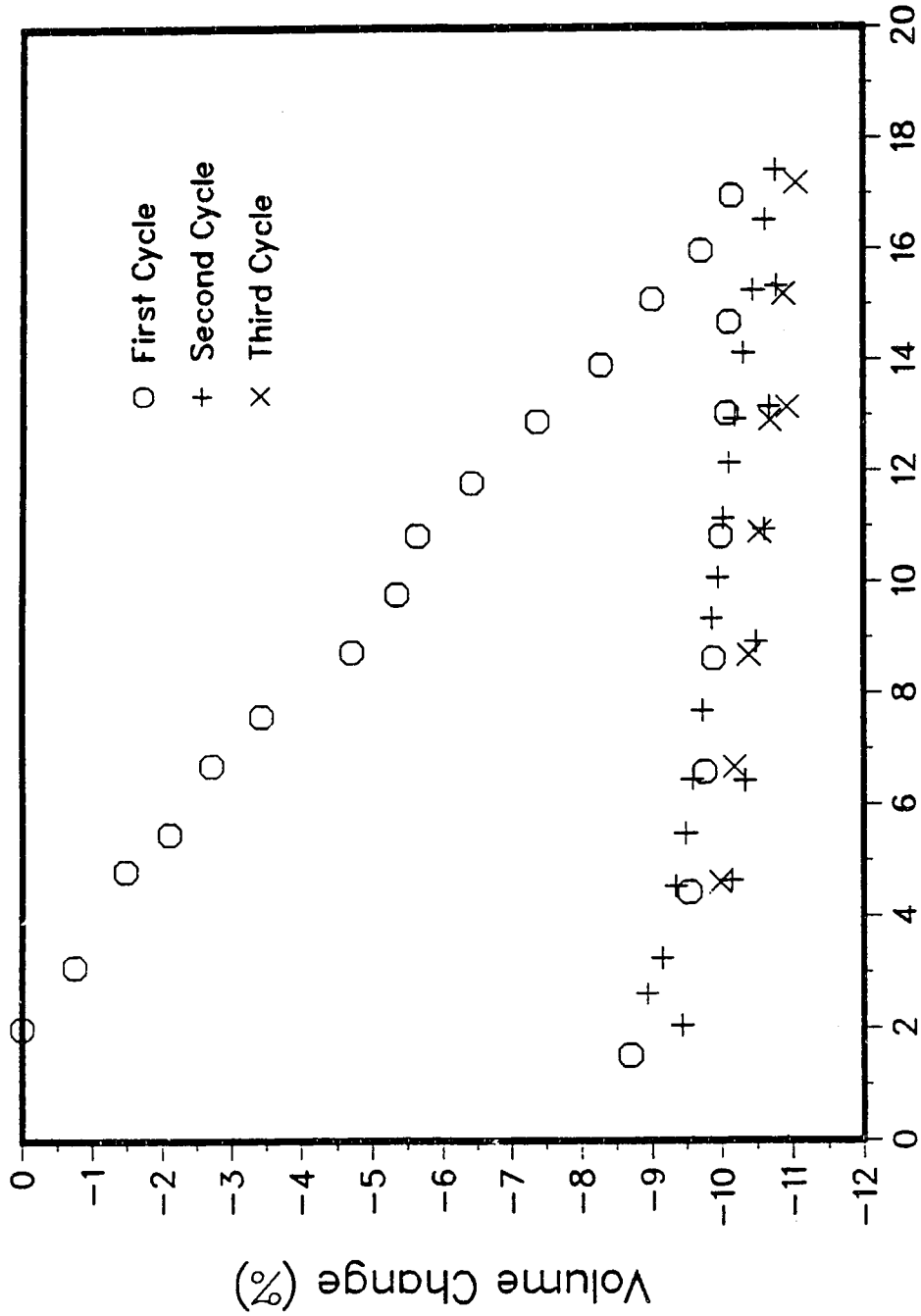

Figure E.31 One Dimensional Compressibility Test CL4COS1 250 °C

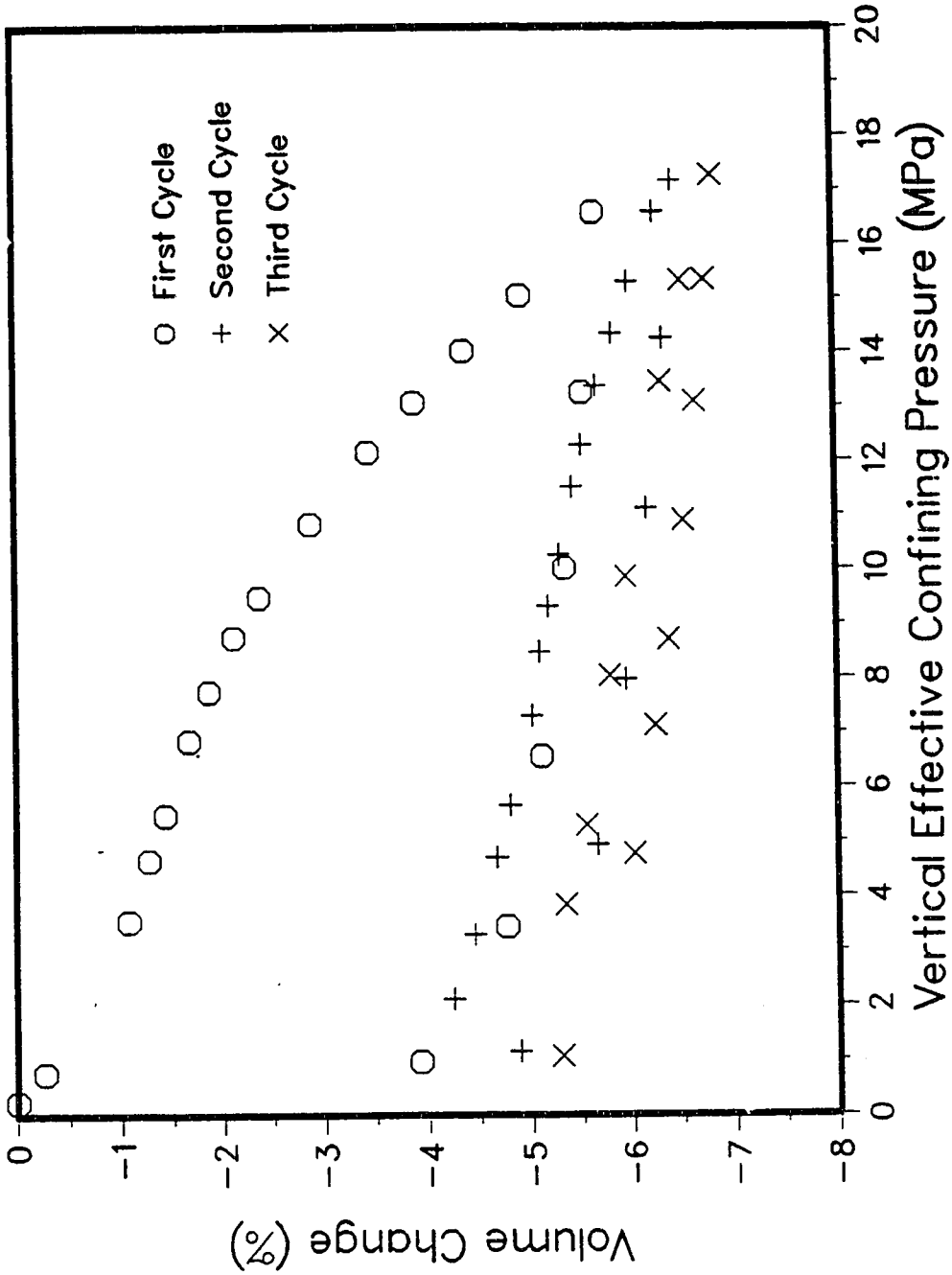

Figure E.32 One Dimensional Compressibility Test CL4CO52

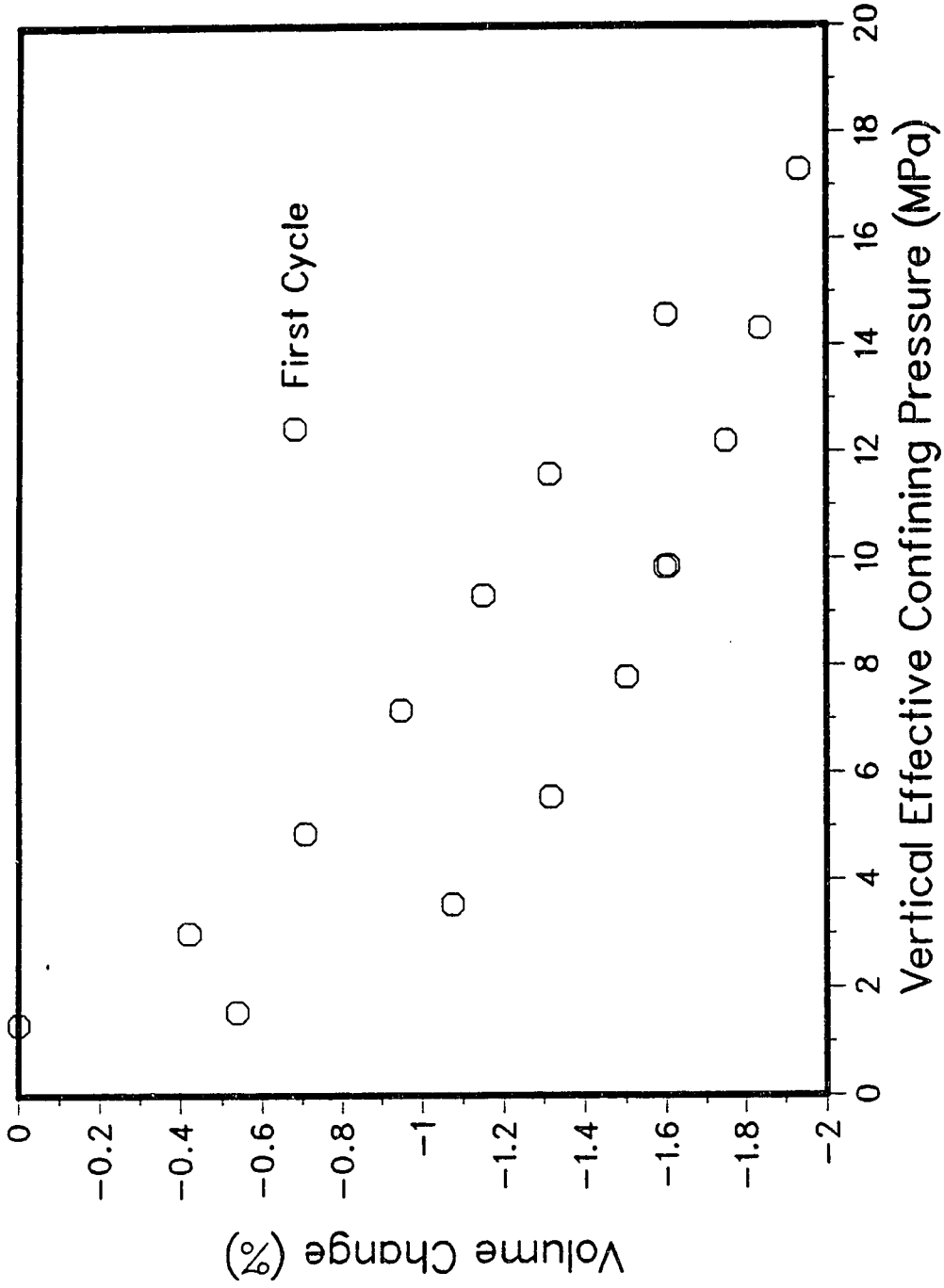

Figure E.33 One Dimensional Compressibility Test C14CO52 100 °C

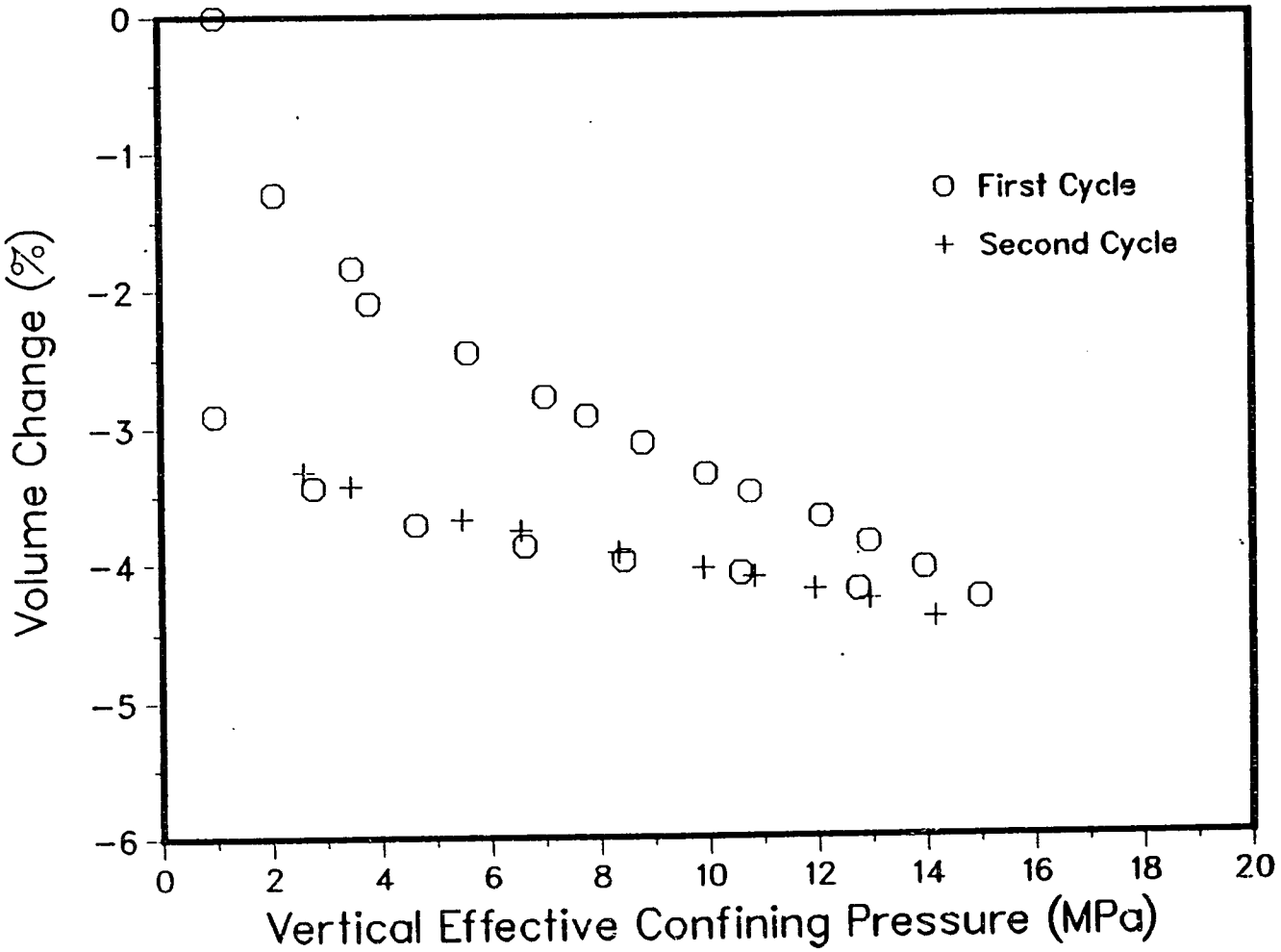

Figure E.34 One Dimensional Compressibility Test CL4COS2 200 °C

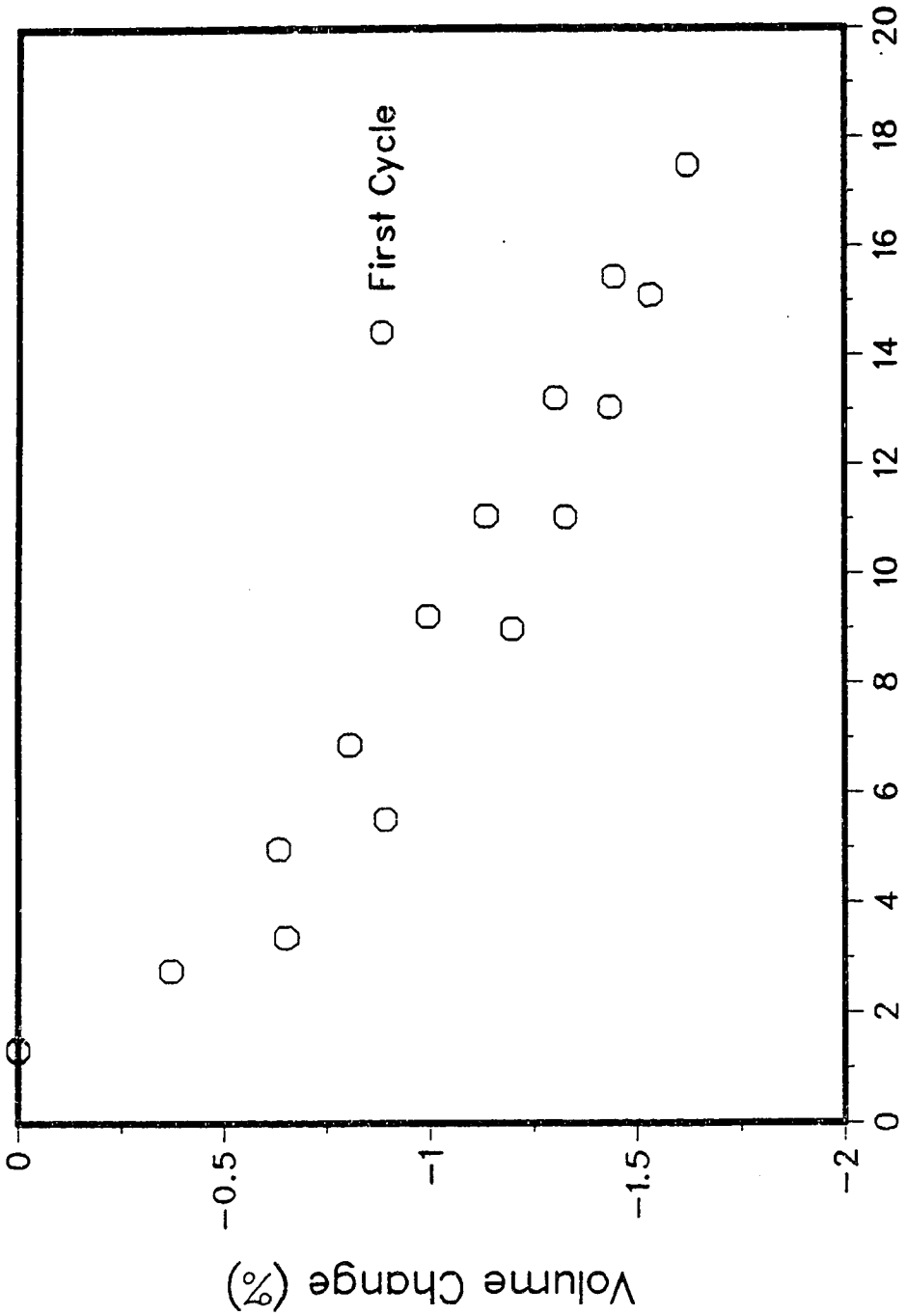

Figure E.35 One Dimensional Compressibility Test CL4COS2 200 °C

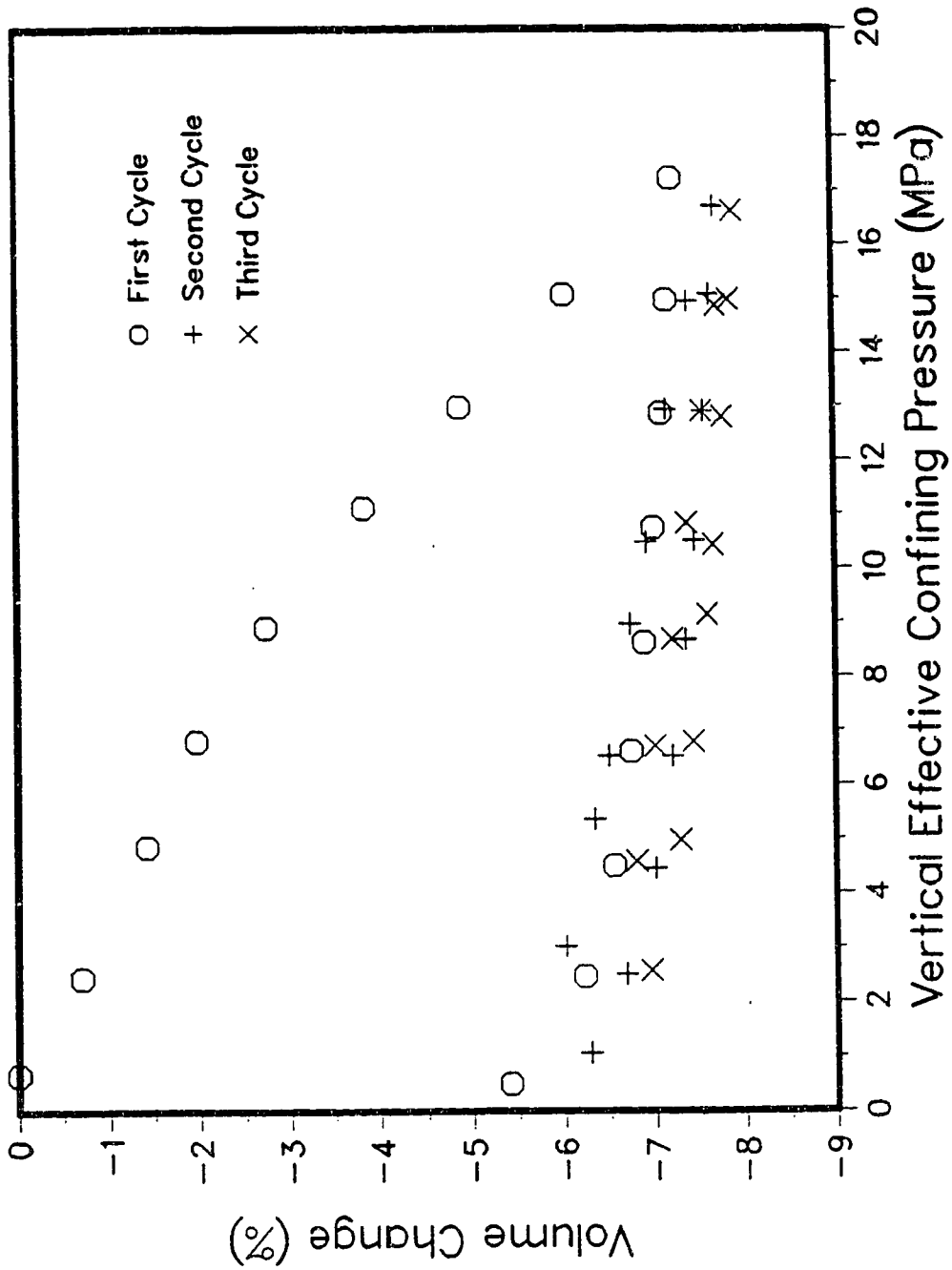

Figure E.36 One Dimensional Compressibility Test CL4COS3 200 °C

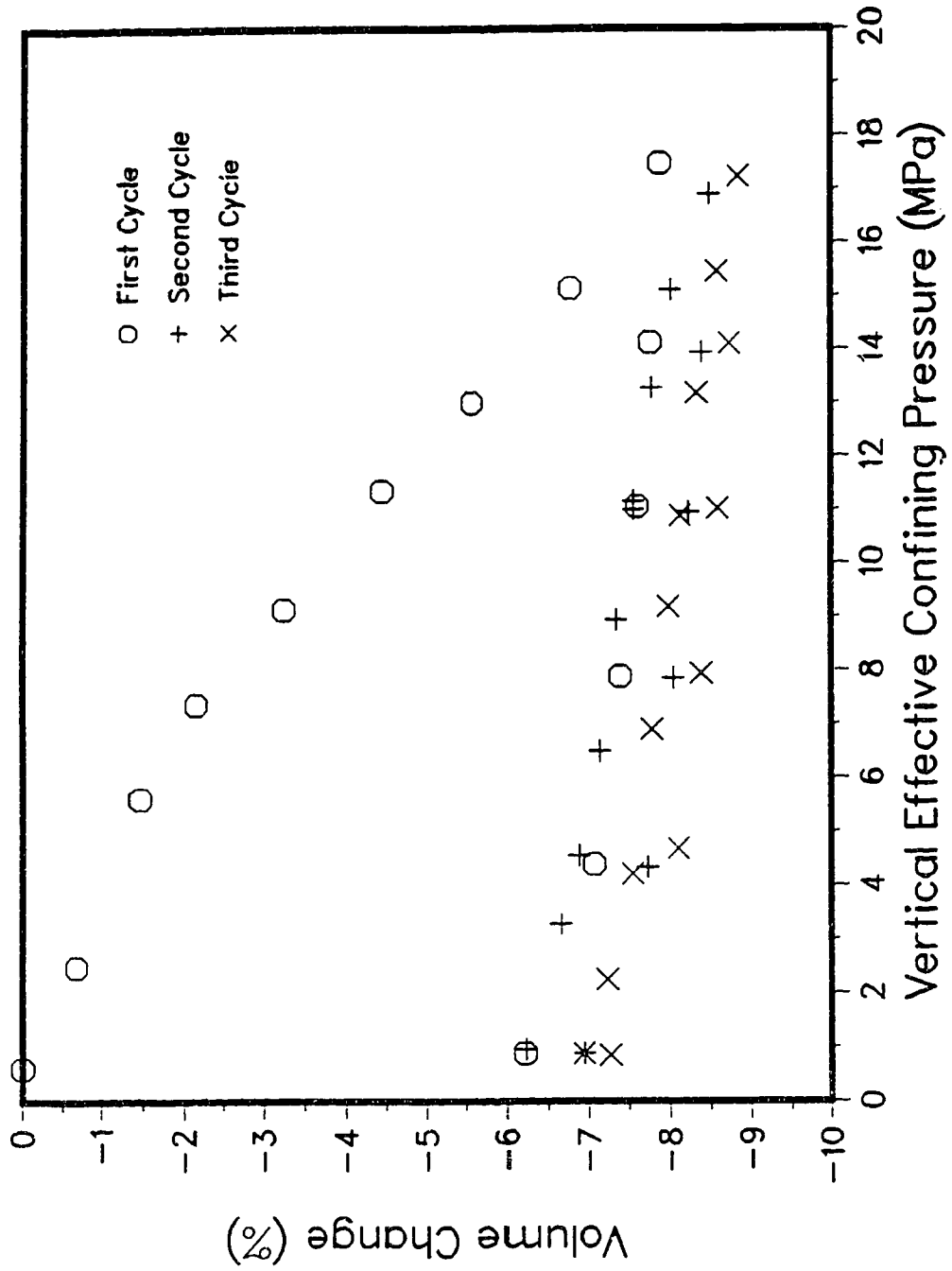

Figure E.37 One Dimensional Compressibility Test CL4COS4

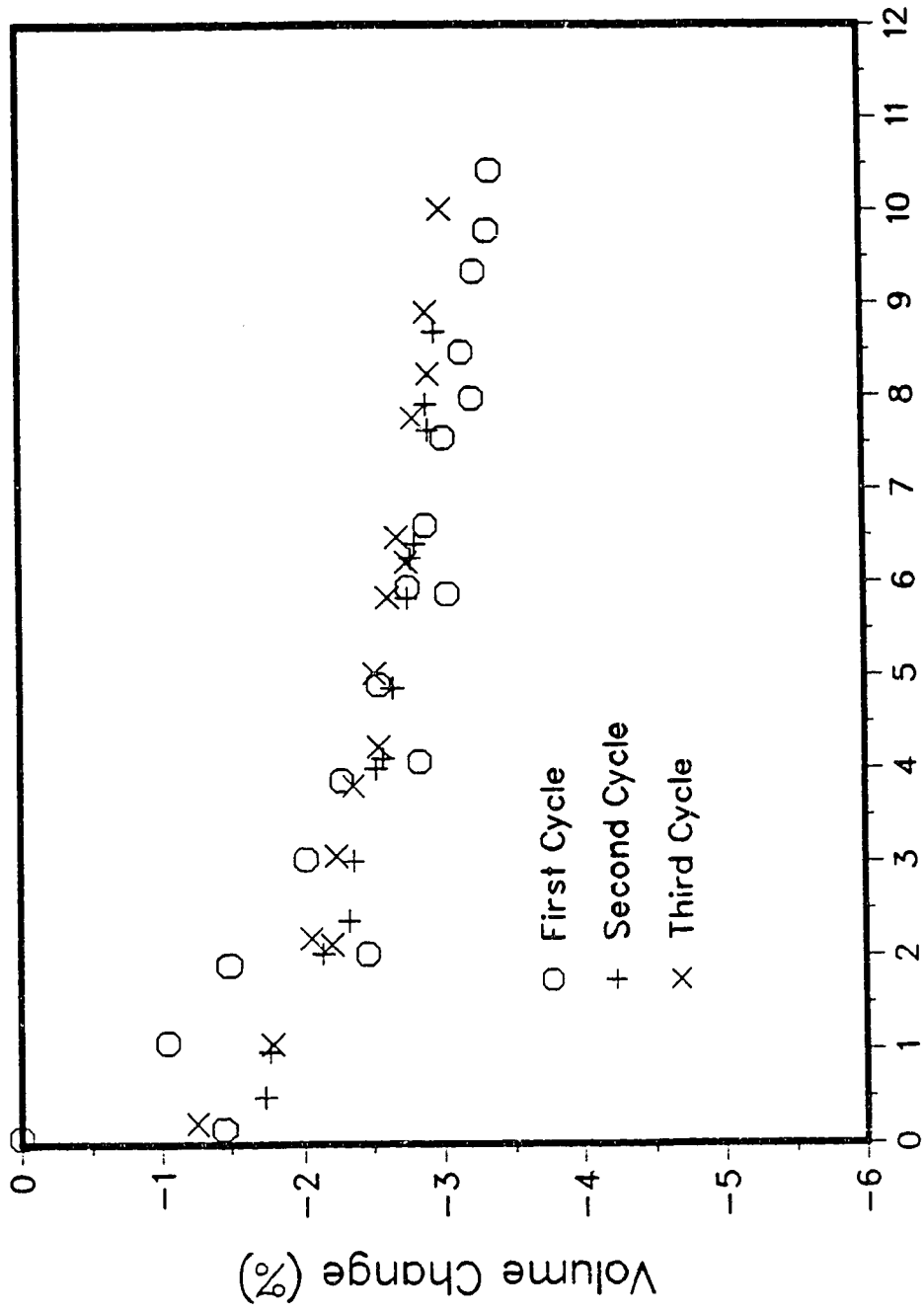

Figure E.38 Isotropic Compressibility Test CL4TOS1

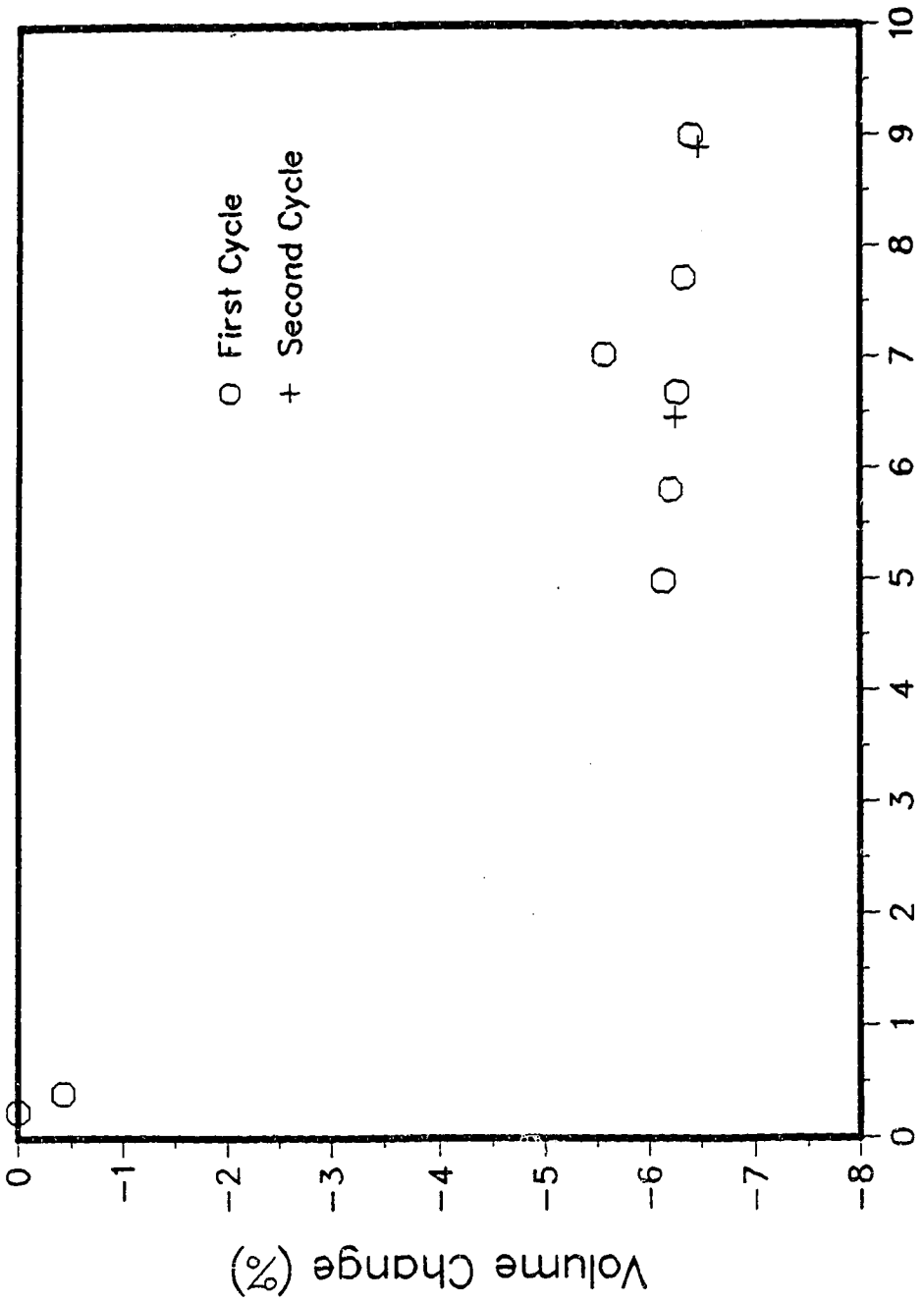

Figure E.39 Isotropic Compressibility Test CL4TOS2

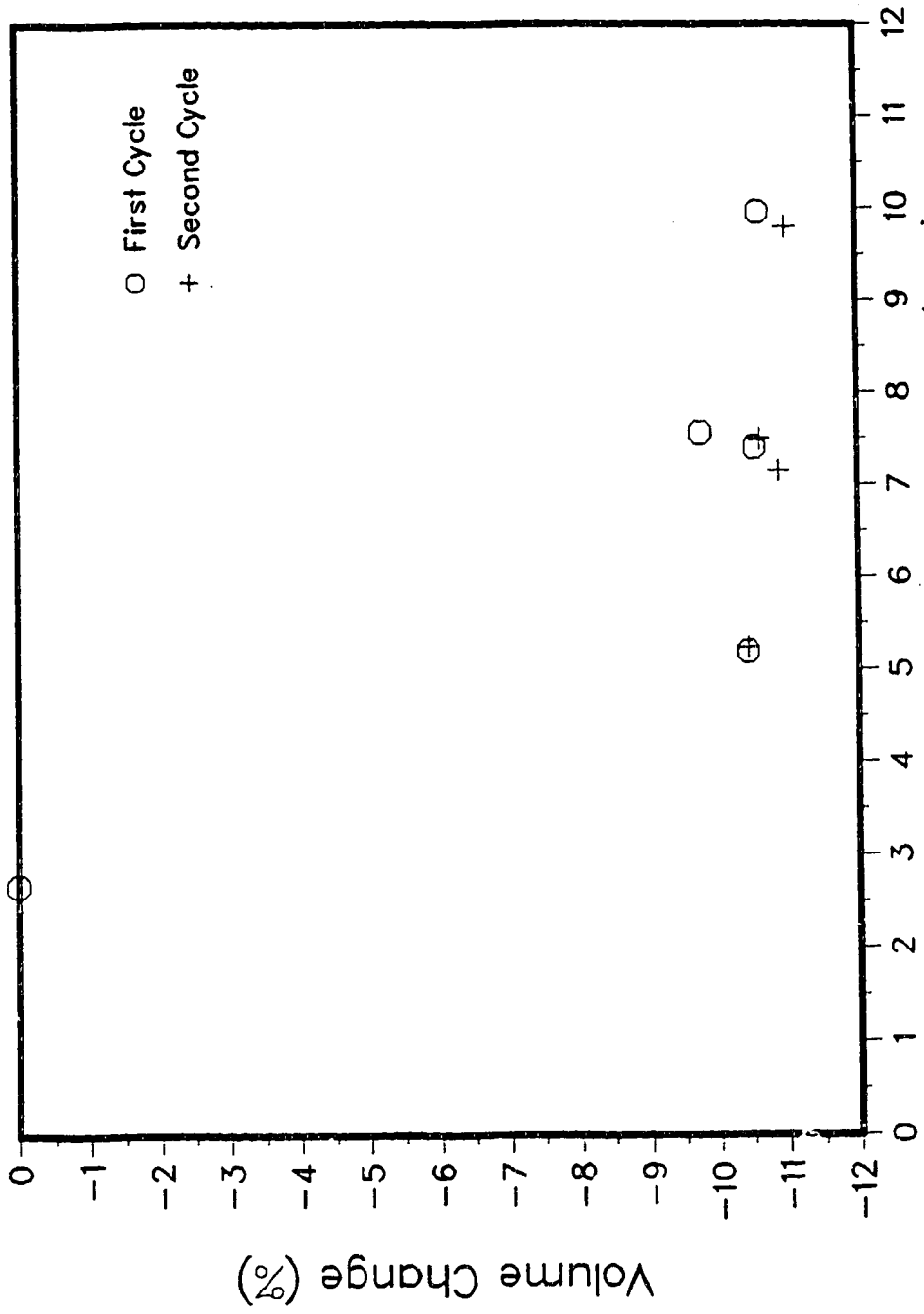

Figure E.40 Isotropic Compressibility Test CL4TOS3 225 °C

F. SPECIMEN DATA

Specimen Data Summary Sheet

Test Number: AMTOS1
Apparatus: Triaxial Cell

Specimen Dimensions

Before Test			After Test		
Diameter	5.11	cm	Diameter		cm
Height	9.89	cm	Height		cm
Area	20.47	cm^2	Area		cm^2
Volume	202.53	cm^3	Volume		cm^3
Mass	374.20	gm	Mass		gm
Density	1.85	gm/cm^3	Density		g/cm^3

Results of Soxhlet Extraction

% water = 2.6 % sand = 82.5 % bitumen = 14.9

Results of Specific Gravity G_s = 2.65

Grain Size Analysis

Size of Opening (mm)	Percent Finer than
2.000	
0.840	
0.420	100.00
0.250	99.36
0.149	27.70
0.074	5.61
0.044	4.12

Hydrometer Analysis

D (mm)	Percent Finer than
0.094	17.7
0.070	6.9
0.050	5.9
0.036	5.2
0.025	5.0
0.018	4.8
0.013	3.8
0.0095	3.7
0.0066	3.5
0.0047	2.9
0.0037	2.6
0.0025	2.4
0.00135	2.2

After Test Sketch

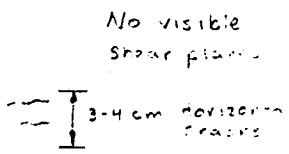

Specimen Data Summary Sheet

Test Number: AMTOS2
Apparatus: Triaxial Cell

Specimen Dimensions

Before Test			After Test		
Diameter	5.07	cm	Diameter	4.98 - 5.10	cm
Height	10.15	cm	Height	10.01	cm
Area	20.20	cm^2	Area		cm^2
Volume	205.00	cm^3	Volume		cm^3
Mass	383.50	gm	Mass	390.57	gm
Density	1.87	gm/cm^3	Density		g/cm^3

Results of Soxhlet Extraction

% water = 2.3 % sand = 82.2 % bitumen = 15.5

Results of Specific Gravity

G_s = 2.65

Grain Size Analysis

Size of Opening (mm)	Percent Finer than
2.000	
0.840	100.00
0.420	99.98
0.250	98.80
0.149	30.10
0.074	5.43
0.044	3.63

Hydrometer Analysis

D (mm)	Percent Finer than
0.098	13.3
0.070	7.1
0.050	5.8
0.036	3.6
0.025	3.5
0.018	3.3
0.0132	3.2
0.0096	3.0
0.0067	2.9
0.0047	2.6
0.0033	2.5
0.0025	2.2
0.00135	2.1

After Test Sketch

No visible shear plane
Uniform [illegible]

Specimen Data Summary Sheet

Test Number: AMTOS3
Apparatus: Triaxial Cell

Specimen Dimensions

Before Test			After Test		
Diameter	5.03	cm	Diameter	4.94 - 5.12	cm
Height	10.09	cm	Height	10.27	cm
Area	19.87	cm^2	Area		cm^2
Volume	200.50	cm^3	Volume		cm^3
Mass	379.11	gm	Mass	390.55	gm
Density	1.89	gm/cm^3	Density		g/cm^3

Results of Soxhlet Extraction

% water = 3.3 % sand = 81.2 % bitumen = 15.5

Results of Specific Gravity $G_s = 2.65$

Grain Size Analysis

Size of Opening (mm)	Percent Finer than
2.000	
0.840	
0.420	100.00
0.250	99.51
0.149	30.38
0.074	9.19
0.044	5.56

Hydrometer Analysis

D (mm)	Percent Finer than
0.095	16.3
0.067	8.7
0.050	6.6
0.035	5.3
0.025	4.9
0.018	4.8
0.013	4.1
0.0095	3.9
0.0067	3.2
0.0047	3.1
0.0033	2.8
0.0027	2.6
0.0014	2.4

After Test Sketch

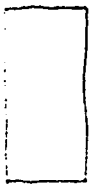

No visible shear planes
Uniform oil sands

Specimen Data Summary Sheet

Test Number: ACTOS1
Apparatus: Triaxial Cell

Specimen Dimensions

Before Test			After Test		
Diameter	5.11	cm	Diameter	5.02 - 5.18	cm
Height	10.43	cm	Height	10.12	cm
Area	20.47	cm^2	Area		cm^2
Volume	213.48	cm^3	Volume		cm^3
Mass	406.03	gm	Mass	406.49	gm
Density	1.90	gm/cm^3	Density		g/cm^3

Results of Soxhlet Extraction

% water = 5.4 % sand = 83.2 % bitumen = 11.4

Results of Specific Gravity $G_s = 2.68$

Grain Size Analysis

Size of Opening (mm)	Percent Finer than
2.000	
0.840	
0.420	100.00
0.250	99.93
0.149	88.50
0.074	21.00
0.044	15.49

Hydrometer Analysis

D (mm)	Percent Finer than
0.088	30.82
0.067	19.66
0.048	15.67
0.035	14.71
0.025	13.44
0.0177	12.16
0.0130	11.37
0.0093	10.25
0.0065	8.78
0.0047	7.48
0.0033	6.66
0.0025	5.99
0.0014	4.89

After Test Sketch

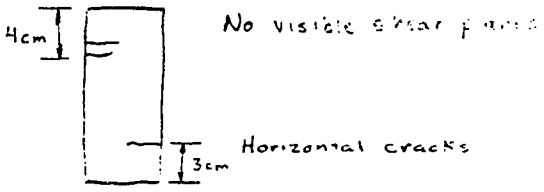

Specimen Data Summary Sheet

Test Number: ACTOS2
Apparatus: Triaxial Cell

Specimen Dimensions

Before Test			After Test		
Diameter	5.08	cm	Diameter	4.98-5.06	cm
Height	10.39	cm	Height	10.19	cm
Area	20.30	cm^2	Area		cm^2
Volume	210.98	cm^3	Volume		cm^3
Mass	402.05	gm	Mass	400.34	gm
Density	1.91	gm/cm^3	Density		g/cm^3

Results of Soxhlet Extraction

% water = 5.0 % sand = 83.0 % bitumen = 12.0

Results of Specific Gravity $G_s = 2.68$

Grain Size Analysis

Size of Opening (mm)	Percent Finer than
2.000	100.00
0.840	99.93
0.420	99.90
0.250	99.78
0.149	89.59
0.074	17.28
0.044	13.94

Hydrometer Analysis

D (mm)	Percent Finer than
0.088	28.58
0.065	17.48
0.048	14.98
0.035	13.59
0.022	12.62
0.018	11.93
0.013	10.96
0.0085	9.96
0.0064	9.13
0.0033	6.52
0.0024	6.27
0.00135	4.58

After Test Sketch

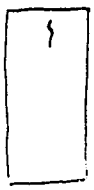

Small vertical crack

No visible shear plane

Specimen Data Summary Sheet

Test Number: ACTOS3
Apparatus: Triaxial Cell

Specimen Dimensions

Before Test			After Test		
Diameter	5.08	cm	Diameter	4.93 - 5.04	cm
Height	10.25	cm	Height	10.03	cm
Area	20.27	cm^2	Area		cm^2
Volume	207.82	cm^3	Volume		cm^3
Mass	367.74	gm	Mass	378.58	gm
Density	1.77	gm/cm^3	Density		g/cm^3

Results of Soxhlet Extraction

% water = 6.7 % sand = 81.4 % bitumen = 11.9

Results of Specific Gravity $G_s = 2.66$

Grain Size Analysis

Size of Opening (mm)	Percent Finer than
2.000	
0.840	100.00
0.420	99.96
0.250	99.39
0.149	43.13
0.074	5.03
0.044	4.11

Hydrometer Analysis

D (mm)	Percent Finer than
0.090	27.06
0.070	8.64
0.050	6.55
0.036	6.23
0.025	6.07
0.016	4.95
0.013	4.63
0.0088	4.29
0.0067	4.13
0.0047	3.53
0.0033	3.04
0.0025	2.88
0.0014	2.66

After Test Sketch

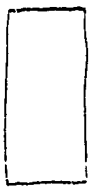

No visible shear plane

Specimen Data Summary Sheet

Test Number: ACTOS4
Apparatus: Triaxial Cell

Specimen Dimensions

Before Test			After Test		
Diameter	5.08	cm	Diameter	4.93 - 5.11	cm
Height	10.35	cm	Height	10.59	cm
Area	20.30	cm^2	Area		cm^2
Volume	210.30	cm^3	Volume		cm^3
Mass	391.77	gm	Mass	403.63	gm
Density	1.87	gm/cm^3	Density		g/cm^3

Results of Soxhlet Extraction

% water = 6.6 % sand = 81.9 % bitumen = 11.5

Results of Specific Gravity $G_s = 2.67$

Grain Size Analysis

Size of Opening (mm)	Percent Finer than
2.000	
0.840	
0.420	100.00
0.250	99.83
0.149	76.67
0.074	19.90
0.044	15.72

Hydrometer Analysis

D (mm)	Percent Finer than
0.084	32.77
0.065	20.26
0.047	16.78
0.034	14.83
0.024	13.72
0.017	12.89
0.0128	11.78
0.0100	10.82
0.0054	9.15
0.0046	8.87
0.0032	7.79
0.0024	6.84
0.00135	5.28

After Test Sketch

No visible shear plane

Specimen Data Summary Sheet

Test Number: UFCOS1
Apparatus: High Temperature Consolidometer

Specimen Dimensions

Before Test			After Test	
Diameter	5.31	cm	Diameter	cm
Height	2.74	cm	Height	cm
Area	22.15	cm^2	Area	cm^2
Volume	60.68	cm^3	Volume	cm^3
Mass	119.48	gm	Mass	gm
Density	1.97	gm/cm^3	Density	g/cm^3

Results of Soxhlet Extraction

% water = 9.4 % sand = 86.3 % bitumen = 4.3

Results of Specific Gravity $G_s = 2.66$

Grain Size Analysis

Size of Opening (mm)	Percent Finer than
2.000	
0.840	100.00
0.420	99.99
0.250	99.51
0.149	68.11
0.074	47.51
0.044	45.59

Hydrometer Analysis

D (mm)	Percent Finer than
0.078	63.82
0.059	50.09
0.043	47.80
0.031	45.51
0.022	42.07
0.015	39.10
0.012	35.89
0.0079	31.06
0.0062	27.17
0.0044	23.74
0.0031	19.46
0.0024	17.40
0.0013	13.87

After Test Sketch

Specimen Data Summary Sheet

Test Number: UFCOS2
Apparatus: High Temperature Consolidometer

Specimen Dimensions

Before Test			After Test	
Diameter	5.31	cm	Diameter	cm
Height	2.80	cm	Height	cm
Area	22.15	cm^2	Area	cm^2
Volume	61.85	cm^3	Volume	cm^3
Mass	118.34	gm	Mass	gm
Density	1.91	gm/cm^3	Density	g/cm^3

Results of Soxhlet Extraction

% water = 9.4 % sand = 86.3 % bitumen = 4.3

Results of Specific Gravity $G_s = 2.66$

Grain Size Analysis

Size of Opening (mm)	Percent Finer than
2.000	
0.840	100.00
0.420	99.99
0.250	99.51
0.149	68.11
0.074	47.51
0.044	45.59

Hydrometer Analysis

D (mm)	Percent Finer than
0.078	63.82
0.059	50.09
0.043	47.80
0.031	45.51
0.022	42.07
0.015	39.10
0.012	35.89
0.0079	31.06
0.0062	27.17
0.0044	23.74
0.0031	19.46
0.0024	17.40
0.0013	13.87

After Test Sketch

Specimen Data Summary Sheet

Test Number: UFCOS3
Apparatus: High Temperature Consolidometer

Specimen Dimensions

Before Test			After Test	
Diameter	5.30	cm	Diameter	cm
Height	2.77	cm	Height	cm
Area	22.06	cm^2	Area	cm^2
Volume	61.11	cm^3	Volume	cm^3
Mass	115.90	gm	Mass	gm
Density	1.90	gm/cm^3	Density	g/cm^3

Results of Soxhlet Extraction

% water = 9.4 % sand = 86.3 % bitumen = 4.3

Results of Specific Gravity G_s = 2.66

Grain Size Analysis

Size of Opening (mm)	Percent Finer than
2.000	
0.840	100.00
0.420	99.99
0.250	99.51
0.149	68.11
0.074	47.51
0.044	45.59

Hydrometer Analysis

D (mm)	Percent Finer than
0.078	63.82
0.059	50.09
0.043	47.80
0.031	45.51
0.022	42.07
0.015	39.10
0.012	35.89
0.0079	31.06
0.0062	27.17
0.0044	23.74
0.0031	19.46
0.0024	17.40
0.0013	13.87

After Test Sketch

Specimen Data Summary Sheet

Test Number: UFCOS4
Apparatus: High Temperature Consolidometer

Specimen Dimensions

Before Test			After Test		
Diameter	5.31	cm	Diameter	5.08	cm
Height	3.09	cm	Height	2.99	cm
Area	22.15	cm^2	Area	20.27	cm^2
Volume	68.32	cm^3	Volume	60.60	cm^3
Mass	135.98	gm	Mass	132.02	gm
Density	1.99	gm/cm^3	Density	2.18	g/cm^3

Results of Soxhlet Extraction

% water = 6.9 % sand = 88.2 % bitumen = 4.9

Results of Specific Gravity $G_s = 2.62$

Grain Size Analysis

Size of Opening (mm)	Percent Finer than
2.000	
0.840	100.00
0.420	99.99
0.250	99.78
0.149	69.56
0.074	44.83
0.044	41.03

Hydrometer Analysis

D (mm)	Percent Finer than
0.081	45.78
0.059	40.93
0.043	38.01
0.031	34.93
0.022	31.21
0.016	28.10
0.012	25.99
0.0086	23.35
0.0062	18.74
0.0045	16.88
0.0032	14.25
0.0025	12.47
0.00081	7.06

After Test Sketch

Specimen Data Summary Sheet

Test Number: UFCOS5
Apparatus: High Temperature Consolidometer

Specimen Dimensions

Before Test			After Test		
Diameter	5.32	cm	Diameter	5.33	cm
Height	3.11	cm	Height	2.90	cm
Area	22.23	cm^2	Area	22.30	cm^2
Volume	69.13	cm^3	Volume	64.81	cm^3
Mass	137.48	gm	Mass	136.57	gm
Density	1.99	gm/cm^3	Density	2.11	g/cm^3

Results of Soxhlet Extraction

% water = 5.3 % sand = 86.4 % bitumen = 8.3

Results of Specific Gravity $G_s = 2.62$

Grain Size Analysis

Size of Opening (mm)	Percent Finer than
2.000	
0.840	100.00
0.420	99.99
0.250	99.81
0.149	73.46
0.074	51.76
0.044	48.52

Hydrometer Analysis

D (mm)	Percent Finer than
0.069	54.73
0.052	50.51
0.038	47.00
0.028	42.08
0.020	38.57
0.015	35.06
0.011	31.24
0.0082	28.12
0.0060	25.12
0.0042	22.14
0.0031	19.55
0.0022	17.63
0.0013	14.92

After Test Sketch

Specimen Data Summary Sheet

Test Number: UFTOS1
Apparatus: Triaxial Cell

Specimen Dimensions

Before Test			After Test		
Diameter	5.07	cm	Diameter	5.11 - 5.20	cm
Height	10.27	cm	Height	10.33	cm
Area	20.19	cm^2	Area		cm^2
Volume	207.34	cm^3	Volume		cm^3
Mass	412.50	gm	Mass	423.09	gm
Density	1.99	gm/cm^3	Density		g/cm^3

Results of Soxhlet Extraction

% water = 8.3 % sand = 84.1 % bitumen = 7.6

Results of Specific Gravity $G_s = 2.66$

Grain Size Analysis

Size of Opening (mm)	Percent Finer than
2.000	
0.840	100.00
0.420	99.98
0.250	98.20
0.149	63.33
0.074	41.23
0.044	

Hydrometer Analysis

D (mm)	Percent Finer than
0.077	41.23
0.056	40.20
0.046	38.88
0.040	38.22
0.033	36.65
0.029	36.65
0.025	32.70
0.0195	30.30
0.0143	26.59
0.0103	23.29
0.0076	20.37
0.0061	18.47
0.0045	15.71
0.0029	13.07
0.0013	10.43

After Test Sketch

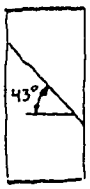

Specimen Data Summary Sheet

Test Number: UFTOS2
Apparatus: Triaxial Cell

Specimen Dimensions

Before Test			After Test		
Diameter	5.10	cm	Diameter		cm
Height	10.20	cm	Height		cm
Area	20.41	cm^2	Area		cm^2
Volume	208.06	cm^3	Volume		cm^3
Mass	428.40	gm	Mass	437.71	gm
Density	2.06	gm/cm^3	Density		g/cm^3

Results of Soxhlet Extraction

% water = 8.3 % sand = 86.1 % bitumen = 5.6

Results of Specific Gravity $G_s = 2.69$

Grain Size Analysis

Size of Opening (mm)	Percent Finer than
2.000	
0.840	
0.420	
0.250	100.00
0.149	72.88
0.074	55.18
0.044	

Hydrometer Analysis

D (mm)	Percent Finer than
0.077	56.45
0.055	54.35
0.038	52.59
0.028	50.16
0.020	47.68
0.015	42.76
0.011	37.63
0.0083	33.88
0.0050	28.14
0.0038	26.16
0.0029	25.05
0.0024	22.40
0.0013	19.26

After Test Sketch

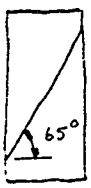

Specimen Data Summary Sheet

Test Number: UFTOS3
Apparatus: Triaxial Cell

Specimen Dimensions

Before Test			After Test		
Diameter	5.08	cm	Diameter		cm
Height	10.22	cm	Height	10.70	cm
Area	20.29	cm^2	Area		cm^2
Volume	207.33	cm^3	Volume		cm^3
Mass	729.50	gm	Mass		gm
Density	2.07	gm/cm^3	Density		g/cm^3

Results of Soxhlet Extraction

% water = 8.5 % sand = 84.9 % bitumen = 6.6

Results of Specific Gravity $G_s = 2.69$

Grain Size Analysis

Size of Opening (mm)	Percent Finer than
2.000	
0.840	
0.420	100.00
0.250	99.63
0.149	66.64
0.074	53.96
0.044	50.16

Hydrometer Analysis

D (mm)	Percent Finer than
0.065	53.63
0.047	50.87
0.034	49.48
0.025	45.61
0.018	42.56
0.014	38.41
0.0105	35.23
0.0076	31.77
0.0055	28.86
0.0040	24.71
0.0029	22.19
0.0024	20.51
0.0013	16.18

After Test Sketch

Specimen Data Summary Sheet

Test Number: UFTOS4
Apparatus: Triaxial Cell

Specimen Dimensions

Before Test			After Test		
Diameter	5.06	cm	Diameter	5.08 - 5.12	cm
Height	10.26	cm	Height	9.80	cm
Area	20.11	cm^2	Area		cm^2
Volume	206.32	cm^3	Volume		cm^3
Mass	436.36	gm	Mass	441.6	gm
Density	2.12	gm/cm^3	Density		g/cm^3

Results of Soxhlet Extraction

% water = 6.4 % sand = 87.1 % bitumen = 6.5

Results of Specific Gravity $G_s = 2.67$

Grain Size Analysis

Size of Opening (mm)	Percent Finer than
2.000	
0.840	
0.420	
0.250	100.00
0.149	75.05
0.074	52.91
0.044	

Hydrometer Analysis

D (mm)	Percent Finer than
0.085	58.23
0.061	51.59
0.044	48.84
0.032	47.46
0.022	41.32
0.0175	37.88
0.0120	33.70
0.0088	30.26
0.0063	26.30
0.0045	23.54
0.0032	20.32
0.0024	18.84
0.0013	15.98

After Test Sketch

Specimen Data Summary Sheet

Test Number: UFTOS5
Apparatus: Triaxial Cell

Specimen Dimensions

Before Test			After Test		
Diameter	5.08	cm	Diameter	5.14-5.16	cm
Height	10.24	cm	Height	10.06	cm
Area	20.27	cm^2	Area		cm^2
Volume	207.55	cm^3	Volume		cm^3
Mass	442.64	gm	Mass	455.01	gm
Density	2.13	gm/cm^3	Density		g/cm^3

Results of Soxhlet Extraction

% water = 6.4 % sand = 87.1 % bitumen = 6.5

Results of Specific Gravity $G_s = 2.67$

Grain Size Analysis

Size of Opening (mm)	Percent Finer than
2.000	
0.840	
0.420	
0.250	100.00
0.149	75.05
0.074	52.90
0.044	

Hydrometer Analysis

D (mm)	Percent Finer than
0.085	58.20
0.061	51.59
0.044	48.84
0.032	47.46
0.022	41.32
0.0175	37.89
0.0120	33.70
0.0088	30.26
0.0063	26.30
0.0045	23.54
0.0032	20.32
0.0024	18.84
0.0013	15.98

After Test Sketch

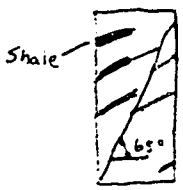

Specimen Data Summary Sheet

Test Number: UFTOS6
Apparatus: Triaxial Cell

Specimen Dimensions

Before Test			After Test		
Diameter	5.07	cm	Diameter	5.00-5.10	cm
Height	10.39	cm	Height	10.43	cm
Area	20.19	cm^2	Area		cm^2
Volume	209.69	cm^3	Volume		cm^3
Mass	402.81	gm	Mass	409.43	gm
Density	1.92	gm/cm^3	Density		g/cm^3

Results of Soxhlet Extraction

% water = 2.8 % sand = 83.0 % bitumen = 14.1

Results of Specific Gravity $G_s = 2.68$

Grain Size Analysis

Size of Opening (mm)	Percent Finer than
2.000	
0.840	100.00
0.420	99.92
0.250	97.73
0.149	35.79
0.074	3.46
0.044	2.07

Hydrometer Analysis

D (mm)	Percent Finer than
0.099	13.96
0.072	6.88
0.051	5.81
0.036	5.46
0.025	5.28
0.018	4.93
0.0133	4.75
0.0096	4.576
0.0088	4.39
0.0048	4.22
0.0034	3.86
0.0025	3.69

After Test Sketch

No visible shear planes

Specimen Data Summary Sheet

Test Number: UFTOS7
Apparatus: Triaxial Cell

Specimen Dimensions

Before Test			After Test		
Diameter	5.16	cm	Diameter	5.09 - 5.40	cm
Height	10.18	cm	Height	10.40	cm
Area	20.91	cm^2	Area		cm^2
Volume	212.94	cm^3	Volume		cm^3
Mass	411.48	gm	Mass	425.52	gm
Density	1.93	gm/cm^3	Density		g/cm^3

Results of Soxhlet Extraction

% water = 4.1 % sand = 81.9 % bitumen = 14.0

Results of Specific Gravity $G_s = 2.67$

Grain Size Analysis

Size of Opening (mm)	Percent Finer than
2.000	
0.840	100.00
0.420	99.96
0.250	97.09
0.149	36.22
0.074	3.43
0.044	2.30

Hydrometer Analysis

D (mm)	Percent Finer than
0.093	16.71
0.070	3.50
0.051	1.42
0.037	1.36
0.025	1.28
0.0180	1.28
0.0130	1.25
0.0095	1.03
0.0066	0.89
0.0047	0.61
0.0025	0.61

After Test Sketch

No visible shear plane
Vertical cracks
Bucking at base

Specimen Data Summary Sheet

Test Number: UFTOS8
Apparatus: Triaxial Cell

Specimen Dimensions

Before Test			After Test		
Diameter	5.05	cm	Diameter	5.05 - 5.25	cm
Height	10.21	cm	Height	10.10	cm
Area	20.04	cm^2	Area		cm^2
Volume	204.56	cm^3	Volume		cm^3
Mass	420.18	gm	Mass	429.64	gm
Density	2.05	gm/cm^3	Density		g/cm^3

Results of Soxhlet Extraction

% water = 7.3 % sand = 85.3 % bitumen = 7.4

Results of Specific Gravity $G_s = 2.67$

Grain Size Analysis

Size of Opening (mm)	Percent Finer than
2.000	100.00
0.840	99.98
0.420	99.95
0.250	99.63
0.149	79.23
0.074	57.35
0.044	52.04

Hydrometer Analysis

D (mm)	Percent Finer than
0.065	55.45
0.047	51.28
0.035	48.49
0.025	45.98
0.019	45.84
0.0128	37.34
0.0087	33.00
0.0077	31.88
0.0056	28.82
0.0040	25.62
0.0029	22.95
0.0023	21.42
0.00122	17.42

After Test Sketch

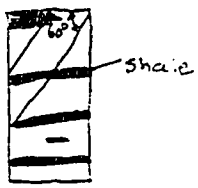

Specimen Data Summary Sheet

Test Number: UFTOS9
Apparatus: Triaxial Cell

Specimen Dimensions

Before Test			After Test		
Diameter	5.08	cm	Diameter	5.06 - 5.29	cm
Height	10.31	cm	Height	10.15	cm
Area	20.31	cm^2	Area		cm^2
Volume	209.38	cm^3	Volume		cm^3
Mass	410.50	gm	Mass	419.02	gm
Density	1.96	gm/cm^3	Density		g/cm^3

Results of Soxhlet Extraction

% water = 7.8 % sand = 83.4 % bitumen = 8.8

Results of Specific Gravity $G_s = 2.67$

Grain Size Analysis

Size of Opening (mm)	Percent Finer than
2.000	
0.840	
0.420	100.00
0.250	99.33
0.149	65.19
0.074	36.16
0.044	33.21

Hydrometer Analysis

D (mm)	Percent Finer than
0.072	44.46
0.055	37.51
0.040	35.84
0.029	33.48
0.020	32.09
0.0150	29.17
0.0110	27.50
0.0075	24.11
0.0042	19.58
0.0030	17.21
0.0023	15.54
0.0013	12.89

After Test Sketch

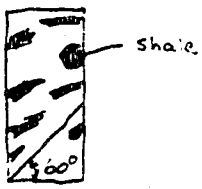

Specimen Data Summary Sheet

Test Number: UFTOS10
Apparatus: Triaxial Cell

Specimen Dimensions

Before Test			After Test		
Diameter	5.09	cm	Diameter	5.01-5.28	cm
Height	10.41	cm	Height	10.24	cm
Area	20.35	cm^2	Area		cm^2
Volume	211.72	cm^3	Volume		cm^3
Mass	435.29	gm	Mass	441.15	gm
Density	2.06	gm/cm^3	Density		g/cm^3

Results of Soxhlet Extraction

% water = 6.6 % sand = 86.1 % bitumen = 7.3

Results of Specific Gravity $G_s = 2.67$

Grain Size Analysis

Size of Opening (mm)	Percent Finer than
2.000	100.00
0.840	99.97
0.420	99.63
0.250	99.37
0.149	86.01
0.074	71.86
0.044	66.73

Hydrometer Analysis

D (mm)	Percent Finer than
0.024	55.24
0.019	48.29
0.014	44.11
0.011	40.75
0.007	37.27
0.0056	33.10
0.0040	30.02
0.0030	26.65
0.0023	24.11
0.0017	20.16

After Test Sketch

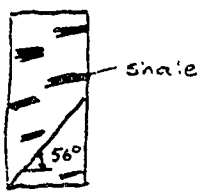

Specimen Data Summary Sheet

Test Number: UFTOS11
Apparatus: Triaxial Cell

Specimen Dimensions

Before Test			After Test		
Diameter	5.08	cm	Diameter	5.00-5.09	cm
Height	10.27	cm	Height	10.35	cm
Area	20.31	cm^2	Area		cm^2
Volume	208.57	cm^3	Volume		cm^3
Mass	411.87	gm	Mass	420.60	gm
Density	1.98	gm/cm^3	Density		g/cm^3

Results of Soxhlet Extraction

% water = 6.0 % sand = 84.5 % bitumen = 9.5

Results of Specific Gravity $G_s = 2.64$

Grain Size Analysis

Size of Opening (mm)	Percent Finer than
2.000	
0.840	100.00
0.420	99.99
0.250	98.91
0.149	62.03
0.074	42.52
0.044	39.34

Hydrometer Analysis

D (mm)	Percent Finer than
0.075	44.72
0.053	41.92
0.039	39.12
0.028	33.52
0.020	30.03
0.015	27.92
0.011	25.22
0.0081	25.22
0.0057	22.42
0.0042	19.84
0.0030	17.01
0.0023	14.80
0.0013	12.04

After Test Sketch

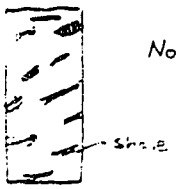

Specimen Data Summary Sheet

Test Number: UFTOS12
Apparatus: Triaxial Cell

Specimen Dimensions

Before Test			After Test		
Diameter	5.09	cm	Diameter	5.00 - 5.09	cm
Height	10.36	cm	Height	10.49	cm
Area	20.31	cm^2	Area		cm^2
Volume	210.43	cm^3	Volume		cm^3
Mass	417.49	gm	Mass	426.02	gm
Density	1.98	gm/cm^3	Density		g/cm^3

Results of Soxhlet Extraction

% water = 7.0 % sand = 83.4 % bitumen = 9.5

Results of Specific Gravity $G_s = 2.66$

Grain Size Analysis

Size of Opening (mm)	Percent Finer than
2.000	
0.840	
0.420	100.00
0.250	97.40
0.149	58.20
0.074	37.70
0.044	34.30

Hydrometer Analysis

D (mm)	Percent Finer than
0.076	41.73
0.056	36.14
0.041	34.05
0.029	32.23
0.021	29.86
0.0150	27.76
0.0114	25.67
0.0082	23.99
0.0058	21.70
0.0042	19.44
0.0030	16.79
0.0023	15.28
0.0013	12.35

After Test Sketch

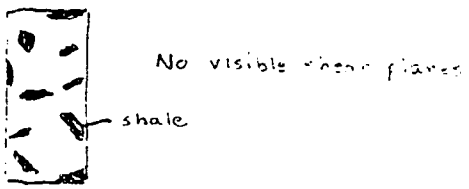

Specimen Data Summary Sheet

Test Number: UFTOS14
Apparatus: Triaxial Cell

Specimen Dimensions

Before Test			After Test		
Diameter	5.07	cm	Diameter	4.90- 5.04	cm
Height	10.19	cm	Height	10.30	cm
Area	20.19	cm^2	Area		cm^2
Volume	205.62	cm^3	Volume		cm^3
Mass	392.29	gm	Mass	390.75	gm
Density	1.91	gm/cm^3	Density		g/cm^3

Results of Soxhlet Extraction

% water = 2.7 % sand = 81.8 % bitumen = 15.5

Results of Specific Gravity $G_s = 2.66$

Grain Size Analysis

Size of Opening (mm)	Percent Finer than
2.000	
0.840	100.00
0.420	99.96
0.250	97.63
0.149	25.84
0.074	2.99
0.044	2.10

Hydrometer Analysis

D (mm)	Percent Finer than
0.092	16.32
0.070	5.17
0.050	4.89
0.036	3.08
0.025	2.94
0.0180	2.94
0.0130	2.80
0.0095	2.80
0.0066	2.80
0.0047	2.80
0.0039	2.55
0.0024	2.55
0.0014	2.56

After Test Sketch

No visible shear plane

Specimen Data Summary Sheet

Test Number: UFHTTOS1
Apparatus: High Temperature Triaxial Cell

Specimen Dimensions

Before Test			After Test		
Diameter	5.40	cm	Diameter	5.32-5.53	cm
Height	10.89	cm	Height	10.23	cm
Area	22.86	cm^2	Area		cm^2
Volume	249.06	cm^3	Volume		cm^3
Mass	495.62	gm	Mass	491.50	gm
Density	1.99	gm/cm^3	Density		g/cm^3

Results of Soxhlet Extraction

% water = 6.2 % sand = 86.8 % bitumen = 7.0

Results of Specific Gravity G_s = 2.66

Grain Size Analysis

Size of Opening (mm)	Percent Finer than
2.000	100.00
0.840	99.97
0.420	99.90
0.250	99.58
0.149	71.72
0.074	51.35
0.044	45.29

Hydrometer Analysis

D (mm)	Percent Finer than
0.068	51.30
0.050	47.12
0.036	45.73
0.026	43.50
0.019	40.16
0.0140	35.98
0.0116	32.91
0.0073	29.26
0.0056	27.45
0.0040	23.17
0.0030	20.16
0.0023	17.97
0.0013	13.93

After Test Sketch

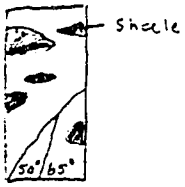

Specimen Data Summary Sheet

Test Number: UFHTTOS2
Apparatus: High Temperature Triaxial Cell

Specimen Dimensions

Before Test			After Test		
Diameter	5.34	cm	Diameter	5.26 - 5.29	cm
Height	10.95	cm	Height	10.60	cm
Area	22.35	cm^2	Area		cm^2
Volume	244.78	cm^3	Volume		cm^3
Mass	477.99	gm	Mass	465.95	gm
Density	1.95	gm/cm^3	Density		g/cm^3

Results of Soxhlet Extraction

% water = 0.8 % sand = 84.4 % bitumen = 14.8

Results of Specific Gravity $G_s = 2.67$

Grain Size Analysis

Size of Opening (mm)	Percent Finer than
2.000	
0.840	100.00
0.420	99.95
0.250	98.48
0.149	30.53
0.074	5.17
0.044	2.91

Hydrometer Analysis

D (mm)	Percent Finer than
0.096	16.38
0.071	3.86
0.050	3.59
0.036	3.17
0.025	2.61
0.0180	2.61
0.013	2.61
0.0095	2.61
0.0066	2.59
0.0047	2.56
0.0033	2.59
0.0027	2.50
0.0014	2.43

After Test Sketch

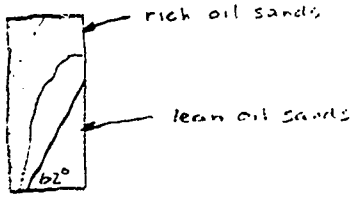

Specimen Data Summary Sheet

Test Number: UFHTTOS3
Apparatus: High Temperature Triaxial Cell

Specimen Dimensions

Before Test			After Test		
Diameter	5.35	cm	Diameter	5.43 - 5.58	cm
Height	11.05	cm	Height	10.48	cm
Area	22.48	cm^2	Area		cm^2
Volume	248.41	cm^3	Volume		cm^3
Mass	480.61	gm	Mass	496.20	gm
Density	1.94	gm/cm^3	Density		g/cm^3

Results of Soxhlet Extraction

% water = 5.2 % sand = 82.4 % bitumen = 12.4

Results of Specific Gravity $G_s = 2.67$

Grain Size Analysis

Size of Opening (mm)	Percent Finer than
2.000	
0.840	100.00
0.420	99.94
0.250	97.72
0.149	36.51
0.074	4.49
0.044	2.41

Hydrometer Analysis

D (mm)	Percent Finer than
0.098	12.09
0.073	8.54
0.052	6.77
0.037	6.41
0.025	5.88
0.0180	5.35
0.0133	5.17
0.0095	5.13
0.0068	4.96
0.0048	4.78
0.0033	4.56
0.0025	4.28

After Test Sketch

Specimen Data Summary Sheet

Test Number: UFHTTOS4
Apparatus: High Temperature Triaxial Cell

Specimen Dimensions

Before Test			After Test		
Diameter	5.35	cm	Diameter	5.31 - 5.47	cm
Height	10.75	cm	Height	10.36	cm
Area	22.48	cm^2	Area		cm^2
Volume	241.66	cm^3	Volume		cm^3
Mass	492.03	gm	Mass	485.30	gm
Density	2.04	gm/cm^3	Density		g/cm^3

Results of Soxhlet Extraction

% water = 4.5 % sand = 86.9 % bitumen = 8.6

Results of Specific Gravity G_s = 2.64

Grain Size Analysis

Size of Opening (mm)	Percent Finer than
2.000	
0.840	
0.420	100.00
0.250	99.66
0.149	68.98
0.074	48.44
0.044	44.38

Hydrometer Analysis

D (mm)	Percent Finer than
0.067	50.25
0.050	47.87
0.037	44.65
0.027	41.57
0.019	37.65
0.0140	34.16
0.011	30.94
0.0080	27.16
0.0057	23.77
0.0042	20.77
0.0030	17.95
0.0023	15.29
0.0013	12.35

After Test Sketch

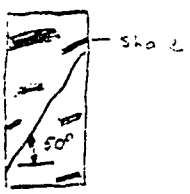

Specimen Data Summary Sheet

Test Number: UFHTTOS5
Apparatus: High Temperature Triaxial Cell

Specimen Dimensions

Before Test			After Test		
Diameter	5.40	cm	Diameter	5.23-5.51	cm
Height	10.92	cm	Height	10.42	cm
Area	22.86	cm^2	Area		cm^2
Volume	249.55	cm^3	Volume		cm^3
Mass	513.56	gm	Mass	504.60	gm
Density	2.06	gm/cm^3	Density		g/cm^3

Results of Soxhlet Extraction

% water = 7.2 % sand = 87.6 % bitumen = 5.2

Results of Specific Gravity $G_s = 2.65$

Grain Size Analysis

Size of Opening (mm)	Percent Finer than
2.000	
0.840	
0.420	100.00
0.250	99.45
0.149	74.58
0.074	56.68
0.044	53.97

Hydrometer Analysis

D (mm)	Percent Finer than
0.045	54.47
0.033	53.07
0.024	51.12
0.017	47.48
0.013	43.57
0.0100	39.66
0.0074	35.73
0.0055	30.64
0.0040	26.87
0.0029	22.64
0.0022	19.57
0.0013	15.18

After Test Sketch

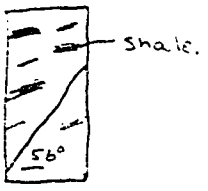

Specimen Data Summary Sheet

Test Number: UFHTTOS6
Apparatus: High Temperature Triaxial Cell

Specimen Dimensions

Before Test			After Test	
Diameter	5.39	cm	Diameter	cm
Height	10.86	cm	Height	cm
Area	22.79	cm^2	Area	cm^2
Volume	247.52	cm^3	Volume	cm^3
Mass	504.58	gm	Mass	gm
Density	2.04	gm/cm^3	Density	g/cm^3

Results of Soxhlet Extraction

% water = 7.8 % sand = 85.9 % bitumen = 6.3

Results of Specific Gravity $G_s = 2.64$

Grain Size Analysis

Size of Opening (mm)	Percent Finer than
2.000	
0.840	100.00
0.420	99.91
0.250	99.45
0.149	79.86
0.074	65.46
0.044	59.35

Hydrometer Analysis

D (mm)	Percent Finer than
0.050	59.13
0.036	56.71
0.026	52.69
0.020	48.66
0.014	44.80
0.011	40.91
0.008	37.52
0.0057	33.50
0.0042	28.62
0.0030	26.75
0.0025	25.15
0.0013	20.12

After Test Sketch

Specimen Data Summary Sheet

Test Number: UFHTTOS7
Apparatus: High Temperature Triaxial Cell

Specimen Dimensions

Before Test			After Test		
Diameter	5.43	cm	Diameter	5.37 - 5.39	cm
Height	10.95	cm	Height	11.11	cm
Area	23.12	cm^2	Area		cm^2
Volume	252.99	cm^3	Volume		cm^3
Mass	522.27	gm	Mass	528.20	gm
Density	2.06	gm/cm^3	Density		g/cm^3

Results of Soxhlet Extraction

% water = 6.7 % sand = 85.1 % bitumen = 8.2

Results of Specific Gravity G_s =

Grain Size Analysis

Size of Opening (mm)	Percent Finer than
2.000	
0.840	100.00
0.420	99.98
0.250	99.15
0.149	75.72
0.074	50.87
0.044	47.69

Hydrometer Analysis

D (mm)	Percent Finer than
0.065	52.99
0.048	50.19
0.035	46.84
0.026	43.63
0.019	40.14
0.014	36.65
0.011	33.43
0.0078	30.78
0.0056	27.54
0.0040	24.47
0.0029	21.20
0.0022	19.25
0.00125	16.16

After Test Sketch

Specimen Data Summary Sheet

Test Number: UFHTTOS8
Apparatus: High Temperature Triaxial Cell

Specimen Dimensions

Before Test			After Test		
Diameter	5.32	cm	Diameter	5.32-5.35	cm
Height	10.80	cm	Height	9.71	cm
Area	22.20	cm^2	Area		cm^2
Volume	239.81	cm^3	Volume		cm^3
Mass	482.75	gm	Mass		gm
Density	2.01	gm/cm^3	Density		g/cm^3

Results of Soxhlet Extraction

% water = 6.7 % sand = 85.1 % bitumen = 8.2

Results of Specific Gravity G_s =

Grain Size Analysis

Size of Opening (mm)	Percent Finer than
2.000	
0.840	100.00
0.420	99.98
0.250	99.15
0.149	75.72
0.074	50.87
0.044	47.69

Hydrometer Analysis

D (mm)	Percent Finer than
0.065	52.99
0.048	50.19
0.035	46.84
0.026	43.63
0.019	40.14
0.014	36.65
0.011	33.43
0.0078	30.78
0.0056	27.54
0.0040	24.47
0.0029	21.20
0.0022	19.25
0.00125	16.16

After Test Sketch

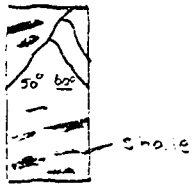

Specimen Data Summary Sheet

Test Number: UFCCS1
Apparatus:

Specimen Dimensions

Before Test			After Test	
Diameter	5.25	cm	Diameter	cm
Height	3.29	cm	Height	cm
Area	21.65	cm^2	Area	cm^2
Volume	71.22	cm^3	Volume	cm^3
Mass	144.50	gm	Mass	gm
Density	2.03	gm/cm^3	Density	g/cm^3

Results of Soxhlet Extraction

% water = % sand = % bitumen =

Results of Specific Gravity $G_s = 2.70$

Grain Size Analysis

Size of Opening (mm)	Percent Finer than
2.000	
0.840	
0.420	
0.250	
0.149	
0.074	
0.044	

Hydrometer Analysis

D (mm)	Percent Finer than

After Test Sketch

Specimen Data Summary Sheet

Test Number: UFCCS2
Apparatus:

Specimen Dimensions

Before Test		After Test	
Diameter	cm	Diameter	cm
Height	cm	Height	cm
Area	cm^2	Area	cm^2
Volume	cm^3	Volume	cm^3
Mass	gm	Mass	gm
Density	gm/cm^3	Density	g/cm^3

Results of Soxhlet Extraction

% water = % sand = % bitumen =

Results of Specific Gravity G_s =

Grain Size Analysis

Size of Opening (mm)	Percent Finer than
2.000	
0.840	
0.420	
0.250	
0.149	
0.074	
0.044	

Hydrometer Analysis

D (mm)	Percent Finer than

After Test Sketch

Specimen Data Summary Sheet

Test Number: UFCCS3
Apparatus: Consolidometer

Specimen Dimensions

Before Test			After Test	
Diameter	5.32	cm	Diameter	cm
Height	3.17	cm	Height	cm
Area	22.23	cm^2	Area	cm^2
Volume	70.47	cm^3	Volume	cm^3
Mass	149.43	gm	Mass	gm
Density	2.12	gm/cm^3	Density	g/cm^3

Results of Soxhlet Extraction

% water = % sand = % bitumen =

Results of Specific Gravity $G_s = 2.70$

Grain Size Analysis

Size of Opening (mm)	Percent Finer than
2.000	
0.840	
0.420	
0.250	
0.149	
0.074	
0.044	

Hydrometer Analysis

D (mm)	Percent Finer than

After Test Sketch

Specimen Data Summary Sheet

Test Number: UFCCS4
Apparatus: Consolidometer

Specimen Dimensions

Before Test			After Test	
Diameter	5.32	cm	Diameter	cm
Height	2.61	cm	Height	cm
Area	22.19	cm^2	Area	cm^2
Volume	57.98	cm^3	Volume	cm^3
Mass	120.70	gm	Mass	gm
Density	2.09	gm/cm^3	Density	g/cm^3

Results of Soxhlet Extraction

% water = % sand = % bitumen =

Results of Specific Gravity

G_s =

Grain Size Analysis

Size of Opening (mm)	Percent Finer than
2.000	
0.840	
0.420	
0.250	
0.149	
0.074	
0.044	

Hydrometer Analysis

D (mm)	Percent Finer than

After Test Sketch

Specimen Data Summary Sheet

Test Number: UFCCS5
Apparatus: Consolidometer

Specimen Dimensions

Before Test			After Test	
Diameter	5.32	cm	Diameter	cm
Height	3.00	cm	Height	cm
Area	22.23	cm^2	Area	cm^2
Volume	66.69	cm^3	Volume	cm^3
Mass	137.87	gm	Mass	gm
Density	2.07	gm/cm^3	Density	g/cm^3

Results of Soxhlet Extraction

% water = % sand = % bitumen =

Results of Specific Gravity $G_s = 2.70$

Grain Size Analysis

Size of Opening (mm)	Percent Finer than
2.000	
0.840	
0.420	
0.250	
0.149	
0.074	
0.044	

Hydrometer Analysis

D (mm)	Percent Finer than

After Test Sketch

Specimen Data Summary Sheet

Test Number: UTFCL1
Apparatus: Consolidometer

Specimen Dimensions

Before Test			After Test	
Diameter	5.31	cm	Diameter	cm
Height	3.14	cm	Height	cm
Area	22.12	cm^2	Area	cm^2
Volume	69.38	cm^3	Volume	cm^3
Mass	182.53	gm	Mass	gm
Density	2.63	gm/cm^3	Density	g/cm^3

Results of Soxhlet Extraction

% water = % sand = % bitumen =

Results of Specific Gravity G_s =

Grain Size Analysis

Size of Opening (mm)	Percent Finer than
2.000	
0.840	
0.420	
0.250	
0.149	
0.074	
0.044	

Hydrometer Analysis

D (mm)	Percent Finer than

After Test Sketch

Specimen Data Summary Sheet

Test Number: UFTCS1
Apparatus: Triaxial Cell

Specimen Dimensions

Before Test			After Test	
Diameter	6.60	cm	Diameter	cm
Height	13.53	cm	Height	cm
Area	34.18	cm^2	Area	cm^2
Volume	462.32	cm^3	Volume	cm^3
Mass	962.70	gm	Mass	gm
Density	2.08	gm/cm^3	Density	g/cm^3

Results of Soxhlet Extraction

% water = % sand = % bitumen =

Results of Specific Gravity $G_s = 2.73$

Grain Size Analysis

Size of Opening (mm)	Percent Finer than
2.000	
0.840	
0.420	
0.250	100.00
0.149	99.71
0.074	99.49
0.044	
0.0023	
0.0011	

Hydrometer Analysis

D (mm)	Percent Finer than
0.073	38.60
0.052	37.44
0.043	37.09
0.037	36.86
0.029	36.63
0.021	36.40
0.0188	35.67
0.0140	30.79
0.0108	26.72
0.008	24.16
0.0057	20.44
0.0041	17.51
0.0030	15.65
	13.91
	11.49

After Test Sketch

Specimen Data Summary Sheet

Test Number: UFTCS2
Apparatus: Triaxial Cell

Specimen Dimensions

Before Test			After Test	
Diameter	5.47	cm	Diameter	cm
Height	10.39	cm	Height	cm
Area	23.49	cm^2	Area	cm^2
Volume	243.96	cm^3	Volume	cm^3
Mass	528.60	gm	Mass	gm
Density	2.17	gm/cm^3	Density	g/cm^3

Results of Soxhlet Extraction

% water = % sand = % bitumen =

Results of Specific Gravity G_s =

Grain Size Analysis

Size of Opening (mm)	Percent Finer than
2.000	
0.840	
0.420	
0.250	
0.149	
0.074	
0.044	

Hydrometer Analysis

D (mm)	Percent Finer than

After Test Sketch

Specimen Data Summary Sheet

Test Number: UFTCS3
Apparatus: Triaxial Cell

Specimen Dimensions

Before Test			After Test		
Diameter	5.54	cm	Diameter	5.50-5.70	cm
Height	10.93	cm	Height	10.46	cm
Area	24.06	cm^2	Area		cm^2
Volume	262.87	cm^3	Volume		cm^3
Mass	563.40	gm	Mass	563.0	gm
Density	2.14	gm/cm^3	Density		g/cm^3

Results of Soxhlet Extraction

% water = % sand = % bitumen =

Results of Specific Gravity

G_s =

Grain Size Analysis

Size of Opening (mm)	Percent Finer than
2.000	
0.840	
0.420	
0.250	
0.149	
0.074	
0.044	

Hydrometer Analysis

D (mm)	Percent Finer than

After Test Sketch

Specimen Data Summary Sheet

Test Number: UFTCS4
Apparatus: Triaxial Cell

Specimen Dimensions

Before Test			After Test		
Diameter	5.42	cm	Diameter	5.49-5.59	cm
Height	10.92	cm	Height	10.75	cm
Area	23.09	cm^2	Area		cm^2
Volume	252.10	cm^3	Volume		cm^3
Mass	546.63	gm	Mass	555.0	gm
Density	2.17	gm/cm^3	Density		g/cm^3

Results of Soxhlet Extraction

% water = % sand = % bitumen =

Results of Specific Gravity G_s =

Grain Size Analysis

Size of Opening (mm)	Percent Finer than
2.000	
0.840	
0.420	
0.250	
0.149	
0.074	
0.044	

Hydrometer Analysis

D (mm)	Percent Finer than

After Test Sketch

Specimen Data Summary Sheet

Test Number: UFTCS5
Apparatus: Triaxial Cell

Specimen Dimensions

Before Test			After Test		
Diameter	5.43	cm	Diameter	5.48 - 5.71	cm
Height	10.74	cm	Height	10.30	cm
Area	23.12	cm^2	Area		cm^2
Volume	248.14	cm^3	Volume		cm^3
Mass	540.60	gm	Mass	539.3	gm
Density	2.18	gm/cm^3	Density		g/cm^3

Results of Soxhlet Extraction

% water = % sand = % bitumen =

Results of Specific Gravity

G_s =

Grain Size Analysis

Size of Opening (mm)	Percent Finer than
2.000	
0.840	
0.420	
0.250	
0.149	
0.074	
0.044	

Hydrometer Analysis

D (mm)	Percent Finer than

After Test Sketch

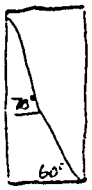

Specimen Data Summary Sheet

Test Number: UFTCS6
Apparatus: Triaxial Cell

Specimen Dimensions

Before Test			After Test		
Diameter	5.15	cm	Diameter	5.17 - 5.40	cm
Height	10.66	cm	Height	10.10	cm
Area	20.81	cm^2	Area		cm^2
Volume	221.86	cm^3	Volume		cm^3
Mass	460.35	gm	Mass	465.10	gm
Density	2.08	gm/cm^3	Density		g/cm^3

Results of Soxhlet Extraction

% water = % sand = % bitumen =

Results of Specific Gravity

G_s =

Grain Size Analysis

Size of Opening (mm)	Percent Finer than
2.000	
0.840	
0.420	
0.250	
0.149	
0.074	
0.044	

Hydrometer Analysis

D (mm)	Percent Finer than

After Test Sketch

Specimen Data Summary Sheet

Test Number: UFTCS7
Apparatus: Triaxial Cell

Specimen Dimensions

Before Test			After Test		
Diameter	5.12	cm	Diameter	5.15 - 5.28	cm
Height	10.22	cm	Height	10.06	cm
Area	20.62	cm^2	Area		cm^2
Volume	210.69	cm^3	Volume		cm^3
Mass	463.58	gm	Mass	467.53	gm
Density	2.20	gm/cm^3	Density		g/cm^3

Results of Soxhlet Extraction

% water = % sand = % bitumen =

Results of Specific Gravity

G_s =

Grain Size Analysis

Size of Opening (mm)	Percent Finer than
2.000	
0.840	
0.420	
0.250	
0.149	
0.074	
0.044	

Hydrometer Analysis

D (mm)	Percent Finer than

After Test Sketch

Specimen Data Summary Sheet

Test Number: UFHTTCS1
Apparatus: High Temperature Triaxial Cell

Specimen Dimensions

Before Test			After Test		
Diameter	5.40	cm	Diameter	5.38-5.46	cm
Height	10.95	cm	Height	0.26	cm
Area	22.86	cm^2	Area		cm^2
Volume	250.32	cm^3	Volume		cm^3
Mass	527.87	gm	Mass	518.30	gm
Density	2.11	gm/cm^3	Density		g/cm^3

Results of Soxhlet Extraction

% water = % sand = % bitumen =

Results of Specific Gravity

G_s =

Grain Size Analysis

Size of Opening (mm)	Percent Finer than
2.000	
0.840	
0.420	
0.250	
0.149	
0.074	
0.044	

Hydrometer Analysis

D (mm)	Percent Finer than

After Test Sketch

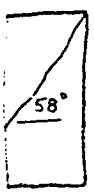

Specimen Data Summary Sheet

Test Number: UFHTTCS2
Apparatus: High Temperature Triaxial Cell

Specimen Dimensions

Before Test			After Test		
Diameter	5.40	cm	Diameter	5.32-5.37	cm
Height	10.82	cm	Height	9.76	cm
Area	22.87	cm^2	Area		cm^2
Volume	247.34	cm^3	Volume		cm^3
Mass	506.00	gm	Mass	479.69	gm
Density	2.05	gm/cm^3	Density		g/cm^3

Results of Soxhlet Extraction

% water = % sand = % bitumen =

Results of Specific Gravity

G_s =

Grain Size Analysis

Size of Opening (mm)	Percent Finer than
2.000	
0.840	
0.420	
0.250	
0.149	
0.074	
0.044	

Hydrometer Analysis

D (mm)	Percent Finer than

After Test Sketch

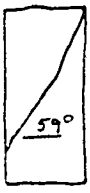

Specimen Data Summary Sheet

Test Number: UFHTTCS3
Apparatus: High Temperature Triaxial Cell

Specimen Dimensions

Before Test			After Test		
Diameter	5.40	cm	Diameter	5.30 - 5.35	cm
Height	10.83	cm	Height	10.00	cm
Area	22.90	cm^2	Area		cm^2
Volume	247.92	cm^3	Volume		cm^3
Mass	502.83	gm	Mass	480.16	gm
Density	2.03	gm/cm^3	Density		g/cm^3

Results of Soxhlet Extraction

% water = % sand = % bitumen =

Results of Specific Gravity G_s =

Grain Size Analysis

Size of Opening (mm)	Percent Finer than
2.000	
0.840	
0.420	
0.250	
0.149	
0.074	
0.044	

Hydrometer Analysis

D (mm)	Percent Finer than

After Test Sketch

Specimen Data Summary Sheet

Test Number: UFTL1
Apparatus: Triaxial Cell

Specimen Dimensions

Before Test			After Test	
Diameter	5.99	cm	Diameter	cm
Height	5.84	cm	Height	cm
Area	28.18	cm^2	Area	cm^2
Volume	164.58	cm^3	Volume	cm^3
Mass		gm	Mass	gm
Density		gm/cm^3	Density	g/cm^3

Results of Soxhlet Extraction

% water = % sand = % bitumen =

Results of Specific Gravity

G_s =

Grain Size Analysis

Size of Opening (mm)	Percent Finer than
2.000	
0.840	
0.420	
0.250	
0.149	
0.074	
0.044	

Hydrometer Analysis

D (mm)	Percent Finer than

After Test Sketch

Specimen Data Summary Sheet

Test Number: UFHTTL1
Apparatus: High Temperature Triaxial Cell

Specimen Dimensions

Before Test			After Test	
Diameter	5.40	cm	Diameter	cm
Height	10.99	cm	Height	cm
Area	22.90	cm^2	Area	cm^2
Volume	251.70	cm^3	Volume	cm^3
Mass	658.53	gm	Mass	gm
Density	2.59	gm/cm^3	Density	g/cm^3

Results of Soxhlet Extraction

% water = % sand = % bitumen =

Results of Specific Gravity G_s =

Grain Size Analysis

Size of Opening (mm)	Percent Finer than
2.000	
0.840	
0.420	
0.250	
0.149	
0.074	
0.044	

Hydrometer Analysis

D (mm)	Percent Finer than

After Test Sketch

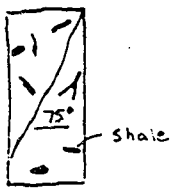

Specimen Data Summary Sheet

Test Number: UFTL2
Apparatus: Triaxial Cell

Specimen Dimensions

Before Test			After Test	
Diameter	5.20	cm	Diameter	cm
Height	5.15	cm	Height	cm
Area	21.21	cm^2	Area	cm^2
Volume	109.31	cm^3	Volume	cm^3
Mass	288.20	gm	Mass	gm
Density	2.64	gm/cm^3	Density	g/cm^3

Results of Soxhlet Extraction

% water = % sand = % bitumen =

Results of Specific Gravity

$G_s = 2.70$

Grain Size Analysis

Size of Opening (mm)	Percent Finer than
2.000	
0.840	
0.420	
0.250	
0.149	
0.074	
0.044	

Hydrometer Analysis

D (mm)	Percent Finer than

After Test Sketch

Specimen Data Summary Sheet

Test Number: CL1COS1
Apparatus: Consolidometer

Specimen Dimensions

Before Test			After Test	
Diameter	7.57	cm	Diameter	cm
Height	2.78	cm	Height	cm
Area	44.97	cm^2	Area	cm^2
Volume	125.16	cm^3	Volume	cm^3
Mass	223.43	gm	Mass	gm
Density	1.78	gm/cm^3	Density	g/cm^3

Results of Soxhlet Extraction

% water = 8.2 % sand = 84.5 % bitumen = 7.3

Results of Specific Gravity $G_s = 2.68$

Grain Size Analysis

Size of Opening (mm)	Percent Finer than
2.000	100.00
0.840	99.90
0.420	99.48
0.250	98.93
0.149	93.71
0.074	22.39
0.044	13.58

Hydrometer Analysis

D (mm)	Percent Finer than
0.083	33.55
0.062	21.06
0.046	16.48
0.032	12.87
0.024	10.92
0.017	8.24
0.0127	6.94
0.0092	5.29
0.0065	4.30
0.0046	3.98
0.0031	3.71
0.0026	3.50
0.00135	3.08

After Test Sketch

Specimen Data Summary Sheet

Test Number: CL1COS2
Apparatus: Consolidometer

Specimen Dimensions

Before Test			After Test	
Diameter	7.61	cm	Diameter	cm
Height	2.59	cm	Height	cm
Area	45.42	cm^2	Area	cm^2
Volume	117.50	cm^3	Volume	cm^3
Mass	213.83	gm	Mass	gm
Density	1.82	gm/cm^3	Density	g/cm^3

Results of Soxhlet Extraction

% water = 8.2 % sand = 84.5 % bitumen = 7.3

Results of Specific Gravity $G_s = 2.65$

Grain Size Analysis

Size of Opening (mm)	Percent Finer than
2.000	
0.840	100.00
0.420	99.98
0.250	98.80
0.149	30.10
0.074	5.43
0.044	3.63

Hydrometer Analysis

D (mm)	Percent Finer than
0.098	13.3
0.070	7.1
0.050	5.8
0.036	3.6
0.025	3.5
0.018	3.3
0.0132	3.2
0.0096	3.0
0.0067	2.9
0.0047	2.6
0.0033	2.5
0.0025	2.2
0.00135	2.1

After Test Sketch

Specimen Data Summary Sheet

Test Number: CL1COS3
Apparatus: Consolidometer

Specimen Dimensions

Before Test			After Test	
Diameter	7.60	cm	Diameter	cm
Height	2.56	cm	Height	cm
Area	45.36	cm^2	Area	cm^2
Volume	116.22	cm^3	Volume	cm^3
Mass	219.38	gm	Mass	gm
Density	1.88	gm/cm^3	Density	g/cm^3

Results of Soxhlet Extraction

% water = 9.9 % sand = 84.0 % bitumen = 6.1

Results of Specific Gravity $G_s = 2.66$

Grain Size Analysis

Size of Opening (mm)	Percent Finer than
2.000	
0.840	
0.420	100.00
0.250	99.96
0.149	96.21
0.074	19.37
0.044	12.81

Hydrometer Analysis

D (mm)	Percent Finer than
0.087	33.23
0.066	20.41
0.049	15.29
0.035	12.40
0.025	10.80
0.018	9.20
0.013	8.40
0.0094	7.11
0.0066	6.22
0.0047	5.32
0.0033	4.55
0.0025	4.45
0.00135	3.93

After Test Sketch

Specimen Data Summary Sheet

Test Number: CL1TOS1
Apparatus: Triaxial Cell

Specimen Dimensions

Before Test			After Test		
Diameter	5.08	cm	Diameter	4.97-5.48	cm
Height	10.18	cm	Height	9.25	cm
Area	20.23	cm^2	Area		cm^2
Volume	205.93	cm^3	Volume		cm^3
Mass	388.91	gm	Mass	395.33	gm
Density	1.89	gm/cm^3	Density		g/cm^3

Results of Soxhlet Extraction

% water = 10.0 % sand = 83.5 % bitumen = 6.5

Results of Specific Gravity

G_s = 2.68

Grain Size Analysis

Size of Opening (mm)	Percent Finer than
2.000	99.92
0.840	99.83
0.420	99.71
0.250	99.47
0.149	94.29
0.074	20.31
0.044	15.75

Hydrometer Analysis

D (mm)	Percent Finer than
0.080	37.48
0.065	20.13
0.047	16.38
0.033	14.30
0.024	12.91
0.017	12.35
0.013	11.94
0.0092	10.66
0.0065	9.79
0.0046	8.65
0.0032	7.88
0.0025	7.31
0.0013	6.47

After Test Sketch

Specimen Data Summary Sheet

Test Number: CL1TOS2
Apparatus: Triaxial Cell

Specimen Dimensions

Before Test			After Test		
Diameter	5.06	cm	Diameter	5.04 - 5.25	cm
Height	10.18	cm	Height	9.45	cm
Area	20.12	cm^2	Area		cm^2
Volume	204.87	cm^3	Volume		cm^3
Mass	388.03	gm	Mass	389.77	gm
Density	1.89	gm/cm^3	Density		g/cm^3

Results of Soxhlet Extraction

% water = 12.9 % sand = 82.6 % bitumen = 4.5

Results of Specific Gravity $G_s = 2.68$

Grain Size Analysis

Size of Opening (mm)	Percent Finer than
2.000	
0.840	100.00
0.420	99.90
0.250	99.50
0.149	93.41
0.074	29.13
0.044	22.31

Hydrometer Analysis

D (mm)	Percent Finer than
0.072	47.55
0.058	32.29
0.041	26.05
0.032	22.58
0.022	21.06
0.016	19.61
0.012	18.62
0.0087	16.77
0.0062	15.63
0.0044	13.32
0.0032	11.61
0.0022	10.43
0.0013	8.32

After Test Sketch

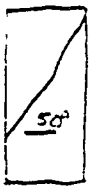

Specimen Data Summary Sheet

Test Number: CL1TOS3
Apparatus: Triaxial Cell

Specimen Dimensions

Before Test			After Test		
Diameter	5.02	cm	Diameter	5.02-5.06	cm
Height	10.08	cm	Height	10.20	cm
Area	19.82	cm^2	Area		cm^2
Volume	199.90	cm^3	Volume		cm^3
Mass	379.35	gm	Mass	392.65	gm
Density	1.90	gm/cm^3	Density		g/cm^3

Results of Soxhlet Extraction

% water = 7.3 % sand = 83.5 % bitumen = 9.2

Results of Specific Gravity $G_s = 2.69$

Grain Size Analysis

Size of Opening (mm)	Percent Finer than
2.000	
0.840	100.00
0.420	99.98
0.250	99.76
0.149	95.23
0.074	29.08
0.044	21.27

Hydrometer Analysis

D (mm)	Percent Finer than
0.077	341.36
0.060	28.90
0.045	24.75
0.032	20.73
0.023	17.83
0.015	14.37
0.012	13.67
0.0090	10.77
0.0063	9.92
0.0046	8.26
0.0033	6.89
0.0023	6.06
0.0013	5.20

After Test Sketch

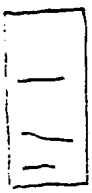

No visible shear planes
Horizontal cracks

Specimen Data Summary Sheet

Test Number: CL1TOS4
Apparatus: Triaxial Cell

Specimen Dimensions

Before Test			After Test		
Diameter	5.07	cm	Diameter	4.97 - 5.07	cm
Height	10.07	cm	Height	9.29	cm
Area	20.19	cm^2	Area		cm^2
Volume	203.30	cm^3	Volume		cm^3
Mass	370.87	gm	Mass	365.75	gm
Density	1.82	gm/cm^3	Density		g/cm^3

Results of Soxhlet Extraction

% water = 8.9 % sand = 81.7 % bitumen = 9.4

Results of Specific Gravity $G_s = 2.69$

Grain Size Analysis

Size of Opening (mm)	Percent Finer than
2.000	100.00
0.840	99.97
0.420	99.90
0.250	99.77
0.149	92.38
0.074	16.80
0.044	9.71

Hydrometer Analysis

D (mm)	Percent Finer than
0.083	33.35
0.068	15.35
0.050	12.58
0.035	10.50
0.025	10.08
0.018	9.72
0.013	8.55
0.0093	6.86
0.0065	6.20
0.0047	5.37
0.0033	5.17
0.0027	4.89
0.0014	4.53

After Test Sketch

No visible shear planes
Buckling of specimen

Specimen Data Summary Sheet

Test Number: CL1TOS5
Apparatus: Triaxial Cell

Specimen Dimensions

Before Test			After Test		
Diameter	5.08	cm	Diameter	4.96 - 5.04	cm
Height	10.20	cm	Height	9.72	cm
Area	20.27	cm^2	Area		cm^2
Volume	206.74	cm^3	Volume		cm^3
Mass	378.02	gm	Mass	377.02	gm
Density	1.83	gm/cm^3	Density		g/cm^3

Results of Soxhlet Extraction

% water = 7.2 % sand = 82.6 % bitumen = 10.2

Results of Specific Gravity $G_s = 2.69$

Grain Size Analysis

Size of Opening (mm)	Percent Finer than
2.000	100.00
0.840	99.97
0.420	99.90
0.250	99.77
0.149	92.38
0.074	16.80
0.044	9.71

Hydrometer Analysis

D (mm)	Percent Finer than
0.083	33.35
0.068	15.35
0.050	12.58
0.035	10.50
0.025	10.08
0.018	9.72
0.013	8.55
0.0093	6.86
0.0065	6.20
0.0047	5.37
0.0033	5.17
0.0027	4.89
0.0014	4.53

After Test Sketch

Specimen Data Summary Sheet

Test Number: CL1TOS6
Apparatus: Triaxial Cell

Specimen Dimensions

Before Test			After Test		
Diameter	5.09	cm	Diameter	5.09-5.45	cm
Height	10.24	cm	Height	9.92	cm
Area	20.31	cm^2	Area		cm^2
Volume	207.86	cm^3	Volume		cm^3
Mass	382.20	gm	Mass	394.84	gm
Density	1.83	gm/cm^3	Density		g/cm^3

Results of Soxhlet Extraction

% water = 12.6 % sand = 81.5 % bitumen = 5.9

Results of Specific Gravity $G_s = 2.65$

Grain Size Analysis

Size of Opening (mm)	Percent Finer than
2.000	
0.840	
0.420	100.00
0.250	99.55
0.149	91.25
0.074	33.24
0.044	28.90

Hydrometer Analysis

D (mm)	Percent Finer than
0.078	40.35
0.057	34.76
0.042	31.41
0.030	29.03
0.021	26.52
0.015	24.85
0.010	21.54
0.0083	20.53
0.0058	18.13
0.0043	16.38
0.0031	14.40
0.0023	13.28
0.0013	10.71

After Test Sketch

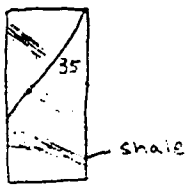

Specimen Data Summary Sheet

Test Number: CL1TOS7
Apparatus: Triaxial Cell

Specimen Dimensions

Before Test			After Test		
Diameter	5.07	cm	Diameter	4.98-5.18	cm
Height	10.41	cm	Height	10.38	cm
Area	20.15	cm^2	Area		cm^2
Volume	209.75	cm^3	Volume		cm^3
Mass	387.23	gm	Mass	395.55	gm
Density	1.85	gm/cm^3	Density		g/cm^3

Results of Soxhlet Extraction

% water = 9.3 % sand = 81.4 % bitumen = 9.3

Results of Specific Gravity

$G_s = 2.67$

Grain Size Analysis

Size of Opening (mm)	Percent Finer than
2.000	
0.840	100.00
0.420	99.99
0.250	99.41
0.149	69.77
0.074	9.43
0.044	6.57

Hydrometer Analysis

D (mm)	Percent Finer than
0.087	25.90
0.068	11.44
0.049	9.22
0.033	8.11
0.025	7.55
0.018	6.44
0.013	5.74
0.0093	5.16
0.0066	4.81
0.0047	4.39
0.0033	3.93
0.0025	3.77
0.0013	3.42

After Test Sketch

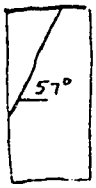

Specimen Data Summary Sheet

Test Number: CL1TOS8
Apparatus: Triaxial Cell

Specimen Dimensions

Before Test			After Test		
Diameter	5.09	cm	Diameter	5.09 - 5.28	cm
Height	10.18	cm	Height	9.82	cm
Area	20.32	cm^2	Area		cm^2
Volume	206.82	cm^3	Volume		cm^3
Mass	381.41	gm	Mass	384.48	gm
Density	1.84	gm/cm^3	Density		g/cm^3

Results of Soxhlet Extraction

% water = 12.8 % sand = 82.0 % bitumen = 5.2

Results of Specific Gravity $G_s = 2.68$

Grain Size Analysis

Size of Opening (mm)	Percent Finer than
2.000	100.00
0.840	99.77
0.420	99.75
0.250	99.51
0.149	94.47
0.074	48.54
0.044	43.61

Hydrometer Analysis

D (mm)	Percent Finer than
0.067	50.99
0.048	48.22
0.036	45.45
0.027	41.58
0.019	39.78
0.014	36.55
0.011	33.51
0.0078	30.42
0.0056	27.31
0.0040	24.48
0.0029	22.27
0.0022	19.87
0.0013	15.75

After Test Sketch

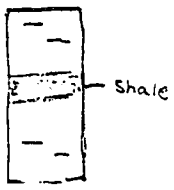

No visible shear plane

Specimen Data Summary Sheet

Test Number: CL1TOS9
Apparatus: Triaxial Cell

Specimen Dimensions

Before Test			After Test		
Diameter	5.07	cm	Diameter	4.95 - 5.10	cm
Height	10.42	cm	Height	10.10	cm
Area	20.20	cm^2	Area		cm^2
Volume	210.56	cm^3	Volume		cm^3
Mass	384.50	gm	Mass	384.78	gm
Density	1.83	gm/cm^3	Density		g/cm^3

Results of Soxhlet Extraction

% water = 8.2 % sand = 81.1 % bitumen = 10.7

Results of Specific Gravity $G_s = 2.68$

Grain Size Analysis

Size of Opening (mm)	Percent Finer than
2.000	100.00
0.840	99.97
0.420	99.89
0.250	99.74
0.149	92.84
0.074	18.72
0.044	13.07

Hydrometer Analysis

D (mm)	Percent Finer than
0.080	34.60
0.063	21.42
0.048	15.45
0.034	12.68
0.024	11.71
0.017	10.29
0.013	8.77
0.0092	7.77
0.0064	6.94
0.0046	6.13
0.0032	5.58
0.0026	5.30
0.0013	4.33

After Test Sketch

No visible shear plane

Specimen Data Summary Sheet

Test Number: CL1TOS10
Apparatus: Triaxial Cell

Specimen Dimensions

Before Test			After Test		
Diameter	5.09	cm	Diameter	4.94-5.27	cm
Height	9.94	cm	Height	9.46	cm
Area	20.31	cm^2	Area		cm^2
Volume	201.86	cm^3	Volume		cm^3
Mass	377.38	gm	Mass	380.75	gm
Density	1.87	gm/cm^3	Density		g/cm^3

Results of Soxhlet Extraction

% water = 9.9 % sand = 82.9 % bitumen = 7.2

Results of Specific Gravity $G_s = 2.67$

Grain Size Analysis

Size of Opening (mm)	Percent Finer than
2.000	
0.840	
0.420	100.00
0.250	99.94
0.149	89.76
0.074	20.38
0.044	14.18

Hydrometer Analysis

D (mm)	Percent Finer than
0.085	37.38
0.065	22.99
0.048	16.76
0.035	14.20
0.024	12.92
0.018	9.88
0.013	7.32
0.0095	6.52
0.0067	5.69
0.0047	5.18
0.0034	4.81
0.0025	4.59
0.0014	4.27

After Test Sketch

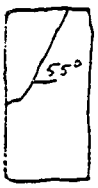

Specimen Data Summary Sheet

Test Number: CL1TOS11
Apparatus: Triaxial Cell

Specimen Dimensions

Before Test			After Test		
Diameter	5.38	cm	Diameter	5.24-5.31	cm
Height	10.17	cm	Height	9.71	cm
Area	22.76	cm^2	Area		cm^2
Volume	231.45	cm^3	Volume		cm^3
Mass	426.82	gm	Mass	421.67	gm
Density	1.84	gm/cm^3	Density		g/cm^3

Results of Soxhlet Extraction

% water = 7.4 % sand = 82.7 % bitumen = 9.9

Results of Specific Gravity $G_s = 2.68$

Grain Size Analysis

Size of Opening (mm)	Percent Finer than
2.000	100.00
0.840	99.99
0.420	99.94
0.250	99.55
0.149	79.87
0.074	14.00
0.044	8.83

Hydrometer Analysis

D (mm)	Percent Finer than
0.085	29.85
0.065	17.37
0.049	12.23
0.036	8.77
0.023	4.19
0.018	3.50
0.013	2.43
0.0095	2.43
0.0067	2.36
0.0047	2.33
0.0033	2.19
0.0025	2.01
0.0013	2.08

After Test Sketch

No visible shear plane

Specimen Data Summary Sheet

Test Number: CL1TOS12
Apparatus: Triaxial Cell

Specimen Dimensions

Before Test			After Test		
Diameter	5.38	cm	Diameter	5.34-5.39	cm
Height	10.62	cm	Height	10.62	cm
Area	22.69	cm^2	Area		cm^2
Volume	240.91	cm^3	Volume		cm^3
Mass	443.65	gm	Mass	436.75	gm
Density	1.84	gm/cm^3	Density		g/cm^3

Results of Soxhlet Extraction

% water = 7.8 % sand = 82.6 % bitumen = 9.7

Results of Specific Gravity $G_s = 2.68$

Grain Size Analysis

Size of Opening (mm)	Percent Finer than
2.000	
0.840	100.00
0.420	99.94
0.250	99.61
0.149	81.61
0.074	12.85
0.044	7.55

Hydrometer Analysis

D (mm)	Percent Finer than
0.085	28.88
0.067	13.62
0.049	10.84
0.036	8.07
0.025	5.02
0.018	4.05
0.013	3.63
0.0096	3.63
0.0067	3.33
0.0047	2.84
0.0033	2.75
0.0027	2.77
0.0013	2.77

After Test Sketch

Specimen Data Summary Sheet

Test Number: CL1TOS13
Apparatus: Triaxial Cell

Specimen Dimensions

Before Test			After Test		
Diameter	5.39	cm	Diameter	5.40-5.75	cm
Height	10.69	cm	Height	9.75	cm
Area	22.83	cm^2	Area		cm^2
Volume	243.98	cm^3	Volume		cm^3
Mass	472.99	gm	Mass	449.91	gm
Density	1.95	gm/cm^3	Density		g/cm^3

Results of Soxhlet Extraction

% water = 10.2 % sand = 83.6 % bitumen = 6.2

Results of Specific Gravity

G_s = 2.69

Grain Size Analysis

Size of Opening (mm)	Percent Finer than
2.000	100.00
0.840	99.99
0.420	99.94
0.250	99.61
0.149	84.17
0.074	21.10
0.044	13.30

Hydrometer Analysis

D (mm)	Percent Finer than
0.081	30.82
0.063	22.86
0.046	16.22
0.035	7.09
0.025	3.90
0.018	3.49
0.013	3.00
0.0095	2.70
0.0066	2.52
0.0047	2.33
0.0033	2.33
0.0028	2.28
0.0013	2.28

After Test Sketch

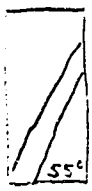

Specimen Data Summary Sheet

Test Number: CL1TOS14
Apparatus: Triaxial Cell

Specimen Dimensions

Before Test			After Test		
Diameter	5.39	cm	Diameter	5.28 - 5.38	cm
Height	10.81	cm	Height	9.62	cm
Area	22.79	cm^2	Area		cm^2
Volume	246.27	cm^3	Volume		cm^3
Mass	424.72	gm	Mass	438.38	gm
Density	1.73	gm/cm^3	Density		g/cm^3

Results of Soxhlet Extraction

% water = 8.3 % sand = 81.2 % bitumen = 10.4

Results of Specific Gravity $G_s = 2.69$

Grain Size Analysis

Size of Opening (mm)	Percent Finer than
2.000	100.00
0.840	99.99
0.420	99.97
0.250	99.81
0.149	81.60
0.074	10.37
0.044	7.10

Hydrometer Analysis

D (mm)	Percent Finer than
0.085	28.96
0.067	12.32
0.049	9.86
0.035	8.33
0.025	7.09
0.018	6.67
0.013	6.12
0.0094	5.26
0.0066	4.84
0.0047	4.25
0.0033	3.70
0.0025	3.29
0.0014	2.84

After Test Sketch

No visual shear plane
Specimen barrelled at top

Specimen Data Summary Sheet

Test Number: CL1TOS15
Apparatus: Triaxial Cell

Specimen Dimensions

Before Test			After Test	
Diameter	7.61	cm	Diameter	cm
Height	15.12	cm	Height	cm
Area	45.52	cm^2	Area	cm^2
Volume	688.47	cm^3	Volume	cm^3
Mass	1325.1	gm	Mass	gm
Density	1.93	gm/cm^3	Density	g/cm^3

Results of Soxhlet Extraction

% water = 8.9 % sand = 83.3 % bitumen = 7.8

Results of Specific Gravity $G_s = 2.64$

Grain Size Analysis

Size of Opening (mm)	Percent Finer than
2.000	100.00
0.840	99.97
0.420	99.80
0.250	99.10
0.149	96.38
0.074	30.50
0.044	19.26

Hydrometer Analysis

D (mm)	Percent Finer than
0.075	48.80
0.062	29.21
0.047	22.50
0.034	19.56
0.024	17.32
0.017	15.47
0.013	15.05
0.0092	13.24
0.0064	11.19
0.0046	9.37
0.0033	7.99
0.0025	7.48
0.0014	6.60

After Test Sketch

Specimen Data Summary Sheet

Test Number: CL2COS1
Apparatus: Consolidometer

Specimen Dimensions

Before Test			After Test	
Diameter	7.54	cm	Diameter	cm
Height	2.93	cm	Height	cm
Area	44.65	cm^2	Area	cm^2
Volume	130.83	cm^3	Volume	cm^3
Mass	232.74	gm	Mass	gm
Density	1.78	gm/cm^3	Density	g/cm^3

Results of Soxhlet Extraction

% water = 7.8 % sand = 81.1 % bitumen = 11.1

Results of Specific Gravity $G_s = 2.69$

Grain Size Analysis

Size of Opening (mm)	Percent Finer than
2.000	100.00
0.840	99.98
0.420	99.82
0.250	78.39
0.149	19.90
0.074	9.97
0.044	8.84

Hydrometer Analysis

D (mm)	Percent Finer than
0.097	14.54
0.067	10.11
0.048	8.86
0.033	8.17
0.024	8.03
0.017	7.72
0.013	7.27
0.0090	7.07
0.0064	6.41
0.0046	5.66
0.0033	4.71
0.0025	4.02
0.0008	3.41

After Test Sketch

Specimen Data Summary Sheet

Test Number: CL2TOS1
Apparatus: Triaxial Cell

Specimen Dimensions

Before Test			After Test		
Diameter	5.16	cm	Diameter	4.78-5.23	cm
Height	10.09	cm	Height	8.75	cm
Area	20.91	cm^2	Area		cm^2
Volume	210.99	cm^3	Volume		cm^3
Mass	351.95	gm	Mass	354.20	gm
Density	1.67	gm/cm^3	Density		g/cm^3

Results of Soxhlet Extraction

% water = 8.4 % sand = 81.9 % bitumen = 9.7

Results of Specific Gravity

$G_s = 2.69$

Grain Size Analysis

Size of Opening (mm)	Percent Finer than
2.000	
0.840	100.00
0.420	99.89
0.250	79.70
0.149	18.07
0.074	10.62
0.044	8.97

Hydrometer Analysis

D (mm)	Percent Finer than
0.097	14.25
0.068	11.17
0.045	10.61
0.035	9.77
0.024	8.51
0.017	8.23
0.013	8.09
0.0092	7.94
0.0065	6.97
0.0046	6.54
0.0033	5.74
0.0025	5.56
0.00135	5.22

After Test Sketch

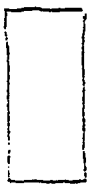

Specimen Data Summary Sheet

Test Number: CL2TOS2
Apparatus: Triaxial Cell

Specimen Dimensions

Before Test			After Test	
Diameter	5.13	cm	Diameter	cm
Height	10.28	cm	Height	cm
Area	20.67	cm^2	Area	cm^2
Volume	212.48	cm^3	Volume	cm^3
Mass	378.33	gm	Mass	gm
Density	1.78	gm/cm^3	Density	g/cm^3

Results of Soxhlet Extraction

% water = 8.4 % sand = 81.9 % bitumen = 9.7

Results of Specific Gravity $G_s = 2.64$

Grain Size Analysis

Size of Opening (mm)	Percent Finer than
2.000	
0.840	100.00
0.420	99.89
0.250	79.70
0.149	18.07
0.074	10.62
0.044	8.97

Hydrometer Analysis

D (mm)	Percent Finer than
0.097	14.25
0.068	11.17
0.045	10.61
0.035	9.77
0.024	8.51
0.017	8.23
0.013	8.09
0.0092	7.94
0.0065	6.97
0.0046	6.54
0.0033	5.74
0.0025	5.56
0.00135	5.22

After Test Sketch

Specimen Data Summary Sheet

Test Number: CL2TOS3
Apparatus: Triaxial Cell

Specimen Dimensions

Before Test			After Test	
Diameter	5.07	cm	Diameter	cm
Height	10.46	cm	Height	cm
Area	20.19	cm^2	Area	cm^2
Volume	211.07	cm^3	Volume	cm^3
Mass	351.00	gm	Mass	gm
Density	1.66	gm/cm^3	Density	g/cm^3

Results of Soxhlet Extraction

% water = 6.7 % sand = 81.0 % bitumen = 12.3

Results of Specific Gravity $G_s = 2.77$

Grain Size Analysis

Size of Opening (mm)	Percent Finer than
2.000	
0.840	100.00
0.420	99.86
0.250	73.24
0.149	13.32
0.074	10.62
0.044	5.78

Hydrometer Analysis

D (mm)	Percent Finer than
0.090	5.70
0.066	5.38
0.047	4.92
0.034	4.18
0.024	3.68
0.017	3.04
0.013	2.37
0.0090	2.01
0.0065	1.62
0.0046	1.48
0.0033	1.23
0.0025	1.06
0.00135	0.94

After Test Sketch

Specimen Data Summary Sheet

Test Number: CL2TOS4
Apparatus: Triaxial Cell

Specimen Dimensions

Before Test			After Test		
Diameter	5.37	cm	Diameter	5.15 - 5.20	cm
Height	10.68	cm	Height	10.03	cm
Area	22.65	cm^2	Area		cm^2
Volume	241.89	cm^3	Volume		cm^3
Mass	433.94	gm	Mass	430.58	gm
Density	1.79	gm/cm^3	Density		g/cm^3

Results of Soxhlet Extraction

% water = 8.2 % sand = 81.1 % bitumen = 10.7

Results of Specific Gravity

G_s = 2.66

Grain Size Analysis

Size of Opening (mm)	Percent Finer than
2.000	
0.840	100.00
0.420	99.77
0.250	76.77
0.149	16.46
0.074	8.37
0.044	6.75

Hydrometer Analysis

D (mm)	Percent Finer than
0.095	15.68
0.068	9.41
0.050	8.29
0.035	7.59
0.024	7.18
0.017	6.69
0.012	6.17
0.0093	5.71
0.0065	5.17
0.0047	4.88
0.0033	4.60
0.0025	3.94
0.00145	3.72

After Test Sketch

No visible shear planes

Specimen Data Summary Sheet

Test Number: CL3COS1
Apparatus: Consolidometer

Specimen Dimensions

Before Test			After Test	
Diameter	7.06	cm	Diameter	cm
Height	2.54	cm	Height	cm
Area	45.37	cm^2	Area	cm^2
Volume	115.23	cm^3	Volume	cm^3
Mass	223.00	gm	Mass	gm
Density	1.94	gm/cm^3	Density	g/cm^3

Results of Soxhlet Extraction

% water = 8.9 % sand = 85.1 % bitumen = 6.0

Results of Specific Gravity

G_s = 2.65

Grain Size Analysis

Size of Opening (mm)	Percent Finer than
2.000	
0.840	100.00
0.420	99.95
0.250	73.06
0.149	15.00
0.074	9.98
0.044	

Hydrometer Analysis

D (mm)	Percent Finer than
0.086	31.66
0.067	15.60
0.049	12.22
0.035	9.33
0.025	8.37
0.018	7.56
0.013	6.76
0.0095	5.96
0.0065	5.72
0.0047	4.50
0.0038	3.60
0.0025	3.15
0.0014	2.51

After Test Sketch

Specimen Data Summary Sheet

Test Number: CL3COS2
Apparatus: Triaxial Cell

Specimen Dimensions

Before Test			After Test	
Diameter	7.59	cm	Diameter	cm
Height	2.54	cm	Height	cm
Area	45.25	cm^2	Area	cm^2
Volume	114.70	cm^3	Volume	cm^3
Mass	221.50	gm	Mass	gm
Density	1.93	gm/cm^3	Density	g/cm^3

Results of Soxhlet Extraction

% water = 6.4 % sand = 84.6 % bitumen = 9.0

Results of Specific Gravity $G_s = 2.65$

Grain Size Analysis

Size of Opening (mm)	Percent Finer than
2.000	
0.840	100.00
0.420	99.92
0.250	99.55
0.149	72.51
0.074	19.74
0.044	13.43

Hydrometer Analysis

D (mm)	Percent Finer than
0.088	31.70
0.067	18.05
0.048	12.91
0.035	10.82
0.024	9.38
0.018	8.42
0.013	7.29
0.0094	6.49
0.0065	6.20
0.0047	4.66
0.0033	4.60
0.0025	3.95
0.00136	2.65

After Test Sketch

Specimen Data Summary Sheet

Test Number: CL3CO33
Apparatus: Triaxial Cell

Specimen Dimensions

Before Test			After Test	
Diameter	7.61	cm	Diameter	cm
Height	2.55	cm	Height	cm
Area	45.48	cm^2	Area	cm^2
Volume	115.85	cm^3	Volume	cm^3
Mass	244.11	gm	Mass	gm
Density	2.11	gm/cm^3	Density	g/cm^3

Results of Soxhlet Extraction

% water = 11.7 % sand = 84.4 % bitumen = 3.9

Results of Specific Gravity $G_s = 2.67$

Grain Size Analysis

Size of Opening (mm)	Percent Finer than
2.000	100.00
0.840	99.99
0.420	99.85
0.250	99.29
0.149	68.07
0.074	27.09
0.044	21.73

Hydrometer Analysis

D (mm)	Percent Finer than
0.087	31.27
0.062	27.80
0.045	22.95
0.033	19.90
0.023	18.65
0.017	16.85
0.012	15.43
0.0089	14.05
0.0063	12.11
0.0045	10.69
0.0033	9.61
0.0024	8.83
0.0013	7.52

After Test Sketch

Specimen Data Summary Sheet

Test Number: CL3COS4
Apparatus: Consolidometer

Specimen Dimensions

Before Test			After Test	
Diameter	7.57	cm	Diameter	cm
Height	2.55	cm	Height	cm
Area	45.05	cm^2	Area	cm^2
Volume	114.92	cm^3	Volume	cm^3
Mass	221.50	gm	Mass	gm
Density	1.93	gm/cm^3	Density	g/cm^3

Results of Soxhlet Extraction

% water = 12.3 % sand = 84.5 % bitumen = 3.2

Results of Specific Gravity $G_s = 2.61$

Grain Size Analysis

Size of Opening (mm)	Percent Finer than
2.000	
0.840	100.00
0.420	99.92
0.250	98.75
0.149	73.87
0.074	29.48
0.044	23.02

Hydrometer Analysis

D (mm)	Percent Finer than
0.078	42.99
0.062	29.58
0.045	24.36
0.033	20.98
0.023	19.14
0.017	17.56
0.012	16.25
0.0089	14.67
0.0064	13.01
0.0046	10.99
0.0033	9.17
0.0025	8.89
0.0008	6.43

After Test Sketch

Specimen Data Summary Sheet

Test Number: CL3TOS1
Apparatus: High Temperature Triaxial Cell

Specimen Dimensions

Before Test			After Test	
Diameter	4.99	cm	Diameter	cm
Height	10.06	cm	Height	cm
Area	19.56	cm^2	Area	cm^2
Volume	196.70	cm^3	Volume	cm^3
Mass	368.00	gm	Mass	gm
Density	1.87	gm/cm^3	Density	g/cm^3

Results of Soxhlet Extraction

% water = 8.9 % sand = 83.1 % bitumen = 8.0

Results of Specific Gravity $G_s = 2.65$

Grain Size Analysis

Size of Opening (mm)	Percent Finer than
2.000	
0.840	100.00
0.420	99.88
0.250	97.72
0.149	54.30
0.074	14.24
0.044	
0.0015	

Hydrometer Analysis

D (mm)	Percent Finer than
0.086	13.02
0.062	12.16
0.046	10.03
0.034	7.89
0.022	5.75
0.016	4.63
0.012	3.51
0.0083	2.76
0.0068	2.34
0.0055	2.13
0.0048	1.92
0.0039	1.71
0.0030	1.53
	0.97

After Test Sketch

Specimen Data Summary Sheet

Test Number: CL3TOS2
Apparatus: High Temperature Triaxial Cell

Specimen Dimensions

Before Test			After Test		
Diameter	5.38	cm	Diameter	5.26-5.31	cm
Height	10.83	cm	Height	10.41	cm
Area	22.69	cm^2	Area		cm^2
Volume	245.74	cm^3	Volume		cm^3
Mass	467.31	gm	Mass	454.84	gm
Density	1.90	gm/cm^3	Density		g/cm^3

Results of Soxhlet Extraction

% water = 10.4 % sand = 81.8 % bitumen = 7.9

Results of Specific Gravity $G_s = 2.68$

Grain Size Analysis

Size of Opening (mm)	Percent Finer than
2.000	
0.840	100.00
0.420	99.90
0.250	99.30
0.149	55.63
0.074	16.70
0.044	12.43

Hydrometer Analysis

D (mm)	Percent Finer than
0.085	26.47
0.065	16.76
0.046	13.98
0.034	12.59
0.024	11.76
0.017	11.49
0.012	10.38
0.0088	9.64
0.0062	7.59
0.0045	7.01
0.0031	6.59
0.0024	5.90
0.0013	5.08

After Test Sketch

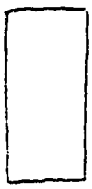

No visible shear planes

Specimen Data Summary Sheet

Test Number: CL4COS1
Apparatus: Consolidometer

Specimen Dimensions

Before Test			After Test		
Diameter	7.57	cm	Diameter	7.62	cm
Height	2.54	cm	Height	2.24	cm
Area	44.97	cm^2	Area	45.60	cm^2
Volume	114.22	cm^3	Volume	102.15	cm^3
Mass	213.00	gm	Mass	200.50	gm
Density	1.87	gm/cm^3	Density	1.96	g/cm^3

Results of Soxhlet Extraction

% water = 8.6 % sand = 82.0 % bitumen = 9.4

Results of Specific Gravity $G_s = 2.69$

Grain Size Analysis

Size of Opening (mm)	Percent Finer than
2.000	99.98
0.840	99.96
0.420	99.93
0.250	99.90
0.149	99.08
0.074	25.99
0.044	17.08

Hydrometer Analysis

D (mm)	Percent Finer than
0.087	29.86
0.063	25.01
0.047	17.39
0.035	15.45
0.024	14.34
0.017	13.65
0.013	11.96
0.0090	10.78
0.0064	9.88
0.0045	8.47
0.0032	8.22
0.0024	7.62
0.0014	6.82

After Test Sketch

Specimen Data Summary Sheet

Test Number: CL4COS2
Apparatus: Consolidometer

Specimen Dimensions

Before Test

Diameter	7.57	cm
Height	2.55	cm
Area	44.97	cm^2
Volume	114.82	cm^3
Mass	214.00	gm
Density	1.86	gm/cm^3

After Test

Diameter	7.62	cm
Height	2.28	cm
Area	45.60	cm^2
Volume	103.98	cm^3
Mass	204.15	gm
Density	1.96	g/cm^3

Results of Soxhlet Extraction

% water = 12.4 % sand = 84.8 % bitumen = 2.8

Results of Specific Gravity $G_s = 2.67$

Grain Size Analysis

Size of Opening (mm)	Percent Finer than
2.000	100.00
0.840	99.98
0.420	99.97
0.250	99.93
0.149	99.40
0.074	43.29
0.044	24.31

Hydrometer Analysis

D (mm)	Percent Finer than
0.072	49.87
0.057	36.72
0.044	27.00
0.033	20.64
0.024	17.04
0.017	15.65
0.012	13.49
0.0090	11.67
0.0065	10.77
0.0046	9.44
0.0033	7.89
0.0025	7.11
0.0014	6.15

After Test Sketch

Specimen Data Summary Sheet

Test Number: CL4COS3
Apparatus: Consolidometer

Specimen Dimensions

Before Test			After Test		
Diameter	7.58	cm	Diameter	7.62	cm
Height	2.68	cm	Height	2.40	cm
Area	45.21	cm^2	Area	45.60	cm^2
Volume	121.16	cm^3	Volume	109.36	cm^3
Mass	228.00	gm	Mass	215.20	gm
Density	1.88	gm/cm^3	Density	1.97	g/cm^3

Results of Soxhlet Extraction

% water = 11.4 % sand = 85.4 % bitumen = 3.2

Results of Specific Gravity

$G_s = 2.68$

Grain Size Analysis

Size of Opening (mm)	Percent Finer than
2.000	100.00
0.840	99.90
0.420	99.52
0.250	98.33
0.149	95.51
0.074	41.11
0.044	

Hydrometer Analysis

D (mm)	Percent Finer than
0.077	35.45
0.057	30.33
0.043	22.72
0.032	16.96
0.021	12.48
0.016	9.41
0.011	7.49
0.0076	6.3
0.0062	5.25
0.0052	4.33
0.0045	3.94
0.0015	2.18

After Test Sketch

Specimen Data Summary Sheet

Test Number: CL4COS4
Apparatus: Consolidometer

Specimen Dimensions

Before Test			After Test		
Diameter	7.58	cm	Diameter	7.62	cm
Height	2.71	cm	Height	2.39	cm
Area	45.16	cm^2	Area	45.60	cm^2
Volume	122.25	cm^3	Volume	108.99	cm^3
Mass	229.00	gm	Mass	218.20	gm
Density	1.87	gm/cm^3	Density	2.00	g/cm^3

Results of Soxhlet Extraction

% water = 11.4 % sand = 85.4 % bitumen = 3.2

Results of Specific Gravity $G_s = 2.67$

Grain Size Analysis

Size of Opening (mm)	Percent Finer than
2.000	100.00
0.840	99.90
0.420	99.52
0.250	98.33
0.149	95.51
0.074	41.11
0.044	

Hydrometer Analysis

D (mm)	Percent Finer than
0.077	35.45
0.057	30.33
0.043	22.72
0.032	16.96
0.021	12.48
0.016	9.41
0.011	7.49
0.0076	6.3
0.0062	5.25
0.0052	4.33
0.0045	3.94
0.0015	2.18

After Test Sketch

Specimen Data Summary Sheet

Test Number: CL4TOS1
Apparatus: High Temperature Triaxial Cell

Specimen Dimensions

Before Test			After Test		
Diameter	5.05	cm	Diameter	5.03 - 5.12	cm
Height	10.28	cm	Height	9.84	cm
Area	20.01	cm^2	Area		cm^2
Volume	205.56	cm^3	Volume		cm^3
Mass	398.00	gm	Mass	398.05	gm
Density	1.94	gm/cm^3	Density		g/cm^3

Results of Soxhlet Extraction

% water = 9.5 % sand = 82.6 % bitumen = 7.9

Results of Specific Gravity

G_s = 2.70

Grain Size Analysis

Size of Opening (mm)	Percent Finer than
2.000	
0.840	
0.420	100.00
0.250	99.98
0.149	93.62
0.074	22.02
0.044	

Hydrometer Analysis

D (mm)	Percent Finer than
0.079	19.84
0.055	17.42
0.044	12.99
0.032	10.96
0.021	9.34
0.015	8.13
0.011	7.08
0.0077	6.20
0.0064	5.67
0.0043	5.16
0.0036	4.76
0.0031	4.46
0.0013	3.23

After Test Sketch

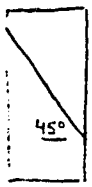

Specimen Data Summary Sheet

Test Number: CL4TOS2
Apparatus: High Temperature Triaxial Cell

Specimen Dimensions

Before Test			After Test		
Diameter	5.03	cm	Diameter	4.92-5.21	cm
Height	10.12	cm	Height	9.75	cm
Area	19.83	cm^2	Area		cm^2
Volume	200.70	cm^3	Volume		cm^3
Mass	379.25	gm	Mass	385.49	gm
Density	1.89	gm/cm^3	Density		g/cm^3

Results of Soxhlet Extraction

% water = 10.7 % sand = 82.0 % bitumen = 7.3

Results of Specific Gravity $G_s = 2.68$

Grain Size Analysis

Size of Opening (mm)	Percent Finer than
2.000	
0.840	
0.420	100.00
0.250	99.87
0.149	96.80
0.074	34.70
0.044	19.25

Hydrometer Analysis

D (mm)	Percent Finer than
0.076	44.40
0.058	31.92
0.044	22.76
0.033	18.05
0.022	15.27
0.017	13.33
0.013	11.53
0.0089	10.14
0.0062	9.04
0.0045	7.96
0.0032	6.94
0.0024	6.66
0.0013	5.06

After Test Sketch

Specimen Data Summary Sheet

Test Number: CL4TOS3
Apparatus: High Temperature Triaxial Cell

Specimen Dimensions

Before Test			After Test	
Diameter	5.32	cm	Diameter	cm
Height	10.80	cm	Height	cm
Area	22.19	cm^2	Area	cm^2
Volume	229.65	cm^3	Volume	cm^3
Mass	442.51	gm	Mass	gm
Density	1.85	gm/cm^3	Density	g/cm^3

Results of Soxhlet Extraction

% water = 9.0 % sand = 82.8 % bitumen = 8.2

Results of Specific Gravity

$G_s = 2.67$

Grain Size Analysis

Size of Opening (mm)	Percent Finer than
2.000	99.97
0.840	99.96
0.420	99.92
0.250	99.76
0.149	96.90
0.074	29.36
0.044	

Hydrometer Analysis

D (mm)	Percent Finer than
0.080	41.28
0.061	29.46
0.047	20.42
0.035	16.25
0.025	12.08
0.018	11.08
0.013	9.79
0.0095	8.40
0.0066	7.40
0.0047	7.09
0.0035	5.76
0.0026	5.39
0.0014	4.55

After Test Sketch

Specimen Data Summary Sheet

Test Number: THERM1
Apparatus:

Specimen Dimensions

Before Test			After Test	
Diameter	7.49	cm	Diameter	cm
Height	15.48	cm	Height	cm
Area	44.06	cm^2	Area	cm^2
Volume	682.06	cm^3	Volume	cm^3
Mass	1152.2	gm	Mass	gm
Density	1.69	gm/cm^3	Density	g/cm^3

Results of Soxhlet Extraction

% water = % sand = % bitumen =

Results of Specific Gravity G_s =

Grain Size Analysis

Size of Opening (mm)	Percent Finer than
2.000	
0.840	
0.420	
0.250	
0.149	
0.074	
0.044	

Hydrometer Analysis

D (mm)	Percent Finer than

After Test Sketch